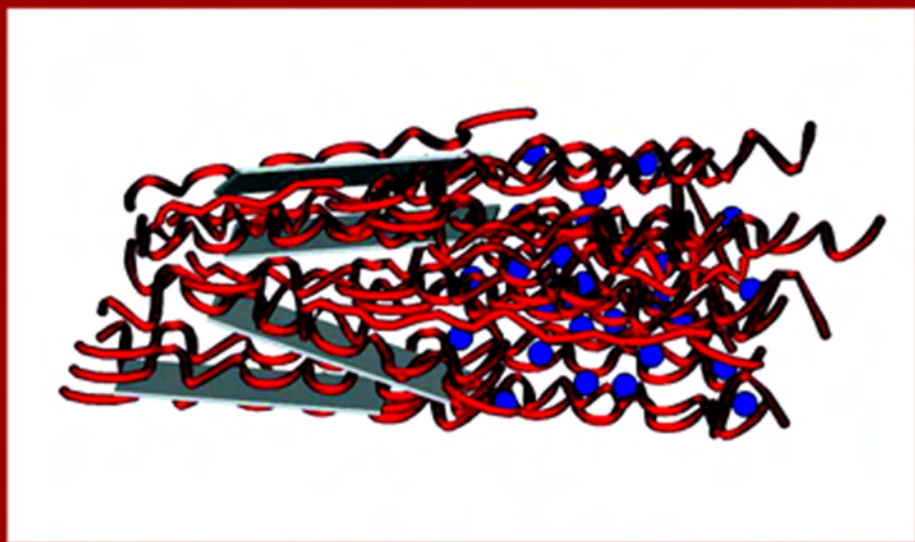




POLYMER-LAYERED SILICATE and SILICA NANOCOMPOSITES



Y.C. KE AND P. STROEVE

Polymer-Layered Silicate and Silica Nanocomposites

Cover illustration made by Jie-Ren Ku, University of California, Davis

Polymer-Layered Silicate and Silica Nanocomposites

Y.C. Ke

*China University of Petroleum
Beijing, China*

and

P. Stroeve

*Chemical Engineering and Materials Science Department
University of California, Davis, USA*

2005



ELSEVIER

Amsterdam – Boston – Heidelberg – London – New York – Oxford
Paris – San Diego – San Francisco – Singapore – Sydney – Tokyo

ELSEVIER B.V.
Radarweg 29
P.O. Box 211, 1000 AE
Amsterdam, The Netherlands

ELSEVIER Inc.
525 B Street, Suite 1900
San Diego, CA 92101-4495
USA

ELSEVIER Ltd
The Boulevard, Langford Lane
Kidlington, Oxford OX5 1GB
UK

ELSEVIER Ltd
84 Theobalds Road
London WC1X 8RR
UK

© 2005 Elsevier B.V. All rights reserved.

This work is protected under copyright by Elsevier B.V., and the following terms and conditions apply to its use:

Photocopying

Single photocopies of single chapters may be made for personal use as allowed by national copyright laws. Permission of the Publisher and payment of a fee is required for all other photocopying, including multiple or systematic copying, copying for advertising or promotional purposes, resale, and all forms of document delivery. Special rates are available for educational institutions that wish to make photocopies for non-profit educational classroom use.

Permissions may be sought directly from Elsevier's Rights Department in Oxford, UK: phone (+44) 1865 843830, fax (+44) 1865 853333, e-mail: permissions@elsevier.com. Requests may also be completed on-line via the Elsevier homepage (<http://www.elsevier.com/locate/permissions>).

In the USA, users may clear permissions and make payments through the Copyright Clearance Center, Inc., 222 Rosewood Drive, Danvers, MA 01923, USA; phone: (+1) (978) 7508400, fax: (+1) (978) 7504744, and in the UK through the Copyright Licensing Agency Rapid Clearance Service (CLARCS), 90 Tottenham Court Road, London W1P 0LP, UK; phone: (+44) 20 7631 5555; fax: (+44) 20 7631 5500. Other countries may have a local reprographic rights agency for payments.

Derivative Works

Tables of contents may be reproduced for internal circulation, but permission of the Publisher is required for external resale or distribution of such material. Permission of the Publisher is required for all other derivative works, including compilations and translations.

Electronic Storage or Usage

Permission of the Publisher is required to store or use electronically any material contained in this work, including any chapter or part of a chapter.

Except as outlined above, no part of this work may be reproduced, stored in a retrieval system or transmitted in any form or by any means, electronic, mechanical, photocopying, recording or otherwise, without prior written permission of the Publisher.

Address permissions requests to: Elsevier's Rights Department, at the fax and e-mail addresses noted above.

Notice

No responsibility is assumed by the Publisher for any injury and/or damage to persons or property as a matter of products liability, negligence or otherwise, or from any use or operation of any methods, products, instructions or ideas contained in the material herein. Because of rapid advances in the medical sciences, in particular, independent verification of diagnoses and drug dosages should be made.

First edition 2005

Library of Congress Cataloging in Publication Data
A catalog record is available from the Library of Congress.

British Library Cataloguing in Publication Data
A catalogue record is available from the British Library.

ISBN: 0-444-51570-4

∞ The paper used in this publication meets the requirements of ANSI/NISO Z39.48-1992 (Permanence of Paper). Printed in The Netherlands.

Contents

Preface vii

Acknowledgments ix

Chapter 1 Background on Polymer-Layered Silicate and Silica Nanocomposites 1

- Introduction 2
- 1.1. Layered silicate 3
- 1.2. Silica 21
- 1.3. Physical properties of layered silicate and silica 29
- 1.4. Polymers and polymerizations 44
- 1.5. Preparation and technology for nanocomposites 52
- 1.6. Recent phenomena in polymer-silicate and silica nanocomposites 62
- 1.7. Prospect 63
- References 65

Chapter 2 Modification and Dispersion of Silicate and Silica 69

- Introduction 70
- 2.1. Modification of silicate 70
- 2.2. Silica modification 84
- 2.3. Melt intercalation 100
- 2.4. Intercalation in media 105
- 2.5. Modification particles for polymerization 107
- References 117

Chapter 3 Polymer-Layered Silicate and Silica Nanocomposites 119

- Introduction 120
- 3.1. PA-silicate nanocomposites 120
- 3.2. PEO-silicate nanocomposites 135
- 3.3. Polyolefin-silicate nanocomposite 155
- 3.4. Polyester-silicate nanocomposite 172
- 3.5. Polyaniline-silicate nanocomposites 190
- 3.6. Other kinds of polymer-inorganic nanocomposites 197
- 3.7. Polymer-silica nanocomposites 201
- References 206

Chapter 4 Morphology, Assembly and Properties	211
Introduction	212
4.1. Nanostructure and morphology	212
4.2. Crystallization	228
4.3. Thermal properties	237
4.4. Mechanical properties	243
4.5. Special properties of nanocomposites	246
4.6. Functional properties by nanoparticle assemble and doping	256
4.7. Rheology and dynamic behavior	263
4.8. Nucleation and order	265
References	271
Chapter 5 Characterization and Techniques	275
Introduction	276
5.1. Particle Characterization	276
5.2. Structure and properties	278
5.3. Characterization techniques for structure and properties	285
5.4. Multiple structures of nanocomposites	308
5.5. Relationship between structure and property	310
5.6. Nanoeffects in nanocomposites	312
References	326
Chapter 6 Applications and Products	329
Introduction	330
6.1. Applications of nanocomposites	330
6.2. Products of nanomaterials	368
6.3. Nanocomposites and traditional industries	378
6.4. Prospects	384
References	387
Subject Index	389

Preface

Nanotechnology can be dated back to the 1860s when the field of colloid science was first established and when the colloid size range was defined from 1 to 1000 nm. Colloid scientists have studied materials in the nm range since that time. Over 80 years ago, life scientists, interested in the internal properties and functions of cells, began to look at structures at the nanoscale inside the cell. In the 1980s, the synthesis and investigation of new materials with size scales below a fraction of a micron became popular in many other fields. Some scientists predicted that, on the nanoscale, the properties of materials are quite different from those on the bulk scale. The preparation and study of nanoparticles became an active area of research. The use of nanoparticles in materials has become a central issue. The main problem in the application of nanoparticles is how to disperse the superfine particles into a matrix. When reviewing the technologies related to the dispersion of nanoparticles, it can be observed that the previous technology used for the dispersion of μm -sized particles is often employed. Many works deal with the surface treatment and interfacial design of nanoparticles, but the effective dispersion of nanoscale powders is still a major problem. Nanoscale particles with extremely high surface area and energy have a strong tendency to cluster. Agglomerated nanoparticles still account for a large part of nanoparticles dispersed in a matrix.

To deal with the dispersion problem, we took an opposite approach. We used a layered compound as an intermediate or precursor to prepare nanoscale materials through a step-by-step process, in which the μm particles are exfoliated into particles of a smaller size. In our approach, the larger particles become smaller and smaller, forming nanoscale particles, which is opposite to the agglomeration process in which the smaller nanoparticles become larger and larger. Fortunately, when naturally nanostructured layered silicates are used as the precursor, their interlayer distance can be pillared larger by the intercalation of foreign molecules or cations into the gallery space through an ion exchange reaction, and the silicate can be completely exfoliated by in situ polymerization.

Since 1994, research on polymer-layered silicate nanocomposites was started in China with support from the Natural Science Foundation of China (NSFC). The research was led by Prof. Z.N. Qi and F.S. Wang and, due to their and related scientists' efforts, nanotechnology and science on organic-inorganic nanocomposite became an emerging field in China. At the same time, several similar materials were developed by A. Usuki at Toyota, T. J. Pinnavaia at Michigan State University and P. Giannelis at Cornell University. Today, advanced research on organic-inorganic nanocomposites is conducted in different parts of the world.

Polymer-layered silicate and silica nanocomposites are important in China because of their applications to engineering, electronics, plastics and petrochemical fields. With

financial support from the Ministry of Science and Technology (MOST), the China Academy of Sciences (CAS), the Natural Science Foundation of China (NSFC) and corporations such as BASF (Germany), Sinopec (China) and CNPC (China), we have prepared and studied many advanced materials. Since 1996, we have applied for more than 20 patents in China for a series of nanocomposite materials, including polyesters (PBT, PET), polyolefins (PP, PE), polyamide and PI with layered silicates and silica. These materials have been used to make functional films, plastic bottles, coatings and engineering plastics. Some of these applications are summarized in our final reports to the financial organizations supporting the research, in postdoctoral reports, doctoral dissertations and the book *Polymer-Inorganic Nanocomposites* published in Chinese by China Chemical Industry Press.

When developing a series of polymer-layered silicate and silica nanocomposites, we made a breakthrough in fabricating plastic barrier bottles. Inspired by the success of silica nanoparticle preparations at a large scale developed by L.D. Zhang at the China Academy of Sciences (CAS), we prepared several nanocomposite materials with assembled, or array patterns, of monodisperse silica nanoparticles. Additional nanocomposite materials with arrays of silica were prepared with our collaborators. Composites with silica particles as small as 20 nm were also prepared.

We first attempt to present the nanocomposite materials with advanced properties, explore nanoeffects and develop the dispersion technology. As is shown above, our research obtained strong financial backing from MOST, NSFC and the national corporations. Meanwhile, at the University of California, Davis, layer-by-layer film technology was being studied in order to create nanoparticle/ultrathin film structures. We decided to join forces and combine our research efforts. We made a book proposal to Elsevier for publishing our research and partial related works from our collaborators.

This research monograph deals with nanocomposite materials of organic polymer-layered silicate, organic polymer-silica and layer-by-layer polyion nanoparticles. It focuses on the nanomaterial's classifications, preparations, characterization, applications and material properties. It also reports on our development of nanotechnology and processing of the polymer-layered silicate and silica nanocomposites.

The authors
Changping, Beijing, China
August 21, 2004

Acknowledgements

This research monograph reviews our research and the research of colleagues with whom we have collaborated. In addition, review the work of researchers who have had a significant impact on our own work. Thus, this book is a reflection of the research of many individuals and groups in the area of nanocomposites and nanoparticles. A number of years ago, Prof. Z.N. Qi and Prof. F.S. Wang conducted their ground-breaking research on polymer– inorganic nanocomposites in China and they wrote a book – *Preparations and Theory of Polymer-Layered Silicates Nanocomposites*, which was published by China Chemical Industry. Their work has had a tremendous impact on our research. Further, they have given us helpful advice and memorable guidance.

Most of the work in this research monograph comes from the final reports of several projects, which were supported by the Ministry of Science and Technology (MOST), the China Academy of Sciences (CAS), the Natural Science Foundations of China (NSFC), and the companies BASF (Germany), PetroChina, CNPC (China) and Sinopec (China). Some pictures and graphs in the book are from postdoctoral reports written by Prof. Y. C. Ke, the senior author of this book.

Some researchers and professors provided original material and gave us permission to publish their work in our book. We thank our colleagues Prof. Q. Li, Prof. L.D. Zhang, Prof. P. Dong, Prof. J.N. Yan, Prof. Y. Cai Ke, Dr. Z.J. Xue, Y.M. Ma and others for providing us with such information. We appreciate their kindness.

We thank our students and postdoctorates who collaborated with us in the research: C.J. Yan, D.Y. Zheng, T.B. Wu, H. Wang, Y.X. Song, M.Z. Sun, G.F. Yang, W.K. Liu, Y. Wang, S. Dante, A.M. Fojas, E. Murphy, L. Zhang, A. Dutta, G. Jarero, A.K. Dutta, T. Ho, Z. Hou and others. The following students also assisted us in typing and drawing figures: C.J. Yan, D.Y. Zheng, T.B. Wu, H. Wang, Y.X. Song, M.Z. Sun and G.F. Yang.

Financial support from the State Key Lab of Heavy Oil Processing in China for writing this book is specially appreciated. Supports from native and abroad media and magazines have been mentioned in separate figures of the book.

This page intentionally left blank

CHAPTER 1

Background on Polymer-Layered Silicate and Silica Nanocomposites

OUTLINE

- Introduction 2
- 1.1. Layered silicate 3
 - 1.1.1. *Nanostructures in nature* 3
 - 1.1.2. *Classifications of silicate* 8
 - 1.1.3. *Layered structures of silicate* 10
 - 1.1.4. *Natural mineral resources of silicate in China* 20
 - 1.1.5. *The world mineral resources for silicate* 21
- 1.2. Silica 21
 - 1.2.1. *Precursor of silica* 22
 - 1.2.2. *Resources of silica* 25
 - 1.2.3. *Monodisperse silica* 25
- 1.3. Physical properties of layered silicate and silica 29
 - 1.3.1. *Condensed structure* 29
 - 1.3.2. *Silica colloid crystals and opals* 32
 - 1.3.3. *Particle and porosity* 32
 - 1.3.4. *Diffuse electrical double layer* 36
 - 1.3.5. *Zeta potential* 38
 - 1.3.6. *Coagulation and flocculation* 39
- 1.4. Polymers and polymerizations 44
 - 1.4.1. *Multiple structure of polymers* 44
 - 1.4.2. *Polymer classification* 47
- 1.5. Preparation and technology for nanocomposites 52
 - 1.5.1. *Brief introduction to nanocomposite preparation* 52
 - 1.5.2. *General design and aspects for nanocomposite* 54
 - 1.5.3. *Technology for composite nanoparticles or nanocomposites* 58
 - 1.5.4. *Intercalation chemistry for nanocomposites* 60
 - 1.5.5. *Some reviews on nanocomposites* 61
- 1.6. Recent phenomena in polymer-silicate and silica nanocomposites 62
 - 1.6.1. *The types of microstructure in PLS nanocomposites* 62

1.7. Prospect 63

1.7.1. Prospect of nanocomposites and their applications 63

References 65

In this chapter we introduce general concepts, the methods of preparation of nanoparticles and nanocomposites and classifications of different technologies, e.g., intercalation chemistry and sol–gel processes. Classical colloidal theory and its applications to nanocomposites are also discussed.

Introduction

In polymer-layered silicate and silica nanocomposites, the polymers used are those that are universal. Layered silicate are those minerals that assemble regularly with the unit crystalline layer, usually at the nanoscale. Minerals are montmorillonite (MMT), kaolinite, sepiolite, etc. In this book, the word clay is a general name for layered silicate minerals, and specifically refers to MMT if not otherwise pointed out. Silica in this book refers to multiple dispersed silicon oxides, monodispersed silica particles and its powders.

The book mainly deals with the preparation of polymer-layered silicate and silica nanocomposites, their structure–property relationships and the related nanoeffects. Some key aspects are specifically emphasized, such as the in situ preparation of solid precursors for nanoparticles and nanocomposites, the proper dispersion of nanoparticles in selected inorganic or organic matrixes, particle surface treatment and in situ polymerization. With the development of ultrafine particles and their applications, the dispersion techniques for micrometer particles are introduced for nanoparticles to obtain ideal homogeneous morphology [1]. From the previous literature, the dispersions of both nanoparticles and micrometer particles are mentioned in several sections of this book. Our primary goals are to show how to enhance the organic polymer properties by making nanocomposite materials of polymers and silicate. We think of nanocomposites as materials to improve the properties of traditional organic polymers. Improved properties of polymer materials are of great importance in applications in the petrochemical industry, the chemical industry, materials and allied fields.

In this book, layered silicates are designed by in situ dispersion into polymer matrixes through a method called “intercalation,” in which polymer monomers are intercalated into the gallery space of layered silicates, causing the layers to exfoliate before polymerization reactions are initiated. Finally, the polymer-layered silicate nanocomposites are discussed. Most layered silicates themselves have strong dispersion and cation exchange properties in many media, e.g., water and ethanol, which is why silicate are selected as raw materials for fabricating nanocomposites. Layered silicate contains certain quantities of non-metals, such as silicon, proteins, iron oxides and titanium elements. These materials can be harmful and lead to unstable or not useful crystalline structures. Thus, silicate should be purified and transformed into “polymer grade clay” [2]. To a large extent, intercalation polymerization based on layered silicates creates a way to prepare and disperse nanoparticles in organic polymer matrixes. Preparation techniques are designed to avoid nanoparticle agglomeration during dispersion. However, dispersed particles tend to form

aggregates during dispersion. Particles piled together without separation or particles forming interconnected agglomerations have to be avoided in order to enhance the material properties of the nanocomposite. Thus, researchers have sought ways to avoid the agglomeration of particles. At present, *in-situ dispersion* is an established technology for dispersing fine particles in materials. In this book, we show how layered silicates are fabricated by in situ dispersion in a polymer matrix by a method called *intercalation*, in which polymer monomers are intercalated into the spacing of layered silicates, after which the layers are exfoliated once the polymerization reaction is initiated. In this manner, nanocomposites of polymer silicates can be prepared.

According to our previous works [3–5], a layered silicate as a candidate for preparing a nanocomposite must meet requirements based on its structural unit, stable ingredients, reactive properties, high-performance–cost ratio and available resources in nature. We give more details below.

Structural units. The most important reason for layered silicates to be a candidate in preparing nanocomposites is their unit layer structure. The unit structure scale is 1 nm or so, and usually forms a nanophase in situ in a polymer matrix during its compounding or polymerization. There is also a requirement that the layers be expandable and easily exfoliated during formation of the nanocomposite. Generally, the layer interdistance must be expandable in solvents such as water and alcohol.

Stable ingredients. Most layered silicates have no stable ingredients, but they have ambiguous features such as unknown compositions, variable elements or transitional elements such as Fe, Ti and their oxides.

Reactive properties. Reactive properties refer to the layered structure taking part in different reactions including copolymerization reaction with the surface hydroxyl groups, catalytic reaction, etc. Specifically, the layered silicate should not pose an obstacle to polymerization during the exfoliation process.

High performance–cost ratio, and readily available resources in nature. The selected mineral as a candidate in preparing nanocomposites on an industrial scale requires that the cost is appropriate based on the performance of the nanocomposite. This depends on a good performance to cost ratio.

In this book, a great number of nanocomposites of polymer silica are introduced and discussed. This will naturally lead to questions about the suitability of silica for nanocomposites. Similar to the layered silicates with surface hydroxyl groups, ultrafine silica is also suitable for in situ polymerization through proper surface treatment. This silica is generally prepared in a form called “core–shell” structures, where the silica is in the core position, while polymer or oligomer film is outside of the particles. The core–shell particles have their scale usually greater than pristine silica but they exfoliate during further compounding, or during in situ polymerization with polymer monomers.

1.1. Layered silicate

1.1.1. Nanostructures in nature

Nanostructures in nature can be found in various forms. Naturally formed nanostructures exist not only in non-living forms but in living forms as well. In biological systems, there

exist a great variety of complex self-assembled nanostructures in organelles, cells, tissues and organs. Nature tends to arrange itself into nanostructures. Nature's ordered structures and patterns are very useful for study. Organic macromolecules and biological molecules have been designed by nature to build nanostructures or composite structures in biological systems [5]. Molecular self-assembly is of great interest to scientists and has stimulated research in nanotechnology and nanoscience.

In this book, nanostructures in nature refers specifically to those found in minerals, and specifically to layered silicates. In different minerals, such as MMT, illite, talc, saponite, attapulgite and mica, layered structures of nanometer size can be found. The natural nanostructures in layered silicates are also seen in man-made materials such as the carriers ZSM-5, MCM-42, MCM-41 and zeolite [6], which are used in the petrochemical industry. These materials have either nanometer-size pores or nanoscale particle structures. The carrier materials are prepared by copying natural nanostructures such as the zeolites, which have pore diameters from several nanometers to several tens of nanometers. When catalysts such as P_d , P_t and R_h are dispersed as nanoclusters on the surfaces of the carrier materials, the resulting catalytic materials are used for oil cracking. In particular, when Ziegler–Natta catalysts are deposited on the carrier $MgCl_2$ [5], or its mixture with silica, the active catalyst components are from 1 nm to several tens of nanometers thick and are suitable for polyolefin polymerization.

Extensive work in the literature indicates whether the minerals are of natural occurrence or man-made, and if the natural nanostructures can be identified. The International Union of Pure and Applied Chemistry (IUPAC) [7] has given a definition for the pore diameter of these materials (see Table 1.1). According to this definition, porous carriers are called nanoporous and are different from nanoparticles themselves. Materials with either nanopores or nanoparticles are generally defined as nanomaterials.

1.1.1.1. Some milestones in nanoscale science and technology

In 1959, the Nobel Prize Physicist Richard Feynman asked “what would happen if we could arrange the atoms one by one the way we want them?” in one of his question lectures at the University of California. His question is thought to be the theoretical origin of the creation of modern nanotechnology and nanoscience. The development of the atomic force microscope (AFM) and the scanning tunneling microscope (STM) by IBM in the 1980s was another milestone [8,9]. The invention of scanning nanoprobe microscopies has stimulated the development of nanotechnology and nanoscience in the last 20 years.

In 1989, the Argonne National Laboratory (USA) facilitated the establishment of a company based on nanophase materials and also organized a meeting on nanometer

Table 1.1
IUPAC classification for pores

Pore classification	Pore diameter (nm)
Micro-pore	< 2
Medium pore	20–50
Large pore	> 50

science and technology. In 1992, the first scientific magazine on nanomaterials, *Nanostructured Materials*, appeared. In the 1980s and 1990s, the synthesis of carbon nanotubes and C₆₀ Buckey Balls stimulated the interest in nanotechnology and nanoscience. Around 1997, several companies were created that produced nanomaterials (e.g., Nanophase Technologies and Nanocor).

In the 1980s, scientists in China suggested that new alloys with new metal crystalline phases could be made using metal superfine powders below micrometer scale [11]. Research in this area was published in a book on nanomaterial science [12]. These events are thought to be the beginning of nanomaterials and their applications in China. Work on nanomaterials and nanotechnology in China has been discussed in several recent books, [5,10].

On the other hand, one can easily find discussions of many chemical methods for preparing nanoparticles, nanopowders and nanoscale materials in the literature of the past century. For example, the sol-gel technique is well known for preparing different forms of nanomaterials. Historically speaking, colloid chemistry has been known for more than a century, and in this field one can find procedures for the preparation of many nanomaterials. Colloid chemistry defines colloidal particles as particles that range in from 1×10^{-9} to 1×10^{-6} m (or 1–1000 nm), which is partly in the nanoscale. This proves that concepts such as nanosize, nanoscale and nanoscience have, an effect, been known for more than a hundred years.

1.1.1.2. Formation of concepts for nanomaterials and nanotechnology

While it might seem to be too early to, give a complete definition of nanomaterials and nanotechnology, we have to present such concepts in our teaching, lectures and books for engineering students. Together with other related literature, this book will use the following expressions to describe nanoscience and nanotechnology.

- (1) Nanometer: a unit for nanomaterials, often abbreviated as nm.
- (2) Nanoscale: a scale within nanometers.
- (3) Nanoparticle: a nanoscale particle.
- (4) Nanostructure: a nanoscale structure, usually a structure revealed under scanning probe microscopy, e.g. TEM and AFM.
- (5) Nanomaterial: a material in which many nanoparticles with nanoscale structures are dispersed or aggregated.
- (6) Superfine or ultrafine powder: refers to powder materials with their particles at the nanometer scale.
- (7) Nanotechnology: The U.S. National Nanotechnology Initiative (NNI, 2000) and other sources describe nanotechnology as a technology for synthesizing nanomaterials by controlling single atom behavior at the molecular level and creating new molecular structures. Nanotechnology deals with matter showing novel and markedly improved character when the structure and composition of the matter system within 1–100 nm. Nanotechnology falls aims at the development of information on nanostructures, the invention of analytical equipment to investigate the characteristics of nanostructures based on groups of atoms, molecules and supramolecules, and the creation of processes to produce nanostructures for useful applications.

1.1.1.3. Nanocomposites

1.1.1.3.1. Definition of composites In polymer science, the word composite is well known. In brief, composites are generally two or more closely interacting materials in intimate contact with each other. Intimate contact can be down to the atomic or molecular level. Polymer science uses the concept of a composite as a material formed by combining different phases. There are many ways of combining phases and these are: filling, blending, compounding, mixing, melting and assembling. These terms are well known in scientific papers dealing with composites, especially those related to material or polymer science. Though a composite is not easily defined or briefly described, this book will adopt the definition of the concept of a composite as it is used in polymer science.

1.1.1.3.2. Composite materials According to the International Organization for Standardization, composite materials are solid ones with multiple phases, which is a combination of two or more materials with different physical and chemical properties [12]. In composite materials, one phase is usually continuous and called the matrix, while the other phase is a reinforcing material called the dispersed phase. In self-assembled systems, the ordered structure is the dispersed phase, while the template film can be the continuous phase.

Organic–inorganic composite materials. This refers to composite materials in which one phase is made up of organic molecules or polymers and the other of inorganic molecules or polymers. Thus, polymer–inorganic composites belong to this category.

Organic–inorganic nanocomposites. In organic–inorganic composites, nanocomposites refer to composites in which the inorganic phase has nanoscale morphology such as particles, fibers and tubes. There is an additional type of organic–inorganic nanocomposite, where either the organic phase or the inorganic phase has nanoscale morphology in an organic–inorganic composite [5,12]. For example, in emulsion systems of W/O or O/W, clay nanoparticles and silica are often used to stabilize the emulsions, which then form an organic–inorganic nanocomposite. In designing a system of thiol/FeOOH, heating the mixture would lead to the formation of thiol/Fe₂O₃ or thiol/Fe₃O₄ nanocomposites [5].

Polymer–Inorganic nanocomposites. Generally, it refers to a nanocomposite in which organic polymer forms a composite with inorganic nanoparticles, e.g., BiI₃–nylon nanocomposite [13], and montmorillonite–nylon (polyester) nanocomposites [7].

1.1.1.4. The classification of nanocomposites

This book gives our classifications of nanocomposites based on a review of the literature.

- (1) *Classification 1.* This classification is based on the nanomaterial's dimensional (D) morphology.
 - (a) 0-D nanopowder or nanoparticle;
 - (b) 1-D nanowire, nanowisp, nanosilk, nanotube or nanocrystalline whisker;
 - (c) 2-D nanomaterial with morphology of layer, lamellar or belt structure;
 - (d) 3-D nanomaterial with morphology of cylinder, solid or block structure.
- (2) *Classification 2.* This classification is based on polymer morphology, shape or state in the nanocomposites, in which the inorganic particle is a 0-D nanoparticle [5,14].

- (a) 1-D nanocomposite when the polymer in the composite is in solution;
 - (b) 2-D nanocomposite when the polymer in the composite is in film or membrane shape;
 - (c) 3-D nanocomposite when the polymer in the composite is in a powder state or morphology;
 - (d) 0-D nanocomposite formed with two different nanopowders.
- (3) *Classification 3*. This classification is based on a nanophase of tube- or non-tube-like material in the nanocomposites.
- (a) *Tube-like*, e.g., single-wall carbon nanotube, TiO₂ Tube, or Al₂O₃ tube.
 - (b) *Non-tube-like*, e.g., layer of clay, lamellar, silk, belt or band-like shape.

Sometimes, the classifications are mixed to describe nanocomposites, e.g., carbon nanotubes or nanocrystalline whiskers with polymer powder construct a 1–3 type nanocomposite. Nanolayers of clay with polymer powder form 2–3 type of nanocomposites, etc. The classifications for nanomaterials or nanocomposites are of definite significance with respect to the so-called “nanoeffect,” which is related to the material properties of the composite (mechanical, optical, thermal and magnetic) and the dependence of the properties on the size of the nanoparticles in the nanocomposite.

1.1.1.5. *Nanoeffect*

Besides the particle’s shape, surface or morphology, dispersion and aggregation in a matrix, attention needs to be paid to the properties and performance of a composite. How nanoparticles affect the properties of nanocomposite materials is of concern to engineers and scientists who are interested in the applications of nanocomposites.

1.1.1.5.1. Critical scale The nanomaterials or nanocomposites and the theories related to them are based on a concept of “critical scale,” or nanoscale. For a critical scale of nanoparticles, the nanocomposite properties produce a superior property compared with the pure counterpart matrix if the nanoparticles are below a critical size. When a material structure has one dimension less than the critical scale of 100 nm, can appear totally different the behavior of its material properties. Based on such phenomena, scientists determined the abnormal phenomena to be produced on the scale level between single-atom molecules and clusters of many thousands of molecules. Properties of any nanocomposite must include two aspects: “nanoscale” and “nanoeffect.” At a critical scale, the properties of nanocomposite materials can sometimes produce an inverse transition of a property, e.g., the conduction behavior of the metal Ag will change into that of an insulator at a particle scale less than 14 nm, while ferric magnetic performance is transformed into supermagnetic if the cluster size becomes less than several nanometers.

1.1.1.5.2. Nanoeffect in nanocomposites Nanoeffects in nanocomposites have several forms such as acceleration of polymer crystallization, induction of crystallization in a polymer, induction of liquid crystalline phenomenon, abnormal optical phenomenon, e.g., a blue shift, and abnormal multiple melting behavior, e.g., double-melting behavior in PET-layered clay nanocomposites. In addition, several forms of nanoeffects related to optical–electrical transition, electrical–magnetic transition and system properties are introduced in the book.

A nanoeffect can result from the transition of the performance due to aggregation, change of morphology or interactions, which leads to subsequent changes in the materials' properties. As for nanocomposites, with many nanoeffects were not seen in each single composition, nanoeffects occurred during mixing, blending, compounding or in situ polymerization of the selected nanoparticles with the matrix (matrix usually refers to macromolecules or polymers). Only after two kinds of matter come together to make a composite, where one phase is composed of nanoparticles, a nanoeffect can occur. Examples of these nanoeffects are numerous and are described in this book. Specific examples will be given in later chapters.

Example 1.1.1.1. Nanoeffect in BiI₃-nylon11 nanocomposites. BiI₃ is a semiconductor and Nylon11 is a polyamide II [13] with good insulating properties. Neither conducts electricity, but do conduct once they are melted together. When the BiI₃ mass % reaches 50% of the composite, the composite materials will produce strong electrical conducting properties. In these composites, BiI₃ is divided into 20 nm-sized particles, dispersed in the nylon matrix.

Example 1.1.1.2. Blue transfer of ZnO particle. The blue transfer occurs when nanocomposites containing ZnO nanoparticles absorb violet light. After nanoparticles of ZnO are treated with different surfactants, the absorption wavelength shows different blue transfer compared with the naked particles. Some results of blue transfer caused by treated ZnO nanoparticles are shown in Table 1.2.

1.1.2. Classifications of silicate

1.1.2.1. Classifications of layered silicate and related compounds

Classifications of layered silicates and related compounds are made based on their layered structure, to better understand their properties and effects in nanocomposites. The layered materials and related compounds may be separated into several types as follows:

- (1) Non-metal graphite, asphalt mesophases
- (2) Layered silicates, natural and/or artificial clay minerals (see Table 1.3)
- (3) Transition metal dichalcogenides
- (4) Transition metal oxides
- (5) Layered compounds (see Table 1.3)
- (6) Layered double hydroxides (LDH)
- (7) Phosphates and metal phosphates

Table 1.2

Blue transition characters of treated ZnO nanoparticles after absorption of ultraviolet light

No.	Surfactant	Particle size (nm)	Absorption (nm)	Transmittance (%)
1	—	4–15	300–380	85
2	Span-80 ^a	40–70	220–280	96
3	PEG-400 ^b	100–250	250–300	90
4	PEG-200	100–200	250–290	89

^aPolyethylene glycol.

^bNon-ionized commercial surfactant.

Table 1.3
Classifications of layered silicate and compounds

Inorganic	Examples
Layered compounds	MoS ₂ , V ₂ O ₅ , MoSe ₂ , WS ₂ , WSe ₂ , SnS ₂ , ZrSe ₂ , PbI ₂ , BN, BiI ₃
Layered silicates	Magadiite, bentonite, kaolinite, montmorillonite, clay saponite, sepiolite, vermiculite, talc (OH), hectorite, attapulgite, fluoromica, illite, chlorite

Table 1.4
Classifications of layered silicate crystals

Unit crystal lamellae type	Family of clay	Examples of clay
1:1	Family of kaolinite Family of illite	Kaolinite, perlite clay, etc. Illite, etc.
2:1	Family of saponite ^a Family of hydromica	Montmorillonite, saponite, vermiculite Illite, glauconite
2:2	Chlorite family and others	Chlorite
Mixed layer and chain structure	Family of saponite	Sepiolite, palygorskite, attapulgite

^aPreviously also named as a family of MMT while called montosaponite, since 1975, by the name committee of the international clay investigation committee.

The classifications of layered silicates and compounds are shown in Table 1.3. In our investigations of layered silicates, these minerals are briefly classified according to the types and the relative content of the unit crystal lamellae (Table 1.4).

According to the relative ratio of two unit crystal sheets in Table 1.4, the layered silicates are divided into three types:

- 1:1 *type*. Its unit lamellar crystal is composed of one crystal sheet of silica tetrahedron combined with one-crystal lamellae of alumina octahedron.
- 2:1 *type*. Its unit lamellar crystal is composed of two crystal sheets of silica tetrahedron combined with one crystal sheet of alumina octahedron between them.
- 2:2 *type*. Its unit lamellar crystal is composed of four crystal sheets, in which crystal sheets of silica tetrahedron and alumina or magnesium octahedron are alternately arranged.

Mixed lamellar and chain-like structure. In this structure, the lamellar hexagon rings composed of silica tetrahedron sheets are arranged opposite to one another in a right direction from the top down.

1.1.2.2. The chemical composition of layered silicate minerals

Attention is paid to the chemical composition of layered silicates when they are used as candidates for preparing nanocomposites. Stable compositions directly lead to the final properties of the nanocomposite products. The most popular or practical layered silicates of clay are of three types: kaolinite, MMT and illite (hydro-mica). Their chemical compositions are shown in Table 1.5.

Table 1.5
Chemical compositions of layered silicate of clay minerals

Name of clay	Chemical composition	$n\text{SiO}_2/n\text{Al}_2\text{O}_3$
Kaolinite	$\text{Al}_4[\text{Si}_4\text{O}_{10}] (\text{OH})_8$ or $2\text{Al}_2\text{O}_3 \cdot 4\text{SiO}_2 \cdot 4\text{H}_2\text{O}$	2:1
Montmorillonite	$(\text{Al}_2\text{Mg}_3)(\text{Si}_4\text{O}_{10}) (\text{OH})_2 \cdot n\text{H}_2\text{O}$	4:1
Illite	$(\text{K}, \text{Na}, \text{Ca}_2)_m (\text{Al}, \text{Mg})_4 (\text{Si}, \text{Al})_8 \text{O}_{20} (\text{OH})_4 \cdot n\text{H}_2\text{O} (m < 1)$	4:1

Clays have different chemical compositions: kaolinite has a high content of alumina and low content of silica; MMT has a low content of alumina and a high content of silica; illite has a high content of K_2O . The chemical composition of layered silicates of clay minerals in nature is a reference parameter for their applications and is also important as evidence for chemical analysis in order to identify the type of clay.

1.1.3. Layered structures of silicate

1.1.3.1. Crystal structure of some layered silicates of clay minerals

1.1.3.1.1. Silica tetrahedron and its crystal sheet Silica tetrahedron as a unit structure is obtained from the results of X-ray diffraction and is shown in Figure 1.1. The four oxygen atoms are located at the corner of the silica tetrahedron linked by covalent bonds to a silicon atom at the center. The silicon atom has the same distance from three oxygen atoms. In most layered silicate minerals, the silica tetrahedron forms a hexagonal structure in planar form by sharing oxygen atoms at three corners (Figure 1.1(b)). The silica tetrahedron is actually a network stereostructure (Figure 1.1(c)) or a silica tetrahedron crystal sheet.

1.1.3.1.2. Alumina octahedron and octahedral crystal sheet Six hydroxyl ions situated at the corners of the octahedron, in which aluminum, ferric or magnesium ion is in the central position, are shown in Figure 1.2(a). Figure 1.2(b) indicates that only octahedral sites are occupied by Al^{3+} ions in the octahedral sheet, and the asterisk signifies one-third of the unoccupied position. If trivalent metal ions like Al^{3+} and Fe^{3+} just hold two-thirds of the central positions of octahedral sheets and the other one third centers are empty, this kind of crystal sheet is known as a dioctahedral crystal sheet. When all octahedral centers of the crystal sheet are occupied by a divalent metal ion such as Mg^{2+} or Fe^{2+} , a trioctahedral crystal sheet is formed, which is shown in Figure 1.2(c).

1.1.3.1.3. Combination of crystal sheets Tetrahedral and octahedral sheets are linked with shared oxygen atoms and held together, forming crystal layers. When this layer structure is composed of one tetrahedral sheet and one octahedral sheet (say kaolinite), the hexagonal network formed by oxygen atoms is exposed in the same plane.

When the structure of clay minerals consists of two tetrahedral and one octahedral sheet, the octahedral sheet is sandwiched between the two tetrahedral sheets, and the oxygen atoms at the apex of the silica tetrahedrons extend into and are part of the octahedral sheet, where two hydroxyls in each octahedron are replaced with the shared oxygen atoms. In this case, the hexagonal oxygen-atom network is exposed as the upper and

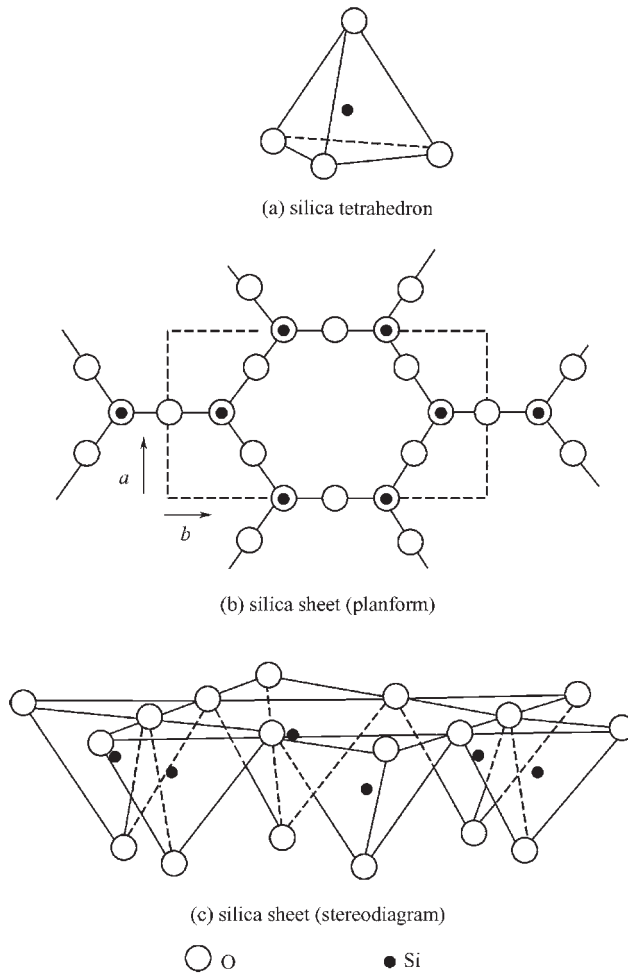


Fig. 1.1. Sketch map of silica tetrahedron and silica sheet.

lower surface of the crystal layer. The tetrahedral silica sheet and the octahedral alumina sheet are linked by covalent bonds to form a unit crystal layer. The crystal layers stack up to form the crystal structure. The mark C is used to represent the vertical distance between adjacent layers. Figure 1.3 shows a diagrammatic sketch of the kaolinite layer, where $C = 0.72$ nm.

1.1.3.2. Crystal structures of some major clay minerals

1.1.3.2.1. Kaolinite Kaolinite is composed of a tetrahedral silica sheet and an octahedral alumina sheet (Figure 1.3). The basal oxygen atoms of the tetrahedral sheet form a hexagonal pattern and the apical or top oxygen atoms of all tetrahedra are perpendicular to the sheet. The tetrahedral and octahedral sheets are connected with shared oxygen

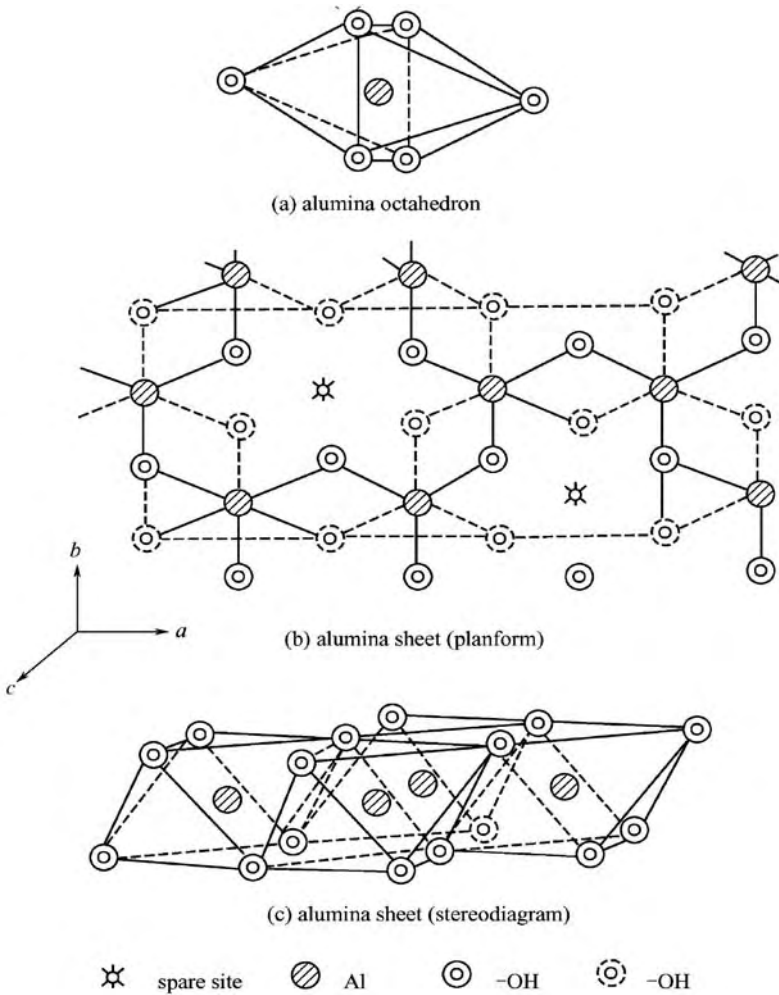


Fig. 1.2. Sketch map of alumina octahedron and alumina sheet.

atoms. The charge within the layers is nearly balanced, and the chemical formula is $\text{Al}_4[\text{Si}_4\text{O}_{10}](\text{OH})_8$ or $2\text{Al}_2\text{O}_3 \cdot 4\text{SiO}_2 \cdot 4\text{H}_2\text{O}$. Kaolinite is called a 1:1 type of layered mineral since its structure is composed of one tetrahedral sheet and one octahedral sheet, where layers are stacked up along the c -axis and extend to the plane made up of a - and b -axes. The hexagonal scale structure can be observed microscopically.

Successive kaolinite layers are held together by hydrogen bonds formed by the OH–O pairing between octahedral hydroxyl ions at the top of the layer and tetrahedral oxygen atoms at the base of the overlying layer. The distance between adjacent layers reaches 7.2×10^{-1} nm. The closely stacked structure of kaolinite results in favorable stability, low dispersion degree and no substitution.

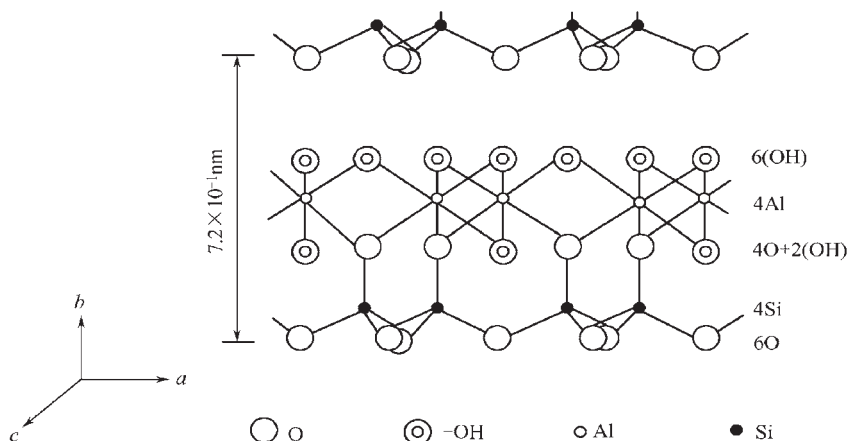


Fig. 1.3. Diagrammatic sketch of kaolinite. (permitted and provided from Press of University of Petroleum)

Owing to the nature of the kaolinite structure, the cation exchange capacity of these mineral is relatively low, and it is difficult for water molecules to enter the interlayer space. Consequently, kaolinite belongs to the non-swelling type of clay minerals. Therefore, kaolinite cannot be used to prepare nanocomposite materials through cation exchange (like MMT) because of its poor hydration and unsatisfying mud-making ability. However, there are other methods that can be applied to the preparation of nanomaterials by making use of kaolinite. For example, before kaolinite is used to produce nanocomposite materials, polar organic molecules can be embedded in it (see the latter part of this chapter).

1.3.2.2. Montmorillonite MMT is a derivative of pyrophyllite. The formula for pyrophyllite is $\text{Al}_4[\text{Si}_4\text{O}_{10}](\text{OH})_2$. Pyrophyllite has a 2:1 layer structure consisting of two fused silica tetrahedral sheets sandwiching an edge-shared octahedral sheet of alumina, as shown in Figure 1.4. The apical oxygen atoms of the tetrahedral sheet are all shared with the octahedral sheet. Such layers extend continuously in the plane constituted by the *a*- and *b*-axes and are stacked up in the *c*-axis direction, thus forming the whole crystal structure.

The difference between the crystal structure of MMT and pyrophyllite is that the latter is neutral, while the former has layer charges due to isomorphous substitution. Isomorphous substitution occurs when some atoms in the crystal structure are replaced with other atoms with different valence without any change in the sketch of the crystal structure. For instance, when there is an isomorphous substitution of Mg^{2+} for Al^{3+} in the octahedral lattice, a negative charge of minus one (-1) is generated, which is normally counterbalanced by cations adsorbed from the ambient solution. Isomorphous substitution can take place in both octahedral and tetrahedral lattices, for example, a portion of Si^{4+} in tetrahedral sheets can be replaced with Al^{3+} , and a part of Al^{3+} in octahedral sheets can be substituted with Mg^{2+} , Fe^{2+} or Zn^{2+} . If one-fourth Al^{3+} in octahedral sheets and one-eighth of the Si^{4+} in tetrahedral sheets are replaced with Mg^{2+} and Al^{3+} , respectively, the chemical formula of this kind of MMT is $(\text{Al}_{3.34}\text{Mg}_{0.66})(\text{Si}_{7.0}\text{Al}_{1.0})\text{O}_{20}(\text{OH})_4$. The crystal structure of MMT is shown in Figure 1.5.

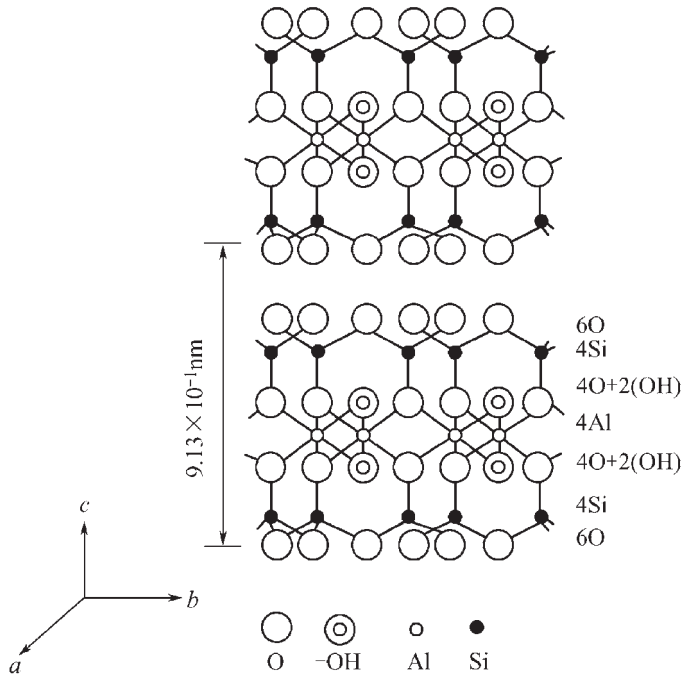


Fig. 1.4. Diagrammatic sketch of pyrophyllite. (permitted and provided from Press of University of Petroleum)

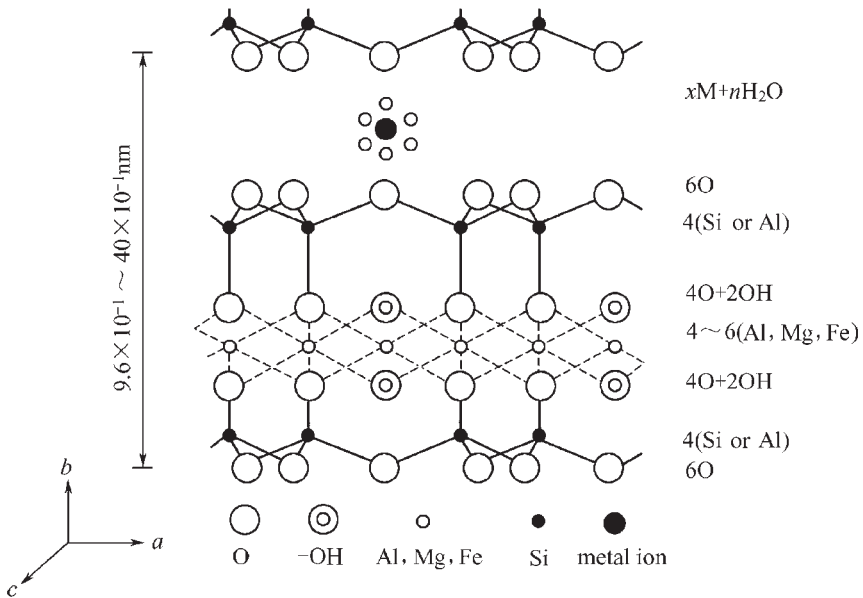


Fig. 1.5. Diagrammatic sketch of MMT. (permitted and provided from Press of University of Petroleum)

All positions at the top and base of the lattice layers of MMT are completely occupied by oxygen atoms. These layers are held together by a relatively weak intermolecular force. As a result, water molecules easily penetrate the interlayer region and can cause the expansion of the lattice. Owing to isomorphous substitution between metals, MMT with negative charges can adsorb cations with an electric quantity equal to that of montmorillonite. Hydrated cations enter the interlayer region, which then leads to an increase in the distance between adjacent layers. Accordingly, MMT is an expandable clay mineral and has colloidal activity. The whole surface of layers including the internal surface and external surface can be hydrated and the exchange reaction of cations can occur there (Figure 1.6). MMT possesses a specific surface area as large as $800 \text{ m}^2 \text{ g}^{-1}$.

The degree of expansion of MMT is determined by the category of the exchangeable cations. The expansion pressure of MMT in which sodium ions constitute the majority of the adsorbed cations (called Na-MMT) is very high, leading to the exfoliation and dispersion of the crystal in the manner of fine particles or even single layers. The size of the particle has been measured, but this is difficult because the clay mineral is very thin, its shape is irregular and the range of sizes is very wide. Kahn has used a supercentrifuge and modern optical apparatuses to study the size of Na-MMT and the results are listed in Table 1.6. The data in Table 1.6 indicate that the width and thickness of the clay particles decrease with the decrease in the equivalent spherical radius. The same result is also obtained from X-ray diffraction and optical scattering measurements. Images obtained by electron microscopy of the edge of coarse Na-MMT particles (separated by supercentrifuge) illustrate that 3–4 unit layers stack up orderly and make up a slice. When Ca^{2+} , Mg^{2+} and ammonium are the dominant exchangeable cations, the dispersion degree is relatively low and the size of the particle is relatively large.

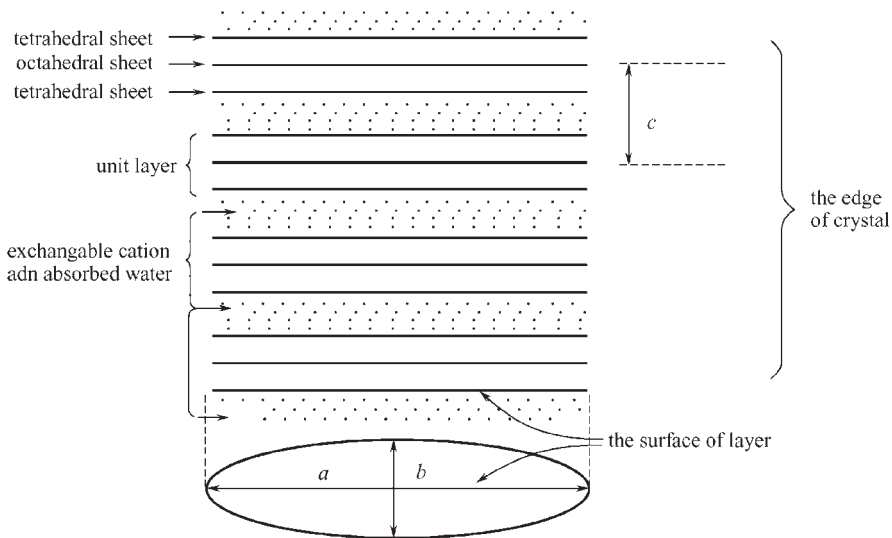


Fig. 1.6. Diagrammatic sketch of 2:1 layer clay.

Table 1.6
Distribution of Na-MMT particles in water

Rank	Mass ratio (%)	R_E equivalent spherical radius (μm)	L (μm)		B (10^{-1} nm)	Average number of layers in each particle
			By electron optics birefracton	By electron microscope		
1	27.3	> 0.14	2.5	1.4	146	7.7
2	15.4	0.14–0.08	2.1	1.1	88	4.6
3	17.0	0.08–0.04	0.76	0.68	28	1.5
4	17.9	0.04–0.023	0.51	0.32	22	1.1
5	22.4	0.023–0.007	0.49	0.28	18	1.0

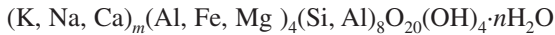
Note: R_E is the equivalent spherical radius of layered silicate of clay (or briefly, clay), L the measured maximum width of clay and B the measured thickness of clay.

Kahn has used the concept of “equivalent sphere” in his study to describe the average properties of layered silicates of clay. A sphere whose volume is equal to that of an irregular clay particle is called the equivalent sphere. The method for calculating the size of equivalent sphere is stated here. The clay particle is assumed to be a flat but square body, whose volume is approximately calculated by the following equation:

$$V_g = L^2B \quad (1.3.1)$$

where V_g is the volume of clay particle (μm^3), L is the measured maximum width of the clay particle and B is the measured thickness of the clay particle (μm). For a layered silicate of clay suspended in water, the measured result is shown as a reference sample as listed in Table 1.6.

1.1.3.2.3. *Illite* Illite is also called hydromica. The theoretical formula of illite is



where $m < 1$. Illite’s host minerals are muscovite and biotite. During the process that gradually turns mica into illite, the mica particle gets finer by degree, and, as a result, its specific surface increases. Potassium ions exposed on the surface are more easily hydrated and exchanged with other cations than those inside the layer structures. A portion of K^+ between layers is replaced by Ca^{2+} , Mg^{2+} and $(\text{H}_3\text{O})^+$. Chemical analysis shows that illite contains less potassium and more water molecules than its host mineral, thus the name hydromica.

The crystal structure of illite is similar to that of MMT. The major difference is that in illite, the isomorphous substitutions generally occur in the tetrahedral sheet with Al^{3+} for Si^{4+} . In most cases, up to one-fourth of the tetrahedral coordinated cations is Al^{3+} . Isomorphous substitution can also be found in the octahedral sheet, typically, Mg^{2+} and Fe^{2+} for Al^{3+} . The average negative charge of the unit cell in illite is 0.6–1.0, which is larger than that in MMT, which is 0.25–0.6, and the generated negative charge is counterbalanced by K^+ [6].

The lattice of illite is difficult to expand because water molecules have great difficulty in approaching the interlayer region. The reason for this is that the negative charge is situated mainly on the tetrahedral sheet close to the surface, resulting in strong electrostatic attraction between K^+ and the negative charge in the layers. In addition, K^+ ions are embedded in the hole formed by the surface oxygen atoms in adjacent layers and are 12 number-coordinated with the surrounding oxygen atoms, causing the K^+ ions to link the adjacent layers. As a result, the linkage is usually very firm. However, cation exchange can take place on the external surface of each clay particle. Therefore, hydration is limited to the external surface, and the volume increment caused by hydration in illite is far less than that in MMT.

Illite may be dispersed in water and the equivalent spherical radius of particles is $0.15\ \mu\text{m}$ and the width is about $0.7\ \mu\text{m}$. Some illite may also exist in a degraded form, resulting from the fact that some of the K^+ ions escape from the interlayer regions, making some layers hydrated and some lattices expanded. Nevertheless, illite cannot reach a level of hydration similar to that of MMT.

Illite is one of the most abundant layered silicates of clay minerals in China or perhaps in the world, and exists in sediments from all geological ages, especially in the Paleozoic sediments. Its expansibility and dispersibility are essentially and necessary properties in the preparation of nanosystems. When illite is suspended in an aqueous solution of surfactant, the surfactant can penetrate into the layer spacing causing enlargement. Using post-heating processes or polymerization with organic monomers, composite materials with dispersed nanoscale illite layers can be prepared. In some applications, such as oil drilling, it is necessary to protect the surface of the well wall, and suspensions of illite are used as a drilling fluid.

Generally, the properties of clay minerals are closely associated with the crystal structure, and it is essential to know the surface properties. A comparison of the characteristics of three common layered silicates of clay minerals is given in detail in Table 1.7 and Figure 1.7. One can usually determine the expansion properties of clay by calculating the distance variation between adjacent layers before and after the reactions with clay.

1.1.3.2.4. Chlorite The layer structure of chlorite consists of alternately stacked pyrophyllite-like sheets and brucite sheets (Figure 1.8). The negative charge is created by the substitution of Al^{3+} for Si^{4+} in the tetrahedral sheet, but the net charge is very small. Al^{3+} substitutes for Mg^{2+} in the brucite sheet and produces some positive charge, which is balanced by the negative charge above it. The formula is $2[(Si, Al)_4(Mg, Fe)_3O_{10}(OH)] + (Mg, Al)_6(OH)_{12}$.

Table 1.7

Crystal structure and physical and chemical properties of three kinds of clay minerals

Clay mineral	Layer type	Distance between adjacent layers ($10^{-1}\ \text{nm}$)	Attraction force between layers	CEC (mmol/100 g clay)
Kaolinite	1:1	7.2	Hydrogen bond, very strong	3–15
MMT	2:1	9.6–40.0	Intermolecular force, weak	70–130
Illite	2:1	10.0	Electrostatic, strong	20–40

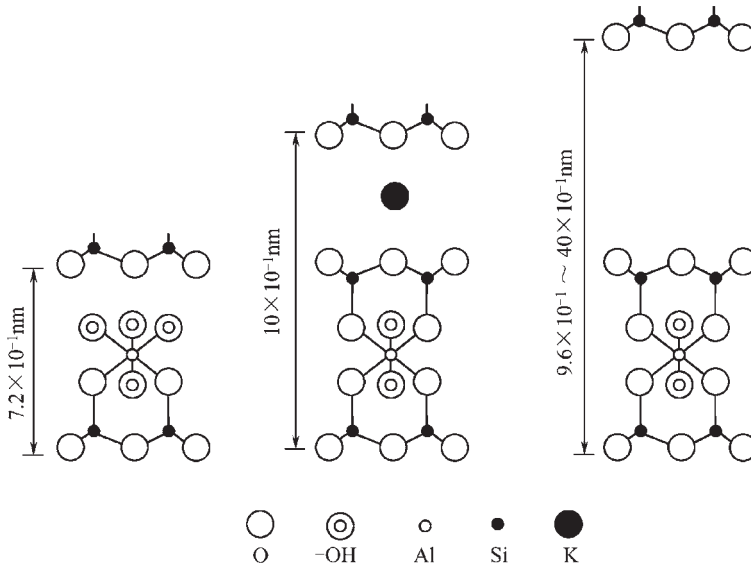


Fig. 1.7. Characteristics of structure of kaolinite, illite and MMT.

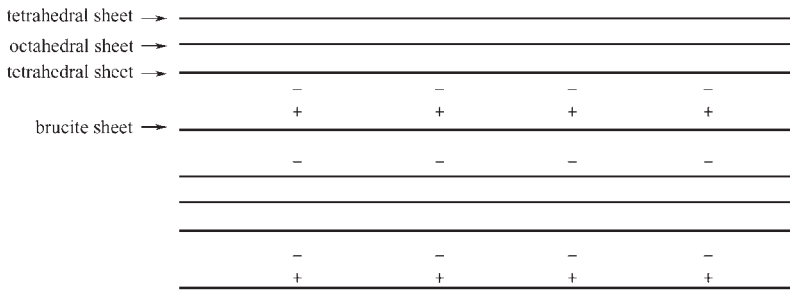


Fig. 1.8. Diagrammatic sketch of chlorite.

In general, there is no interlayer water in chlorite. However, in some degraded chlorite a portion of the brucite sheets are removed. Consequently, interlayer water and lattice expansion are present to some extent. Chlorite is most abundant in the Paleozoic sediments.

1.1.3.2.5. Sepiolite The popular name of the sepiolite group is “anti-salt” clay, which belongs to “chain structure” -hydrated Al-Mg silicates including sepiolite, attapulgite and palygorskite. So far, the literature related to these clay minerals is not rich. Sepiolite is a type of Al-Mg silicate that contains water and has a fibrous structure. The tetrahedral sheets extend to considerable distances in the *a* and *b* directions. However, at periodic intervals, along the *b*-axis, the tetrahedral sheets invert, forming checkerboard

patterns that are linked together by octahedral sheets, in which the main cations are primarily Al^{3+} and Mg^{2+} . The clay mineral has a very large internal surface due to the many hollow channels in its structure through which water molecules can penetrate. Figure 1.9 gives the sketch map of the palygorskite crystal structure.

Sepiolite is a hydrated magnesium silicate, where the ratio of SiO_2 to MgO is approximately 1.5. Because the composition of sepiolite from different regions is remarkably distinct, its formula cannot be accurately determined, but it is usually expressed as $4\text{MgO}\cdot 6\text{SiO}_2\cdot 2\text{H}_2\text{O}$. Sepiolite has a unique fibrous crystal structure. In a suspension of sepiolite, the fibers intersect each other to form a network frame, which is an important factor to keep the suspension stable. As a result, the rheological behavior of the suspension of the sepiolite group depends on the fibrous structure rather than the electrostatic attraction between particles.

The physical and chemical properties of the layered clay mineral are different from other minerals due to the special crystal structure, which leads to the adsorption of comparatively larger quantities of water (Table 1.8). It has good thermostability and it is suitable as a deep-well drilling fluid. Moreover, its mud-making ability with salt water is as good as with fresh water. Drilling fluids containing sepiolite exhibit excellent suspension capacity when used in ocean drilling and in high-pressure salt-water bed drilling, or rock salt bed drilling.

1.1.3.2.6. Mixed-layer clay minerals In some clays, different types of clay layers are stacked up in the crystal structure of the same clay mineral. These clays are called mixed-layer clay minerals. In mixed-layer structure, different types of layers mutually overlap. The layer sequence is generally irregular. Occasionally, however, regular stacking can be found. Illite/MMT and chlorite/vermiculite layers are the most familiar mixed-layer structures. Mixed-layer clay minerals usually disperse and expand in water more easily than other clay minerals, especially when one component of the mixed-layer clay is expandable.

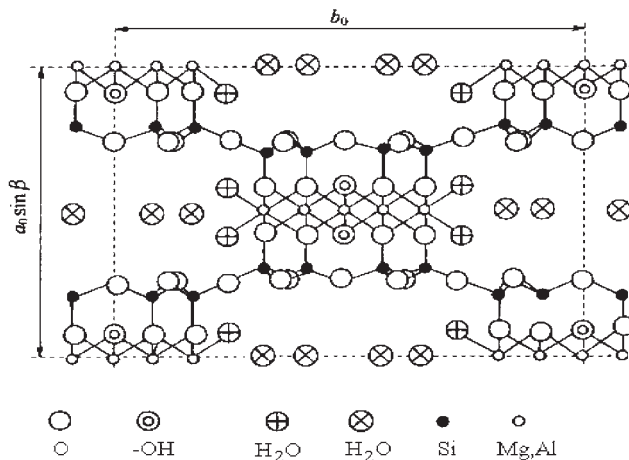


Fig. 1.9. Diagrammatic sketch of palygorskite.

Table 1.8
Content of adsorbed water in some clay minerals

Clay mineral	Mass ratio of adsorbed water (%)	Clay mineral	Mass ratio of adsorbed water (%)
Palygorskite	24.3	Muscovite	5.4
MMT	20.2	Kaolinite	2.0

Table 1.9
Important layered silicate and their producers

Name of silicate	Producer
Palygorskite (Kaolinite, Talc)	Jiashan, Anhui Province, China
Synthetic analogues of smectites, i.e. Saponite	Sumecton SA, Kunimine Ind. Co., Japan
Hectorite (MMT)	Laporte, Laporte Ind. Co., UK
Swelling mica or sodium fluor tetrasilic mica	Topy Ind. Co., India

Notes: Contents of some silicates are (1) Kaolinite, $\text{Al}_2(\text{Si}_2\text{O}_5)(\text{OH})_4$ with $\text{Al}_2(\text{Si}_2\text{O}_5)(\text{OH})_4 \cdot 2\text{H}_2\text{O}$; (2) Talc, $\text{Mg}_3(\text{Si}_4\text{O}_{10})(\text{OH})_2$; (3) Sepiolite, $\text{Mg}_8\text{H}_6(\text{Si}_{12}\text{O}_{30})(\text{OH})_{10} \cdot 6\text{H}_2\text{O}$; (4) MMT $[\text{Al}_{(2-x)}\text{Mg}_x]_2[\text{Si}_4\text{O}_{10}]_2(\text{OH})_2 \cdot n\text{H}_2\text{O}$.

Table 1.10
Statistical data of MMT yield in China

No.	Year	Total yield (million tons)
1	1992	1.20
2	1994	1.58
3	1995	1.60
4	1998	2.00
5	2000	3.00
6	2002	No exact data

1.1.4. Natural mineral resources of silicates in China

Owing to the importance of clays in making nanocomposites for industrial applications, a variety of corporations have produced layered silicates in the pure state as shown in Table 1.9. MMT resources are very rich in China, and have become number one in the world. The total mineral resource quantity of montmorillonite is 7 billion tons, of which 2 billions tons are being explored. Statistical data show that 41.5% of these explored MMTs (or bentonites) are composed of 80% (by wt) of Ca-MMTs and 20% (by wt) of Na-MMTs. At present, there are 250 mines including 30 state-run plants in China, and the remaining ones are non-state run (Table 1.10).

In 1998, whitened or acidized (purified) MMTs constituted 20% of the total yield. A small part of the purified MMTs are now being used as precursors for nanocomposites. These types of MMTs for nanoparticle materials are regarded as polymer-grade, which

Table 1.11
Consumption composition

No.	Application field	Quantity (%)
1	Foundry industry	52
2	Drilling fluid	24
3	Additives for puddling	6
4	Petrochemical, light industry, textile, agriculture, construction	16
5	Superfine powder	No exact data

means that they are suitable for polymerization or copolymerization with monomers in preparing nanocomposites. Except for these polymer-grade MMTs, there are several applications for MMT, as shown in Table 1.11.

Although rich in MMT, the Ca-MMTs dominate in the total resources of China's MMT minerals. There are many techniques for converting Ca-MMTs into Na-MMTs through ion-exchange reactions with the salt Na_2CO_3 .

1.1.5. The world mineral resources for silicates

The mineral resources of different layered silicates exist and are produced in several countries. The resources provide the raw materials for preparing particles of different sizes including nanoparticle size. The United States of America is the largest producer, consumer and exporter of bentonite, most of which are MMTs. Recent statistical data from the 1990s show that the USA produces 4 million tons per year of the total world production of 9.6 million tons per year. In the total yield, the Na-MMTs or Na-bentonite accounts for 89%, while Ca-MMTs or Ca-bentonite accounts for 11%. The composition of MMTs produced in the USA is completely different from that in China. The composition of MMTs varies depending on their location in nature, which directly affects the final quality of the prepared nanocomposites, and is thus considered when MMTs are used as a precursor for nanocomposites.

From 1998 to the present, the yearly consumption of MMTs in USA was approximately 3 million tons per year. At present, the yearly consumption of MMTs has surpassed 4.0 million tons. The export price varies from \$100/ton for Na-MMTs or Na-bentonite (in 1998) to \$7,300/ton for superfine powder or nanoscale powder (in 2002). In the early 1990s, the latter product was mainly exported to Canada and Japan, but is now also exported to China. The rapid expansion of the uses of superfine powder and the development of nanoparticles, suggests a promising future for nanocomposites based on MMTs.

1.2. Silica

Sands cover a large quantity of the Earth and are the source from which most silica is made. Different ultrafine particles of silica with different sizes are prepared mainly from the corresponding precursors. The preparation of nanoscale silica has been published in

Table 1.12
Characteristic index for silica

Parameters	Index
Specific surface area (m^2g^{-1})	640 ± 50
Particle size (nm)	$(10-30) \pm 5$
Silica content (%)	> 99.9
Stirring density (gm^{-3})	< 0.15
Impurities (%)	Cl < 0.02 , metal < 0.001
Content of surface hydrogen (%)	$(30-40)$

the literature [15–18], and tetraethoxysilane (TEOS) is often used as the precursor in preparing nanoparticles of different morphologies and size.

Two methods have been used in preparing nanoscale silica: the gas-phase (or the drying method) and the deposition preparation method (or the wet method). The particle sizes in both the gas-phase and the deposition method are quite different in that the former produces silica with a smaller particle size than that produced by the latter method. The particle sizes are less than 40 nm as shown in Table 1.12.

The production of silica has been industrialized, and it has been applied to producing composites with rubber, fibers, resins and nanocomposites. At present, silica is mainly used in fields such as coatings, engineering plastics, automobile tires and electronic components. The consumption of silica is increasing in China because of the emergence of nanotechnology. In 2001, the yield of both silica and TiO_2 in China was about 15,000 tons, of which about one-third was silica. At the same time, the silica yields in both USA and Europe has surpassed 200,000 tons. These silica usually have high specific surface area and appropriate hydrogen content.

1.2.1. Precursor of silica

The preparation of silica particles involves several precursors or intermediate reagents such as TEOS, Na_2SiO_3 , CH_3SiCl_3 and SiCl_4 . Selecting a proper precursor depends mainly on the practical requirements of silica quality and function. The use of the gas-phase method (drying method) or deposition method (wet method) depends on the application.

The principle of the gas-phase method is burning the silica precursor under an atmosphere of pure hydrogen gas and purified air (oxygen). This burning process is shown below:



In the burning process, the temperature inside the furnace will reach 1000–1200°C. Silica particles of 20 nm are produced by this method.

The second method is to aggregate the nanoparticles with a depositing reagent such as ammonia or amine. First, a precursor of either Na_2SiO_3 or CaSiO_3 is used to prepare

nanoparticles of silica by reaction with hydrochloric acid:



The precipitate of CaCl_2 is separated, and then the depositing reagent is added to the silica suspending solution to obtain silica aggregates. The purified silica particles are obtained after washing the aggregates several times.

At present, TEOS is used to prepare silica particles through a sol-gel process. To trace the silica particle growth, the concentration of TEOS obtained from FTIR spectroscopic measurement was used to deduce the kinetics of TEOS hydrolysis. In this investigation, the concentration of water was always kept significantly in excess in order to stabilize the silica particles in the solution. In an excess of water, the rate of TEOS hydrolysis can be treated as first order with respect to the TEOS concentration and follows an exponential decay:

$$[\text{TEOS}](t) / [\text{TEOS}](0) = \exp(-k_h t) \quad (1.2.1)$$

where $[\text{TEOS}](t)$ and $[\text{TEOS}](0)$ are the concentrations of TEOS at reaction time t and at the start of reaction, respectively, and k_h is the specific rate constant for TEOS hydrolysis. The rate of silica particle growth can be deduced from the increase in the volume of silica particles measured by TEM and light scattering methods. For a first-order reaction, the rate of silica-particle growth follows

$$1 - (V_p(t) / V_p(\infty)) = \exp(-k_c t) \quad (1.2.2)$$

where k_c is the specific rate constant for silica-particle growth, and $V_p(t)$ and $V_p(\infty)$ are the volumes of silica particles at time t and at the end of reaction, respectively.

1.2.1.1. Hydrolysis of TEOS characterized by several techniques

In FTIR spectra, the absorption bands of TEOS's Si-O-C group, located at both 795 and 967 cm^{-1} , decrease with reaction time and eventually disappear, indicating that TEOS has been completely reacted. The formation of ethanol is seen by the increase with reaction time of the ethanol's C-C-O stretching bands located at 882 and 1,050 cm^{-1} . A small absorption peak at 950 cm^{-1} remains unchanged during TEOS hydrolysis, which most likely corresponds to the vibration of $(\text{SiO}_4)_n$ [20].

Consumption of water is observed in that the decrease of the 1,640 cm^{-1} band is not as significant as that of TEOS due to the initial excessive amount of water. Moreover, it is known that $\text{RSi}(\text{OH})_n$ has a strong Si-OH absorption band located between 910 and 830 cm^{-1} . The lack of a noticeable Si-OH band in FTIR shows that most of the TEOS molecules, after being hydrolyzed, immediately condense into polymeric silica species.

The concentrations of the TEOS, ethanol and water at different reaction times, were calculated from the intensities of the 967, 1,050 and 1,640 cm^{-1} bands, respectively. The TEOS concentration decreases exponentially while the ethanol concentration increases exponentially. Over the reaction period, the increase in $(\text{C}_2\text{H}_5\text{OH})$ is approximately four

times greater than the decrease in TEOS, which is consistent with the ethanol TEOS stoichiometric ratio in the TEOS hydrolysis reaction. Thus, FTIR spectroscopic analysis provides quantitative information on the consumption of TEOS and water, and the production of ethanol from the hydrolysis of TEOS in microemulsions.

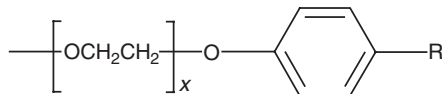
1.2.1.2. Light-scattering tracing hydrolysis of TEOS

Light-scattering measurements were used to study the growth of silica particles in the same microemulsion solution as used in the above FTIR studies [19]. The steady increase in the scattered light intensity with hydrolysis time reflects the formation of silica particles in the solution. The data points measured at the final reaction period appear more scattered due to the higher experimental uncertainty. The apparent specific rate constants, k_h for TEOS hydrolysis and k_c for silica-particle growth, were determined to be, k_c (FTIR) = 0.031 h^{-1} , k_c (TEM) = 0.032 h^{-1} , and k_c (light scattering) = 0.034 h^{-1} by different measurement techniques. The fact that the calculated k_c values are virtually the same demonstrates that the growth of silica particles is rate-controlled by the extremely slow hydrolysis of TEOS. This hydrolysis reaction is carried out through the mass transfer of TEOS molecules from the oil phase into microemulsion droplets. The subsequent contact of TEOS molecules with water forms hydrolyzed silica monomers, which then condense with other silica species. There are many similar investigations, for example, by Chang et al. [19] which light-scattering measurements for tracing the hydrolysis of TEOS in water as,

$$1 - [F_p(\infty) (\langle I(t) \rangle - \langle I(0) \rangle) / (F_p(t) (\langle I(\infty) \rangle - \langle I(0) \rangle))]^{1/2} = \exp(-k_c t) \quad (1.2.3)$$

where $\langle I(0) \rangle$, $\langle I(t) \rangle$ and $\langle I(\infty) \rangle$ are the scattering intensities of solution at the start, at time t , and at the end of the reaction, respectively, and $F_p(\infty)$ and $F_p(t)$ are the form factors of the silica particles at the end of reaction and at time t [19].

Example 2.1.1. Preparing silica nanoparticles in W/O microemulsion. By controlling the rates of TEOS hydrolysis, silica-particle growth in a single-phase W/O microemulsion (aqueous ammonia in heptane) with the following composition is obtained: [NP4] = 0.126 M (NP4 is an aromatic alkyl ether, see below in this section), [TEOS] = 0.0357 M; [NH₃] = 0.104 M, and [H₂O] = 0.235 M (here M = mol dm⁻³). The NP4 is first mixed with water and then TEOS and NH₃ are added by dipping. The reaction time is 1–4 h at temperatures ranging from 30 to 90°C. Silica nanoparticles with a size below 50 nm are obtained. NP x has a molecular formula as follows:



NP means non-ionic polyoxyethylene nonylphenyl ether surfactants. NP4 or NP6 is often used for emulsions to prepare SiO₂ (Table 1.13).

Table 1.13
The nanoparticle size of silica based on NP_x

Water/(NP _x)	Particle size (nm)	Year	Reference
—/(<i>x</i> = 6)	40–50	1986	[1]
1.4/(<i>x</i> = 5)	35–70	1990–1992	[2]
1.9/(<i>x</i> = 4)	26–43	1996	[3]

1.2.2. Resources of silica

The precursor resources for silica nanoparticles are abundant in China; they are listed in the following order based on their richness in nature:



1.2.3. Monodisperse silica

1.2.3.1. Preparation of high-quality SiO₂ opals

Silica has other applications such as in patterning materials and photonic crystals. The synthetic SiO₂ opals and polystyrene opals, which are photonic crystals, possess an incomplete photonic band gap in the visible region [21–26]. The so-called opals are template materials with ordered arrays. Monodisperse SiO₂ and polystyrene submicrospheres have been used because they can be prepared easily and the opals can be fabricated relatively simply from these materials. Further, opals can be used as a template for creating inverse opals [27–29], which have a complete photonic band gap.

Our work [30] shows that the monodispersity of submicrospheres is one of the most important factors for the fabrication of high-quality opals. Imperfect monodispersity of submicrospheres can cause serious disorders and dislocations of lattices in opals, especially when opals are fabricated by sedimentation in a gravitational field. These defects lead to strong random scattering of incident light so that the transmission of the opals becomes very low, influencing their photonic properties. In our work, we developed a submicrosphere selection technique separating single spheres from aggregated spheres to improve the monodispersity of the submicrospheres. Higher quality silica opals were fabricated from the selected submicrospheres.

1.2.3.2. A new submicrospheres selection technique

1.2.3.2.1. Preparation of monodisperse SiO₂ submicrospheres Monodisperse SiO₂ submicrospheres were prepared by a seeding technique [31–36] on the basis of the hydrolysis and condensation of tetraethoxysilane (TEOS) in a mixture of water, ammonia and ethanol. The seeding technique was developed and improved by our studies on the formation, mechanisms and kinetics of silica monodisperse systems.

In one experiment, commercial silica sol particles were dispersed in ethanol aqueous solution, which contained 2 M NH₃ and 6 M H₂O. TEOS was added to the stirring suspension by continuous feeding at 35.8°C with a fixed flow rate and then the mixture

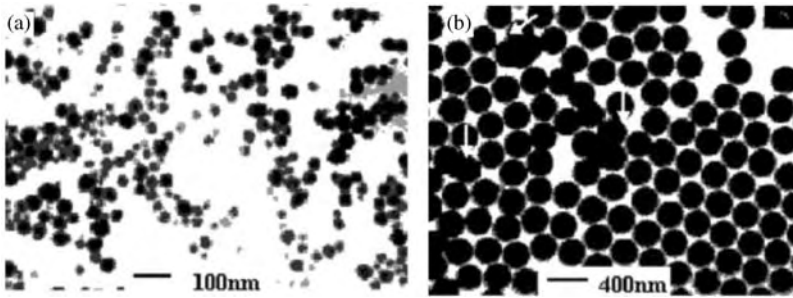


Fig. 1.10. TEM images of (a) commercial sol particles and (b) our SiO_2 submicrospheres (fused pairs of spheres are indicated by arrows).

was continually stirred for 2 h. The resulting silica submicrospheres were separated from the suspension by centrifuge and ultrasonically washed with water. TEM images of commercial silica [37] sol particles and our silica submicrospheres are shown in Figure 1.10 separately. The average diameter of commercial sol particles is ~ 27 nm, and the relative standard deviation (RSD) of diameters distribution is $\sim 28.4\%$. The diameter of the silica submicrospheres is 310 nm, and the RSD of diameters distribution is 4.50%. Compared with other methods, monodispersity of the silica submicrospheres grown by the seeding technique are more perfect. However, in solution, the aggregation and adhesion between the same single spheres can be seen from time to time, as shown in Figure 1.10.

1.2.3.2.2. Reselection of monodisperse SiO_2 submicrospheres Stokes' law can be applied for the sedimentation of particles in a gravity field as given by the equation $v = (2r^2/9\eta) (\rho - \rho_0)g$. Our previous work indicates that the sedimentation of submicrospheres with a diameter larger than 200 nm can obey Stokes' law in which the calculated diameter is identical with the diameter measured by TEM. Aggregated clumps, containing a number of spheres with diameter d_s , have an apparent diameter d_a , and they have a settling velocity v_a according to Stokes' law, i.e., the aggregated spheres with various numbers of the single spheres have different relative settling velocities. The aggregated spheres have higher settling velocities. Therefore, different regions are formed during sedimentation in a transparent glass tube of the initial suspension of monodisperse spheres with partial aggregation, as shown in Figure 1.11.

In Figure 1.11, region 1 contains only single sphere. The height of region 1 is dependent on the settling velocity ratio of doublets (region 2) to single spheres and the settling time. We used glass spheres aggregated by two single spheres with the same diameter (of ~ 1 mm) and uniform density as models of doublets to measure the settling velocity ratio of doublets to single spheres (v_a/v_s) at various low Reynolds numbers. Then we correlated the settling velocity ratio v_a/v_s with the Reynolds number. Since the Reynolds number is very small and approximates to zero in our experimental suspension system of submicrospheres, we extrapolated the correlation to the point where the Reynolds number is equal to zero, as shown in Figure 1.12.

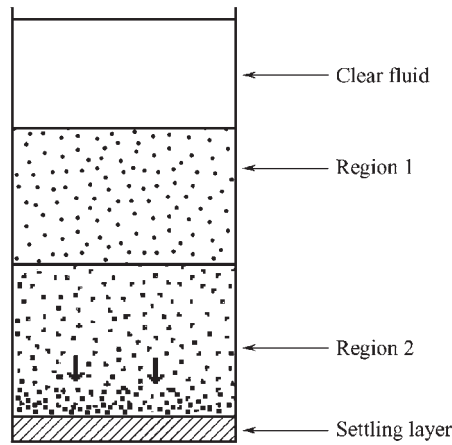


Fig. 1.11. Schematic illustration of the regions that develop during sedimentation of monodisperse spheres with partial aggregation.

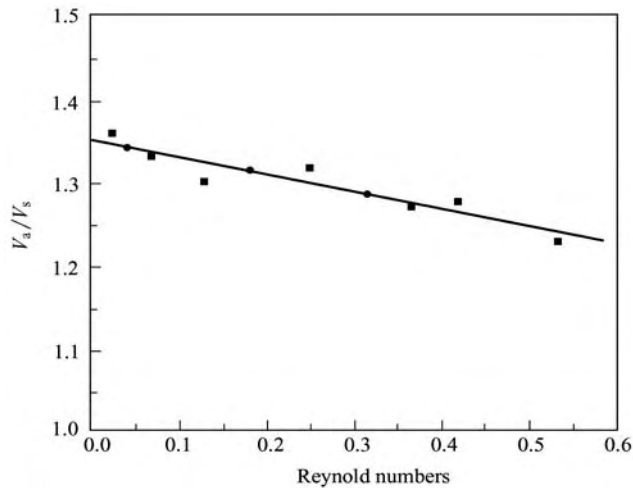


Fig. 1.12. Correlation between the settling velocity ratio of doublets to single spheres (v_a/v_s) and the Reynolds number.

From Figure 1.12 we can determine the settling velocity ratio of doublets to single spheres at the zero Reynolds number to calculate the height of region 1. The settling velocity ratio ranges from 1.3 to 1.35 according to the actual experiments. Finally, single spheres are collected from region 1 to be separated from aggregated spheres in the form of doublets, triplets, etc. A TEM image of the selected spheres is shown in Figure 1.13.

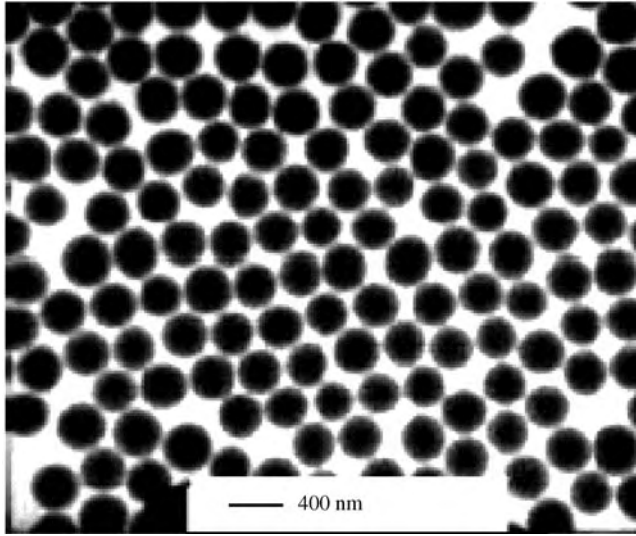


Fig. 1.13. TEM image of selected SiO_2 submicrospheres with a diameter of 290 nm.

1.2.3.3. Fabrication of SiO_2 opals from colloidal SiO_2 submicrospheres

SiO_2 opals were fabricated from colloidal SiO_2 submicrospheres prepared by the method of sedimentation in a gravitational field. We used the following procedure. In order to eliminate the interaction between submicrospheres, the suspension of SiO_2 submicrospheres was diluted so that the concentration of SiO_2 submicrospheres was below 1 wt%. Then the diluted suspension was placed in a tube with a polished surface. The diameter of the tube was 2.5 cm, which is large enough to eliminate wall effects. After a few weeks, the aqueous solution was extracted carefully when sedimentation was complete. The opals were taken out of the tube, dried at room temperature and annealed at 900°C for 4 h. The opals had better mechanical and optical properties after the thermal annealing. Diffractive colors from green to red could be readily seen when the opals were placed under a lamp and the observation angle was changed. An SEM image of an annealed and then cleaved opal sample is shown in Figure 1.14, where the opal has face-centered cubic structure symmetry. With our selection procedure for spheres, the size of a single crystal of the opals was substantially larger than without using the selection procedure, and its mechanical and optical properties were also better.

The photonic band structure of the opals was probed experimentally as shown in Figure 1.15. By measuring the transmission spectra of opals' using electromagnetic waves with different wavelengths, the transmission spectra between the opals fabricated from the selected silica spheres and the unselected spheres can be compared. Because the diameters of the spheres used in the two cases were slightly different, the position of the midgap (1 min) was not exactly identical. Because lesser defects and dislocations are present in the opals using the selection procedure, the random scattering decreases and the coherent scattering increases. After the selection procedure of spheres was used, the maximum attenuation of the gap (I_{\max}/I_{\min}) characterizing the bandgap increased

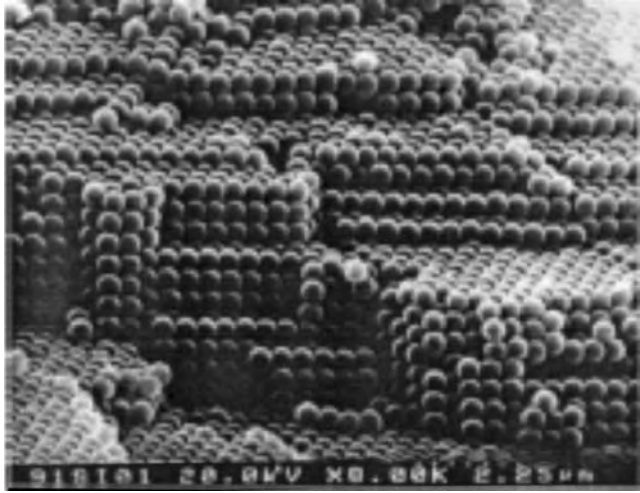


Fig. 1.14. SEM image of typical boundaries of the cleaved facets in the SiO_2 opal.

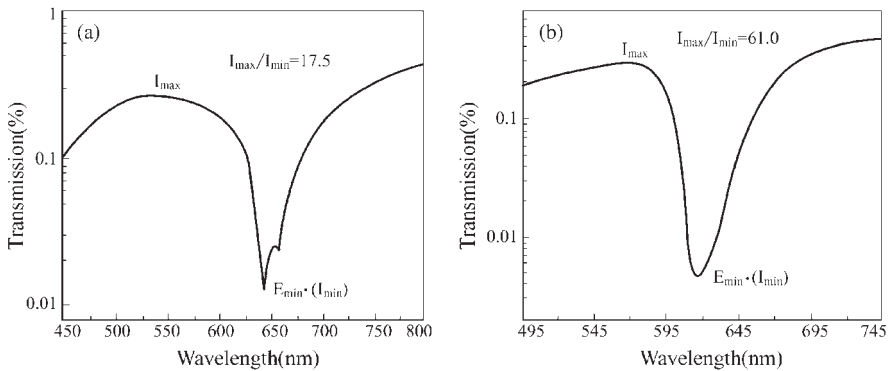


Fig. 1.15. Transmission spectra of two SiO_2 opals: (a) without the selection procedure of spheres; (b) with the selection procedure of spheres.

from 17.5 (Figure 1.15(a)) to 61.0 (Figure 1.15(b)), which further indicates the effectiveness of the selection procedure of spheres for fabricating opals.

1.3. Physical properties of layered silicate and silica

1.3.1. Condensed structure

1.3.1.1. General aspects of layered silicate and silica

The unique properties of the layered silicates of clay, such as their swelling behavior and cation exchange performance, make them applicable in several fields. Silicates form a stable thixotropic gel when dispersed in water. When the gel is moderately evaporated,

the clay silicate particles pile up with their crystal a - b plane parallel to the layer substrate to form a transparent self-supporting film. As for the electric charge properties, the cations adsorbed in the layered silicate layers with negative charge are usually exchanged with foreign cations. Through such a cation exchange reaction, layered silicates of clay can be modified for practical applications.

Intercalation of guest compounds into the host of the layered silicates of clay can be done in two ways. One is through a cation exchange reaction with interlayer exchangeable cations, and the other is through the adsorption of polar molecules into the space gallery of layered silicates. These polar molecules can be alcohols, ketones and amides. The polar molecules have ion-dipole interactions with the interlayer cations and hydrogen bonding with the surface oxygen atoms on the layered silicate sheets.

In the intercalation reaction, the layer sheets of the layered silicates of clay tend to exfoliate. In water, the condensed structure is broken down or restructured; their condensed character disappears in the XRD patterns. It is thought that exfoliated layered silicates become amorphous. Exfoliated layers form the so-called "colloidal crystals" in solvents such as water and alcohol, or they form mixed crystals when melt-mixed with polymers such as polyester and polyamide. Obviously, whether the exfoliated layers are crystals or not is still debated.

Silica also has both crystal and amorphous forms in its applications as nanocomposites and emulsions. Silica morphology in the matrix is expressed in a way similar to the layered silicates.

1.3.1.2. Crystal structure variation of layered silicate during heating MMTs

The crystal structure of the layered silicates is expressed by powder crystal diffraction, and its diffraction peak and interlayer spacing is calculated by the Bragg equation. Due to the swelling properties of layered silicates, their crystal structure changes or expands as the reagents react with the cations in the layers through a cation exchange process.

In an example of layered silicates, the pristine clay has its diffraction peak at $2\theta = 7.0^\circ$. Based on the diffraction peak of MMTs, under different thermal temperatures, their X-ray peaks are calculated to obtain the interlayer distance change as shown in Table 1.14. The characteristic peak for the pristine clay is that of the diffraction at (001), such peak interdistance is expressed by d_{001} , which is calculated from the Bragg equation

$$\lambda = 2d_{001} \sin\theta \quad (1.3.1)$$

where λ is the wavelength of X-rays, d_{001} the interlayer spacing of (001) crystal face, and θ is half of the diffraction angle.

It is clear that the condensed clay has transmitted from crystal form to amorphous state: during the process the interlayer distance changes from 1.556 to 0.974 nm.

The condensed structure of the layered silicates will vary with the heating temperature. Thermal analysis of MMTs reveals the different forms of water in MMT structures. Figure 1.16 shows a typical differential thermal analysis (DTA).

Some specifications on the different thermal adsorption peaks of MMTs are stated here based on Figure 1.16. The first value of thermal adsorption appears at 126–139°C.

Table 1.14
Diffraction peak variation of MMTs under heating characterized by X-ray

Heat temperature (°C)	Diffraction peak d_{001} (nm)	Matter composition
RT (untreated)	1.556 (d_{001})	MMTs
500	0.996 (d_{001})	MMTs
600	0.955 (d_{001})	MMTs
700	0.974 (d_{001})	MMTs
900	0.343 nm	μ -cordierite/dichroite
1000	0.426, 0.335 and 0.182 nm	α -quartz or weak μ -dichroite, strong diffraction of square quartz
1200	0.4117 and 0.2514 nm	
1350	0.8566 and 0.315 nm	Fe-dichroite

Note: μ -dichroite, a metastable dichroite phase; composition, $\text{MgAl}_2\text{O}_4\text{-SiO}_2$.

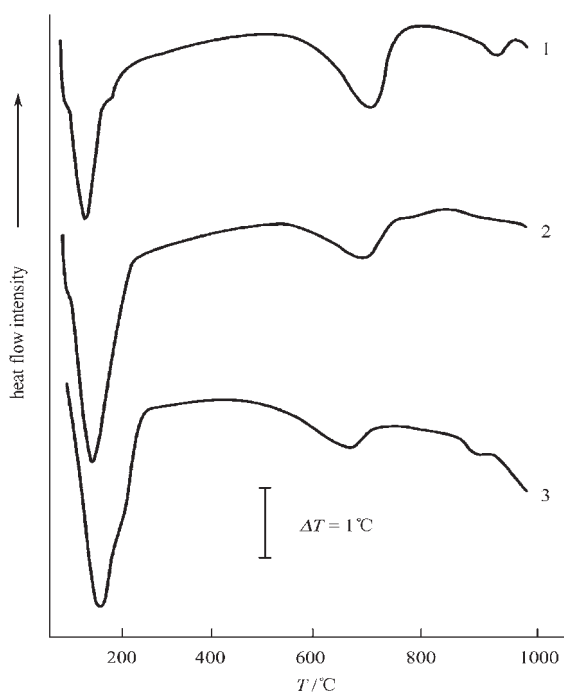


Fig. 1.16. DTA curves for MMTs; 1. Na-MMTs; 2. mixed Na-MMTs and Ca-MMT; 3. Ca-MMT.

In this temperature range, the surface water is adsorbed and interlayer water is desorbed. The shape and size of the peak are related to the cations adsorbed in the layer space. The peak area will reflect the type of MMTs, e.g., the wider and bigger the peak area, the higher the probability is for Na-MMTs. It is noted that the above peak shows Ca-MMTs with interlayer water loss of 17.1%.

The second value of thermal adsorption appears at 650°C. This peak shows that the hydroxyl groups are degenerated, which shows a loss of bound water in the crystal. The weight loss of the hydroxyl group is 1.97%. This temperature peak reflects the thermal stability of MMTs and is thus used as a method to determine thermal stability. The temperature of such dehydrolysis is a function of the cation composition and the ore crystal degree. The MMTs with a high content of ferric element are low in hydroxyl groups, while those with a low content of ferric element have a higher content of hydroxyl groups.

The third decalescence value at 906°C is a measure of the collapse of the MMTs structure. MMTs become amorphous according to X-ray diffraction patterns.

1.3.1.3. *The variations of the characteristic structure of layered silicate of MMTs with heating*

MMTs display a characteristic structure variation when different temperatures are used. For layered silicates of MMT there are some characteristic aspects for heating of MMT:

- (1) The dehydration process of MMT is reversible for treatment temperatures of 126–139°C.
- (2) The hydroxyl groups in the octahedral position are unstable and driven off at temperatures of ~650°C, but the layered structure of the silicate is maintained. The change is irreversible. Also at this temperature there is a transition from Al^{VI} to Al^{IV}, which is revealed by NMR.
- (3) The layered structure of MMTs collapses totally at 900°C, and the collapse is accompanied by the formation of a new phase of μ -dichroite. When the temperature reaches 1200°C, the μ -dichroite is degenerated into a cristobalite phase. When the temperature reaches 1350°C, the content of cristobalite will decrease slightly and more ferric μ -dichroite appears.

1.3.2. *Silica colloid crystals and opals*

Silica particles in a solvent usually form colloidal crystals. Colloidal crystals have ordered array patterns on templates or substrates. Opals can be organized either from the selected silica submicrospheres or from the unselected submicrospheres. When comparing opals fabricated from selected silica submicrospheres with those from unselected submicrospheres, the top surfaces of the opals fabricated from unselected submicron spheres have good alignment (Figure 1.17(a)), while their bottom surfaces do not have good alignment. However, with the selection procedure of spheres, both surfaces have good alignment (Figure 1.17(b)). This selection procedure of spheres is very successful at improving the monodispersity of spheres. It also confirms that the monodispersity of spheres is one of the most important factors for fabricating opals.

1.3.3. *Particle and porosity*

In organic polymer–inorganic particle nanocomposites, silica and layered silicates have been widely used as the inorganic phase. Several concepts and principles describe the structure and properties for particles of silica and layered silicates, which are introduced here for better understanding. These concepts are based on classical descriptions for micrometer particles.

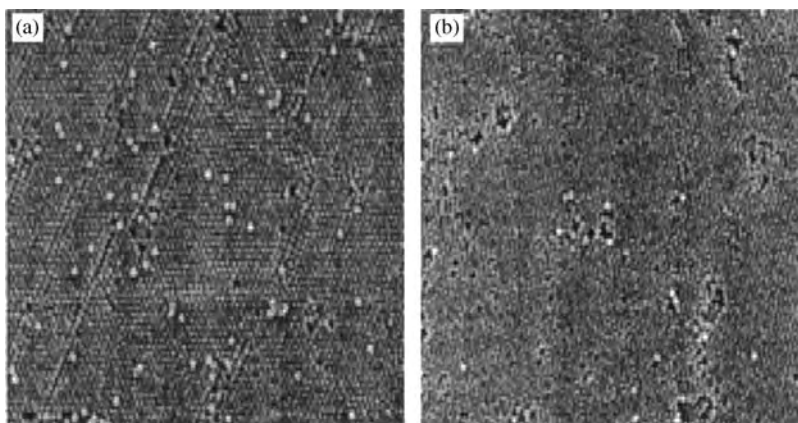


Fig. 1.17. SEM image of top surfaces of silica opals: (a) top surface of the opals without selection procedure of spheres; (b) top surface of the opals with the selection procedure of spheres.

Particle porosity structure and pore distribution are of importance in various applications. According to the definition given by IUPAC on porosity, the diameters of micropores and mesopores are all less than 50 nm, and the diameter of macropores or large pores is above 50 nm. Particles with pore diameter less than 100 nm should be thought of as nanomaterials.

Besides organic–inorganic nanocomposites, there are two other kinds of nanocomposites, e.g., inorganic–inorganic nanoparticle composites or mixtures, or organic–organic nanocomposites. In all nanocomposites, a description of the phases and the interfaces can give information on the nanocomposite.

1.3.3.1. Phase and phase interface

The word phase refers to a completely even or uniform region of a matter's physical and chemical properties. Two or more phases in a system are known as a multiple phase system. The domain or region between one phase and another phase is called the interface. The interface is usually not fixed but transitional. If an interface in a material is not seen, the material is said to have a homogeneous phase. Figure 1.18 shows the morphology of nanoparticles of silica in copolymers of MXD6/PET. The bright and white region is an air phase in the copper grid, while the material in the dark region is composed of silica and copolymers. The silica particles and copolymer matrix form a misty morphology.

1.3.3.2. Dispersion phase and media

In a system of multiple phase dispersion, the material dispersed is called the dispersion phase; the other phase used to disperse it is called the dispersion medium. In suspensions of clay in water, the clay particle is the dispersion phase while water is the dispersion medium. The media for dispersing silica and silicates are water, ammonia, alcohol and related solvents.

To improve the dispersion effect, different media can be mixed together. For example, mixed solvents of water and toluene are used to disperse silica or silicate into

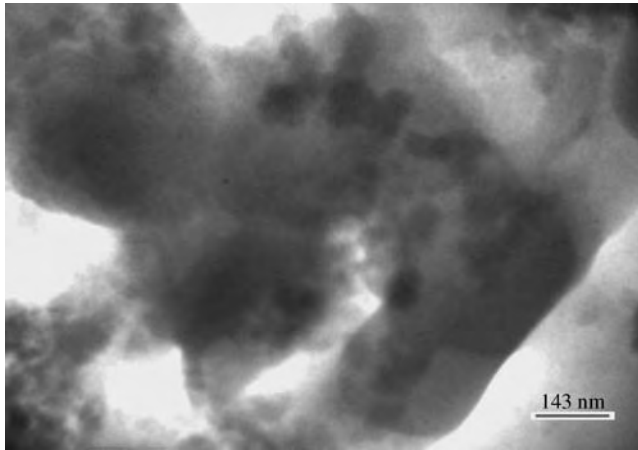


Fig. 1.18. Nanocomposites of silica (20%, by wt) with copolymer of MXD6-PET.

oligomers of copolymer of MXD6 (nylon6 with *m*-xylydine) with PET, which provides good nanoparticle dispersion morphology. Results show that polarity compatibility between solvent and nanoparticles leads to better dispersion. Besides water and ethanol, the solvents of ethylene glycol (EG), polyethylene glycol with different polymeric degree (PEG), nonionic polyoxyethylene nonylphenyl ether surfactants (NP4 or NP6), etc., have the closest polarity to silica and layered silicate particles and thus these are often selected as dispersion media. Nanoparticles dispersed in a solvent are used for dispersion into organic polymers.

1.3.3.3. Dispersion degree and specific surface area

We use the dispersion degree (D) to measure the difficulty of dispersing nanoparticles. It is simply expressed as the reciprocal value or length of the particles' mean diameter in a dispersion phase:

$$D = 1/a. \quad (1.3.2)$$

The smaller the particle size (a) the more difficult is its dispersion into the polymer matrix. Nanoparticle agglomerations are unavoidable in some cases. We also use the specific surface area (S_s) to measure the dispersion degree of particles, which is the ratio of total area to the total mass (or volume) of overall particles in a dispersion phase,

$$S_s = S/V \quad (\text{or } = S/m) \quad (1.3.3)$$

where S is the overall area, V is the total volume and m the total mass. Ultrafine particles have large specific interfacial area when dispersed. The total interface energy of the nanocomposite changes as the particle size or the specific interfacial area S_s changes.

Dispersions are classified as either fine or coarse dispersions. Colloids are fine dispersion systems, with specific surface area of the dispersion phase $\geq 10 \text{ m}^2 \text{ g}^{-1}$, and particle

lengths of 1 nm–1 μm (in one dimension). S_s for nanoparticles of silica are generally $> 100 \text{ m}^2 \text{ g}^{-1}$. S_s for precursor particles of MMTs is $> 150 \text{ m}^2 \text{ g}^{-1}$, while S_s for dispersed nanoparticles of MMTs is $> 200 \text{ m}^2 \text{ g}^{-1}$. As for suspending systems belonging to the coarse dispersions, the specific surface area or S_s may not be $> 10 \text{ m}^2 \text{ g}^{-1}$, and the dispersion phase is about 1–4.0 μm in length.

1.3.3.4. Adsorption behavior

Nanoparticles, or colloids, have a strong tendency to accumulate spontaneously on the interphase between two phases: the concentration at the interphase is higher than that inside the bulk solution, which is known as adsorption. Adsorption is classified as either physical or chemical adsorption according to the properties of the adsorbing force. The adsorption caused by van der Waals forces is defined as physical adsorption, which generally has no selectivity and a small adsorbing heat, and exhibits easy desorption in a coarse dispersion. In fine dispersions, such as layered silicates, physical adsorption may lead to high adsorbing heat and desorption is more difficult because of the high interfacial area. In the intercalation reaction of layered silicates with both organic and inorganic cations, the interaction between adsorbing matter and adsorbent forms a chemical bond, which is chemical adsorption. Chemical adsorption has selective properties, high adsorbing heat and very difficult desorption. Quaternary ammonia salts are fixed by chemisorption in the gallery of clay and are thus incapable of being removed. Their adsorption behavior is slightly different from that of amine chemical adsorption on clay particle surfaces, as shown in Figure 1.19.

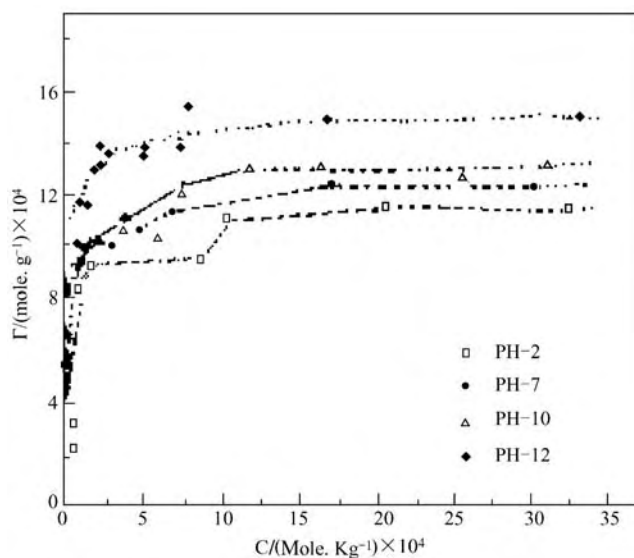


Fig. 1.19. Isothermal adsorption behavior of trimethylcetyl amine on the surface of Na-MMTs as a function of pH: Γ is adsorption quantity and C is the concentration of the solute in the bulk.

1.3.4. Diffuse electrical double layer

Several principles and theories dealing with silica and layered silicate particles are introduced here to better understand their properties[38–40]. These principles are obtained from electrostatic interactions between particles in suspension and are described by classical colloid science.

1.3.4.1. The physical and chemical properties of clay colloids

1.3.4.1.1. Sedimentation and its equilibrium Particles in a suspending solution may sediment when subjected to gravity or centrifugal forces. During sedimentation, the concentration of particles in the lower part of the system increases, while the concentration in the upper part decreases. This concentration difference breaks the systems homogeneity, which in turn causes a diffusion process (Brownian movement) to make the system more homogeneous. Sedimentation and diffusion are two aspects of a contradictory system. If the particles in gel state are spherical with radius of r , density ρ and dispersion media's density ρ_0 , then at steady state the sedimentation force F_1 is set to be equal to the resistance force F_2 , opposing particle sedimentation. When $F_1 = F_2$, a particle settles down with velocity v , and the Stokes' law has the form $v = (2r^2/9\eta) (\rho - \rho_0) g$, where g is the acceleration constant due to force, and η is the medium viscosity. The Stokes' law is quite suitable for describing the sedimentation of spherical silica particles in solvents such as water, ethanol, etc., while it has an obvious limitation in describing nanoparticle sedimentation of layered silicates in selected media. However, a revised form of the Stokes' equation can express the velocity of sedimentation of suspended clay nanoparticle in a media as

$$v = (2 r^2/9 k_c \eta) (\rho - \rho_0) g \quad (1.3.4)$$

where $k_c = 1.1-1.56$.

1.3.4.1.2. The electromotion in aqueous suspension of clay particles Colloidal electromotion of clay particles includes electrophoresis, electro dialysis, flow (streaming) and sedimentation electrical potentials. In electrophoresis, the charged colloidal particles move toward an electrode with opposite charge when an outside electrical field is exerted. In electro dialysis, a liquid moves parallel to a fixed and charged solid surface when exposed to an electrical field. Streaming potentials are produced when two phases move oppositely under exerted mechanical forces. Sedimentation potentials are created when colloids settle in a media due to an external force such as gravity or centrifugal acceleration. The electromotion of clay particles in media is due to the charged nature of the colloids. The charges on the surfaces of clay particles originate mainly from ionization, lattice substitution, ionization, adsorption and unsaturated bonds.

1.3.4.2. Theory of diffusion and electromotion (zeta) potentials

1.3.4.2.1. The formation and structure of diffuse electrical double layers In the diffuse electrical double layers, the distribution of counter-ions is not homogeneous, and the distribution density close to the particle surface is relatively high, which constitutes

a compact layer or adsorbing layer, as shown in Figure 1.20. Shown in the figure is the Stern model (1924) for diffuse electrical double layers.

Charged nanoparticles in water (e.g., hydrated layers of clay) have an equal but opposite charge of counter-ions dispersed to form diffuse electrical double layers in the interfacial region between the particles and the medium. The counter-ions in the electrical double layers are attracted by the opposite charges on the surfaces of the layers or particles. On the other hand, the counter-ions have the capability of diffusing in the liquid due to kinetic motion. The diffusion of counter-ions is influenced by the electrical field in the liquid created by the charge on the surface of the particles. For clays, the adsorbed ions on the particle surfaces are negative. The counter-ions are, in this case, cations. The layer of adsorbed anions and the region in the liquid adjacent to the surface where cations are in excess is known as the diffuse electrical double layer. The region from the particle surface to a point where the excess of adsorbed counter-ions is negligible is known as the Debye length.

The interphase where the bound layer of solvent hydration is in contact with the bulk liquid is a sliding plane (Figure 1.20(a)). The potential difference from the sliding plane to the potential location in bulk liquid phase is known as the zeta potential, or electro-motion potential (ζ potential). The thermodynamic potential (ϕ_0) is the potential difference between the particle surface and the bulk liquid phase. The thermodynamic potential depends on the total charge of the particle surface, while the ζ potential depends on the charge difference between the particle surface and charges in the adsorption layer of solvent hydration (the adsorbed counter-ions).

For clay layers in a suspension, two different diffuse electrical double layers may form as a result of the difference between the charge on the crystalline layer surface and the charge on the edge surface of the clay. The diffuse electrical double layers of clay

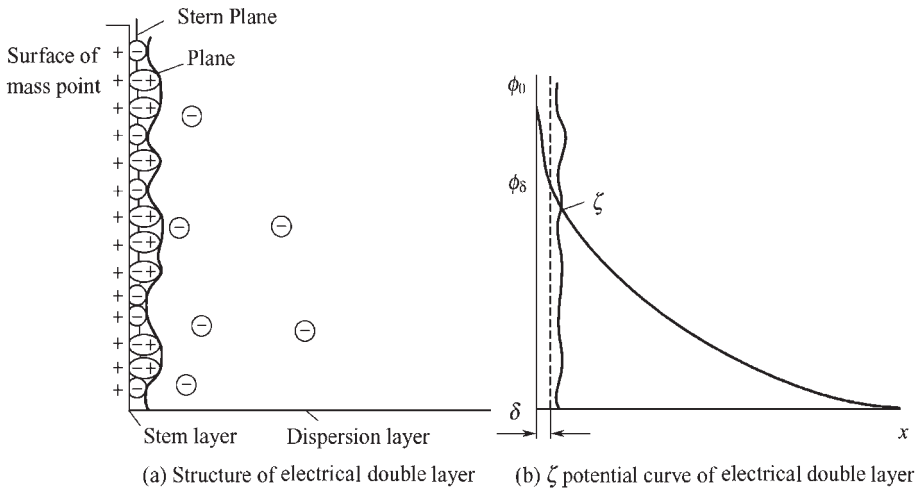


Fig. 1.20. Stern model of diffuse electrical double layers.

have dual properties. This feature is different from other colloidal particles and is described below.

1.3.4.2.2. The electrical double-layer structure for clay surfaces In the lattices of MMTs and illite there occurs the replacement of Si^{4+} by Al^{3+} in the silicon–oxygen tetrahedron crystalline layers and the replacement of Al^{3+} by Mg^{2+} or Fe^{2+} in the aluminum–oxygen octahedron. The lattice replacement creates a permanent negative charge on the surface of the clay, which then attracts cations such as Na^+ , Ca^{2+} and Mg^{2+} . When clay is dispersed in water, the cations move and diffuse outwards. This results in the formation of diffuse electrical double layers on the colloid particles. Part of the water on the clay surface is firmly bound (connected by hydrogen bonds) and so is part of the shell of hydrated cations, both of which form a solvent hydration layer. The other cations diffuse into the liquid surrounded by hydration water, which forms a diffuse electrical layer.

1.3.4.2.3. Double electrical layer structure on the end surface of clay The exposed atoms on the end surface of the clay particles are different from those on the layer surface. On the end surface, the original bonds in the aluminum–oxygen octahedron and silicon–oxygen tetrahedron are broken. The end surface of the octahedron is equivalent to that of the particles of aluminum bauxite $[\text{Al}(\text{OH})_3]$. Several investigators pointed out that when the pH value of the media is less than 9, the OH groups will expose the aluminum ions to a positive charge thus forming a diffuse electrical double layer as for a positive colloid. In basic media, the hydrogen will expose the negatively charged surface ($>\text{Al}-\text{O}^-$).

The formation of an electrical double layer due to a positive charge on the clay end surface is not in conflict with the negatively charged clay particles. The positive charge on the end surface of the clay layers is much lower than the negative charge on the clay particle's surface. The net charge of a clay particle is still negative, so it moves towards a positive pole in an electrical field.

1.3.5. Zeta potential

1.3.5.1. Potential of the diffuse electrical double layers

1.3.5.1.1. Zeta (ζ) potential The electrical potential is an important characteristic parameter of the diffuse electrical double layer and is a criterion for describing the stability of the colloidal system. According to the Stern model, the electric potential (ζ potential) depends on the net charge on the sliding interphase next to the adsorbed layer of counter-ions (Figure 1.20).

1.3.5.1.2. Potential in the diffuse double layer If the surface potential ϕ_0 is less than 25 mV and there is no adsorbed layer of counter-ions, the surface potential ϕ in the diffuse layer is given by the Debye–Huckel equation [41]

$$\phi = \phi_0 \exp(-K \cdot X) \quad (1.3.5)$$

where K is the Debye parameter, $1/K$ the thickness of ionization atmosphere (thickness of the diffuse electrical layer) and X the distance from the particle surface. Obviously,

when $X = 1/K$, $\varphi = \varphi_0/e$; at a distance of $X = 1/K$, the potential exponentially decreases to $1/e$ times φ_0 or $[1/e]\varphi_0$. When $X \rightarrow \infty$, $\varphi \rightarrow 0$, and $X = 0$, $\varphi = \varphi_0$.

1.3.5.1.3. Factors for the thickness of the diffuse electrical double layer and the zeta potential The stability of a colloid against aggregation is closely related to the thickness of the diffuse electrical layer. The thicker the diffuse electrical layer, the greater the electrostatic repulsion between particles and the more stable the colloid. The thickness of the diffuse electrical layer depends mainly on the valence of the counter-ions in solution and the concentration of the electrolyte. If the concentration of the electrolyte increases, or if the valence of the counter-ion is increased, the thickness of the diffuse electrical layer will decrease. Increases in concentration and valence of the counter-ions in solution effectively compress the diffusive electrical layers. A decrease in the thickness of the diffuse electrical layer will in turn lead to a drop in the electrostatic repulsion between the charged particles. The colloid is stable and will not aggregate as long as the electrostatic repulsion is greater than the attractive van der Waals forces between the particles. The colloidal particles usually aggregate when the electrical double layer is compressed down to the thickness of the adsorbed solvation layer by the addition of electrolyte. Predictions on the stability of colloids can be obtained from the DLVO (Derjaguin, Landau, Verwey, Overbeek) theory, which models the competition between electrostatic repulsion and van der Waals attraction among the colloidal particles.

1.3.6. Coagulation and flocculation

The colloid is a thermodynamically unstable system. Stability is a core problem for clay colloids or particles of silica. When clays are exfoliated or dispersed into nanoscale particles, they have a large surface area with high energy. As the surface energy increases, the colloids have a spontaneous tendency to aggregate and grow bigger in order to reduce the surface energy.

Although the colloidal system is unstable, it may remain in a metastable state for a long time because the kinetics to form aggregates may be extremely slow. For example, a sol of gold can be stable for several years or several decades. Colloids of $\text{Fe}(\text{OH})_3$ are stable for several months or 1 year. Colloids eventually become unstable and coagulate and then flocculate. To adjust their stability, one can add treating agents (e.g., surfactants, polymers) to the colloidal system. The factors that affect the stability of colloids and the principles of breaking or stabilizing the colloid systems? are discussed in the following sections.

1.3.6.1. Colloid stability

Colloid stability can be classified into dynamic stability and aggregation stability.

1.3.6.1.1. Dynamic stability Dynamic stability refers to whether a dispersed particle is easy to sediment or not due to an external force such as gravity or centrifugal acceleration. Generally, the sedimentation rate is used to describe a particles dynamic stability. For example, a glass container is filled with a clay suspension and stays undisturbed for 24 h; then the suspending densities on the upper part and lower part, respectively, are determined. The smaller the density difference, the higher the dynamic stability of the system, because the particle sedimentation rate is very slow.

1.3.6.1.2. Aggregation stability Aggregation stability refers to whether a particle of dispersion phase is easy to aggregate. Dynamic stability and aggregation stability are different concepts, but are interrelated. When the particles of the dispersion phase gather together and become larger, they must settle due to an increase in weight. To decrease the aggregation trend, the inorganic particles (e.g., silica or MMT) are usually covered or treated with organic molecules. These molecules form protecting layers or spaces between nanoparticles in order to prevent direct contact and increase the dynamic stability of the system. The protective layers will avoid the formation of extreme negative potential energy or the first minimum potential energy, as seen in Figure 1.21.

1.3.6.1.3. The factors affecting dynamic stability

(1) *External force.* Since gravity (or centrifugal force) is an important factor affecting dynamic stability, its effect is first analyzed. The net gravity of a solid particle in liquid media is expressed as

$$F_1 = (4/3)\pi r^3(\rho - \rho_0)g \quad (1.3.6)$$

where parameters π and g are constants. The net gravity of a mass point of dispersion phase in a gel system depends mainly on the radius of the solid particles and the density difference between the dispersion phase and the dispersion media.

(2) *The effect of Brownian movement.* The smaller the particle radius, the more tempestuous is its Brownian motion. Brownian motion plays an important role in determining the

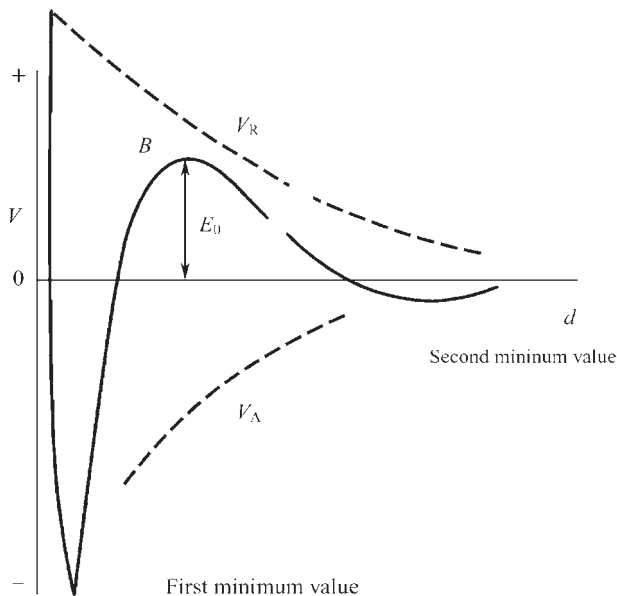


Fig. 1.21. Plot of potential energy of colloidal particles vs. interdistance between particles. (With permission from Press of the University of Petroleum.)

dynamic stability of colloids. When the radius of a particle is greater than 5 μm Brownian motion disappears.

(3) *The effect of media viscosity on the dynamic stability.* According to Stokes' law (Eq. (1.3.4)), the sedimentation velocity of a solid particle in liquid media is inversely proportional to the media's viscosity. In practice, increasing the media viscosity increases the dynamic stability of a colloidal system.

1.3.6.1.4. The aggregation stability

(1) *Theory of electrostatic stability.* In the classical theory by Derjaguin, Landau, Verwey and Overbeek (DLVO theory), the effect of electrolyte valence and concentration on colloid stability has been discussed. There exist two kinds of opposite acting forces: attractive force (V_A) and repulsive force (V_R). If colloidal particles collide during the Brownian motion and the attractive force of the particles is greater than the repulsive force, the sol will aggregate. Conversely, the particles will remain separate and maintain a dispersed state when the repulsive force is greater than the attractive force.

(2) *The attractive force between two colloid particles.* The attractive force is essentially a van der Waals force, which is different from that a single molecule. The colloid particles are ensembles of many molecules. The attractive force between two colloid particles is the summation of all molecular attractive forces. According to the classical theory [42,43], for particles of the same matter and radius a , the attractive potential energy of two spherical colloidal particles is expressed as

$$\begin{aligned} V_A &= -Aa/12H \quad \text{for spherical particles such as silica} \\ V_A &= -A/12\pi D^2 \quad \text{for plate-like particles such as MMT} \end{aligned} \quad (1.3.7)$$

where H is the shortest distance between two spherical particles, A the Hamaker constant (10^{-19} – 10^{-20} J), a the radius of the sphere and D the distance between two parallel plates. These equations describe the interaction between two colloidal particles at a distance in a vacuum.

When the particle size is in the nanoscale, Eq. (1.3.7) has to be corrected as follows: for spherical nanoparticles such as silica,

$$V_A = -4A/[12(1/(k_s^2 + 4k_s) + 1/(k_s + 1)^2 + 1/2 \ln(k_s^2 + 4)/(k_s + 2)^2)] \quad (1.3.8)$$

where $k_s = H/a$. For plate-like nanoparticles such as MMT,

$$V_A = -2A/\delta^2[12\pi k_1(k_1 + 1)(k_1 + 2)] \quad (1.3.9)$$

where $k_1 = D/\delta = d_{001} = \lambda/2\sin\theta_{001}$ as obtained from Eq. (1.3.1). The Hamaker constant for nanoparticles can be obtained from both Eqs. (1.3.8) and (1.3.9) or from the interfacial tensions of the nanoparticle and the medium. When the colloidal particles are dispersed in a medium, e.g., water, the effective Hamaker constants are decreased. For a particle 1 submerged in medium 2, the Hamaker constant is $A_{121} = A_{11} + A_{22} - 2A_{12}$,

where $A_{12} = (A_{11} A_{22})^{1/2}$, so that A_{121}

$$A_{121} = (A_{11}^{1/2} - A_{22}^{1/2})^2 \quad (1.3.10)$$

where A_{121} is an effective Hamaker constant for a colloidal particle in the medium, and A_{11} and A_{22} are the Hamaker constant of the colloidal particle and A_{22} of the medium, respectively. Generally, $A_{\text{H}_2\text{O}} = 3.0-6.1 \times 10^{-20}$ J, $A_{\text{SiO}_2} = 8.0-8.8 \times 10^{-20}$ J [45], $A_{\text{PS}} = 5.6-6.4 \times 10^{-20}$ J and $A_{\text{MMT}} = 15.0-18.0 \times 10^{-20}$ J (this work). It is seen that A_{121} is always a positive value, so that dispersed particles in one media are usually attractive, resulting in an unstable colloidal system. The attractive force between particles when submerged in the medium is usually diminished. In practice, media with the properties closest to the properties of the particle are usually selected so that the interattractive force tends to be the weakest, thereby avoiding aggregations or settling in the media.

(3) *The repulsive force between nanoparticles.* Similar to colloidal particles, the repulsive force between nanoparticles originates from two sources, one is the electrostatic repulsive force and the other is the repulsive force of the solvating film or hydration film on the outside of particles. Usually, these attractive forces are expressed in terms of the attractive potential energy V_A . The magnitude of the repulsive energy depends on the zeta potential (ζ) and the thickness of the ionized hydration film. Generally, the thickness of the hydration film is less than that of the diffuse electrical layer. If counter-ions in the diffuse electrical layer enter the adsorbed layer and stay, the zeta potential will decrease, and this can lead to agglomeration. Molecules inside the hydration film are oriented. When nanoparticles or colloidal particles approach each other, the hydration film deforms because of compression. The hydration film displays an elastic behavior, producing a mechanical hindering force when the nanoparticles approach very closely. The viscosity of water inside the hydration film is higher than that in the bulk state. The increased mechanical resistance in these particles due to hydration films gives rise to a repulsive force.

1.3.6.1.5. *The factors of the agglomeration and flocculation stability* When the colloids are in a relatively stable state, the attractive energy (V_A) is counteracted by the repulsive energy (V_R). The electrolyte concentration and valence state affect the repulsive potential energy of the particles. The total interaction energy between the particles is

$$V_T = V_A + V_R \quad (1.3.11)$$

where $V_R = C_k a e^{-\kappa H}$ (a is the particle radius, $1/\kappa$ is the Debye length and H the distance), $C_k = 64\pi\gamma_0^2 n_0 kT/\kappa^2$ (γ_0 is potential function on the particle surface, n_0 the ion concentration, k the Boltzmann constant and T the temperature). The classical V_T-H curve is plotted in Figure 1.21.

(1) *The effect of electrolyte concentration.* The relationship between the interaction potential energy and the interdistance between particles is given in Figure 1.21. From the overall potential energy of the colloidal particles, the coagulation process can occur at the second minimum value while flocculation occurs at the first minimum value.

If the particles at flocculation are loosely interconnected or if the interparticle coupling force is weak, then the flocculation may be reversible. When, at the first minimum potential energy, the particles are closely connected, the flocculation process is irreversible.

The electrolyte concentration has a great effect on the minimum potential energy. At high concentrations of electrolyte, the attractive energy dominates except at very short distances. At moderate concentrations of electrolyte, the effect of a “long distance” repulsive energy delays the coagulation process. At low electrolyte concentrations, the effect of the “long distance” repulsive energy makes the coagulation process of the particles much slower.

(2) *The effect of the valence of the counter-ions – the critical flocculation concentration.* Coagulation value and rate are used to quantitatively denote the effect of the electrolyte on the stability of sol. The critical or the lowest concentration of electrolyte capable of settling the sol is defined as the coagulation value or the critical flocculation concentration (CFC), which depends on the type and concentration of the electrolyte. The CFC refers to the lowest ion concentration required to flocculate the nanoparticles or colloids under set conditions, and is expressed as mmol l^{-1} . The lower the value of the CFC, the stronger the coagulation capability of the electrolyte. Schulze (1882) and Hardy (1900)[45] have experimentally determined the CFC of sol with different electrolytes with different valences. Their results show that the effect of electrolyte on flocculation originates from the counter-ions having opposite charges compared with colloidal particles. The higher the number of counter-ions, the lower is the coagulation value higher is the coagulation rate. The ratio of the empirical CFC determined by Schulze–Hardy is

$$[M^+]:[M^{2+}]:[M^{3+}] = 100:1.6:0.3 = (1/1)^6:(1/2)^6:(1/3)^6 \quad (1.3.12)$$

where the superscripts in the brackets is the reciprocal valence of the counter-ions. It is seen that the CFC of an electrolyte is inversely proportional to the sixth power of the valence of counter-ions. The attractive van der Waals force for colloids is inversely proportional to the distance to the third power. It can act at positions from 1 to 100 nm or more from the particle surface and is considered to be long range.

The general equation for the CFC (v_c) of a sol based on the DLVO theory according to the Schulze–Hardy principle

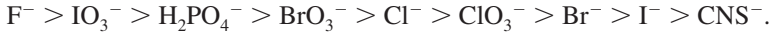
$$v_c = K/Z^6 \quad (1.3.13)$$

where $K = C\varepsilon^3(kT)^5\gamma_0/A^2$, C is a constant related to the symmetrical property of anions and cations in an electrolyte, ε the dielectric constant, A the Hamaker constant, and Z the valence of the counter-ions.

(3) *The effect of ion size – lyotropic effects.* The CFC of ions with the same valence is similar but small differences exist. These differences are called lyotropic effects. The order of the CFC for cations of valence



The order of the CFC for anions of valence 1 is



The order of the CFC with the same valence is approximately identical to the order of the hydration ion radius of the ions (from large to small). For ions of high valence, the CFC depends on the valence of the ions; the effect of ion size is not significant.

(4) *The effect of the ion with the same charge and symbol.* An ion with the same charge as a colloidal particle is called an ion of identical symbol. If these ions do not adsorb on the particles then they only have a secondary effect on colloids and can only reduce the CFC slightly, except in the case of organic polymer ions (polymeric electrolyte). Polymer ions can be adsorbed by the colloidal particles even though they may have the same charge as the colloidal particles.

(5) *The interconglomeration phenomenon.* Generally, two kinds of sol with the same charge will not flocculate when mixed together. If two types of sols with opposite charges are mixed together, flocculation will occur, which is a phenomenon of interagglomeration.

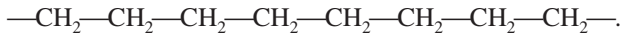
1.4. Polymers and polymerizations

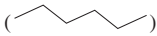
1.4.1. Multiple structure of polymers

1.4.1.1. Polymers and polymer classifications in nanocomposites

In polymer-inorganic nanocomposites, the organic polymers are characterized by a molecular chain structure composed of repeat units or monomers. Flory [46] classified polymers based on his investigations of the features of the chain structure. Combining Flory's classification together with classifications in other works, the three levels for polymer structure are classified as follows:

1.4.1.1.1. *First level of chain structure* The first level refers to the chain structure, e.g., the simple chains of polyethylene molecules have the structure



This chain often takes a zigzag structure () . Polymer chain structure depends on its surrounding or medium, e.g., it is a coil when in solution. The average square end distance is seen in Figure 1.22 and is shown by the two arrows.

To measure the molecular weight of polyamide or polyester nanocomposites, a small-angle light-scattering method is often used together with gel permeation chromatography (GPC). These nanocomposites with appropriate molecular weight (e.g., $\eta_{iv} = 0.6\text{--}0.7$ g dl) will dissolve well in a common solvent so that their molecular weight can be determined. The inorganic phase is thought to affect the final result. However, it is difficult to separate the inorganic phase from the solvent.

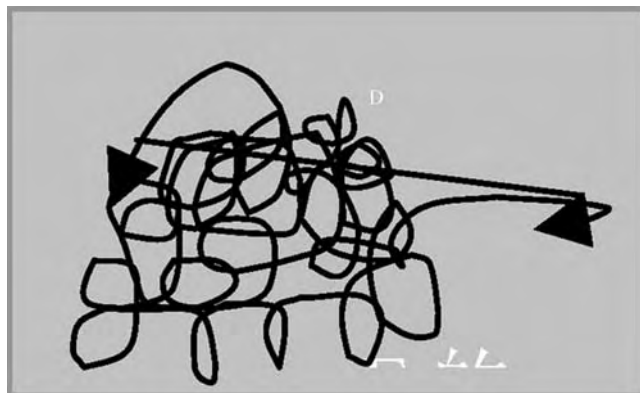


Fig. 1.22. Polymer coil model in solution.

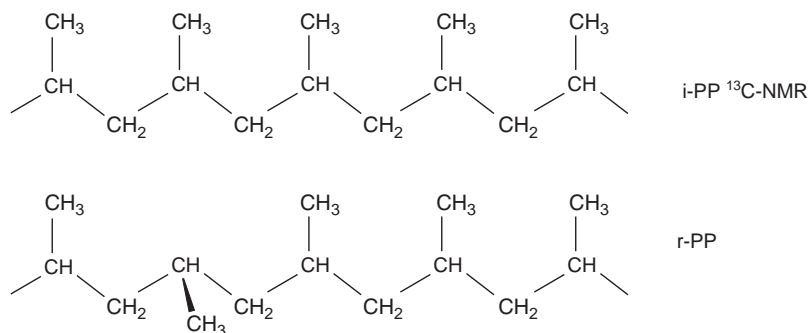


Fig. 1.23. Chain structure of isotactic and atactic polypropylene.

1.4.1.1.2. Second level: the chain conformation The second level is the chain conformation, which is directly related to the polymer property. For example, isotactic polypropylene (*i*-PP) and atactic or random polypropylene (*r*-PP), with the chain conformation as shown in Figure 1.23, have totally different physical properties.

The atactic polypropylene is not suitable for the preparation of nanocomposites with silica or MMT, while *i*-PP is used to prepare many nanocomposites. The chain conformations of *i*-PP or *a*-PP by ^{13}C -NMR expressed by their monomer unit, and determined are shown in Figure 1.24.

1.4.1.1.3. Third level of condensed state structure The third level of structure is the condensed structure of polymers. In these condensed structures, crystal spherulitic structures are usually seen in semi-crystalline polymers, e.g., liquid crystalline polymer imides or polyesters (PET). The crystalline morphologies are shown in Figure 1.25 for

semi-crystalline polyaryl ether ether ketone ketone [47] (PEEKmK, *m*-meta link aromatic ring) with molecular chain unit structure as

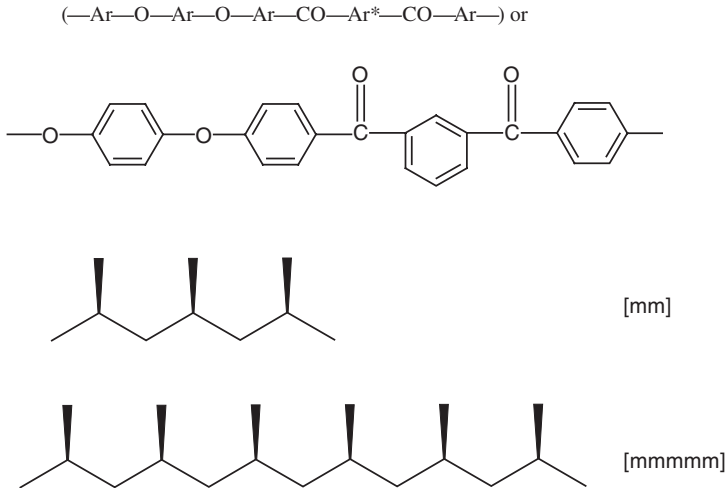


Fig. 1.24. Conformation of PP molecular chains expressed by 3 (above) and 6 unit groups.

The samples were crystallized at 220°C for 15 h from the glassy state without further treatment (the crystal growth has been shown by our investigation by TEM). The morphology is like a shish-kebab morphology of polyethylene, which was produced by stirring a 5% xylene solution of PE at 510 rpm and 104.5°C [48].

Under certain types of flow, molecular chains tend to align parallel to each other. In Figure 1.26, the quadrant angular crystals grow by linking together in the direction of the *b*-axis. Controlling the crystallization conditions can lead to a structure in which highly aligned or linked (or parallel) fibrils can be formed with chain-folded lamellae attached to them at right angles.

In many polymers such as polypropylene (PP), polyethylene (PE) and poly-(butylene terephthalate) (PBT), the spherulitic morphology is observed with TEM. Sometimes, polymers such as *i*-PP often have a perfect spherulitic morphology, as shown in Figure 1.27, using optical microscopy.

In the case of polyethylene (PE), the early growth stage of spherulites is often observed when it is crystallized in solution. Similarly, one can observe the leaf-like growth of PEEK spherulites (Figure 1.28).

Similar morphologies have been discussed in the literature [49]. For the polymer-condensed state, there are four phase states: amorphous, transitional (or meta stable) [50], liquid crystalline and crystalline state. In the crystalline state, polymorphism formation has attracted much attention. When nanoparticles are introduced into organic polymers to make composites, this polymorphism often occurs through their induction (Chapter 3), and is usually a starting point for investigating nanocomposites.

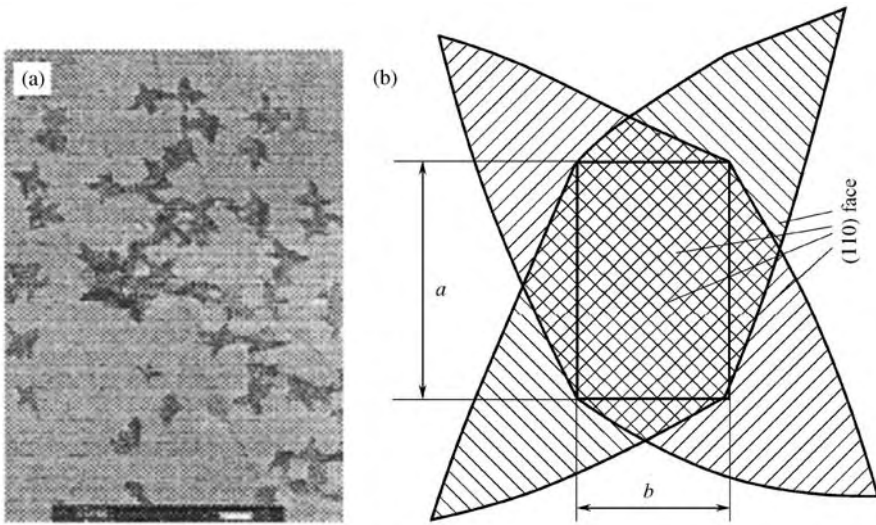


Fig. 1.25. Morphology of quadrant angular single lamella (A), and the predicted growth of single lamella in the direction of (110) face (B) in polymers of PEEKmK.

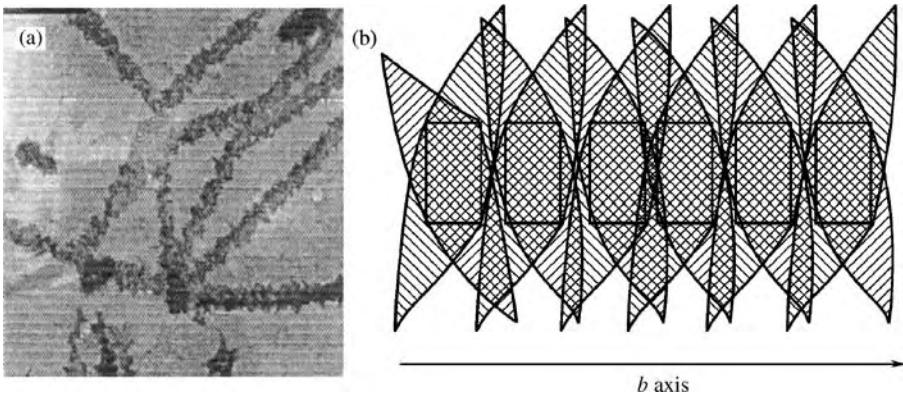


Fig. 1.26. Morphology of quadrant leaf-like single lamella (A) and the predicted growth direction of spherulites along the b -axis of the crystal (B).

1.4.2. Polymer classification

Organic polymer materials are produced in very large yields. Data show that the total polymer yield in 2003 reached 200 million tons. Polymers have become a main application field for ultrafine powders. The polymers are classified by their function and applications.

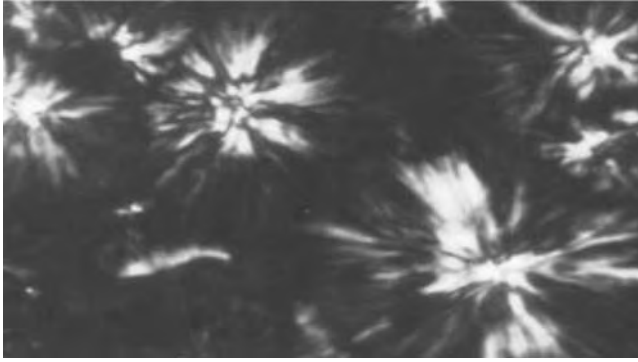


Fig. 1.27. Polarized optical microscopy (POM) spherulitic morphology of a high isotactic fraction sample of i-pp made from the temperature rising elution fractionation device at 140°C.

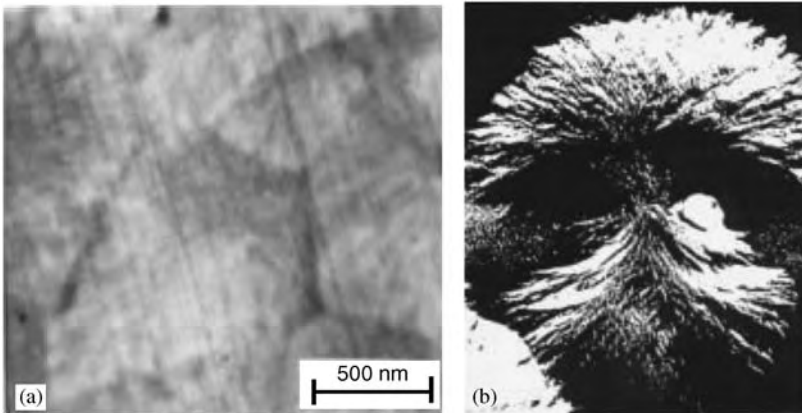


Fig. 1.28. Morphology of collision spherulites in polybutylene terephthalate (PBT) crystallized from the melt, and the leaf-like spherulitic morphology in polyaromatic ether ketone (PEEK) solution, e.g. chloroform.

1.4.2.1. Classification by function and application

Organic polymers are generally divided into plastics, rubber and fibers. Polymers will be divided into polymers for common usage, for special applications, for functional aim and for biological applications.

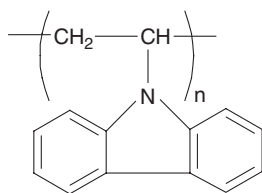
1.4.2.1.1. Polymers for universal or all-purpose usage Universal refers to polymers with large yield and wide applications. These polymers account for 70% of the entire polymer production in the world, but accounts for nearly 90% (by wt) in China. The polymers are mainly polyolefins such as PP, PE, polyvinyl chloride (PVC) and polystyrene (PS); polymer fibers such as terylene used mainly as polyethylene terephthalate (PET), nylon, polyamide, polyacrylonitrile (PAN) and polyvinyl alcohol (PVA); rubbers

such as copolymers of butadiene-styrene (SBR), *cis*-butadiene rubber (*cis*-BR), isoprene rubber (IR) and rubber of ethylene-propylene copolymers (EPR).

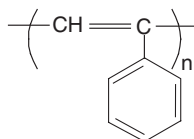
1.4.2.1.2. Polymers of special types with high performance Some polymers are resistant at temperatures over 100°C; these are high-performance polymers and engineering plastics. For example, polymers of polyether ketone (PEK) and polyether sulfone (PES) both have application temperatures above 150°C. The top five engineering plastics are polyformaldehyde (POM), polycarbonate (PC), polyamide (PA), polybutylenes terephthalate (PBT), and polyphenyl ether (PEO). All have application temperatures (usually referred to as heat distortion temperature) above 100°C. Many all-purpose polymers are modified to prepare engineering plastics through diverse approaches including nanocomposites. So far, nanocomposites have been prepared from several main polymers, which are extensively produced in the world, e.g., PP, PE, PC and PET. The success in modifying these polymers can have profound effects on the polymers.

1.4.2.1.3. Functional polymers These polymer materials and composites have useful optical, sonic, electrical and magnetic functions and properties:

- (1) *Optical sensitive polymers.* Polymers sensitive to optics are polyethylene carbazole and polyphenyl ethene:



[Polyethylene carbazole]



[Poly phenyle ethene]

Polyethylene carbazole is an electrically conducting polymer, while polyphenyl ethene is a semiconductor polymer.

- (2) *Diverse liquid crystalline polymers.* These polymers include lyotropic liquid crystals (LLC), such as PPT (Poly(*p*-phenyl terephthalamide)) or polymers of thermotropic liquid crystal (TLC) such as polycarbonate ester.
- (3) *Different kinds of polymer reagents and catalysis.* Polystyrene well known as a catalyst carrier. There are other examples such as polymers for ion-exchange reagents, sulphonate reagents, acryl reagents of polymers and copolymers of sulfonated polystyrene – diethylene benzene as catalysts.

1.4.2.1.4. Biopolymers or biomacromolecules Biomacromolecules are macromolecules in biological systems and man-made polymers for medical applications. Biomacromolecules have become a branch of nanomaterial science.

1.4.2.2. Polymer-based nanocomposites

In the 21st century, nanocomposites will be one of the most rapidly developing and advanced composite materials. Polymer-based nanocomposites are defined as those in which the dispersion phase ranges from 1 to 100 nm. The superfine powder is mixed with polymer matrixes to form polymer-based nanocomposites. Most kinds of composites are prepared from these inorganic powders mixed with polymers through melting, solvent mixing, codeposition assembly and simply blending different block polymers. In Table 1.15, the classification of polymer-based nanocomposites from dispersion phases is shown. The nanocomposite materials have a scale ranging from microcosmic composites of superfine particle dispersions to the molecular scale (scale level for molecular dispersion in Å). According to the dispersion phase, they are classified into polymer/polymer system and polymer/fill system. The classifications are used for understanding the behavior of nanocomposites. The polymer-based nanocomposites have special advantages in their properties and performances, as discussed below.

- (1) *Property enhancement*: The materials have enhanced properties such as heat distortion temperature, crystalline rate, mechanical properties, and other functional properties (optical, sonic).
- (2) *Resources economizing composites*: The main raw materials are readily available (e.g., organic polymers, inorganic MMT, are natural products).
- (3) *Maintaining original technology*: Compounding of these nanomaterials generally involves the use of established techniques without changing equipment. This important characteristic could cause the fabrication of these nanocomposites to become rapidly industrialized.

According to the dispersion-phase classification, there are polymer/polymer or polymer/oligomer systems, and polymer/filler systems. Polymer/filler systems are organic/inorganic systems (Table 1.16), in which filler includes metal particles, non-metal powder, and semiconductor matter or conductor powder, e.g., PET/layered silicate

Table 1.15
Classification of polymer system-based composites for an inorganic/organic phase

Phase 1/phase 2	Dispersion phase scale (nm)		
	~1000	100–1000	0.5–100
Polymer/oligomer	Powder direct mixing	Oligomer as phase miscible agent	Oligomer as modifier of rheology Polymer composites with heat plasticity
Polymer/polymer	Blending composite of macrocosmic phase separation	Polymer alloys of microcosmic phase separation	Molecular composites Miscible polymer alloys Microcosmic miscible polymer composites

Table 1.16
Classification of polymer based composites for a organic–inorganic phase system

Phase 1/phase 2	Dispersion phase scale (nm)		
	1000	100–1000	0.5–100
Polymer/filler	Melt blending polymer with inorganic filler	Composites of polymer/ common fillers	Composites of polymer filled with superfine particles
Polymer/Nanoprecursor ^a	Simply melt blending	Simply melt extruding Melt intercalation	Polymer-based nanocomposite Hybrids Polymerization of Nanocomposites in situ

^aRefers to a precursor of a liquid or a solid state

systems. Polymer/polymer systems can be obtained by the blending of macrocomposites in which the interface scale is in nanometers, e.g., PC/PET, PET/PBT, Nylon6/PET or PEEK/PEEK oligomers. The polymer can also be oligomer, which can be used to modify other polymers that cannot fulfil the properties in polymer/filler systems.

1.4.2.3. Classifications of polymer-inorganic nanocomposites

The dispersion phase has different morphologies or shapes, based on which polymer-inorganic nanocomposites are classified into three types.

- 1-D (one-dimensional) nanocomposites: the dispersion phase is wire-like, e.g., nanowiskers of attapulgite/polyolefin nanocomposites.
- 2-D (two-dimensional) nanocomposites: the dispersion phase is layer-like, e.g., layered silicate/polyimide nanocomposites.
- 3-D (three-dimensional) nanocomposites: the dispersion phase is spherical-like, e.g., polymer SBS/nano-CaCO₃ nanocomposites.

To describe a special structure or morphology, polymer-inorganic nanocomposites were also classified according to these morphologies:

- H-H nanocomposites (H stands for homogeneous phase): consists of two phases.
- H-S nanocomposites (S stands for phase separation): consists of two phases which are partly phase-separated.
- S-S nanocomposites (consists of two phases, which are totally phase-separated or all phases are separated).

These classifications are useful in describing assembling or self-assembling nanocomposites. The particle's morphology in nanocomposites is either ordered, random or aggregated. The distribution of nanoparticles in matrixes is homogeneous, heterogeneous or agglomerated, which are factors affecting the properties of the nanocomposites. In designing of nanocomposites physical parameters, space distribution parameters and volume fractions should be taken into account.

1.5. Preparation and technology for nanocomposites

1.5.1. Brief introduction to nanocomposite preparation

There are several methods for the preparation of nanoparticles or composite nanoparticles. The sol–gel technique, chemical vapour deposition (CVD) and ball-milling techniques are widely applied to nanoparticles. In nanocomposite materials, particle dispersion is one of the most urgent problems to be addressed. The dispersion and related preparations and synthesis are described in a later section. In order to disperse the particles, particle surface treatment may be necessary to match the polymer matrix in compatibility. Surface treatment is directly related to the stability of nanoparticles. There are several dispersion technologies for nanoparticles dispersed in polymers, such as CVD and gas vapor deposition (GVD), which are used for depositing or covering layers on the outside of the particles. The deposited layers can be both organic and inorganic material. Most of the surface treatments are organic, e.g., oligomers, surfactants or polymer films. Polymer powders are also treated by techniques of ionization, degradation or mechanical milling to improve compatibility with superfine inorganic powders.

1.5.1.1. Preparation methods

The preparation of nanoparticles includes surface treatments to disperse them homogeneously in nanocomposite matrixes. These include several aspects, which are briefly introduced and described in detail in the later chapters.

(1) *Sol–gel method.* Using this method, the treating agent is added to the nanoparticle precursors, forming a sol by a hydration process. The sol forms a surface layer on the particle after recovering the gel. Then some monomers of solvent-soluble (e.g., polyvinylpyrrolidone (PVP)) or water-soluble (e.g., polyvinyl alcohol (PVA)) polymers are introduced; nanocomposites are prepared in one pot. This method has a narrower selecting space for organic polymers and nanomaterials, but is very popular for nanocomposites because the polymer is soluble in the media.

(2) *Nanoprecursor methods.* There are many raw materials of layered silicates, layered compounds, metal powders and oxide compounds. Nearly all of the oxide compounds or their particles can be transformed into superfine powders. Some have complicated compositions not suitable for the preparation of nanocomposites or composite nanoparticles. These materials are transformed into an intermediate form, called the precursor, in which the homogeneous raw material with extremely high purity is obtained. Some of the precursors for nanoparticles or nanocomposites are shown in Table 1.17.

(3) *Intercalation method.* For layered compounds or silicates, agents or treating reagents are intercalated into the layer space. These intercalates are nanomaterial precursors with controlled layer morphology and are exfoliated during the polymerization reaction.

(4) *Blending methods.* Nanoparticles are prepared via a sol–gel process and are blended with treating agents such as siloxane, surfactants, lower molecular weight molecules, oligomers or polymers. By blending or mixing, particles covered with the treating agents are obtained. When a treating agent is a polymer, a core (inorganic)–shell (polymer cover)

Table 1.17

Usual inorganic nanoparticle materials and their counterpart precursors for nanocomposites

No.	Nanoparticles	Counterpart	Precursors	Preparation techniques
1	SiO ₂	TEOS		Hydrolysis Centrifugal separation [50–52]
2	SiC	SiH ₄ + CH ₄		LICVD [53,54]
3	Si ₃ N ₄	SiH ₄ + NH ₃		LICVD [53,54]
4	ZrO ₂	ZrOCl ₂ + NH ₄ OH/Zr(OH) ₄		Codeposition [54,55]
5	Y ₂ O ₃	YCl ₃ + NH ₄ OH/Y(OH) ₃		Codeposition [54,55]
6	TiO ₂	Ti(OC ₂ H ₅) ₄	Metal ethylate [58]	
7	M _x O _y	M _x (OC ₂ H ₅) _z	Metal ethylate/ codeposition	

structure is usually obtained. The nanoparticles are not directly mixed with polymers but with an intermediate material. For example, nanosilica treated with maleic anhydride is mixed with polypropylene to prepare the intermediate pellets, in which the silica content is up to 10–30% (by wt); this intermediate is then diluted through dispersion in the polymer matrix.

(5) *Filling methods.* The composite nanoparticles or nanocomposites are prepared by filling organic molecules or polymers into inorganic particle pores, surfaces and interfaces by means of mechanical powder mixing, liquid dissolving or heat melting. This method is versatile and has wide applications for either treating or preparing nanomaterials or nanocomposites. In one of these filling methods, the dry mixing process is similar to the formation of polymer alloys, e.g., polymer–polymer blends, or polymer–rigid particle blends.

1.5.1.2. Synthesis

In polymer-inorganic nanocomposites, the synthetic routes are usually related to the conditions for polymerization. The synthesis of these nanocomposites are that they are economical, easy to realize and reasonable. The polymerization conditions or technologies for the nanocomposites are the same as those for the pristine.

1.5.1.3. Stabilization design for nanocomposites

An important aspect of preparing nanocomposites is the particle surface treatment as described above. Often mentioned in the literature are deposition reaction modification, surface chemical modification, mechanical force chemical modification, modification by high energy and modification by gelation wisp and intercalation. These modifications are to improve the nanomaterial's stability, thereby solving problems of heterogeneous aggregation and preventing agglomeration and phase separation of nanoparticles from the matrix. The interactions between the reacting groups of the polymer and the nanoparticles depend on the chemical structure of the polymer, the nanoparticle surface charge, and the broken and dangling bonds on the nanoparticles. These interactions can be discussed in terms of covalent bonds, ionic bonds, chiral bonds or mixtures of these bonds.

1.5.1.4. Forming covalent bond between nanocomposite materials

Groups on polymer chains can form a polar group interaction by a covalent bond [57, 58]. For example, carboxyl groups, sulfonation groups, amide or amine groups can form a covalent bond with hydroxyl groups on the nanoparticles. The double bond of siloxane copolymerized with a polymer main chain forms a polymer with branched chains of siloxane. The partial hydroxylation of siloxane forms silicon gel nanoparticles combined with the polymer main chains through covalent bonds.

1.5.1.5. Forming nanocomposites by ionic bonds

The ionic bond is a chemical bond formed by coulombic attraction between positive and negative charges. Generally, the selected polymer chains and nanoparticles have opposite charges, and the ionic interaction between them stabilizes the nanocomposites systems. For example, under acid conditions, polyaniline is easily intercalated into MMT interlayer space, forming PAN/MMT nanocomposites through ionic bond interactions between PAN salt and the counter-ions on the layer surface of MMT. It is this ionic bond interaction that stabilizes the PAN/MMT system.

1.5.1.6. Forming nanocomposites by affinity effect

The surface affinity of nanoparticles for groups in polymer chains forms a strong interaction. This affinity ensures the homogenous dispersion of nanoparticles into the polymer matrix.

1.5.2. General design and aspects for nanocomposite

Except for the special requirements of monodisperse particle preparation [59–61], the preparation of most of the nanoparticles and nanomaterials are divided into four methods:

The wet method: In this method, nanoparticles prepared in a medium using the sol–gel approach, the emulsion approach and the intercalation polymerization approach.

The dry method: In this method, nanoparticles are prepared in a direct way and not in a wet medium, using methods such as the abrasive approach, the burning approach, the gas impinging approach, and the collision approach.

The evaporating method: In this method, nanoparticles are prepared using CVD and the gas deposition approach, e.g., the laser gas vapor deposition (GVD) approach.

The sedimentation method: In this method, special approaches, e.g., the heavy weight selection approach and the sedimentation approach. These approaches are of practical significance if skillfully applied in the preparation of nanocomposites and nanomaterials.

1.5.2.1. Sol–gel approach

1.5.2.1.1. Scientific principle The principle of sol–gel synthesis is based on colloid chemistry in which the solid raw materials (usually inorganic materials) are dissolved in selected solvents and are then transmitted into homogeneous solution under controlled conditions (temperature, pressure, etc.). Then the dispersed phase is transferred into gel under similarly controlled conditions. The colloid particles formed are in the size range 1000–1 nm.

1.5.2.1.2. Steps of the sol–gel approach for nanoparticles Preparation of the sol starts by suspending the bulk particles, adding precipitator and filtering the unsolved particles. After the large particles are dissolved, the fine particles are deposited by the addition of a selected precipitator. The filtrated and aggregated particle gels are separated into original fine particles, while the fractions of unsolved particles are filtrated and removed. A homogeneous sol is prepared through these steps.

1.5.2.2. In situ polymerization composites

All components in one system mix, react and form new forms of products in the same system. For in situ polymerization of composites, the formation of nanoparticles and the polymerization occur in the same system and at the same time.

1.5.2.2.1. Organic–inorganic nanocomposites by covalent effect The nanocomposites are prepared using the sol–gel technique. In applications, polysiloxane/SiO₂ (TiO₂) nanocomposites have properties such as low gas permeability and high transparency. In the preparation of these nanocomposites, the precursor of TEOS for silica is mixed with polysiloxane in CH₃Cl₃ to form a film. When dried, a film of nanocomposites is formed. In this design, the covalent bond is formed in situ during the initiating of the polymerization reaction.

1.5.2.2.2. Forming nanocomposites by a chiral bond interaction Organic matrixes usually have pair electrons, which have chiral interactions with empty electron orbitals through which a chemical interaction occur. The chiral interaction effect is used to prepare nanocomposites by in situ polymerization. The preparation of these nanocomposites is to mix the polymer powder with functional inorganic powder in a solution. The selected inorganic materials should interact with the polymer functional groups.

1.5.2.3. Mixing ethylate approach

The mixing ethylate approach is also based on the sol–gel principle. The following examples show that in the preparation of BaTiO₃ particles, the metal barium precursors need to be hydrolyzed as rapidly as possible and that the hydrolyzed products are easily calcinated into nanocomposites.

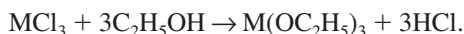
Example 1.5.2.1. Preparation of BaTiO₃ nanoparticles [62,63] and their composites. First, metal barium is reacted with ethanol to obtain ethylate barium. Second, ethanol, ammonia and tetrachlorotitanate react together to form the titanate ethylate which is filtrated from the chloro-ammonium. Third, some precursor of TEOS is added to the system to prepare the nanocomposite particles of BaTiO₃/TiO₂/SiO₂.

The ethylate mixed in benzene solvent has a molar ratio of Ba/Ti = 1:1. It is refluxed for 2 h, and to this solution a small amount of distilled water is added and stirred. White superfine particles are obtained after hydrolysis. The crystalline BaTiO₃ nanoparticles have diameters of 10–15 nm. The alcoholic salts are Ba(OC₃H₇)₂ or Ti(OC₅H₁₁)₄. The BaTiO₃ nanoparticles have a size < 15 nm with a purity of 99.98% suitable for conductor or semiconductor applications.

The use of ethylates and its mixing salts for the preparation of nanoparticle precursors are well known. The preparation process is divided developed into two methods: the

ethanol–ammonia method and the ethanol–metal sodium method. Their operating principles and preparing processes are introduced below.

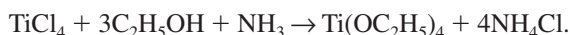
1.5.2.3.1. Ethanol–ammonia approach The metal halides react with alcohol to form its salts; then through the sol–gel process and by the addition of ammonia or amine compound to the system, the nanoparticles are prepared:



In most reactions of metal chlorides with ethanol, only partial Cl^- ion replacement by the RO group (R = alkyl group) takes place. Therefore, ammonia, trialkyl amine, pyridine or alcoholic sodium, are added to complete the reaction. Consider the reaction of $TiCl_4$ as an example:



Next NH_3 is added to the mixture of $TiCl_4$ and C_2H_5OH . Then, further reaction occurs:



In this reaction, the product is flocculated titanate; thus, in this way the nanoprecursor of titanium ester of $Ti(OC_2H_5)_4$ is prepared. Similarly, several alcoholic compounds can be prepared using the metal chlorides of Pt, Rh, P, B, Ti, Si, Ge, Zr, Hf, Nb, Ta, Fe, Sb, V, Ce, U, Th, Pu.

1.5.2.3.2. Alcoholic sodium approach Several active metals such as alkali metals, alkaline-earth metals and the lanthanum system of metals directly react with alcohol to give metal salts and hydrogen, similar to sodium (Na) reacting with alcohol.



where R = $-C_2H_5$, $-C_3H_7$ and $-C_4H_9$ and indicates M metals such as Li, Na, K, Ca, Sr, Ba, Be, Mg, Al, Tl, Sc, Yb, Ga, In, Si and Ni. Metals of weak positive charges, such as Be, Mg, and Al need to react in the presence of catalysts of I_2 , Hg or HgI.

1.5.2.4. Microemulsion approach

The microemulsion approach is a sol–gel approach. This system has added surfactant in the nanoparticle sol system. The surfactant forms an in situ cover on the nanoparticles, which forms a so-called nanoparticle core–shell colloid wisp. The inner core consists of nanoparticles and the shell layer of surfactants.

The microemulsion approach is excellent for the preparation of particles of small diameter, narrow size distribution and large specific surface area. The method requires that a properly matched microemulsion should be designed, and that suitable deposition system and economical posttreatment be provided. Its composition should include nanomaterial precursors (organic reagents, e.g., metal alcoholic compound), surfactants and their matching additives. The greater the solubility capacity of the microemulsion

for the organic reagents, the better the microemulsion is for obtaining a high yield rate of nanoparticles. After the microemulsion system is prepared, measures should be taken to control the preparation conditions of nanoparticles. These measures control the relative ratio of water/surfactant and pH value of the system in order to control the particle size.

The nanoparticles obtained from the microemulsion approach have core-shell structures, which have a direct effect on their subsequent applications. In W/O microemulsion systems, the synthetic SiO_2 particles have a size ranging from 30 nm to 70 nm. Silica particle size stability and its final size distribution are affected by factors such as water, surfactant concentration and surfactant properties. The narrow dispersed silica nanoparticles are prepared through hydration of TEOS in the tri-composition system of W/O microemulsion or a system of 29% (by wt) ammonia/hexane/non-ionic surfactant. The non-ionic surfactant is poly(oxyethylene or nonyl) phenyl and its molecular structure is $\text{R-Ar-(OCH}_2\text{CH}_2\text{-)}_x\text{-OH}$ ($\text{R} = \text{-C}_9\text{H}_{19}, \text{-C}_{12}\text{H}_{23}$ Ar = phenyl). When $\text{R} = \text{-C}_9\text{H}_{19}$, the above molecule is written as NP_x , where x is the average number of oxyethylene in each surfactant molecule.

Use of NP6 as a surfactant has produced SiO_2 particles with an average size of 40–50 nm, while, when NP5 is used in W/O microemulsion systems, the dispersed particle size is 35–70 nm. Our investigations also show that, in this W/O system, the molar ratio of water/surfactant at 1.3–1.4 produces the minimum size of SiO_2 particle with a narrow dispersion.

Example 1.5.2.2. Preparation of ultrafine particles of silica by microemulsion with NP_x . NP4 (analytical grade), TEOS (99.999% purity, Aldrich Co.), heptane and ammonia (NH_4OH) solution with 71% (by wt) of water and 29% (by wt) of ammonia as a catalyst are used for mixing. Ammonia and deionized water are mixed with the heptane/NP4 system, which is stirred until it is transparent. Finally, TEOS is added to the microemulsion system and begins to hydrate to form the nanoparticles of silica in a reactor sealed by Teflon at 22°C. The final silica particle size is about 26–43 nm. The minimum silica particle size is obtained at the ratio of water/surfactant of 1:1.9.

Example 1.5.2.3. Preparation of nanoparticles of Rh carried on SiO_2 . The emulsion system is NP5/hexane/ $\text{RhCl}_2/\text{H}_2\text{O}$. The concentration of NP5 is 0.5 mol/l^{-1} in the organic phase and $\text{RhCl}_2/\text{H}_2\text{O}$ is 0.37 mol/l^{-1} . In this emulsion, the volume fraction of water phase is 0.11. At 25°C, the compound $\text{NH}_2\text{-NH}_2$ is added to the emulsion system. The mixture is stirred while the particles of Rh compounds are formed. Dilute ammonia is then added to the mixture to form a suspending emulsion. Finally, zirconium butyl alcohol or TEOS in cyclohexane solvent is added to the mixture while stirring vigorously and heating to 40°C. The yellowish compound of ZrO_2 or SiO_2 is precipitated. By calcination and reduction with high-temperature hydrogen gas, the compound gives the catalysts of oxides carrying Rh.

1.5.2.5. Deposition approach and plasma deposition approach

The deposition approach includes chemical vapor deposition (CVD) and physical vapor deposition (PVD). Recently, CVD, PVD and plasma deposition have been used to prepare high-purity nanoparticles on a small scale. Under an inert gas atmosphere without any

oxygen, nanopowders, such as Co and Ni, are directly deposited on the carriers of polymers or inorganic materials to prepare catalysts capable of substituting precious metal of Pd. The deposition approach is used mainly in the preparation of film catalyst materials such as Ni–Fe, Ni–P, and Ni–Zn, which are combined with that of plasma creating a mixed plasma approach of plasma vapor, reactive plasma vapor and plasma CVD.

1.5.3. Technology for composite nanoparticles or nanocomposites

1.5.3.1. General technology for preparation of raw materials

The technology for the preparation of inorganic–inorganic composite nanoparticles or polymer–inorganic nanocomposites is based on either intercalation methods or on those for inorganic phases such as silica. The technology generally refers to the large-scale preparation processes. As for the natural minerals of clay, it is a mixture of several components depending on their coexistence condition, mineral regions and natural sources. In order to apply them for preparation of nanocomposite materials, they are first purified and kept as relative stable components. So far, the technology for selecting clay ores and purification is very mature and has been industrialized.

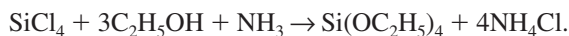
The key to processing clay is to remove the dissociative components such as sand, separate the organic residuals and reduce harmful element contents such as ferric or heavy metals. The purifying process will be discussed in the later part of the book. Similarly, silica is obtained from siliceous ore, willemite ore or quartzite ore. All these ores contain some ferric content, and will remain as intermediates such as SiCl_4 and TEOS. According to different requirements of purity, the precursors of silica have to be purified to remove the harmful elements.

1.5.3.2. Ethanol–ammonia approach

This process is a modification of the preparation process for nanoparticles or composite nanoparticles. The mixture of ethanol, ammonia, the metal halides, and monomers is put in the same autoclave or reactor. Then, the sol–gel process starts after dropping some ammonia or amine additive to the mixture. Taking the reaction of SiCl_4 as an example, its initial reaction is



Then NH_3 is added to the system and further reaction occurs,



In the reaction, the product is a of titanate flocculate. Thus, the nanoprecursor of titanium ester of $\text{Ti}(\text{OC}_2\text{H}_5)_4$ is prepared.

1.5.3.3. Mixing approach or one pot technology

Other methods may use mixing solvents of water and alcohol with mixtures of the precursors of silica and MMT. When the reactive mixture or sol–gel system forms, the nanoparticles are not separated, but are reacted in situ with the modifier or surface-treating agents. The nanocomposites are prepared by initiating the polymerization reaction. The whole reaction is accomplished in one form (not separated any material during the

middle stage), thus it is called the “one-pot” process. This process is both suitable for silica and MMT preparation. The practical “one-pot” technology for preparation of precursors of layered silicate and silica for the corresponding nanomaterials or nanocomposites is shown in Figure 1.29.

In the one-pot process, it is not necessary to dry the nanoparticles or separate them from the solution system; they directly react with the monomers in the mixtures by either a form of silica precursor or MMT precursor. Meanwhile, the modified agents for silica or MMT are mixed with the precursors of silica or MMT to prepare the reactive mixture, which is initialized under the polymerization process to produce the final nanocomposites product.

1.5.3.4. Examples for the preparation of composite nanoparticles or nanocomposite materials

Example 1.5.3.1. Sol-gel approach for preparation of $\text{SnO}_2/\text{SiO}_2$ nanoparticles. For preparation of single SnO_2 particles, the preparation process was as follows: 20 g of SnCl_2 dissolved in 250 ml of ethanol, followed by stirring for 30 min, then refluxed for 1 h, and allowed for aging for 2 h. The mixture was kept at room temperature for 5 d, and dried for 2 d in a water bath at 333 K. The collected particles were oven-dried at 373 K to give nanoparticles of SnO_2 .

Generally, $\text{NH}_3/\text{H}_2\text{O}$ (its molar ratio to ethanol is 1:4) is added to the mixture to adjust the sedimentation or control the particle size. To get a fine or smaller size of composite nanoparticles, an emulsifier such as NP_x is added to the mixtures. In practice, this

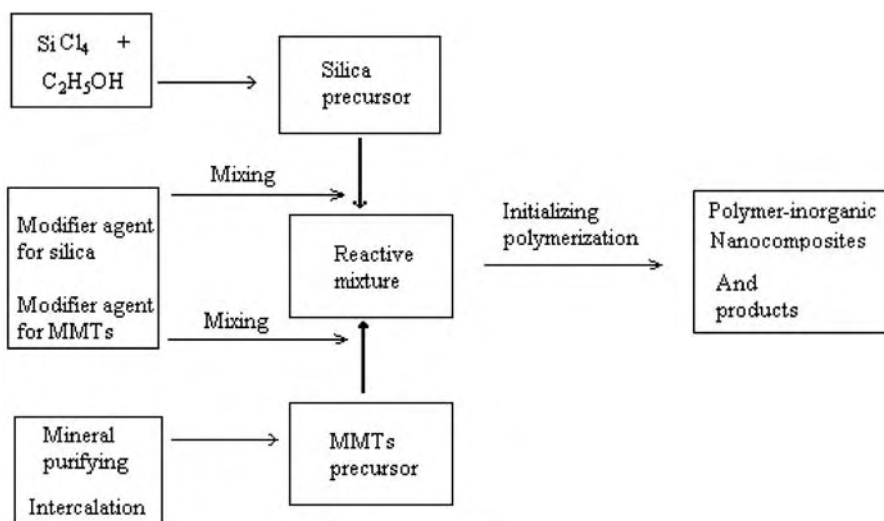


Fig. 1.29. Flow chart of the one-pot process of preparation of fine particle of layered silicate, silica and the related key device.

process is supposed to transform into one-pot technology by the addition of the monomers of polymers to the above mixture during the aging stage. Afterwards, the mixture is moved to another reactor to initialize the polymerization.

Example 1.5.3.2. Sol-gel approach for preparation of nanoparticles and nanocomposites. The preparation is at a temperature of 288 K. First 40 ml TBTT (tetrabutyl titanate, chemical purity of 99.0%, $\rho = 0.99\text{--}1.003$ g ml) is added to distilled water, the water volume is 256 and 480 ml, respectively, to give different sizes of nanoparticles (or nanocomposites, see below). TBTT is added with a controlled stirring rate; the sol forms by hydrolysis. After stirring the system by ultrasonication for 20 min, the collected samples are dried under infrared light. The loose titanium hydroxide gel is obtained. The nanoparticles of TiO_2 are obtained by milling the gel and calcination at 673 and 873 K for 1 h.

In a similar way, TEOS, which is the precursor of silica, is dissolved in a mixed solvent of ethanol and water (weight ratio of ethanol/water is 4:1) and added drop by drop to the mixture used above. The hydration reaction forms composite nanoparticles of $\text{TiO}_2/\text{SiO}_2$. The NP_x as a surfactant is used to prepare the emulsion of the precursors of TiO_2 or SiO_2 , which usually leads to finer nanoparticles with a size less than 50 nm.

1.5.4. Intercalation chemistry for nanocomposites

Generally, in organic polymer-inorganic nanocomposites, layered silicates of clay are a proper choice for the inorganic phase. They have a layer unit structure of $50\text{ nm} \times 100\text{ nm} \times 1\text{ nm}$, where 1 nm is the interlayer distance. The pristine layer structure is further exfoliated and creates nanoparticles in the intercalation polymerization reaction. Most of the polymer-clay nanocomposites are prepared by such an intercalation-polymerization process, which is divided into two stages: the first stage is the treatment of the clay with organic reagents of quaternary ammonia salt, which is called "intercalation," and the second stage is the polymerization at conditions analogous to those used for making pure polymers. This polymerization intercalation has been used to prepare most polymer-MMT nanocomposites. These polymers are PS [64], PA6 [65-67], PI [68], PET [69,71,73], PBT [70-72] and PA66 [74].

There are other polymers that can be used to prepare nanocomposites using a melting intercalation technique. Here the organic polymer pellets and treated clay are directly mixed in an extruder machine and are then melt extruded together to obtain the nanocomposites with exfoliated layers. The polymer matrix for preparation of nanocomposites by such methods is polyethylene (PE [75]), polypropylene (PP) [75-77], polyamide 6 (PA6 [78]) and polystyrene (PS [79]). Some polymers, including water-soluble polymers such as polyvinyl alcohol (PVA), polyvinyl pyrrolidone (PVP) and hydrated polyacrylonitrile (PAN), can accomplish the intercalation reaction in a medium or solvent, a reagent or a gas. The other polymers for this technique are PI [68], PEO [80-82], PLLA and PCL [83] (PLLA, poly(L-lactide), PCL, and poly(ϵ -caprolactone)). So far, PA6-clay nanocomposites [84-89] and PET-clay nanocomposites [68, 69] have been successfully prepared and are used.

1.5.4.1. Intercalation polymerization of polymer-MMT nanocomposites

The preparation of polymer-MMT nanocomposites has many dimensions, but the three main technologies are (1) intercalation polymerization, (2) melt intercalation and (3) media intercalation. These will be described in detail in later chapters.

Intercalation chemistry has been under discussion since the 1980s [90]. In order to improve the dispersion of carbon black in a polymer matrix, solvents and long-chain polymers are intercalated into the treated carbon black. Lately, attention has been paid to the treatment of layered silicate, including the use of coupling reagents and dispersion reagents to reduce the high surface energy and improve compatibility with polymer matrixes [91]. In recent years, clay has been selected as an inorganic phase to form nanocomposites with macromolecules and polymers by different intercalation methods. This improved intercalation technology provides a series of nanocomposites with improved performance [92]. Layered silicates have become the most important inorganic phase for the preparation of the nanocomposites or hybrids by intercalation polymerization methods.

1.5.4.2. The method of nanostructure unit and polymerization formed at the same time

Intercalation chemistry is used to directly intercalate polymer chains into the gallery space of the layered silicate. Specifically designed molecules are used to treat the clay. The treated clay should match the polymer chains so that the long-chain polymers can enter into the layer space of the layered silicate. More recently, the intercalation technique has been developed such that at the first stage, the polymer monomers are intercalated into layered silicates of montmorillonite, and at the second stage the monomers inside the MMT will polymerize in situ. The polymer molecular chains will stimulate the exfoliations of layered sheets of the MMT. Finally, the exfoliated MMT in the polymer matrixes form the nanocomposites. The cations suitable for the intercalation reaction are single nucleus or multiple nucleus, organic cations, organic metal complexes and biocations. They can be introduced into the gallery of the layered silicate.

The polymer monomers suitable for intercalation reactions are those for which the polymerization process is not hindered by the dispersed layer sheets when the polymerizations start. In preparation polyamide-MMT nanocomposites, the monomers are first mixed with MMT treated by a cation exchange reaction. The monomers inside the quasi-two-dimensional layer gallery are polymerized to obtain the nanocomposites.

1.5.5. Some reviews on nanocomposites

We have seen that the nanoparticles are prepared in a similar way to sol-gel or colloid particles, which are 10^{-6} – 10^{-9} m in size. Intercalation chemistry of clay is in essence a sol-gel process. Polymer composites with nanoparticles have many enhanced properties. However not all properties are enhanced. Properties such as impact and transparency are reduced in several cases where the polymers are PET, PP and PS. Table 1.18 lists changes in mechanical, thermal and functional properties of nanocomposite material.

Table 1.18

Advantages and disadvantages of nanocomposites of polymer with layered silicate and silica based on mechanical properties

	Properties enhanced or reduced degree of nanocomposites compared with their pristine polymer matrix
Mechanical property	
Tensile strength	Enhanced 10–50%
Elongation at break	Reduced 100– < 10%
Bending strength	Enhanced 50– > 100%
Elastic modulus (tensile/bending)	Enhanced 1.6–2 times
Impact strength	Reduced 10–50%
Creep at tensile	Enhanced at nylon6, but reduced at PET
Friction coefficient	Reduced 50% at nylon66
Thermal property	
Heat Distortion Temperature	Enhanced 10–20°C in amorphous polymer, and 80–90°C in crystalline polymer
Thermal Expanding Coefficient	Reduced 30% (PEO) ~50% (Nylon 6)
Flow behavior at melt	Increased the length of melted strips at flow
Contractibility	Reduced below 20%
Adhesive strength	Reduced
Crystallinity at annealing	Enhanced 2–5 times in PET, 50% or so in Nylon-6
Functional property	
Permeability at water vapor	Reduced to 1/2–1/5 of the original data
Permeability at gas	Reduced to 1/2–1/5 of the original data; reduced to 1/6 to 1/10 of the original PET data
Inflammability	Reduced heat conducting
Resistance to weather	Enhanced at PET, Reduced at PS
Bio-degradation	Not decided
Transparency	Reduce 10–20% at PET; But enhanced at Nylon6 from 10 to 40%
Scale stability	Sample scale variation rate at 1/3–1/4

1.6. Recent phenomena in polymer-silicate and silica nanocomposites

1.6.1. The types of microstructure in PLS nanocomposites

In general, there are two idealized types of microstructures in PLS nanocomposites, namely, intercalated and exfoliated (or delaminated). In an intercalated hybrid, extended polymer chains reside between the host silicate layers that are typically separated by 1–4 nm (a distance of the order of a typical segment length of a polymer chain). Intercalation results in well-ordered multilayered structures with alternating polymer/inorganic layers. In an exfoliated hybrid, the silicate layers are randomly dispersed in a continuous polymer matrix such that the interlayer distance is comparable to the radius of gyration of the polymer. Real PLS nanocomposites have a hierarchy of morphologies, which fall in between the two idealized microstructures.

However, in the exfoliated or delaminated state, where the periodic arrangement is lost, WAXD does not provide definitive information regarding the structure of the nanocomposite. WAXD can also suffer from problems of weak peak intensity, bias

towards the surface region and poor peak resolution, particularly in those composites where the clay content is small. Recently, SAXS has been used to probe the superstructure of a delaminated polycaprolactone-layered silicate nanocomposite [93].

1.7. Prospect

1.7.1. Prospect of nanocomposites and their applications

1.7.1.1. A versatile matrix for diverse designs

Polymer matrixes provide a number of choices for the design of functional, mechanical, thermal and catalytic materials. They have characteristic properties such as reasonable resistance to high temperature, resistance to harmful radioactive light, high permeability to gas, low expandability and processing flexibility. The most important aspect is that polymers can be processed by well-known methods such as melting, mixing, blending, compressing, polymerizing and assembling. Polymers can satisfy the diverse requirements for films, membranes, automobiles, appliances, electronics and packaging containers.

By compounding PET with layered silicates, the nanocomposite shows a far-infrared reflecting performance. The reflection coefficients reach $R > 85\%$ for wavelengths of 5,000–230,000 nm. Fibers of PET nanocomposites have applications in insulation. PET-inorganic nanocomposites can be used for packaging materials. The nanocomposites have a gas permeability reduced to 20–50% compared with pure PET.

In functional applications, nanocomposites are endowed with bacterial killing properties required by users. The chemicals for killing bacteria are carried on superfine powders, such as SiO_2 or MMTs, and then the powders are mixed with polymers. Production of self-cleaning materials will become a goal for new generations of materials, which can be used in hospitals, at home or at the office.

1.7.1.2. Polymer nanocrystalline or nanoscale interface materials

Many organic polymers are semi-crystalline with sizes changing crystallite from nanometers to millimeters. Large crystallites can make the polymer materials more fragile due to the presence of stress points. To improve polymer properties, polymers are often modified to reduce the size of the crystallites. In PP-based nanocomposites, nanoparticles of SiO_2 act as nucleation centers to form a highly flexible material. This modification causes the crystalline particles to be less than 50 nm. In addition, PP nanocomposite films also have good transparency.

1.7.1.3. Nanocarrier of assembled and self-assembled structure

In inorganic carriers, such as silicates of ZSM-(4)5 and SAPO, the pore structure forms an array. The pore structure can be enlarged from 1 to 50 nm to meet diverse needs in industrial applications. When the pore structure is enlarged, the mechanical strength usually decrease. To counter these disadvantages, polymer carriers, or mixtures with the inorganic carriers, such as starch, cyclodextrins, polystyrene and poly(diene benzene) were prepared.

The independent polymer carriers are not resistant to high temperatures, while their template arrays could create a pattern for inorganic particles and pore structures. In traditional catalysts, of the active component heterogeneous distribution, scalping and

loose properties for the decrease in were the main reasons activity. Further developments for these catalysts focused on the pore structure, where polymers are the most important templates.

1.7.1.4. New engineering plastics with diverse functions

Engineering plastics have a strong tendency to have multiple functions for bacterial killing, ultraviolet shielding, transparency and high refractive index. Some of these functions are obtained by micrometer powders. However, nanoparticles have an obvious advantage over micrometer-sized powders in that the amount needed for addition to the polymer is much less. Nanoparticles of Ag, ZnO or TiO₂ dispersed in polymer matrixes provide a series of functional plastics for bacterial killing, which have been applied to shields in air-conditioners and refrigerators.

Example 1.7.1.1. Substitute additives for traditional ones. The traditional additives such as nucleation agents, stability agents, blocking agents and antioxidant agents were universal for polymers such as PP, PE and PET. These additives were in the form of micrometer powders, but now there are corresponding nanoscale counterparts, which have more versatile properties in conduction, transparency, barrier performance, etc. The interesting properties of nanometer additives include low loading amount for polymers, low coefficients of heat resistance and low change in specific weight.

In electricity-conducting properties, the critical values of polymer matrixes were broken when nanoparticles were introduced. The supertransparency obtained from nanoparticles as a result at the molecular level of composites formed between the polymer matrix and nanoparticles. The word “Nanoplastics” has appeared in some reports [94], although it is not yet seen in textbooks. Today nano-PP and nano-PE are commercial products seen in different media. These include nano-SiO₂ and nano-TiO₂, filled plastics.

1.7.1.5. Nanocomposite functional coatings and shielding

A breakthrough in the coating industry, by using nanoparticles, has brought about completely new phenomena and effects. New nanocomposite coatings have been applied in printing of integrated circuits, shape shielding coatings, wave-absorbing coatings, sonic-insulating coatings, and barrier coatings (e.g., PET/SiO₂ bottle). These coatings have unique properties such as resistance to heat aging and radiation aging. Nanoparticle coatings are resistant to salt and ultraviolet light, and possess the characteristics of smooth surfaces and self-cleaning.

Nanostructured powder coatings are of practical significance. In high-temperature coating processes, the nanostructures in the coatings are maintained even under melting conditions. This discovery has a profound effect on new materials and surface modifications of plastic bottles, appliances, information devices, sealing ports and meters. In these materials, the inorganic particle surfaces can be treated for creating functional effects such as the killing of bacteria and resistance to radiation.

1.7.1.6. The past and future of nanomachines

In nanotechnology, nanomachines have attracted much attention. According to some imaginary designs, two kinds of nanomachines will appear in the future. The first one will be a nanoscale submarine, the size of a cell, which will enter the blood circulation,

find the sick cells, and kill them. The other nanomachine will be a nanoworker for device integration. This machine will create any mechanical structure including its own structure. This nanomachine will work on an atomic scale of “grasp and place.” For example, nanoscale fingers will grasp a single atom and then place it in a set position. It is proposed that these tiny machines will create micro-TV sets or microcomputer sets within 1 h. According to some predictions, our society will change permanently because of the appearance of nanomachines.

The idea of a nanomachine is a product of man’s design and ideas. However, there are nanomachines already at work in the field biology. Inside cells, molecular aggregates, proteins, RNA molecules and organelles carry out specific tasks of enormous diversity and complexity. The creation of nanomachines by man needs much more thought and discussion to determine the feasibility and the use of such devices.

References

- [1] S.C. Lu, Powder Processing Technology, Light Industry Press of China, Beijing, 1999.
- [2] Nanocor Patent: (1) Method of manufacturing polymer-grade clay for use in nanocomposites, USP 6,050,509, April 2000; (2) Process for purifying clay by the hydrothermal conversion of silica impurities to a dioctahedral or trioctahedral smectite clay, USP 6,090,734, July 2000.
- [3] Y.C. Ke, Polyester-layered silicate nanocomposites and their industrial preparation technology, Postdoctoral Report, Institute of Chemistry, China Academy of Sciences, Beijing, 1998.
- [4] Y.C. Ke, Polyester (PET, PBT) and PA6-layered clay nanocomposites, Report to BASF, 1997.
- [5] Y.C. Ke, Polymer-Inorganic Nanocomposites, Chemical Industry Press, Beijing, 2003.
- [6] Y.X. Zhao, Clay Minerals, Geological Press of China, Beijing, 1980.
- [7] Q. Li, Postdoctoral Dissertation, Inst. Chem., China Academy of Science, Beijing, 1997.
- [8] J.H. Yin, Z.S. Mo, Modern Polymer Physics, China Science Press, Beijing, 2001 (Chapter 15).
- [9] C.L. Bai, Techniques of Scanning Tunneling Microscopy and its Applications, China Science Press, Beijing, 1994.
- [10] (a) L.D. Zhang, C.M. Mo, Nanomaterials and Nanostructure, China Science Press, Beijing, 2000, (b) T.J. Pinnavaia, G.W. Beall, Polymer-Clay Nanocomposites, Wiley, NewYork 2000.
- [11] Germany scientist Gleiter for academic exchange, metal crystalline phase.
- [12] L.D. Zhang, Q. M. Mo, Nanomaterial Science, Press of Liaoning Science and Technology, Shenyang, 1994.
- [13] Y. Wang, N. Herron, Science, 273, (1996) 632.
- [14] L.D. Zhang, Y. Sheng, D.Q. Zhu, J.D. Chen, Polym. Bull. (Chin.) 4, (2001) 9.
- [15] L.D. Zhang, The Technology of Ultra Fine Powder Preparation and Application, Sinopec Press, Beijing, 2001 (Chapter 3).
- [16] M. Yanagi, Y. Asano, et al., Proceedings of the 1986 Shikizai Technical Conference, Osaka, Japan, 1986, p. 86.
- [17] K. Osseo-Asare, Arriagada, Colloids Surf. 50, (1990) 321; K. Osseo-Asare, Arriagada, Colloid Surf. 69 (1992) 105.
- [18] C.-L. Chang, H.S. Fogler, AIChE J. 42 (11) (1996) 3153.
- [19] C.-L. Chang and H.S. Fogler, AIChE J. 42(11) (1996) 3153–3163.
- [20] N.B. Colthup, D.L. Hand, S.E. Wiberley, Introduction to Infrared and Raman Spectroscopy, Third ed., Academic Press, San Diego, 1990.
- [21] I.I. Tarhan, G.H. Watson, Phys. Rev. Lett. 76 (1996) 315.
- [22] H. Miguez, F. Meseguer, C. Lopez, A. Mifsud, J.S. Moya, L. Vazquez, Langmuir 13 (1997) 6009.
- [23] B. Gates, D. Qin, Y. Xia, Adv. Mater. 11 (1999) 466.
- [24] K. Busch, S. John, Phys. Rev. Lett. 83 (1999) 967.
- [25] Y.A. Vlasov, V.N. Astrolov, O.Z. Astratov, A.A. Kaplyanskii, V.N. Bogomolov, A.V. Prokofiev, Phys. Rev. B 55, (1997) R13357.
- [26] D. Mei, P. Dong, H. Li, B. Cheng, D. Zhang, Chin. Phys. Lett. 15 (1998) 21.

- [27] L.V. Woodcock, *Nature* 385 (1997) 141.
- [28] A.A. Zakhidov, R.H. Baughman, Z. Iqbal, C. Cui, I. Khayrullin, S.O. Dantas, J. Marti, V.G. Ralchenko, *Science* 282 (1998) 897.
- [29] J.E.G.J. Wijnhoven, W.L. Vos, *Science* 281 (1998) 802.
- [30] B. Cheng, P. Ni, C. Jin, Z. Li, D. Zhang, P. Dong, X. Guo, *Opt. Commun.* 170 (1999) 41.
- [31] T.B. Wu, Ph. D. Reports, University of Petroleum, 2003, p. 11.
- [32] P. Dong, *Acta Physico-Chim. Sin.* 14 (1998) 109.
- [33] R. Zhao, P. Dong, W. Liang, *Acta Physico-Chim. Sin.* 11 (1995) 612.
- [34] Y.C. Ke, *Chem. Ind. Eng. Prog. (Chin.)* 22(8) (2003) 833.
- [35] S. Chen, P. Dong, G. Yang, J. Yang, *J. Colloid Interf. Sci.* 180 (1996) 273.
- [36] Y.C. Ke, T.B. Wu, *Particology (Chin.)* 1(6) (2003) 41.
- [37] Q. Li, et al., *Colloids Surf. A: Physicochem. Eng. Aspects* 1 (2002) 62.
- [38] J.N. Yan, *Drilling Fluid Technology*, Press of Petroleum Industry, Beijing, 2002.
- [39] L.D. Zhang, *Nanomaterial Science*, press of Liaoning Sci. & tech., Sheng Yang, 1994.
- [40] G.V. Chilingarian, P. Voraburt, *Drilling and Drilling Fluids*, Elsevier Scientific Publishing Company, Amsterdam, 1981.
- [41] Y.C. Ke, *Polymer Physics and Experiments, Nanocomposites of Montmorillonite with Polymers*. Press of the University of Petroleum, Beijing, 2002.
- [42] E.J.W. Verwey and T.Th.G. Overbeek, *Theory of the Stability of Lyophobic Colloids*, Elsevier, New York, 1948.
- [43] Tatsuo Sato and R. Ruth, *Stabilization of Colloidal Dispersions by Polymer Adsorption*, Marcel Dekker, New York, 1980.
- [44] R.J. Hunter, *Zeta Potential in Colloid Science*, Academic Press, New York, 1981.
- [45] Z.K. Zhou, T.R. Gu, J.M. Ma, *Colloid Chemistry Basis*, Second ed., Press of Beijing University, Beijing, 1987, pp. 46–47.
- [46] P.J. Flory, *Principles of Polymer Chemistry*, Cornell University Press, Ithaca, 1953.
- [47] Y.C. Ke, Y.B. Zheng, Z.W. Wu, S.J. Zhang, J.Z. Wang, *Chem. J. Chin. Univ.*, 17 (1996) 6; Y.C. Ke, J.K. Feng, Y.B. Zheng, Z.W. Wu, *Chem. J. Chin. Univ.* 17 (1996) 485.
- [48] D. Bower, *An Introduction to Polymer Physics*, Cambridge University Press, UK, 2002, p.138.
- [49] (a) R.M. Ho, S.Z.D. Chen, B.S. Xiao, *Macromolecules*, 27 (1994), 2136, 5787; (b) A.J. Lovinger, S.D. Hudson, *Macromolecules*, 25 (1992) 1752.
- [50] P. Dong, *Chin. J. Phys. Chem.* 14(2) (1998) 109.
- [51] R.Y. Zhao, P. Dong, W.J. Liang *Chin. J. Phys. Chem.* 11(7) (1995) 612.
- [52] S.L. Chen, P. Dong, G.H. Yang, et al. *Ind. Eng. Chem. Res.* 35 (1996) 4487.
- [53] L.D. Zhang, C.M. Mo, *Nanomaterial Science*. Liaoning Press; Shenyang City, China 1994.
- [54] K. Haberko, A. Ciesla, *A Pron. Ceram. Int.* 1 (1975) 111–116.
- [55] D.W. Johnson, *Am. Ceram. Soc. Bull.* 60 (1981) 221.
- [56] K.S. Mazdiyaski, *Ceram. Int.* 8(2) (1982) 42.
- [57] J.E. Blendell, H.K. Bowen, R.L. Coble, *Am. Ceram. Soc. Bull.* 63(6) (1984) 797.
- [58] X.N. Bao, *Preprints of National Academic Meetings on Nanometer Solids, Eighth Session, China, Changchun*, 1991.
- [59] P. Dong, *Chin. J. Phys. Chem.* 14 2 (1998) 109.
- [60] R.Y. Zhao, P. Dong, W.J. Liang, *Chin. J. Phys. Chem.* 11(7) (1995) 612.
- [61] S. Chen, P. Dong, G. Yang et al., *Ind. Eng. Chem. Res.* 35 (1996) 4487.
- [62] P.S. Su, *Superfine Nanomaterials (Chin.)*, Fuhun Press, North Taiwan, 1989.
- [63] K. Kiss, J. Magder, M.S. Vukasovich, et al., *J. Am. Ceram. Soc.* 49 (1955) 91.
- [64] B. Hoffman, C. Dietich, R. Thomann, C. Fredrich, R. Mulhaupt, *Macromol. Rapid Commun.* 21 (2000) 57.
- [65] Z. Qi, Q. Li; Y. Zhou, CN139643.6, 03, 1996.
- [66] R.A. Vaia, H. Ishii, E.P. Giannelis, *Chem. Mater.* 5 (1993) 1694.
- [67] R.A. Vaia, S. Vasudevan, W. Krawiec, L.G. Scanlon, E.P. Giannelis, *Adv. Mater.* 8 (1) (1996) 29.
- [68] Z.K. Zhu, Y. Yang, J. Ying, X.Y. Wang, Y.C. Ke, Z.N. Qi, *J. Appl. Polym. Sci.* 73 (1999) 2063
- [69] Z.N. Qi, Y.C. Ke, Y.Z. Zhou, *Chin. Pat. Appl.* 971040559.
- [70] Z.N. Qi, Y.C. Ke, Y.Z. Zhou, *Chin. Pat. Appl.* 971041964.

- [71] Y.C. Ke, Z.N. Qi, C.F. Long, *J. Appl. Polym. Sci.* 71 (1999) 1139.
- [72] Y.C. Ke, C.F. Long, International Symposium on Polymer Physics, November 25–29, Guilin City, China, 1997, p. 158.
- [73] Y.C. Ke, Z.B. Yang, C.F. Zhu, *J. Appl. Polym. Sci.*, 85(13) (2002) 2677–2691.
- [74] Y.C. Ke, submitted to the patent office of China, 2002.
- [75] S.D. Hudson, Polyolefin nanocomposites, US5910523, 06,08, 1999.
- [76] M. Kawasumi, N. Hasegawa, M. Kato, A. Usuki, A. Okada, *Macromolecules* 30 (1997) 6333.
- [77] Q. Zhang, Q. Fu, L.X. Jiang, Y. Lei, *Polym. Int.* 49(12) (2000) 1561.
- [78] D.M. Lincoln, R.A. Vaia, Z.-G. Wang, B.S. Hsiao, *Polymer* 42 (2001) 1621.
- [79] Y.T. Lim, O.Ok. Park, *Macromol. Rapid Commun.* 21, (2000) 231.
- [80] H.J. Choi, S.G. Kim, Y.H. Hyun, M.S. John, *Macromol. Rapid Commun.* 22 (2001) 320.
- [81] J.K. Lu, Y.C. Ke, X.S. Yi and Z.N. Qi, *J. Polym. Sci., Part B: Polym. Phys.* 39 (2001) 115.
- [82] Y.C. Ke, J.K. Lu, X. S. Yi, J. Zhao and Z.N. Qi, *J. Appl. Polym. Sci.* 78 (2000) 808.
- [83] N. Ogawa, G. Jimenez, H. Kawai, T. Ogihara, *J. Appl. Polym. Sci. Part B: Polym. Phys.* 35 (1997) 389.
- [84] Y. Kojima, A. Okada, *J. Appl. Polym. Sci. Part B: Polym. Phys.*, 32 (1994) 625.
- [85] T.M. Wu, C.S. Liao, *Macromol. Chem. Phys.* 201, (2000) 2820.
- [86] Y. Kojima, A. Usuki, M. Kawasumi, A. Okada, Y. Fukushima, T. Kurauchi, O. Kamigato, *J. Mater. Res.* 8 (1993) 1185.
- [87] Y. Kojima, A. Usuki, *J. Polym. Sci. Part A: Polym. Chem.* 31 (1993) 1755.
- [88] A. Usuki, Kabushiki Kaisha Toyota Chuo Kenkyusho, US4889885, 12, 1989.
- [89] Hutton Jr., A.E., Burke R.E. Monadnock Paper Mills, Inc., US4920171, (1990).
- [90] M.S. Whilingham, and A.J. Jacobson, *Intercalation Chemistry*, Academic Press, New York, 1982.
- [91] B.K.G. Theng, *Formation and Properties of Clay – Polymer Complexes*, Elsevier, Amsterdam, 1979.
- [92] T.J. Pinnavaia, *Polymer–Clay Nanocomposites*, Wiley, New York, 2002.
- [93] R.A. Vaia, D.D. Lincoln, Z.-G. Wang, B.S. Hsiao, *Polym. Mater. Sci. Eng.* 82 (2000) 257.
- [94] Z.N. Qi, et al. *Chem. Indus. & Eng. Progress (Chin.)*, 20(2001)1–4.

This page intentionally left blank

CHAPTER 2

Modification and Dispersion of Silicate and Silica

OUTLINE

- Introduction 70
- 2.1. Modification of silicate 70
 - 2.1.1. *Compositions of layered silicate* 70
 - 2.1.2. *Purification of silicate and granule preparation* 71
 - 2.1.3. *Surface treatment and dispersion* 77
- 2.2. Silica modification 84
 - 2.2.1. *Particle grade for polymerization* 84
 - 2.2.2. *Silica modification* 88
 - 2.2.3. *Monodisperse silica modification* 89
 - 2.2.4. *Self-assembly mechanism and defect analysis of colloidal silica photonic crystals* 98
- 2.3. Melt intercalation 100
 - 2.3.1. *Precursor intermediate preparation for nanocomposites* 101
 - 2.3.2. *Melting intercalations* 103
- 2.4. Intercalation in media 105
 - 2.4.1. *Intercalation in solvent* 105
 - 2.4.2. *Intercalation in monomer* 106
 - 2.4.3. *Intercalation in emulsions* 107
- 2.5. Modification of particles for polymerization 107
 - 2.5.1. *Oligomer–silica mixtures* 107
 - 2.5.2. *Oligomer-silicate mixtures* 111
 - 2.5.3. *In situ polymerization in media* 113
 - 2.5.4. *Comparison of dispersion behavior in different precursors* 115
- References 117

The goals of modification of layered silicate and silica are flexible dispersion and application to different matrixes. The design principles for the modification of selected particles are to improve their compatibility with the matrix and to accelerate the homogeneous distribution.

Introduction

Nanoparticles of prepared layered silicate and silica can be modified to form intermediate materials using a number of techniques. One example is the solid nanoparticle precursor (NPP) [1] technique, which has been developed by us. The modification of particles involves several aspects, such as preparation, synthesis and mechanical blending. The intermediates are designed to be endowed with good dispersion behavior and desirable functional properties such as catalytic, radiation shielding, optical and barrier properties. Traditional polymerization methods such as free radical polymerization, condensation polymerization, melt blending or composite and reactive injection or extrusion are directly used to meet different requirements in particle modification and dispersion. Other techniques such as surface coverage, core-shell structure, sonochemical, mechanical shearing and supercritical and fluid techniques will also be presented.

Evaluation of particle dispersion is based on electron and scanning probe microscopy techniques, such as transmission electron microscopy (TEM), scanning electron microscopy (SEM) and atomic force microscopy (AFM). Additional techniques such as optical transparency, dynamic light scattering and X-ray are reference techniques used for investigating particle dispersions. We prefer to use TEM and related statistical methods to obtain results for particle size and distribution.

2.1. Modification of silicate

2.1.1. Compositions of layered silicate

In modifications of superfine particles, their chemical compositions are initially measured. This is specially needed for the layered silicate of montmorillonite (MMT), which is composed of complicated oxides and organic residuals. In these compositions, some cations are usually hydrated inside the layer space of MMTs. These hydrated cations, such as cations of Na^+ , K^+ , Ca^{2+} , Mg^{2+} , Al^{3+} , H^+ , Li^+ , Cs^+ , Rb^+ and NH_4^+ are exchangeable. The type of MMT is usually classified by its exchangeable cations, such as Li-MMTs, in which the MMT contains the exchangeable cations of Li inside its interlayer space, Na-MMTs, which refers to MMTs with Na^+ inside its interlayer space and the Ca-MMTs, which are MMTs with an exchangeable Ca^{2+} inside their layer gallery. Usually, Na-MMTs have a gelatin value of 100% compared to a value of 50% for Ca-MMTs, which shows that the former have higher swelling performance than the latter.

2.1.1.1. Natural composition of MMTs

MMTs in nature are intergrowth minerals with complicated compositions. They have to be purified depending on their application in the nanomaterial field. Their compositions [1] are shown in Table 2.1.

It is evident from the table that it is necessary to use precise purification to prepare MMTs with homogeneous compositions in order to upgrade them for high-grade products, especially for nanocomposites.

2.1.1.2. Raw material composition variation of MMTs

The variation in the chemical composition of MMT originates from the replacement of their electrical charges, including the replacement of Al^{3+} ions in the octahedron by Mg^{2+} ,

Table 2.1
Compositions of MMT minerals

Main composition	Secondary composition	Color
Montmorillonite, glass chipping, rock chipping, quartzite, tuff, lava gravel of montmorillonite	Crystalloid chipping, quartz, feldspar, zeolite, chipping melting tuff, andesite, felstone, plagioclase, biotite-glass chipping, sand, mud, epicontinental chipping (pyrite, calcite), gravel-quartzite, inclined grown zeolite, lava rock	Gray, rosiness, whiteness

Note: some data are from literature [2,3].

or by a few $\text{Fe}^{2+}/\text{Fe}^{3+}$ ions. Al^{3+} can also replace the Si^{4+} ion in the tetrahedron. Due to these replacements, MMTs have different electric charges on their crystal layers. As shown in Table 2.1, intergrowth minerals such as quartz, zeolite, calcite, feldspar and pyrite have a great effect on the composition of MMTs and consequently on the purification technology. Table 2.2 shows typical chemical compositions of MMTs in China.

The industrial applications of MMTs depend mainly on the treatment technology, crystal structure, chemical composition and the crystal chemical properties. Treatment and purification enhance the quality of MMTs. The technology includes purification steps for enhancing the mass fraction of MMTs in the minerals and modifications for improving performance. The compositions of MMTs and their quality are important in the preparation of nanocomposites and their applications to the fine chemical and the petroleum industry.

2.1.2. Purification of silicate and granule preparation

2.1.2.1. Measurements and control of the quality of MMTs

The common quality indexes for evaluating MMTs are blue adsorption quantity and cation exchange capacity (CEC) [2–4]; the former is related to the relative content of MMTs, while the latter refers to the reaction properties of MMTs.

(1) *Blue adsorption quantity.* This index can be converted into the content of MMT as follows:

$$M = B/K \times 100 \quad (2.1.1)$$

where M is the relative content of MMTs in its minerals (%), B is the blue adsorption quantity of a sample (mmol (100 g)^{-1}) and K is a conversion coefficient (usually = 150).

(2) *CEC.* CEC refers to the total quantity of adsorbed cations (e.g., K^+ , Na^+ , Ca^{2+} and Mg^{2+}) at a pH value of 7, and its unit of measurement is mmol/100 g of layered silicate (or MMT). The higher the value of the negative charge of a layered silicate, the stronger is the capacity for hydration, swelling and dispersion. On the contrary, the lower the negative charge, the lower is the capacity of hydration, swelling and dispersion. Not only are

Table 2.2
Chemical compositions of MMTs in partial typical area (% , by wt)

Producing area	SiO ₂	Al ₂ O ₃	Fe ₂ O ₃	TiO ₂	MgO	CaO	K ₂ O	Na ₂ O	Cauterization
ShiGangZi, HeiShan, LiaoNing	73.06	16.17	1.63	0.16	2.72	2.01	0.41	0.39	4.81
XiaWanZi, HeiShan, LiaoNing	71.39	14.41	1.71	1.52	1.20	0.44	1.98	—	5.25
PingShan, LinAn, ZheJiang	70.94	15.26	1.38	0.05	2.26	1.65	1.51	2.00	4.57
LanJin, LinAn, ZheJiang	65.14	18.56	3.01	0.52	3.09	2.84	0.88	1.58	4.66
QiuShan, ZheJiang/ Na-MMTs	68.01	15.4	3.94	3.0	2.50	—	—	—	5.90
QiuShan, ZheJiang/ Ca-MMTs	70.66	17.58	2.59	0.24	2.54	2.04	0.86	0.30	4.47
SanTai, SiChuan	57.64	16.24	1.60	0.02	3.92	1.99	0.51	0.40	7.76
ZhangJiaKou, HeBei	61.14	20.11	3.10	0.62	3.31	2.42	1.63	2.11	5.19
XuanHua County, HeBei	68.18	13.03	1.24	0.25	5.07	3.89	0.44	0.78	6.78
WuTuDian, XinYang, HeNan	72.02	15.76	1.44	0.21	3.27	2.19	0.38	0.22	5.91
DaCaoTan, JiuQuan, GanSu	62.50	18.61	5.37	1.86	1.35	2.38	1.25	—	6.31
XiangYang Area, HuBei	50.14	16.17	6.84	0.88	6.24	4.73	1.84	0.19	11.56
QuXian County, SiChuan	60.47	20.21	2.76	3.8	3.3	1.3	0.4	—	8.25
WuJiaZi, ShuangYang, JiLin	71.58	14.56	2.95	0.37	2.72	2.30	0.25	0.37	4.58
PengKou, LianCheng, FuJian	65.92	20.72	1.70	0.31	2.66	0.14	1.14	0.32	6.7

the cations (e.g., K⁺, Na⁺, Ca²⁺ and Mg²⁺) inside the MMT layers exchangeable, but the cations such as H⁺, multiple nuclei (e.g., hydroxyl aluminum or monomer or inorganic clusters) and organic cations (e.g., dimethyl, dioctadecane chlorite ammonia) can exchange with the cations inside the MMT layers. Measurement of the CEC data and the exchangeable cations of layered silicate are important in evaluating the quality of the minerals and classifying the minerals.

When an organic reagent is used to react with MMT, two types of adsorption can occur: ion-exchange adsorption and hydrophobic bonding. When the dose of organic cation reagent is less than or equal to the CEC value of the MMT, all the organic cations are adsorbed by the MMT by ion exchange, and the ions are not forced out except in high concentrations of strong salt solutions. When the quantity of the organic cations is greater than the CEC of the MMT, those already existing in the layers of MMT will further adsorb organic compounds in the solution by hydrophobic bonds. Similarly, in the practical preparation of organo-clay or organo-MMTs, the added quantity of organic cation reagent should be less than the CEC value of the MMTs. An overload of surfactant will reduce

the stability of organo-MMTs or organo- clay. The organic cations are usually cationic surfactants of the quaternary ammonia salt, such as $((\text{CH}_3)_3\text{NR})^+$ or $((\text{CH}_3)_2\text{NR}_2)^+$, where R stands for alkyl or aromatic groups; their permanent positive charges do not vary with the pH value of some solution. The R group is a chain with different length.

2.1.2.2. Purification of MMTs

Purification of MMTs becomes necessary in order to maintain a constant composition of MMTs for applications. Based on industrial technology and dispersion methods [5–7], several processing routes have been proposed for making MMTs with high purity.

Example 2.1.2.1. Purification of MMTs by magnetic selection. In one practical example, we use magnetic materials to purify the MMT particles. A raw bentonite with 70–75% MMT is used and suspended in the water. Selection of minerals aims at the preparation of good raw materials such as pillared MMTs. Purification and separation, using strong magnetism-stirring gradation technology, are shown with a flowchart in Figure 2.1, and the final results are tabulated in Table 2.3.

Example 2.1.2.2. Modification of MMTs by cation exchange. A sample from HeiShan, Liaoning, is an example (the sample has a yield capacity of 100 kt, practical yield per year is 50 kt or so of MMTs). To modify this layered silicate of MMTs, an alkali of Na_2CO_3 solution with a concentration of 3–4% (by mass) is applied to treat the Ca-MMTs. The flowchart of this technology is shown in Figure 2.2.

A wet slurry is formed and then extruded, which transforms the Ca-MMTs into Na-MMTs. This transformation effect is achieved by mixing Ca-MMTs and Na-MMTs with the water-soluble polymer, polyacrylamide, and is then observed using an ion-emitting spectrum such as the inductive coupled plasma-Auger electronic spectroscopy (ICP-AES) method, in which the Na^+ is easily detected. The results before and after

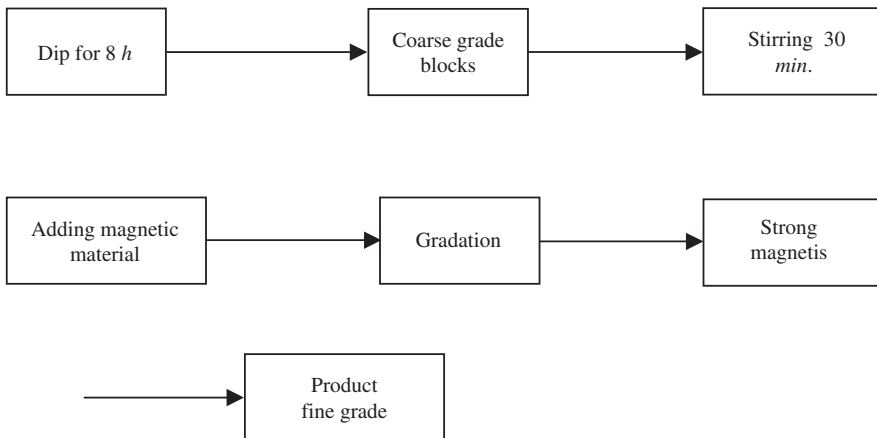


Fig. 2.1. Flowchart of strong magnetic gradation of block minerals.

Table 2.3
Particle grade by strong magnetic stirring of the block minerals

Product grade	Productivity (%)	MMTs (%)
Fine	45.86	95.60
Coarse	48.85	85.33
Magnetic mineral	5.29	79.33
Pristine mineral	100.00	88.00

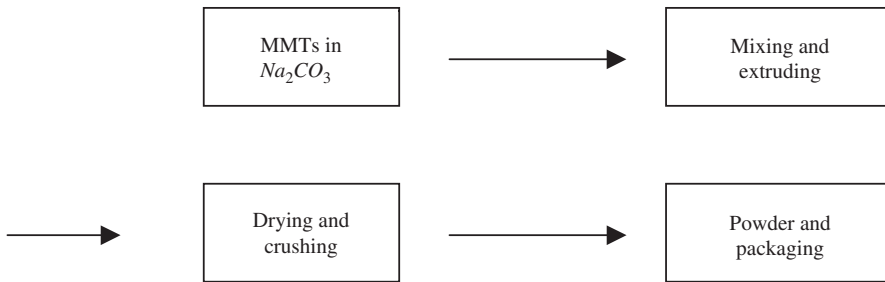


Fig. 2.2. Flowchart of converting Ca-MMTs into Na-MMTs by Na⁺ exchange reaction and extrusion process.

Table 2.4
Comparison of properties before and after treating the layered silicate by Na⁺ exchange and then extrusion

Items	Before Na ⁺ ^a	After Na ⁺ ^b
Strength at wet pressure (kPa)	38.25	48.1
Strength at dry pressure (kPa)	490.33	582.60
Swelling multiple	8–12	21
Gelatin value (%)	72.34	100
pH value	6.8	9.5

^aMMTs before treating with Na₂CO₃. ^bMMTs after treating with Na₂CO₃.

treatment are compared and shown in Table 2.4 for layered silicate of MMTs reacted with sodium salt such as Na₂CO₃.

A different equipment is available for influencing the transformation of MMTs. For example, a treatment equipment is shown in Figure 2.3, where the Na⁺ exchanging reaction together with wet extrusion is presented.

The raw minerals are crushed (1) into powder and transported by a conveyer belt (2), enter a tank (4) where they are mixed with fluid (3) and suspended in a mixing tank (5). Finally, the slurry is transported into a settling tank to separate the heavy fractions. After this, the slurry in the upper part of (6) is transported into a spray drier and a powder

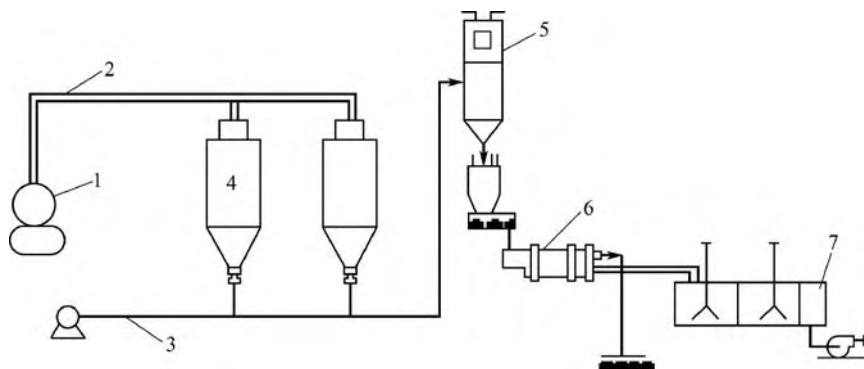


Fig. 2.3. Technology for treating pristine minerals of MMT. 1 – crusher, 2 – conveyer belt, 3 – tank, 4 – transport belt, 5 – mixing tank, 6 – sedimentation tank.

Table 2.5
Quality standard for commercial organo-clay

Commercial product	Moisture (%)	Fine degree (m)	Weight loss (%)	Viscosity (MPas)
BT-881 ^a	≤ 3.0	74	—	≥ 1,000
BS-IA	≤ 3.01	10	—	< 1,000
BS-IB ^b	≤ 3.01	10	—	> 1,500
BS-4	≤ 3.01	20	—	≥ 3,000
HG/T2248-91 ^c	≤ 3.5	76	≤ 40.0	≥ 900

^aLinAn, ZheJiang. ^bAnJi, Zhejiang. ^cStandard of the Chemical Industry of China.

product is obtained. When the slurry reacts with organic surfactants, the final products are transformed further into organo-silicates, such as organo-clay and organo-MMTs. By such a process, commercial products shown in Table 2.5 can be prepared.

2.1.2.3. Quality control of the layered silicate slurry

The slurry quality is characterized by its viscosity. Viscometry is the measurement of the friction between the slurry and the cylinder barrel. A viscometer is the usual NDZ NDG-79 type six-velocity rotary measurement meter (Hisense Corp. Limit, China and Tongji University, Shanghai). When the NDZ meter is used, the viscosity data measured for a sample are expressed by the scale value of $\phi 600$ velocity multiplied by 10, and the apparent viscosity is expressed as follows:

$$\eta_a = \phi 600 / 2 \quad (2.1.2)$$

where η_a is the apparent viscosity with a dimension of mPas, and $\phi 600$ is the scale data for the measured sample.

In order to control the layered silicate gel quality for the preparation of nanoparticles, we have proposed experimental indexes for the test standards that meet the basic

requirements for the preparation of nanomaterials from the layered silicate of MMT and attapulgite. The experimental indexes are shown in Table 2.6.

2.1.2.4. Basic reactions and reagents for the preparation of nanomaterials

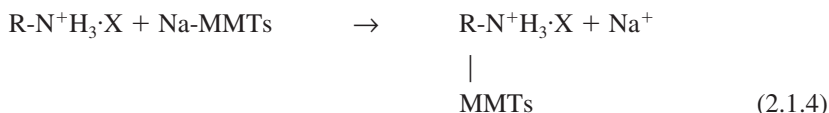
The purified layered silicate can be converted into two forms: gel and fine powder. These forms become the raw materials for the preparation of nanoparticles and nanocomposites. During preparation, the basic reactions are cation exchange reactions. The reaction processes are divided into quaternary ammonia reactions and cation exchange dispersion reactions, which are discussed below.

(1) Preparation of quaternary ammonia:



In this reaction, the organic quaternary ammonia salt is formed, which is used as a dispersion reagent in a solution of layered silicate of MMTs. In the formula, R = HOOCAr (Ar = 1,4-phenylene, hereafter), HOCH₂CH₂, CH₃(CH₂)₁₅N(CH₃)₂ or CH₃(CH₂)₁₁ and X = Cl, H₂PO₄ or H₂PO₃.

The quaternary ammonia salt is then suitable for reacting with the layered MMTs by an exchanging process:



By this process, organo-MMTs or organo-clays are formed. They are polymerized with polymer monomers. The organo-MMTs for polymerization are called polymer-grade MMTs, which are solid nanoprecursors for nanocomposites.

(2) *Cation exchange dispersion reactions.* The cation exchange dispersion reactions of MMTs take several forms. The common reaction is usually completed in aqueous solution when the molar quantity of organic reagent is similar to the CEC value of MMT. The

Table 2.6
Physicochemical standard of MMTs for the preparation of nanoparticle gel

Items	Pristine MMTs	MMTs after treatment
CEC (mmol (100 g) ⁻¹) ^a	70–110	100–130
Free sand content (% by mass) ^b	< 0.1	0.05
Whiteness/spectrophotometer	> 80	> 70
Fe ₂ O ₃ + FeO (% by mass) ^c	< 0.5	< 0.1
Solid content in gel (% by mass)	5	5–15
Viscosity value (φ 600) ^d	> 20	> 200

^aInductively coupled plasma - Auger electron spectroscopy (ICP-AES). ^bSedimentation. ^cElement analysis of plasma absorption spectroscopy. ^dRotary viscometer with 6-velocity. The requirements for water as such, the hardness of water: [Ca²⁺ or Mg²⁺] < 100 ppm; [Cl⁻] < 20 ppm.

reaction medium is stirred for 4–5 h, and then the powder is prepared. A second type of reaction for the cation exchange process occurs when an organic compound is first mixed with MMT, followed by mechanical milling. The third type of reaction for *cation exchange dispersion reactions* involves melting the organic compound and intercalate the compound into the layers of MMT to prepare organic MMTs. Further purification of MMTs will be introduced in a later chapter. The basic inorganic raw materials for the preparation of nano-materials include multiple phase nanoprecursors with a core–shell structure and processed clay such as layered double hydroxides (LDH), MMTs and mica.

The basic organic treatment reagents are organic amine, amide, ammonia and metal cations. When treated clay is used for polymerization with polyester (e.g., PET), the organic quaternary ammonia salt or organic amine is used to react with organic acids selected from Table 2.7. This acid reaction (usually, HX) is called protonation.

2.1.3. Surface treatment and dispersion

2.1.3.1. The design of particles surface treatment

The inorganic particles with core–shell structure are prepared according to the above methods. In the preparation, inorganic particles are treated in several steps including surfactant adsorption (or reactions of relevant organic molecules), and the treated particles are mixed with organic oligomers of polymers (see later description). In a similar way, core–shell structures are also obtained in two steps: inorganic particles are first treated by organic molecules, and then these particles are further reacted with oligomers, by which the oligomer film adheres to the particles surfaces by bonding reactions between the organic molecules and the organic oligomers. The films on the particles surfaces are thick enough to be comparable with the polymer chain length. The adsorbed films on the particles surfaces become thicker and thicker up to ~20 nm during reaction or blending processes and, finally, particles with a core–shell structure are formed, as shown in Figure 2.4.

When mixing the particles with an organic polymer matrix, the particles agglomeration tendency should be avoided. The dispersion stability can be qualitatively assessed with the values of the Hamaker constants [3] by using the following equations:

$$A_{131} \cong (\sqrt{A_{11}} - \sqrt{A_{33}})^2$$

Table 2.7
Physical parameters for acid protonation in MMTs intercalation reaction

Series of acetic acid	M.p. (°C)	B.p. (°C)	K_a (S) ^a	pK_a
HCOOH	8.4	101	$1.77 \times 10^{-5}(\infty)$	3.77
CH ₃ COOH	17	118	$1.75 \times 10^{-5}(\infty)$	4.76
CH ₃ CH ₂ COOH	-22	141	$1.32 \times 10^{-5}(\infty)$	4.88
CH ₃ CH ₂ CH ₂ COOH	-5	163	$1.52 \times 10^{-5}(\infty)$	4.82
CH ₃ CH ₂ CH ₂ CH ₂ COOH	-35	187	(3.7)	

Ar, phenyl ring; m.p., melting point; b.p., boiling point; K_a , separation coefficient of ions in solution; pK_a , the logarithm data of the reciprocal K_a ; S, solubility of the compound in (a) 100 g of water.

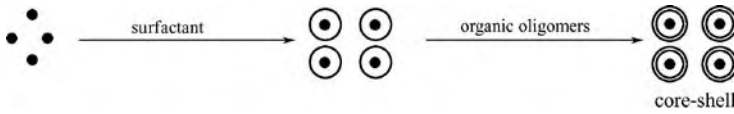


Fig. 2.4. Fine particle dispersion by forming a core-shell structure.

and

$$A_{132} \cong (\sqrt{A_{11}} - \sqrt{A_{33}})(\sqrt{A_{22}} - \sqrt{A_{33}}) \quad (2.1.5)$$

where A_{11} and A_{22} are the Hamaker constants for particles 1 and 2 in vacuum, respectively; A_{33} is the Hamaker constant for organic solid polymers in vacuum; A_{131} is the Hamaker constant between similar particles 1 and 1 in an organic 3; and A_{132} is the Hamaker constant between the different particles 1 and 2 in organic 3. Based on the above definitions, the Hamaker constants for the particles are used to predict the interacting force (F_M) between similar or different particles:

$$F_M \propto (-A_{131}) \quad \text{or} \quad F_M \propto (-A_{132}) \quad (2.1.6)$$

Generally, if A_{131} or A_{132} are > 0 , the F_M is < 0 , and the acting force between the particles is attractive. When superfine particles are blended with polymer monomers and the in situ polymerization reaction is then initiated, nanocomposites with dispersed particles are obtained when the attractive force between the particles is either weak or if the force is repulsive. For the interaction between unlike particles, an ideal situation is when $A_{11} < A_{33} < A_{22}$, which will make $A_{132} < 0$ or $F_M > 0$, producing a repulsive force between particles.

2.1.3.2. Particle dispersion

2.1.3.2.1. Control of ultrafine particle dispersion The homogeneous dispersion of ultrafine particles is the most important problem in the preparation of nanocomposites. To disperse the particles homogeneously, their surfaces should be properly treated. There are molecular deposition techniques, assembly and self-assembly techniques for the small-scale treatment of fine particles. In large-scale applications, ultrafine particles dispersion and its control in polymer melts is of great significance in industry. The dispersion process of particle's is classified into three steps: selection of the dispersion media and surfactant, the use of external power for dispersion and collection and redispersion of the treated particles.

(1) *Media and surfactant.* Solid inorganic particles dispersed in liquid media, such as water, acetone and ethanol, will react with the surfactant and be transformed into core-shell structure particles. The particles are only primary particles, which will be further dispersed in liquid media or polymer melt by external power dispersion techniques. The surfactants used for the layered silicate and silica, such as the commercial products, KH-550, KH-560 and siloxane ($\text{H}_3\text{Si}(\text{NHSiH}_2)_n\text{NHSiH}_3$), are listed in Table 2.8.

Table 2.8
Surfactants for treating ultrafine particles

Ultrafine particles	Neutral reagents	Positive-charge reagent	Negative-charge reagent
Carbon materials	PEO thiol, alkyl phenol	WSP ⁺	WSP ⁻
Metal materials	PEO thiolamine, fatty acid	Bezoar acid salt WSP ⁺	
Oxides	KH-550, KH-560, amine, imidazoline, siloxane	Quaternary ammonia salt WSP ⁺	Benzyl sulfonate Phosphate
Salt materials	Pear oil, CH ₃ CO ₂ C ₅ H ₁₁ , etc.	Quaternary ammonia salt	WSP ⁻

WSP, water-soluble polymer; WSP⁺ and WSP⁻, water-soluble polymers with positive and negative charges, respectively, KH-550 and KH-560, organic silanes.

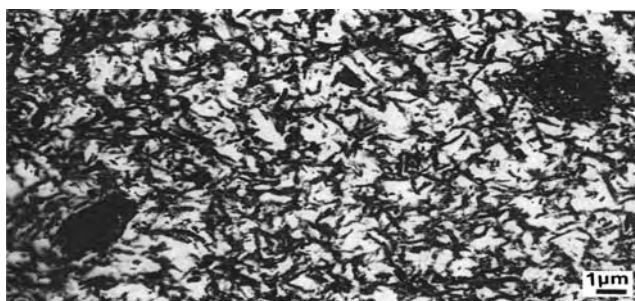


Fig. 2.5. Fine particle agglomeration during dispersion.

(2) *The external power dispersion techniques.* Any dispersion process needs external force, such as electrical power stirring, mechanical crushing and ultrasound mixing.

(3) *Collection of the treated particles and redispersion.* When the particles are dried, they will be in an aggregated state. To avoid the formation of agglomerated particles in this dried state, special collection techniques have been designed. The freezing–drying method provides a small-scale approach for powder collection, while the spray-drying machine provides a large-scale approach for the collection of particles.

2.1.3.2.2. Design of a homogeneous dispersion system From an analysis of the relative values of the Hamaker constants, it is seen that there can be strong attractive forces between untreated (naked) particles so that the particles have a strong tendency to come together to form agglomerated particles. The assembly process is shown in Figure 2.5 where the dark dots stand for untreated particles. TEM morphology of agglomerations is shown in Figure 2.6.

Figure 2.6 shows that the particles form agglomerations even though they are initially exfoliated and reacted with organic molecules. This will lead to about 10% (in number) of agglomerated particles greater than 2 μm in diameter as shown in Figure 2.6. The agglomerated particles are not exfoliated any more, a condition which is called

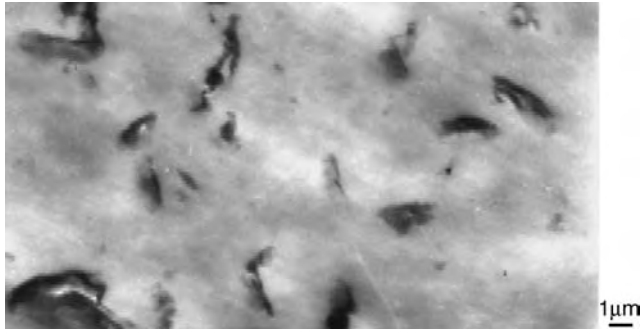


Fig. 2.6. TEM morphology of agglomerated layered silicate particles in poly(ethylene terephthalate) under improperly treated conditions.

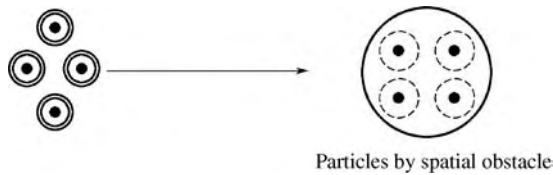


Fig. 2.7. Particle dispersions with spatial obstacles.

“rigid agglomeration” in contrast to “soft agglomeration.” In the latter case, the particles are capable of being further exfoliated or separated again.

(1) *The steric effect of organic polymer oligomers.* Properly treated particles mixed with polymer oligomers can produce superfine particles and form a homogeneous distribution morphology. The steric effect of oligomers adsorbed on the particles surfaces can provide stability against agglomeration. The adsorbed polymers exert a steric effect. Thin films (20 nm or so thick) provide a steric barrier effect against particles approaching each other. Even though the particles may be merged closely, the protective surface films separate them (Figure 2.7).

A new kind of composite precursor of NPP has been invented [1,8]. The NPP surface is covered by surfactant and polymer oligomers and their particle sizes range from 100 to 500 nm (Table 2.9). They can be further exfoliated or dispersed by polymerization or blending.

(2) *The comparison of different NPP dispersing in PET.* Organo-MMTs are similar to NPP, in that the inorganic particles can be further dispersed. The NPP particles prepared from both layered silicate of MMTs and from silica are used for blending or polymerization with PET matrix to obtain nanocomposites [8–18]. In the preparation of these nanocomposites, NPP01 from layered silicate are mixed with PET monomers in the first step, and in the second step this mixture is polymerized to obtain the nanocomposites (Figure 2.8). This process is called an intercalation polymerization process. It is

Table 2.9

Physical properties of submicron precursors of NPP by dry powder (DP) addition method

Parameters	NPP0	NPP01	NPP02
Whiteness	> 70 (spectrophotometer)	> 70	> 70
Powder scale	100–500 nm (first/TEM)	100 nm–1 μm	\leq 500 nm
	< 10 μm (Secondary/D50)	< 10 μm	< 10 μm
Fe content	\leq 500 ppm	\leq 500 ppm	\leq 300 ppm
Density	1.8–2.2	1.8–2.3	1.8–2.4
Surface treat/ organic content	\leq 75%	\leq 80%	\leq 70%
Composition	$\text{SiO}_2 \cdot \text{Al}_2\text{O}_3 \cdot n\text{H}_2\text{O}$	$\text{Al}_2\text{O}_3(\text{Mg}, \text{Na}, \text{Ca})_n \cdot x\text{SiO}_2 \cdot y\text{H}_2\text{O}$	
$\text{SiO}_2 \cdot \text{Ti}_2\text{O}_3 \cdot m\text{H}_2\text{O}$			

First, the first or primary structure of particles; second, the accumulated particles.

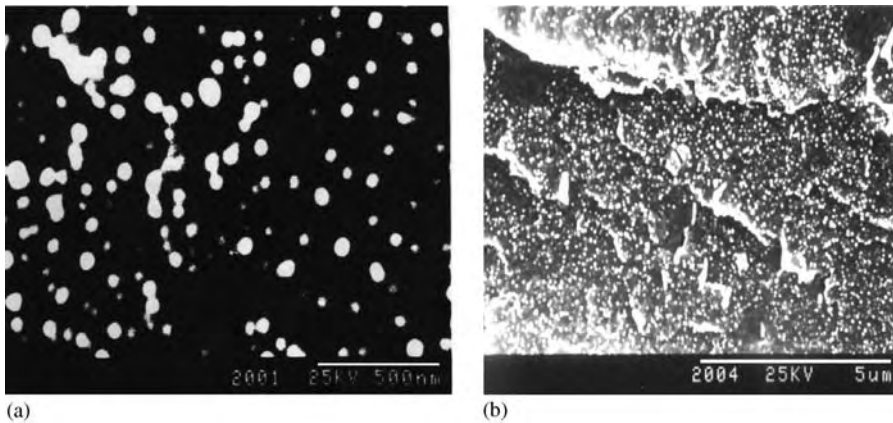


Fig. 2.8. SEM morphology of layered silicate (2.5% load, (by wt)) in PET-NPP01 nanocomposites: (a) particle dispersion in PET matrix; (b) particle dispersion in fractured surface.

seen that particles are exfoliated into about 100 nm size layers with relatively narrow size distribution (Figure 2.8a). The morphology is maintained in large-scale dispersion. The morphology for the large-scale dispersion of particles from a fractured surface is shown in Figure 2.8(b), where the particles are homogeneously spread in the whole polymer matrix.

The dispersing of the superfine particle NPP02 containing silica is achieved by direct mixing with oligomers of PET (bihydroxyl ethylene terephthalate, or BHET). They are then polymerized together to obtain the nanocomposites. The morphology is shown in Figure 2.9. It is seen that the particles can be dispersed homogeneously, but there appears some particle stacking, and some agglomerations are produced. In TEM equipment, electron diffraction (ED) can be used to detect the crystallization behavior of particles. In Figure 2.9(b), nanoparticles in PET-based nanocomposites are detected by ED to show whether these particles are crystallized or not. The ED patterns show a particle

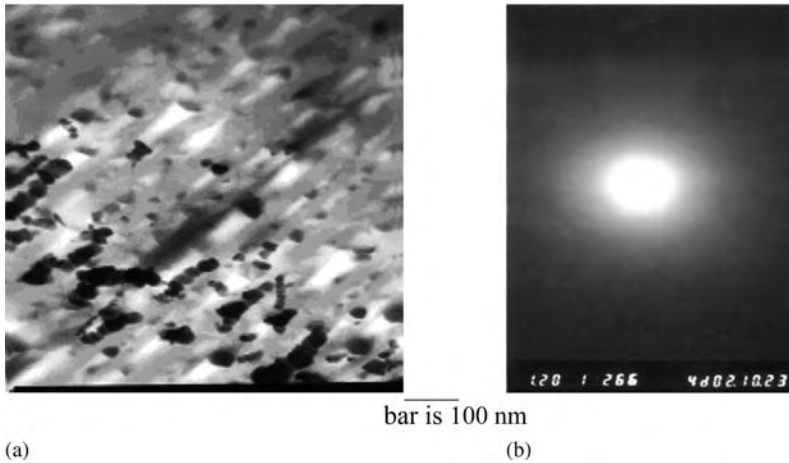


Fig. 2.9. TEM morphology of silica (1% load, (by wt)) in PET-NPP02 nanocomposites: (a) silica dispersion; (b) ED patterns for silica particles.

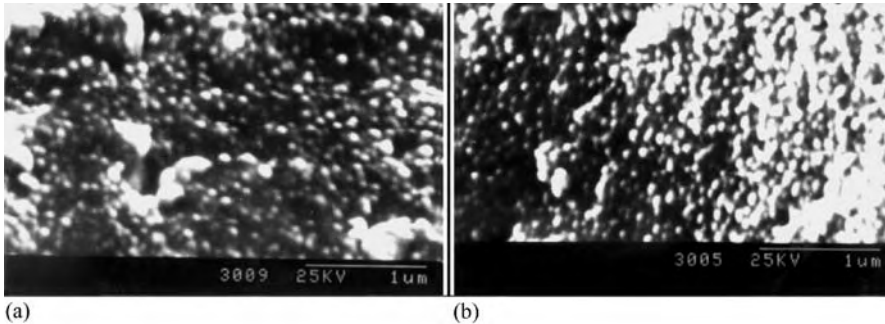


Fig. 2.10. Particle distribution morphology in PET-5% load, (by wt) layered silicate nanocomposites: (a) Near the center; (b) near the edge.

dispersion ring, which is a feature of amorphous particles. These silica particles are not crystalline but amorphous. Based on this result, it is believed that the layered silicate is not crystalline in PET-based nanocomposites when exfoliated.

If samples of PET-based nanocomposites are not fractured but cut into a slice with a special knife, then the particles have a distribution morphology as shown in Figure 2.10. The particles disperse homogeneously and are separated from the polymer PET matrix. The stacked bright area is a characteristic of the PET matrix. The particles have similar morphology with only slight differences throughout the image between the center and edge.

(2) *The particle exfoliation goes beyond the steric effect.* The transformation of submicron particles into nanoparticles is an interesting phenomenon when NPP is dispersed

into PET. In the dispersion process, the NPP's particle size becomes smaller and smaller by blending or polymerization with the PET matrix. Particles in NPP in the intercalated state are shown in Figure 2.11.

In Figure 2.11, the parallel lines represent the layered silicate of MMTs and the zigzag lines represent organic molecular chains. Core-shell particles in PET-based nanocomposites are further exfoliated into random layers of nanoscale size, as shown in Figure 2.12. In large-scale particle dispersion, the interlayer distance is 2–3 nm, which is 2–3 times that of the layered silicate MMTs basal space by WAXD (not shown here).

The data in Figure 2.12 show bright particles with diameters of 150 nm, which account for about 3% in number. Most of the superfine particles can be percolated into nanoscale particles, forming a homogeneous morphology. This type of particle dispersion morphology will improve the polymer films transparency and barrier properties [19].

By SEM, it is not easy to observe the particles agglomeration morphology, and thus SEM may not reflect the whole description of the particles structures. TEM shows this morphology in Figure 2.13. The TEM morphology of the layered silicate-PET

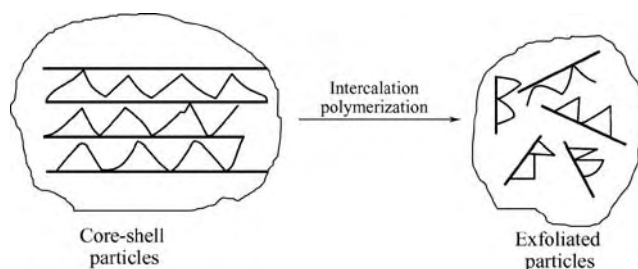


Fig. 2.11. Submicron core-shell particles in NPP are exfoliated into nanoparticle layers in PET-based nanocomposites by the intercalation polymerization process.

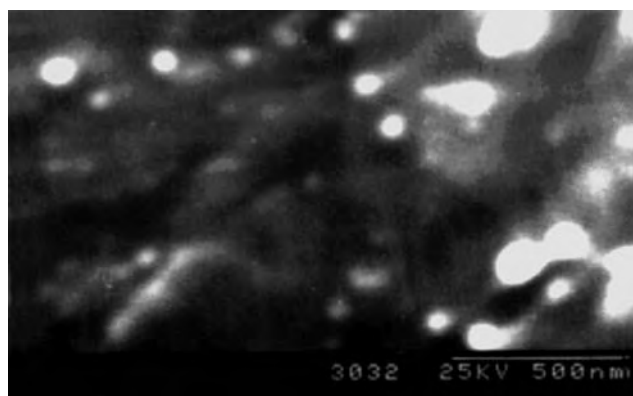


Fig. 2.12. SEM morphology of superfine core-shell particles exfoliated by intercalation polymerization (2.5% load, (by wt).

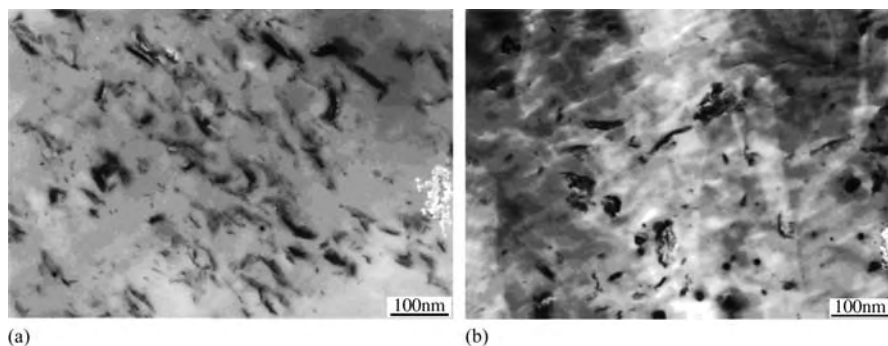


Fig. 2.13. Morphology of layered silicate particles in PET matrix with a load of 1% (by wt): (a) exfoliated 1.0% (by wt); (b) agglomerated 1.0% (by wt).

nanocomposite shows a distorted fiber-like pattern (Figure 2.13(a)). In Figure 2.13(b), agglomerated particles are seen and account for 3–4% by number.

2.2. Silica modification

2.2.1. Particle grade for polymerization

2.2.1.1. Preparation of monodisperse

Monodisperse colloidal silica has become one of the most widely investigated monodisperse systems since Stöber et al. reported on its preparation by hydrolysis and condensation of alkoxy silanes in a mixture of alcohol, water and ammonia [20,21]. The particles prepared in this way have high monodispersity, well-defined morphology and controlled size and the particles surfaces are functionalized with silane groups. Surface modification offers new opportunities for expanding the applications of monodisperse silica.

Our group has investigated the preparation and application of monodisperse colloidal silica. First, based on Stöber's method, we developed a method for the preparation of particles, aimed at extending the size range of the particles and improving the monodispersity of the system. From studies on the formation conditions, mechanisms, and kinetics of monodisperse systems, a seeding technique was developed and improved. Particles with diameters ranging from dozens of nanometers to 2.5 μm can be prepared by the seeding technique, as shown in Figure 2.14. The relative standard deviation of size distribution is less than 5% for particles ≥ 150 nm. The final concentration of the dispersed phase in the reaction systems can reach 10%. The surface modifications of particles with $\text{Al}(\text{OH})_3$, Al_2O_3 , NiO , MoO_3 , TiO_2 , C_8 and C_{18} aliphatic groups, amino propyl and phthalocyanine (tpps4 or CuTsPc) were investigated. Moreover, it was found that the pore of the particle can be closed by hydrothermal treatment. The functionalized particles and particle systems and their optical properties have been utilized in various fields such as non-porous rapid high-performance liquid chromatographic (HPLC) packing, model catalysts for hydrogenation of heavy oil,

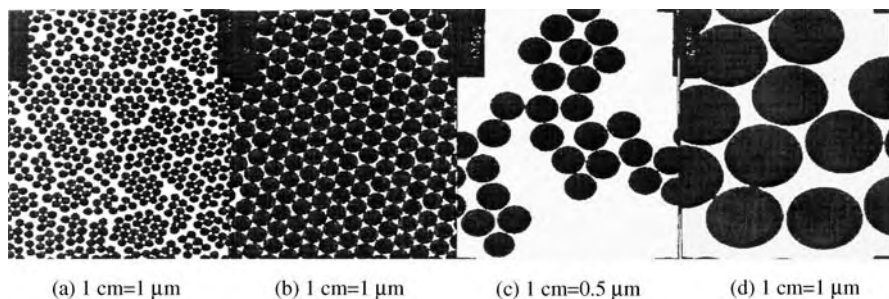


Fig. 2.14. TEM of monodisperse silica particles with different sizes: (a) 1 cm = 1 μm ; (b) 1 cm = 1 μm ; (c) 1 cm = 0.5 μm ; (d) 1 cm = 1 μm .

monodisperse electrorheological fluids, colloidal crystals. The particles can also be used as standard or reference particles for the calibration of particle analyzers.

2.2.1.2. Fundamental aspects on the preparation of monodisperse particles

The formation of the monodisperse systems is a multidimensional and dynamic process that is very sensitive to preparation conditions and is restricted by many complicated factors. As a result, some reaction mechanisms or processes have not yet been understood, and the preparations of monodisperse particles are still confined to the laboratory. In this section, several fundamental subjects concerned with their preparation have been suggested, including the reaction kinetics of the hydrolysis and condensation of precursor tetra ethyl orthosilicate (TEOS), the growth mechanism of monodisperse particles and the critical conditions of new particle formation.

(1) *Kinetics of hydrolysis and condensation of TEOS under conditions of forming monodisperse sol.* The reactions involved in the formation of the monodisperse silica system are the hydrolysis of alkoxy silanes and the condensation of silicic acid. The overall reactions can be written as follows:



Although these reactions are well known in sol-gel processing and the kinetics of the reactions has been studied, there are essential differences in reaction conditions and direction between sol-gel processing and monodisperse sol production. The kinetics data of the former cannot be extrapolated to the latter. Although TEOS hydrolysis is the rate-limiting step of the reaction, the monodispersity of the system will be destroyed once the supply of TEOS exceeds the rate of TEOS hydrolysis under the reaction conditions. Maintaining an appropriate rate of hydrolysis and condensation is a prerequisite for the effective control of the formation process of monodisperse particle systems. By means of extraction/gas chromatography and conduction measurements, respectively [20], the rate constants of TEOS hydrolysis and condensation can be determined.

The relationships of the hydrolysis rate constant (K_H) and condensation rate constant (K_C) with the reaction condition variables in a wide range were empirically found as

$$K_H = 74.36 \exp(-25,211/RT) [\text{H}_2\text{O}]^{1.267} [\text{NH}_3]^{0.971}$$

or,

$$K_C = 19,408 \exp(-33,202/RT) [\text{H}_2\text{O}]^{1.196} [\text{NH}_3]^{0.785} \quad (2.2.1)$$

where, from Eq. (2.2.1), the disappearance rate of TEOS and silicic acid during the formation of monodisperse systems under the reaction conditions can be calculated, providing a means for investigating the relationship between the reaction rates of particles.

(2) *Process of new particle formation and particle growth.* The condensation of silicic acid can be divided into two stages, particle nucleation and nuclear growth. Monodisperse particles are a result of nuclear growth. However, the detailed process of particle growth is still not fully understood. It has been suggested that particle growth should be limited by diffusion or by surface reaction. In order to solve this problem, the relationship between the growth rate of monodisperse particles and particle diameter is investigated. In the case of diffusion-controlled growth, the equation of growth rate of each particle can be derived from Fick's law:

$$dL/dt = 4DV(C_\infty - C_s/L) \quad (2.2.2)$$

where L is the particle diameter, V the molar volume of growth fraction deposited onto the particle, D the diffusion coefficient of the diffusing material, C_∞ the bulk concentration and C_s the saturation concentration on the particle surface. In the case of surface reaction-limited growth, the particle growth rate in volume is proportional to the external surface area of the particle. One can derive the growth rate equation as

$$dL/dt = 2K_s V(C_m - C_s) \quad (2.2.3)$$

where K_s is the surface reaction rate constant and C_m the concentration of growth intermediate. From Eqs. (2.2.2) and (2.2.3), one can conclude that the growth rate is independent of particle size in the surface reaction-limited process and is inversely proportional to particle size in the diffusion-limited process. Therefore, the growth rates of the particles in a suspension of silica particles with a bimodal size distribution are analyzed. It was found that when there was no formation of new particles, the diameter difference between the particles with two sizes was constant during the growth process. This means that particles with different sizes grow at the same rate, which demonstrates the properties of the surface-reaction-limited process.

When the formation of new particles takes place, however, curves as in Figure 2.15 are obtained, which show that smaller particles grow faster than the larger ones during the nucleation period, i.e., the growth proceeds by a diffusion-limited process. However, both smaller and larger particles grow at the same rate before and after the formation of new particles. In the meantime, the growth mechanism changes into a

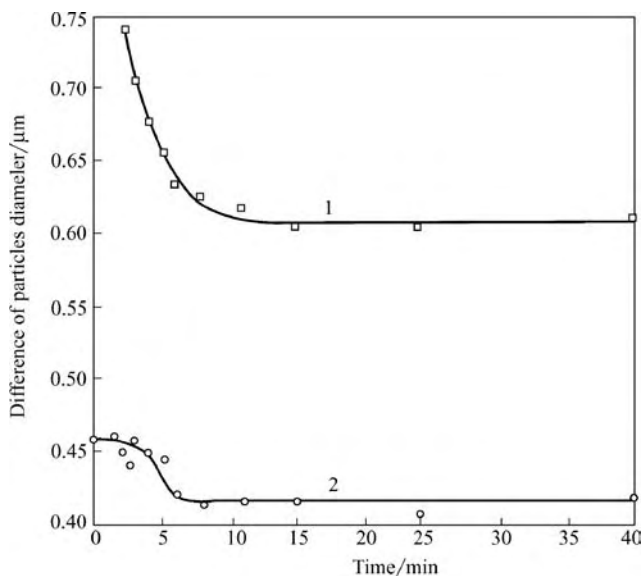


Fig. 2.15. Diameter differences vs. time during growth of particles. Curve 1 – diameter difference between seeds and new particles; curve 2 – diameter difference between larger and smaller particles. (With the permission of Press of Elsevier in the article, S.L. Chen et al., *J. Colloid & Inter. Sci.*, 180(2) (1996) 237–241.)

surface-reaction-limited process. This kind of transition of growth mechanism has not been reported before.

The key factor resulting in the formation of new particles is the insufficient surface area of seed particles, which increases the concentration of silicic acid-condensed species, so that the latter tends to condense to form larger subparticles. Some of the subparticles partly aggregate to form new particles independent of seed particles, while others are partly condensed onto the surface of seed particles by a diffusion-controlled process because of their low diffusion coefficient. In order to prepare the particle systems with high monodispersity, the formation of new particles must be avoided during the growth process. By experiments, we have determined the critical conditions for seeds with different sizes, i.e., the critical specific surface area, S_{pc} , at which new particles are found. The curve in Figure 2.16 indicates that S_{pc} is proportional to the size of seed particles. This result agrees with the foregoing conclusion about diffusion-controlled growth during the formation of new particles.

On the basis of these studies, we have developed a seeding technique to grow monodisperse particles continuously, in which either commercial silica sol or the silica sol prepared by us is selected to be the seeds. Under the typical Stöber's conditions, the seed particles grow by feeding stock continuously until the monodisperse system is formed. This method can precisely control and predict the particle size and size distribution. The deviation of the particle sizes between practical and predictive values is usually less than 10%, and the quantity of one batch of particles can reach the scale of a hundred grams.

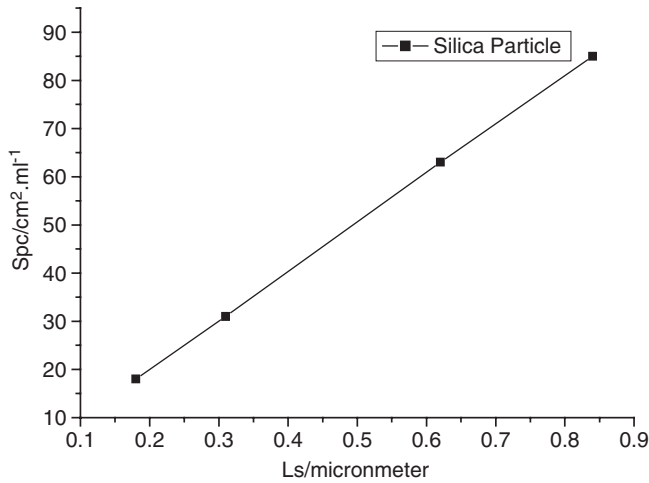


Fig. 2.16. Critical specific surface area S_{pc} vs. L_s (seed diameter). (With the permission of Press of Elsevier in the article, S.L. Chen et al., J. Colloid & Inter. Sci., 180(2) (1996) 237–241.)

Table 2.10
Physical parameters of nanometer silica

Parameters	Properties indexes	
	MN1P	MN1S
Surface area (m^2/g)	640 ± 50	160 ± 20
Particle size (nm)	10 ± 5	15 ± 5
Surface hydroxyl (%)	48	36
Reflect rate of ultraviolet (%)	> 85	> 80
SiO ₂ content (%)	> 99.9	—
Loose density ($g\ cm^{-3}$)	> 0.15	—
Stirring density ($g\ cm^{-3}$)	< 0.22	—
Condensed phase	Amorphous white loose powder	
Impurities (%)	Al < 0.001, Fe < 0.001, Ca < 0.002, Sn < 0.001, Cu < 0.003, Mg < 0.001	

Note: MN1P or MN1S is a sample symbol.

2.2.2. Silica modification

2.2.2.1. Multiple dispersed particles

The multiple dispersed particles of silica are usually prepared via chemical deposition (CD) and vapor oxidation reaction such as silica particles from SiCl₄ reacting with O₂. In these preparations, silica is collected in a heavily aggregated form. To obtain the nanoparticles of silica, there must be a post-treatment, or calcinations at temperatures as high as 1000°C and above. These kinds of silica particles have their properties as shown in Table 2.10.

2.2.2.2. *The monodisperse particles dispersed in electric rheological fluid*

After the silica particles are selected from the mixed aggregated ones by sedimentation method in the designed settling slot, they will be in the form of regular packaging and show a vivid color under visible light. This packaging morphology is seen in Figure 2.17.

Electrical rheological fluids (ERF) are composed of insulating oil and solid particles suspended in ERF, which are easily polarized. Under an electric field, the electric polarized dipole of the particles will interact and arrange into linear chains along the electric direction, which will change the apparent viscosity and shear stress of the liquids. With proper design and control, the ERF properties are capable of being transformed, quickly and continuously, between liquid and solid properties. Previously, most researchers used multiple dispersed particles to investigate the ERF properties of a particle–liquid system, but conclusions for their behavior were difficult to reach. For the same particle size and concentration, the viscosity at zero field of the spherical suspended particles is the lowest, and the response to electric rheology is the most rapid. Monodisperse particles will exclude the difference between response time and viscosity at zero shear field observed for the multiple dispersed particles. For synthesized monodisperse particles with a size of 200, 300, 1,000 nm, etc., their surface is treated properly if they are suspended in amino benzene or propyl amine compound solution. A series of model ERF were measured under direct and alternating currents. The monodisperse particles of silica are interconnected into chains when exerted with electric fields. Their SEM morphology is shown in Figure 2.18.

2.2.3. *Monodisperse silica modification*

2.2.3.1. *Higher quality SiO₂ opals*

Previous work shows that there exist deviations among prepared SiO₂ opals. Thus, different improvements on the size and modification of opals have been reported. The synthetic

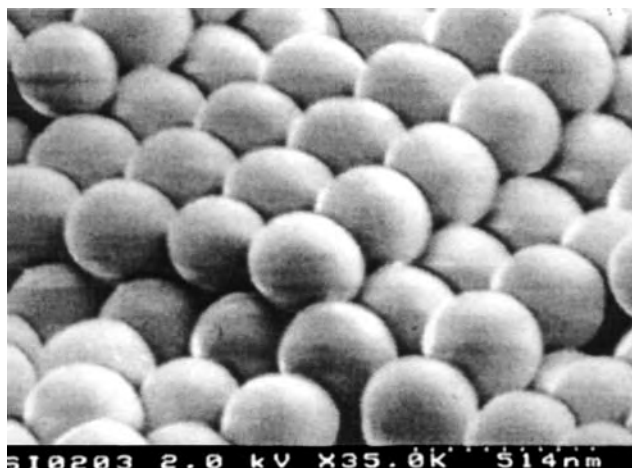


Fig. 2.17. Packaging morphology of monodisperse particles from deposition–selection process.

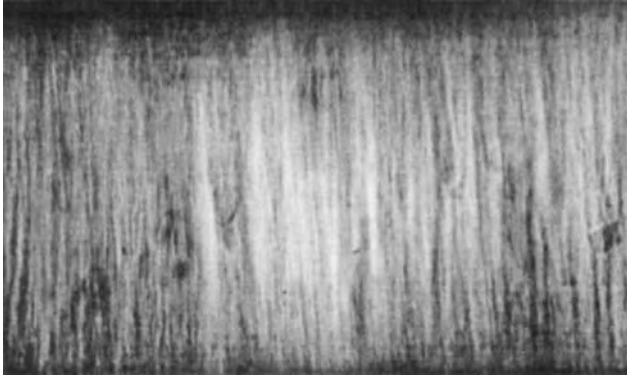


Fig. 2.18. ERF of monodisperse particles subjected to an electric field, with the particles treated by propyl amine compounds. The particles are interconnected into chains due to the electric field.

SiO_2 opals and polystyrene opals, a kind of currently available photonic crystal, possessing an incomplete photonic band gap in the visible region, have been of increasing concern [22–28]. This is because not only can monodisperse SiO_2 and polystyrene submicrospheres be prepared comparatively easily but because opals can also be fabricated relatively simply from them. More importantly, these opals can be used as a template for creating inverse opals [29–34], promising a complete photonic band gap. However, many factors influence the quality of synthetic opals. Our previous work [35] indicates that the monodispersity of submicrospheres is one of the most important factors governing the fabrication of high-quality opals. Imperfect monodispersity of submicrospheres can cause serious disorders and dislocations of lattice in opal, especially when opals are fabricated by sedimentation in a gravitational field. These defects lead to strong random scattering of incident light so that the transmission of the opals becomes very low and influences their photonic properties.

Recently, we developed a submicrospheres selection technique of separating single spheres from aggregated spheres to improve the monodispersity of the submicrospheres. Higher quality silica opals were fabricated from the selected submicrospheres. In this way, the preparation of higher quality SiO_2 opals based on this submicrospheres selection technique has practical value.

2.2.3.2. Preparation of higher quality SiO_2 opals

(1) *Preparation of monodisperse SiO_2 submicrospheres.* Monodisperse SiO_2 submicrospheres were prepared via a seeding technique based on the hydrolysis and condensation of tetraethoxysilane $\text{Si}(\text{OC}_2\text{H}_5)_4$ (TEOS) in a mixture of water, ammonia and ethanol. The technique was developed and improved by our studies on the formation, mechanism and kinetics of silica monodisperse system [35–40]. In one experiment, commercial silica sol particles were dispersed in an ethanol aqueous solution that contained 2 M NH_3 and 6 M H_2O . TEOS was added to the stirring suspension by continuous feeding at 35.8°C at a certain velocity and then the mixture was stirred for 2 h. The

resulting silica submicrospheres were centrifugally separated from the suspension and ultrasonically washed with water. TEM images of commercial silica sol particles and the resulting silica submicrospheres are shown in Figure 2.19 separately.

The average diameter of commercial sol particles is about 27 nm, and the relative standard deviation (RSD) of the diameters distribution is about 28.4%. The diameter of the resulting silica submicrospheres is 310 nm, and the RSD of the diameters distribution is 4.50%. Compared with other methods, the monodispersity of these resulting silica submicrospheres grown by the seeding technique is more perfect. However, in solution, aggregation and adhesion between the same single spheres can be seen from time to time, as shown in Figure 2.19.

(2) *Reselection of monodisperse SiO₂ submicrospheres.* Stoke's law is applied to the sedimentation of particles in a gravity field, as seen in Chapter 1, as $v = gd^2(\rho - \rho_0)/18\eta$, where d is the diameter of a particle with a uniform density ρ , v the constant settling velocity, and ρ_0 and η , respectively, the density and viscosity of fluid media, i.e. water in the present work. Our previous work indicates that the sedimentation of submicrospheres with a diameter larger than 200 nm obeys Stoke's law, in which case the diameter calculated is identical with the diameter measured by TEM. Aggregation of spheres with similar diameter d_s have an apparent diameter d_a , and the aggregate has a settling velocity v_a according to the Stokes law [41].

Moreover, aggregated spheres have higher settling velocities than single spheres of the same size. Therefore, different regions are formed in a transparent glass tube during the sedimentation of the initial suspension of monodisperse spheres with partial aggregation, as shown in Figure 2.20.

In Figure 2.20, region 1 contains only single spheres. The height of region 1 is dependent on the velocity ratio of doublets to single spheres and settling time. We used glass spheres aggregated by two single spheres with the same diameter (about 1 mm and uniform density) as models of doublets to measure the settling velocity ratio of doublets to single spheres v_a/v_s at various low Reynolds numbers. Then, we correlated the settling velocity ratio of doublets to single spheres v_a/v_s with the Reynolds numbers, and

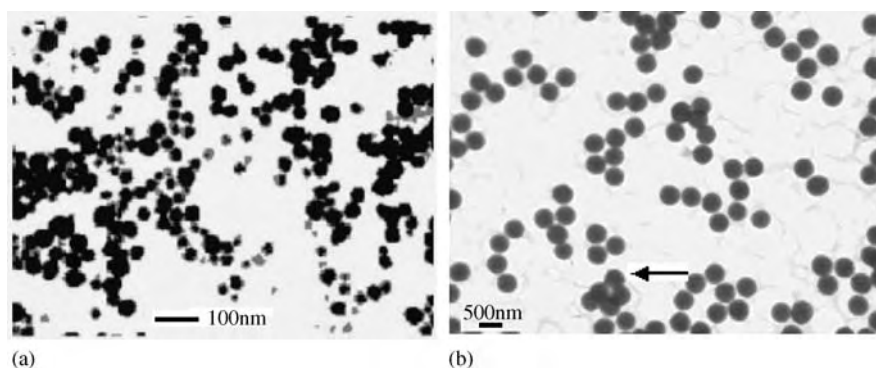


Fig. 2.19. TEM images of (a) commercial sol particles and (b) SiO₂ submicrosphere. Adhered pairs of spheres are indicated by arrows.

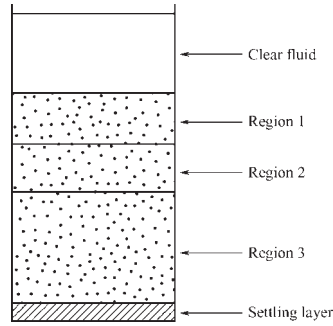


Fig. 2.20. Schematic illustration of the regions that develop during sedimentation of the monodisperse spheres with partial aggregation.

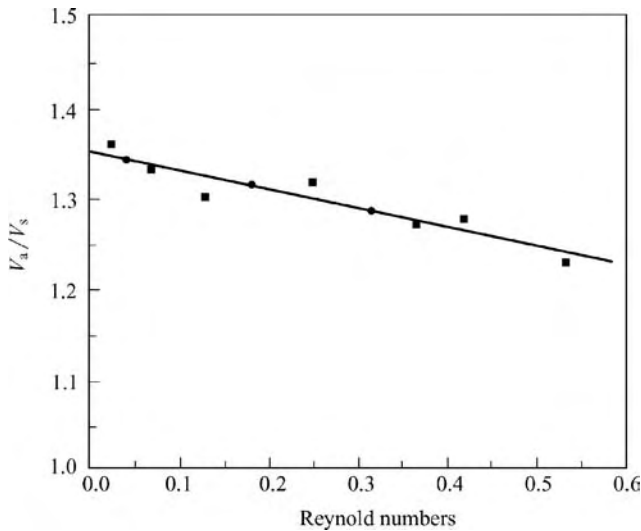


Fig. 2.21. Correlation between the settling velocity ratios of doublets to single spheres v_d/v_s and Reynolds numbers.

because the Reynolds number is very small and approximates to zero in our experimental suspension system of submicrospheres, we extrapolated the correlation to the point where the Reynolds number is equal to zero, as shown in Figure 2.21.

From Figure 2.21, we can read the settling velocity ratio of doublets to single spheres at the zero Reynolds number to calculate the height of region 1; the settling velocity ratio ranges from 1.3 to 1.35 according to the actual experiment. Finally, single spheres were collected from region 1 and separated from aggregated spheres in the form of doublets, triplets, etc. A TEM image of the selected spheres is shown in Figure 2.22.

(3) *Fabrication of SiO_2 opals from colloidal SiO_2 submicrospheres.* SiO_2 opals were fabricated from colloidal SiO_2 submicrospheres (preparation discussed in section 2.2.1)

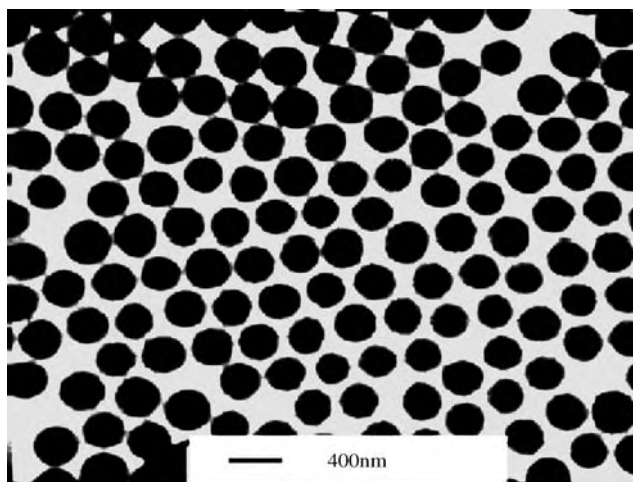


Fig. 2.22. TEM image of selected SiO_2 submicrospheres with a diameter of 290 nm.

by the method of sedimentation in a gravitational field. We used the following procedure: In order to eliminate interaction between submicrospheres, the suspension of SiO_2 submicrospheres was diluted so that quality concentration of SiO_2 submicrospheres was below 1 wt%. Then the diluted suspension was filled into a tube with a polished substrate. The diameter of the tube was 2.5 cm, which is large enough to eliminate edge effect. The aqueous solution was extracted carefully when sedimentation was complete after a few weeks. After they were dried naturally at room temperature, the opals, which were very easy to crack, were taken out of the tube and annealed at 900°C for 4 h. The opals had better mechanical and optical properties after annealing. Diffractive colors from green to red could be readily seen when the opals were put under a lamp and the observation angle was changed. An SEM image of the annealed sample shows that the opals have face-centered cubic structure symmetry. Using the selection procedure for spheres, the size of a single crystal in the opals obtained was substantially larger and their mechanical and optical properties also became better. A comparison of SEM images between the opals fabricated from selected silica submicrospheres and the unselected submicrospheres is shown in Figure 2.23. The top surfaces of the opals fabricated from both selected and unselected submicrospheres have good alignment, while their bottom surfaces (Figure 2.23(a) and (b)) have different morphologies. The opals fabricated by the selected procedure show a good alignment of particles on both of their sides, while the opals fabricated from unselected submicrospheres have good order patterns only on one side of the top face but a bad order on the bottom face. This shows that the selection procedure for spheres is very successful in improving the monodispersity of spheres, and this selection will help particles packaging regularly.

The monodispersity of spheres is one of the most important factors governing the fabrication of opals. The photonic band structure of the opals can be probed experimentally by measuring its transmission spectra using electromagnetic waves with different

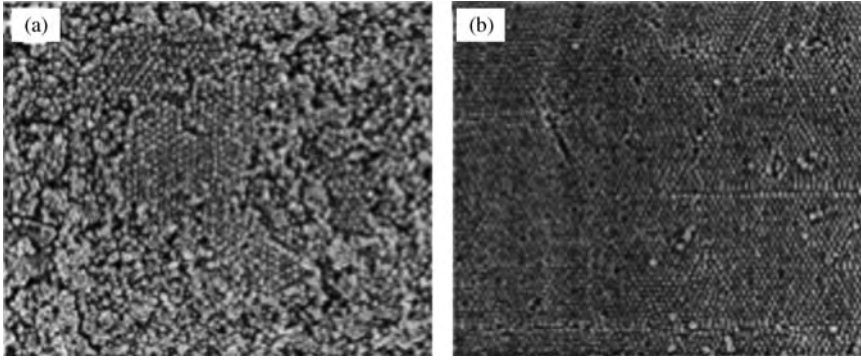


Fig. 2.23. SEM image of top and bottom surfaces of silica opals. (a) Bottom surface of the opals without selection procedure for spheres; (b) bottom surface of the opals with the selection procedure for spheres.

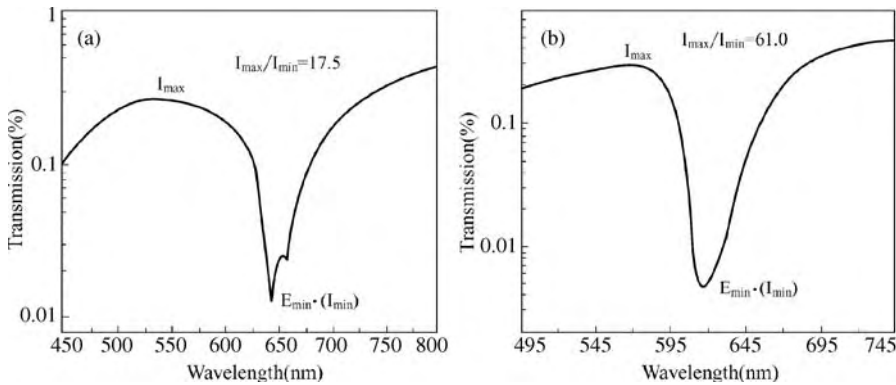


Fig. 2.24. Transmission spectra of two SiO_2 opals: (a) without selection procedure for spheres; (b) with the selection procedure for spheres. (With the permission of Press of Elsevier in the article, Q.Y. Li et al. *Colloid & Surfaces*. 216(2) (2003) 123–128.)

wavelengths. Transmission spectra between the opals fabricated from the selected silica spheres and the unselected spheres are compared, as shown in Figure 2.24. Because the diameters of the spheres used in the two cases were slightly different, the position of the midgap (I_{\min}) was not exactly identical. Because fewer defects and dislocations are present in the opals with the selection procedure, the random scattering decreases and the coherent scattering increases. On using the selection procedure for spheres, the maximum attenuation of the gap (I_{\max}/I_{\min}) characterizing the band gap increased from 17.5 (Figure 2.24(a)) to 61.0 (Figure 2.24(b)), which further indicates the effectiveness of using the selection procedure for spheres while fabricating opals.

2.2.3.3. Core-shell particles of monodisperse silica with polymers

2.2.3.3.1. Core-shell particles of monodisperse silica with polystyrene Both silica and polystyrene are suitable for the preparation of monodisperse particles [42,43]. As

for silica, a particle size greater than 100 nm usually gives good sphere-like particles with high sphericity, while for polystyrene, any particle size seems to give a good sphere-like shape (Figure 2.25).

If inorganic silica particles are covered by organic polystyrene, then the core-shell structure formed from them depends on the silica particle size. When the particle size is < 100 nm, there is a greater probability that a core-shell where many silica particles will squeeze in the same single particle will form, as in Figure 2.26(a). When the particle size is large (say 500 nm), the particles are homogenous and the sphere-like core-shell particle will usually contain one silica particle.

2.2.3.3.2. Core-shell particles formed by proper surface treatment In order to make monodisperse silica suitable for different matrixes, the silica surface is usually treated

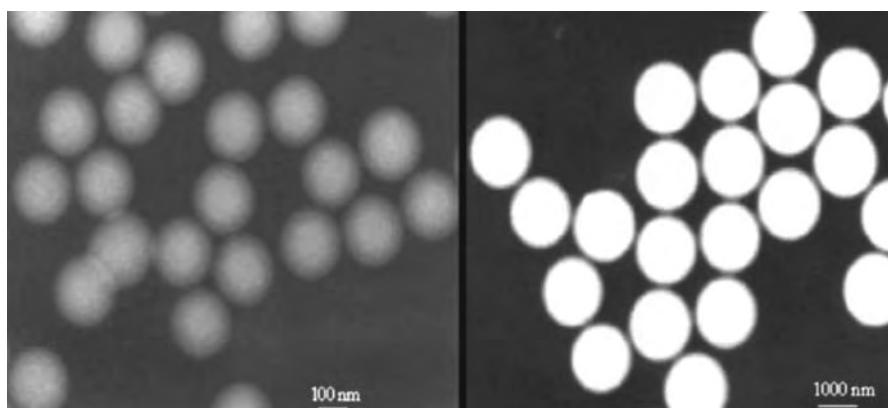


Fig. 2.25. TEM morphology of the monodisperse silica and polystyrene particles (left, monodisperse silica; right, monodisperse PS particle).

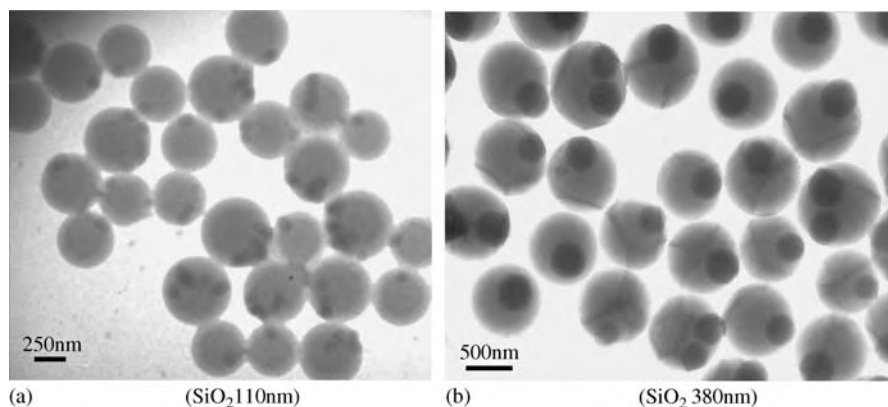


Fig. 2.26. Core-shell particles of monodisperse silica and polystyrene (a) silica particle size of 72 nm, (b) silica particle size of 629 nm.

with silane. This treatment will increase the original particle size of monodisperse silica, but the particles of good sphere-like morphology are usually retained, as shown in Figure 2.27, where the silica particles are 20–50 nm larger than the pristine silica particle after treatment with silane. The sphericity of the silica sphere-like particle is improved under some circumstances (see Figure 2.28).

When the silica is polymerized with polystyrene, core-shell structure particles with good sphericity have been obtained. The treated particles have a much smaller size deviation than the untreated silica.

2.2.3.3.3. Core-shell particles of monodisperse silica with polypropylene Polypropylene is a common plastic material produced in high yield in China and the rest of the world. Its additives need to be dispersed in a polypropylene matrix for the preparation of high-performance materials. In one practice, silica is used as a carrier for additives such as

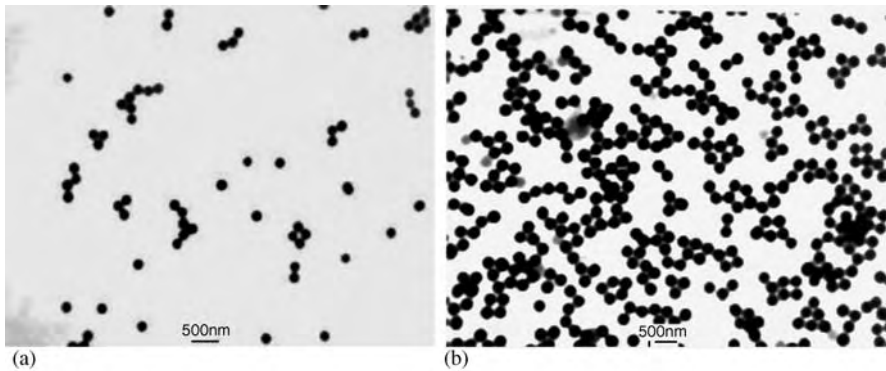


Fig. 2.27. The morphology of monodisperse silica particles: (a) silica before treatment with silane; (b) silica after treatment with silane.

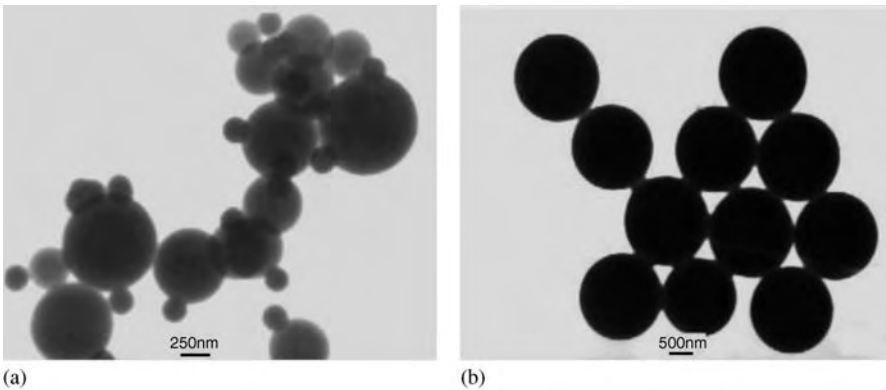


Fig. 2.28. The morphology of nanocomposites of silica with PS: (a) silica before treatment with silane; (b) silica after treatment with silane.

stabilizing, antioxidation, nucleation and antistatic electricity agents. The additives are called composite additives when silica is used as a carrier. The nanocomposite of polypropylene with composite additives has enhanced processing and antioxidation properties (Figure 2.29).

2.2.3.4. Silica particle dispersion and properties in PET melt

Core-shell nanoparticle precursors (NPP) with silica (or layered silicate) as a core material have been applied for mixing with PET melt. The NPP mixed with PET melt has produced different properties, as shown in Table 2.11. There, the crystallization degree of NPPs-PET nanocomposites is much lower than that of NPPI-PET nanocomposites with layered silicate loads of 0.5 to 1.5% (by wt). This is due to more nucleation centers formed from the exfoliated silicate layers than those formed from silica. In other words,

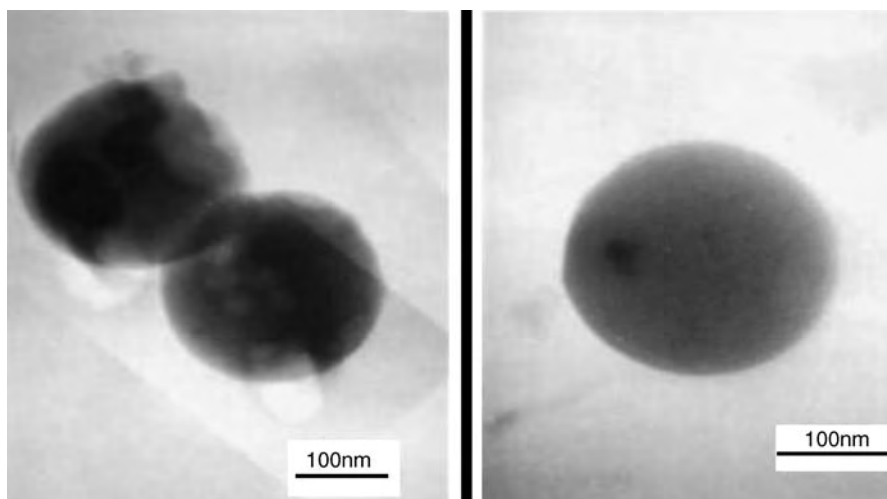


Fig. 2.29. Core-shell structure of silica particle with polypropylene by compounding or melt mixing with a designed composite additive containing silica nanoparticles (the compounding temperature is from 170°C to 240°C).

Table 2.11
The properties of NPP-PET composites

Properties	Silica + PET (NPPs)			Layered silicate + PET (NPPI)		PET
	0.5	1.0	1.5	0.5	1.5	
LW (%)	0.5	1.0	1.5	0.5	1.5	0
ΔH ($J g^{-1}$)	37.3	40.1	40.3	50.2	56.9	50.1
T_m (°C)	246.0	247.3	247.7	254.7	250.6	254
Tr	Y	Y	Y/N	Y	Y/N	Y
$t_{1/2}$ (min)	—	—	0.81	—	0.72	1.8

LW, Load weight, ΔH , heat of fusion, Tr, transparency, $t_{1/2}$, the time at which the crystallization degree reaches 50% of the whole. Y, Yes, N, No.

nanoparticles of silica tend to accumulate and become large particles, while silicate particles become smaller and smaller from the layer exfoliation. It can be seen from the comparison that both of the composites have lower $t_{1/2}$ than that of PET ($t_{1/2} = 0.81$ min for NPETs with silica; $t_{1/2} = 0.72$ min for NPET with MMTs). This strongly reflects the rapid crystallization of PET–silica (silicate) nanocomposites. Nanocomposites with an inorganic particle load of up to 1.5% (by wt) are not transparent. The inorganic particle load affects film transparency, which is limited below the load of 1.5% (by wt).

Finally, the crystallization rate of NPPI with PET nanocomposite is obviously higher than that of NPPs-PET. This makes it possible for NPP to be used as a nucleation reagent to replace high-cost chemical reagents.

2.2.3.5. *Monodisperse silica coated by titanium*

To enhance the sphericity of the silica, silica particles coated with titanium can be made. One may use codeposition and multiple step methods to prepare core–shell structure particles. In the codeposition method, the precursors for mixtures of particles are reacted in a vessel for some time. The modified silica has a better sphere-like shape (Figure 2.30).

2.2.4. *Self-assembly mechanism and defect analysis of colloidal silica photonic crystals*

The modified Stober method for the preparation of SiO_2 particles can be used for self-assembly mechanism. To control their formation and nucleus number, the original raw materials are added by a two-step procedure instead of a one-step procedure. Preparation conditions are as follows: 200 ml of ethanol and 16 ml ammonia are placed in a three-necked flask; the flask is immersed in a 34°C water bath. After heat equilibrium is reached, TEOS is added to the reactor at a rate of 6–8 drops min^{-1} . Meanwhile, the reaction mixtures are kept homogeneous and heated at 34°C for 2 h. Degassing this reacting solution causes NH_3 to be volatilized. To obtain the ideal structure pattern, the SiO_2 solution in ethanol is injected into a glass tube (diameter \times height = 2 cm \times 7 cm). The bottom of this tube is polished to avoid the growth of too many defects in the photonic crystals. Then the tube is kept in a desiccator, which lets the particles sediment while shaking or vibrating is avoided. After 2 days, a vivid color can be seen on the wall of the tube. This color changes with the incident ray of common light. When all ethanol is eliminated and the SiO_2 is dried, the SiO_2 settles on the bottom of the glass tube, forming SiO_2 gel photonic crystals.

2.2.4.1. *Calculations of the ordered structure of silica particles by assembly and self-assembly*

The silica forms self-assembly structures by the settling technique. Microscopy data shows that average silica particles of 120–400 nm with a standard deviation of 5.7% are obtained. In the patterns composed of these SiO_2 particles with 230 nm or so, mainly self-assembled fcc crystals are observed. The spheres of SiO_2 particles are stacked in forms of both OPOPOPO.....(hcp) and OPQOPQOPQ.....(fcc) under a heavy force. According to the findings of Woodcock [44], the fcc system has a free energy of $0.005 RT \text{ mol}^{-1}$ lower than the crystals in hcp form. The fcc-packed crystal is the most stable structure. The SiO_2 self-assembly morphology is shown in Figure 2.31, where the (111) and the (100) face images, obtained by SEM, are shown. Some point defects and line

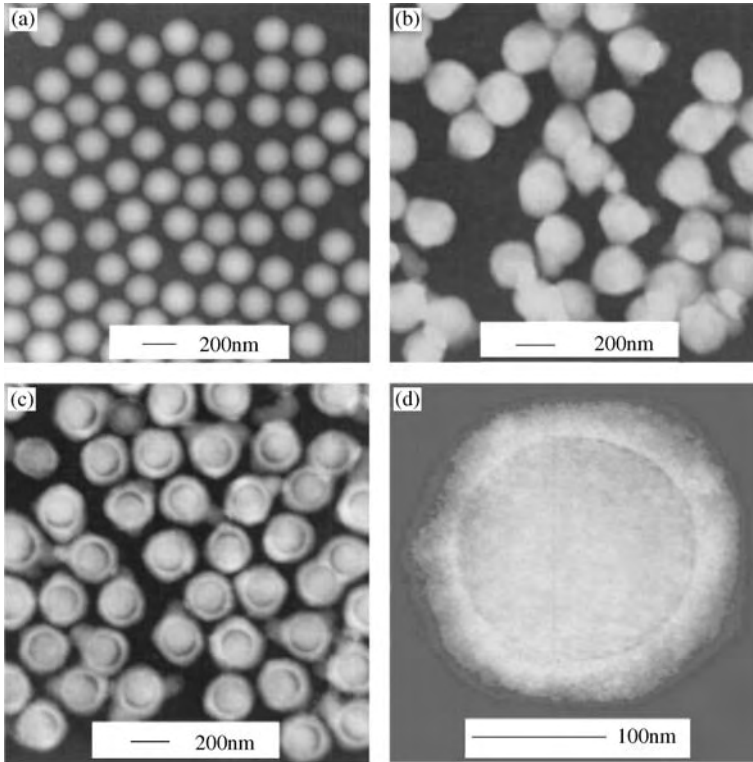


Fig. 2.30. TEM images of spheres and composite particles (a) silica spheres without titania coating, (b) silica spheres with three-step coating of titania, and (c) and (d) titania-coated silica spheres with the outermost, thin coating of silica: (a) Sample A, 1Si-0Ti; (b) sample A, 1Si-3Ti; (c) and (d) sample A, 1Si-3Ti-1Si.

defects were found. The experiments show that in the photonic crystals prepared from 200 nm SiO_2 particles, the strongest absorption occurs at its (111) face with its peak position at 550–600 nm.

The absorption of light follows Bragg scattering. Taking each SiO_2 particle as a lattice atom of crystals, the (111) face has its face interdistance as

$$d_{111} = a/\sqrt{1^2 + 1^2 + 1^2} = \sqrt{2D/3}$$

(where a is the lattice constant and D the diameter of small spheres)
while the Bragg equation is

$$\lambda = 2kn_{\text{SiO}_2}d_{111} \sin 90^\circ = 544k \quad (k = 1, 2, 3, \dots) \quad (2.2.4)$$

The first portion of the incident light is positioned at 544 nm when the silica size is 230 nm, which is in good agreement with the experimental results. However, due to the

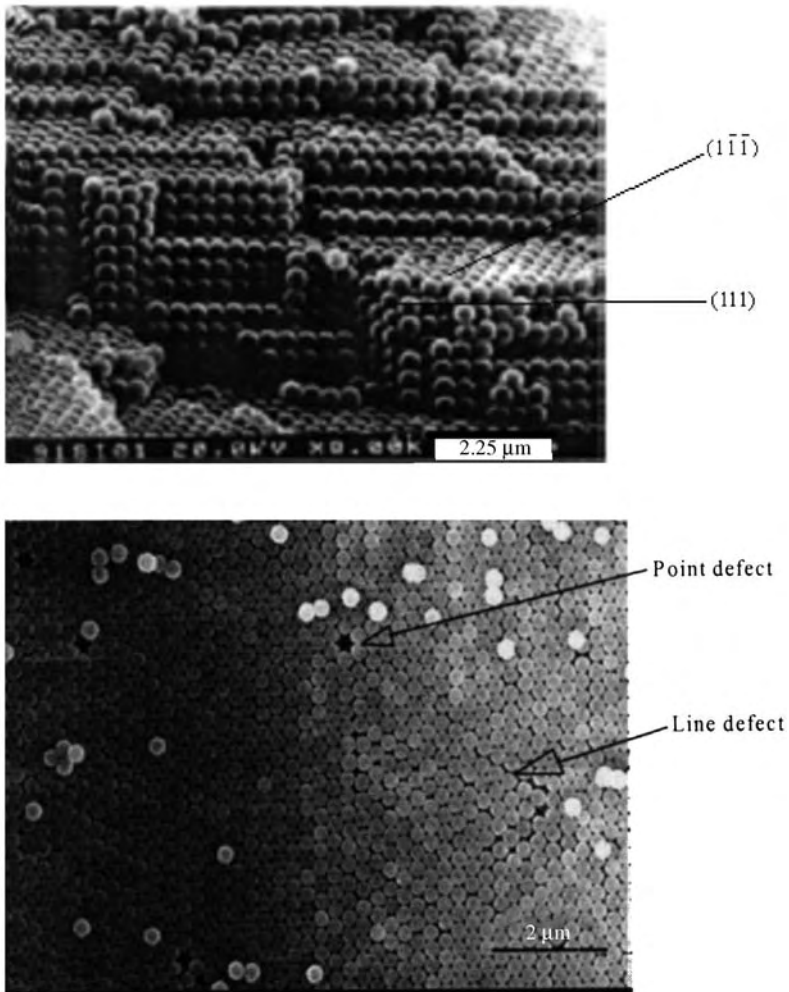


Fig. 2.31. Packed structure of silica particles by a self-assembly process.

rather small refractive index of SiO_2 , the complete light band gap cannot be reached. It is speculated that the second absorption peak is near 1,088 nm, but is very weak.

2.3. Melt intercalation

Based on the previously published work and our own work, we have summarized several approaches for the preparation of polymer-layered silicate nanocomposites. The goal of these methods is homogeneously dispersing or exfoliating the layers of clay into the organic polymer matrix. The morphology of dispersed particles have an inherent relationship with the final properties of the nanocomposites.

(1) *Melting intercalation*. In this method, organic polymer pellets and treated clay are directly mixed in the extruder machine and are then melt-extruded together to prepare the nanocomposite on a large scale to obtain the exfoliated layers. The organic polymer matrix is selected from PP, PE, PA6, PS and others [45–49]. The organo-clay is modified with different surface affinity reagents in order to match the system. For example, in the preparation of PP-MMTs nanocomposites, the organo-clay is first covered by PP oligomer grafted with maleic anhydride, which improves the compatibility of organo-clay with the PP matrix, and the properties of the final nanocomposite. The PET-MMTs nanocomposites are incapable of being prepared via such a technology because of easy degradation. The organo-clay readily adsorbs moisture and usually degrades the polymer chains.

(2) *Polymerization intercalation*. This method requires that the monomer of the polymer be mixed with organo-clay at first because the interlayer space in this organo-clay is already enlarged to let the monomers enter. Then, the prepared mixture is polymerized under the reaction conditions similar to pure polymer, during which clay layers are exfoliated in situ into nanoparticles. This technique is suitable for polymers such as PS, PA6, PI, PET, PBT and PA66 [50–59]. The polymerization medium is the important factor for the reaction and final products. For example, in the preparation of PS-MMTs nanocomposites, the emulsion media must include not only initiator, but also surfactant or dispersant.

(3) *Media intercalation*. The word “media” here refers to solvent, reagent, gas, etc. By using the media, the clay is treated. Polymers for nanocomposites in such a method are PI [54], PET [55], PEO [60–62], PLLA and PCL [63] (where PLLA is poly(L-lactide) and PCL is poly(ϵ -caprolactone)).

Among the many reports on polymer-clay nanocomposites, there are several successful ones. For example, PA6-clay nanocomposites [64–68] and PET-clay nanocomposites [55,59,69] have been prepared successfully. The second and third technologies are described in Section 2.4.

2.3.1. Precursor intermediate preparation for nanocomposites

2.3.1.1. Reducing the water quantity in treating clay

As stated, it is possible to disperse the nanoparticles by the intermediate process of using the precursors. This is an important approach to dispersing nanoparticles in the polymer melt. However, in treating clay to prepare the intermediates for nanoparticles, a large amount of water is required to suspend them. For example, the weight (mass) ratio of water to dry clay ranges from 15 to 30, while, the optimized ratio is 15 to 20 in practice. To solve the problem of drying the composites with too much water in the very dilute solutions, a new technology is designed by melting the layered clay with the selected intercalant or treatment agent, forming its precursor.

The selected intercalants or oligomers are usually organic compounds with carbons of C_2 to C_{100} repeat monomer units; or their related polymers are used to mix directly with clay [45] (see also US Patents 4,739,007, 4,810,734 and 5,385,776). The treatment agents are either mixtures of different organic molecules, which contain at least 1–5% (by wt) intercalant oligomer, or intercalant polymer. Recently, about 50–80% (by wt)

oligomer or polymer (based on the oligomer, polymer and carrier) have been used to achieve better sorption of the intercalant polymers between silicate platelets. At these percentages, less drying is required after intercalation (Figure 2.32). Oligomers that cause separation or added space between silicate platelets are organic intercalants or intercalant polymers. Here, the carrier refers to water and solvent. Thus, in this manner, the water-soluble polymers or oligomers will be adsorbed sufficiently to increase the interlayer spacing of the phyllosilicate of clay in the range of $\sim 1.0\text{--}10.0$ nm, for easier and more complete exfoliation, in a commercially viable process, regardless of the particular phyllosilicate or intercalant polymer. These water-soluble polymers or oligomers have the following structures:

The PMAAm is a derivative of poly(methacrylic acid) (PMAA). Exfoliation of the intercalated layered material should provide delamination of at least 90% (by wt) of the intercalated material to provide a composition of a polymeric matrix having platelet particles homogeneously dispersed therein. Some intercalates require a shear rate $> 10\text{ s}^{-1}$ for thorough exfoliation. Other intercalates exfoliate naturally or by heating to the melt temperature of the intercalant polymer or by applying low to moderate pressures, e.g., 0.5–60 atm above ambient, with or without heating. Some reports show that the shear rate should reach $100\text{--}20,000\text{ s}^{-1}$.

Example 2.3.1.1. Preparation of oligomers-layered clay nanocomposites. In the process, Na ion-exchanged MMTs (or Na-MMTs) and a polymer of polyvinyl pyrrolidone (PVP) with molecular weights of 10,000–40,000 are used. Three methods are used to prepare nanocomposites:

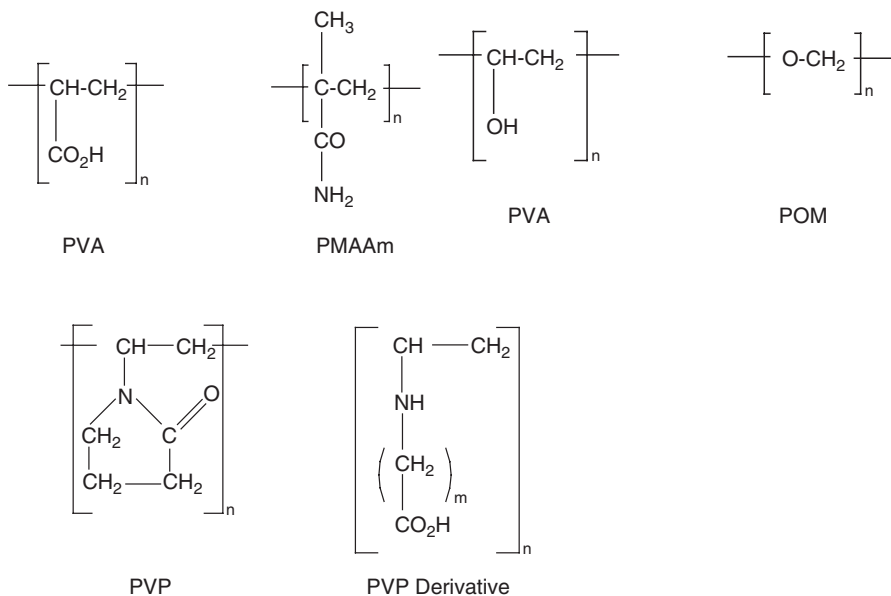


Fig. 2.32. Oligomers and polymers for preparation of treated clay by intercalation.

- (1) PVP 2% in water solution is mixed with 2–5% clay in water suspensions, in which the ratio is sufficient to provide a polymer concentration of at least 15–20% based on the dry weight of the clay. In this way, the gel of treated clay is obtained.
- (2) In the second approach, the dry clay powder (about 8% (by wt). of moisture) is gradually added to 2% PVP in water solution in a ratio sufficient to provide a polymer concentration of at least 15–20% based on the dry weight of the clay.
- (3) In the third approach, dry PVP is mixed with dry clay, the mixture is hydrated with 35–38% of water by spraying or dipping, based on the dry weight of the clay, and then extruded.

The extruder is usually a twin- or single-screw machine. In the final composition, sorption of 20–30% PVP has a d -spacing of clay ranging from 1.2 nm (pristine clay) to 2.4 or 2.5 nm, while it is increased to 3.0–3.2 nm spacing when the sorbed PVP [20] content is increased to 40–60%. Further increasing the sorbed PVP content to 70–80% increases the $d(001)$ values to 4.0 or 4.2 nm. The $d(001)$ reflexes in X-ray patterns of all complexes are shown in Table 2.12. This indicates the regularity of PVP–clay complex structures.

2.3.2. Melting intercalations

In this method, the inorganic phase in composites is dispersed by a melt process and shear force from the extruder. The usual process for melting intercalation in detail is shown in Figure 2.33.

The pristine clay is treated by ion-exchange reaction to form an organo-clay, which forms a precursor intermediate. It also has a core–shell structure with layered silicate as its core material. When it is used for melt mixing with polymers, its layers will be further exfoliated and form nanoparticles in situ in the polymer matrix. Such exfoliation morphology is shown in Figure 2.34, where the traditional composites have coarse fibers, while the nanocomposites have homogeneous distribution of fine particles.

The PA6 (nylon6)–clay nanocomposites have significantly enhanced properties with respect to heat distortion temperature, modulus and gas barrier. These results are from

Table 2.12
The interdistance d (nm) of MMTs intercalated by PVP polymers

No.	PVP (%)	$d(001)$	$d(002)$
1	0.0	1.24	0.62
2	20.0	2.40	1.14
3	30.0	2.50	1.20
4	40.0	3.0	1.52
5	45.0	3.10	1.52
6	50.0	3.0	1.55
7	55.0	3.2	1.65
8	60.0	3.4	1.70
9	70.0	4.0	2.10
10	80.0	4.2	2.10

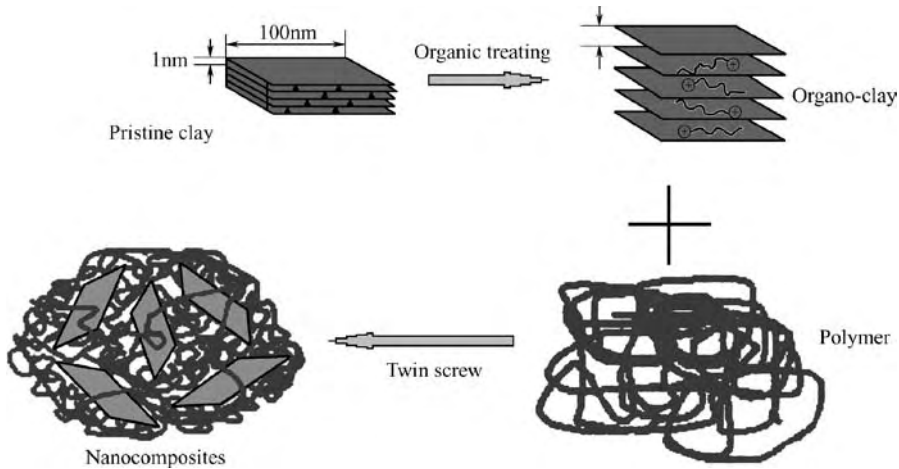


Fig. 2.33. Melt intercalation flow chart for polymer with organo-clay.

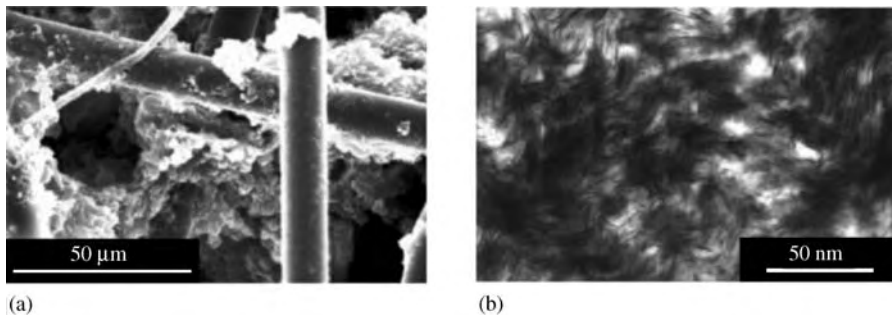


Fig. 2.34. TEM morphology of traditional composites (a) and nanocomposites (b) for PA6 with glass fiber and layered clay of MMTs.

the dispersion of exfoliated layers of clay in the polymer matrix. Some of these results are seen in the comparisons with the pure polymer matrix (Table 2.13).

The modulus of nanocomposites of nylon6 with layered clay is shown to be directly proportional to the clay load (Figure 2.35). As is seen, the strongest bonding effect between the amine group in nylon6 and hydroxyl groups in the MMTs will explain this property enhancement.

While the morphology and high aspect ratio of layered silicate contribute more to the enhancements of these polymer-based nanocomposites, in MMTs, the aspect ratio may reach (50–100): 1, and will disperse in random, parallel, and stacked forms. These dispersions except in parallel ways are always seen in the polymer-MMTs nanocomposites, while the layer dispersion in the parallel way is not always observed in these prepared nanocomposites. Recently, such a dispersion morphology is reached in

Table 2.13
Properties of nylon6-MMT nanocomposites by a melt intercalation

Properties	Nylon6	Nylon6/MMT Nanocomposites (4.2 wt%)
Yield strength (MPa)	68.2	91.3
Tensile modulus (GPa)	3.0	4.1
Flexural strength (MPa)	93.5	150
Flexural modulus (Gpa)	2.4	4.2
Notched Izod impact strength ($J^{-1}m$)	28.0	26.0
Heat distortion temperature ($^{\circ}C$, 1.82 MPa)	62	112

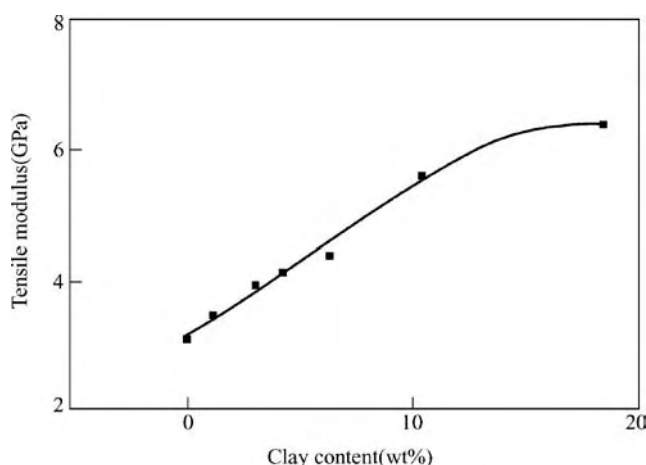


Fig. 2.35. The tensile modulus of nylon6 - MMT nanocomposites.

polypropylene-MMTs nanocomposites. When pristine MMTs are treated with grafted maleic acid, then, they are melt-mixed with polypropylene by an extruder. Under such a shearing interaction, the layers of MMTs may exfoliate and orient with the outside force (Figure 2.36).

2.4. Intercalation in media

2.4.1. Intercalation in solvent

Polar groups on the surface of particles have large effects on their dispersion in the polymer melt. For example, the hydroxyl groups on the silica particles will adhere to their particle surface when they are dried. The hydroxyl groups will take a different angle to the particle surface when they are in different moisture states. The solvent content has a direct effect on the hydroxyl morphology on the surface, which in turn will have a direct effect on the dispersion behavior.

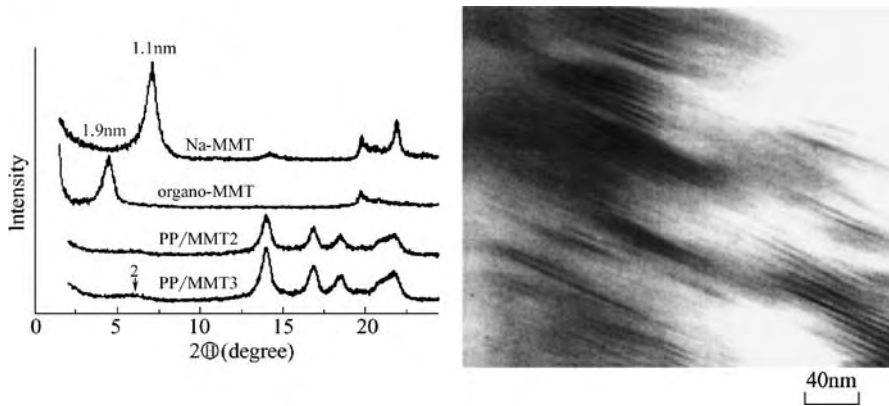


Fig. 2.36. The morphology for PP-layered silicate nanocomposites. Left panel for X-ray pattern, right panel for TEM pattern.

Table 2.14
The MMTs particle agglomeration degree

	BHET	PET
Dried MMTs	+	++
Moisture MMTs (80% H ₂ O)	-	+ -
Solved MMTs (95% H ₂ O)	+ -	+

+, agglomerated particles account for 3–4%; ++, agglomerated particles account for 5%; + -, agglomerated particles account for 2–3%; -, agglomerated particles account for 1%.

Taking polyester-MMTs (or PET-MMTs) nanocomposites as an example, the inorganic phase is derived from the dried MMTs, moisture MMTs (80% H₂O), and dispersed MMTs (95% H₂O), respectively. They are used to polymerize with monomers of ethylene glycol (EG) and *p*-terephthalate (PTA). The obtained products are oligomers of bihydroxyethyl terephthalate (BHET) and polymers of polyester (PET). It is seen that the particles disperse in different ways as shown in Table 2.14.

It is seen that proper water content will benefit particle dispersion in the organic matrix with little agglomeration or without agglomerations.

2.4.2. Intercalation in monomer

When a monomer is used as a medium in the MMTs intercalation reaction, there are several cases of nanocomposites with either good or poor dispersion morphology. There are examples of the monomer as both solvent and intercalant. In some of our practices, the purified pristine MMTs is exposed in a gas atmosphere of ethylene or propylene, and then submerged into the oligomers by a floating-bed device. The produced MMTs

blend is transferred into a reactor for polymerization. In this way the nanocomposite can be prepared.

In the preparation of PA6-MMTs nanocomposites, the monomer also acts as an intercalant at first. The monomer-treated clay is added to the caprolactam monomer of nylon6, and then initiated to polymerize after draining for sometime. In this way, nylon6-clay nanocomposites with good properties are obtained. As shown in the above and following sections, the properties of the PA6-clay nanocomposites are enhanced compared with their pure counterpart.

In the preparation of PET-MMTs nanocomposites, the monomer intercalation and polymerization usually can not produce nanocomposites with satisfactory layer dispersion, because many agglomerated particles appear in the polyester matrix (Figure 2.6) due to the regathering of the exfoliated layers during the long esterification reaction.

2.4.3. Intercalation in emulsions

In preparation of PS-MMTs nanocomposites, an emulsion must be prepared for its polymerization. An ion-exchange process is used to prepare the organo-MMTs, which in turn is mixed with the emulsion. Then this reaction system is initiated by a radical reagent (AIBN or BPO). After the reaction, the pure powder nanocomposites (PS-MMT) are obtained by washing several times (Figure 2.37).

The TEM morphology of the obtained PS-MMTs nanocomposites is shown in Figure 2.38, where the layers are basically homogeneously dispersed in the polystyrene matrix. When this nanocomposite sample is sheared to orient, the probable liquid crystalline phenomenon will occur due to induction or nucleation (see Chapter 4 or 5).

2.5. Modification of particles for polymerization

Particles, including nanoparticles, have heterogeneous surfaces and properties, which cause variability in contacting or reacting with other matrixes. Control of the surface properties gives the best properties for the final nanocomposite. In this section, several modified technologies are suggested to make the particle surface homogeneous and compatible when contacting other organic matrixes.

2.5.1. Oligomer-silica mixtures

As seen from the modifications of silica and silicate particles, the matched organic compounds should be properly treated with the ultrafine particles. The particles to be dispersed in the polymer melt should be carefully chosen to suit the application. In general, the oligomer of one polymer is one of the polymer's best compatibility reagents, and this oligomer acts like an adhesive reagent or lubricant between its counterpart polymer and the inorganic particles. For example, to disperse silica into poly(methyl methacrylate) (PMMA), the treated particles must be further reacted with the oligomers of PMMA. By this reaction, the nanoparticle precursors for silica particles and in turn the final nanocomposites are obtained, which are in situ polymerized or melt-blended with monomers of PMMA or PMMA polymer. The morphology of the mixtures of oligomer PMMA mixed with silica is shown in Figure 2.39.

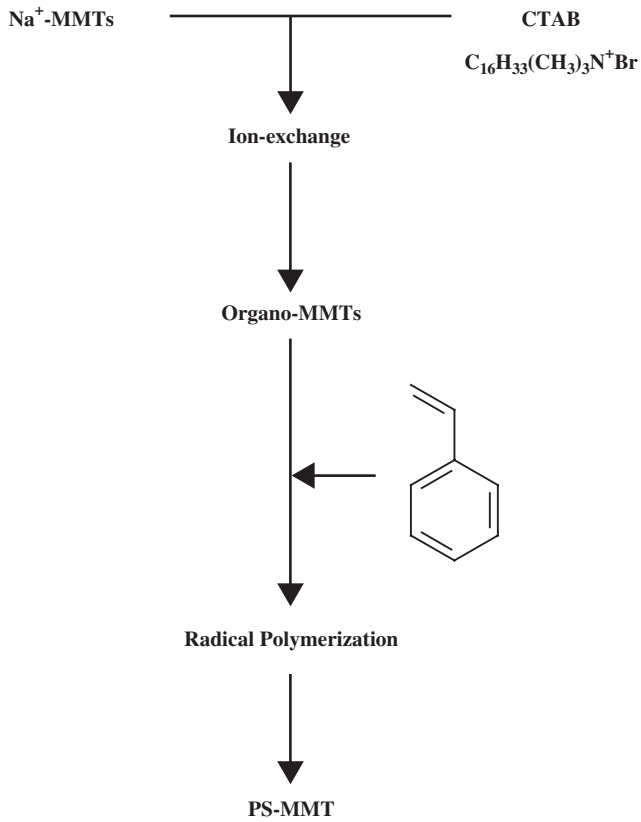
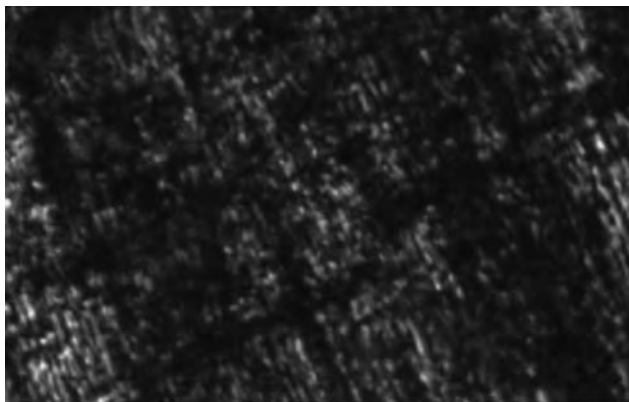


Fig. 2.37. The polymerization process of PS and layered silicate of MMTs in an emulsion.



Room temperature

Fig. 2.38. The dispersion behavior of MMTs in a matrix of PS.

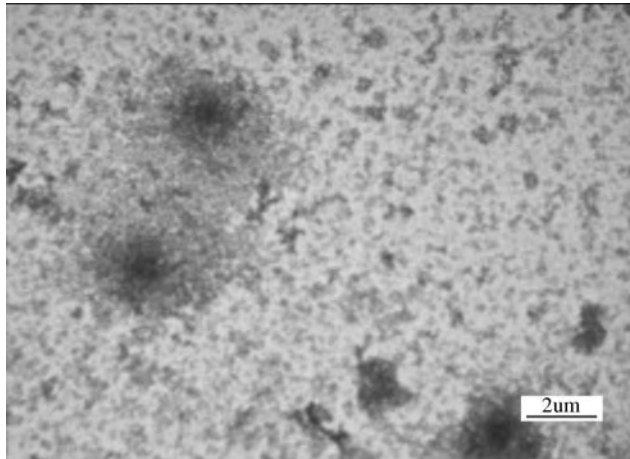


Fig. 2.39. TEM morphology of the nanoprecursors of silica mixed with oligomer PMMA. The pristine silica particles of about 20 nm are treated for 4 h at the boiling temperature of silane in xylene solution before mixing with oligomer PMMA.

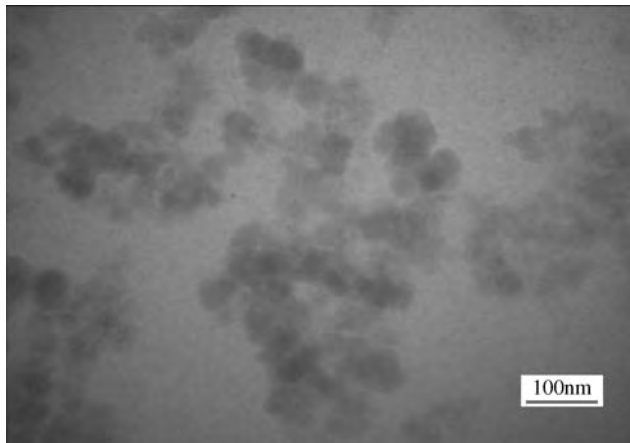


Fig. 2.40. TEM morphology of the nanoprecursors of silica mixed with oligomer PMMA. The pristine silica particles of about 20 nm are treated by silane in xylene solution for 4 h at boiling temperature before mixing with the oligomer PMMA.

In the melt mixing of silica particles treated with oligomer PMMA, there appears to be a bad effect from solvent mixing silica particles in that they agglomerate again. The reason for this is that some particle surfaces might be naked or contain defects in the treatment process. In Figure 2.39 it is clear that the dark areas look like clusters in the melt. To investigate in more detail, we enhanced the observation resolution. The TEM morphology of silica dispersed in oligomers of PMMA is seen above and below (Figures 2.40 and 2.41). Chain-like silica is seen in the composites.

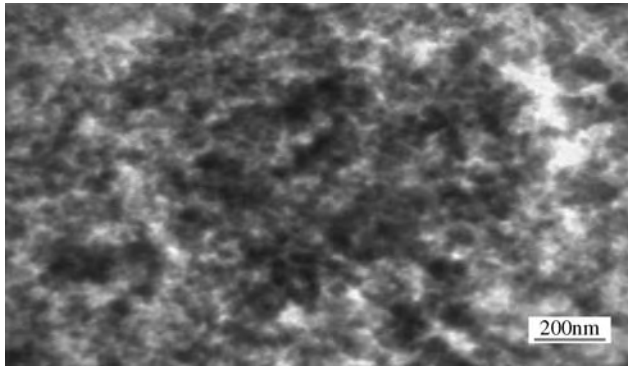


Fig. 2.41. The nanoprecursors of silica mixed with oligomer PMMA. The pristine silica particles, which are about 20 nm, are treated by silane before being mixed with oligomer PMMA.

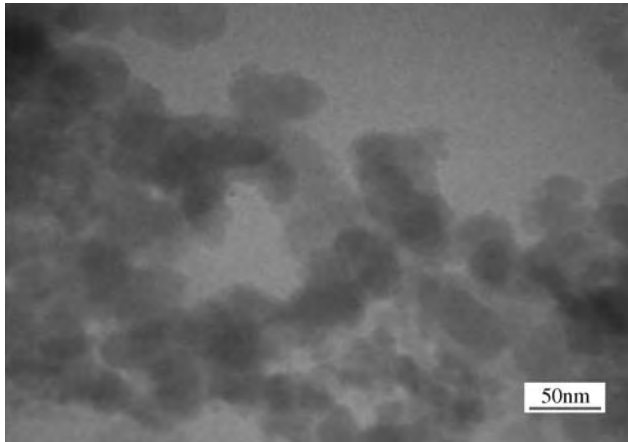


Fig. 2.42. TEM morphology of silica/PMMA nanocomposite.

Similarly, silica dispersed in the polymer PMMA matrix gives a nanocomposite with chain-like morphology is also seen in Figure 2.42. The chain-like morphology of silica will form when the nanoparticle precursor is used to disperse in a polymer matrix such as the polyester of PET (Figures 2.43 and 2.44). Silica dispersion in PET, or its oligomers of BHET and PMMA matrixes is a difficult process due to the formation of the silica chain-like morphology. The chain-like silica is not further exfoliated or dispersed because of its strong binding with the polymer matrix and slow percolation effect. The difference of refractive index, due to the chain-like morphology of silica in dispersion, may explain the reason why silica-based nanocomposites are usually opaque. Otherwise, to obtain a nanocomposite film with high transparency, the dispersion morphology has to be improved by breaking the formation of the chain-like morphology of silica in dispersion.

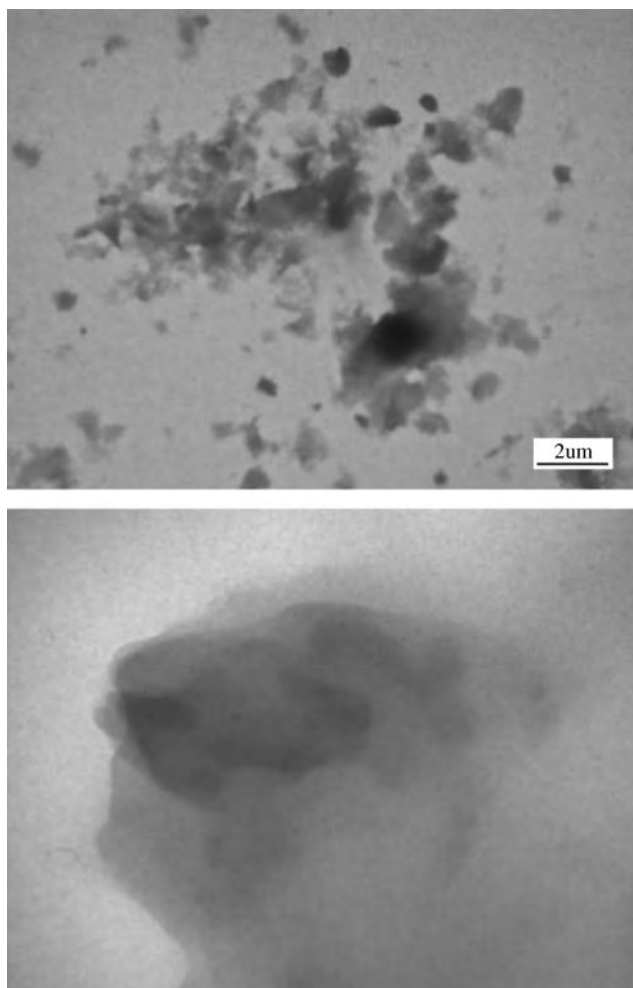


Fig. 2.43. TEM morphology of NPP01. (NPP: silica wrapped inside the polyester matrix under melt compounding at temperatures of 240–260°C).

2.5.2. Oligomer–silicate mixtures

2.5.2.1. The particle exfoliation beyond the steric effect

The transformation of submicron particles into nanoparticles is an interesting phenomenon when dispersing NPP in PET. In the dispersing process, the NPP's particle size becomes smaller and smaller by blending or polymerizing with PET matrix. This dispersion phenomenon goes beyond the steric effect, and it is in fact a creative point and a great progress in nanocomposites, particles in NPP are specially designed in an intercalated state shown in Figure 2.45.

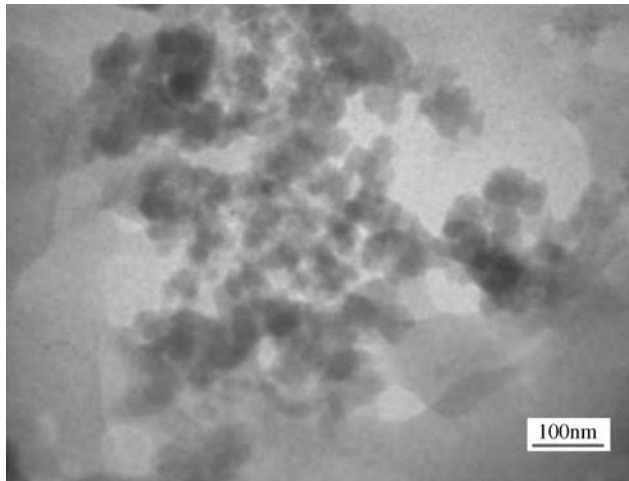


Fig. 2.44. TEM morphology of NPP01 (813 K). (NPP: silica wrapped inside the polyester matrix under melt compounding at temperatures of 240–26°C).

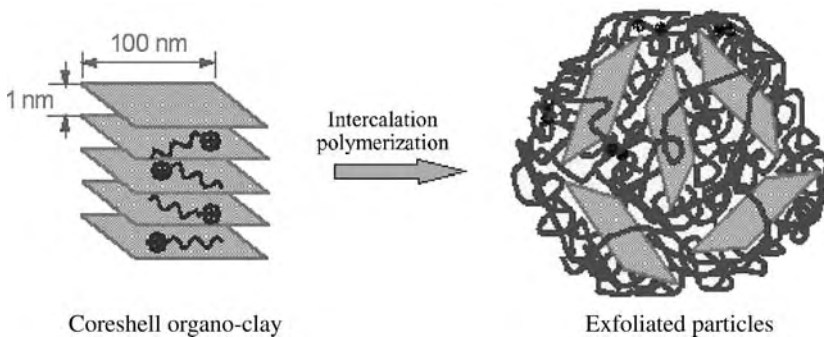


Fig. 2.45. The submicron core-shell particles in NPP are exfoliated into nanoparticle layers in PET-based nanocomposites by an intercalation polymerization process.

In Figure 2.45, the parallel lines represent layered silicate, and the zigzag lines organic molecular chains. It is shown that core-shell particles in PET-based nanocomposites are further exfoliated into random layers with nanoscale size shown in Figure 2.46. In a large scale of particle dispersion, the obtained interlayer distance is 2–3 nm, which is 2–3 times of the layered silicate basal space by WAXD (not shown).

The data in Figure 2.46 show that bright particles have diameters of 150 nm, which account for about 3% in number. Most of the superfine particles are percolated into nanoscale particles, forming a homogeneous dispersion. This type of particle dispersion morphology improves the polymer film's barrier properties as predicted [46,47].

Using SEM, it is not easy to observe the particle agglomeration morphology and thus, SEM may not reflect a complete description of particle inner structure. TEM,

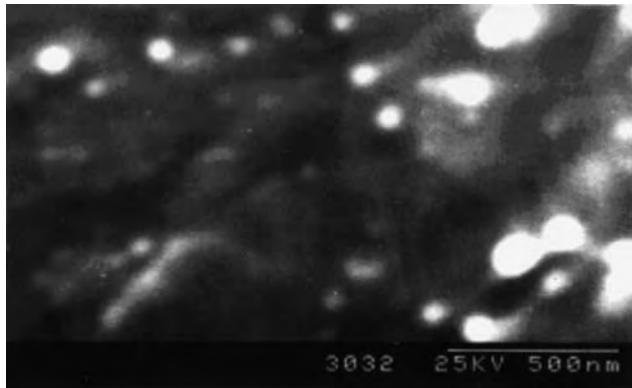


Fig. 2.46. The SEM morphology of superfine core-shell particles exfoliated by intercalation polymerization (load, 2.5% (by wt)).

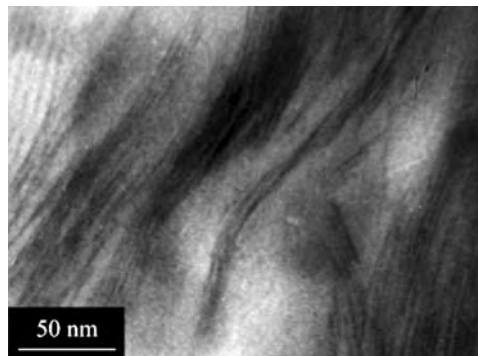


Fig. 2.47. The morphology of layered silicate particles in PET matrix with load 1% (by wt).

however, can give this morphology as shown in Figure 2.47. The TEM morphology of layered silicate-PET nanocomposite shows distorted fiber-like patterns (Figure 2.47(a), whose dispersion morphology makes a great contribution to reinforcements for the nanocomposites. In Figure 2.47, the agglomerated particles are seen and account for 3–4% by number.

2.5.3. *In situ polymerization in media*

Polyolefin-MMTs nanocomposites have been prepared by in situ polymerization in composite carriers such as MMTs-silica-MgCl₂. Such a composite carrier is a nanoparticle precursor, and its X-ray pattern is shown in Figure 2.48.

In in situ polymerization of polyethylene-MMTs nanocomposite, the samples are investigated by TEM, which show two kinds of morphologies (Figure 2.49). The first is the layer structure of MMTs, the second is spherulite-like materials, which is possibly

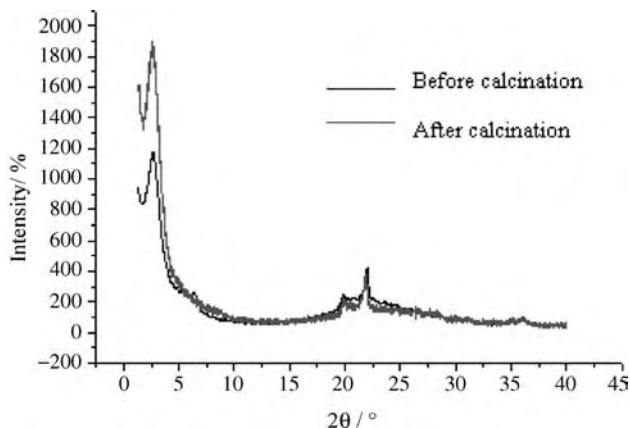


Fig. 2.48. X-ray pattern of composite carrier before and after calcinations.

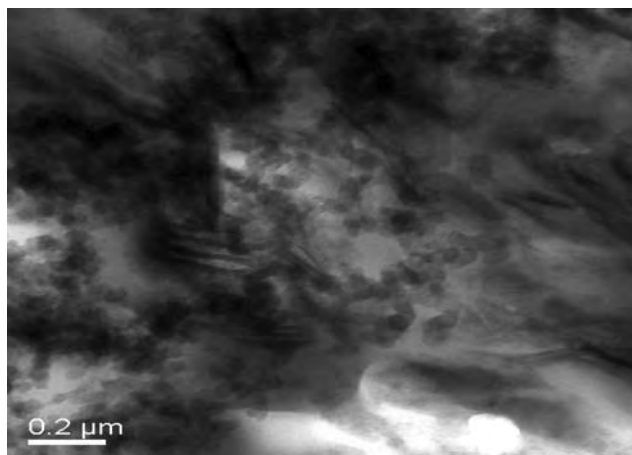


Fig. 2.49. TEM morphology of polyethylene-MMTs nanocomposites. Carriers are composites of MMTs, silica and magnesium chlorite.

silica from hydration of TEOS. In TEM morphology of the PE-based nanocomposites, the MMTs layers are seen to be dispersed in the PE matrix in a random state mixed with other materials (silica or MgCl_2). The layer structure is in a broken or exfoliated state. The SiO_2 particles also disperse randomly inside the layer gallery, and range in size from 60 to 100 nm the nanocomposites.

The finer structure of MMTs layer exfoliation is detected with layers completely exfoliated, but in a completely random but homogeneous state.

The exfoliation morphology of MMTs in the nanocomposites can be characterized by X-ray diffraction patterns. The characteristic peak of the d_{001} disappears completely in the X-ray pattern.

In the polyethylene–MMT nanocomposites, the inorganic phase plays a role in providing rigid and thermal stability, and scale stability which gives PE-based nanocomposites enhanced mechanical properties, high-temperature stability and resistance, and good abrasive aspects (see Figures 2.50 and 2.51).

2.5.4. Comparison of dispersion behavior in different precursors

2.5.4.1. Silica dispersion behavior in polymer melts

The shape or morphology of most of the prepared particles is not round, flat or pointed, but mixed. The particle size is also not homogeneous, as seen in the chain-like forms when the treated particles are polymerized in situ with polyester (Figure 2.52).

Silica with small size (10–30 nm) has been grown in PET melt matrix. The silica particles tend to be connected during their dispersion. Thus, the particle shapes are often irregular. Researchers have also prepared silica particles by a selection process, which produces silica particles with two kinds of surfaces: One is silica with smooth

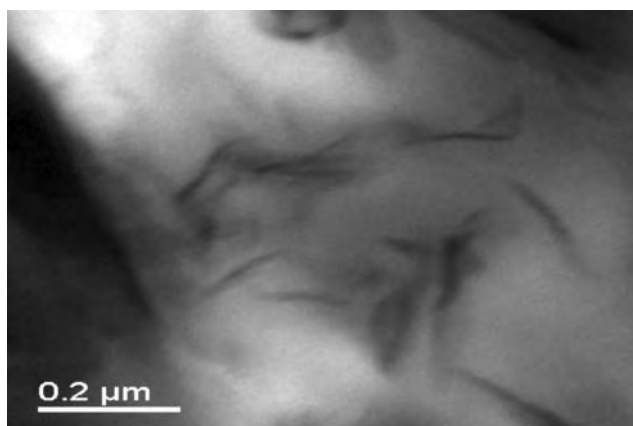


Fig. 2.50. TEM morphology of MMTs layer dispersion in polyethylene-MMT nanocomposites.

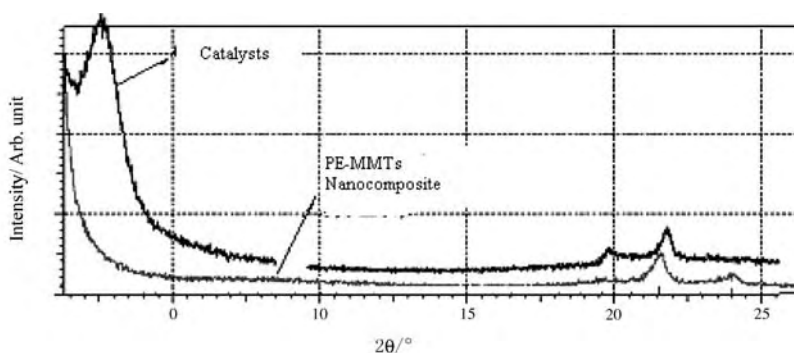


Fig. 2.51. X-ray patterns of polyethylene–MMT nanocomposites.

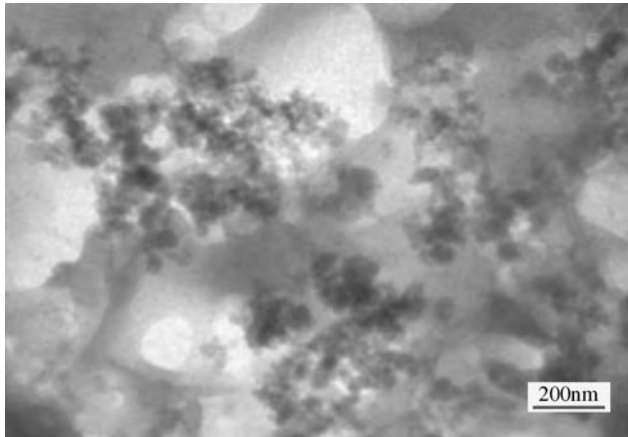


Fig. 2.52. The silica morphology dispersed in PET matrix by melting/blending.

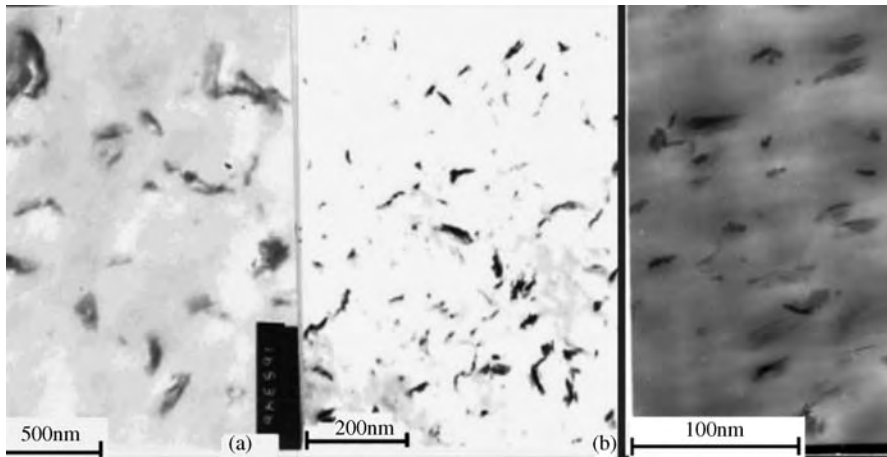


Fig. 2.53. The MMT particles exfoliated gradually from 500 to 200 to 100 nm.

surfaces, which is used for dispersion or suspension in solutions; the other is silica with porous surfaces, which serves as a template to prepare other kinds of particles, such as nanoparticles of Ni, Pd or Ag, etc. Whether silica has a smooth surface or is in a porous state, its dispersion in polyester melt is a process of accumulation or interconnecting.

2.5.4.2. Silicate dispersion behavior in polymer melts

MMTs dispersed in different stages during polyester polymerization will have particle sizes ranging from 500 to below 200 or 100 nm (Figure 2.53). The layered silicate particles decrease in size during dispersion because of the existence of layer exfoliation or

nanoparticle precursor structure. The dispersion of MMTs in the polymer melt is completely different from silica dispersion behavior.

References

- [1] Y.C. Ke, Chin. Pat. Appl. 02153554.X, 2002.
- [2] J.Y. Li, Colloidal Chemistry, Press of Petroleum Industry, Beijing, 1982.
- [3] J.N. Yan, Drilling Fluid Technology, Press of Petroleum Industry, Beijing, 2002.
- [4] Y.C. Ke, Masters Degree Dissertation, Jilin University, Changchun City, China, 1991.
- [5] Z.Q. Yu, Y.C. Wang, Fine Particle Dispersion in Liquid Media, Press of the Petrochemical Industry, Beijing, 1991.
- [6] S.C. Lu, Powder Processing Technology, second ed., China Light Industry Press, Beijing, 2000.
- [7] Y.C. Ke, T.B. Wu, C.J. Yan, China Particuol. 1 (2003) 247–252.
- [8] Y.C. Ke, T.B. Wu, PS-Silica Core–Shell Particles, Petroleum Science, 2 (2005) 70.
- [9] Y.C. Ke, Chin. Pat. Appl. 01131141.8, 2001.
- [10] M. Jiang, S.K. Fu, The Latest Topics of Polymer Science, Press of Fudan University, Shanghai, 1998.
- [11] Y.C. Ke, et al., J. Appl. Polym. Sci. 85 (2002) 2677–2691.
- [12] Y.C. Ke, et al., J. Appl. Polym. Sci. 71 (1999) 1139–1146.
- [13] Y.C. Ke, Polymer-Inorganic Nanocomposites, Press of Chemical Industry, Beijing, 2003.
- [14] Y.C. Ke, Nanostructure in nanocomposites, Symposium of Young Physicists of China, Shanghai, Vol. 10, 1999.
- [15] Z.N. Qi, Y.C. Ke, China Pat. ZL97104194.6.
- [16] Z.N. Qi, Y.C. Ke, CN 1187506A, 1998/07.
- [17] Y.C. Ke, et al., J. Appl. Polym. Sci. 71 (1999) 1139.
- [18] Y.C. Ke, C.F. Zhu, Z.B. Yang, J. Appl. Polym. Sci. 85 (2002) 2677–2691.
- [19] Y.C. Ke, Chin. Pat. Appl. 200410077924.8 (2004).
- [20] P. Dong, Prog. Nat. Sci. 10 (2000) 575.
- [21] P. Dong, et al., Adv. Mater. 13 (2001) 437.
- [22] I.I. Tarhan, G.H. Watson, Phys. Rev. Lett. 76 (1996) 315.
- [23] H. Míguez, F. Meseguer, C. Lopez, A. Mifsud, J.S. Moya, L. Vazquez, Langmuir 13 (1997) 6009.
- [24] T.B. Wu, Y.C. Ke, Acta Polymerica Sinica, 2005 (in press).
- [25] K. Busch, S. John, Phys. Rev. Lett. 83 (1999) 967.
- [26] Y.A. Vlasov, V.N. Astrolov, O.Z. Astratov, A.A. Kaplynanski, V.N. Bogomolov, A.V. Prokofiev, Phys. Rev. B 55 (1997) R13357.
- [27] D. Mei, P. Dong, H. Li, B. Cheng, D. Zhang, Chin. Phys. Lett. 15 (1998) 21.
- [28] B. Gates, D. Qin, Y. Xia, Adv. Mater. 11 (1999) 466.
- [29] L.V. Woodcock, Nature 385 (1997) 141.
- [30] A.A. Zakhidov, R.H. Baughman, Z. Iqbal, C. Cui, I. Khayrullin, S.O. Dantas, J. Marti, V.G. Ralchenko, Science 282 (1998) 897.
- [31] J.E.G.J. Wijnhoven, W.L. Vos, Science 281 (1998) 802.
- [32] A. Rechel, N.P. Johnson, D.W. McComb, Appl. Phys. Lett. 76 (2000) 14.
- [33] G. Subramania, K. Constant, R. Bisway, M.M. Sigalas, K.M. Ho, Appl. Phys. Lett. 74 (1999) 3933.
- [34] K. Busch, S. John, Phys. Rev. E 58 (1998) 3896.
- [35] B. Cheng, P. Ni, C. Jin, Z. Li, D. Zhang, P. Dong, X. Guo, Opt. Commun. 170 (1999) 41.
- [36] P. Dong, Acta Physico-Chim. Sin. 14 (1998) 109.
- [37] R. Zhao, P. Dong, W. Liang, Acta Physico-Chim. Sin. 11 (1995) 612.
- [38] S. Chen, P. Dong, G. Yang, J. Yang, Ind. Eng. Chem. Res. 35 (1996) 4487.
- [39] Y.C. Ke, Chin. J. Chem. Eng. 11 (2003), 701–708.
- [40] (a) S. Chen, P. Dong, G. Yang, J. Colloid Interface Sci. 189 (1997) 268; (b) S. Chen, P. Dong, G. Yang, J. Colloid Interface Sci. 180 (1996) 273.
- [41] Q. Li, et al., Colloids Surf. A: Physicochem. Eng. Aspects 1 (2002) 62.
- [42] Y.H. Wang, Graduate Thesis, University of Petroleum, Beijing, China, 2004, p. 6.

- [43] T.B. Wu, Y.C. Ke, Y.H. Wang, A proceedings of Symposium by China Material Research Society, Nov. 22–26 (2004), Beijing (www.c-mrs.org.cn)
- [44] L.V. Woodcock, *Nature* 385 (1997) 141.
- [45] (a) Y.C. Ke, China Pat. Appl. 02153554.X; (b) Y.C. Ke, *Polymer-Inorganic Nanocomposites*, Chemical Industry, Beijing, 2003, p. 1.
- [46] Z.N. Qi, Y.C. Ke, *Proceedings on the Industrialization of Polymer-Inorganic Nanocomposites*, Railway Buildings, Beijing, 2004, p. 3.
- [47] Y.C. Ke, *Reports to the Meeting of the China National Petroleum Co.*, Beijing, 2004, p.8.
- [48] L. Liu, Z.N. Qi, X. Zhu, *J. Appl. Polym. Sci.* 71 (1999) 1133.
- [49] G.M. Chen, Q. Li, Z.N. Qi, F.S. Wang, *Chin. Polym. Rapid. Bull.* 4 (1999) 1.
- [50] B. Hoffman, C. Dietich, R. Thomann, C. Fredrich, R. Mulhaupt, *Macromol. Rapid Commun.* 21 (2000) 57.
- [51] Z.N. Qi, Q. Li, Y. Zhou, CN139643.6,03, 1996.
- [52] R.A. Vaia, H. Ishii, E.P. Giannelis, *Chem. Mater.* 5 (1993) 1694.
- [53] R.A. Vaia, S. Vasudevan, W. Krawiec, L.G. Scanlon, E.P. Giannelis, *Adv. Mater.* 8(1) (1996) 29.
- [54] (a) Z.N. Qi, F.S. Wang, Y.M. Ma, China Pat. Appl. 98103038.6, 1998/10; (b) Z.N. Qi, F.S. Wang, Y.M. Ma, China Pat. Appl. 98103041.6, 1998/10.
- [55] Z.N. Qi, Y.C. Ke, Y.Z. Zhou, *Chin. Pat. Appl.* 97104055.9.
- [56] Z.N. Qi, Y.C. Ke, Y.Z. Zhou, *Chin. Pat. Appl.* 97104196.4.
- [57] Y.C. Ke, Z.N. Qi, C.F. Long, *J. Appl. Polym. Sci.* 71 (1999) 1139.
- [58] Y.C. Ke, C.F. Long, *Internatational Symposium on Polymer Physics*, November 25–29, Guilin City, China, 1997, p. 158.
- [59] Y.C. Ke, Z.B. Yang, C.F. Zhu, *J. Appl. Polym. Sci.* 85(13) (2002) 2677–2691.
- [60] H.J. Choi, S.G. Kim, Y.H. Hyun, M.S. Jhon, *Macromol. Rapid Commun.* 22 (2001) 320.
- [61] J.K. Lu, Y.C. Ke, X. S. Yi, Z.N. Qi, *J. Polym. Sci. Part B: Polym. Phys.* 39 (2001) 115.
- [62] J.K. Lu, Y.C. Ke, Z.N. Qi, *Chin. J. Polym. Sci.* 1 (2000) 85.
- [63] N. Ogawa, G. Jimenez, H. Kawai, T. Ogiwara, *J. Polym. Sci. Part B: Polym. Phys.* 35 (1997) 389.
- [64] Y. Kojima, A. Okada, *J. Appl. Polym. Sci. Part B: Polym. Phys.* 32 (1994) 625.
- [65] T.M. Wu, C.S. Liao, *Macromol. Chem. Phys.* 201 (2000) 2820.
- [66] Z.N. Qi, Q. Li, Z.D. Zhao, China Pat. ZL 96105362.3, 1996.
- [67] Y. Kojima, A. Usuki, *J. Polym. Sci. Part A: Polym. Chem.* 31 (1993) 1755.
- [68] (a) Z.N. Qi, Y.C. Ke, Q. Li, China Pat. ZL 97104055.9, 1997 (b) Z.N. Qi, Y.C. Ke, Y.K. Ding, China Pat. CN1187506A, 1998.
- [69] Y.C. Ke, China Pat. Appl. 02157993 (2002).

CHAPTER 3

Polymer-Layered Silicate and Silica Nanocomposites

OUTLINE

- Introduction 120
- 3.1. PA-silicate nanocomposites 120
 - 3.1.1. PA6, PA66 and PA11 120
 - 3.1.2. Preparations 124
- 3.2. PEO-silicate nanocomposites 135
 - 3.2.1. PEO oligomer 136
 - 3.2.2. Layered silicate (clay)-epoxy nanocomposites 140
 - 3.2.3. PEO-clay nanocomposite and layer exfoliation 141
 - 3.2.4. The properties of PEO-clay nanocomposites 154
- 3.3. Polyolefin-silicate nanocomposite 155
 - 3.3.1. PP-inorganic nanocomposites 155
 - 3.3.2. PE-inorganic nanocomposites 162
 - 3.3.3. Preparation and properties of polystyrene-inorganic nanocomposites 167
- 3.4. Polyester-silicate nanocomposite 172
 - 3.4.1. Polyester-clay nanocomposites preparation 173
 - 3.4.2. PBT-clay nanocomposite preparations 182
- 3.5. Polyaniline-silicate nanocomposites 190
 - 3.5.1. PAN and its conductivity 190
 - 3.5.2. Preparation and polymerization of PAN 192
- 3.6. Other kinds of polymer-inorganic nanocomposites 197
 - 3.6.1. PMMA-based nanocomposites 197
 - 3.6.2. Polyimides-based nanocomposites 198
- 3.7. Polymer-silica nanocomposites 201
 - 3.7.1. Assembly and self-assembly 202
 - 3.7.2. Fabrication of SiO₂ opals from colloidal SiO₂ submicrospheres 202
 - 3.7.3. Properties and products 204
- References 206

In this chapter, the preparation and properties of different polymer-layered silicate (silica) nanocomposites are presented.

Introduction

Polyamide is one of the earliest industrial polymers (invented in the 1930s by Caruthers) and also one of the earliest engineering plastics. In the application to products such as films and barrier packaging, polyamide's disadvantages of easily absorbing water, its low modulus and low flexibility need to be solved. Nanocomposite technology is used in the different modifications of polyamide resins. An example is the work from the Toyota Research Laboratory since 1989 on polyamide 6–clay hybrids [1]. At present, PA6–clay nanocomposites are prepared by Amoco, Sinopec (China) and CNPC (China). Results show that the PA6–clay nanocomposite heat distortion temperature (HDT) is enhanced from 140 to 165°C compared to that of 65°C of PA6.

We developed polymer–clay nanocomposites including poly(ethylene terephthalate)–clay (silica) nanocomposites, poly(butylene terephthalate)–clay (silica) nanocomposites, polystyrene–clay (silica) nanocomposites, polyaniline–clay nanocomposites and poly(methyl methyl acrylate)–clay (silica) nanocomposites. Most of them are successful in improving the mechanical, thermal and functional properties. Many nanocomposites have their thermal properties increased at 20–100°C compared to the pure matrix, the barrier properties to gas are lowered from one-third to one-sixth, and the modulus is enhanced 2–10 times compared to the pure polymer matrix. Polyolefin–inorganic composites are not only prepared through melting the organo-clay with polymer matrix but they are also prepared through in situ polymerizations. In the nanocomposites, only 1–10% (by wt) of the inorganic-phase material in the polymer matrix produces improved properties. The properties are obtained without the need to change traditional industrial production technology. Many attempts have been made to apply the nanocomposites to other areas such as barrier, functional and electronics materials. For example, polyimide–clay nanocomposite film is used in microelectronic circuits [2] because of its low linear expansion coefficient.

3.1. PA-silicate nanocomposites

The commercial name of polyamide is nylon. As a thermoplastic, it has developed into diverse types such as PA6, PA66, PA610, PA612, PA1010, PA11, PA12 and PA1414. China has been consuming more and more polyamides since 1998. The consuming share percentage for polyamide in different fields is plotted in Figure 3.1. Polyamide materials for appliances, communications and machinery account for 70% (by wt).

3.1.1. PA6, PA66 and PA11

PA6 and PA66 are the most important types of nylon, accounting for 90% (by wt) of the total yield of polyamide polymers. PA66 is mainly produced in the United States, while PA6 and PA1010 are mainly produced in Western Europe and in China, respectively. [Shenma Co., (Pindingshan, Henan province) produces most of the PA1010, and Liaoyang Petrochemical (CNPC) produces most of the PA1010]. However, the yields of nylons are unable to meet the demand. Some of polyamides, including PA11, rely on

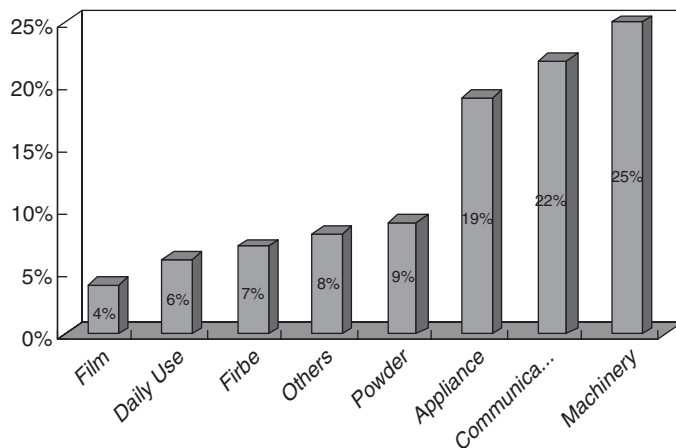
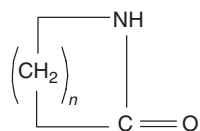


Fig. 3.1. Percentage of polyamide used in products.

imports from other countries. This book deals mainly with polyamide (PA6, PA66 and PA11)–inorganic (MMTs, silica) nanocomposites. PA6- or PA66–inorganic nanocomposites are used for engineering plastic materials, while PA11 is used for functional material.

3.1.1.1. Monomers of polyamides

3.1.1.1.1. There are several nylon monomers [3–4], including caprolactam, amino acids, alkyl(benzyl) diamine and alkyl(benzyl) di-acid. Caprolactam has the molecular formula



Several monomers used in the preparation of polyamide–inorganic nanocomposites are shown in Table 3.1.

Amino acids are another series of monomers for polyamide, and their molecular formulae can be represented as



PA11 made from ω -amino-11-carbon acid has a melting point of 185°C and a density of 1.1 g cm⁻³. The most widely applied polyamides are produced with diamide and diacid monomers. These monomers have their molecular structure as follows:



Table 3.1
Monomers of polyamide and their properties

Polyamide (PA _m) ^a	Monomers		Properties of polyamides			
	Monomer type	T _{mm} (°C)	T _m (°C)	Density (g cm ⁻³)	Humidity rate	
					RH=65%/20°C	RH=100%/20°C
PA4	Butylene lactam	24.5	260	1.22–1.24	9.1	28
PA6	Caprolactam	69	223	1.14–1.16	4.3–4.7	9.5–11
PA7	Heptane lactam	25	233	1.10	2.6–2.8	5.0
PA8	Octane lactam	71–72	200	1.08	1.7–1.8	3.9–4.2
PA9	Nonane lactam	—	209	1.06	1.45–1.5	2.5–3.3
PA10	Decane lactam	128–135	188	—	1.25–1.4	1.9
PA11	Undecane lactam	155.6	190	1.04	1.2–1.3	1.8–2.8
PA12	Dodecane lactam	153–154	179	1.03	1.3	1.5–2.7

^am = n (carbon number in caprolactam); T_{mm}, the melting point of monomer; RH, relative humidity.

Table 3.2
Polyamides from diamine and diacid based on fatty acid and the amine family and their properties

Carbon number in PA unit (PA _{mn})	Monomers	T _m (°C)
PA610	Hexane diamide/decane diacid	209
PA66	Hexane diamide/hexane diacid	251
PA86	Octane diamine/hexane diacid	235
PA810	Octane diamine/decane diacid	197
PA102	Decane diamine/ethane diacid	229
PA1010 ^a	Decane diamine/decane diacid	194

Note: m, carbon number of diamine monomers; n, carbon number of diacid monomers [3–5].

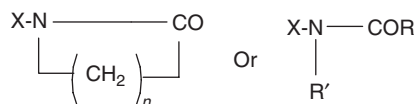
^afirst industrially produced in China.

Some of the polymers from these monomers are shown in Table 3.2 for reference. The industrial polyamides have been developed into different types of nylon: nylon1010, nylon66 and nylon11 [6–8].

3.1.1.2. The catalysts and additives for polyamides

(1) *Catalysts*. Both base catalysts and acid catalysts are used for ring-opening polymerizations of caprolactam. Under the base catalyst, the caprolactam anion forms a catalyst center, the reagents for which are metals of Na, NaH, Na(RO), NaOH and Na₂CO₃. Acid catalysts contain 6-aminohexane acid, lauryl amino acid or amino acid with carbon numbers 4–19.

(2) *Additives for catalysts*. Some additives can stimulate the effectiveness of the catalysts. These additives include two types; the first type has molecular structures as follows:



where X is a polar group, e.g., X is $-C=O$ or $-COCl$, etc. The second type of additives are diverse, some of which have their molecular structure as follows:

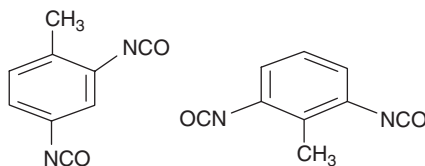
(a) Acetyl caprolactam



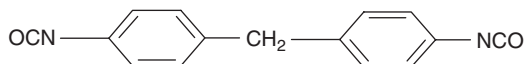
(b) Hexamethylene diisocyanate (HDI)



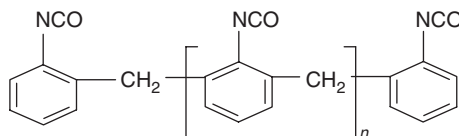
(c) (2,4/2,6)Diisocyanatoluene (2,4-TDI/2,6-TDI)



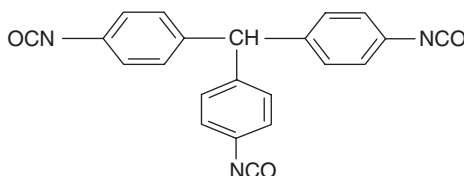
(d) Diphenylmethane-4,4'-diisocyanate (MDI)



(e) Polymethylene polyphenylene polyisocyanate (PAPI)



(f) Tritanetriisocyanate

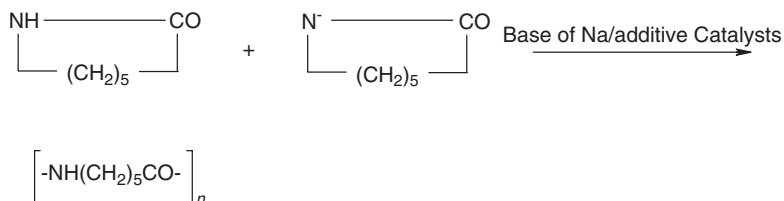


In the preparation of polyamide-based nanocomposites, amino acids and dihexanoic acid are also used.

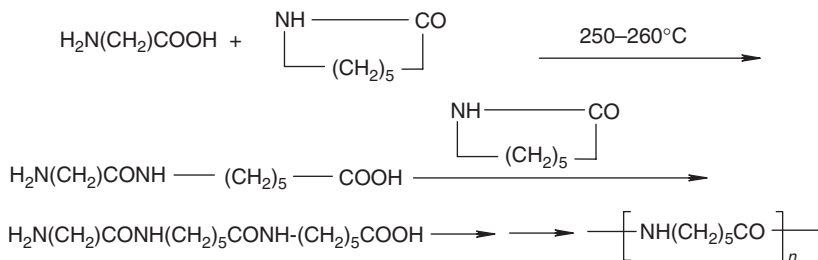
3.1.2. Preparations

3.1.2.1. Polymerization of polyamide and its nanocomposites

(1) *Polymerization process.* In the preparation of nylon6, the base amino acid catalysts are used while the monomers are either amino or caprolactam monomers. The base catalysis process for PA6 is



Before polymerization starts, a strong base is used to prepare the salt of caprolactam monomers, as the catalyst. The metal of sodium reacts with caprolactam to form an anion as the catalyst center in the preparation of nylon6. If an acid catalyst is used, the polymerization process is different from the previous one and is shown below:



where the amino acid of $\text{H}_2\text{N(CH}_2\text{)}_5\text{COOH}$ acts as a catalyst. The catalyst opens the ring of caprolactam monomers producing the active center for further condensation reaction.

(2) *Preparation of PA6-MMTs nanocomposites.* The polymerization process of nylon6 is suitable for the preparation of PA6-MMTs nanocomposites. The difference between the preparation of PA6 and its nanocomposites is that the latter needs treatment of the inorganic phase, prohibiting the oxidation reaction and loading the related inhibitor, thus slightly modifying the preparation. Considering these factors, we recommend using the acid catalyst process, its components are given in Table 3.3 for PA6-MMTs nanocomposites.

Similarly, the components of the raw materials and the loads in base catalyst for the preparation of PA6-MMTs nanocomposites are shown in Table 3.4.

The quality of MMTs should meet the following requirements: the content of both ferric compound and dissociated sand in the MMTs should be below 500 ppm. Thus, 85–93% (by wt) MMTs in the clay are selected as the inorganic phase. The MMTs are known as “polymerization-grade MMTs,” which means that they have the required

Table 3.3
Components of raw materials and content in acid catalyst for the preparation of PA6-MMTs nanocomposites

Component	Load share by weight
Monomers	100.0
MMTs	0.05–60 (0.5–10)
Acid catalyst	0.01–20 (0.1–2)
Disperse media	1–1,200 (10–15)
Protonization agent	0.001–1.0 (0.1–0.5)
Additive	0.05–5

Note: The data within parentheses are preferred.

Table 3.4
Components of raw materials and loads in base catalyst for the preparation of PA6-MMTs nanocomposites

Components	Load share by weight
Monomers	100
MMTs	0.05–60
Base catalyst	0.01–20
Disperse media	1–1200
Organic cation reagent	0.001–1.0
Inorganic base	0.01–10
Additives	0.05–5

quality standards for preparation of gels and are suitable for polymerization with monomers. In practice, MMTs with CEC of 50–200 mmol (100 g)⁻¹ are selected.

The advantages of the preparation of PA-MMTs nanocomposites relies on the fact that the monomer itself is suitable for the preparation of the quaternary salt through reaction with protonated reagents such as phosphorous salt, chloric acid, sulfuric acid or acetic acid. The salt is then directly applied to treat the MMTs and take part in the polymerization reaction. There are many additives for polyamide such as chain extenders of hexane diamine, or nucleation reagents of phosphoric acid and phosphoric salts.

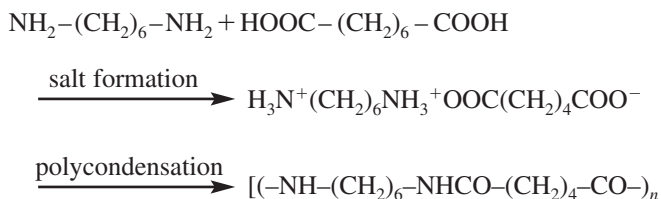
Example 3.1.2.1. Preparation of nylon6-MMTs nanocomposites. First, 0.05–60 parts of MMTs with cation exchange capacity (CEC) of 50–200 mmol (100 g)⁻¹ are dispersed into 1–1000 parts of dispersion media with vigorous stirring to form a stable suspending system. Then, 100 parts of caprolactam monomers are dispersed in the solution composed of 5–200 parts of media and 0.001–1 parts of protonation reagents. This solution is mixed with a clay-suspending solution, forming a colloidal system through vigorous stirring. In the stable colloidal system, the cation exchange reactions are carried out. Finally, 0.01–20 parts of 6-aminohexane acid and 0.05–5 parts of hexane diamine are dissolved in the colloidal solution. After vacuum-drying, until the water content of the reactive system is < 0.5% (by wt) the temperature increases to 250–260°C during polymerization for 6–10 h to give the final product. In this example, after the layer interdistance is increased through intercalating the MMTs, the nylon6 monomers are introduced into the layer space. Then,

the monomers polymerize inside the layer gallery of MMTs. Such a polymerization method is called a one-step method, or an in situ intercalation polymerization method. The treatment of the MMTs through a cation exchange reaction, the polyamide monomer intercalation and polymerization or copolymerization is completed in the same reactor. Finally, the product is obtained. In the product, the layers from MMTs disperse into the polyamide matrix by coulombic forces. A special process for the preparation of nanocomposites of nylon6–MMTs is given in Example 3.1.2.2.

Example 3.1.2.2. Preparation of nylon6–MMTs nanocomposites. MMTs (3 g) with CEC of 100 mmol (100 g)⁻¹ are dispersed in 100 g water, stirred vigorously for 0.5 h after dipping in water, then stored for 24 h giving the dispersion solution A. Then 100 g of caprolactam and 0.3 g of phosphorous acid are added to 20 g of water, allowing the temperature to increase to 80°C while stirring to form a homogeneous protonated solution of B. While stirring solution A, solution B is added to A while maintaining the mixture at a temperature of 80°C for 0.5 h; then this mixture is dewatered under reduced pressure to a temperature of 135°C, at which point the mixture has a water content less than 0.5% (by wt). To this mixture, 13 g of 6-aminohexal acid and 0.18 g of hexane diacid are added while stirring, gradually raising the temperature to 250°C and the mixture is polymerized for 6 h. This final mixture is extruded under pressure, smashed mechanically, washed with hot water and dried to obtain the composites.

3.1.2.2. Preparation of nylon66–clay of MMTs nanocomposites

(1) *Polymerization of nylon66.* Nylon66 is prepared from the reaction of hexane diamine and hexane diacid in two steps; salt formation and polycondensation:



The polycondensation of diamine and diacid is carried out by dissolving them in a solvent such as methanol at 180–300°C. The water produced from the reaction is continuously removed. However, this reaction usually gives a product with poor color. Diamine and diacid will form equimolar nylon66 salts through the primary reaction. In practice, the produced salts are separated from the reaction system to be applied to the polycondensation process. The preparation of nylon66 salts is aimed at disposing of the impurities from the original monomers. The factors that influence nylon66 polymerization are well recognized. The following are few other factors governing the preparation of the nylon66–inorganic nanocomposites.

- (a) *The preparation of salt of hexane diamine and hexane diacid.* In the preparation of the mixture salt, the pH value should be controlled at 6.7–7.2.
- (b) *The precipitation of nylon66 salt.* The salt of nylon66 is precipitated from the solvent of the ethanol and methanol, during which the reaction system should be

- controlled in order for it not to boil violently and cause unnecessary loss. The salt can be collected through centrifugal filtration (it does not need drying).
- (c) *Polycondensation and the extrusion and cutting of the melt into strips and pellets.* In polycondensation of nylon66, 0.9% (by wt) of hexane diacid (or acetic acid) is added to the reaction system, acting as capping reagent. The reactive pressure, that is, loading pressure at first stage is controlled, while water is removed during the latter stage.
- (d) *The control of drying.* The system dries at 200°C for 3 h. The discoloring probably occurs at the drying stage and must be avoided.

The preparation of nylon66 can be classified into the continuous method and the step-in-step method (or the discontinuous method). The step-in-step preparation method for nylon66 has been described [8]. Nylon66 salts, reagents for modulating molecular weight and stabilization reagents of phosphorous triphenyl ester, are mixed in a high-pressure autoclave, which is cleaned with a highly pure nitrogen gas. Usually, this reactor begins the polycondensation reaction through heating, the temperature increases up to 260–265°C and the autoclave pressure reaches 1.6–1.7 Mpa, while maintaining the pressure constant, disposing moisture and continuing to raise the temperature up to 270–275°C. Then, at temperatures of 270–275°C within 1 h, the pressure at the reaction system reduces to the normal level, and thus loads a vacuum to remove water and enhance the molecular weight. The dewatering time lasts 3–4 h, and the pellets are then collected through a cutter.

The polycondensation reaction of nylon66 has been reported [9,10]. A secondary reaction has been noticed, and the corresponding the active energy is 22 kcal mol⁻¹. The reactive rate constants of nylon66 increase with increase in temperature but become decrease as the water concentration increases. The reaction rate constants decrease rapidly as the water concentration increases as can be seen in Table 3.5.

This implies that in the preparation of the nylon66–MMT nanocomposites, the water in the gel of nanomaterials is controlled before being added to the nylon66 monomer mixtures to ensure the high molecular weight of nylon66. The flowchart for the continuous method for nylon66 [11,12], is shown in Figure 3.2.

Example 3.1.2.3. The general preparation process of nylon66. An aqueous solution of nylon66 salt (100 kg) 50–60%, (by wt) is solved in pot 1; then 0.5% (by wt) of hexane

Table 3.5
Dependence of the reaction rate constant of polycondensation of nylon66 in water medium on the water content

Water concentration (mol mol ⁻¹)	Reactive rate constant (g mol ⁻¹ h)	
	< 220°C	220°C
0.5	1000	2620
1.0	825	2200
3.8	390	1020
6.25	195	510
10.0	–	395

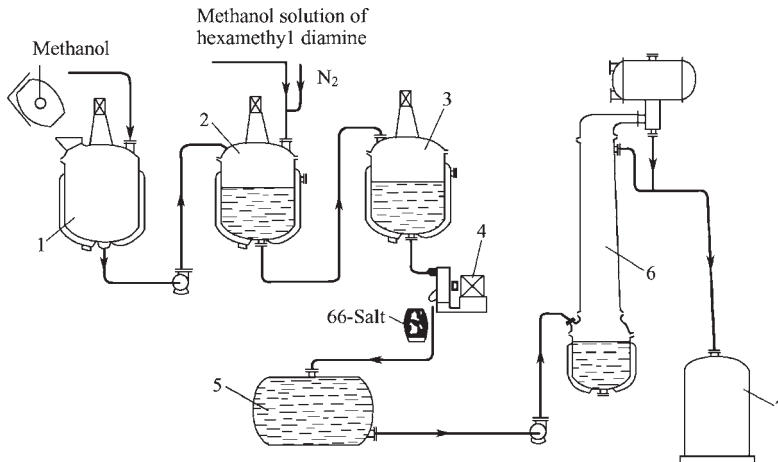


Fig. 3.2. The flowchart of our pilot plant for continuous polycondensation of nylon66: 1 – tank for hexamethyl diacid, 2 – Sedimentation tank, 3 – intermediate tank, 4 – Centrifugal machine, 5 – parent solution tank, 6 – distilled tower for methanol, 7 – tank for pure methanol.

diacid and 2% (by wt) of caprolactam (according to nylon66), are heated to 80–90°C, solved, and then compressed into a store tank by filtration. Through unit 4, the reaction material in the store tank is compressed into pipeline 6 at a temperature of 210–215°C. These materials are conveyed continuously from pipeline 6 into pipelines 7 and 8; meanwhile, the temperature continues to rise while the water is discharged from pipeline 9. The concentration of nylon66 also increases, and begins to pre-condensate with system pressure at 1.8 MPa. The reaction material enters from the horizontal pipeline into pipeline 9 with its central temperature reaching 225°C, and is then conveyed quantitatively from pressure reducing pump 10 to the evaporation device 11. The materials may stay in the evaporation machine for 3–5 s and the pressure is reduced from 1.8 MPa to normal pressure. The temperature of the evaporation device is controlled at 285°C and continues to discharge water, which enters into a unit smashing bulb 12, and the water is discharged. The polymer product flows into post-condensation autoclave 13 in the form of a film with its temperature controlled at 275–280°C and reacts under the vacuum condition, during which the water is discharged in large amounts; these reaction takes place rapidly and reaches equilibrium after 30 min. The product polymer melt is discharged out from vertical pipeline 14 to be cut into pellets or to be made into silk directly. The whole pre-condensation time is controlled at 2–3 h and post-condensation time is controlled at 30–40 min.

(2) *Preparation of nylon66 nanocomposites.* The equipment for the preparation of nanocomposites of nylon66-MMTs has the following device and conditions. The 10 L of stainless pressure autoclave is attached with a vacuum and cooling system; the experimental materials use nylon66 salt (e.g., dry nylon66 salt from Liaoyang Petrochemical

Industry, Liaoning Province, China). Here, MMTs is a purified white clay, which acts as a precursor (e.g., white clay from Hebei Province, China). These materials are amorphous when they are exfoliated through an intercalated treatment and are in colloidal form.

Example 3.1.2.4. Preparation of nylon66–MMTs nanocomposites. Nanomaterials or nanoprecursors in an amorphous or colloidal state are mixed well and added to 10 L autoclave. Nylon66 salt (3.0 kg) is added together with the 1–4% (by wt) nanomaterial load (w/w) relative to nylon66 salt. The water of the system is discharged gradually from the autoclave while the temperature increases slowly. During heating and stirring, the mixtures are very easily oxidized, especially when the temperature increases up to 250°C or above, because the ferric component in the MMTs accelerates oxidation. Finally, the molecular weight of nylon66–MMTs nanocomposite reaches the required level.

Besides oxidation, there are other problems. The nanocomposites easily condense and clog the discharging pipelines or valves. Further, the molecular weight may not reach as high as desired. Optimization of the operating conditions and control of components of the reaction mixtures are necessary. Optimization may involve the control of the clay component, especially its iron content ($\text{FeO}/\text{Fe}_2\text{O}_3$) and the dissociate sand (or quartz) content and monomer load. The molecular weights of the nanocomposites can be controlled reasonably well although discoloring, due to partial oxidation, may occur. Oxidation can be controlled by the addition of antioxidants.

3.1.2.3. Physical and chemical properties of polyamide–MMTs nanocomposites

The factors affecting the molecular weight of polyamide are quite complicated, not only due to the introduction of MMTs, which introduce an obstacle to the polymerization, but also because the present technology cannot isolate the nanoparticles from the polyamide matrix. Therefore, irrespective of what the molecular weight is from the GPC or from the Ullman viscometer experiments, the measured molecular weight deviates from the true value due to the presence of the nanoparticles. A relative method is used to analyze the molecular weight of the nanocomposite and the end titration method is used to analyze the logarithm molecular weight. Considering 12-amino acid treatment or intercalating MMTs as an example, with the increase in MMTs treated by 12 amino acid, the number average molecular weight (M_n) of polyamide6 has a tendency to decrease. When the load of MMTs is lower than 5% (by wt), M_n of the nanocomposite reduces by relatively a small amount (for example, 4.0% MMT load produces an M_n of 10,000 dl g^{-1} ; 1.5% MMT load gives an M_n of 17,200 dl g^{-1}), but when the MMT load is over 5% the molecular weight decreases rapidly (for example, 6.8% (by wt) MMT load gives an M_n of 6,340 dl g^{-1} ; 13.0% (by wt) MMT load gives an M_n of 3,800). The trend is that 12-amino acid-treated MMTs reduce the molecular weight of nylon6. So, the introduction of MMTs into nylon6 for polymerization definitely produces some difficulties in polyamide polymerization.

Silica has a different effect on the two-step nylon66 polymerization from MMTs. MMT gel has a greater tendency to be an obstacle to nylon66 polymerization than silica gel at the nanoparticle scale.

Table 3.6
Effect of different protonated reagents on the nanocomposites

Protonated reagent	M_n (10^4)	Tensile modulus (Gpa)
H ₃ PO ₄	5.2	1.0
H ₂ SO ₄	3.3	0.9
HCl	3.0	0.9
HA _C	2.5	0.8

3.1.2.4. The effect of additives on the properties of nylon6–MMTs nanocomposites

Acting as protonated reagents for the intercalant, some acids such as phosphorous acid, chloric acid, sulfuric acid, acetic acid or their composite acids are usually used. Different protonated acid reagent also has some effect on the molecular weight and mechanical properties of nanocomposites (e.g., rigidity) as shown in Table 3.6. It is clearly seen that phosphorous acid [5,7] is the best protonated reagent.

(1) *The effect of protonated reagent.* Acidic protonated reagents have effects on the nanocomposites as shown in Table 3.6.

(2) *The effect of chain extender.* During polycondensation of nylon6, the addition of different amino acids and hexane diamine will exert different effects on the molecular weight of its nanocomposites and its distribution as shown in Table 3.7. It is seen that with an increase of hexane diamine to 0.44% (by wt) the nanocomposites have increased impact strength while maintaining a nearly constant heat distortion temperature.

The MMT load is limited in the preparation of the nanocomposites. As seen in Table 3.8, as the MMT load increases, the mechanical properties of the nanocomposites become crisp or fragile, and their heat distortion temperature increases gradually. These results are related to the filling effect of the inorganic particles.

(3) *The mechanical property relationship between clay type and nanocomposite.* There are many types of clay (see Chapter 1). To meet the needs of the intercalation reaction, a clay with high CEC, such as MMTs, synthetic mica, Li-MMTs, talc, sepiolite, etc, is chosen as an inorganic phase. In clays having a very low CEC value ($50 \text{ mmol (100 g)}^{-1}$), the CEC value has to be enhanced to $70\text{--}200 \text{ mmol (100 g)}^{-1}$ through a post-sodium exchange reaction. As for mica, it has too high a CEC to be a candidate for the preparation of nanocomposites. Mica can be modified, through a fluorite reaction, to synthetic mica to reduce the charges inside the layers to a suitable level. As for the talc, it has a low CEC or anions inside its layers and thus needs to be transformed into hydro-talc. In the preparation of nylon6–clay nanocomposites, the properties of the nanocomposites [7] depend on the clay, as shown in Table 3.9).

From Table 3.9, it is seen that nylon6–MMTs nanocomposites (NPA6) have higher impact properties than the others. Other clay minerals have unsatisfactory intercalation effects or only produce some simple composites or mixtures. The nylon6–clay composites have enhanced HDT from 65 to 152°C over the pure PA6. Obviously, the type of MMTs used has the most significant effect on the composites' HDT and is a factor influencing the nanoeffect.

Table 3.7

Properties of nanocomposites of nylon6–MMTs (NPA) using a chain extender reagent (weight ratio of MMTs to caprolactam is 5/100)

Hexane diamine ^a	Tensile strength (MPa)	Elongation at break (%)	Tensile modulus (GPa)	Tensile-impact strength (kJ m ⁻²)	HDT (°C) (18.6 Kg cm ⁻²)
0.0	79.0	29.0	1.0	63.0	148.0
0.30	80.0	34.0	1.1	90.0	148.0
0.44	80.0	35.0	1.1	113.0	150.0
0.58	82.0	23.0	1.1	68.0	146.0

^aThe chain extender reagent of hexane diamine is calculated relative to caprolactam, which has 100 parts; all samples have 5% (by wt) clay load.

Table 3.8

Mechanical properties of PA6–clay of MMTs nanocomposites (NPA)

MMT load (g)	Tensile strength (MPa)	Elongation at break (%)	Tensile modulus (GPa)	Tensile impact strength (KJ m ⁻²)	HDT (°C)
0	73	110	0.8	90	65
3	78	30	0.9	67	140
5	79	29	1.0	63	148
7	88	13	1.1	57	151
10	89	12	1.2	51	154
20	98	6	1.4	34	156

Table 3.9

Comparison of nylon6–clay nanocomposites and their mechanical properties^a

Types of clay	MMTs	SM	Li-MMTs	Talc	Sepiolite	None
Properties/nanocomposites	MMTs–Nylon6	SM–Nylon6	Li-MMTs–Nylon6	Talc–Nylon6	Saponite–Nylon6	Nylon6
Tensile strength (Mpa)	97.2	93.1	89.5	84.7	90.6	68.6
Tensile modulus (Gpa)	1.87	2.02	1.65	1.59	1.26	1.11
Elongation at break (%)	7.3	7.2	100	100	10.2	100
Charpy impact strength (KJ m ⁻²)	6.1	—	—	—	6.2	—
HDT (°C)	152	145	93	107	101	65

^a5% (by wt) clay load; SM, synthetic mica; Li-MMTs, MMTs with Li ion intercalated inside its layers.

(4) *The effect of intercalation method on nanocomposites.* Large-scale production of polyamide–MMT nanocomposites needs to be considered for reducing cost. Melt intercalation and composition methods are usually used. One method is to mix the organo-clay with melted polymer pellets in the extruder, which directly gives extruded products. In such nanocomposites, the nanoparticle phase forms with particle sizes smaller than 100 nm and is homogeneously dispersed in the nylon6 matrix. Table 3.10 gives the properties of nylon6–clay nanocomposites and industrial products using different intercalation methods.

Table 3.10
Properties of nylon6-clay nanocomposites and industrial products using different intercalation methods

Intercalation	Techniques	Polyamide-clay	Barrier performance NPA/PA	HDT NPA/PA (°C/°C)
Melt intercalation	RTP, USA	PA6-clay	1/3	160/65
	Honeywell	PA6-clay	1/3-1/4	160/65
	Unichika	PA6-clay	1/3	152/70
Polymerization intercalation	TOYOTA	PA6-clay	1/3	155/65

Note: NPA/PA is the ratio of the barrier properties of nylon6-based nanocomposite to polyamide; HDT, heat distortion temperature.

When MMTs are intercalated with caprolactam, the diffraction peaks in the nanocomposites generally reduce from 7° to 1.3° (2θ), while the corresponding interdistance of layers increases from 1.0 nm (1.26 nm) to 6.2 nm. The relatively low MMT load in the nanocomposite promotes the enlargement of the interdistance of the silicate layers inside the nanocomposites [6]. When the MMT load is $<10\%$ (by wt) with satisfactory intercalation, the diffraction peak of MMTs is not detected because of the layer exfoliation. The exfoliated layers disperse in the nylon6 matrixes, which is necessary for improved properties of nanocomposites of NPA6.

(5) *Property relationship between the intercalant and NPA6.* Investigations have shown that the chain length of the intercalant has an effect on the properties of NPA6 [6]. In fact, both the type and chain length of the intercalant have effects on the treatment of the MMTs and the properties of the final NPA6s. These effects are mainly seen in the layer exfoliation morphology and the final thermal performance of the nanocomposites. The effects of the intercalant type on the nanocomposites are described in this book.

Example 3.1.2.4. Intercalation reaction of different chain length intercalants. A 5% (by wt) Na-MMTs aqueous solution is stirred at 80°C , to which tridecane trimethyl bromide ammonia (TTBA) is added in chloric acid (HCl) solution (molar ratio of TTBA/HCl is 1:1). After 1 h, this solution is filtered and washed with water until no $\text{Cl}^{-\text{ion}}$ is detected (or no white precipitate material is detected by 0.1 N AgNO_3 solution). The final material is then vacuum-dried until its weight remains constant and is grounded into 500 μm powder. The ω -amino acid has the formula $\text{H}_2\text{N}(\text{CH}_2)_n\text{COOH}$. When $n < 7$, or $n > 10$, the molecular morphology inside the interlayer gallery takes either a horizontally arranged form or a slit angle to the layer direction. The morphology affects the layer exfoliation of MMTs. When an intercalant with a fixed carbon number is selected, the layer exfoliation morphology will be realized by enhancing the heating temperature. For example, when the temperature increases from 25 to 100°C , the interdistance of the layered silicate results from the same intercalant is varied. The increase in this layer interdistance implies that the more perfect exfoliation has been reached. The relationship of layer exfoliation and the intercalant carbon number is shown in Figure 3.3, which can be used as a reference in selecting an intercalant.

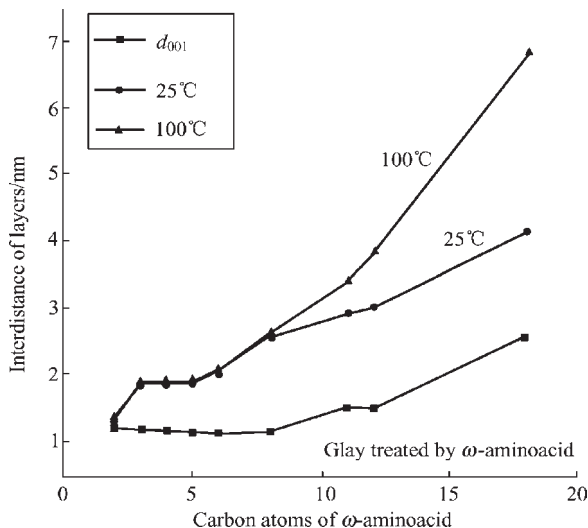


Fig. 3.3. Plot of layer exfoliation vs. intercalant carbon.

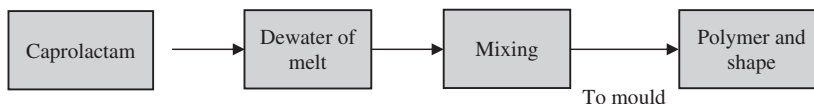


Fig. 3.4. Flowchart for casting and shaping caprolactam monomers.

3.1.2.5. Casting nylon

Casting nylon technology is a typical one under the base catalyst. Such technology requires that the nylon mixtures be directly cast into mold under normal pressure and take shape directly in the mold as shown in Figure 3.4.

Figure 3.4 shows the process in which caprolactam reacts with its sodium salt (melt dewater). By the addition of additives into the polymer melt, and direct entry into the mold, the product will be obtained. The equipment and flowchart for casting caprolactam monomers are shown in Figure 3.5. In the figure, caprolactam and additives enter directly into designed mold 8, which is active and replaceable. The products can take different shapes and are processed into different forms by means of sawing, abrasion, cutting, etc., similar to processing wood. The casting technology for nylon is suitable for the preparation of nylon6–MMT nanocomposites. The organo-MMTs are mixed with caprolactam monomers and polymerized before they entering the mold. They are directly cast into shapes and the products are processed, as is the casting nylon. Recently, a new kind of NPA6 nanocomposite film [5] was obtained whose barrier properties were improved 3–4 times that of the pure nylon6.

We have also made efforts to modify NPA6. Glass fibers are used to reinforce the nylon6-based nanocomposite. The modification of NPA6 has obvious advantages over the common glass- or mineral-reinforced nylon6 in that the former (NPA6) has lower specific gravity, better resistance to abrasion and superior composite performance compared to the latter. The NPA6 reinforced by glass fibers has applications in automobile parts, thermal-resistant engine parts, electronic parts, pipelines, etc. Some properties of the nanocomposites are seen in Table 3.11.

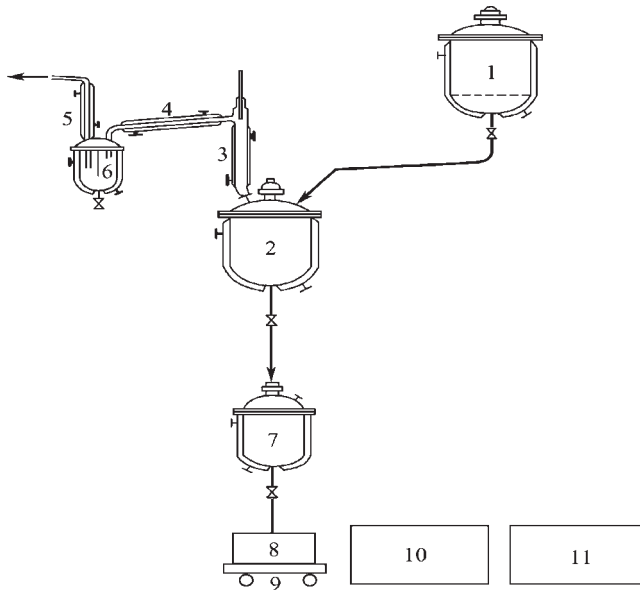


Fig. 3.5. Casting device and flowchart for caprolactam monomers. 1 – autoclave for melted monomers; 2 – dehydration autoclave; 3 – Circumfluence tube; 4 – heating tube; 5 – Condensation tube; 6 – Acceptor; 7 – Additive autoclave; 8 – mould; 9 – moving vehicle; 10 – heater; 11 – attenuator.

Table 3.11
Properties of nylon6–MMT nanocomposites

Measuring items	References	Sample names		
		NPA6-G10	NPA6-G20	NPA6-G30
Tensile strength (MPa)	GB/T-1040	123	164	190
Tensile modulus (GPa)	GB/T-1040	6.5	9.2	11.9
Elongation at break (%)	GB/T-1040	3.6	4	3.7
Bending strength (MPa)	GB8341	206	225	247
Bending modulus (GPa)	GB9341	5.1	7.5	10.2
Notched impact strength (J m ⁻¹) (IZOD 23°C)	GB1843	104	169	191
HDT (°C) (1.82 MPa)	GB1634	190	206	210
Melting point (°C)		220–230	220–230	220–230
Degradation temperature (°C)		469	453	448

3.1.2.6. Physical and chemical properties of nylon66-based nanocomposites

The physical and mechanical properties of some nylon66-layered silicate nanocomposites are characterized according to the ASTM or GB (China) standard. Some of the related standards are seen in Table 3.11, some others include the initial modulus standard of ASTM D-638, stretch ability standard of ASTM D-638, bending modulus and strength standard of ASTM D-790, impact strength standard of ASTM D-256, and hardness standard of ASTM D-65, etc; ASTM D-648 is used as a standard in measuring the HDT of the nanocomposites. The experimental results for the properties of nylon66–inorganic nanocomposites are listed in Table 3.12.

In the nylon66–MMT nanocomposites, the nanoparticle precursor (NPP) is used to disperse the larger particles into nanoparticles with a narrow particle size distribution. The NPP particles are designed and prepared according to the core–shell structure shown in Chapter 2. Although the molecular weight of nylon66 in the nylon66–MMT nanocomposites is difficult to control, because some residuals in the outlet valve easily form to clog up the pipeline, the problem can be solved using different NPP particle sources. So far, the physical-mechanical properties of the nylon66–MMT nanocomposites are the best and the nylon66–MMT nanocomposites can be produced on a large scale.

Different nylon11–inorganic nanocomposites can also be prepared. For example, the nylon11–BiI₃ nanocomposites are prepared through melt mixing with high-purity BiI₃ (purity 99.99%). The film sample is compressed at temperatures of 20–50°C above the melting point of nylon11. This nanocomposite has good electroconductive properties for X-ray sources. Nylon11–silica nanocomposites [10] (PA11/SiO₂) can be prepared and milled into special particles, which are used to coat aluminum plates as electroconductive materials. The nanocomposites form firm adhesive coatings.

3.2. PEO–silicate nanocomposites

Polyethylene oxide (PEO) or epoxy resin is one of the most common thermosetting materials. Its molecular chain is composed of a repeat unit of atomic oxygen and a

Table 3.12
Properties of nylon66-silicate and silica nanocomposites

Inorganic phase	None	Silica	Silica	Silica	MMTs
Inorganic load	0	1%	2%	3%	4%
Tensile strength (MPa)	80.00	121.0	141.1	129.0	109.0
Stretch rate (%)	29.0	12.1	18.4	13.5	11.2
Bending modulus (MPa)	2,810.0	3,106.0	3,810.0	3,257.3	3,005.0
Impact strength (Kg cm cm ⁻¹)	8.4	9.7	12.5	10.2	9.4
Hardness (D)	105.8	127.1	138.4	136.2	123.4
Molecular weight (mol g ⁻¹)	14,600	14,400	14,530	14,540	14,450
Melting point (°C)	251	261	264	262	258
Appearance	Transparent	Half-transparent	Half-transparent	Opaque	Half-transparent

Note: Test standards: tensile strength – ASTM D-638; initial modulus – ASTM D-638; stretch rate – ASTM D-638; bending strength – ASTM D-790; bending modulus – ASTM D-790; impact strength – ASTM D-256; hardness – ASTM D-65; HDT – ASTM D-648.

methylene group. It has been used to make sensors, integrated circuits and plastic sealing materials. The PEO properties are versatile because of the complicated curing technology. PEO has many advanced mechanical, dielectric and adhesive properties. Glass fiber, carbon fiber and other inorganic particles are often added to its matrix to reinforce its strength, rigidity, thermoresistance and barrier properties. Poor interfacial adhesion and particle agglomerations can be countered by surface treatment of the filler with coupling agents of silane or titanate ester. If the ideal interfacial property is realized, stress convergence and severe fracture does not occur.

PEO-MMT nanocomposites are useful for making epoxy. Because of the low molecular weight of epoxy resins, they are easy to mix with organo-clays, and are then cured, which is often the method used to prepare PEO-MMT nanocomposites. For high-molecular weight PEO (e.g. 10,000 g mol⁻¹), which is in powder form, it is first dissolved in order to mix it with organo-clay to prepare the nanocomposite after removing the solvent and followed by a curing process. The monomers of PEO (diphenol-A) are preliminarily mixed with clay, then the gas of phosgene (carbonyl chloride) is introduced to start polymerization, from which the final nanocomposites are obtained.

Exfoliated clay added to PEO is beneficial in improving its properties. The polymerization-curing reaction in PEO-MMT nanocomposites and the related structure-relationship properties are discussed in this chapter.

3.2.1. PEO oligomer

PEO is generally prepared by reacting bisphenol-A with chloro-epoxy propane in the presence of a catalyst of strong alkali. It is necessary to design the monomer ratio in the reaction such that one of the monomers is in excess of the other species. Generally, the chloro-epoxy propane is the material in excess because it is easy to distill from the reaction mixture.

The molar ratio of chloro-epoxy propane to bisphenol-A can reach 10/1 in the preparation of PEO oligomers (see Table 3.13). The number of epoxy groups in each PEO molecule rapidly decreases as the molecular weight of the epoxy resin increases. Based on this, the preparation of epoxy resin-clay nanocomposites also requires PEO oligomers for mixing with clay to form the mixture, in which the organo-clay treated with primary or quaternary ammonium salt acts as the curing agent.

3.2.1.1. Curing reagents for low-molecular weight epoxy resin

Epoxy monomer is stable under general conditions, e.g., bisphenol-A will not be cured at a temperature of 20°C. But its epoxy group on the chain has a high activation in the

Table 3.13
The properties of epoxy resin oligomer

Property	10/1	1.48/1	1.22/1
M_w^a	370	900	1,400
Epoxy equivalent value per 100 g	0.5	0.2	0.1
Soft point (°C)	9	69	98
No. epoxy group per molecule	1.85/1	1/2	1.44/3.7

^aWeight average molecular weight.

Table 3.14
Curing agents selected for epoxy resin–clay nanocomposites

Type of agent	Molecular structure	Examples	Features
Amine	Primary/secondary/tertiary amine, aromatic amine, unsaturated amine	Triethylamine, dimethyl benzo-methyl amine, di-ethylene triamine, triethylene tetraamine, <i>m</i> -phenylene diamine, di-ammonia diphenylene (methyl) 4,4'-diamine diphenyl methane (DDM)	Rapid curing, exothermal, cracking superior thermal product property
Acid anhydride	Maleic anhydride, benzo anhydride, other anhydrides	Maleic anhydride, phthalic anhydride, poly (nonyl di-anhydride), 2,3,5,6-benzene tetra formic anhydride, China wood oil anhydride (resin)	Slow curing with temperature, slow exothermal, tough product
Resin	Active end group of ammonia, hydroxyl (methyl) and carboxylate	Phenol formaldehyde resin, urea-formaldehyde resin, tri-polycyanamide formaldehyde resin, polyamide- <i>co</i> -dimaleic anhydride oligomer resin, or the intermediate	High-performance composites or nanocomposites

presence of curing reagents, which play a key role in determining the product properties, especially in the exfoliated-type (comparing to the intercalation-type) epoxy–clay nanocomposites. The curing reagents are divided into two types: alkali (e.g., amine type) and acid (anhydride) as seen in Table 3.14.

Some curing reagents catalyze the reaction and also act as addition agents for epoxy resins, e.g., imidazole (imidazole, imidazoline, imidazoline phosphor amide or 2-ethyl-4-methyl imidazole etc.), dicyandiamide, diamine and BF_3 , etc., which are catalyst-type curing agents. Organic acid, acid anhydride and primary amine are addition-type curing agents. The type of curing agent selected depends on its match with a nanocomposite system. In the preparation of the exfoliation-type, epoxy resin–clay nanocomposites, the choice of the curing agents is more important than the preparation of epoxy resin itself. We and other researchers have investigated the effects of different curing agents on the exfoliation process of clay in the nanocomposites (see later) [11–17]. Results from different investigators show that there are no definite principles in selecting the curing agents. Some curing agents are listed in Table 3.14.

The doses of the curing agents are summarized in Table 3.15. To overcome porosity and cracking, which cause brittle performance during curing, fillers and elasticizers (plasticizer) are added to the matrix, or the viscosity of the system is controlled to give satisfactory rheological properties.

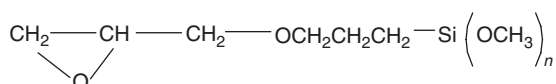
3.2.1.2. Additives for epoxy nanocomposites

Most of the additives play a catalytic role or have a filler effect in reinforcing the matrix or improving the matrix's rheological properties. For example, silica is usually used as a filler in the preparation of epoxy-based nanocomposites. A surfactant such as silane is used to treat the silica surface, making it to be a good adhesive for the epoxy matrix.

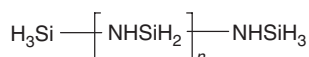
Table 3.15
Curing agents, their dose and curing conditions

Type of curing agent	Dose (wt%)	Curing condition		Additives
		T (°C)	Time (h)	
Tri-ethylamine, dimethyl benzomethyl amine,	5–15%	100–140	4–6	Phenol
di-ethylene tri-amine, tri-ethylene tetraamine	8–15%	100–140	4–6	Alcohols
<i>m</i> -phenylene diamine	14–16%	150–	—	Imidazole, BF ₃
Maleic anhydride, phthalic anhydride,	30–40%	160–200	2–4	Tertiary amine
poly(nonan-edioic anhydride)/	30–45%	—	—	(1–3%)
2,3,5,6-benzene tetra formic anhydride	20–25%	100	12	Imidazole/Pyridine
China wood oil anhydride (resin)	100–200%	80–100	20–5	(0.5–1.5%)
Phenol or urea formaldehyde resin,	30–200%	—	—	Tertiary amine
tri-polycyanamide formaldehyde resin,				(0.5–1.5%)
oligomers of polyamide or maleic amide				

The most popular silanes are KH-550 or KH-560. KH-550 has the molecular formula $H_2N-CH_2CH_2CH_2-Si(OC_2H_5)_n$ and KH-560 has the molecular formula



In the two formulas, $n = 3$. Another surfactant of siloxane is shown below:



The organo-clay also acts as a filler to overcome the environmental disadvantages of silica (silica dust can cause the disease pneumoconiosis). The curing accelerator is introduced into the interlayer of clay to catalyze the reaction of epoxy molecules. The reaction rate is more rapid inside than outside the clay gallery. Thus, the epoxy solidification rate outside of the clay interlayer is controlled to delay the hardening inside the clay gallery; otherwise, it prevents the clay layer from exfoliation. The curing accelerators are tertiary amine, phenylene methylamine, quaternary ammonium salt, diacetone methyl salt, alcohol/phenol, imidazole and others. They are used to reduce the curing temperature and accelerate the curing rate. Besides the accelerator, several other additives are summarized here based mainly on our work, such as matching agents, diluting agents and ductility agents. The molecular regulators of the monomer of epoxy, chloropropane, etc., aim at controlling the molecular weight when extra additives are added. The fillers of metal powder include active SiO₂, clay or MMTs and mica powder, and are used to reduce the product shrinkage rate. The fillers are treated with siloxane, hexamethyl siloxane, KH-550 and KH-560 for compatibility with PEO. Diluting agents such as epoxy propane derivatives, including glycerol epoxy, epoxy propane phylene(butyl) ether, and xylene, acetone, are

added to reduce the PEO viscosity due to the addition of the fillers. Finally, ductility agents or plasticizers, such as phosphate, *o*-diphenyl formate, polyamine, vulcanized, silicon or thiokol rubber, polyvinyl alcohol or its acetals and polyester are added to the PEO system to increase its ductility and improve its brittleness.

3.2.1.3. Examples of the preparation of epoxy with different molecular weight

Three examples of the preparation of epoxies with low-, intermediate- or high-molecular weight are shown.

Example 3.2.1.1. Preparation of low-molecular weight epoxy. The process includes the following steps: (1) the preparation of a 30% (by wt) NaOH solution; (2) bisphenol-A, epoxy chloropropane and alkali are mixed at the molar ratio of 1:2.75:2.42, respectively, and dissolved at 70°C for 30 min; (3) the alkali is added in two steps: at first, it is added at 50–55°C, dissolved for 4 h and reacted at 55–60°C for 4 h. Epoxy chloropropane is recovered under vacuum for 2 h at a temperature lower than 85°C and the vacuum higher than 600 mmHg, and then the epoxy chloropropane is dissolved at 70°C by the addition of benzene for 30 min; (4) the second addition of alkali is at 55–70°C for 1 h and is maintained for another 3 h, cooled and water is removed, making the benzene solution transparent. The mixture is allowed to stand for 4 h. Then benzene is removed at temperatures up to 110°C and further 140–143°C under vacuum.

Example 3.2.1.2. Preparation of the intermediate- and high-molecular weight epoxy. The raw material of bisphenol-A, epoxy chloropropane and alkali at a molar ratio of 1: n_1 (= 1.473): n_2 (= 1.598) are mixed; and are dissolved in 10% (by wt) of alkali; the rest of the experiment is the same as in Example 3.2.1.1. The dissolving temperature is regulated at 70°C for 30 min. All of the epoxy chloropropane is added to the mixture at 47°C, and the temperature is raised to 80–85°C for 1 h, then 85–90°C for 2–3 h. Then the product is washed to make it neutral and water is removed by vacuum drying up to 115°C under normal pressure; drying is then continued at 135–140°C under vacuum.

Example 3.2.1.3. Preparation of high-molecular epoxy. Is similar to Example 3.2.1.2. The bisphenol-A, epoxy chloropropane and alkali at a molar ratio of 1: n_1 (= 1.218): n_2 (= 1.185) are mixed, and are then dissolved in 10% (by wt) alkali; The rest of the experiment is same as in Example 3.2.1.1. However, the dissolving temperature is adjusted to 70°C for 30 min; then all of the epoxy chloropropane is added once the temperature is at 47°C and then reacted at 80–85°C for 1 h, and 95°C for 2–3 h. After dissolving, the product is washed to make it neutral, and the water is removed by vacuum drying up to 115°C under normal pressure; drying is then continued at 135–140°C under vacuum.

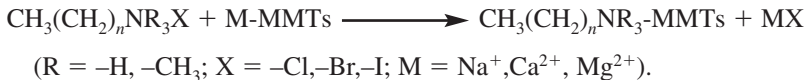
The epoxy chloropropane acts as a molecular regulator in the reaction. The strong concentrated alkali serves to improve the yield rate of the epoxy chloropropane. This epoxy chloropropane is mixed with bisphenol-A in the alkali solution producing a low-molecular-weight epoxy [14–17]. This is then cured to obtain the epoxy nanocomposites possessing properties such as chemical stability, thermal behavior, hardness and electronic aspects, which are directly related to the curing process besides additives. In the curing process, the matched curing agents such as tertiary amine, imidazole, composite quarter ammonium salt and the resin with the amine or ammonia as end groups

react with the epoxy group. The amine-treated clay, mixed with epoxy, produces an interaction with the charged clay platelet and accelerates the curing rate.

3.2.2. Layered silicate (clay)–epoxy nanocomposites

As one of the most important layered silicates, purified clay usually plays an important role in the preparation of the nanocomposites, improving the overall properties of the epoxy resins. Using intercalation–polymerization technology, the preparation of the epoxy–clay nanocomposites provides exfoliated layers with a thickness of 9.6 Å and an aspect ratio of 100–1000 nm dispersed in the epoxy matrix. The layered silicates enhance the resin's mechanical, thermal and heat-resistant properties.

3.2.2.1. The organo-clay. The clay layers are negatively charged in water. They absorb positive ions (cations). In Na-MMTs, the clay layer has adsorbed Na ions on its surface. Na-MMTs have many superior properties to these of Ca-MMTs in that the Na-MMTs are swelled because of their high CEC, which is higher than 70 mmol (100 g)⁻¹ clay. Usually, clay with a CEC from 80 to 120 mmol (100 g)⁻¹ clay [15] is used for mixing with PEO. The clay treated by organic molecules is called an organo-clay. The organic reagents are quaternary ammonium salt with alkyl chains such as octadecanoic alkyl trimethyl quaternary ammonium salt. The reaction process of clay with organic molecules is represented as



The interlayer distance enlarged through this intercalation process is measured by X-ray diffraction (XRD) using the diffraction peak at d_{001} . The organo-clay interlayer distance treated by alkyl trimethyl quaternary ammonium ranges from 1.0 to 1.35–2.0 nm of pristine clay. The organo-clay has its wettability reversed from a hydrophilic surface to a hydrophobic one and vice versa. This reversion process makes the clay suitable for diverse polarity systems. The organo-clay is more compatible with polymers or macromolecules than the pristine clay. For the PEO–clay nanocomposites, three different molecular arrangement morphologies in the clay gallery are hypothesized: (a) monolayer arrangement (unilayer); (b) double layer arrangement (bilayer); and (c) tilted or inclined arrangement (paraffin-like). These models are as shown in Figure 3.6.

The interlayer distance (the basal space plus the aliphatic chains) is $d_{001} = k(n-1) + d_c + d_m$, where n is the carbon number in the chain, d_c the interdistance of pristine clay and d_m the van der Waals radius at the end of methyl group (0.4 nm) [12]; k is a constant equal to 0.126 [12] calculated from increasing length of each C–C bond in the chain direction. When organic cations with alkyl group adopt a total extension molecular chain conformation or *trans–trans* form conformation vertical to the clay surface, the interdistance is thus calculated. The experimental d_{001} values help in evaluating the arrangement of organic molecules in the interlayer.

When experimental d_{001} values are higher than those calculated using the third model in Figure 3.6, the original structure of clay is exfoliated into nanolayers. Generally, d_{001} values > 3 nm denotes the exfoliation state. Naturally, the final organo-clay takes

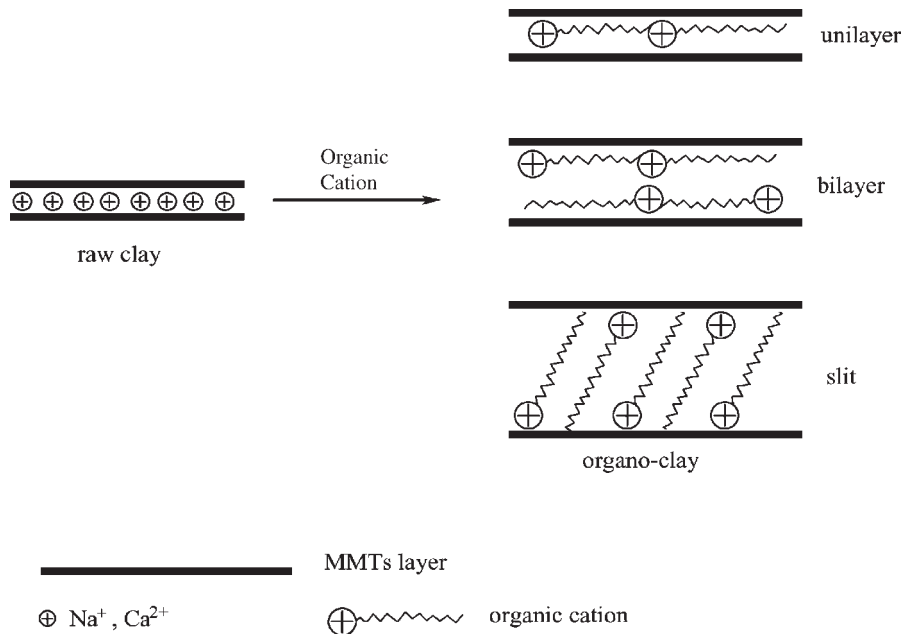


Fig. 3.6. Organic molecular structure models for organo-MMTs.

the three corresponding morphologies: intercalation, exfoliation and their mixed state according to both the calculation and layers dispersion as revealed by TEM. In PEO–clay nanocomposites, the exfoliation state is required for obtaining homogeneous materials with good properties.

3.2.3. PEO–clay nanocomposite and layer exfoliation

3.2.3.1. Preparation examples

In high-performance epoxy–clay nanocomposites, layer exfoliation of clay into a homogeneous but random dispersion is a benefit. To meet this requirements, the monomers or oligomers are intercalated into the internal surface or gallery of the clay. After that, the in situ polymerization-exothermal reaction stimulates the layers to exfoliate and disperse into the epoxy matrix. The intercalation polymerization method can be extended to the preparation of the thermal setting resin nanocomposites, such as polyimides and epoxy resins [18–22]. The preparation process for epoxy–clay or MMT nanocomposites involves the following steps: first, the epoxy or its oligomer is added to organo-clay to be mixed together. Second, the epoxy molecules are intercalated into the internal layer gallery of clay by heating and mechanical stirring. Third, the mixtures are cured with curing agents.

As a thermosetting resin, the epoxy composite molding process is static, unlike the preparation process of the thermoplastic rubber resin–clay nanocomposites with a shearing force. The homogeneous dispersion of clay in the epoxy matrix may be rather difficult. It is important that the clay is sufficiently mixed with epoxy by mechanical stirring before curing.

There are two ways of mixing clay with epoxy: one is to mix the clay with epoxy directly; the other is to choose a suitable solvent in which to dissolve the epoxy and swell the clay, promoting the intercalation of epoxy molecules intercalating into the clay's interlayer gallery. The direct mixing technique is practical, but the solvent mixing method is used if the molecular weight of the epoxy is rather high or its curing agent takes a solid state at room temperature. To illustrate these preparations, some practical examples of the preparation of epoxy-clay nanocomposites are given.

Example 3.2.3.1. Direct mixing method for preparation of epoxy/organo-clay nanocomposites. First, a suitable amount of organo-clay (the organo-clay preparation method will refer to Section 3.3.1 in this chapter) and epoxy resin of E-51 (molecular weight of 390, EP, bisphenol-A type of glycol ether) is taken, in a 250 ml flask and mixed under certain temperature ranging from 70 to 260°C, and stirred at different times (1–200 min). By this mixing, the mixture is kept in a liquid state. A small amount of this mixture is used to coat on a glass slice to produce a sample for XRD measurement.

Example 3.2.3.2. The preparation of low-molecular weight epoxy/organo-clay nanocomposites via direct mixing. A small amount of the mixture in Example 3.2.3.1 is taken, to which the curing agent of methyl tetrahydroxy phthalic anhydride (MeTHPA) is added together with the curing accelerator agent dimethyl benzyl amine (DMBA) in a beaker. Then, the mixture is stirred thoroughly under 50°C, the bubbles removed and is finally poured into a polytetrafluoroethylene (PTFE) mold to shape a sample whose mechanical properties are then measured.

The recipe of the preparation of the mixture is as follows: the mass ratio of epoxy/curing agent/curing accelerator is 100:80:2. Thereby, the organo-clay accounts for 1–10% (by wt) of the whole mixture. The curing process is either direct or step by step. The direct or one-step process for the mixture requires curing at 80°C for 2 h or pre-curing at 80°C for 2 h, and then curing at 160°C for another 3 h to obtain the final product.

Example 3.2.3.3. The preparation of high-molecular weight epoxy/organo-clay nanocomposites via co-mixing. Ten grams of dried PEO ($M_w = 2 \times 10^5 \text{ g mol}^{-1}$) powder is dissolved in 200 ml of chloroform for 2 days; then, 0.2, 0.5, 1 and 2 g of powered organo-clay (treated by dimethyl-hydroxy, 2-ethyl tallow quaternary ammonia sulfuric salt) are weighed and dissolved in 200 ml of chloroform for 2 days, and are dispersed by ultrasonic technique. The organo-clay is mixed with a PEO-suspending solution of chloroform for 2 days, and the chloroform is then removed by heating to obtain the nanocomposites. The powder is hot-pressed into 170- μm -thick film by the press machine under 120°C, which is for the post-direct measurement.

3.2.3.2. Epoxy intercalation behavior in the clay

Investigations show that epoxy resin is compatible with organo-clay [20,26]. Both the direct and solution mixing techniques produce homogeneous composites. XRD analysis of the composite has shown that epoxy molecules are intercalated into the interlayer gallery of clay. Figure 3.7 is an XRD pattern, in which 10 parts of organo-clay (or $\text{CH}_3(\text{CH}_2)_{17}\text{NH}_3^+$ -MMTs) are mixed with epoxy under direct or solution mixing for different lengths of time. XRD patterns show that the clay's interlayer distance d_{001}

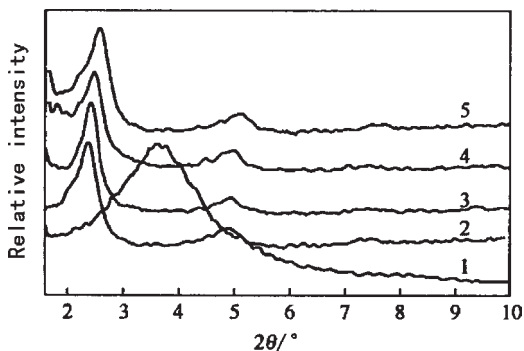


Fig. 3.7. The interlayer distance changes with the mixing of $\text{CH}_3(\text{CH}_2)_{17}\text{NH}_3^+$ -MMTs with epoxy: (1) $\text{CH}_3(\text{CH}_2)_{17}\text{NH}_3^+$ -MMTs; (2) the $\text{CH}_3(\text{CH}_2)_{17}\text{NH}_3^+$ -MMTs/EP mixture under direct mixing in the temperature range 70–80°C for 20 min; (3) $\text{CH}_3(\text{CH}_2)_{17}\text{NH}_3^+$ -MMTs/EP mixture under direct mixing in the temperature range 70–80°C for 60 min; (4) $\text{CH}_3(\text{CH}_2)_{17}\text{NH}_3^+$ -MMTs/EP mixture after solution mixing; and (5) $\text{CH}_3(\text{CH}_2)_{17}\text{NH}_3^+$ -MMTs/EP mixture after storage for 2 months.

increases from 2.4 to 3.7 nm in the mixture, showing epoxy molecules intercalated into the clay interlayer space. The intercalation reaction occurs in the temperatures range 70 to 80°C under stirring and mixing for 20 min. Secondly, at certain mixing temperatures, this clay interlayer space can accommodate only a limited amount of epoxy resin, as the saturated amount of epoxy fills up its interlayer gallery. However, the final saturated state for epoxy filling takes a long time to reach equilibrium, especially during low-temperature mixing. At temperatures of 70–80°C, the mixing time should last for 60 min for the mixture to reach the apparent saturated state; otherwise, the solvent mixing technique cannot increase the interlayer distance of clay in the mixture. If not mixed thoroughly, epoxy molecules will be steadily present in the interlayer of clay and keep the interlayer distance nearly unchanged for 2 months in storage.

Previously, the intercalation behavior of the organo-clay by the epoxy molecules was investigated [11,23] and it has been shown that the interlayer distance is closely related to the chain length of organic cation molecules but not related to the original interdistance of the organo-clay. In Table 3.16, the original interlayer distances of the organo-clay and its nanocomposites are compared. As the chain length of organic quaternary ammonia cation increases, the interlayer distance of clay intercalated by epoxy molecules increases. The different initial interlayer distance of organo-clay creates nearly the same interdistance of clay in nanocomposites.

It is supposed that the alkyl chains of the organic ammonia in the organo-clay extend to the ultimate degree to accommodate the most epoxy molecules. In such a conformation, the organic surfactant cations orient vertically with clay layers to form an intercalated type of “brush” structure. The interlayer distance intercalated by epoxy is estimated from the chain length of the organic ammonia cation. This is seen in Table 3.16 and refers to the molecule orientation morphology [21]. The alkyl chain steric hindrance of the arrangement in the interlayer gallery creates mutual exclusion of these molecules under steady entropy and heat release from self-polymerization. The heat

Table 3.16
Effect of intercalate agent on epoxy intercalation behavior

Organo-cation	Initial interlayer distance of organo-clay (nm)	Interlayer distance of organo-clay-epoxy ^a (nm)	Calculated ^b (nm)	Reference
CH ₃ (CH ₂) ₇ NH ₃ ⁺	1.38	2.72	2.47	[13]
CH ₃ (CH ₂) ₉ NH ₃	1.38	3.00	2.72	[11–12]
CH ₃ (CH ₂) ₁₁ NH ₃	1.56	3.19	2.98	[12]
CH ₃ (CH ₂) ₁₅ NH ₃ ⁺	1.76, 1.2	3.41, 2.2	3.49	[11–12]
CH ₃ (CH ₂) ₁₇ NH ₃ ⁺	1.80	3.67	3.74	[14–17]
CH ₃ (CH ₂) ₁₇ N(CH ₃) ₃ ⁺	2.21	3.69	3.74	[11–12]
CH ₃ (CH ₂) ₂₃ N(CH ₃) ₃ ⁺	—	—	—	[14–17]

^aInterlayer distance of initial organo-clay. ^bInterlayer distance calculated using the formula $d_{001} = k(n-1) + d_c + d_m$.

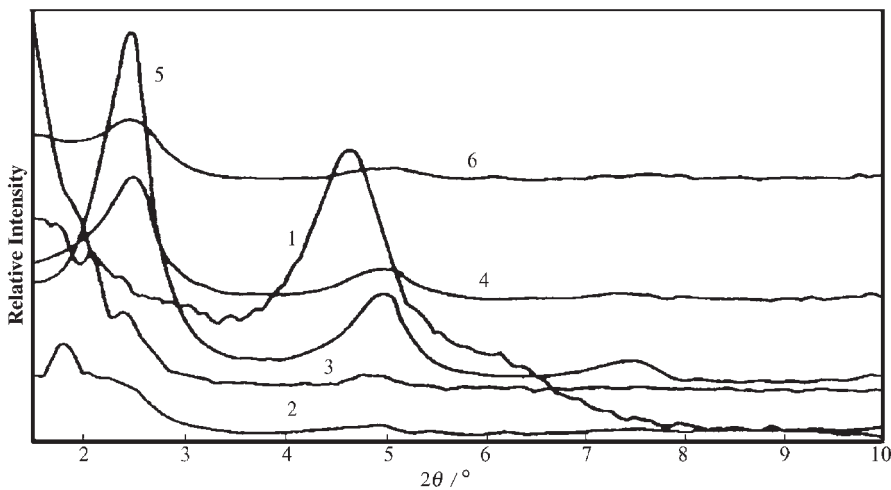


Fig. 3.8. XRD pattern of 1–9% (by wt) of CH₃(CH₂)₁₅NH₃⁺-MMTs mixture with epoxy (1) CH₃(CH₂)₁₇NH₃⁺-MMTs; (2)–(5) the mixture load of organo-clay of 1, 3, 5 and 7% (by wt), mixed at 225°C for 1 min; (6) organo-clay load of 9% (by wt) mixed at 80°C for 2 h.

releases further push forward, expanding the interlayer space and doubling the interlayer distance in the alkyl chain length.

Figure 3.8 shows an XRD pattern of different 16-alkyl primary amine-treated MMT load in the nanocomposite under different temperatures for a certain time. The intercalate mixture is obtained irrespective of the increase in mixing temperature from 80 to 225°C or increase in the organo-clay load from 1 to 9% (by wt). The mixture's interlayer distance increases from the original 1.9 nm of organo-clay to 3.5 nm of the intercalated clay, coinciding with the calculated value of 3.2 nm, while in epoxy, 1 and 3% (by wt) of organo-clay mixture, and their interlayer distance expand to 4.9 nm, which is double the alkyl amine chain length of 2.5 nm.

3.2.3.3. The factors influencing exfoliation behavior in epoxy-clay nanocomposites

The exfoliation behavior in nanocomposites is investigated to reveal how the different factors influence the exfoliation of clay during epoxy curing. Besides X-ray, transmission electron microscopy (TEM) is also used to match the final results.

To produce an exfoliated type of nanocomposite, it is necessary that there should be enough epoxy molecules participating in the reaction in the clay microreaction system and that the reaction rate inside be more rapid than outside the interlayer gallery in order to discharge enough heat in the inside space, overcoming the van der Waals force between the interlayer, exfoliating the clay into a monolayer and dispersing it in the epoxy matrix.

(1) *The chain length of organic cations.* The exfoliation degree of clay in the epoxy depends on the chain length of the organic quaternary ammonia salt. This principle has been observed by several researches including our group [11–12,26,28–29,31]. When the carbon number of the alkyl chain of the organic ammonia salt is over 11, the bilayer orientation of the organic cation in the interlayer enhances the layer exfoliation of clay. On the basis of Table 3.16, it can be seen that a longer alkyl chain creates a larger interlayer distance in clay and intercalates more epoxy molecules into its interlayer space. By sufficient mixing, the long chain of the organic cation can take a vertical orientation in the interlayer space, which thus accommodates more epoxy resin. This orientation enables more epoxy molecules there to participate in the polymerization reaction and releases more heat to produce the layer exfoliation.

In one case [22] it has been observed that after several ion-exchange reactions replaced all of the inorganic cations, the exfoliation type of nanocomposite was obtained, although the carbon number of the organic ammonia cation was < 3 . The treated clay makes contain enough vacant space occupied by metal cations for accommodating more epoxy molecules in the clay layer space. Irrespective of the treatment technology used, proper chain length is beneficial for treating clay and forming exfoliated nanocomposites.

(2) *The effect of the curing agent and its load on the exfoliation of the nanocomposites.* The curing agent is the key factor influencing the exfoliation behavior of the epoxy–clay nanocomposites and the product quality. There are different criteria from researchers, including Pinnavaia [11–17], as how to choose a suitable curing agent for an exfoliation type of epoxy-clay nanocomposites.

In the case of octadecanoic alkyl dihydroxyethyl methyl as a reagent for treating layered silicate ($\text{CH}_3(\text{CH}_2)_{17} \text{N}^+(\text{CH}_3)(\text{HOCH}_2\text{CH}_2)_2\text{-MMTs}$) and its mixture with epoxy resin, the nanocomposites form after the curing agent is added. Curing agents such as anhydride or tertiary amine (benzyl dimethyl amine, BDMA) produce exfoliated layers. When the reactive amine curing agent of 4,4'-diamine diphenyl methyl (DDM) is used for the mixture, the clay is not exfoliated. However, our investigations show that [11] a DDM- $\text{CH}_3(\text{CH}_2)_{15}\text{NH}_3^+\text{-MMTs}$ complex system mixed with epoxy resin produces an exfoliated nanocomposite as shown in Figure 3.9. Similarly, tetrahydroxy phthalic anhydride (MeTHPA)/*N,N*-benzyl dimethyl amine (BDMA) is suitable for the preparation of exfoliated layers in nanocomposites.

Different investigators, including Giannelis et al. [13,16–17], show that one of the reasons that DDM is incapable of causing some clay mixtures to exfoliate, is that the active group at the two ends of this amine has surface interactions with adjacent layers,

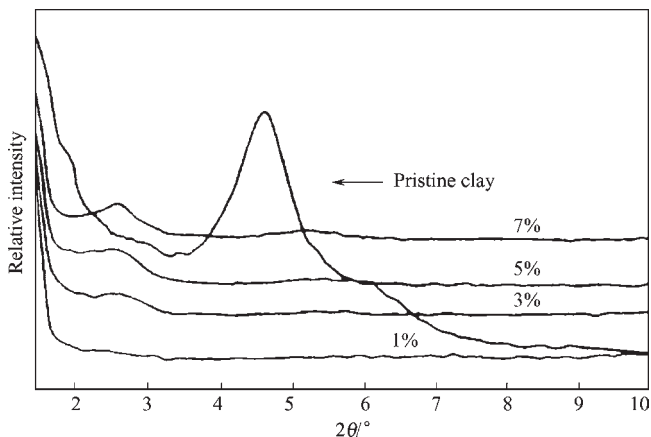


Fig. 3.9. XRD patterns of nanocomposites for different clay loads of epoxy- $\text{CH}_3(\text{CH}_2)_{15}\text{NH}_3^+$ -MMTs cured by DDM at an initial temperature of 80°C for 2 h, at a temperature of 160°C for 3 h. (With the permission of Acta Polymerica Sinica, China Chemical Association.)

producing a bridging connection to deter the layers from further exfoliation. Another reason is that this amine has very strong polarity and makes the exfoliated layers agglomerate together.

Exfoliation of clay is related to both the acidity of the organic cations and the curing temperature. For example, for the two complexes $\text{CH}_3(\text{CH}_2)_{17}\text{NH}_3^+$ -MMTs and $\text{CH}_3(\text{CH}_2)_{17}\text{N}(\text{CH}_3)_3^+$ -MMTs, different exfoliation behavior is observed when the two complex mixtures are cured with *m*-phenylene diamine, even though the chain lengths of the organic molecules are the same and their interlayer distances in the organo-clay are equal. The former organo-clay produces exfoliated layers, while for the latter organo-clay, the formation of exfoliation layers depends on the curing temperature. $\text{CH}_3(\text{CH}_2)_{17}\text{N}(\text{CH}_3)_3^+$ -MMTs are not exfoliated either at a temperature lower than 120°C for slow curing, or at a temperature of 140°C for fast curing. Only at temperatures from 100 to 125°C , with an intermediate rate of curing, can the clay be exfoliated. Similarly, when the two complexes are cured with DDM, it is found that in the $\text{CH}_3(\text{CH}_2)_{17}\text{N}(\text{CH}_3)_3^+$ -MMT mixture, the clay layer is incapable of exfoliation, while the clay layers in the $\text{CH}_3(\text{CH}_2)_{17}\text{NH}_3^+$ -MMT mixture are exfoliated under the same conditions [11]. Thus, when the $\text{CH}_3(\text{CH}_2)_{17}\text{NH}_3^+$ -MMT mixture is cured at temperatures from 80 to 160°C , the organo-clay produces complete layer exfoliation.

The $\text{CH}_3(\text{CH}_2)_{17}\text{NH}_3^+$ reagent is used as a Bronsted acid to catalyze the amine-curing agent and increases the curing rate of epoxy molecules in the interlayer of clay. The ammonia cation of $\text{CH}_3(\text{CH}_2)_{17}\text{N}(\text{CH}_3)_3^+$ in the organo-clay has no acidity and cannot act as a catalyst in the $\text{CH}_3(\text{CH}_2)_{17}\text{N}(\text{CH}_3)_3^+$ -MMTs. The $-\text{N}(\text{CH}_3)_3^+$ group has a radius similar to that of the hexagon space composed of silica tetrahedron and alumina octahedron preventing clay from exfoliation.

Evidence for the above statement can be obtained by DSC experiments as seen in Figure 3.10. Only the epoxy/ $\text{CH}_3(\text{CH}_2)_{17}(\text{NH}_3)^+$ -MMT mixture cured by DDM decreases

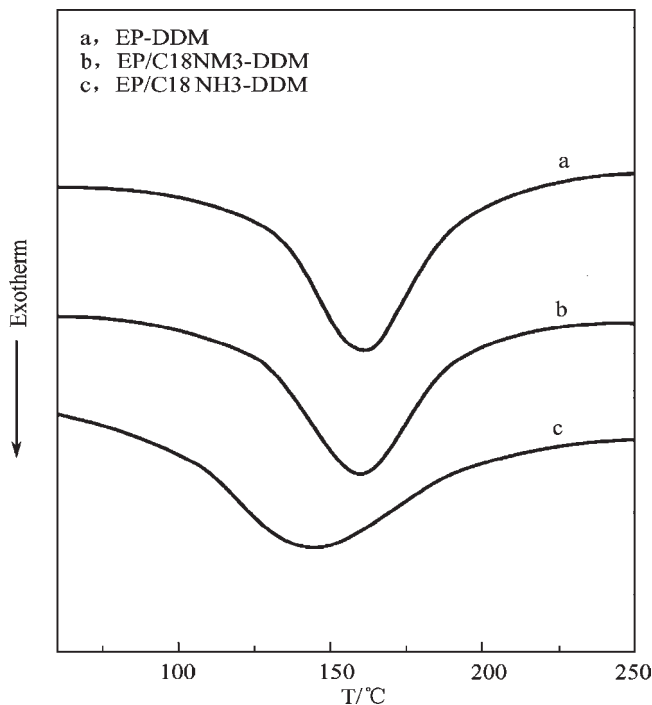


Fig. 3.10. DSC patterns of three mixtures of epoxy cured by DDM: (a) epoxy/DDM; (b) epoxy/CH₃(CH₂)₁₇(CH₃)₃⁺-MMTs/DDM; (c) epoxy/CH₃(CH₂)₁₇(NH₃)⁺-MMTs.

the curing temperature, while the curing temperature of the epoxy/CH₃(CH₂)₁₇N(CH₃)₃⁺-MMTs mixture cured by DDM is nearly unchanged, showing that only organic ammonia cations with acidic proton catalyze the amine curing reaction of epoxy system. The acidity of the organic cation in the clay interlayer accelerates the amine curing process of epoxy, which explains the clay exfoliation behavior. There is another example. Although CH₃(CH₂)₁₅NH₃⁺-MMT mixture has a strong acid proton, it is only intercalated, without exfoliation, under DDM curing. However, it is easily exfoliated with MeTHPA as a curing agent.

Too high or low temperatures and overlong curing times make the resins outside the clay interlayer freeze too quickly, preventing the resin molecules from penetrating into the clay's interlayer space. Thus, the concentration of DDM inside the clay gallery is relatively lowered occurring while its curing rate is lower than that outside space, preventing exfoliation from occurring. Taking anhydride as a curing agent, exfoliated nanocomposites of two mixtures of epoxy/CH₃(CH₂)₁₇(NH₃)⁺-MMTs and epoxy/CH₃(CH₂)₁₇N(CH₃)₃⁺-MMTs under different temperatures are obtained. FTIR results show that the anhydride concentration inside the interlayer is higher than the concentration outside under which the clay layers are exfoliated.

The exfoliation of clay in an epoxy matrix is also related to the anhydride content [24]. A high load of anhydride and an excessive curing rate outside the clay does not make clay

exfoliation easy, but exfoliation does take place, when the curing agent concentration is low and when the curing rate inside the interlayer is more rapid than that outside.

(3) *Effect of the organic cation acidity on accelerating the clay exfoliation.* The organic cations acidity catalyzes the organic amine curing agent by enhancing the curing rate of epoxy inside the clay gallery than that on the outside of it. The interlayer distance is enlarged by the heat swelling before the epoxy outside the gallery reaches the curing gel point. The uncured resin outside the gallery is capable of flowing into the interlayer space, which makes the interlayer distance to swell continuously and exfoliate fully. This results from acidity proton catalysis [25]. The acidic proton H^+ , and the ammonia cation NH_4^+ treated MMTs are similar to those of the organo-MMTs treated with $[H_3N(CH_2)_nNH_2]^+$, $[H_3N(CH_2)_nNH_3]^{2+}$, $[H_3N(CH_2)_{n-1}COOH]^+$, $[H_3N(CH_2)_{n-1}CH_3]^+$ ($n = 6$ or 12). There appears a “self-polymerization exfoliation temperature” that occurs at such a temperature as to produce the maximum exothermal peak on DSC scanning curve, decreasing as the acidity intensity of the organic cations decreases. Thus, the acid catalyzes the epoxy polymerization inside the interlayer space benefiting balance of the curing rate inside and outside the interlayer space. Adding the curing accelerator to this mixture enhances the clay exfoliation during the curing process [26]. Figure 3.11 shows an XRD pattern of the curing mixture of epoxy/ $CH_3(CH_2)_{15}NH_3^+$ -MMTs/MeTHPA as a curing agent without the BDMA accelerator. Where, the diffraction peak at $2\theta = 4.66^\circ$ reflects $d_{001} = 1.9$ nm. It is found that the clay is exfoliated only at 1% (by wt) load in the composites, while it is unexfoliated at over 3% (by wt) load.

The maximum reaction rate of these mixtures (Figure 3.11) occurs at $186^\circ C$ without the accelerator. This temperature is $30^\circ C$ higher than the mixture system with BDMA (Figure 3.12). Thus, the organic cation acid proton exhibits its catalytic effect at a certain temperature for which the reaction inside the interlayer space is accelerated for the layer exfoliation.

In Figure 3.13, the solid lines represent different loads of organo-MMTs or clay treated by primary amine mixing with epoxy at $225^\circ C$ for 1 min. To get these exfoliated

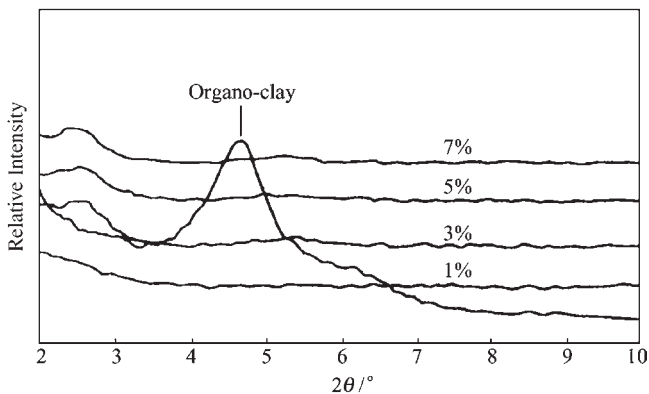


Fig. 3.11. XRD patterns for mixture of epoxy/ $CH_3(CH_2)_{15}NH_3^+$ -MMTs/MeTHPA, cured at $80^\circ C$ for 2 h, $160^\circ C$ for 3 h (organo-clay load of 1, 3, 5 and 7% (by wt) respectively). (With the permission of Acta Polymerica Sinica, China Chemical Association.)

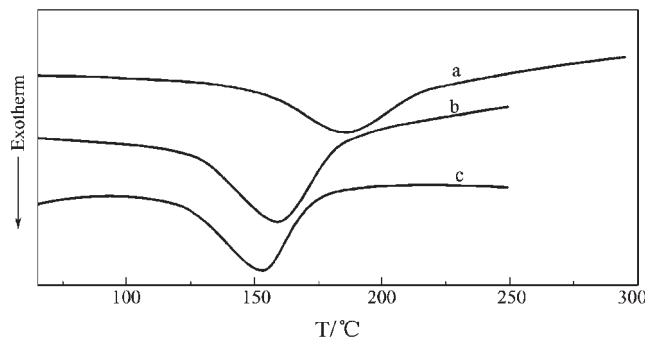


Fig. 3.12. DSC pattern of epoxy/ $\text{CH}_3(\text{CH}_2)_{15}\text{N}^+(\text{NH}_3)_3^+$ -MMTs-MeTHPA (5%, by wt) system: (a) without BDMA, (b) with BDMA and (c) with BDMA and coupling agent.

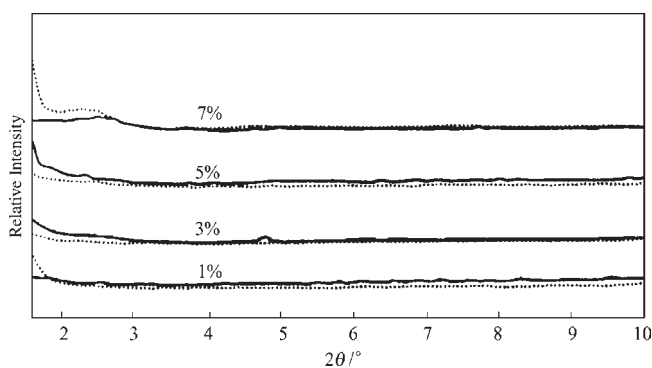


Fig. 3.13. XRD patterns for cured nanocomposites of epoxy/ $\text{CH}_3(\text{CH}_2)_{15}\text{N}^+(\text{NH}_3)_3^+$ -MMTs/MeTHPA- $\text{CH}_3(\text{CH}_2)_{15}\text{N}^+(\text{NH}_3)_3^+$ -MMTs (curing condition are the same as in Figure 3.11). (—), with BDMA; (...) with BDMA and coupling agent). (With the permission of John Wileys & Sons in the article, Y.C. Ke et al., *J. Appl. Polym. Sci.*, 78 (2000) 808–895.)

composites, the curing agent and its accelerator are added to this mixture, curing at 80°C for 2 h and at 160°C for 3 h. Further addition of the curing accelerator BDMA to this mixture makes its featured diffraction peaks all disappear showing a complete clay exfoliation in the epoxy/organo-clay, (1–5%, by wt) except 7% (by wt) load. In X-ray curves, the position of $2\theta = 1.5^\circ$ is for the interlayer distance of 6 nm for the organo-clay which is roughly consistent with that from the TEM morphology shown in Figure 3.14, where the interlayer distance of clay–clay is 8.0 nm (the arrow shows the d_{001} distance between layers).

The BDMA accelerator, as a nucleophilic reagent, has an affinity for protonated organic cation. Its catalytic effect greatly reduces the peak temperature corresponding to the maximum reaction rate and accelerates the reaction heat release (see the exfoliation shown by dotted lines in Figure 3.13).

(4) *The effect of mixing conditions on intercalation and exfoliation behavior.* Accurate control of the composition of the epoxy-based mixtures should be maintained. The

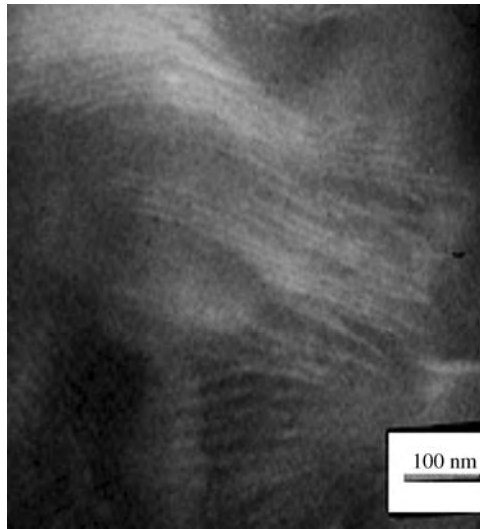


Fig. 3.14. TEM morphology of 5% epoxy nanocomposites. The bright lines show the interlayer distance.

relationship among the curing temperature, time and curing gel transition has been studied [31].

In some cases, high-quality, epoxy-based nanocomposites are prepared by prolonging the mixing time at a low temperature. However, these materials are more easily obtained by mixing at high temperatures at which the interlayer distance is increased by acidic proton catalysis of epoxy's self-polymerization reaction in the organo-clay. When 7% (by wt) of $\text{CH}_3(\text{CH}_2)_{15}\text{NH}_3^+$ -MMTs is mixed with epoxy at 180°C , the diffraction peak at XRD pattern moves to a small angle position as the mixing time and its intensity is attenuated, indicating a partial exfoliation. If the mixing time is prolonged, the mixture transforms from liquid to solid due to complete self-polymerization (called "liquid-powder transition") while forming a nanocomposite that is difficult to process and exfoliate. The XRD patterns at different mixing times are shown in Figure 3.15 and 3.16 for mixtures of epoxy/organo-clay (7%, by wt) mixed at 225°C . The mixing time is controlled; otherwise the transition from liquid to solid is impossible.

When the samples are mixed at 210 and 235°C for different times, similar XRD patterns or exfoliation behavior are observed. If clay overloads (e.g., 7%, by wt), the epoxy molecules overcome the van der Waals attractive force to swell gradually by penetrating into the interlayer gallery under relatively high temperature and long time. The curing process is set up for different temperatures and times together with the concentrations of the curing agent and accelerator as additives in order to observe the effect of the mixing and curing condition on the layer intercalation and exfoliation in the epoxy-clay mixture.

(5) *The effect and the criterion of the curing process and gelation time on clay exfoliation.* Epoxy resin changes from a reactive liquid to an elastomer and finally cross-linked solid materials in different stages. The reaction mechanism at each stage is governed by

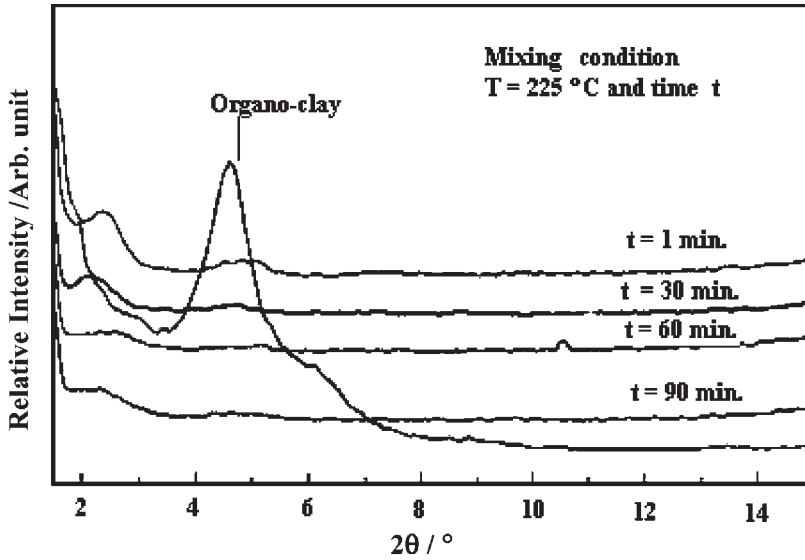


Fig. 3.15. XRD patterns of nanocomposites of epoxy/clay (7%, by wt) mixing at 225°C for different times. (With the permission of Acta Polymerica Sinica, China Chemical Association in the article, Y.C. Ke et al., 6 (2000) 768.)

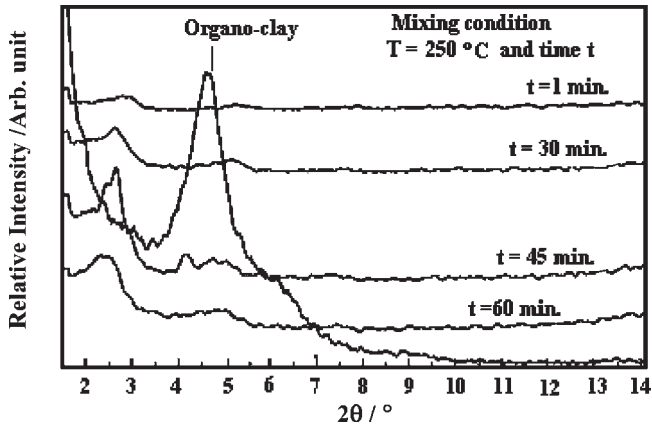


Fig. 3.16. XRD patterns of nanocomposites of epoxy/clay (7%, by wt) load mixing at 250°C for different times. (With the permission of Acta Polymerica Sinica, China Chemical Association in the article, Y.C. Ke et al., 6 (2000) 768.)

both the dynamic and expanding process in the mixture. The complex processes definitely influence the exfoliation behavior of clay in the epoxy matrix. At what stage does the clay produce a complete exfoliation during the curing process? To answer this question, the effects of curing on clay exfoliation in the nanocomposites are shown in Figure 3.17(a) and (b). Clay exfoliation behavior changes as the curing time in the mixture of 3

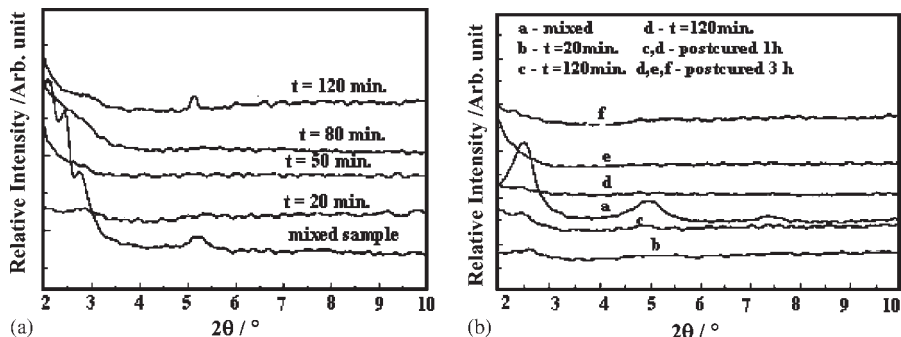


Fig. 3.17. XRD pattern of (a) epoxy/ $\text{CH}_3(\text{CH}_2)_{15}\text{NH}_3^+$ -MMTs (3%, by wt) curing at 80°C . (b) epoxy/ $\text{CH}_3(\text{CH}_2)_{15}\text{NH}_3^+$ -MMTs (5%, by wt) (e and f obtained from d by post-curing at 160°C). (With the permission of John Wileys & Sons in the article, Y.C. Ke et al., *J. Appl. Polym. Sci.*, 78 (2000) 808–815.)

or 5% (by wt) of $\text{CH}_3(\text{CH}_2)_{15}\text{NH}_3^+$ -MMTs/epoxy resin/THPA/BDMA cured at 80°C [26]. As the curing reaction proceeds, its characteristic diffraction peak (d_{001}) diminishes and moves toward the small-angle position indicating the end of the exfoliation. The clay layers are completely exfoliated at the critical time of curing.

The complete exfoliation time for the two samples in Figure 3.17 is approx. 50 min, and occurs at either the gelation point, or before this point (Table 3.17). The clay in $\text{CH}_3(\text{CH}_2)_{17}\text{NH}_3^+$ -MMTs-epoxy/DDM mixture (7%, by wt) needs 15 min to completely exfoliate at 100°C (Figure 3.18). So, only at the critical time of curing does the clay exfoliate completely, while the exfoliation occurs definitely before or at the mixture's gelation point.

The degree of clay exfoliation during curing does not depend on the temperature, but does depend on the curing degree (time). The analysis based on DSC and FTIR techniques shows that when the epoxy resin curing degree reaches 20–30%, the interlayer distance expands to the complete exfoliation extent [14].

(6) *Some principles.* Based on the several factors affecting clay exfoliation, it is concluded that the reactive heat released from the interlayer intercalation should be high enough to overcome the van der Waals attractive force to completely exfoliate the clay. It is necessary that the interlayer space accommodates as many epoxy resin and curing agents as possible. The final interlayer distance depends on the size and type of the organic cation molecules, the curing agent and the clay's treatment. The reaction rate inside the interlayer should be greater than outside, which is a sufficient condition for clay exfoliation. This condition also depends on the properties of the organic cations (with acid catalytic function) and the accelerator. The accelerator lowers the temperature at the maximum reactive heat released from the interlayers, while the polymerization reaction inside the interlayer gallery causes it to swell and release heat before the resin outside the interlayer space cures and gels. The organo-clay property, the gelling time and the curing degree have effects on the complete exfoliation of clay. For the thermocuring nanocomposites, two criteria for the complete exfoliation of clay are suggested.

Criterion 1. The thermodynamic criterion, or condition, is that complete exfoliation of the clay occurs when its free energy variation is lower than or equal to zero (0) so that the reaction proceeds spontaneously. The free energy variation (ΔG) is composed

Table 3.17

The gelation time for epoxy/CH₃(CH₂)₁₅NH₃⁺-MMTs-MeTHPA and epoxy/CH₃(CH₂)₁₇NH₃⁺-MMTs-DDM mixtures

Clay load (wt%)	Gel time t_g (min) at				E (kJ (mol K) ⁻¹)
	80°C	100°C	120°C	140°C	
Composite with BDMA					
0	71.17	17.55	5.98	1.75	17.66
1	61.67	14.43	4.80	1.30	18.49
3	48.33	11.52	3.30	1.00	18.67
5	41.13	10.82	2.82	1.00	17.88
7	14.53	4.75	1.48	0.45	16.75
5 ^a	280.0	—	—	—	—
7 ^b	62	15.4	8.5	—	—

Note: E , active energy; composite with BDMA, epoxy-CH₃(CH₂)₁₅NH₃⁺-MMTs-MeTHPA/BDMA.

^aEpoxy-CH₃(CH₂)₁₅NH₃⁺-MMTs-MeTHPA without BDMA. ^bEpoxy-CH₃(CH₂)₁₇NH₃⁺-MTs/DDM.

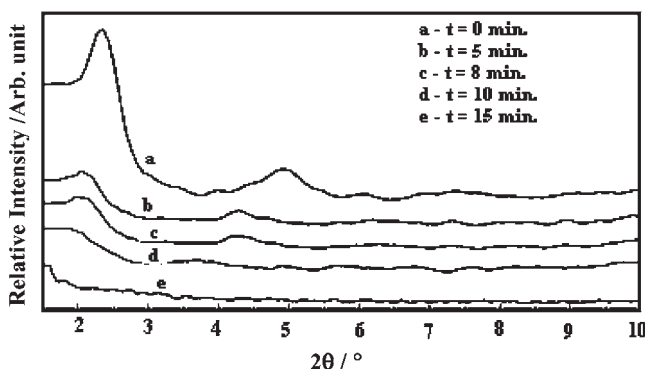


Fig. 3.18. XRD patterns of the mixture of epoxy/CH₃(CH₂)₁₇NH₃⁺-MMTs/DDM curing at 100°C for different times. (With the permission of John Wiley in the article, J.K. Lu, Y.C. Ke, Z.N. Qi, X.S. Yi, J. Polym. Sci.: Part B-Polym. Phys. 39 (2001) 115–120.)

of the independent enthalpy variation (ΔH) and entropy variation (ΔS), which is the sum of the contributions by both the polymer and the clay. The general free energy variation ΔG_t has the following form:

$$\Delta G_t = (\Delta H_m + \Delta H_c) - T(\Delta S_m + \Delta S_c) = \Delta H_t - T\Delta S_t \tag{3.2.1}$$

where ΔH_m and ΔH_c are the heats of fusion for matrix epoxy and clay, respectively, and ΔS_m and ΔS_c are the entropy variations of the matrix and clay, respectively. When epoxy resin or polymer penetrates into the interlayer space, the molecular chains are confined by the interlayer space to give a negative entropy variation ΔS_m , or a reduction of the entropy variation, which produces a resistance to the intercalation process. The penetrated molecules swell the clay interlayer creating the clay's positive exfoliation entropy variation ΔS_c , or an increase in the entropy, which counteracts the previous reduction

in the entropy. If the increase in the entropy is greater than or equal to its reduction during the clay exfoliation, the exfoliation inside the interlayer depends on the system's general enthalpy variation of ΔH_t . Once the heat releases from the epoxy, the ΔH_m at constant pressure produces complete exfoliation with the interlayer distance greater than 8 nm (the disappearance of Bragg diffraction peak in XRD), or if the van der Waals attractive energy in ΔH_c is endothermic, the clay's exfoliation proceeds spontaneously.

Criterion 2. When the reaction rate inside and outside the layers is relatively equal, and the system gelling time is largely decreased or once the gel point is reached, the mixture viscosity rapidly increases and prevents the epoxy molecules and curing agent from penetrating into the interlayer space. The heat release is high enough to exfoliate the clay. These are sufficient conditions for the complete exfoliation of clay.

In other words, the condition for the complete exfoliation interlayer is possible only when the epoxy curing releases a large amount of heat before gelling to overcome the van der Waals force, or

$$\Delta H_m(t \leq t_g) \gg \Delta H_c \quad (3.2.2)$$

where t_g is a gelation time.

3.2.4. The properties of PEO-clay nanocomposites

Under certain mixing conditions, a mixture of epoxy–MMTs appears at an intercalation–exfoliation transition after curing. Compared with epoxy, the mixture's nanocomposite properties are obviously enhanced, and their properties with exfoliated layers are best improved. The property comparison of the epoxy with the intercalation type of nanocomposite and exfoliation type of nanocomposites [26,31] is shown in Table 3.18, where the curing agent, accelerator and dosage are the same in each sample.

Whether the nanocomposite is the exfoliation or intercalation type, its property is enhanced greatly over the pure epoxy resin. The exfoliation type of nanocomposites has higher tensile strength of σ_b , tensile modulus of E_T and bending modulus of E_f and impact strength higher than those of the intercalation type. Note that the bending strength and HDT of σ_f have not been significantly improved, the reason for which remains to be solved.

Table 3.18

Comparison of properties of epoxy/organo-clay (7%, by wt) nanocomposites with the pure epoxy resin

T (°C)	t (min)	Type	σ_b (MPa)	E_T (GPa)	σ_f (MPa)	E_f (GPa)	Impact (kJ m ⁻²)	HDT (°C)
225	1	Intercalation	32	1.25	100	3.01	5.0	113
225	60	Exfoliation	40	1.30	113	3.21	5.5	108
235	1	Intercalation	30	0.95	115	3.25	4.4	107
235	40	Exfoliation	47	1.24	109	3.41	5.7	107
250	1	Exfoliation	40	1.27	105	3.24	6.4	105
Pure epoxy ^a				1.09	120	2.34	4.5	103

Note: Curing, 80°C for 2 h, 160°C post-curing for 3 h.

^aPure resin curing at room temperature.

3.3. Polyolefin–silicate nanocomposite

With their wider application fields, different modifications of polyolefins have been suggested to meet the versatile requirements for them. These modifications include melt-blending matrix resin with inorganic phase, using composite carrier for their catalyst, filling or in situ polymerization, etc. As for polyolefin catalyst, it focuses on two aspects: one is in the new active components, and the other is to find a high new effective carrier, and the matched technology to carry the active material on it.

Polypropylene (PP) is one of the most widely applied polyolefins but has many disadvantages, e.g., brittleness at low temperature, ductility, low resistance to temperature in application, etc. To improve PP properties such as process ability, rigidity, scale stability, impact, etc., PP is modified by a proper inorganic phase. A new route of in situ preparation of the nanocomposite of polyolefin-layered silicate of MMTs is suggested, based on reports [28,29], for example, polyolefin nanocomposites are synthesized in situ via a newly designed carrier, instead of traditional carriers such as $MgCl_2$ and $(RO)_n-Mg$ for Ziegler–Natta catalyst. The chlorite element in $MgCl_2$ does not match the new active centers, e.g., metallocene or post-transitional metal catalysts, eroding the equipment, hence it is necessary to design new carriers. These carriers are prepared using nanotechnology. The advantage of using nanotechnology is that the nanocomposite material is obtained in situ without modifying any polymerization technology, and without washing any residual materials. Such a process is environment-friendly is, flexible, and provides integration of blending and polymerization of the nanocomposites, etc. The nanocomposite of this in situ filling polymerization has not only improved the traditional melt-blending technology for polyolefins, but also the nanomaterial powder used in mixing with polyolefins.

Thus, using nanomaterial powder or nanoprecursor as the carrier for olefin polymerization is one means of optimizing the preparation of polyolefin-based nanocomposites. Such a technology integrates the nanoparticle carriers, creating new functions [30].

3.3.1. PP-inorganic nanocomposites

In the preparation of PP-based nanocomposites, a composite carrier of layered silicate is prepared. For example, MMTs react with TEOS forming a so-called pillared structured composite, which has satisfactory activity. In similar works [31–33], particles with a pore size of 1.4–2.2 nm and particle size of 200 nm are prepared and used as carriers in cracking raw petroleum. The carrier is also used in in situ preparation of the PP–inorganic nanocomposite.

3.3.1.1. Preparation of the composite carrier of MMTs/oxides

Considering the carrier of MMTs/ SiO_2 as an example, its heterogeneous porosity structure is prepared via an intercalating quaternary ammonia salt and neutral amine in the MMT layer space, where the neutral amine acts as the template. The silica is intercalated and hydrated in the space there using TEOS as a precursor. The final pillared structure of MMTs is prepared by calcinating the mixture to remove the organic compounds.

In the preparation of this composite carrier, controlling the interlayer enlargement depends on the types of quaternary ammonia salt and neutral amine selected (e.g., chain length of the reagents), and the level of control over the polymerization reaction.

(1) *General process of the preparation of the carrier.* This is divided into several steps as follows:

- (a) MMTs react with the organic intercalants (e.g., dodecyl trimethyl ammonia bromide), giving intercalated MMTs (I-MMTs).
- (b) I-MMTs then mix with the amine of (C₆–C₁₂) and TEOS, and the composites of organic-treated MMTs/SiO₂ are prepared once hydration is initiated. When I-MMTs are mixed with MgCl₂ in an alcoholic solution such as butyl alcohol, ethanol, etc., the MMTs/MgCl₂ carrier is obtained. Regardless of the order of mixing i.e., of whether MMTs are added to MgCl₂ solution or MgCl₂ solution is added to MMTs, nearly the same carrier is obtained.
- (c) These composites are washed several times with ethanol, pure water or a mixture of both in order to remove the residual ions, and then dried in a vacuum stove to obtain homogeneous white powders. The powders are calcinated to give a primary carrier, whose basic physical properties are shown in Table 3.19, as well as catalysts, properties of which are shown in Table 3.20.

The calcination of the composite carriers usually decreases their specific surface area, and pore volume, and may also produce more defective regions in the carriers. Therefore, Ti metal is carried on the defective position and provides more space for the active matter, increasing the catalyst's activity. The specific surface area of the catalysts is reduced as expected.

(2) *The nanostructure of the composite carrier.* The nanostructure of the carrier is characterized by X-ray diffraction. The diffraction pattern of MMTs/SiO₂ mixture is shown in Figure 3.19, where the peaks at a position below 5° (2θ) denote the formation of nanostructures in the carriers. The maximum peak intensity is in the range of 2.64°–2.68°, reaching upto 2.56° after calcinations. When θ decreases, d₀₀₁ increases

Table 3.19
Basic physical properties of primary carriers (BET method)

Carriers	Interlayer distance (nm)	SSA (BET) (m ² g ⁻¹)	Pore volume (ml g ⁻¹)	Mean pore size (nm)
Composite	3.29	721	0.45	4.5
Counterpart	2.8	680	—	1.8

Note: SSA, specific surface area; counterpart carrier refers to LeBord and Wang [34].

Table 3.20
Basic physical properties of catalysts (BET method)

Catalysts	SSA (m ² g ⁻¹)	Pore volume (cm ³ g ⁻¹)	Pore area (m ² g ⁻¹)	10 Å pore volume (cm ³ g ⁻¹)
C-2	190.39	0.15	146.20	0.097
C-5	140.74	0.11	100.60	0.083
C-6	253.97	0.21	185.83	0.15
C-10	227.90	0.20	155.01	0.16

Note: SSA, specific surface area; 10 Å pore volume, total pore volume from those diameters above 10 Å.

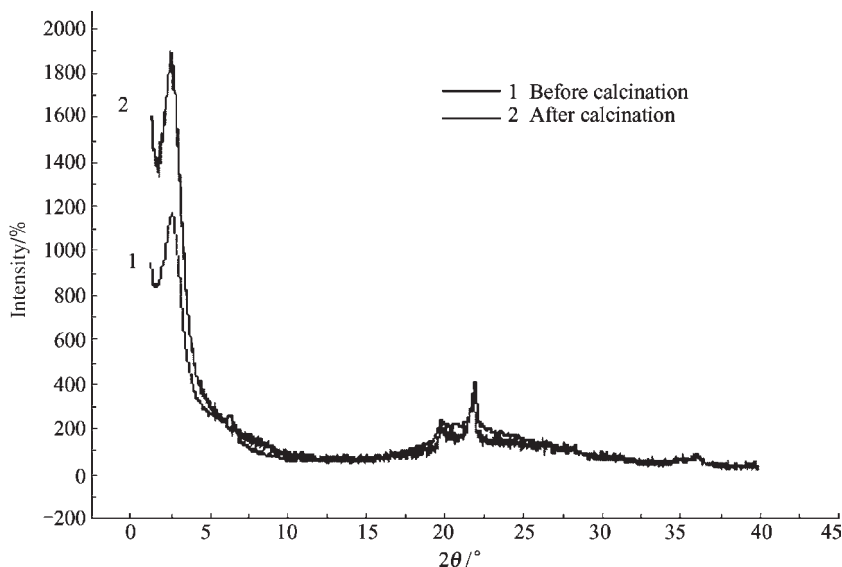


Fig. 3.19. XRD patterns of composite carriers of MMTS/silica.

according to the Bragg equation $\lambda = 2d_{001} \sin \theta_{001}$ (θ is half-angle of diffraction position at X-ray diffraction peak). At the 2θ position, the calculated interlayer distance is 3.8 nm. In Figure 3.19, the layer structure is maintained after calcinations but is slightly enlarged. This enlarged structure provides a foundation for creating an exfoliated layer during in situ polymerization.

3.3.1.2. Carrying the active ingredient

The complexity of the preparation of the Ziegler–Natta catalyst necessitates a careful examination of each preparation step on the nanoparticle carriers.

(1) *Preparation of solvents.* In an inert solvent such as hexane from which residual water and oxygen has been removed, the zeolite dipping for at least 24 h. Then, under an N_2 atmosphere, the solvent of hexane, benzophenone and sodium metal are added to the three-necked flask, and heated to boil for 6 h. Finally, the purified hexane is separated and sealed inside the desiccator for further use as a solvent. This freshly prepared solvent is beneficial for catalyst activity.

(2) *Carrying process.* Under N_2 atmosphere, 1.5087 g of the carrier is added to the freshly prepared hexane solvent, which has been cooled to below 0°C . Then, to this mixture, 130 ml of cold $TiCl_4$ solution ($M_w = 189.71$, density = 1.726 g ml^{-1}) below 0°C is added and stirred. This solution is gradually heated to $70\text{--}80^\circ\text{C}$. Another additive (0.8 ml of *o*-benzene dicarboxylic dibutanoate, BDD) is added to it and heated to 120°C for 3 h. Finally, the solution is filtered out under the N_2 atmosphere, and washed several times with hexane solvent. The collected materials are dried and sealed inside a glass bottle. Several catalysts are prepared in this way, as shown in Table 3.21.

Table 3.21
Several typical catalysts and their preparation conditions

No.	Carrier (g)	TiCl ₄ (ml)	<i>o</i> -BDD (ml)	Reaction time (h)	Ti content (%)
C-2	1.5087	130	0.8	3	8.1
C-3	1.5090	140	0.8	3	—
C-5	1.5070	170	0.8	3	5.0 ^a
C-7	1.5056	130	0.6	3	7.5
C-8	1.5030	130	1.0	3	—
C-10	1.5037	130	0.8	4	—

^aMean value.

Table 3.22
The effect of Ti/Al(Si) ratio on the catalyst's activity

Catalysts	Ti/Al (Si)	Activity (g g ⁻¹ catalyst h ⁻¹)
C-3	55	50.5
C-4	60	54.24
C-5	65	76.57
C-6	70	61.42

(3) *Effect of Ti/Al(Si) ratio on the catalysts.* When fixing the carrier load, several catalysts with different *Ti/Al(Si)* ratios are prepared for polymerization reaction at normal pressure (Table 3.22).

It is seen from Figure 3.20, that initially as the *Ti/Al(Si)* ratio increases, the number of atoms of Ti creates more active centers and increases the polymerization activity accordingly. Under such conditions, propylene on the surface of TiCl₄ (at the edge of crystallites) produces a coordination effect [32], as a result of which the monomer polymerizes and intercalates into the interlayer space. When the Ti load increases more, the more empty orbitals create more coordination causing the monomer polymerization to be more difficult. How the MMTs affect the Ti activity centers needs further investigation.

The effect of the inner electronic donor on the effectiveness of the catalyst is still under investigation. During PP polymerization, the proper electronic donor not only makes the catalyst active, but also produces PP of high iso-tacticity. One of the effects of the inner electronic donor is that it forms a complex with the carrier on the location of the random active center, where active TiCl₄ does not function, and prevents forming such a random active center. In addition, the inner electronic donor promotes polymerization activity, enhancing the yield of PP with high iso-tacticity. The inner electronic donor *o*-BDE is often preferred in experiments.

3.3.1.3. Polymerization process

(1) *Polymerization of polypropylene.* The polymerization process of polypropylene on MMT carriers is similar to that on MgCl₂. A Hexane or heptane is used as solvent for polymerization. This polymerization may make use of slurry technology, with the help

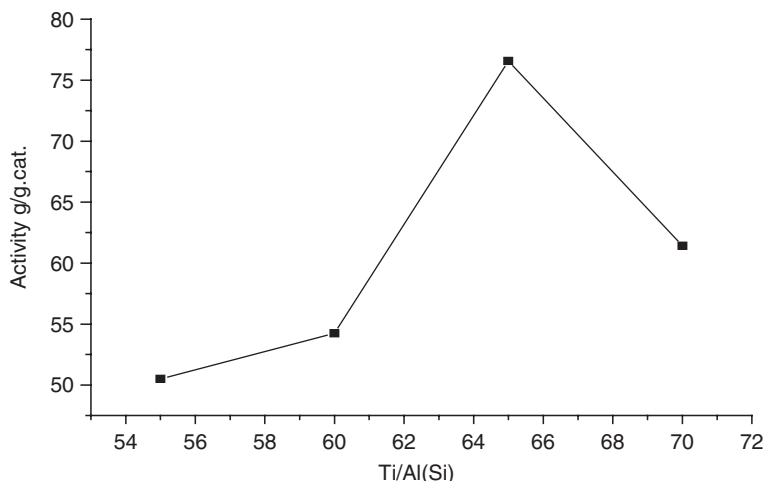


Fig. 3.20. Plot of catalyst's activity vs. Ti/Al (Si) ratio.

of which the products are formed and precipitated in the mixture. The solvents in the slurry are beneficial to the intercalation of propylene monomers into the gallery of MMTs. The details are provided below.

Example 3.3.1.1. Polymerization of polypropylene. The process is briefly described here. A three-necked flask equipped with a stirrer and a constant temperature device is set to 66°C and purged with N₂ gas for 10 min. The propylene monomer is then poured into the flask, to which a 150 ml of hexane is added together with 3.3 ml of AlEt₃ catalyst while stirring. Further, 5 mg of catalyst and the outer electronic donor in 1 ml pure hexane are added to the flask, and then the remaining catalyst (3.3 ml) is added to the system; the slurry mixture reacts for 1 h at 66°C before stirring is stopped. A mixture of the hydrophilic chloric acid and ethanol is added to the polymerization system to terminate the reaction. The reactive system is cooled to room temperature; polypropylene separates out, which is dried at 50°C for 2 h. The material composition is: in Al/Ti = 300, Ti% = 0.05, additives, 0.54 ml of benzyl ethyl ester and 19.46 ml of hexane. The properties of the catalysts and the products are shown in Table 3.23.

In the polymerization of propylene, the activity is rather moderate though it is not as high as that of MgCl₂. The inorganic phase accounts for 1–2% (by mass) of the whole nanocomposite. At such contents of inorganic loading, the mechanical properties will meet the needs of applications.

(2) *Polymerization of ethylene.* Similar to the process of propylene polymerization, polyethylene polymerization also uses heptane as a solvent on MMT carrier. Slurry technology is used as described below.

Example 3.3.1.2. Polymerization of ethylene. An autoclave equipped with a stirrer and a constant temperature device is heated to 50°C and purged with N₂ gas for 10 min.

Table 3.23

Properties of propylene polymerization in the catalysts under a reaction temperature at 66°C and pressure of 1 atm

Catalyst	Load (mg)	AlEt ₃ (mmol)	Benzyl ethyl ester (mmol)	Time (h)	Activity (g g ⁻¹ cat h ⁻¹)
C-3	7	3.760	0.188	1	50.5
C-4	7.3	3.760	0.188	1	54.24
C-5	7	3.760	0.188	1	76.57
C-6	5	3.760	0.188	1	61.42
C-7	5	3.760	0.188	1	71.74
C-10	5	3.760	0.188	1	92.16
C-5-1	5	3.760	0.188	0.5	83.9
C-5-2	6.6	3.760	0.376	1	62.67
C-5-3	7.4	3.760	0.094	1	90.78

Note: Load, catalyst load; time, polymerization time.

Table 3.24

Effect of the outer electric donor on the activity of catalysts

Catalyst	Load (mg)	AlEt ₃ (mmol)	Benzyl ethyl ester (mmol)	Time (h)	Activity (g g ⁻¹ cat h ⁻¹)
C-5	6.6	3.760	0.376	1	62.67
C-5	7	3.760	0.188	1	76.57
C-5	7.4	3.760	0.094	1	90.78

Note: load, catalyst load; time, polymerization time.

Then, ethylene gas is flushed into the autoclave, to which heptane, AlEt₃ additive and TiCl₄ are added while stirring at 50°C and 1 atm for 1 h. The stirring is stopped and acidized ethanol is added to terminate the reaction to give the final product, which is filtered out and dried under vacuum. The polymerization gives the low activity of 10–30 g of the product per g of catalyst.

(3) *The effect of the outer electric donor on propylene polymerization activity.* The effect of addition Catalyst C-5 with different loads of outer electric donor on polymerization activity is shown in Table 3.24. The increase in load of the outer electric donor decreases the activity of the propylene polymerization. One of the functions of benzyl ethyl ester is to form a complex with the AlEt₃ additive, reducing the production of the free AlEt₃ or the formation of the active centers. It also has other roles in controlling the activity of the propylene reaction.

In polyolefin–inorganic phase nanocomposites, the inorganic load usually reaches 1% (by wt), which is the critical load at which this nanocomposite shows a “nanoeffect.” That is, the nanoparticle load reaches or accumulates to a critical extent, at which the nanoparticles will demonstrate an unusual effect in their properties or physical functions. Thus, the overall design of such a catalyst carried on MMTs is taken into consideration, which requires enough load of inorganic phase to produce the nanoeffect.

(4) *The effect of polymerization time on the propylene reaction.* Attempts have been made to investigate the effect of reaction time on propylene polymerization. The results show that as the reaction time increases, the polyolefin yield increases but its activity decreases. The reasons for such a decrease in activity may be due to two aspects: (1) as polymerization proceeds, the structure of the active center varies or its activity is lost; and (2) as far as the monomer dispersion is concerned, during the formation of polymer products on the surface of the catalysts, it is difficult to spread monomer from the catalyst surface into its inner space. For solvent precipitation or slurry polymerization, there exists a possibility of mass transfer resistance from the gas phase to the liquid state [30].

(5) *The physical properties of propylene polymerization.* The morphology of clay exfoliation, its crystallization and inorganic layer dispersion in PP–MMT nanocomposites is characterized by different techniques such as TEM, AFM, or XRD. Their structure information reflects the properties of the nanocomposites. In XRD pattern, there is no diffraction peak between diffraction angle from 0–5°, indicating that the interlayer distance is enlarged during monomer penetration and polymerization. This interlayer distance approaches the ultimate level so as to produce nanocomposites with complete layer exfoliation morphology (see Figure 3.21 for TEM and X-ray). Obviously, the disappearance of the diffraction peaks shows complete exfoliation of the clay layer.

The nanocomposites of PP–MMTs usually have a high density of 1.01 g cm^{-3} indicating the high density of 2.3 g cm^{-3} clay filling into the composite. In the DSC curve, the phase transfer turning points appear at 93 and 181°C, quite different from the melting point of pure PP at 165°C.

The nanocomposites are very antisolvent. They do not dissolve in nearly all solvents, except some strong acids such as, H_2SO_4 and CF_3COOH . When they are dissolved in *o*-dichloric benzene, *o*-dimethyl benzene, or 1,2,4-trimethyl benzene at 140–160°C for 4–8 h, partial solution of polymers is detected with gel permeation chromatography (e.g., Waters-220), which shows that it is difficult to determine the sample's molecular weight using the usual techniques. In some cases, if the PP oligomers with low molecular weights are obtained and cross-linked by the MMT layers, their molecular weights are

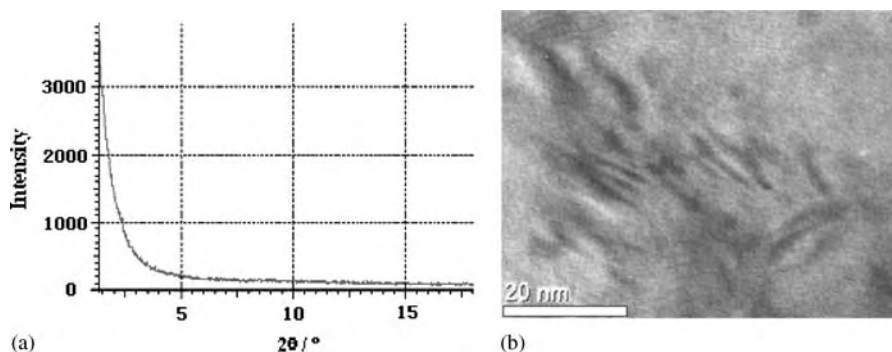


Fig. 3.21. X-ray patterns of PP-based nanocomposites: (a) X-ray diffraction pattern; (b) TEM pattern.

easily detected but their iso-tacticity is lower than that of the high molecular weight PP-MMT nanocomposites. The data on these nanocomposites are still under investigation.

(6) *Some temporary conclusions.*

- (a) Using a prop-up and intercalation techniques, layered silicate/oxides nanocomposite carrier for olefin (propylene, ethylene, etc.) polymerization are prepared. In the nanocomposites, the inorganic load reaches 1–2.0% (by wt) dispersing in 20–80 nm in the polyolefin matrix. Polymerization under normal pressure shows catalyst activity of 20–100 g yield g^{-1} cat h^{-1} , which is suitable for olefin polymerization.
- (b) The carrier has surface area of $721 \text{ m}^2 \text{ g}^{-1}$, pore volume of $0.4536 \text{ cm}^3 \text{ g}^{-1}$ and pore diameter distribution from 40 to 400 Å, while their catalysts still have a surface area of 140.47–300 $\text{m}^2 \text{ g}^{-1}$, and pore volume of $0.1519\text{--}0.2597 \text{ cm}^3 \text{ g}^{-1}$ with wide pore diameter distribution of 10–400 Å. In the catalysts, the Ti/Al(Si) ratio, reaction time, outer electric donor, etc., have effects on polymerization activity and the nanoeffect.

3.3.2. PE–inorganic nanocomposites

3.3.2.1. Features of polyethylene

Polyethylene (PE) production is over 100 million tons per year worldwide as a result of its wide application. Low cost, good recycling performance, good processability, non-toxicity and biocompatibility of PE are its outstanding advantages over other similar polymers. These days PE is only an abbreviation of different PE products. That is, PE belongs to a family of products with diverse performance, such as high-density polyethylene (HDPE), linear low-density polyethylene (LLDPE), middle-density polyethylene (MDPE), linear high-density polyethylene (LHDPE), etc. If PE is divided according to its applications, there are PEs for special applications, such as PE for cable application, blown-film PE, casting-film for food package, ultra-high-molecular-weight polyethylene (UHPE) for pipelines or man-made skins [38], etc. At present, there are thousands of PEs for different applications.

Although it has so many applications and advantages, PE has its disadvantages, such as poor stiffness, low-temperature toughness and low melting behavior, which have left a great opportunity for investigators to improve the PE properties. Modifications of PE through PE-MMTs nanocomposites have been introduced. We have invented several PE-MMTs or clay nanocomposites [39–42] for pipelines, films, etc., and other researchers have also prepared PE nanocomposites by ethylene homo- and copolymerization in the presence of organophilic layered silicate treated by various quaternary alkyl ammonium cations. An incomplete exfoliation of silicate layers is obtained, which leads to a poor reinforcement of PE, e.g. HDPE [40]. Similar modifications of PE use meso-porous silica, MCM-41, etc. as the support of polymerization catalysts, in which metal complexes are attached to the inner walls of uniform pores with a hexagonally arranged array. Some special examples are given in detail [40–41]. National Petroleum Corporation of China's has also supported the research of metallocene catalysts carried on MMTs.

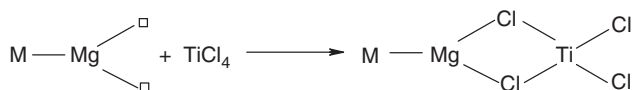
The carriers for metallocene catalysts are MMTs, saponite, Li-MMTs, synthetic mica, etc., which are treated under different intercalants such as amino acids. It is a nanosize carrier, has a specific surface area of $640\text{--}100 \text{ m}^2 \text{ g}^{-1}$, and the active metal

accounts for 0.1–5 wt% of the whole catalysts. The polyolefin resins on the nanosize carrier have properties superior to the similar metallocene catalysts on MgCl_2 carriers, while the cost of the former catalysts is reduced.

Similarly, researches supported by Sinopec have prepared magnetic catalysts for α -olefin polymerization (Chin. Appl. No.97106208.0). Such a magnetic catalyst is made up of approximately 4.0–11.3 wt% TiCl_4 or 6.7–11.7 wt% alkyl aluminum. The catalysts have a particle size of 1–300 nm. The magnetic materials are Fe_2O_3 , $\text{Cr}_x\text{Fe}_{3-x}\text{O}_4$, etc.

Exxon Chemical Patents Inc. has presented a polyolefin prepared from 5 nm silica carrier (US 5902766, 1999), which is applied to polypropylene polymerization under the gas phase. The products are of good appearance and show the good particle morphology. In the catalyst, the molar ratio of aluminum oxygen-alkyl compound to porous carrier is designed to optimize the reaction.

Ziegler–Natta catalysts were also supported on the surface of nanoscale whiskers of palygorskite; subsequently, ethylene was supplied to the activated surface, and polymerization was initiated on the surface of the fibers. As the polymerization proceeded, the surface of the nanowiskers was gradually covered by polymer until the fiber was fully encapsulated by PE. The role of palygorskite was to act as a support of the catalyst for initiating polymerization, and as a reinforcement material after polymerization. The simplest coordinated catalyst, $\text{TiCl}_4/\text{AlR}_3$ was used as active centers when composite carrier had some Mg element in it. Its proposed mechanism is



where M represents layered silicate of clay such as MMTs or palygorskite. On the calcined surface of whiskers with low OH group, the active titanium species were generated. Thus, the Ti content may be low but its activity is high (Table 3.25). This is different from SiO_2 support, in which the reaction of TiCl_4 with Si–OH predominates even calcined SiO_2 .

3.3.2.2. Direct carrier catalyst for PE

The composite carrier of MMT-silica was used to directly carry the TiCl_4 . The effect of the TiCl_4 load on its activity is shown in Figure 3.22. As the TiCl_4 load increases, the catalyst activity has a maximum value. The reasons for this behavior are under investigation, but the TiCl_4 overload (say, 8.0% Ti) shields the active centers.

Table 3.25
Ti content and activity of activated palygorskite

CT (°C)	100	200	300	500	800
Ti (wt%)	8.97	7.14	2.03	1.06	0.54
Activity <i>G</i> PE (g Ti h) ⁻¹	32	75	256	966	904

Note: Polymer conditions, 40°C; molar ratio of Al/Ti, 15; CT, calcination temperature.

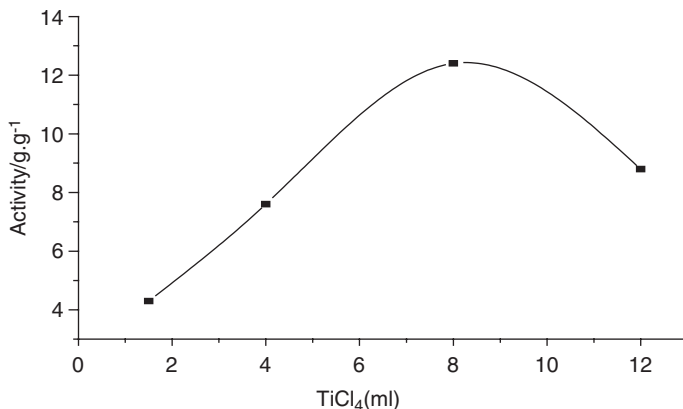


Fig. 3.22. Plot of activity vs. TiCl_4 load of catalyst. (polymerization condition: temperature, 50°C ; ethylene-pressure, 1 atm; time, 1h; activity, g yield g^{-1} catalyst). (With permission from Press of Petroleum Industry.)

3.3.2.3. Composite carrier modified with MgCl_2 -ethanol

MgCl_2 -ethanol-modified catalyst also increases the Ti load on the carrier (see Table 3.26) because TiCl_4 in the catalyst reacts with both MgCl_2 and the hydroxyl groups on the MMT surface, forming groups of $-\text{Si}-\text{O}-\text{TiCl}_3$. These groups obviously enhance the Ti load in the catalyst. This too high Ti load also yields a lower activity of catalyst at normal pressure from a similar shielding effect. Besides, the low ratio of Mg/Ti in the catalyst cannot reach a level of activity as high as that of a pure MgCl_2 carrier. The less active catalysts are also a result of the complicated composition of MMTs.

3.3.2.4. Catalysts of $\text{MgCl}_2/\text{TiCl}_4/\text{THF}$ (tetra hydro furan) carried on the composite carrier

(1) *The effect of temperature and pressure on activity.* The activity of $\text{MgCl}_2/\text{TiCl}_4/\text{THF}$ carried on the composite carrier is shown in Figures 3.23 and 3.24, where the catalyst activity decreases as the temperature increases, and increases as the pressure increases. In the slurry technique, polymerization temperature is limited by the solvent's boiling point and ethylene solubility in the solvent. From 60 to 90°C , the catalyst activity decreases as the temperature increases, indicating that ethylene concentration is a factor affecting polymerization.

(2) *Effect of THF content on catalyst activity.* The effects of the THF content on the catalyst activity areas shown in Table 3.27. In the case of $\text{MgCl}_2/\text{TiCl}_4/\text{THF}$ catalysts carried on the composite carriers, the activity of the catalyst increases along with the reduction of THF content because of the formation of $\text{THF}-\text{Al}(\text{OC}_2\text{H}_5)_3$ complexes.

Table 3.26
Compositions and activity of catalysts

Catalyst	1#	2#	3#
Ti (% by wt)	8.95	8.47	9.45
Mg (% by wt)	1.39	2.86	3.54
Activity (g yield g ⁻¹ cat.)	3.5	5.5	4.0

Note: polymerization temperature, 50°C; ethylene pressure, 1 atm; time, 1 h.

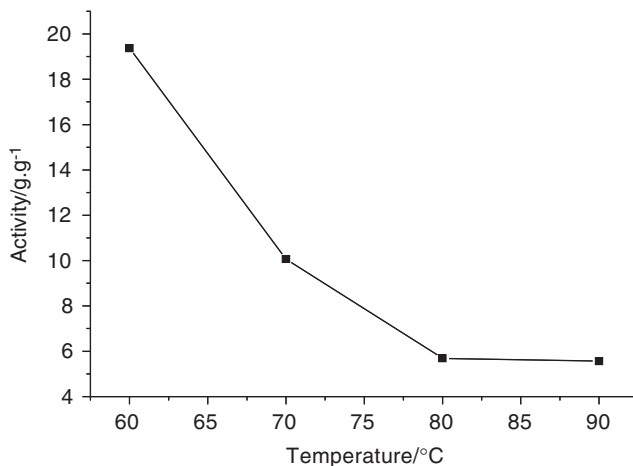


Fig. 3.23. Plot of activity vs. temperature (polymerization pressure; 0.5 MPa, time, 1 h).

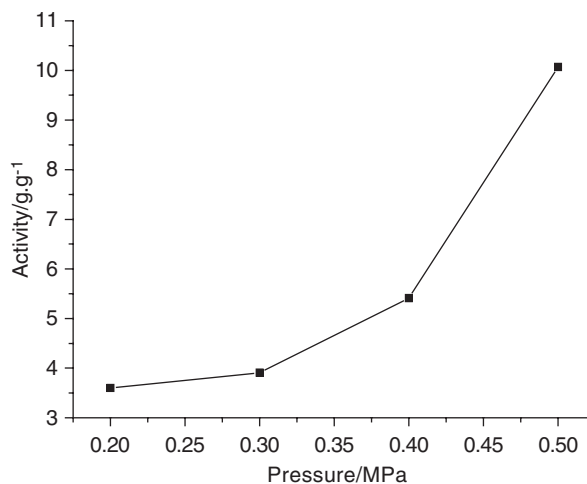


Fig.3.24. Plot of activity vs. pressure (polymerization temperature; 70°C; time, 1 h).

Table 3.27
The effect of THF content on catalyst activity

Catalyst	THF content % (by wt)	Activity (g g ⁻¹)	Drying process
1#	22.3	10.1	N ₂ sweeping
2#	12.74	20.7	N ₂ sweeping and heating at 50 V
3#	6.36	22.0	N ₂ sweeping and heating at 100 V

Note: polymerization temperature, 60°C; ethylene pressure, 0.5 MPa.

Table 3.28
The composition and the activity of MgCl₂/TiCl₄/THF catalysts carried on the composites carrier

Catalyst	1	2	3	4	5
Mg (%by wt)	1.12	2.03	3.01	3.58	6.34
Ti (%by wt)	2.83	2.86	3.02	2.74	2.38
Mg/Ti (mole ratio)	0.78	1.40	1.96	2.57	5.25
Activity (g g ⁻¹)	23.6	20.2	38.7	22.0	14.4

Note: polymerization condition: temperature, 60°C; pressure, 0.5 MPa; activity, g yield g⁻¹ cat.

(3) *Effect of Mg/Ti ratio on catalyst activity.* The Mg/Ti ratio affects catalyst activity as shown in Table 3.28. When the Mg/Ti ratio = 1–3, the catalyst activity reaches a higher level. This indicates that the Mg/Ti ratio has an optimized value, which contributes its activity to the catalyst. Why the catalysts are not similar to the traditional catalyst on pure MgCl₂ is a result of the clay composition and their interaction with the active component.

3.3.2.5. The dispersion of inorganic phase in PE

The exfoliated layer dispersions in polyethylene have their TEM morphology as shown in Figure 3.25. It is observed that MMT layers disperse randomly in the polyethylene matrix, but show an ideal exfoliated state. SiO₂ particles in the composite carriers connected with the exfoliated layers are shown in Figure 3.26, where SiO₂ particles are agglomerated in areas such as the interlayer space of clay. MMT exfoliation in the nanocomposites was investigated with X-ray diffraction, and the characteristic peak of MMT at d_{001} disappeared, showing the exfoliation of nanocomposites.

3.3.2.6. Properties of polyethylene–MMT nanocomposites

The properties of the polyethylene–MMT nanocomposites are compared with similar counterpart materials (see Table 3.29). The materials from melt-blending and in situ polymerizations are also listed in Table 3.29. Under a similar inorganic load, the properties of the nanocomposites by in situ polymerizations are higher than those from their counterparts made from mechanical blending, but similar to those from the in situ polymerized nanocomposites based on palygorskite.

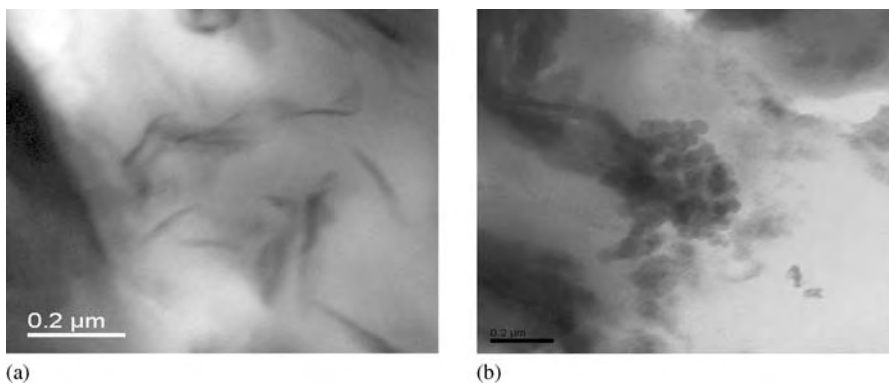


Fig. 3.25. TEM morphology: of inorganic phase dispersion in polyethylene. (a) MMTs exfoliation morphology in PE; (b) silica dispersion in PE.

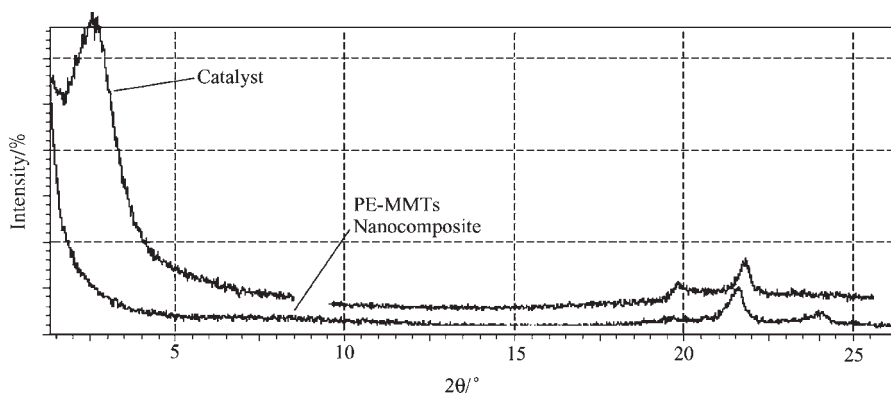


Fig. 3.26. X-ray diffraction of polyethylene-MMT nanocomposites.

3.3.3. Preparation and properties of polystyrene-inorganic nanocomposites

Polystyrene (PS) is an amorphous polymer. Under external conditions, its condensed structure transforms between different transitional states. Thus, the preparation of PS-based nanocomposites is of significance not only in the composite materials themselves, but also in revealing the essence of possible amorphous crystallizations as well. Taking MMTs as an inorganic phase, PS MMT nanocomposites also are prepared via an in situ intercalative polymerization method. When viewed within the microscope a unique shear-inducing ordered structure and self-assembly behavior with increasing temperature [43] were unexpectedly observed in the samples in pellet form. By means of SEM characterization technique, a completely exfoliated morphology is observed in the PS-MMT nanocomposites.

PS is one of the best choices for the preparation of single dispersion of particles with size varying from nanometer to micrometer or millimeter. Using these particles, some

Table 3.29
Mechanical properties of PE-layered silicate nanocomposites

Type of composites	Yield strength (MPa)	Elongation at break (%)	Tensile strength (MPa)	Yield stretch (%)	Inorganic load (% by wt)
Blends [42]	14	5.2	—	—	3.0 ^a
Blends [43]	—	147.0	—	30.4	3.3 ^b
Nanocomposite (this work)	20.9	206.0	20.5	16.0	2.9 ^c
Nanocomposite [42]	22.4	266.9	—	—	3.1 ^d

^aPalygorskite [42]. ^bMontmorillonite [43]. ^cMontmorillonite/SiO₂ composites. ^dpalygorskite [42].

assembled patterns of PS with single-dispersed silica particles are formed, which are introduced here.

3.3.3.1. Preparation of PS-MMTs nanocomposites

The ion exchange of Na⁺ in MMTs with cetyl trimethyl ammonium bromide (CTAB), the synthesis of the PS-MMTs nanocomposite via the in situ intercalative polymerization method and the preparation of their pellet specimens have been described in our previous studies [44]. CTAB-MMTs were prepared by the conventional ion-exchange method, that is, an amount of CTAB equivalent to the CEC of the Na-MMTs was added to an MMT suspension and stirred for 1 day. Then the suspension was filtered, washed three times with distilled water, dried in a vacuum oven and powdered in a miller.

Generally, the styrene monomer was purified by distillation under reduced pressure in a nitrogen atmosphere before use because of its possible pre-polymerization in the container.

Example 3.3.3.1. Preparation of PS-MMT nanocomposites. PS-MMT nanocomposites containing 5 wt% CTAB-MMTs were prepared by in situ intercalative polymerization process. CTAB-MMTs were dispersed in the styrene monomer and dispersed fully into a transparent container, which allowed the styrene monomer to intercalate into the CTAB-MMT galleries. Then, an aqueous mixture of ammonium salt of [(NH₄)₂S₂O₈] as a radical initiator and sodium dodecyl sulfate as an emulsifying agent was added. The resulting mixture was stirred vigorously at room temperature for 30 min. and subsequently polymerized at 70–80°C for 5 h under an N₂ atmosphere. Then it was washed, dried and crushed to finally, obtain the product. The pellet specimens of the PS-MMTs nanocomposites are prepared by extrusion of the nanocomposites powder at 200°C with a common extruder.

A CEC CTAB solution, 1.5 times equivalent to clay, was added to 5 wt% Na-MMT suspension. The mixture was stirred vigorously for 1.5 h at 80°C, filtered off and washed with hot water repeatedly until no Br⁻ was detected on addition of 0.1 mol L⁻¹ AgNO₃ solution. Then, the product was dried in vacuum to a constant weight at ambient temperature and smashed into particles of size smaller than 70 μm.

Use of CTAB improves the wetting between clay and polymers or monomers [43]. The swelling and interlayer distance of MMTs was revealed by XRD.

3.3.3.2. Some properties of PS-MMT nanocomposites

(1) *Specifications and properties of PS-MMT nanocomposites.* In PS-inorganic nanocomposites, the inorganic phase is selected from MMTs, silica and other metal oxide particles. The selection of the inorganic phase depends on improving PS properties and on the formation of regular patterns.

NA-MMT samples from the Source Clay Repository, the Department of Geology at the University of Missouri, from American Southern Clay Corporation, from Jianping, Liaoning Province, from Jiashan, Anhui Province, and from Zhangjiakou, Hebei province were collected. MMTs with CEC from 70 to 100 mmol (100 g)⁻¹ were selected.

For determining properties, some PS-clay nanocomposite samples were made into films with a thickness of about 1.5 mm, a length of 20–25 mm and a width of 12 mm. The PS-MMTs nanocomposites were melt-pressed between two glass slides at about 200°C, and subsequently quickly cooled in cold water and chemically etched in toluene. The synthesized powder sample was fully dispersed in distilled water, and deposited on an aluminum film. The pellet samples were fractured after immersion in liquid nitrogen. Parts of the samples were coated with gold, and other parts of the samples were coated with gold after being etched with toluene to expose possibly concealed MMT nanosize particles.

SEM of the nanocomposite samples shows the morphology of the dispersed CTAB-MMT powder in an aqueous suspension. The planar MMT aggregates are prevalent in the morphology. The MMT aggregates have high aspect ratios. Unlike rigid plates, most of the aggregates are dark at the center and light at the boundary, showing some flexibility. Figure 3.27 represents the SEM micrographs of the PS-MMT nanocomposite powder sample. The synthesized product via emulsion polymerization is in the form of the monodispersed spherical particles, about 200 nm in diameter.

The fracture surface of the extruded pure PS pellet is also detected (not shown here). The fracture surface is relatively even and smooth showing a typical brittle feature before it was chemically etched. The PS-MMT nanocomposite samples are further stretched to reveal their strain–stress behavior. Fibrils leading to stress whitening are prevalent in Figure 3.28, indicating localized plastic deformation. The nanocomposites have some degree of toughness in comparison with pure PS.

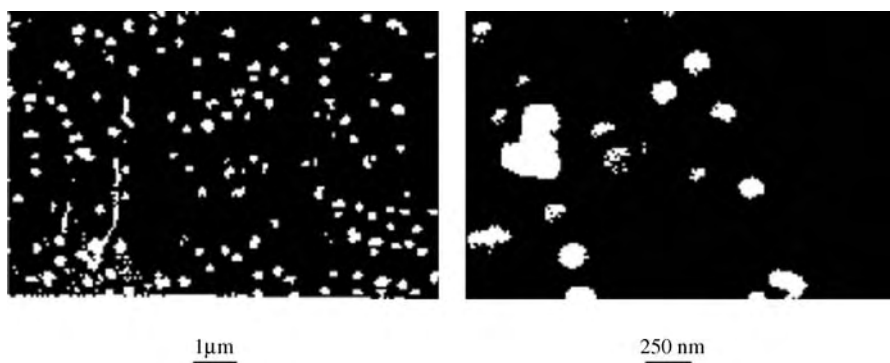


Fig. 3.27. SEM micrographs of the PS-MMT nanocomposite powder sample.

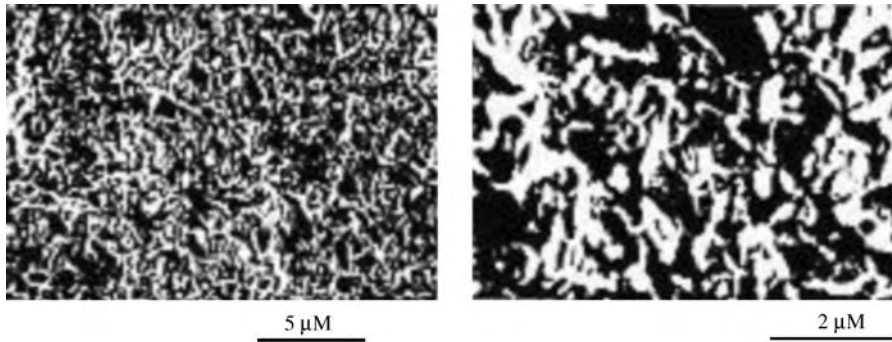


Fig. 3.28. SEM morphology of the fractured surface of the PS-MMT nanocomposite pellet sample before it is chemically etched.

After the fractured pellet sample of the PS-clay nanocomposite was chemically etched by toluene, the fibrils dissolved, and the MMT primary particles can be clearly observed, as shown in Figure 3.29.

During the intercalative polymerization process, the layer structure of the MMT suffers damage and is exfoliated from expansion induced by the PS molecular increasing and the exothermic reaction between the galleries. It is seen that, after polymerization, the micron MMT aggregates are broken into small particles and dispersed homogeneously in the PS matrix. This is in agreement with our previous TEM studies [43]. To observe more details of these silicate primary particles, we present with a higher magnification in Figure 3.29(b). The length of the primary particles is less than 350 nm. Because the planar silicate primary particles disperse in every direction and appear to be flexible, it is difficult to determine the thickness directly from SEM micrographs.

Figure 3.30 presents the surface morphology of the PS-MMTs nanocomposites film specimen. Because the specimen was prepared via melt pressing, the MMT primary particles prefer an orientation parallel to the film surface. It is seen from Figure 3.30 that the diameter of the planar montmorillonite primary particles is less than 350 nm. This is quite consistent with the morphology in Figure 3.29. The distribution of the MMT primary particles in Figure 3.30(a) was aided by an energy-dispersive X-ray probe. An image of elemental mapping for Si is shown in Figure 3.30(b). The domains of the little white dots in Figure 3.30(b), representative of Si, correspond to the dispersed phase in Figure 3.30(a). This indicates that the domains are the images of the MMT primary particles.

(2) *The Morphology of PS-MMTs nanocomposites.* In some examples, it was found that the synthesized PS-MMT powder was composed of monodispersed spherical particles about 200 nm in diameter [44]. Before the PS-MMT nanocomposite pellet was chemically etched, the fracture surface showed many fibrils in comparison with the smooth surface of pure PS. After the PS-MMT pellet fracture surface was chemically etched, the homogeneously dispersed MMT primary particles could be clearly observed. As for the etched film sample, the primary particles preferred an orientation parallel to the surface.

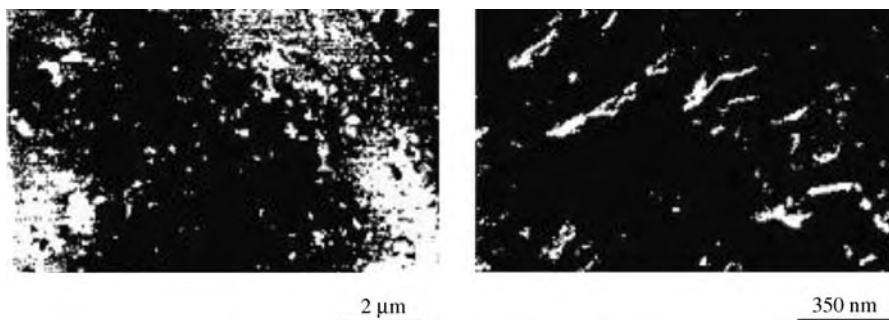


Fig. 3.29. SEM morphology of the fractured surface of a PS-MMT nanocomposite pellet sample after it was chemically etched.

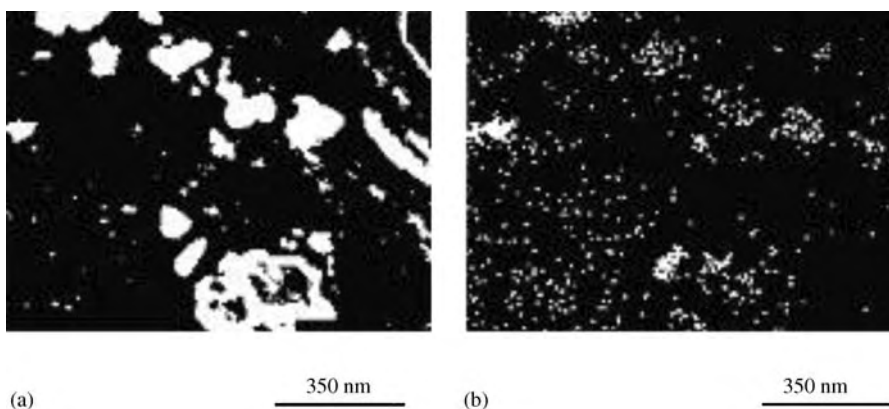


Fig. 3.30 (a) SEM morphology of etched PS-MMT nanocomposite films, and (b) X-ray mapping of such a sample, showing the distribution of the silicon.

An exfoliated PS-MMT nanocomposite has been prepared via an in situ intercalative polymerization process. In the WAXD patterns, an absence of any sharp peaks at low angle ($2\theta < 10^\circ$) is shown. The TEM images present the nanoscale MMT particles narrower than 40 nm in lateral dimension and a heterogeneous disordered microstructure within the primary particles. These morphology observations have confirmed the success of preparation of an exfoliated PS-MMT nanocomposite.

(3) *A complete exfoliation of PS-MMTs.* Because of the nanoscale effect, high interface areas, and strong interfacial interaction between dispersed phases with the polymer matrix, nanocomposites possess unique properties typically not reached by their conventional macro- or micro-composite counterparts, and therefore may open new opportunities in high technology.

Organo-MMT (organo-clay) obtained through a cation exchange reaction with alkyl ammonium or other organic cations is used as an inorganic phase. During in situ intercalative polymerization or melt intercalative process, MMTs are broken down into their

nanoscale building blocks and dispersed uniformly in polymer matrix to form polymer or PS-MMT hybrids or nanocomposites. Their unusual physical properties are normally attributed to the homogeneous dispersion of the nanoscale MMT particles.

Besides the emulsion polymerization process of the preparation of the PS-MMTs, there is another direct intercalation of PS between silicate layers from PS melt. However, research on exfoliated PS-MMTs hybrids has been minimal. We found that the silicate layers became exfoliated and disordered during the polymerization process. After polymerization, the Na-MMTs, about 10–70 μm in diameter were broken into small primary particles of 30–70 nm in lateral dimension, and dispersed in a random direction in the PS matrix. Unlike compact face-to-face stacking characteristic of original clay mineral or intercalated polymer-MMT nanocomposites, a heterogeneous disordered microstructure is observed. The gallery distance ranges 5–20 nm within the primary particles, containing a defect structure (not shown) of about 10 nm. Near the boundary of the primary particle (not shown), the interlayer distance is in the range of 5–18 nm. It is quite interesting that there exists such an order and orientation morphology in PS-MMT nanocomposites, when such nanocomposites are simply sheared in the extruder.

3.4. Polyester–silicate nanocomposite

Poly(ethylene terephthalate) (PET) is a polymer material with many applications, such as fibers, film, packaging, functional matrix materials and engineering plastics. Caruthers invented it in the 1960s. At present, the production of PET in China has reached 75 million tons, accounting for 30% of the global yield. Versatile modifications of PET through nanocomposites have been launched. All these modifications aim at meeting the needs of improving PET melt strength and its crystallization rate for improved processing.

At present, PET materials are applied to fields such as functional films, barrier materials and engineering materials. Through its mixing or in situ polymerizing with different nanoparticles such as TiO_2 , SiO_2 and layered silicate, the nanocomposites are endowed with different properties and functions such as shielding harmful lights and poring a barrier to O_2 and CO_2 gases etc. PET-layered silicates of MMT nanocomposites are prepared mainly through the above mentioned intercalation–polymerization technique. The work in this field is unique in the world.

Several practical approaches to the preparation of polymer–inorganic nanocomposites are introduced below, some of which are suitable for the preparation of PET-MMT nanocomposites.

(1) *Melting blending.* This technique is used to prepare nanocomposites on a large scale. Polymer pellets and organo-clay are blended in the extruder and are melt-extruded together to obtain materials with exfoliated layers. These methods are applied to the preparation of nanocomposites of layered silicate with polymers including PP [46–48], PE [46], PA6 [49], PS [50], etc. The organo-clay suitable for this technology is specially modified to be suitable for different polymers. For example, the organo-clay is treated with polymer oligomers grafted with other functional groups to improve its compatibility with polymer matrix, and the properties of the final nanocomposites. However, this technique is not popular for the preparation of PET-MMT nanocomposites because PET absorbs water and thus degrades.

Silica particles, are made into core-shell structure via radiation-cross-linking grafting, and then melt-blended with polymer matrix to prepare nanocomposites. During this melt blending, silica disperses homogeneously. Under improper blending, the silica tends to agglomerate, so this method should be implemented carefully.

(2) *In situ polymerization blending.* When organo-clay acts as an inorganic phase, the monomer of polymer is blended with the organo-clay to form a suspension solution. This mixture is then initiated to polymerize under reaction conditions similar to pure polymer, during which layered silicates of clay are dispersed in situ into nanoparticles. The polymerization media is designed to prepare most kinds of polymers [51–55,57–61] such as PS, PA6, PI, PET, PBT and PA66.

Similarly, when silica is used to polymerize with polymers such as PS, the emulsion media, which include initiator and surfactant, or dispersant of PVP, are prepared for the polymerization of PS with treated silica. The silica may be treated with a coupling agent such as silane of KH-560, KH-570.

(3) *Media blending.* In the selected solvent, reagent, gas, organic polymer or oligomer, the superfine inorganic phase is usually dispersed. By using media blending or suspension, the clay is modified and applied for different purposes.

The proper content media remaining inside the inorganic particles of silica or layered silicate benefit their dispersion. Example of polymer-inorganic nanocomposites prepared via such a method include PI [54]-MMTs, PET-MMTs or silica [56], PEO-MMTs or silica [62–64], PLLA and PCL-MMTs [65] (PLLA, poly(L-lactate); PCL, poly(ϵ -caprolactone)). PA6-clay nanocomposites [66–70] and PET-clay nanocomposites [56,60,61] are successful and practical examples.

Polyesters such as poly(ethylene terephthalate) (PET) and poly(butylene terephthalate) (PBT) are the top five engineering plastics with improved properties such as, high transparency (PET), high crystallization (PBT) and high electrical and mechanical properties (PBT), which make them applicable for reinforced plastics, bottle packaging, computer parts and automobiles, and in other machine parts as gears, engine cylinders, shells of mobiles and voltage adjusters. However, both have disadvantages of low HDT, poor thermal properties and sensitive variation to processing conditions, which have limited their wider application and the market share of products of engineering plastics in the world. So, modification of their processing behavior is of special importance. To solve this problem, the oligomers of PET are used to treat the inorganic phase such as clay or silica. Then, these oligomers are used to polymerize with PET monomers in the preparation of the final nanocomposites with proper dispersion morphology.

Generally, organic polyester polymer nanocomposites with an inorganic phase is one of the most popular modification methods today. MMTs with a layer unit structure of 50 nm \times 100 nm \times 1 nm are selected as the inorganic phase for the preparation of the nanocomposite.

3.4.1. Polyester-clay nanocomposites preparation

The preparation of nanocomposites of polyester, including PET and PBT, with inorganic phase of MMTs or silica, through either different technologies mentioned or its oligomers-inorganic nanoprecursors is described in this section.

(1) *Silica pretreatment.* Silica particles with a size of 20–50 nm and purity higher than 99.9% (by wt) are used. The phosphorous acid is used as a reagent of hydration, which reacts with amine ($\text{CH}_3(\text{CH}_2)_{15}\text{N}^+(\text{CH}_3)_3$) to produce ammonia salt. This salt reacts with silica pre-treatment, and is again suspended and dispersed, in the polyacrylic amide ($M_w = 15$ million g mol^{-1}) solution with a concentration of 1/100,000 to obtain the treated particles after freeze-drying.

(2) *Particles mixed with oligomers and in situ polymerization.* The treated particles are mixed with oligomers to obtain different particle-based precursors. The precursors are then polymerized with PET monomers by following the processes mentioned earlier with a slight modification, and the final composites are prepared in a 10 l autoclave. The details of the preparation process are as follows:

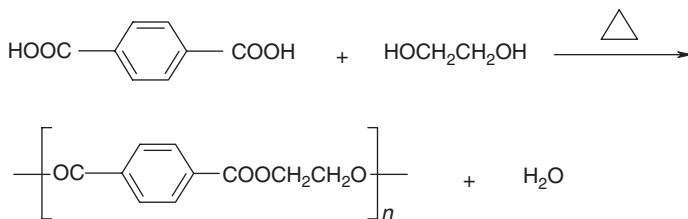
Example 3.4.1.1. Preparation of nanocomposites. 4000 g of BHET (bihydroxyl ethyl terephthalate) oligomers is first melted, then 120 g of the treated silica powder is added to the melt in a stepwise manner within 30 min. Meanwhile, water, ethanol or oligomers are discharged under nitrogen (N_2). During the process, the temperature increases gradually from 230 to 270°C for 30–60 min. When the melted mixture becomes clear, it is kept under vacuum of 40–80 Pa for 2 h to polymerize. After that, N_2 is used to squeeze the melt into strips, which are then cut into pellets in cold water. Pellets are vacuum-dried to obtain samples below 70°C. These PET-silica nanocomposites (NPETs) are characterized.

In the same way, solid precursors of silica or MMTs (i.e., treated silica) are mixed with PET oligomers to polymerize under PET reaction conditions. The solid nanoparticle precursors are named NPP (e.g., NPP00, NPP01, NPP02, etc.)

Example 3.4.1.2. Preparation of NPET film samples. The composite pellet samples are vacuum-dried at 100–120°C for 4 h. The dried pellets are then set in a compressor, processed with a melt-quench process, with a heating temperature of 10°C above the sample melting point at a pressure of 5 MPa in an oil hydraulic press and melted for 5 min. After that, the films formed are withdrawn rapidly from the compressor and put immediately into a mixed solvent of water and ice. Thus, a film thickness of 1 mm is obtained.

3.4.1.1. Direct esterification

There are several methods of polymerizing polyesters. In the preparation of poly(ethylene terephthalate), direct esterification is used to synthesize high-molecular-weight polymers. The process is shown below:

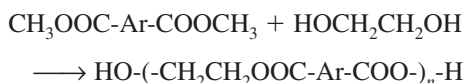


Based on the technology, the poly(ethylene terephthalate)–MMT nanocomposites are prepared by mixing organo-clay with monomers of ethylene glycol (EG) and *p*-terephthalic acid (PTA) under same polymerization conditions as for PET. The reaction reveals that when PET oligomers form, the ester exchange reaction occurs in any section of the molecular chains. That is, during the formation of the resultant nanocomposites, the molecular chain-grafting reaction with silicate layers accompanies an ester exchange reaction as shown below:

A similar process to that shown in Figure 3.31 is reported in the literature [58,60]. By this process, PET-MMT nanocomposite samples are prepared with improved properties including the functional ones to be investigated in the later part.

3.4.1.2. Indirect esterification

Similar to the direct esterification reaction for the polymerization of polyester, indirect esterification takes the monomers of dimethyl terephthalate (DMT) and EG as its monomers. The reaction is as shown below:



where Ar = 1,4-phenylene. During the polymerization process, methanol is produced and has to be recovered for recycling. During the copolymerization of organo-clay with these monomers, it is found that, in some cases, this reaction is sometimes hindered by improperly treated clay. This phenomenon is thought to result from the methanol absorbed on the MMT layers, which prevents it from discharging. That is, such an indirect esterification polymerization process is not suitable for some organo-clay (MMTs) intercalation polymerization to prepare the nanocomposites. When MMT is treated with

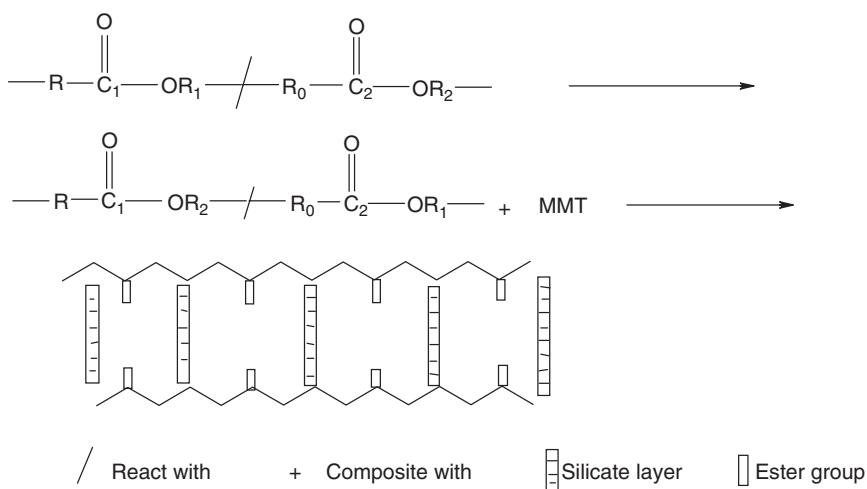


Fig. 3.31. The PET intercalation reaction in MMT gallery with the esterification (C_1 is equal or not equal to C_2 , R, R_0 , R_1 or R_2 are molecular chains connected with ester group, aromatic ring and hydroxyl group).

laurylamine quaternary ammonia chlorite, the polymerization goes well and the nanocomposites possess good property in modulus compared with their counterpart PET. Decreases in the other mechanical properties resulted from the unsatisfactory interface morphology between exfoliated layers and PET matrix. The properties of PET nanocomposites with organo-clay (MMTs) are shown in Table 3.30.

3.4.1.3. Different intercalation reagents

The intercalants usually act as the interfacial modifier when intercalated into the MMT layer gallery. They are important factors affecting the exfoliated morphology of layers in the polymer matrix. The intercalants prove to be intercalated into the interlayer gallery via element analysis of the composites; the results are shown in Table 3.31.

3.4.1.4. Different intercalation technology

In the actual preparation of PET-MMT nanocomposites, there are some precepts.

(1) *Solvent intercalation.* In practice, the mixed solvents of ethylene glycol and water (or EG + H₂O) are used for the intercalation of MMTs. The suspension of EG, water and MMTs is prepared through mixing and stirring. Then, the solution is heated to react between the boiling points of the mixed solvents of EG and water, during which the water produced is gradually discharged through an outlet for draining. As the reaction proceeds, the gel of MMTs becomes viscous and the temperature of the system increases gradually. It is noted that such a reaction aims at producing PET oligomer–MMTs or silica solid nanoprecursors. The PET oligomer containing MMTs or silica particles has satisfactory layer dispersion morphology in the oligomer matrix. There have been other

Table 3.30
Properties of PET-MMT nanocomposites in indirect esterification process

No.	LLC (g)	DMT + EG (g)	IZOD (J M ⁻¹)	σ_t (MPa)	σ_b (MPa)	E_b (MPa)
1	0.0	100	28	58	108	1400
2	3.0	100	26.5	49	79	3540

Note: LLC, load weight of layered silicate; (DMT+EG), total weight of monomers; IZOD, notched izod impact strength; σ_t , tensile strength; σ_b , bending strength; E_b , bending modulus.

Table 3.31
Element analysis of intercalants inside the MMT gallery

Intercalant	C/N	
	(Calculated data)	(Experimental data)
CN-16	18.8	19.6
M-6A	6.96	6.97
M-2H	2.30	2.19
CN-12	11.2	11.3

Note: CN-16, CH₃(CH₃)₂(N)-(CH₂)₁₃; M-6A, HOOC(CH₂)₅NH₂; M-2H, HO(CH₂)₂NH₂; CN-12, CH₃(CH₂)₁₁NH₂; C/N, element weight ratio.

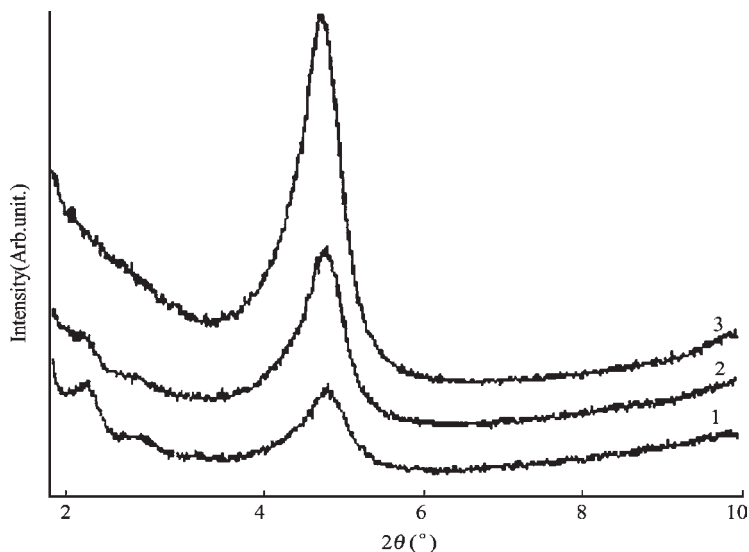


Fig. 3.32. X-ray patterns of PEG ($M_n = 2000$)-MMT composites through a melt intercalation (1 – 1–2% (by wt) MMTs; 2 – 2–5% (by wt) MMTs; 3 – 3–20% (by wt) MMTs.) (With the permission of Acta Polymerica Sinica, China Chemical Association)

attempts to intercalate the organic molecules into MMTs through other oligomers of polyethylene glycol (PEG), and their X-ray patterns are shown in Figure 3.32.

(2) *Oligomer intercalation.* Bihydroxyl ethylene terephthalate (BHET) is an oligomer of PET polymer; it is our experience that the BHET intercalation technique for the nanocomposites is usually successful. Based on BHET, many experiments for the properties of final PET–inorganic composites are made preliminarily to predict the properties of the final products. The properties of some of the BHET–inorganic composites are shown in Table 3.32.

The treated MMTs can be copolymerized with monomers of PET in the same autoclave. Compared with other inorganic phases, this PET-MMT composite has good surface property. Even so, some of the nanocomposites have some agglomerated particles (2–5%, by number; see Table 3.32). The PET-MMT nanocomposites, through an in situ intercalation polymerization process, maintain a good transparency and show enhanced thermal and mechanical properties when the inorganic phase has proper load and treatment. Under these conditions, MMT is often selected to enhance PET properties, such as crystallization behavior and other functional aspects.

A mixture of BHET with MMTs, using a mechanical mixing technology, can be prepared. The treated MMTs can be blended with BHET powder and extruded to prepare a composite in which the MMT layers are partially intercalated and exfoliated. The X-ray patterns are shown in Figure 3.33. X-ray patterns show that the simple mechanical mixing can produce some intercalated intermediates but cannot produce the exfoliated nanocomposites.

Table 3.32

Comparison of PET-based composites with different inorganic particles

Inorganic–organic phase	BHET surface	PET surface (agglomerated particle)	Film transparency
Mixed micrometer SiO ₂ -PET ^a	Homogeneous	Heterogeneous (many)	No
Gas-phase SiO ₂ -PET ^b	Homogeneous	Heterogeneous (many)	No
Deposited nanometer SiO ₂ -PET ^c	Homogeneous	Heterogeneous (many)	No
TiO ₂ -PET	Homogeneous	Homogeneous (little)	No
Talc-PET	Homogeneous	Homogeneous (many)	No
i-MMT-PET	Homogeneous	Homogeneous (no)	Yes
MMT-PET blends	Heterogeneous	Heterogeneous (many)	No
PET	Homogeneous	Homogeneous	Yes
APET	Homogeneous	Homogeneous	Yes

^aMixed micrometer of SiO₂, prepared by step-by-step dispersion and recovery.^bGas-phase SiO₂, prepared by SiCl₄ (g) reacting with H₂.^cDeposited nanometer of SiO₂, prepared by Na₂SiO₃/TEOS as a precursor, and through a sol-gel process

Note: i-MMTs, the montmorillonite (MMT) treated by intercalants, i-MMT-PET, PET-MMT nanocomposite; APET, amorphous morphology of PET; BHET, bihydroxyl ethylene terephthalate; No, less than 70% under visible light; Yes, transmitting 80% over under visible light.

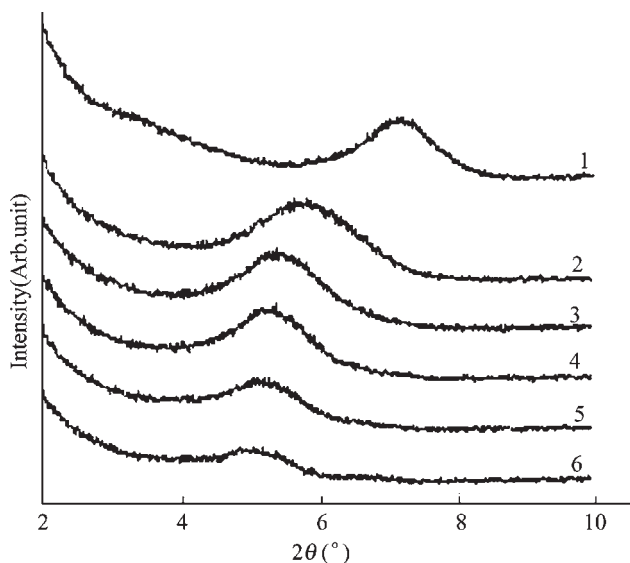


Fig. 3.33. Mechanical intercalation of oligomer BHET into MMTs (1 – BHET; 2 – 30% (by wt) MMTs; 3 – 20% (by wt) MMTs; 4 – 10% (by wt) MMTs; 5 – 5% (by wt) MMTs; 6 – 2% (by wt) MMTs). (With the permission of Acta Polymerica Sinica, China Chemical Association)

(3) *Melt intercalation.* MMTs may be intercalated with monomers or oligomers of PET by another method. That is, MMTs or MMTs treated with organic reagents can be directly melt-mixed with BHET over the temperature range 30–40°C above its melting point. By such a method, the MMT load can reach 30% (by wt) or more. The X-ray patterns show the intercalation results as in Figure 3.34.

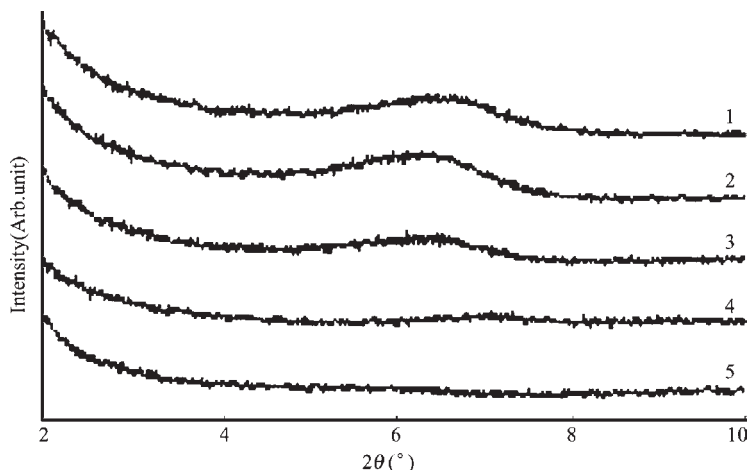


Fig. 3.34. Melt intercalation of oligomer BHET into MMTs (1 – 30% (by wt) MMTs; 2 – 20% (by wt) MMTs; 3 – 10% (by wt) MMTs; 4 – 5% (by wt) MMTs; 5 – 2% (by wt) MMTs). (With the permission of Acta Polymerica Sinina, China Chemical Association)

By such an intercalation technology, a good result is obtained for these oligomer-treated MMTs. However, PET itself is not suitable for this melt intercalation technology because it degrades very easily.

(4) *Physical properties of PET-MMT nanocomposites.* The physical properties of PET-MMTs are given in Table 3.33, and Figure 3.35. The molecular-weight distribution of NPET becomes narrow, but its molecular weight is high compared with pure PET. X-ray results show that the interlayer distance becomes enlarged to an average layer size of 30–100 nm homogeneously (TEM not shown) dispersed in the PET matrix.

(5) *Mechanical properties of PET-MMTs nanocomposites.* The mechanical properties of NPET show that its bending modulus increases with that of the MMTs load. When the MMT load is at 5.0% (by wt), its modulus is enhanced nearly three times, which is not possible for the macroscopic blending materials. The load of MMTs at 3.0% (by wt) appear to be optimized, such that some properties are enhanced while the other properties are maintained.

So far, the izod-notched impact results are unsatisfactory, i.e., MMTs at a load of 1% (by wt) enhance or preserve the impact property of the pure PET, while this impact property inexplicably decreases rapidly when the MMT load is greater than 1% (by wt) (Figure 3.36). The interface between MMTs and the PET matrix is not adhesive, which poses a difficulty in the preparation of PET-MMT nanocomposites.

(6) *HDT of PET-MMT nanocomposites.* HDT is related to both mechanical and thermal properties, and is thus an important parameter in material application under high-temperature conditions. In NPET, the way MMTs are treated, intercalants and the quantity of and load of MMTs have effects on HDT corresponding to the results shown in Table 3.34.

Table 3.33
Molecular weight and their distribution for NPET prepared by direct etherification

No.	LLC (g)	(PTA+EG) (g)	d_{001} (nm)	M_w (g/mol) $\times 10^4$	M_w/M_n	η_a (dl g ⁻¹)
1	0.0	100	—	3.7	2.0	0.57
2	0.5	100	—	4.7	2.0	0.69
3	1.0	100	3.0	4.0	2.0	0.65
4	2.0	100	>3.0	4.1	1.8	0.62
5	3.0	100	>3.0	4.5	1.9	0.68
6	5.0	100	>3.0	4.2	1.7	0.63

Note: η_a , apparent viscosity; d_{001} , (001) interface distance by X-ray diffraction; $2d_{001} \sin \theta_{001} = \lambda$.

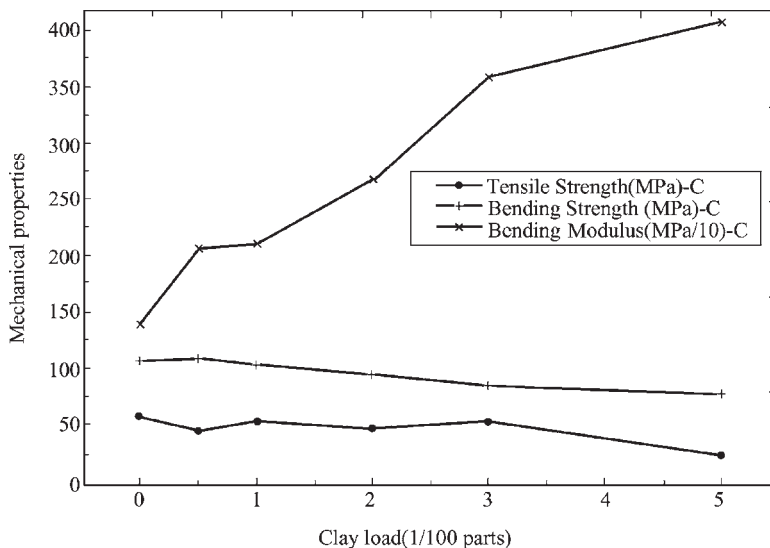


Fig. 3.35. Plot of mechanical properties (σ_t, σ_b, E_b) vs. clay load.

Long-chain intercalants are selected to enhance the intercalation effect. Otherwise, in the case of a short-chain intercalant, the enhancement of HDT is not obvious though the MMT load is high. For example, when treated with short-chain ethanolamine (EA) or a long-chain laurylamine (LLM), the PET-MMT nanocomposites have an HDT of 89°C for EA and 105°C for LLM. It is thought that the chain length of the intercalant must be greater than 8-carbon atoms for the preparation of satisfactory MMTs and their nanocomposites with good HDT property.

(7) *Isothermal crystallization.* The thermal and crystallization behavior of PET-MMT nanocomposites investigated by dynamic scanning calorimetry (DSC). The results are discussed through theories of both glassy and melting transitions the Avrami equation and related techniques. From the isothermal crystallization data detected by DSC, the T (temperature)– X (% crystallinity rate) is determined, based on which the t (time)– $X(t)$ relationship is obtained. Then the $\ln t$ vs. $\ln[-\ln(1-x(t))]$ is calculated from the equation

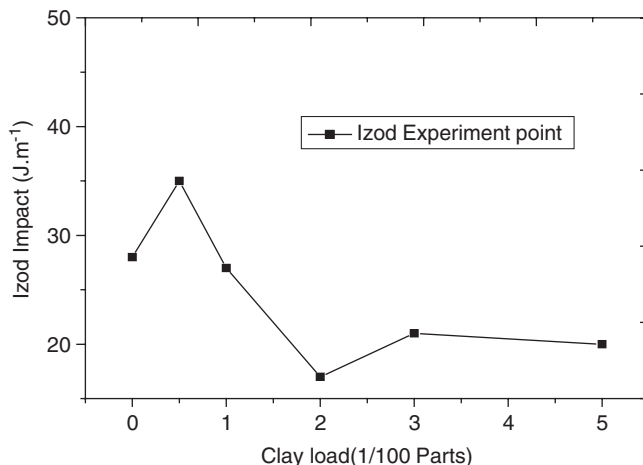


Fig. 3.36. Plot of izod impact–clay load relationship for PET-clay nanocomposite.

Table 3.34
Thermal and optical properties of MMTs treated by different intercalants

Intercalants	HDT (°C)	transparency of PET films
EA (1%)	84	Yes
EA (3.0%)	89	Yes
EA (5.0%)	95	Yes or no
OT (3.0%)	92	Yes
LLM (3.0%)	105	Yes
CPL (5.0%)	-102	No
PET (pure)	76	Yes

Note: The data within parentheses is the load weight of clay; EA, ethanalamine; OT, cetyl trimethyl ammonium salt; LLM, laurylamine; CPL, 1,6-hexanediamine.

$\ln[-\ln(1-x(t))] = \ln k + n \ln t$. From this curve of $\ln t$ vs. $\ln[-\ln(1-X(t))]$, the parameters k, n are obtained. The final $t_{1/2}$ is obtained from the equation $t_{1/2} = (\ln 2/k)^{1/n}$. The results can be seen in Table 3.35.

As the MMT load increases the crystallization rate increases, and at a adequate MMT load of 2–3% (by wt), the crystallization rate reaches the maximum. NPET’s crystallization rate is 2–6 times more than that of pure PET, while the nanocomposite films have overall properties enhanced when the MMT load falls below 3.0% (by wt).

(8) *Processing properties.* When PET is applied to engineering plastics, the processing have a vital effect on the product’s surface properties. The properties also depend on MMT load and processing conditions (MMT load at 3.0% (by wt) is assumed to be a critical point). In NPET processing, the molding temperature decreases by 30–50°C

Table 3.35

Crystallization behavior of NPET prepared by direct etherification reaction

No.	LLC (g)	PTA+EG (g)	$v_j(201^\circ\text{C})$ (s)	$v_{ni}(205^\circ\text{C})$ (s)	$v_j(215^\circ\text{C})$ (s)	Film transparency
1	0.0	100	132	108	192	Transparent
2	0.5	100	97	56	101	Transparent
4	2.0	100	78	42	90	Transparent
5	3.0	100	66	48	42	Transparent
6	5.0	100	60	36	36	Opaque

Note: LLC, load weight of layered silicate; PTA + EG, total weight of monomers; v_{ni} , crystallization rate of non-isothermal crystallization; v_j , rate of isothermal crystallization.

Table 3.36

Processing properties of NPET by direct etherification reaction

No.	LLC (g)	PTA+EG (g)	$T_{cc}-T_{ch}$ ($^\circ\text{C}$)	T_{inj} ($^\circ\text{C}$)	D_n (nm)	Sample surface by molding
1	0.0	100	75	110		Bright and smooth
2	0.5	100	87	70	10–50	Bright and smooth
4	2.0	100	90	70	30–70	Bright and smooth
5	3.0	100	101	65	30–100	Not bad
6	5.0	100	107	60	30–100	Bad

Note: LLC, load weight of layered silicate; PTA+EG, total weight of monomers; $T_{cc}-T_{ch}$, crystallization peak from the melt T_{cc} ; T_{ch} , the crystallization peak from the glassy state; T_{inj} , injection molding temperature; D_n , the average particle size for the molding NPET sample.

compared with pure PET. Such a critical MMT load is also suitable for the preparation of NPET through an indirect esterification reaction (Table 3.36).

3.4.2. PBT-clay nanocomposite preparations

As one of the five top engineering plastics, poly(butylene terephthalate) has several desirable properties like good processing behavior and superior properties in electricity, molding and crystallization. Thus, it finds its use in computers and gears.

The preparation of PBT and its nanocomposite with MMTs (NPBT) and comparison of their properties are discussed in this section. The determination of some of their properties, including flexural (bending) and breaking strength, according to ASTM 790, and notched izod impact strength, according to ASTM D256, are detailed in the literature [58].

3.4.2.1. Materials

In the preparation of NPBT, raw clay with an original size of 100 μm , average CEC of 70–110 mmol (100g^{-1}) and total Fe_2O_3 content lower than 0.5% (by wt) was used. The clay was milled to 2–30 μm particle size, and particles smaller than 17 μm accounted for 58% (by vol), as characterized by Zeta Sizer 2000HS PCS (V14 type), Malvern Co. Then the treated clay was directly used to produce NPBT. Monomer of 1,4-butylene diol (industrial grade) was collected, while DMT (dimethyl terephthalate) (industrial grade) from SINOPEC was used. The $\text{Ti}(\text{OC}_4\text{H}_9)_4$ catalyst was of analytical grade; all

other solvents and reagents used were of chemical grade from SINOPEC. These chemicals were collected to both treat the clay and polymerize it with monomers of PBT.

Example 3.4.2.1. Pretreatment of clay for polymerization. Clay was treated with organic reagents as described in previously [14,16–18], with only a slight modification. Considering laurylamine as an example, the treatment process is as follows: first, 20.0 g of MMTs with CEC of 90 mmol (100 g)⁻¹ was added to 400.0 g of pure water and wetted for 60 min; then the suspension was rapidly stirred. The reaction product of 2.40 g of laurylamine with 1.51 g (85%, mass concentration) of phosphorus acid dissolved in 50.0 g of pure water was added to the suspension. Finally, the intercalated clay was obtained after 6–12 h. The procedure was the same for different treatment reagents. The treated clay was then prepared for polymerization.

Example 3.4.2.2. Preparation of PBT-clay nanocomposites (NPBT). Into a 50 l autoclave equipped with an anchor stirrer of ϕ 270 and a magnetic driving and stabilizing system (to ensure high vacuum level), 2,426.25 g of DMT (dimethyl terephthalate) and 1,573.15 g of 1,4-butylene diol (BD) were added (molar ratio of BD/DMT was 1.4–2.2). The treated clay suspension was added to the mixture while the mixer temperature began to rise. Then, TBTT (tetrabutyl titanate, Ti(OC₄H₉)₄) was added in a total quantity ranging from 40 to 70 ppm Ti/DMT to the mixed solution together with the additive catalyst SnO(OH)(*n*-C₄H₉O) made by CIBC (Chemical Institute of Beijing City, Beijing). The catalysts were added in two steps. In the first step, half of the catalyst was added. After the temperature increased to 90°C, the mixture dewatering started until the water content reached < 1.0%. Then, the transesterification reaction was initiated and continued for 2–4 h at 140 to 220°C. At the end of this stage, another additive, 0.05 g of hexal diamine (H₂N-(CH₂)₆-NH₂), was added to the ester product to adjust the polymer's molecular weight, and the other half of the catalyst was added immediately. The polymerization reaction lasted for 1–3 h at 240–270°C and a vacuum below 80 Pa. The final product was obtained, by pouring the reaction mixture into cold water, and cut into pellets.

Example 3.4.2.3. Preparation of film samples. NPBT pellet samples were vacuum-dried at 100–120°C for 4 h. Then, they underwent a melt-quench process at a heating temperature of 10°C above their melting points at 50 MPa under an oil hydraulic pressure compressor. After melting for 5 min, they were withdrawn from the compressor rapidly, and transferred immediately into a mixture of water and ice to prepare amorphous films. When the melt-quench is done in a 1 mm mold, a film with a thickness of 1 mm can be prepared for further measurement.

3.4.2.2. Properties of nanocomposites

The properties of NPBT nanocomposite samples with MMT load from 1 to 10% (by wt) are listed in Table 3.37. In NPBT, the layer interdistance is expanded from 1.12 to 2.5 nm. That is, the polymer chains are intercalated into the MMT interlayer space. This interdistance enlargement determines the particle size of the final nanocomposites. The NPBT viscosity is usually above 0.85, with MMTs load up to 10% (by wt), which proves that PBT accommodates more MMT than other polymers such as PET [60], or that it is insensitive to MMT load during in situ polymerization.

Table 3.37
Properties and structure of NPBT when MMTs are treated with laurylamine

Clay loading (%)	d_{001} (nm)	η (dl g ⁻¹)	D (nm)	σ_b (MPa)	E_b (MPa)	Izod (J m ⁻¹)
0 (PBT)	—	0.90	—	105	1,700	44.3
1.0	—	0.92	20–100	110.9	2,650	45.1
2.0	—	0.86	30–100	106.8	2,900	41.2
5.0	2.5	0.87	30–100	104	3,700	37.4
10.0	2.6	0.85	no results	95.2	brittle	brittle
(MMTs)	1.12	—	—	—	—	—

Note: D , particle diameter by TEM statistics; Izod, notched izod impact strength; σ_b and E_b , bending strength and modulus; η , intrinsic viscosity, (dl g⁻¹ = 10³ ml g⁻¹). (To determine η , NPBT samples are dissolved in mixed solvents of 50/50 (w/w) of 1,1,2,2-tetrachloro ethane ($n_0^{25} = 1.5250$) and phenol. Then the viscosity is measured with an Ullman viscometer at a concentration

of 0.1 g (100 ml⁻¹) at 25 ± 0.1°C, and calculated using the equation, $[\eta] = \left(1 + \frac{\eta_{sp}}{0.7C}\right)^{1/2} - 1$,

where $\eta_{sp} = (t - t_0)/t_0$; t , t_0 are the flow time for sample and pure solvent in the viscometry, and C , is the concentration of solution (from 1 × 10⁻³ to 10 × 10⁻³ g ml⁻¹)

The mechanical properties of NPBT, such as its modulus, are enhanced greatly; its modulus is about two times more than that of pure PBT when MMT load is up to 5% (by wt). The bending strength is slightly higher than PBT's. Moreover, the tensile strength of NPBT with 5% MMT load is enhanced and its tensile modulus increases from 790 MPa of PBT to 1,300 MPa of NPBT. The notched test shows that the izod value remains unchanged within 2% (by wt). To balance the properties, 2–5% MMT load seems advantageous to PBT.

3.4.2.3. Thermal properties

(1) *HDT*. HDT is a key index of resistance to heat conditions. A plot of HDT–MMT load is shown in Figure 3.37, where, the addition of a small quantity of MMTs enhances HDT of PBT as obvious nanoparticle effect and also increases the strong interaction between dispersed MMT layers in PBT matrix. The selected reagents also have a large effect on HDT. These organic or intercalation reagents are listed in Table 3.38; it is seen that HDT increases from 30 to 50°C in NPBT compared with PBT within 5% (by wt). Such an increase in the level of HDT of NPBT is even greater than that of NPET, giving a new type of PBT material for further modification.

The relationship of HDT with intercalation reagents shows that in the different kinds of reagents selected for treating clay (in Table 3.38), not only the chain length but also the chain polarity of treating reagents, their compatibility with polymer chains, and the treated MMT clay load, contribute to the HDT of NPBT samples. These results differ from those reported in the previous reports on other polymer–clay nanocomposites [66–71]. Thus, NPBT with high HDT depends on these reagents.

(2) *Non-isothermal crystallization property*. The crystallization property for both PBT and NPBT is investigated with DSC and compared. Non-isothermal crystallization is

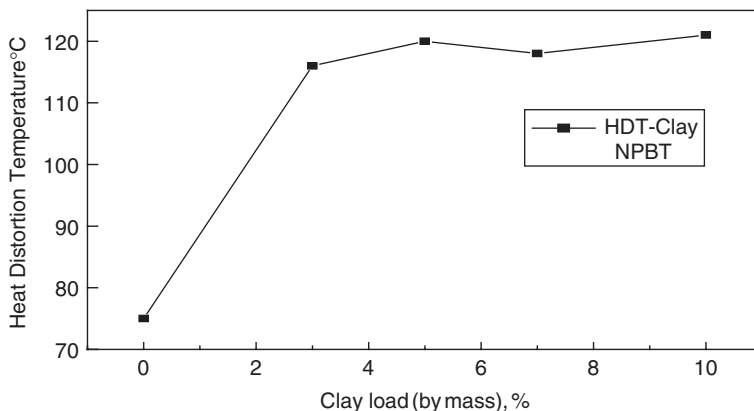


Fig. 3.37. Plot of HDT vs. clay load for NPBT (clay treated with laurylamine; see Section 3.2).

Table 3.38
HDT of NPBT with different clay loads and intercalation reagents

Intercalation reagents	MMTs (clay) content (by mass) (%)	HDT ^a (°C)
No	0.0	75
HOOC(CH ₂) ₅ NH ₂	3.0	112
HOOC(CH ₂) ₃ NH ₂	5.0	120
CH ₃ (CH ₂) ₁₁ NH ₂	3.0	116
CH ₃ (CH ₂) ₁₁ NH ₂	5.0	120
CH ₃ (CH ₂) ₁₅ NH ₂	3.0	118

^aMeasured under the load of 1.84 MPa.

analyzed and described by the Avrami equation, as shown in Chapter 5, as $[-\ln(1-X(t))] = \ln k + n \ln t$ (where $X(t)$ is the crystallization degree at time t , k the crystallization dynamic parameter and n the Avrami number that reflects the growth of crystallites). The reciprocal value of time t at $X(t) = 50\%$ is applied to express the crystallization rate, and then the Avrami equation is transformed into the formula

$$t_{1/2} = \left(\frac{\ln 2}{k}\right)^{1/n} \quad \text{or} \quad \frac{1}{t_{1/2}} = \left(\frac{\ln 2}{k}\right)^{1/n}$$

By using the Avrami equation to calculate the non-isothermal crystallization data in the DSC patterns, the plots of $\ln[-\ln(1-X(t))]$ vs. $\ln t$ are obtained and shown in Figure 3.38 (a) and (b).

It is seen that under non-isothermal crystallization at different scanning rates, NPBT (b) and PBT (a) show slightly different crystallization processes at a higher scanning rate from 20 to 40°C min⁻¹. The NPBT crystallization curves at 30 and 40°C min⁻¹ intersect, while PBT curves within 20 to 40°C min⁻¹ intersect. At a low scanning rate, NPBT and PBT have similar crystallization behavior.

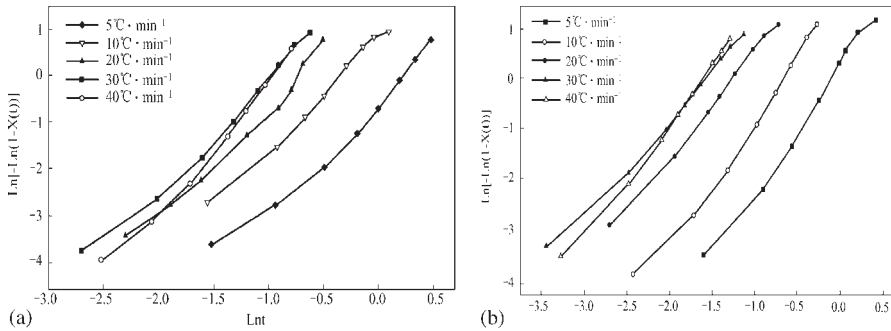


Fig. 3.38. Non-isothermal crystallization behavior from DSC heating by the Avrami equation, for PBT (a) and NPBT (b) with a clay load of 5% (by wt) (its preparation is similar to that in Figure 3.31).

Table 3.39
Dynamic parameters for PBT and NPBT under non-isothermal crystallization

Sample		5 (°C min ⁻¹)	10 (°C min ⁻¹)	20 (°C min ⁻¹)	30 (°C min ⁻¹)	40 (°C min ⁻¹)
NPBT0	$t_{1/2}$	1.063	0.592	0.407	0.317	0.334
	n	2.24	2.38	2.34	2.36	2.69
NPBT5	$t_{1/2}$	0.832	0.478	0.262	0.191	0.187
	n	2.39	2.31	2.05	1.86	2.20

Note: NPBT0, pure PBT; NPBT5, PBT with 5% (by wt) clay load, where clay is treated with laurylamine as mentioned in section 3.2.3.

Based on the intercept and slope of the curves in Figure 3.38, k and n are calculated and listed in Table 3.39 according to the Avrami equation. The plot of crystallization rate ($1/t_{1/2}$) vs. scanning rate under non-isothermal crystallization is shown in Figure 3.39.

It is clearly seen in Figure 3.39 that the crystallization rate ($1/t_{1/2}$) for NPBT increases rapidly with the DSC rate, and the increase becomes larger with the scanning rate, strongly showing that the crystallization behavior of NPBT is higher than that of PBT. The average increase in NPBT crystallization rate is about 50% higher at all non-isothermal crystallization case than that of PBT within 5% loading of clay. Introducing nanoparticles into its matrix to act as new nucleation centers has a direct effect on the crystallization rate. However, comparison of all values of n for both PBT and NPBT in Table 3.39 shows that the crystallites grow in a similar manner, implying that these nanoparticles are of similar size.

(3) *Crystallization degree.* The crystallization degree is one of the parameters describing NPBT crystallization behavior. It is expressed as $\Delta H/\Delta H_f^0$ in DSC investigation, where ΔH is the heat of fusion and changes with scanning rate and crystallization time, while ΔH_f^0 is the heat of fusion at equilibrium state. ΔH_f^0 is a constant value for both PBT and NPBT. The plot of ΔH vs. DSC rate is shown in Figure 3.40.

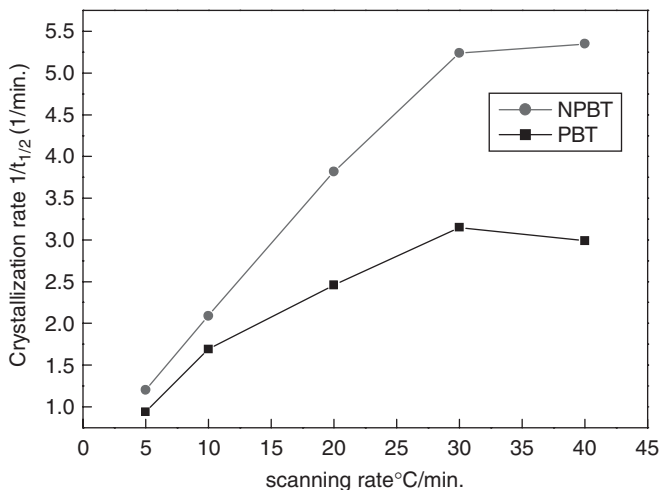


Fig. 3.39. Plot of crystallization rate vs. scanning rate under non-isothermal crystallization for both PBT and NPBT with 5% (by wt) clay load (its preparation similar to that in Figure 3.37).

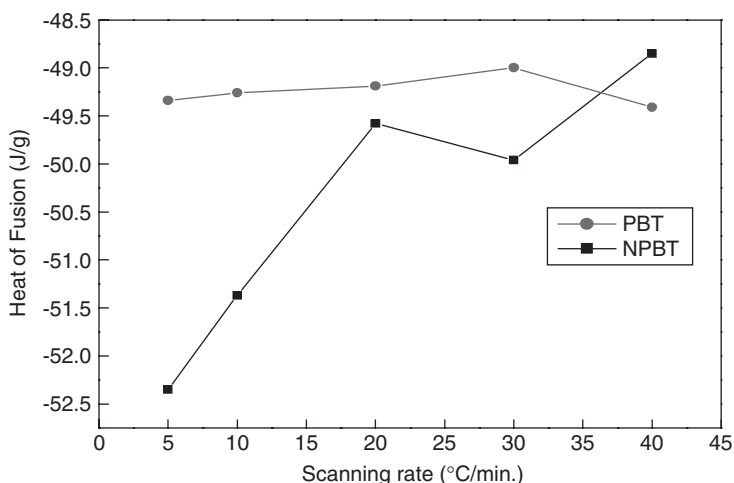


Fig. 3.40. Plot of heat of fusion (ΔH) vs. scanning rate under non-isothermal crystallization for PBT and NPBT with a clay load of 5% (by wt) (its preparation is similar to that shown in Figure 3.37).

In Fig. 3.40, the difference occurs in the heat of fusion between PBT and NPBT. The ΔH of NPBT increases more rapidly than that of PBT as well as the scanning rate. Either the ΔH of PBT remains nearly unchanged under non-isothermal crystallization or PBT is slow to respond to the scanning rate.

(4) *Thermal degradation and melting.* The thermal degradation behavior of both PBT and NPBT is shown in Figure 3.41. Both decompose at a similar temperature at the

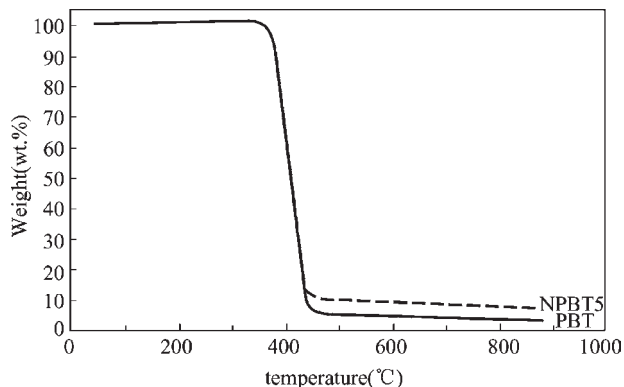


Fig. 3.41. TGA scanning patterns of PBT(a) and NPBT(b) with 5% (by wt) of clay load

Table 3.40
Thermal and processing properties of NPBT^a

Sample	Clay load (%)	T_d (°C)	T_m (°C)
NPBT0	0.0	389	231
NPBT5	5.0	391	230
NPBT7	7.0	401	221
NPBT10	10.0	395	223

Note: The organo-clay is treated with laurylamine; T_m , melting point; T_d , thermal degradation temperature; NPBT0, NPBT5, NPBT7 and NPBT10 represent PBT with 0.0, 5, 7 and 10% (by wt) clay load, respectively.

initial stage. The degradation of NPBT is improved and better than PBT at a higher heating temperature (see Table 3.40).

3.4.2.4. The processing properties

The superior thermal behavior of NPBT to PBT is of much significance to PBT processing properties, especially its injection-processing property (Inject T) shown in Table 3.41. In injection technology, low mold temperature is the key to improving the yield efficiency. In Table 3.41, Inject T of PBT is much higher than that of NPBT implying a higher production efficiency. In fact, the production efficiency of NPBT is three times that of PBT. The improvement results from the formation of the smaller spherulitic crystallites and more nucleation centers in NPBT than PBT, thereby lowering the PBT melting point and accelerating its crystallization.

3.4.2.5. Structure and properties

The nucleation effect of clay is shown by the TEM morphology in Figure 3.42, where spherulite and lamellae in PBT matrix are clear, but their growth is hindered, and spherulite disappears after introducing clay (see Figure 3.42(b)). Dispersed particles

Table 3.41
Processing properties of NPBT with clay load

Sample	Load clay (%)	Inject T^a (°C)	Product surface
NPBT0	0.0	110	Bright and smooth
NPBT5	5.0	55	Bright and smooth
NPBT7	7.0	57	Bright and smooth
NPBT10	10.0	58–60	Little bright

^aRepresents the injection mold temperature for a molded sample capable of being separated from the mold. The sample nomenclature is the same as in Table 3.40.

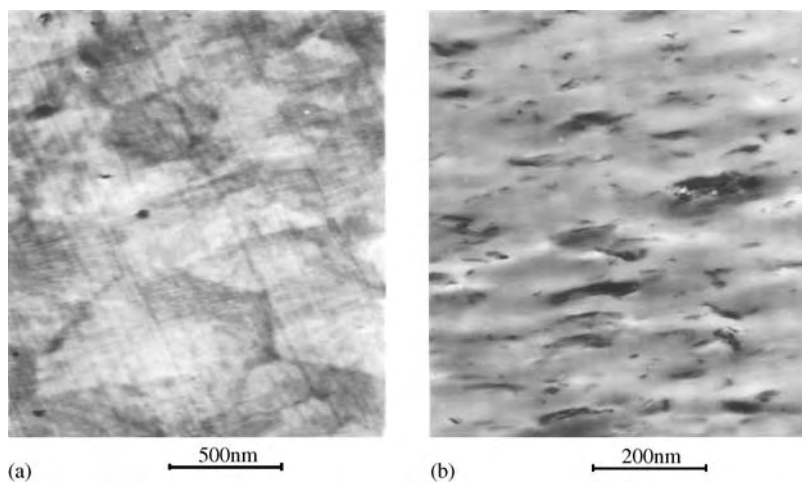


Fig. 3.42. The TEM morphology of PBT spherulitic (a), of NPBT with 2% (by wt) clay load by any polarized reagent (b).

prevent the spherulite from growing (attempts to find spherulites in NPBT have not revealed their spoke).

It is difficult to distinguish the nanoparticle contribution to NPBT morphology from that of the non-nanoparticle. Clay itself has different forms including crystallized and amorphous areas. In PBT, there exists at least two kinds of spherulites, normal and abnormal ones; only one kind of these spherulites is shown by TEM. When the polar reagent ethanolamine is used to treat clay, its layers are exfoliated partially with some stacked layers. When clay is treated with the non-polar reagent laurylamine, TEM morphology of NPBT shows very little layer agglomeration. That is, a long chain (e.g., laurylamine) or polarization chain (e.g., short chain of ethanolamine) has different effects on the properties of NPBT.

In NPBT, when the clay load surpasses 5.0% (by wt), layer agglomeration increases from 200 to 1000 nm. By TEM statistical data [60], 3% (by wt) of agglomerations with

μm -sized layers are obtained, which are phase separated from the polymer matrix. They affect PBT properties at impact and the interface. In PBT, the clay load can reach up to 10% (by wt). This advantage is of much significance in modifying PBT, indicating that NPBT is not very sensitive to clay load and accommodates more clay than other polymers such as PET, PS, etc. It is believed that NPBT with variable clay load meets engineering requirements and provides a new materials for further application.

By loading clay to PBT matrix from 1 to 10% (by wt), the NPBT samples have enhanced properties: e.g., higher HDT of 30–50°C, two times higher modulus, better processing of low mold injection temperature and a 50% higher crystallization rate than that of PBT. PBT has higher capacity to accommodate clay than the other polymers. NPBT nanoparticles range from 30 to 100 nm with 3% agglomeration of layers in phase separation from the PBT matrix. The agglomerations and phase separations affect NPBT properties.

3.5. Polyaniline–silicate nanocomposites

Polyaniline (PAN) is a functional polymer and has applications in dye, cell and additives. We begin our investigation of PAN focussing on conductive materials and anti-electronic materials, which are either used directly or mixed with other polymers. So far, many conjugated polymer/inorganic host hybrid composites have been synthesized and investigated, such as those of PAN/MoO₃, PAN/V₂O₅, polypyrrol/mordenites and polythiophene/mordenites [76]. The PAN-MMT nanocomposites are thus prepared to find ways to improving its electronic behavior.

3.5.1. PAN and its conductivity

3.5.1.1. The structure of PAN at eigenstate

According to early results from MacDiarmid, the PAN polymer is assumed to be a linear with head-end linkage, composed of an alternative structure of phenyl–quinine ring. Later, in 1987, a more widely accepted structure [77] of PAN was accepted, which was not an alternative phenyl–quinine ring structure, but a structure of 3-phenyl rings connected to one quinine ring. The 3:1 structure of PAN with its molecular structure is shown in Figure 3.43.

The structure proposed by MacDiarmid was first proven by us using IR, without any scattering, and ¹³C-NMR methods in solution [78,79].

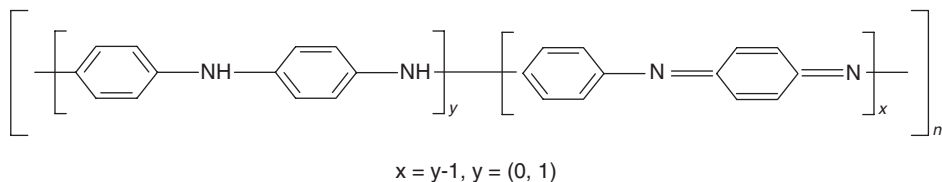


Fig. 3.43. The structure of PAN at eigenstate.

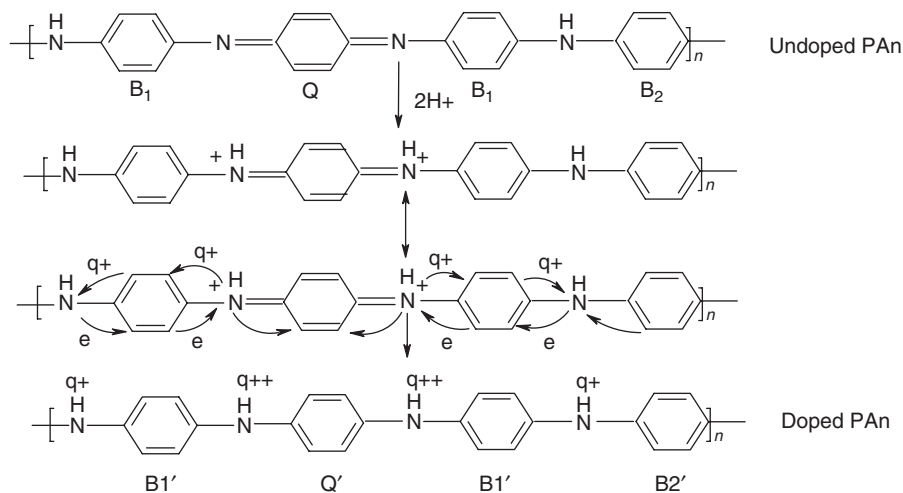


Fig. 3.44. Four-ring BQ transformation model for doping PAN.

3.5.1.2. The doping structure and conductivity

The conductivity of PAN at eigenstate will be transformed into conductive PAN by chemical or electrochemical doping. Such conductivity depends on the doping rate or quantity of the doped materials. Beside the MacDiarmid model for the doping conductivity of PAN, we have suggested the following model, which is called a “4-rings BQ transformation model” [79] (Figure 3.44). In the model, there are two states of PAN polymers: B1, Q, B1 and B2 for undoped and B1', Q', B1' and B2' for its doped state.

3.5.1.3. Conductivity through doping

The doped PAN will have different conductivity with the doping load. For chemical doping, the reagents may be protonic acid, neutral salts, e.g., LiCl, or some other oxides, such as FeCl₃, SnCl₄ and I₂ [80–81]. As ecological problems arise, a water-soluble system for processing conducting PAN becomes more and more essential. Besides the complicated process of grafting groups into PAN main chains, we selected sulfonic acid with a long chain of methyl oxygen or ethyl oxygen groups, or phosphine acid as a doping agent for PAN. The conducting PAN in such a water-soluble or dispersion system is obtained with its highest conductivity at 10⁻¹ S cm⁻¹, and has significant oxidation–reduction properties. The structures of sulfonic acids or phosphoric acids are shown in Figure 3.45.

3.5.1.4. Processing of PAN

From a solution of eigenstate PAN in *N*-methyl pyrrolidone (NMP), a high-density PAN membrane is prepared. The tensile strength, Young's modulus and elongation at break of the film was determined to be 87.9 MPa, 1564 MPa and 10.2%, respectively. The electric conductivity of films doped with protonic acid is similar to that of the compressed powder samples. When the PAN film is doped with protonic acid and stretched

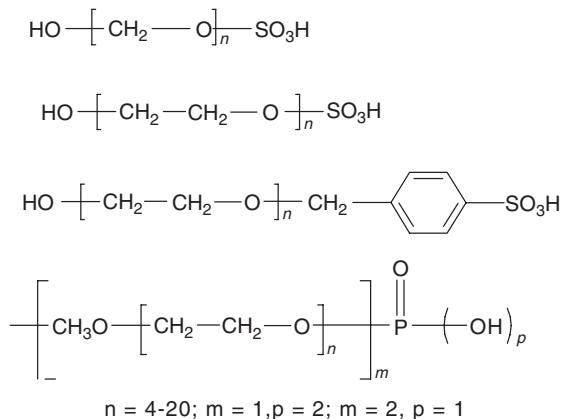


Fig. 3.45. The structure of some hydrophilic doping agents with long chains.

up to 10%, its electric conductivity reached 36.7 S cm^{-1} . These conductivity and mechanical properties are suitable for anode materials [82].

There are a few reports on PAN-based conductive composites applied to coatings in anticorrosion and shielding different waves. Several corporations in our country, seem to wait for progress due to the relative poor processing levels. Under such circumstances, we launched the preparation of PAN/MMT nanocomposites.

3.5.2. Preparation and polymerization of PAN

3.5.2.1. Selecting MMTs as doping agents and confined template

As conjugated polymers usually have high electric conductivity with many potential applications, the insertion of such conjugated polymers into layered (two-dimensional) or microporous (three-dimensional) inorganic hosts has received extensive attention. In intercalation polymerization, the inorganic host serves as a template within which a guest molecule of nanometer dimension is assembled. The constrained environment is expected to lead to a high degree of polymer ordering and to useful properties such as high anisotropy of electric conductivity of more than 10^3 S cm^{-1} , and increasing capacity and reversibility when PAN/MoO₃ nanocomposites serve as the cathode of lithium rechargeable batteries [76]. Owing to the complexity to the heterogeneous systems, some key problems still remain, and some problems related to the structure and properties of the nanocomposite still need to be solved. We selected MMT as the host because of its important advantages:

- (1) The natural MMT mineral with layer structure consists of two silica tetrahedral sheets and one alumina octahedral sheet. The stacking of the layers of ca 1 nm thickness by weak dipolar forces leads to the formation of interlayer distances or galleries between the layers [83]. The galleries occupied by hydrated cations that balance the charge deficiency provide an ideal space for the monomer of aniline, where it is introduced via an ion-exchange process and is hardly separated from the galleries [84].

- (2) MMT is an inactive inorganic host without redox character, so polymerization can be controlled.
- (3) MMT is a well-ordered host in two dimensions and after the intercalation of monomer, an extrinsic initiator can enter and be initiated in the interlayers; this is important for probing the polymerization mechanism by various tools. However, in a three-dimensional ordered host, a similar method is unrealistic due to the blocking tunnel. These favorable characters can assist us in avoiding interference, which often occurs in other intercalate systems.
- (4) Intercalation polymerization is a good strategy by which to study the chain structure of PAN and polymerization mechanism. So far, our understanding of the PAN structure is still fragmentary due to its amorphous or poor crystalline nature and its insolubility in common organic solvents, and important structural problems associated with single chain and macromolecule aggregation remain to be solved. However, when PAN is inserted into the inorganic galleries of MMTs, the strong intermolecular interactions of PAN chains are eliminated by the host barriers and single-chain PAN can be obtained, which is impossible during the normal polymerization of aniline. In addition, the polymerization rate is much slower in a confined environment. Aniline polymerization is a complicated process and a typical precipitation polymerization with a high reaction rate. These features make it difficult to obtain and characterize the reaction intermediates and monitor the reaction rate. In intercalation polymerization however, the slow kinetic diffusion retards the reaction rate, thereby providing a unique opportunity for studying the polymerization mechanism of the induction period, the formation of dimers, and the propagation of polymer chains.

3.5.2.2. *In situ polymerization of PAN with MMTs*

In the preparation of PAN–MMT nanocomposites, sodium montmorillonite (Na-MMT) was preferred due to its specific surface area of $600\text{--}800\text{ m}^2\text{ g}^{-1}$ and a CEC of $80\text{ mmol (100 g)}^{-1}$. In our preparation, Na-MMT was washed several times by saturated NaCl solution prior to use. In laboratory preparations, HCl, NaCl and $(\text{NH}_4)_2\text{S}_2\text{O}_8$ were of analytical grade and aniline was distilled under vacuum before using.

Example 3.5.2.1. Synthesis. Five grams of Na-MMT was added into 250 ml deionized water and stirred for 2 h at 80°C ; then 1 ml of aniline and 0.02 mol of HCl were added. After stirring for 6 h at 80°C the mixture was washed several times with large quantities of deionized water. After cooling to room temperature and regulating the pH value with HCl at 2, 0.8 g (0.0035 mol) of ammonium per sulfate ($(\text{NH}_4)_2\text{S}_2\text{O}_8$) was added and the polymerization lasted for more than 10 h. The dark-green precipitate was isolated by filtration, washed with deionized water thoroughly and dried under vacuum.

3.5.2.3. *Structure characterization of PAN–clay hybrid nanocomposite*

In the formation of PAN–clay hybrid nanocomposites, the reaction takes place in two steps: in the first step of the reaction, the excess aniline takes part in the reaction to exchange Na^+ completely inside the gallery of the MMT layers. Then, the reaction is initiated by $(\text{NH}_4)_2\text{S}_2\text{O}_8$ catalyst in such a way that PAN is formed inside the layers and

takes on a zigzag chain conformation. To test the completion of polymerization reaction, the reaction mixture is washed with deionized water, and only the monomer that has been introduced into the galleries remains in the reaction system. The final wash is tested by UV-Vis spectra and found to be free of residual monomer, indicating that the monomer has been removed completely (Figure 3.46, curve c).

Collecting all residual liquid formed at absorbance 280 nm (assigned to the $n-\pi$ transition of neutralized aniline), we can calculate the saturation insertion amount to be 6.8 wt% of MMTs according to the UV-Vis absorption curve of aniline. The insertion amount calculated by CEC was a little higher than the experimental result. The difference is supposed to be due to the slow kinetics of diffusion for $(\text{Aniline})^+$ (or An^+) and the experimental errors caused by these two measurement methods. It is believed that after An^+ is inserted into the galleries, a coordinate bond is formed between the monomer and the inorganic material; theoretically, An^+ is hardly exchanged by other cations [84]. To determine whether any of the An^+ could escape from the interlayer, we placed the washed An-MMT composite in deionized water, regulated the pH to 2 with HCl, kept stirring for 18 h (except for the initiator, the conditions were the same as with the polymerization) and then detected the aniline content of the centrifugal residual liquid by UV-Vis spectrometer (Figure 3.46, curve d). We found that only a small amount of monomer (8% of the total) escaped from the galleries, becoming free monomer. Thus, in the PAN-MMT hybrid, the content of PAN is 7.2%, and, by a conservative prediction, 90% of the polymer is inserted into the MMT galleries. XRD patterns (Figure 3.47) of PAN-MMT nanocomposite powder show an interlayer distance of 14.82 Å and a difference of 5.22 Å from the corresponding 9.6 Å for anhydrous MMT framework. The expansion of the interlayer distance is very close to that reported for PAN in V_2O_5 (5.23 Å) [76], and less than that for PAN in FeOCl (5.94 Å) [85]. The expansion is in agreement with the intercalation of single chains with extended-chain conformation rather

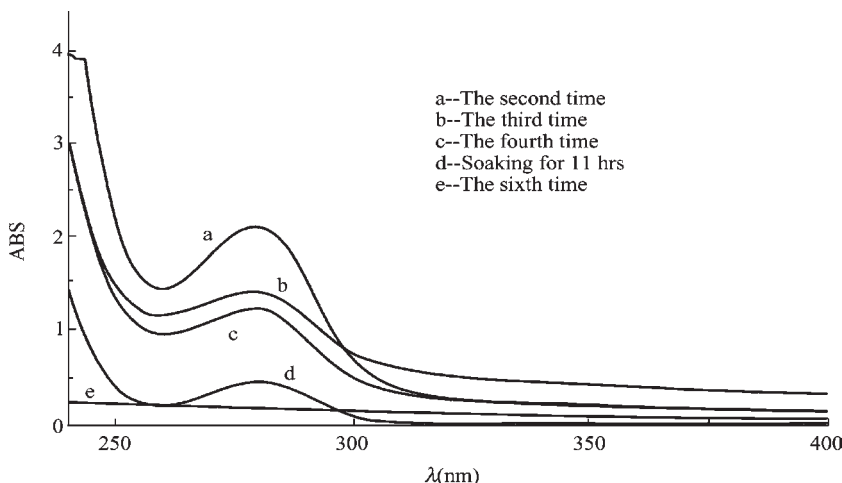


Fig. 3.46. UV absorption of the samples washed out from mixtures of An-MMTs.

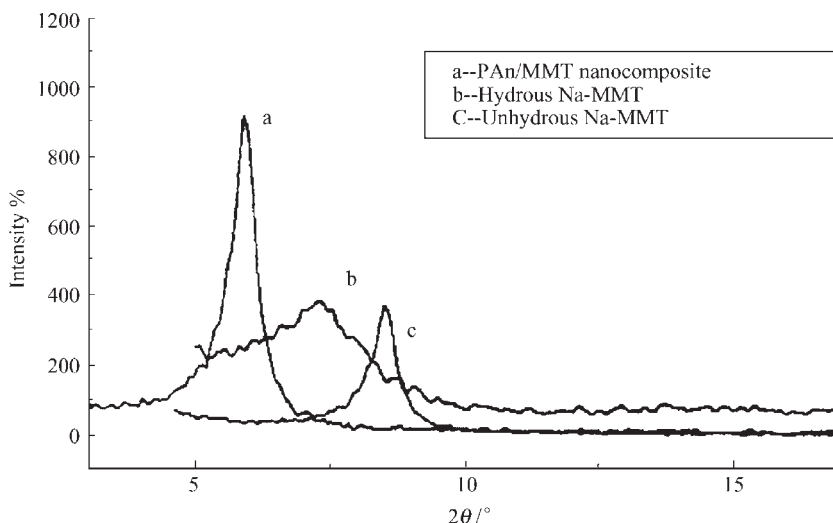


Fig. 3.47. X-ray patterns of PAN-MMT nanocomposites.

than coiled conformation of PAN in the galleries of the host. From these, the structure of PAN-clay hybrid should take a zigzag conformation.

3.5.2.4. Polyaniline chain conformation in PAN/clay hybrid nanocomposite

From the XRD results, it is presumed that in the PAN/clay hybrid nanocomposite the PAN is in extended-chain conformation; direct proof of this is obtained from UV–Vis–NIR and FT-IR spectra.

The UV–Vis–NIR spectra show the obvious difference between PAN-clay hybrid nanocomposite and bulk PAN (Figure 3.48). In bulk PAN a strong absorption peak usually emerges at 700–800 nm ($n-\pi$). But in the PAN/clay hybrid nanocomposite this peak disappears, being displaced by a broad absorption band (called “free-carrier tail” by other authors [86]) in the near-infrared region. This is consistent with the delocalization of electrons in the polar band promoted by an extended conformation of the polymer chains. In bulk PAN, the strong interaction of chains generates π -conjugation defects, and always leads to a “compact coil” conformation. However, in the MMT galleries, the nanometer template not only eliminates the interaction of different PAN chains, but also limits the contraction of the chains. The interaction between the adjacent isolated polarons, therefore, becomes stronger, and the polaron band becomes more dispersed in energy. As a result, the absorption peak disappears and the “free-carrier tail” appears. A similar tail can usually be found in large-size organic acid PAN, i.e., dodecyl benzene-sulfonic acid (DBSA), D,L-camphor sulfonic acid (CSA) as dopant [87], caused by an “expanded coil” conformation and accompanied by a large increase in conductivity. Hence, it is believed that in this PAN/clay hybrid nanocomposite, the extended-chain conformation can give rise to conductivity.

FT-IR spectra (Figure 3.49) also confirm the formation of “free-carrier tail” in the intercalated PAN. In the FT-IR spectra of PAN-MMTs, 917.7 and 840.6 cm^{-1} are the

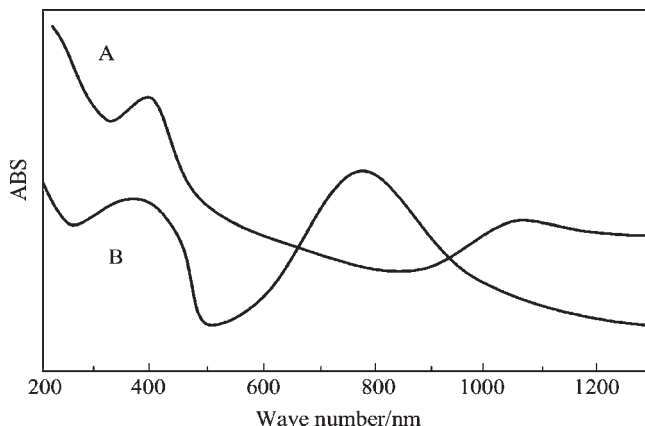


Fig. 3.48. UV-Vis-NIR spectra for (A) PAN-MMTs nanocomposites and (B) bulk polymers.

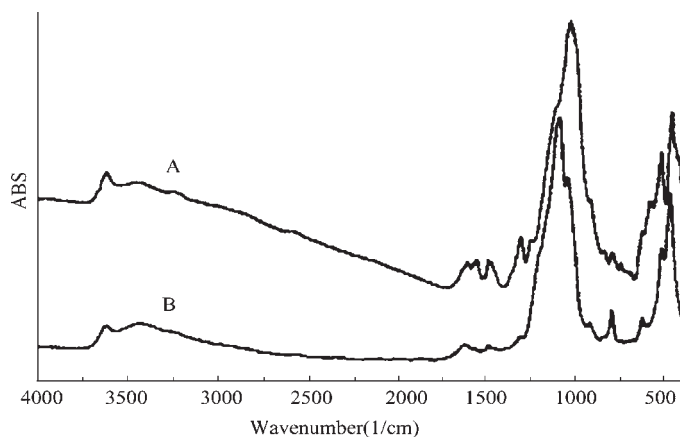


Fig. 3.49. FTIR spectra for (A) PAN-MMT nanocomposites and (B) PAN- Na-MMT blend.

characteristic vibrations of clay; 1489.1, 1562.9 and 1311.5 cm^{-1} are the characteristic vibrations of emeraldine salt [88,89]. In comparison with PAN and Na-MMT blend, its content of PAN is 7.2 wt%, which is the same as the nanocomposite at higher absorption in the high-frequency region. This is caused by the perfect delocalization of electrons [76].

3.5.2.5. Conductivity of the nanocomposite

The room-temperature conductivity of the hybrid nanocomposite is $10^{-3} \text{ S cm}^{-1}$. It has a relatively high conductivity in comparison with other PAN-inorganic host hybrids. The conductivity is controlled by two contradictory reasonings and the model is shown in Figures 3.44 and 3.45. On the one hand, the content of polymer is very low and the confinement of conducting polymers to the interlayer space disrupts the three-dimensional

organization of the polymer chains. On the other hand, the extended PAN chains with high conjugation and small polymer bridges can enhance the conductivity of the hybrid nanocomposite. The PAN bridges are likely to be formed by free monomers (mentioned earlier) and the bridges can electron transform between different layers.

PAN-clay hybrid nanocomposites with relatively high conductivity have been successfully synthesized by the method of intercalation polymerization. In the hybrid nanocomposite, > 90% PAN is inserted between the layers and it is a single chain with an extended-chain conformation owing to the confined environment in the nanometer size gallery.

3.6. Other kinds of polymer–inorganic nanocomposites

There are many organic polymers that are modified with MMTs and silica, such as polymethyl–methacrylate (PMMA), polyimides (PI), polyurethane (PU), etc. Due to their small contribution in the application field, the polymers and their oligomers are used to treat the inorganic phase in the preparation of the nanoprecursors.

3.6.1. PMMA-based nanocomposites

PMMA as a transparent matrix [90] is often used to prepare the core–shell structure materials, and is called a nanoprecursor. The PMMA-silica particles are obtained by an in situ polymerization of MMA monomers in the emulsion solution taking alcohol or butyl alcohol as an emulsifying agent. Polymerization is initiated at 50–90°C in the water media. Usually, the silica is modified with coupling agents such as KH-560 (570 or 580). The treated silica may be hydrated inside the emulsion suspension. To solve this problem, the mixing solution of toluene and water is used for the polymerization of the monomers and treated silica.

The PMMA–silica nanocomposite particles are the intermediate materials, which are further used to produce PET, PBT or other polyesters through a simple mixing or in situ polymerization. These composite particles are easy to interconnect because of the different morphology of the porous silica surface. The interconnected particles result from the active hydroxyl groups on the porous silica surface as shown in Figure 3.50.

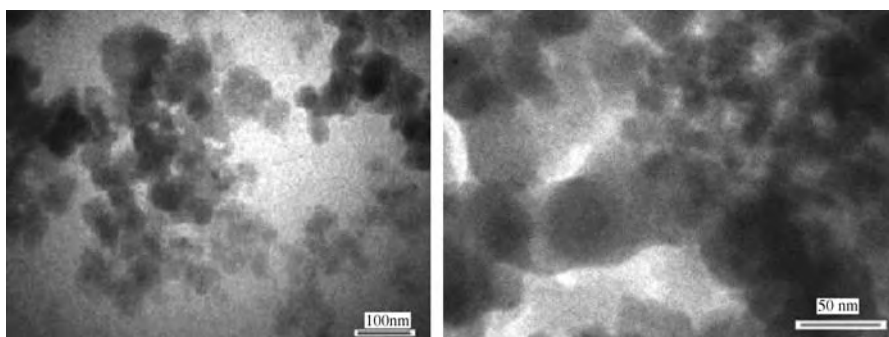


Fig. 3.50. PMMA–silica composite nanoparticles obtained by an in situ polymerization at 60°C.

The solvent dispersion technology is used in the preparation of PMMA–organo-clay nanocomposites.

Example 3.3.1.1. The preparation of PMMA-MMTs nanocomposites. The organo-clay is dissolved in 1–3% molar fraction of mixing solvents of *N,N*-dimethyl propyl amino methyl acrylic amide, or *N,N*-dimethyl acrylic ester. Then, the system is initiated with the initiators of polymerization such as BPO or AIBN for 1–4 h. In this way, the nearly completely exfoliated PMMA-MMT nanocomposites are achieved. The properties of these nanocomposites, when the organo-clay load is 4.0% (by vol), are four times the rigid modulus for the pristine PMMA.

3.6.2. Polyimides-based nanocomposites

Polyimides or aromatic polyimides (PI) exhibit distinguished dielectric and mechanical properties at elevated temperatures. The monomers for different types of PI are pyromellitic dianhydride (PMDA) and 4,4-diaminodiphenylether (ODA). Usually, these PI-MMT hybrids are insoluble through an imidization process. To prepare functional films, there is a strong need to prepare an organo-soluble polyimide [91]. In this preparation, high-performance PI materials are obtained through a monomer intercalation polymerization in solution. The PI-MMT hybrid is expected to show enhanced thermal stability and better solubility, and acquire a lower thermal expansion coefficient than that of their pure counterparts. These materials are specially designed for microelectronics.

3.6.2.1. Flow chart for the preparation of PI-MMTs

The PI polymerization is industrially prepared. A flowchart for the preparation of PI-MMT hybrids is shown in Figure 3.51. The MMTs are mixed with monomers of PI to get the polyamide composites or MMT/PA solution, which is cast into MMT/PA films. Finally, this film is heated to make the MMT/PI films.

3.6.2.2. Recipe for PI-MMTs

The raw materials for PI-MMT mixture are shown in Table 3.42. These materials are mixed (see flowchart) to prepare PI-MMT hybrids or nanocomposites.

3.6.2.3. Examples of the preparation of PI-MMT hybrids

In the preparation of PI-MMT hybrids, the organo-MMTs were specially prepared through an intercalant of quaternary ammonia salt of *p*-aminobenzoic acid with hydrochloric acid.

Example 3.6.2.1. Preparation of organo-MMTs. A mixture of 8.82 g or 0.0584 mol *p*-aminobenzoic acid and 4.8 ml of 37% or 0.0584 mol of hydrochloric acid is dissolved in 100 ml distilled water. This mixture is heated to 80°C, to which the hot (80°C) suspension of MMTs is added. The whole composite is stirred vigorously for 1 h, and organophilic MMTs were prepared through post-filtration and washing several times in order to remove residue such as *p*-aminobenzoic acid. Then dried organo-MMT was obtained in a powder form.

Example 3.6.2.2. Preparation of PI-MMT hybrids. Organo-MMT (3.14 g) was dissolved in a 90.0 g of *N,N*-dimethylacetamide (DMAc). The mixture then was heated to 90°C and stirred for 3 h. Then, 1.017 g or 0.0045 mol of MMDA monomer was dissolved

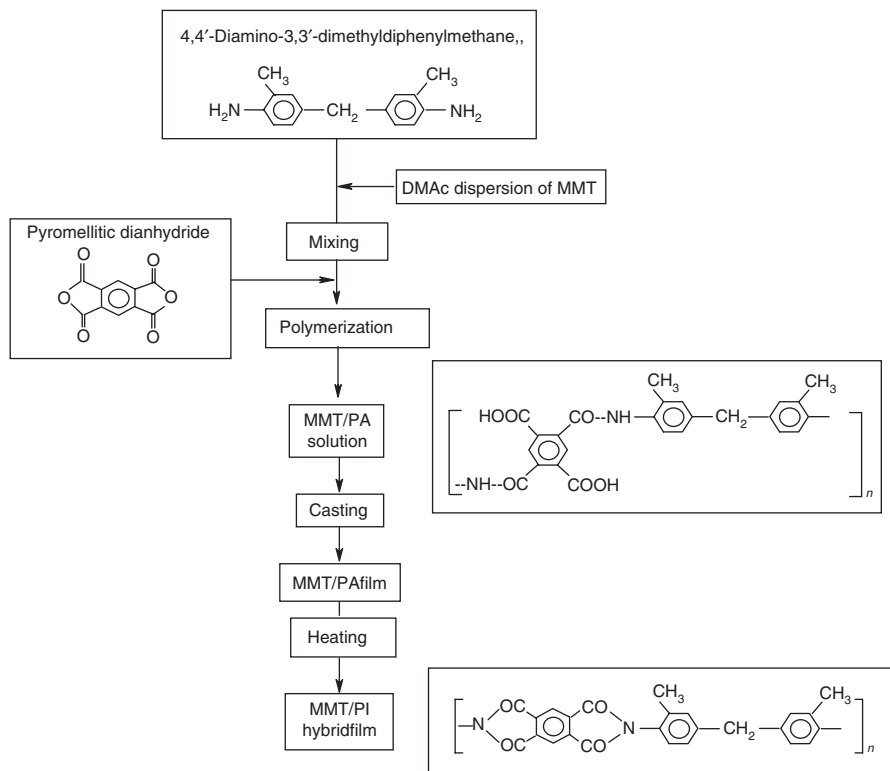


Fig. 3.51. Flowchart for the preparation of PI-MMT hybrids.

Table 3.42
The basic materials, their properties and action for PI-MMTs

Basic materials	Properties and action
Na-MMT	40 μm, CEC = 70–100 mmol (100 g ⁻¹)
<i>p</i> -Aminobenzoic acid	AP grade, intercalants
Pyromellitic dianhydride (PMDA)	CP grade, monomers
4,4'-Diamino-3,3'-dimethyldiphenyl methane (MMDA)	CP grade, monomer
Hydrochloric acid	37% (w/w), catalyst

in 18.6 g of DMAc at room temperature, to which the organo-MMT in DMAc was added and stirred for 30 min. Then, the other monomer, 0.982 g or 0.0045 mol PMDA, was added to react with MMDA. This mixture was then stirred at room temperature for 5 h.

This polyamic acid–MMT hybrid solution was then cast onto a glass substrate, which was heated subsequently at 100°C for 6 h, 150°C for 2 h, and 270°C for 2 h under the nitrogen atmosphere. In this way, the final PI-MMT hybrids were obtained. In these PI-MMT hybrids, the MMT particles were exfoliated into those of 400 nm scale.

3.6.2.4. The properties of PI-MMT hybrids

The properties of the PI-MMT hybrid were measured for powder and film samples. From Table 3.43, it is seen that the treated MMT-PI hybrids have higher thermal degradation temperatures than those of the untreated PI-MMT hybrids or blends. The PI-organo-MMT hybrids have lower thermal expansion coefficients (T_{cc}), demonstrating their thermal stability.

The mechanical properties of the hybrids are listed in Table 3.44. The mechanical properties of the PI-organo-MMT hybrids are much higher than those of the PI-untreated MMTs. The tensile strength increases with an increase in the organo-MMT load.

Notably, the solubility of the hybrids obviously improved in solvents (see Table 3.45).

Table 3.43
Thermal properties of PI-MMT hybrids

Thermal properties	MMT load (by wt)			
	0.0%	1.0%	5.0%	5.0 ^a
$T_d^{\circ}C^b$	510	530	546	501
$T_d^{\circ}C^c$	573	577	581	566
$T_{cc} (\times 10^{-5} K^{-1})^d$	3.60	2.20	1.76	2.40

^a Untreated Na-MMT-PI hybrids. ^b Thermal degradation temperature at a weight loss of 5% (by wt). ^c Thermal degradation temperature at a weight loss of 10% (by wt) (scanning rate, 20°C min⁻¹, nitrogen atmosphere) ^d Thermal expansion coefficients.

Table 3.44
Mechanical properties of PI-MMT hybrids at 25°C

Mechanical properties	MMT load (by wt)			
	0.0%	1.0%	5.0%	5.0% ^a
Tensile strength (MPa)	78	88	95	75
Elongation at break (%)	15	24	20	17

^a Untreated Na-MMT-PI hybrids.

Table 3.45
The solubility of hybrids at room temperature

Solvents	PA-MMT load		PI-MMT load			
	0.0%	5.0%	0.0%	1.0%	5.0%	5.0% ^a
NMP	+	+	+	+	+ -	-
DMAc	+	+	+	+	+ -	-
DMF	+	+	+	+	+ -	-
DMSO	+	+	+	+	+ -	-

Note: soluble; + -, partially soluble; -, insoluble.

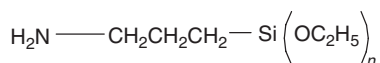
^a Untreated Na-MMT-PI hybrid; NMP, *N*-methyl-2-pyrrolidone; DMAc, *N,N*-dimethylacetamide; DMF, *N,N*-dimethyl formamide; DMSO dimethyl sulfone.

3.7. Polymer–silica nanocomposites

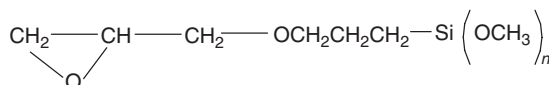
Much attention has to be paid to superfine particles' dispersion and distribution morphology because of their contribution to the final properties of the materials. Most research has focused on the media of gas and liquid for inorganic particle dispersion or suspension. In liquid, submicron silica particles with narrow-size distribution are self-assembled to form an ordered structure used to prepare opals or inverse opals, which are applied to photon crystals [92–93]. So far, the homogeneous dispersion of inorganic particles in organic solid media (e.g., polymers, bio-macromolecules, etc.) has not been considered. Fine particles generally do not disperse directly in the organic polymers, but form clusters, agglomerates or a heterogeneous morphology [94]. These asymmetric states of dispersion must be avoided in order to obtain composite materials with good properties.

Previously, to solve these problems, the inorganic particles' surface was reacted or treated with other organic reagents. In most of the micron particles such as CaCO_3 , talc, saponite, etc., two kinds of reagents were used to modify particle surfaces, KH-550 and KH-560 [95], with their molecular formulae as

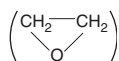
KH-550:



KH-560:



KH-550 and KH-560 have reacting groups of $-\text{NH}_2$ and oxidized ethylene



respectively. Thus, they react with hydroxyl groups on particle surfaces or treated particles; the wettability of the particles surfaces is then reversed, making them compatible to organic polymers with similar hydrophobic surfaces. These two reagents have achieved great success in treating many kinds of inorganic particles' surfaces, and have in turn been applied to the preparation of organic polymer-based composites, such as polymers of polyethylene, polypropylene, polystyrene, etc. All of these polymers have a very large yield in the world.

When inorganic particles decrease in size and are treated by traditional reagents, the ever-present problem of particle agglomeration cannot be avoided, because it has a bad effect on the composite's properties. Most of the organic polymers are mainly used for the preparation of films, whose transparency properties are one of their most important aspects. When superfine particles are mixed with these polymers, film transparency will be lost in most of the cases because of particle agglomeration. Thus, the films are often opaque.

3.7.1. Assembly and self-assembly

In Chapter 2, some theoretical aspects of the preparation of monodisperse silica particles are described. Based on the settling velocity ratio of doublets to single spheres at low Reynolds number, the silica particles with broad distribution are selected through a flotation technique in water media. Single spheres are collected in this way from the designed region of the floatation device [96]. A TEM image of the selected spheres in Figure 3.52 shows that the relative size deviation (RSD) of diameter distribution is 3.22%.

3.7.2. Fabrication of SiO_2 opals from colloidal SiO_2 submicrospheres

In a similar approach, SiO_2 opals were fabricated from colloidal SiO_2 submicrospheres (see Section 2.1) by the method of sedimentation in gravitational field.

3.7.2.1. Details of the preparation of silica opals

In order to eliminate interaction between submicrospheres, the suspension of SiO_2 submicrospheres was diluted so that the concentration of SiO_2 submicrospheres was below 1 wt%. The diluted suspension was then filled into a tube with a polished substrate. The diameter of the tube was 2.5 cm, which is large enough to eliminate edge effects. The aqueous solution was extracted carefully when sedimentation was complete after a few weeks. Then they were dried naturally at room temperature; the opals, which were very easy to crack, were taken out of the tube and annealed at 900°C for 4 h. The opals had better mechanical and optical properties after annealing. Diffractive colors from green to red could be readily seen when the opals were put under a lamp and the observation angle was changed. A scanning electron microscopy (SEM) image of the annealed sample is given in Figure 3.53. It is clearly seen that the opals have face-centered cubic structure symmetry. When the selection procedure of spheres was used, the size of single crystal in the opals was substantially larger and their mechanical and optical properties were also better.

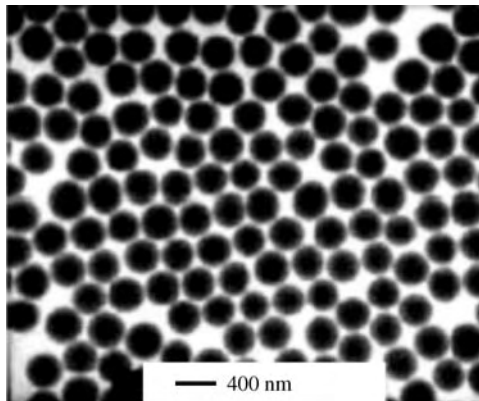


Fig. 3.52. TEM image of selected SiO_2 submicrospheres with a diameter of 290 nm.

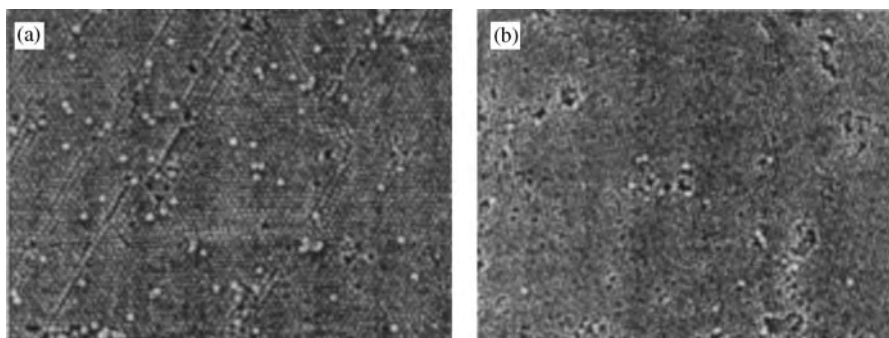


Fig. 3.53. SEM image of top surfaces of silica opals: (a) top surface of the opals without selection procedure of spheres; (b) top surface of the opals with the selection procedure of spheres.

A comparison of SEM images between the opals fabricated from selected silica submicrospheres and the unselected submicrospheres is shown in Figure 3.53. The top surfaces of the opals (Figure 3.53(a)) fabricated from unselected submicrospheres have good alignment, while their bottom surfaces (Figure doesn't provide) do not. However, with the selection procedure of spheres, the two surfaces (Figure 3.53(a) and (b)) have good alignment. This proves that the selection procedure of spheres is very successful in improving the monodispersity of spheres. Meanwhile it also confirms that the monodispersity of spheres is one of the most important factors governing the fabrication of opals. The protonic band structure of the opals can be probed experimentally by measuring their transmission spectra using electromagnetic waves with different wavelengths.

Because fewer defects and dislocations are present in the opals made using the selection procedure, random scattering polystyrene (PS) is one of the best suitable choices for the preparation of the monodisperse particles. Preparation of monodisperse core-shell structured particles of PS with silica is thus naturally suggested based on the reported techniques [96]. These core-shell structured particles have wide application fields in additives, absorbents, composite materials and, especially, polyester composite films. Thus, they are used to directly mix poly(ethylene terephthalate) (PET) to improve their non-fiber applications.

Based on Stöber's method, we developed a method for the preparation of the particles aiming at extending the size range of the synthesized particles and improving the monodispersity of the silica systems. To this end, the seeding technique [100] was also developed and improved, by which particles with diameters ranging from dozens of nanometers to 2.5 μm can be prepared.

3.7.2.2. Raw materials of multiple dispersed particles

The multiple dispersed silica particles are usually prepared from chemical deposition (CD), or vapor oxidation reactions from precursors such as SiCl_4 reacting with O_2 ; the silica collected is heavily aggregated. To obtain the nanoparticles of silica, they are a post-treated, or calcinated at high temperatures $> 1000^\circ\text{C}$. The properties of silica particles are shown in Table 3.46.

Table 3.46
The physical parameters of nanometer silica

Parameters	MNIP	MNIS
Surface area (m ² g)	640±50	160±20
Particle size (nm)	10±5	15±5
Surface hydroxyl (%)	48	36
Reflect rate of ultraviolet (%)	>85	>80
SiO ₂ content (%)	>99.9	—
Loose density (g cm ⁻³)	<0.15	—
Stirring density (g cm ⁻³)	<0.22	—
Condensed phase	Amorphous white loose powder	

Note: Impurities (%): Al <0.001, Fe <0.001, Ca <0.002, Sn <0.001, Cu <0.003, Mg <0.001.

3.7.2.3. The composite monodisperse particles of PS–silica

The multiple dispersed silica nanoparticles usually act as fillers. When they are used to assemble into the ordered patterns, they are either selected from the silica of Table 3.45, or prepared from the sol-gel process together with fine selection. Then, the monodispersed silica particles will be treated with coupling agents such as KH-570 (see Figure 3.54) for use in assembling. The size of the treated monodispersed silica particles are slightly larger than that of the pristine ones.

The modification of the silica surface avoids the interconnecting of particles (Figure 3.55) when they are assembled with monodisperse PS particles.

Then, removing the PS from the solvent (e.g., CH₂Cl₂) will show the patterns with ordered pores as shown in Figure 3.56. This pattern is used as a carrier in cracking the heavy oil, which is dealt later.

3.7.3. Properties and products

3.7.3.1. PET–silica nanocomposites

PET–silica nanocomposites have found applications in functional films, fire retardants, packaging, bottles, plastics, etc. The crystalline particle of PET does not grow homogeneously and is characterized by double melting peaks [97–103], indicating the existence of the unstable crystallites. The preparation of PET–silica nanocomposites aims at making the size of crystallites homogeneous and at bringing about a nucleation effect. The exfoliated silica and layered silicate in PET matrix form more nucleation centers than the micron particles, and this no doubt increases the crystallization rate. These nucleation effects are observed in DSC patterns of NPET. The smaller peak in double melting peaks grows rapidly enough to produce positive enthalpy. The disappearance of smaller peaks suggests that the crystalline nuclei have a similar size. When annealing layered silicate–PET nanocomposites (NPET) at 130°C for different times, all the smaller peaks disappear, which strongly shows the rapid crystallization rate of nanoparticle nucleation, but this is not true in PET–silica nanocomposites.

The nucleation phenomena in the PET–silica nanocomposites are shown in Figure 3.57, where silica particles are mixed with PET oligomers at first, and then polymerized together with PET monomers. When the nanocomposite samples are annealed at

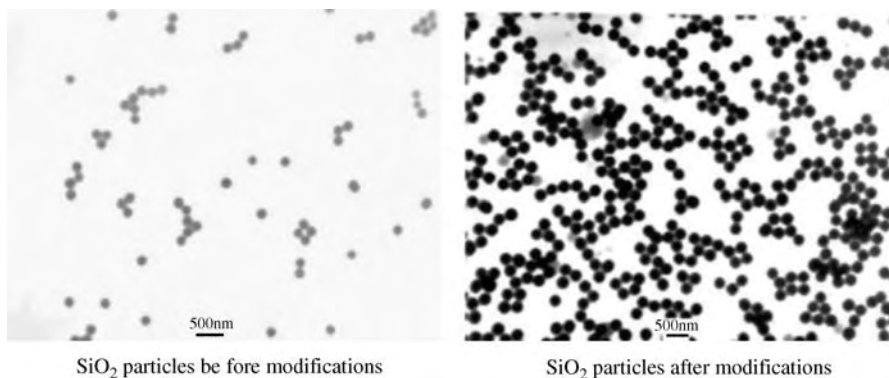


Fig. 3.54. The monodisperse particles of silica and silica modified with silane.

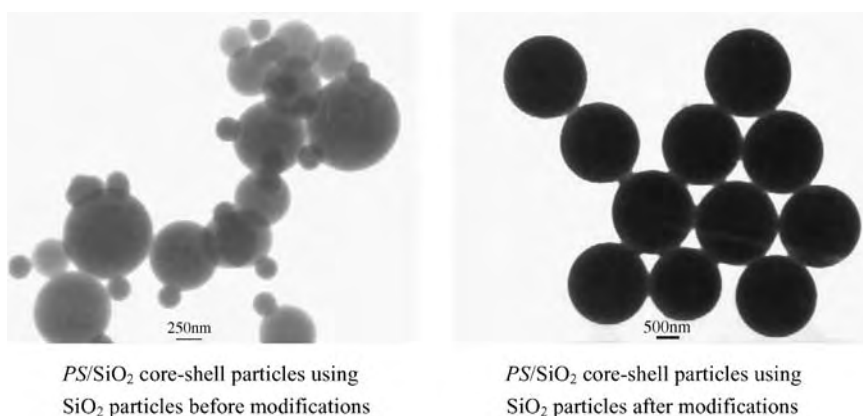


Fig. 3.55. The PS/SiO₂ core-shell particles using SiO₂ particles before and after modifications with silane.

130°C for 45 min, the double melting peaks do not disappear, in contrast to PET-MMT nanocomposites. The PET-silica nanocomposites with different silica loads shrink the double melting peaks at a low position slightly similar to PET. The DSC patterns show that PET-silica nanocomposites have relatively lower crystallization rates than PET-MMT nanocomposites. The heterogeneous dispersion of silica in polymer melt is not beneficial for forming homogeneous nucleation centers.

3.7.3.2. Several products and their properties

By using nanoparticles as carriers, several active additives such as stabilizing agents, antioleto agent, dispersant and nucleation agents can be mixed with silica for the preparation of composite additives. Some products of polypropylene (PP) with silica and nucleation agents have exiting properties, as described in Table 3.47.

The transparent polypropylene plate or flake material is one of the mixtures formed using composite additives. These plate materials are either used in the outer layers of

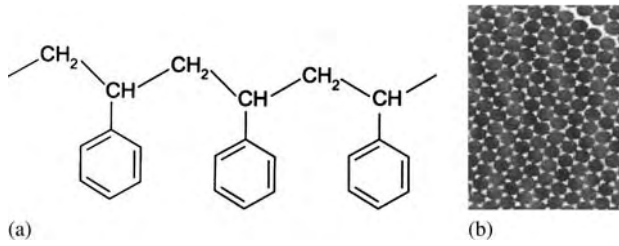


Fig. 3.56. Monodisperse particles of PS–silica composite: (a) polystyrene molecular chains; (b) assembled pattern of silica with monodisperse PS as template.

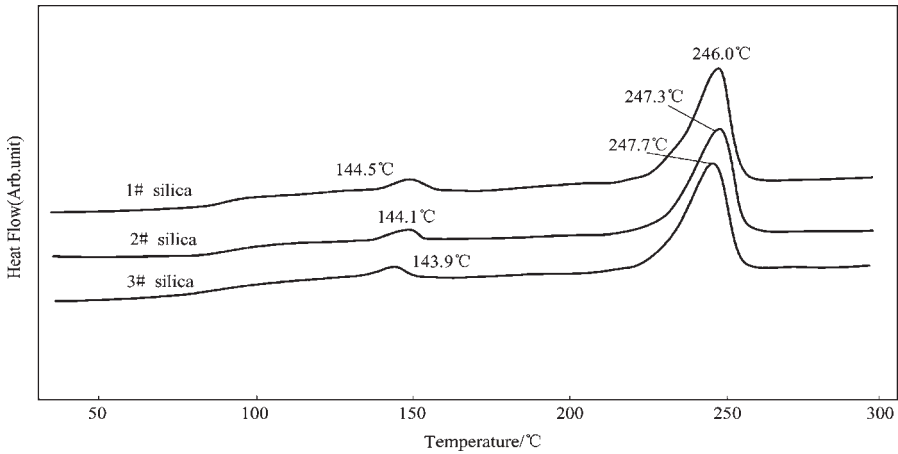


Fig. 3.57. Double melting behavior of silica–PET nanocomposites with a silica load of 0.5–1.5 (by wt) (1#, PET + 0.5% silica; 2#, PET + 1.0% silica; 3#, PET + 1.5% silica).

Table 3.47
Properties of PP and PP–nanosilica composite with nucleation agent

	PP	PP-SiO ₂ (0.5–1%, by wt)
Trans	85%	93%
Haze	30–50%	8–20%
HDT(°C)	80–100	110–150

different steel pipelines or in packaging materials, providing barrier properties to gases such as oxygen or nitrogen.

References

- [1] A. Usuki, T. Mizutani, Y. Fukushima, US Patent 4889885, 1989.
- [2] Z.K. Zhu, Y. Yang, Y.C. Ke, et al., *J. Appl. Polym. Sci.* 73 (1999) 2063.
- [3] Y.H. Wang, *Casting Nylon (Zhu Xing Nylon)*, Academic Press, Beijing, 1973.

- [4] H. Huopuluof, et al., Polyamide, Press of China Industry, Beijing, 1965, 12.
- [5] Q. Li, Postdoctoral Report, Institute of Chemistry, China Academy of Sciences, 1996.
- [6] Honeywell Reports, Eur. Plast. News, 27(11): (2000) 27.
- [7] (a) Z.N. Qi, Q. Li, Z.D. Zhao, Y.Z. Zhou, Q. Fang, ZL96105362.3(1996/6); (b) Z.N. Qi, L.M. Liu, X.G. Zhu, Y.K. Ding, G. Li, ZL 97112237-7 (c) Y.C. Ke, Chin. Pat. Appl. 02153554.X, Vol.11, 2002.
- [8] K.Y. Li, J.H. Zhang, F.R. Xiang, Principles of Polymer Synthesis and Technology, Scientific Press, Beijing, 2001.
- [9] S.A. Lin, Y. Lu, Polymer Chemistry, Scientific Press, Beijing, 1982.
- [10] T.E. Twardowski, Chem. Innovation, 30 (11) (2000) 14.
- [11] T. Lan, P.D. Kaviratna, T.J. Pinnavaia, Chem. Mater. 6 (1995) 2144.
- [12] (a) T. Lan, T.J. Pinnavaia, Chem. Mater. 7 (1994) 2216; (b) Y.C. Ke, Postdoctoral Report, Institute of Chemistry, China Academy of Sciences, 1998.
- [13] (a) P.B. Messersmith, E.P. Giannelis, Chem. Mater., 6 (1994) 1719; (b) H. Wang, Master Degree Dissertation, University of Petroleum, China, 2004.
- [14] J.K. Lv, Y.C. Ke, Z.N. Qi, X.S. Yi, Chin. J. Polym. Sci. 1, (2000) 85.
- [15] J. Zhao, Master Degree Dissertation, Institute of Chemistry, 1998, p. 6.
- [16] J.K. Lv, Y.C. Ke, Z.N. Qi, X.S. Yi, Polym. Bull. (Chin.) 2 (2000) 18.
- [17] J.K. Lv, Y.C. Ke, Z.N. Qi, X.S. Yi, J. Polym. Sci., Part B: Polym. Phys. 39 (2001) 115.
- [18] (a) B.K.G. Theng, Formation and Properties of Clay-Polymer Complexes, Elsevier, New York, 1979, (b) H.J. Choi, S.G. Kim, Y.H. Hyun, M.S. Jhon, Macromol. Rapid Commun. 22 (2001) 320.
- [19] Z.D. Zhao, Z.M. Gao, Z.N. Qi, F. S. Wang, Chin. J. Polym. Sci. 26 (1996) 228.
- [20] M. Kakimoto, Y.I. Yoku, A. Morikawa, H. Yamaguchi, Y. Imai, Polym. Prepr. 35 (1) 1994 393.
- [21] Y.C. Ke, J.K. Lv, X.S. Yi, J. Zhao, Z.N. Qi, J. Appl. Polym. Sci. 18 (4) (2000) 808.
- [22] H.Z. Shi, T. Lan, T.J. Pinnavaia, Chem. Mater. 8 (1996) 1584.
- [23] T.J. Pinnavaia, T. Lan, Z. Wang, et al., in G.M. Chow, K.E. Gonsalves (Eds.) Nanotechnology: Molecularly Designed Materials, ACS Symposium Series 622, ACS, Washington, DC, 1996, p. 250.
- [24] Chin In-Joo, T.-A. Thomas, et al., Polymer 42 (13) (2001) 5947.
- [25] M.S. Wang, T.J. Pinnavaia, Chem. Mater., 6 (1994) 468.
- [26] Y.C. Ke, L. Wang, Z.N. Qi, Chin. J. Polym. Sci., 6 (2000) 768.
- [27] Y.C. Ke, B.H. Su, J.P. Wang, X.L. Tian, R.J. Wu, J. Composites 1 (1984) 16.
- [28] X. Wang, Ph.D. Dissertation, Institute of Chemistry, China Academy of Sciences, 2001.
- [29] J.S. Ma, Ph.D. Dissertation, Institute of Chemistry, China Academy of Sciences, 2001.
- [30] Z.H. Jin, X.Y. Hong, Petrol. Refining Chem. (Chin.) 32 (2001) 10–13.
- [31] Y.C. Ke, Polymer-Inorganic Nanocomposites, Chemical Industry Press, Beijing, 2003.
- [32] B.P. Liu, X.H. Ren, Investigation on polyolefin catalysts carried on silica gel, Chem. reaction Eng. Technol. 13 (1997) 231–238.
- [33] J.F. Rong, Ph.D. Dissertation, China Institute of Petrochemical Science and Technology, 1999.
- [34] P.C. LeBord, Z. Wang, T.J. Pinnavaia, Appl. Clay Sci. 15 (1999) 11–29.
- [35] B.Q. Mao, J.X. Yang, E.C. Yang, et al., CN 1091748A, 1994.
- [36] B.Q. Mao, J.X. Yang, X.Z. Xia, et al., CN 1097597C, 2003.
- [37] X.Y. Hong, L. Ma, X.H. Zhou, J.F. Rong, Z.H. Jin, et al., Chin. Pat. Appl. 1199056A, 1997.
- [38] P. Eyerer, Y.C. Ke, J. Biomed. Mater. Res. 18 (1984) S 1137-1151.
- [39] (a) Y.C. Ke, Chin. Pat. Appl. 03105009.3, Vol.3, 2003; (b) B.C. Zhu, Chin Pat. Appl. 00105161.X, Public No. CN 1268406A, 2000/4/12.
- [40] (a) X. Wang, Ph.D. Dissertation, Institute of Chemistry, China Academy of Sciences, 1999; (b) J.F. Rong, Z.H. Jing, H.Q. Li, M. Shen, Macromol. Rapid Commun. 22 (2001) 329–334.
- [41] (a) Y.L. Hu, J.Y. Dong, Z.N. Qi, Z197120157.9, Vol.11, 1997; (b) Zhe Jiang University, Chin. Appl. No. 97106208.0, Public No. CN 1187497A, 1997.
- [42] (a) J.F. Rong, Ph.D. Dissertation, Institute of Petrochemical Science and Technology, Sinopec, Beijing, 1999, (b) Y.C. Ke, J.R. Hu, H. Wang, Prog. Petrochem., 22 (12) (2003) 1308.
- [43] (a) M. Alexandre, P. Dubois, T. Sun, et al., Polymer, 43 (2002) 2123-2132, (b) H. Wang, Master Degree Dissertation, University of Petroleum, Beijing, 2004, p. 6; (c) Exxon Chemical Patents Inc. US 5902766, 1999, (d) G.M. Chen, D.Y. Shen, Z.N. Qi, Z197120157.9, Vol.11, 1997; (e) G. Chen, S. Liu, S. Zhang, Z.N. Qi, F.S. Wang, Macromol. Rapid Commun. 21 (2000) 746.

- [44] (a) G. Chen, B. Han, H. Yan, J. Colloid Interface Sci. 201 (1998) 158, (b) E.P. Giannelis, Adv. Mater. 8 (1996) 29.
- [45] Y.C. Ke, T.B. Wu, PS-Silica Assemble Patterns, Petroleum Science, 2 (2005) 70.
- [46] S.D. Hudson, Polyolefin Nanocomposites, US5910523, 06, 08, 1999.
- [47] M. Kawasumi, N. Hasegawa, M. Kato, A. Usuki, A. Okada, Macromolecules 30 (1997) 6333.
- [48] Q. Zhang, Q. Fu, L.X. Jiang, Y. Lei, Polym. Int. 49 (12) (2000) 1561.
- [49] D.M. Lincoln, R.A. Vaia, Z.-G. Wang, B.S. Hsiao, Polymer 42 (2001) 1621.
- [50] Y.T. Lim, O.Ok Park, Macromol. Rapid Commun. 21 (2000) 231.
- [51] B. Hoffman, C. Dietich, R. Thomann, C. Fredrich, R. Mulhaupt, Macromol. Rapid Commun. 21 (2000) 57.
- [52] Z.N. Qi, Q. Li, Y. Zhou, CN139643.6,03, 1996.
- [53] R.A. Vaia, H. Ishii, E. P. Giannelis, Chem. Mater. 5 (1993) 1694.
- [54] R.A. Vaia, S. Vasudevan, W. Krawiec; L.G. Scanlon; E.P. Giannelis, Adv. Mater. (1) (1996) 29.
- [55] Y.C. Ke, Chin. Pat. Appl. 02153554.X, 2002, 11.
- [56] Z.N. Qi, Y.C. Ke, Y.Z. Zhou, Chin. Pat Appl. 97104055.9.
- [57] Z.N. Qi, Y.C. Ke, Y.Z. Zhou, Chin. Pat. Appl. 97104196.4.
- [58] Y.C. Ke, Z.N. Qi, C.F. Long, J. Appl. Polym. Sci. 71 (1999) 1139.
- [59] Y.C. Ke, C.F. Long, International Symposium on Polymer Physics. 25–29 November 1997, Guilin City, China, p. 158.
- [60] Y.C. Ke, Z.B. Yang, C.F. Zhu, J. Appl. Polym. Sci. 85 (13) (2002) 2677–2691.
- [61] Y.C. Ke, Patent Office of China, Pat. Appl. 02157993.
- [62] H.J. Choi, S.G. Kim, Y.H. Hyun, M.S. Jhon, Macromol. Rapid Commun. 22 (2001) 320.
- [63] J.K. Lu, Y.C. Ke, X.S. Yi, Z.N. Qi, J. Polym. Sci., Part B: Polym. Phys. 39 (2001) 115.
- [64] Y.C. Ke, Chem. Eng. Oil Gas 33 (1) 2004 50.
- [65] N. Ogawa, G. Jimenez, H. Kawai, T. Ogihara, J. Polym. Sci. Part B: Polym. Phys. 35 (1997) 389.
- [66] Y. Kojima, A. Okada, J. Appl. Polym. Sci. Part B: Polym. Phys. 32 (1994) 625.
- [67] T.M. Wu, C.S. Liao, Macromol. Chem. Phys. 201 (2000) 2820.
- [68] M. Avrami, J. Chem. Phys. 7 (1939) 1103.
- [69] Y. Kojima, A. Usuki, One-pot synthesis of nylon 6—clay hybrid, J. Polym. Sci. Part A: Polym. Chem. 31 (1993) 1755.
- [70] L. Liu, Z.N. Qi, X.G. Zhu, J. Appl. Polym. Sci. 71 (1999) 1133.
- [71] Hutton Jr. A.E., Burke R.E. Monadnock Paper Mills, Inc., US4920171 1990.
- [72] E.R. Kamens, US04460714, 07, 17, 1984.
- [73] M.G. Brereton, G.R. Dowies, R. Fakeways, Polymer 19(1) (1978) 17.
- [74] I.H. Hall, M.G. Pass, Polymer 17, (1976) 807.
- [75] G. Galgali, C. Ramesh, A. Lele, Macromolecules, 34 (2001) 852.
- [76] (a) T.A. Kerr, H. Wu, L.F. Nazar, Chem. Mater. 8 (1996) 2005; (b) M.G. Kanatzidis, C. Wu, J. Am. Chem. Soc. 111 (1989) 4139; (c) G. F. McCann, G. J. Millar, G. A. Bowmaker, R. P. Cooney, J. Chem. Soc. Faraday Trans. 91 (1995) 4321.
- [77] A.G. MacDiarmid, J.C. Chiang, A.F. Richter, A.J. Epstein, Synth. Met. 18 (1987) 285.
- [78] J.S. Tang, X.B. Jing, F.S. Wang, Synth. Met. 24 (1988) 231.
- [79] L.X. Wang, X.B. Jing, F.S. Wang, Synth. Met. 29 (1989) E363.
- [80] L.X. Wang, X.B. Jing, F.S. Wang, Synth. Met. 41 (1991) 739.
- [81] L.X. Wang, X.B. Jing, F.S. Wang, Synth. Met. 41 1991 685.
- [82] H. Jiang, J. Li, L.X. Wang, X.B. Jing; F.S. Wang, Chin. Pat. Appl. 95115519.9.
- [83] C.G. Wu, D.C. Degroot, H.O. Marcy, J.L. Schindler, et al., Chem. Mater., 8 (1996) 1992.
- [84] R. Krishnamoorti; R.A. Vaia; E.P. Giannelis, Chem. Mater. 8 (1996) 1728.
- [85] C.G. Wu, D.C. Degroot, H.O. Marcy, J.L. Schindler, et al., J. Am. Chem. Soc., 117 (1995) 9229.
- [86] G.M. Alan, J.E. Arthur, Synth. Met. 69 (1995) 85.
- [87] Z.J. Xue, Ph.D. Dissertation, Institute of Chemistry, China. Academy of Sciences, 1997.
- [88] Y. Cao, S. Li, Z. Xue, D. Guo, Synth. Met. 16 (1986) 305.
- [89] J. Stejskal, P. Kratochvil, Synth. Met., 61 (1993) 225.
- [90] (a) Y.C. Ke, PMMA-Silica Nanocomposites, submitted; (b) Y. Kojima, A. Usuki, M. Kawasumi, A. Okada, Y. Fukushima, T. Kurauchi, O. Kamigato, J. Mater. Res. 8 (1993) 1185.
- [91] Z.K. Zhu, Y. Yang, J. Yin, X.Y. Wang, Y.C. Ke, Z.N. Qi, J. Appl. Polym. Sci. 73 (1999) 2063.

- [92] Z.N. Qi, F. S. Wang, Y. M. Ma, Chin. Pat. 98103038.6, 1998.
- [93] X.Y. Zhang, L.D. Zhang, et al., Adv. Mater. 17 (2001) 1238.
- [94] S.C. Lu, Powder Processing Technology, Second Ed., China Light Industry Press, Beijing, 2000.
- [95] Z.N. Qi, Y.C. Ke, CN 1187506A, 1998/07.
- [96] (a) Y.C. Ke, T.B. Wu, Particuology 1 (2003) 247–252; (b) P. Dong, et al., Adv. Mater. 13 (2001) 437; (c) P. Dong, Prog. Nat. Sci. 10 (2000) 575.
- [97] S.S. Chang Polym. Commun. 29 (1987) 138.
- [98] Y. Lee, R.S. Porter, Macromolecules 20 (1987) 1336.
- [99] S.Z.D. Cheng, J. Polym. Sci. Polym. Phys. Ed. 28 (1990) 655.
- [100] M. Yagpharov, J. Therm. Anal. 31 (1986) 1073.
- [101] N. Alberola, J. Mater. Sci. 26 (1991) 1856.
- [102] P.J. Holdsworth, A. Turner-Jones, Polymer, 12 (1970) 195.
- [103] H. Marand , A. Prasad, Macromolecules, 25 (1992) 1731.

This page intentionally left blank

CHAPTER 4

Morphology, Assembly and Properties

OUTLINE

- Introduction 212
- 4.1. Nanostructure and morphology 212
 - 4.1.1. *Particle statistical distribution* 212
 - 4.1.2. *Particle size deviation* 217
 - 4.1.3. *Phase separation* 221
 - 4.1.4. *Particle order* 226
 - 4.1.5. *Intercalation dynamics and agglomerations* 226
 - 4.1.6. *Particle morphology–property relationship* 228
- 4.2. Crystallization 228
 - 4.2.1. *Crystallization from nanoparticles* 228
 - 4.2.2. *Isothermal or nonisothermal crystallization* 230
 - 4.2.3. *Phase transformation and polymorphism in crystallization* 232
 - 4.2.4. *Crystallization degree and rate* 234
 - 4.2.5. *Crystallization morphology–property relationships* 237
- 4.3. Thermal properties 237
 - 4.3.1. *Melting behavior* 237
 - 4.3.2. *Heat distortion temperature* 239
 - 4.3.3. *Thermal degradation* 240
 - 4.3.4. *Specific heat and fire retardancy* 241
 - 4.3.5. *Particle load–thermal property relationship* 242
- 4.4. Mechanical properties 243
 - 4.4.1. *Tensile strength and bending modulus* 244
 - 4.4.2. *Brittleness–ductility* 244
 - 4.4.3. *Particle load–mechanical property relationship for PP-MMTs and PEO-MMTs* 245
- 4.5. Special properties of nanocomposites 246
 - 4.5.1. *Assembly and self-assembly* 246
 - 4.5.2. *Optical properties* 254
 - 4.5.3. *Liquid crystal behavior* 255
- 4.6. Functional properties by nanoparticle assemble and doping 256
 - 4.6.1. *Barrier properties* 256
 - 4.6.2. *Optical and reflection properties by assembly and doping* 256

- 4.7. Rheology and dynamic behavior 263
- 4.8. Nucleation and order 265
 - 4.8.1. Nucleation in solution, melt and annealing 265
 - 4.8.2. Nucleation of metal oxide nanoparticles in ultrathin polymeric films 265
- References 271

In this chapter, different properties of polymer–inorganic nanocomposites are discussed. In particular, the property–structure relationship and functional aspects from the perspective of nanoparticle nucleation, assembly and order are described to reveal the laws of nanoparticle dispersion.

Introduction

Most enhanced properties of polymer–inorganic nanocomposites result from the mixing or binding of two different phases [1]. The inorganic phase provides the high-performance thermal and mechanical properties, while the organic phase contributes to the processing and adhesive properties. The dispersion process is usually difficult for nanoparticles in the polymer melt. It is often found that the particles agglomerate during dispersion. In several cases, adding nanoparticles to the polymer matrix has decreased some of its properties while enhancing many of its other properties. The reasons for this are open to debate. Thus, special attention is paid to the mechanical, thermal, rheological, assembling and functional properties of nanocomposites. Besides, if the nanoparticles carry some active or functional reagents and disperse in the polymer melt, some of the functional properties are seen.

4.1. Nanostructure and morphology

4.1.1. Particle statistical distribution

4.1.1.1. Surface morphology

Surface morphology observed by different techniques is briefly presented here [2]. It should be noted that depending on the characterization techniques, different particle distribution morphologies were observed for the same layers of the layered silicate of clay. This morphology is detected by designed experimental techniques. Generally, the particle surface is easily observed on the fractured surface or microtomed films. In Figure 4.1, the layers exfoliated from the MMTs show bright round shapes under SEM observation due to the electrons scanning on the surface of the samples. Due to the fiber-like morphology of the layers, these particles seem imperfectly round even though the film samples of nanocomposites are detected in any direction to the incident electrons.

The statistical results of the particle will be calculated and plotted according to the frequent–log (particle size) or accumulative–particle size model (Chapter 5). Taking advantage of atomic force microscopy (AFM) observation, the film surface of the PET–MMT nanocomposite samples was investigated (Figure 4.2). The AFM image shows

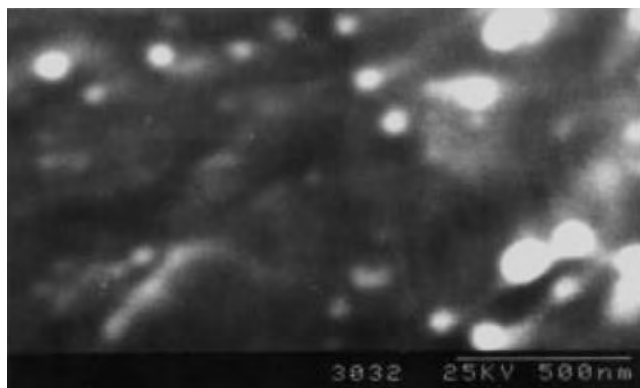


Fig. 4.1. Layer distributions on the fractured surface of nanocomposites of PET-layered silicates of MMTs.

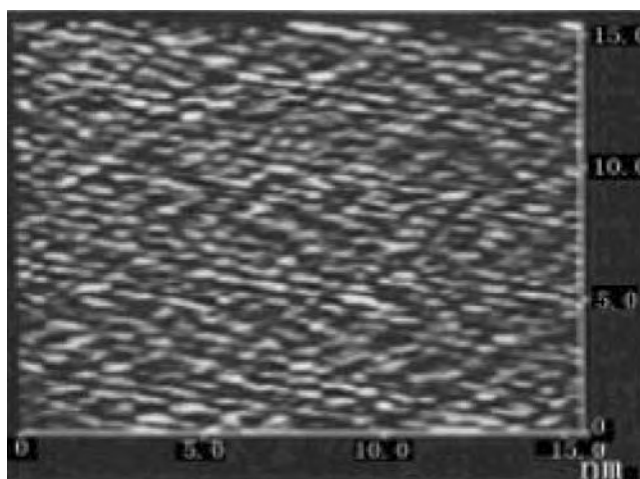


Fig. 4.2. AFM morphology of the film surface of the PET-MMT nanocomposites prepared in the same way as in Figure 4.1.

that there are mixed particles of different shapes in these samples. It is thought that AFM is most suitable for reflecting the true shapes of the exfoliated particles of MMTs.

Some particles have a finer structure than that observable by SEM, which is called the secondary or multiple-degree nanostructure. The layers of the MMTs are further detected by transmission electron microscopy (TEM) under high resolution as shown in Figure 4.3, where a hair- or fiber-like morphology is observed for the PEO-MMT nanocomposites. From these pictures, the interlayer distance, which is often used as a tool of intercalation reactions or treatments, is calculated.

It is noticed that the nanoparticles in nanocomposites are usually encapsulated by an organic cover film, which is sometimes called a “soft cover.” The morphology of such

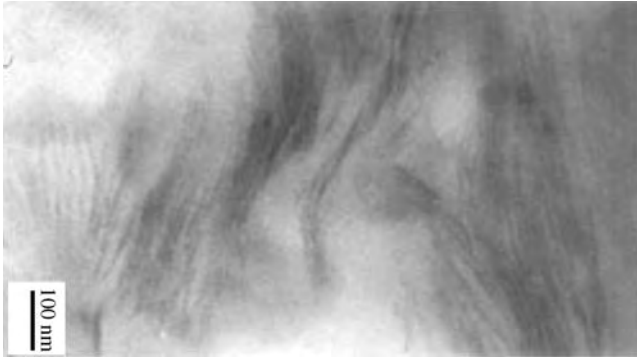


Fig. 4.3. TEM morphology of the epoxy-5% (by wt) $\text{CH}_3(\text{CH}_2)_{15}\text{N}(\text{NH}_3)^+_3$ -MMT nanocomposites samples.

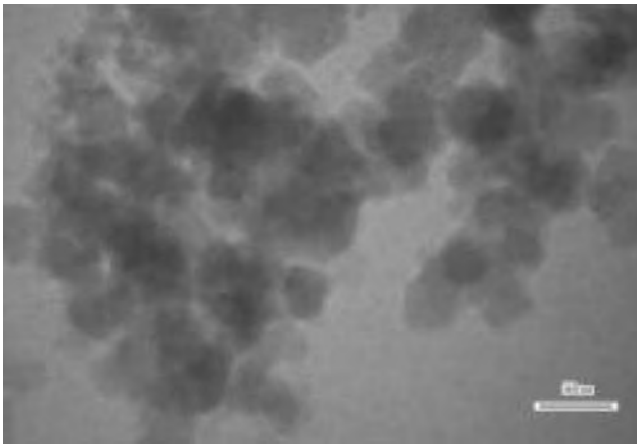


Fig. 4.4. Silica encapsulated by PMMA polymers.

core-shell-structured particles should be carefully observed because much information might be hidden inside the particles. Unfortunately, these core-shell-structured particles cannot be measured directly by the present characterization techniques. The thickness of the film that covers the inorganic particles is not directly measured but only detected by indirect observation methods; TEM is one of them. For example, silica particles covered by PMMA polymers contain particles connected to each other that form a homogeneous film on the surface. Figure 4.4 shows the morphology of silica encapsulated by PMMA polymers.

After further polymerization of PET with silica, it was discovered that silica particle dots were present inside the PET resins. These dots are in fact agglomerated particles. To avoid the possible agglomeration of particles, the particles are further wrapped by other oligomers such as BHET or PET in order to disperse silica homogeneously in the polymer PET melt. Silica particles treated by BHET have a surface morphology as shown in Figure 4.5.

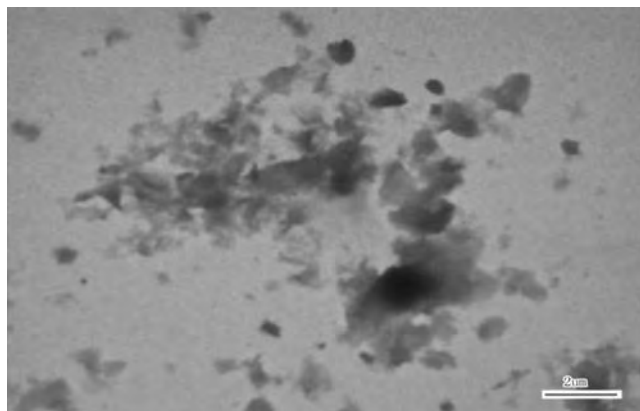


Fig. 4.5. TEM morphology of NPP particles with silica as a core.

In Figure 4.5, the silica particles are “melted” inside the oligomers of BHET or PET. Thus, there appear to be many large particles in which many nanometer silica particles dwell and pile up together.

4.1.1.2. Pore structure and distribution

(1) *The characteristics of mesoporous solids and composites.* Nanoparticles and nanoscale mesoporous solids are important components in nanocomposites. Since the 1990s, research on mesoporous solid and composite has become a notable frontier field [3,4]. The assembly of nanoparticles with mesoporous solids has produced particles with unique and novel properties, which neither nanoparticles nor mesoporous solids themselves have, such as mesoporous fluorescent reinforcing effect [5], non-linear optical reinforcing effect [6] and magnetic abnormal effect [7].

In this chapter, the characterization of the structure and the distribution of the pores are described. There are three kinds of pores. According to IUPAC definition of solid pores, the three kinds of pores are: micropores < 2 nm; mesopores 2–50 nm; and large pores > 50 nm.

However, pore type is not only defined by diameter, but also by shape or morphology. As an independent solid material, mesoporous solids should display a significant difference in properties from microporous solids and non-porous bulky materials. A solid containing few pores does not differ in properties from the bulky materials and therefore cannot be called a mesoporous solid. The mesoporous solid is not only characterized by pore size, but also by porosity. When the porosity becomes large, at a fixed pore diameter, the material can exhibit favorable catalytic properties.

In a nutshell, pore size and porosity are important parameters used to characterize mesoporous solids. The size distribution of the mesopore is a parameter used to characterize mesoporous solids and has the following definitions:

- (a) Porous solids with pore diameter larger than 2 nm and significant surface effect are defined as mesoporous solids.

- (b) Surface effect of porous solids is characterized by the surface atomic fraction (Σ) in the porous solids or the specific surface area S .
- (c) When $\Sigma > \Sigma_0$, porous solids are regarded as having significant surface effect, where Σ_0 is a critical value depending on the properties of solids to be investigated.

(2) *Characterization by specific surface area.* As for porous solids, when their diameters tend to be of a single value, their specific surface area, S , satisfies the following equation:

$$S = \frac{A}{\rho_0} \frac{p}{1-p} \frac{1}{D_p} \quad (4.1.1)$$

where ρ_0 is the backbone density of porous solids, p the porosity, D_p the pore diameter and A a constant or shape factor (for spherulitic shape, $A = 6$; for cylindrical pore shape, $A = 4$). Although the pore shape has many forms, the cylindrical shape is generally used as the approximate morphology, such as in porous solids of SiO_2 , Al_2O_3 and TiO_2 . In this book, $A = 4$ is used for nanoparticles. In statistical calculations, the mean values of different parameters are used. According to the statistical theory [8], the statistical formula for a porous solid is

$$S = \frac{A}{\rho_0} \frac{1}{1+q^2} \frac{p}{1-p} \frac{1}{\overline{D_p}} \quad (4.1.2)$$

where $\overline{D_p}$ is the mean value of pores and $q = \sigma\sqrt{\overline{D_p}}$ with σ being a standard deviation value. Eq. (4.1.2) is an integration of mean pore diameter, size deviation and porosity rate related to specific surface area.

(3) *Surface atomic numbers of Σ .* The Σ of mesoporous solid surface atomic numbers is used to characterize the mesoporous solid. The Σ is closely related to pore size and porosity, and Σ is defined by the following equation:

$$\Sigma \frac{N_s}{N_t} = S\rho_0\delta \quad (4.1.3)$$

where N_s and N_t are the overall atomic numbers of the solid surface and unit mass solid surface, respectively, S the overall specific surface area, and δ the aromatic interdistance in porous solids.

(4) *Characterization and applications.* Calculations based on the above formula show that pore size distribution has no obvious effect on the Σ value. When the value of $1/(1+q^2)$ in Eq. (4.1.2) is located in the range of $[\frac{1}{2}, 2]$ for practical applications, and the intermediate value of $3/4$ is used for the value of $1/(1+q^2)$; then,

$$\Sigma = \frac{3p}{1-p} \frac{1}{\overline{D_E}} \quad (4.1.4)$$

where $\overline{D}_E = \overline{D}_p/\delta$ (δ is the atomic separation); thus, when $\Sigma > \Sigma_0$, a porous solid is defined as a mesoporous solid according to the hypothesis in this section, and the corresponding pore diameter and porosity are determined by the following equation:

$$\overline{D}_E < \frac{3p}{1-p} \frac{1}{\Sigma_0} \quad (4.1.5)$$

Generally, the surface effect becomes significant at a value of $\Sigma_0 > 20\%$ (this is equivalent to a 100 nm size for the particles) (Figure 4.6).

In conclusion, a surface effect is proposed to define mesoporous solids, which are, as mentioned earlier, defined not only by their mean pore diameter, but also by porosity. It is suggested that the critical atomic number of Σ_0 is higher than 20%, while the minimum porosity is higher than 40% for mesoporous solids with a size of 2–50 nm.

4.1.2. Particle size deviation

4.1.2.1. Mechanism of new particle formation and particle growth

The condensation of silicic acid can be divided into two stages: particle nucleation and growth. Monodisperse particles result from particle growth. However, the mechanism of particle growth is still not fully understood and remains open to debate. It has been suggested that particle growth should be limited by diffusion or surface reaction [9,10]. In order to resolve this issue, the relationship between the growth rate of monodisperse particles and particle diameter was studied. In the case of diffusion-controlled growth, the equation of growth rate of each particle can be derived from Fick's law:

$$dL/dt = 4DV(C_\infty - C_s/L) \quad (4.1.6)$$

where L is the particle diameter, V the molar volume of growth fraction deposited onto the particle, D the diffusion coefficient of the diffusing material, C_∞ the bulk concentration and

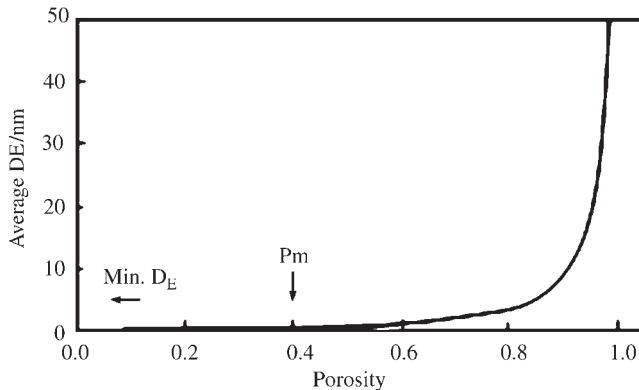


Fig. 4.6. Plot of maximum pore size vs. maximum porosity for mesoporous solid ($\Sigma_0 > 20\%$) (equiv. = equivalent; D is the diameter with arbitrary units).

C_s the saturation concentration on the particle surface. In the case of surface reaction-limited growth, the particle growth rate in volume is proportional to the external surface area of the particle. One can derive the growth rate equation as

$$dL/dt = 2 K_s V(C_m - C_s) \quad (4.1.7)$$

where K_s is the surface reaction rate constant and C_m the concentration of growth intermediate. From Eqs. (4.1.6) and (4.1.7), one can conclude that the growth rate is independent of particle size in the surface reaction-limited process and is inversely proportional to particle size in the diffusion-limited process. The growth rates of the particles in a suspension of silica particles with a bimodal size distribution were analyzed. It is found that when there was no formation of new particles, the diameter difference of the particles with two sizes is constant during the growth process. This means that particles with different sizes grow at the same rate, which demonstrates the properties of a surface reaction-limited process. When new particles are formed, however, the curves in Figure 4.7 are obtained, which show that smaller particles grow faster than the larger ones during the nucleation period, i.e., the growth proceeds by a diffusion-limited process. However, both small and large particles grow at the same rate before and after the formation of new particles. In the meantime, the growth mechanism changes to a surface reaction-limited process. This kind of transition of growth mechanism has not been reported before.

The key factor resulting in the formation of new particles is the insufficient surface area of seed particles, which increases the concentration of silicic acid-condensed

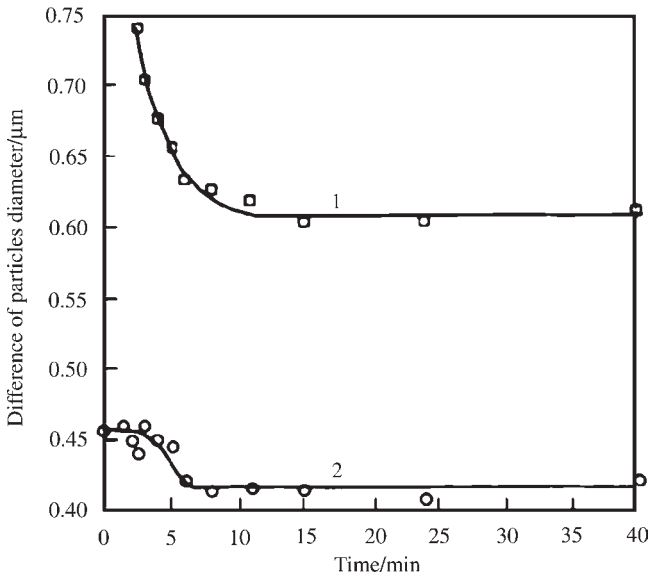


Fig. 4.7. Diameter differences vs. time during growth of particles: curve 1 – diameter difference between seeds and new particles; curve 2 – diameter difference between large and small particles.

species. The latter tends to condense to form large subparticles. Some of the subparticles partly aggregate to form new particles independent of the seed particles, while others are partly condensed onto the surface of seed particles by a diffusion-controlled process because of their low diffusion coefficient. In order to prepare particle systems with high monodispersity, the formation of new particles must be avoided during the growth process. We have determined experimentally the critical conditions for seeds with different sizes, i.e., the critical specific surface area, S_{pc} , at which new particles are found [6]. The straight line in Figure 4.8 indicates that S_{pc} is proportional to the size of the seed particles. This result agrees with the foregoing conclusion about diffusion-controlled growth during the formation of new particles.

In light of these studies, we have developed a seeding technique to grow monodisperse particles continuously in which either commercial silica sol or the silica sol prepared by us was selected as seed. Then, under the typical Stöber's conditions as stated in Chapter 2, the seed particles grow by feeding stock continuously until a monodisperse system is formed. This method can precisely control and predict the particle size and size distribution. The deviation of the particle sizes between practical and predictive values is usually less than 10%.

4.1.2.2. Applications of the particles with monodispersed size

Monodisperse latex (e.g., polystyrene) spheres have been regarded as the standard particles for calibrating particle analyzers for a long time. But the latex spheres have some shortcomings: their size undesirably changes in organic solvents; it is difficult to calibrate

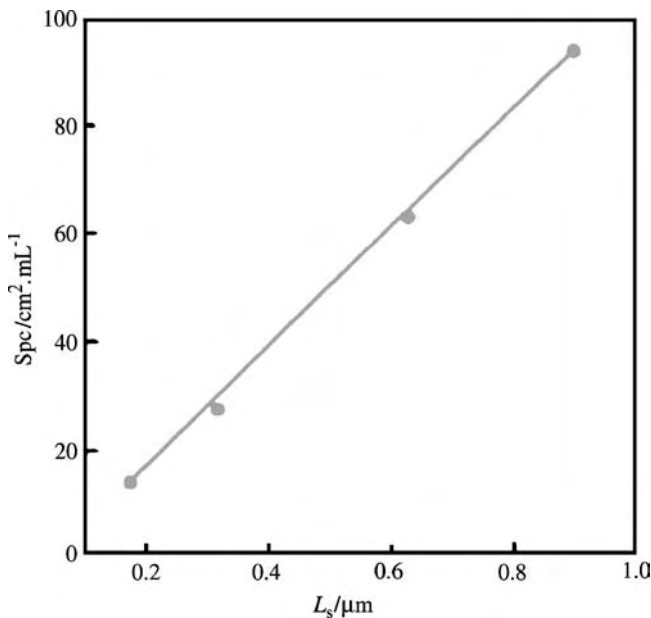


Fig. 4.8. Critical specific surface area S_{pc} vs. L_g (seed diameter).

the particle analyzers of sedimentation type with water because their specific gravity is close to unity; and submicron latex standard particles are rarely available.

In contrast, silica particles have no such disadvantages [11,12]. To test this, a series of suspensions of 1 and 2 μm monodisperse silica particles were prepared as model water samples. The suspensions with known particle concentration and size were used to study the possible harm of the suspending solid particles to model oil reservoirs. The results were satisfactory and provided a base for setting up the standard of water quality in water flooding for oil field recovery. In addition, the study proved that the influence of silica solubility in water on the size of particles could be eliminated at an extremely diluted condition of 10^{-4} wt% concentration.

As is known from the process of particle growth, although mainly monodisperse particles are obtained, there still exists some size deviation. The number-average diameter of monodisperse silica particles is generally obtained by a calibrated transmission electronmicroscopy (TEM), and is consistent with the most probable diameter measured by other equipments such as the Coulter counter (calibrated with polystyrene standard particles). The submicron monodisperse silica particles were used successfully as the standard model dust particles to calibrate the first 0.1 μm dust particle counter (made in China).

When using monodisperse silica particles as the standard particles, partial aggregation between the particles can cause serious errors for the particle analyzers, which cannot accurately measure the most probable diameter expressed in particle count (e.g., sedimentation type particle analyzers). Therefore, 1 μm particles, e.g., S10-1, are synthesized with hardly any aggregated particles for calibration usage. Some results are presented in Table 4.1. The table shows that different measurement techniques give similar results although they are based on different principles.

4.1.2.3. Particle size deviations

Using the preparation process discussed previously, the monodisperse silica particle deviation is about 5% (by size). In the dispersion polymerization of vinyl pyridine (VP) and methacrylic acid (MAA) with the MAA feed ratio = 40 wt%, relatively monodisperse particles are obtained. For these particles, $D_n = 1.67 \mu\text{m}$ (D_n is the number-average size of particles) and $C_v = 8.9\%$ (C_v is a coefficient of variation of the number-average size).

Table 4.1
Diameter of S10-1 measured by different techniques

Method	Diameter (nm)	
TEM	Number-average diameter	1,037
	Most probable diameter	1,033
	Mass median diameter	1,031
Disc centrifuge ^a	Volume-average diameter	1,080
	Geometric-average diameter	1,040
DLS ^b	Effective diameter	1,053

^aDisc centrifuge particle analyzer (BI-XDC). ^bDynamic laser scattering (DLS) particle analyzer (ZetaPlus).

Experimentally, the D_w/D_n ratio is often used to express the polydispersity of particle size. Although monodisperse particles from organic polymers are obtained by several methods, one of the main methods involves polymers with non-polar monomers or hydrophobic monomers such as styrene and methylmethacrylate. Other approaches are based on hydrophilic monomers such as *N*-vinyl formamide and moderately polar monomers by dispersion polymerization, which is especially suitable for the preparation of monodispersed polystyrene particles [13,14].

In the whole preparation process, the stabilizing polymer is the key component. For example, the copolymer of polystyrene–block–polybutadiene (P(St-*b*-Bd)) has a monomer mole ratio of styrene/butadiene as 60:40 (1,2-vinyl unit in PBd segment is 10 mol%; $M_n = 2.8 \times 10^4$ g/mole; $M_w = 1.3 \times 10^5$ g/mole). The copolymer chains contain unsaturated vinyl groups in the side chain. During disperse polymerization, grafting occurs at the reactive sites of the copolymer molecules and the resulting graft copolymer acts as a true stabilizer. In these preparations, as the DMF increases in the mixing solvent, the particle will be gradually enlarged but still preserves its monodisperse morphology. The preparation example is as follows.

Example 4.1.1.1. A mixture of 20 g of monomer, 3 g of polystyrene–block–polybutadiene, 0.4 g of 2,2'-azoisobutyronitrile (AIBN), and 80 g of a solvent was taken in 500 ml three-necked flask, which was deoxygenated with nitrogen. The reaction apparatus was placed on the shelf and shaken at 160 times per minute in a water bath at 70°C for 8 h. After polymerization, the reaction mixture was poured into a large amount of toluene, followed by centrifugation of the dispersion. The particles were resuspended twice in toluene and subjected to successive centrifugation. Through such a process, the organic monomer particles were obtained.

4.1.3. Phase separation

4.1.3.1. Assembled structure from spinodal phase decomposition

Polymer resin systems behaving as complex fluids are defined as soft matter by physicists such as Chaikin and Lubensky [15] and de Gennes [16]. Following the hypothesis developed by de Gennes, several new physical terms such as patterns and pattern assembly are used to describe complex systems of polymer, polymer-based nanocomposites or blends. The block macromolecular copolymers are those with complex morphology during annealing conditions. A polymer matrix is a viscoelastic system and has a very wide time-viscoelasticity relax spectrum, ranging from an order to several decades order. These melt resins reflect an intense non-linear behavior leading to unique patterns characterized by sensitive selection under trivial melt strains by exerted force.

Pattern formation or assembly or pattern selection for polymer complex fluids are closely related to the backbone or chain structure of the polymer. The designs of block chain structure of polymers and their crystallization or crystallized treating condition have provided the most basic foundation for forming phase separation structure, proper morphology and morphology control. Additionally, the formation of patterns in polymer resins as complex fluids has also been governed by the principle of spinodal

phase decomposition, which has developed into an important branch of polymer science.

The basic principles based on spinodal phase decomposition structure have been applied to describe the creation of structure and regular structure growth in polymer-inorganic nanocomposites. Creation of structure will provide stable, low cost and practical ordered structure in nanocomposites. We will discuss the work done by us and others in the following section.

4.1.3.2. The phase separation structure in polymer blends

Polymer resin blending system is one of the main matrix or carrier creating phase separation structures. Polymer block segment structure or proper selection of the segments is a main goal in practical designs. The factors affecting phase separation are controlling factors for growth and formation. For example, in the multicomposition of polymer systems, the volume fraction of each component, the blending conditions, the quench temperature and the rate are the important factors in the preparation of desired structures.

The spinodal phase decomposition is described by the Flory–Huggins theory. Usually, molecular simulation (MSI) based on statistical hypotheses are used to describe the spinodal structure formation process and the related driving force. In describing the free energy (F) by mixing different phases, the equation according to the Flory–Huggins model has the following form:

$$F = \varphi_A \ln \varphi_A / N_A + (1 - \varphi_A) \ln(1 - \varphi_A) / N_B + \chi \varphi_A (1 - \varphi_A) \quad (4.1.8)$$

where N_A and N_B are the chain lengths of polymers A and B, respectively, φ_A the volume fraction of polymer A, and χ is the interacting parameter between chains A and B of polymers. At the phase equilibrium point, $dF/d\varphi_A = 0$ and $dF/d\chi = 0$. Then for a monodisperse system the critical phase point is

$$\varphi_A = (\sqrt{N_A/N_B} + 1)^{-1}, \quad \chi_c = \frac{1}{2} \left[\frac{1}{\sqrt{N_A}} + \frac{1}{\sqrt{N_B}} \right]^2 \quad (4.1.9)$$

Based on these equations, a typical symmetrical phase diagram of polymer blending systems is shown in Figure 4.9.

In Figure 4.9, the solid line represents phase equilibrium and the dashed line represents spinodal phase separation. The arrows show the corresponding critical quench direction in a cool state. In Eq. (4.1.9), when $\varphi_A \neq \chi_c$, the blending system is called a non-critical mixture; otherwise, it is called a critical mixture as shown in the figure. For a symmetrical system, the following exists:

$$\varphi_A = \frac{1}{2}, \chi_c = \frac{2}{N} \quad (4.1.10)$$

The equations and the figure are referred to understand the blending system, in which a true regular structure is created. In practical applications, the equations are much more complicated and may require modifications in special cases. For additional information,

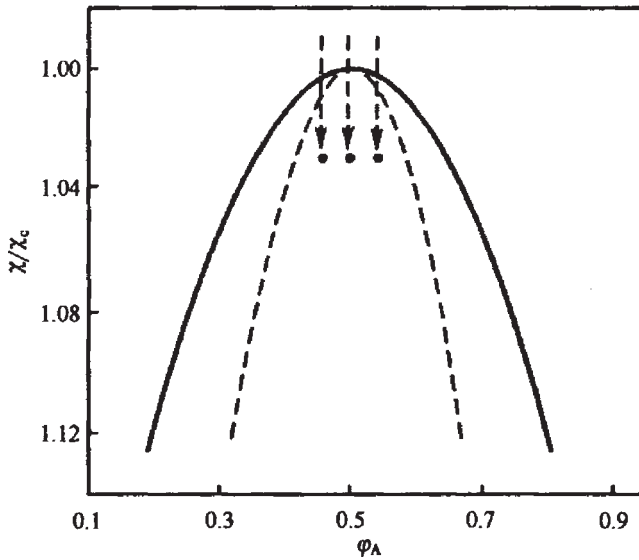


Fig. 4.9. Typical diagram of symmetrical polymer blending systems.

readers may refer to the hypothesis of Flory, the theoretical aspects developed by de Gennes or the Flory–Huggins model [15,16].

4.1.3.3. Examples of regular structure from spinodal phase decomposition

(1) *The morphology of double unit of block copolymers.* For A–B type block copolymers of different monomers, there are several examples of phase separation structure [17,18]. The phase structures can be divided into four types: spherulitic morphology, cylindrical morphology, layer structure and mixed structure. These classifications are based on the blending of block copolymers of polystyrene (S)–butylenes (B)–Methyl methyl acrylic (M) (SBM), each of which shows a different morphology. The overall phase separation process for these double block-copolymers has been described by Matsen and Forster [19] and Matsen and Bates [20]. It was found that interphase curvature has an effect on the free energy within the aggregated region of the intermediate phase.

(2) *The morphology of composites composed of three kinds of tri-block copolymers.* Tri-block copolymers are capable of being mixed together using usual blending technology. Mogi et al. [21] have investigated tri-block-poly(isobutylene-styrene-2-vinylpyridine) (ISVP), in which the addition of end block segments of chains I, S and VP will assemble into different spherical, cylindrical and co-continuous phase networks. When all the components have similar volume fraction, the layer phase structure is obtained. When the block copolymer chain sequence is transformed into ISVP and all the components have similar volume fraction, a cylindrical core–shell structure is created. In such system the interaction between segments of VP and I will be much greater than that between the segments of I and S; thus, VP will become a core pillar.

More examples of ordered phase separation structure in tri-block copolymers have been reported. The tri-block copolymers include the chain sequence PS-block-PB-PMMA (or polystyrene-block-polybutadiene-poly (methyl methyl acrylate)) and hereinafter, S-polystyrene, B-polybutadiene, M-poly(methyl methyl acrylate) and T-poly(tert-butyl methacrylate). There are other tri-block copolymers such as SBM or SBT, which are similar to the PS-block-PB-PMMA sequence. For details of SBM tri-block copolymers, one can refer to Stadler's [22,23] work, in which a series of ordered structures from SBM are shown.

(3) *Blending of tri-block copolymers with other block copolymers.* Recent reports have discussed the blending of tri-block polymers with other block polymers [22]. The prepared composites are dissolved in chloroform (CHCl_3) and then used to form films. The tri-block copolymers are SMT or SBT. The preparation of blending the composites follows several steps. First, each composition of the blends is dissolved in chloroform and stored for several weeks; then, for further equilibration, the dried films are dried at 180°C for 6 h; finally, the films are microtomed into superfine thin films, which are then dyed by OsO_4 vapors. Under TEM observation, the morphology of the B region is black, the S region is dyed into gray and the M or T region is almost white for SBM or SBT copolymers. The S region and the interphase of other components appear black in color [24,25].

Experiments show that blending of layered SBM/layered BM and layered SBT/layered BT gives a core-shell double-screw or core-shell cylindrical morphology, depending on the compositions of the blends. Computer simulations have also predicted the core-shell double-screw morphology. According to the works of Stadler et al., perfect layer morphology is obtained for blends of S(33%)–B(34%)– M_n (33%) ($M_w = 1.53 \times 10^5$ Da) and S (49%)–B (51%) ($M_w = 0.87 \times 10^5$ Da), where S is the styrene segment, B is the butyl diene and M is the methylmethacrylate.

(4) *Self-assembling system in polymer solution.* The block copolymers form phase-separated structures and assemble into ordered structures or superlattices after being subjected to post-treating conditions such as temperature and isothermal crystallization. For example, hydrogen bonds form self-assembling aggregates at different hydration degrees and sequence distributions for vinyl acetyl ester (VAE)–vinyl alcohol (VA) copolymers. Several results reveal that block polymerization benefits the self-aggregates of hydrogen bonds. In random copolymers, the hydrogen bond of OH...OH will have an interaction with that of OH...CO. The hydrogen bond of OH...OC produced in adjacent repeated units will lead to a circular structure of high thermal stability. In the investigation of styrene-vinyl alcohol copolymerized with poly(*N*-methyl-*N*-ethyl amine) to form intermolecular aggregates, the solvent properties and the addition of components to the copolymers have definite effects on the self-assembling structure.

*Example 4.1.3.1. The self-assembly of molecular aggregates in copolymers of polystyrene-vinyl alcohol interacting with poly(*N*-methyl-*N*-ethyl amine).* First, methyl ethyl ketone is selected as a solvent, in which the polystyrene-vinyl alcohol copolymers are dissolved; then poly (*N*-methyl-*N*-ethyl amine) is also dissolved. The two components are designed to be in different fractions, which will form aggregates inside all the copolymer compositions. Then, by vaporizing this solution, a self-assembling composite material is prepared.

In another method, tetra hydrogen furan (THF) is used to dissolve the system. Only when the weight fraction of styrene-vinyl alcohol in copolymers is higher than the others will the two components form aggregates and a self-assembling structure. Dynamic light-scattering experiments show that the hydrogen bonds and hydrophobic interactions are the driving forces.

Once PEO and PMMA solutions are mixed together, a precipitate will form and produce white polymer aggregates of interpolymer complexes. The ether group of the oxygen atoms forming hydrogen bonds with the carboxylic groups causes the formation of the complexes. The number of hydrogen bonds and the stability of the aggregates strongly depend on the chain length, temperature and the solvent. In theoretical calculations, the enthalpy changes as aggregates structure and hydrophobic interaction are both important factors influencing the stability of the aggregates. The increase in macromolecular aggregates affects the formation of polymer blending networks. The molecular aggregates will disappear after the disappearance of mechanical stress and addition of solvent for solvating action.

Hydrogen bonding, coulombic forces and hydrophobic interactions in aqueous solution or solvents all form the polymer aggregates. The interactions are sensitive to temperature, concentration, solvent and polymer chain length. The interactions for polymers dissolved in solvents seem much more intense in comparison with the polymer blends obtained by melting technology.

4.1.3.4. Polymerization and phase separation

The preparation of high-performance polymer-MMT nanocomposites is to create exfoliated morphology and to create phase separation structure by post-treatment. One technique is the polymerization of the corresponding monomers in the presence of organically modified clay particles (guest–host inclusion chemistry). The polymerization of olefins takes place in two steps. First, the clay of MMT particles treated by a plasma polymerization technique is dispersed under vacuum in hydrocarbon solvents. Second, diene monomers are polymerized ionically under vacuum in hydrocarbon solvents with butyl lithium as the initiator. Standard vacuum procedures are used to purify the monomers, initiators and terminator. In the preparation of PS-MMT nanocomposites, anionic synthesis technology is used to polymerize the styrene monomer in the presence of the MMT particles (treated under a plasma environment with styrene monomers under vacuum). The polyisoprene-MMTs, polybutadiene-MMTs and the polystyrene-block-butadiene nanocomposites are also ionically synthesized under vacuum from isoprene and 1,3-butadiene monomers, and with styrene together with butadiene, respectively, again in the presence of the MMT particles treated under a plasma environment.

Another technique is to intercalate chemically different polymer chains in the presence of organically modified MMT particles by melt or solution blending, and then generate the phase-separated domains between layered MMT particles via spinodal decomposition. This approach can yield exfoliated polymer-MMT nanocomposites. Spinodal decomposition occurs when the polymer-MMT nanocomposites are quenched into the two-phase region of the phase diagram of the polymer blend. Polymers (PB-PS and PB-PI)-MMT nanocomposites or blends are designed to show phase-separated structure at room temperature via control of the molecular weight of polymers in polymerization process. Nearly

monodisperse polymers can be synthesized by sequential anionic polymerization of diene monomers. These blends have been studied extensively; information about thermodynamic properties and phase separation is available.

4.1.4. Particle order

Previously, organically modified clay particles were synthesized on a tumbling RF-plasma reactor with comonomer feed control. At present, nanocomposite systems of polymers PS, PB, PI and polyester organo-clay for model investigations are synthesized on a high-vacuum line. With careful design of the segment length and addition order of the monomers in the mixture systems, the copolymers with controllable chain structure or crystallized regions can be synthesized, acting as templates for the preparation of patterns of particle arrays under annealing conditions.

In the future, these difficult copolymers may be replaced by poly(butylene terephthalate) (PBT) in serving as a template. The particle distribution and arrangement order behavior in the poly(butylene terephthalate) (PBT)-layered silicates of clay nanocomposites are shown as in Figure 4.10.

In the distribution process, there also appears particle exfoliation, which has caused complicated situations or morphologies. During annealing, the particles in the PBT matrix are arranged together, and can be formed into ordered structures. In order to avoid the influence of shear force in the preparation of a sample, several trial and error experiments should be performed.

4.1.5. Intercalation dynamics and agglomerations

The intercalation reagent or intercalant entering into the layered silicate gallery occur by mass transfer, in which reagent molecules penetrate at different rates and different mechanisms. Recently, it was found from molecular simulations that the molecular

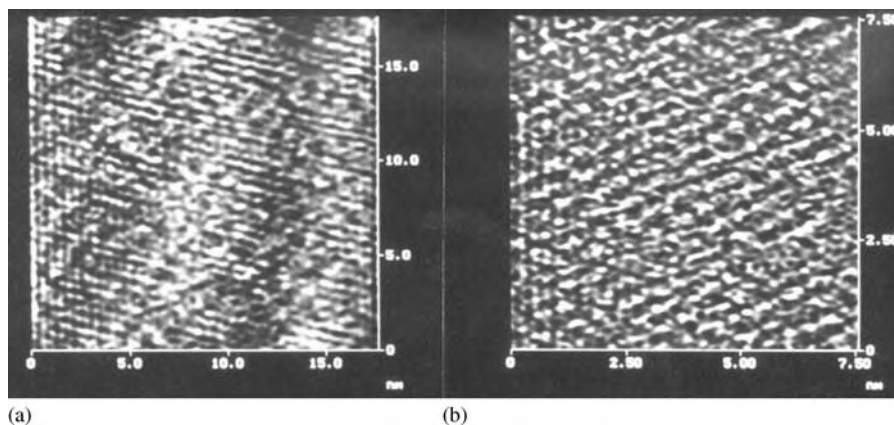


Fig. 4.10. Morphology of exfoliated particles, their distribution and order arrangement: (a) amorphous PBT-clay nanocomposites annealed for several min to several h at 130–200°C after the melt; (b) amorphous sample of PBT.

chains intercalated into the layer gallery have a strong tendency to approach the layer surface with Si–O bonds or hydroxyl groups. This will be shown by model intercalation of polyester oligomer into the layer space of MMTs in Chapter 5. This penetrating tendency is increased by an outer shearing force. The intercalation dynamics process is not yet completely understood, but the obvious effect is that the molecular chains adsorbed on the surface of layers are stiffer than chains in other locations. This leads to a higher T_g of nanocomposites than that of the pure polymers. The details on the molecular simulations from our group have been described elsewhere in the book.

Vaia et al. [26] have described the intercalation process of polymer chains into a primary particle as a diffusion process. Polymer diffusion into the primary particle is modeled as mass transport through a lateral surface by using a cylindrical model. So far, these diffusion processes have been described by Fick's law.

The fraction of silicate MMTs intercalated by reagents, or χ , is expressed by the X-ray diffraction intensities of $I_p(t)/I_i(t)$ (where $I_p(t)$ is the intensity of the nanocomposite and $I_i(t)$ is the intensity of pristine silicate and intercalated silicate). For example, the relationship is given as $\chi \sim D/\bar{a}^2$ (where D is the effective diffusion rate and \bar{a} is the mean radius of the flat impermeable surface of the primary particle). This equation is in good agreement with the Vogel equation or $\log(D^*/T) = A' - B/(T - T_\infty)$ [27] where A' and B are constants, T is the temperature and T_∞ the temperature at equilibrium.

In polymer–inorganic nanocomposites, particle dispersion and exfoliation need to be homogeneous. However, the fact is that particle agglomerations exist in nearly all of the nanocomposite materials. This situation is even worse in the PET-based nanocomposites. That is why PET–MMT nanocomposites with satisfactory properties are difficult to prepare. Figure 4.11 shows that improper treatment of the layered silicate of MMT will lead to a significant phase separation resulting from particle layer stacking or accumulations.

By using atomic force microscopy (AFM), one can also detect the agglomerations from the accumulations of the exfoliated layers in samples of PET–MMT. The exfoliated nanoscale layers will form micrometer-size agglomerations of particles as seen in Figure 4.12.

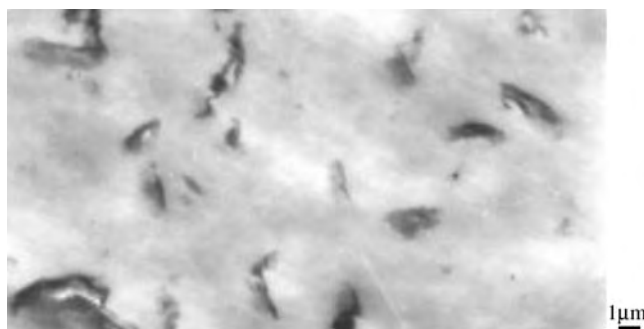


Fig. 4.11. TEM morphology of agglomerated layered silicate particles in poly(ethylene terephthalate) under improper treatment conditions with unique surfactant.

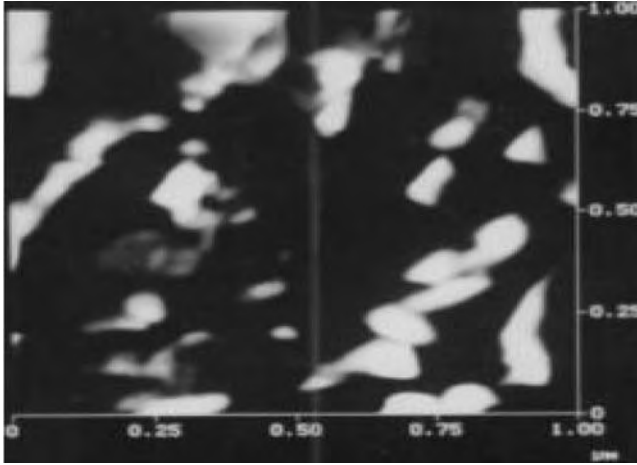


Fig. 4.12. AFM morphology of nanocomposites of PET-layered silicate of MMTs.

4.1.6. Particle morphology–property relationship

It is difficult to clarify the accurate relationship between the particle dispersion morphology and the property in the prepared nanocomposites. The particles will take many possible distributions in the polymer melt, which includes spherical-, fiber-, wire- and triangle-like morphologies. Especially, in polymer-MMT nanocomposites, the MMTs take either an intercalated or an exfoliated morphology, or both. The intercalated state is characterized by sharp or residual peaks of d_{001} in X-ray diffraction patterns, while in the exfoliation state of nanocomposites, peaks of d_{001} disappear. This morphology will have definite effects on the final properties of the prepared nanocomposites.

The complete exfoliated morphology of polymer-MMT nanocomposites contributes greatly to their transparency, impact property, modulus and heat distortion temperature (HDT), while the intercalated state of partially exfoliated state contributes more to the final material's modulus and HDT. In Figure 4.13, the dispersion state of MMTs decides the final properties of izod impact properties. It is often observed that PP-based nanocomposites exhibit both the exfoliated and the intercalated state. These morphologies can be observed in Figure 4.14 for polypropylene–MMT nanocomposites from filling polymerization on the composite carrier containing MMTs and silica.

4.2. Crystallization

4.2.1. Crystallization from nanoparticles

When nanoparticles are introduced into organic polymer matrixes, their crystallization behavior changes to a great extent. Nanoparticles of silica and layered silica particles are often used to mix with the particles to improve their crystallization properties. This

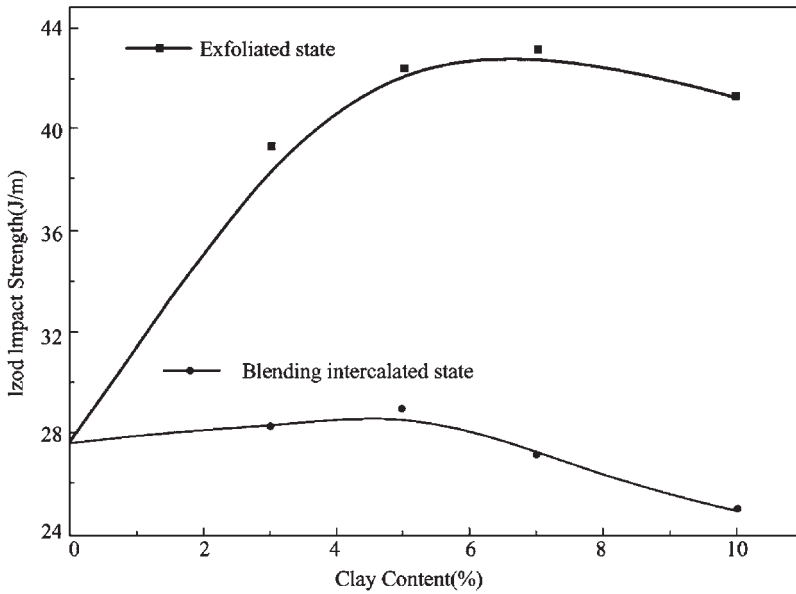


Fig. 4.13. Relationship between the izod impact property–clay load in polypropylene-based nanocomposites.

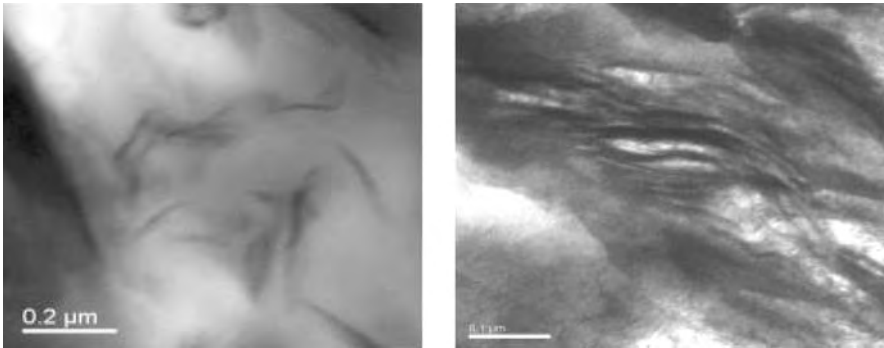


Fig. 4.14. Polypropylene-MMT nanocomposites from filling polymerization on the composite carrier of MMTs and silica (polymerization temperature 50°C, pressure 5 atm, time 1 h).

enhanced crystallization behavior is thought to be a result of the nucleation effect of nanoparticles, which will be described in Chapter 5.

Attention is paid to whether the nanoparticles themselves will crystallize in the composite matrix. In fact, we have shown that the silica particles cannot crystallize inside the nanocomposites via an electron diffraction (ED) technique. But, whether the layers of clay crystallize in the nanocomposites is not clear so far.

Besides the nucleation effects from nanoparticles, the particles can promote the formation of polymorphism, multiple crystallization and crystallization acceleration.

As for thermosetting plastics, their crystallization with nanoparticles is not obvious because of cross-linked molecular chains, while in the case of the thermoplastic resins they have an obvious glass transition temperature that will act as a criterion when to introduce nanoparticles.

4.2.2. Isothermal or nonisothermal crystallization

4.2.2.1. Isothermal crystallization of PET–clay nanocomposites

The crystallization for both the isothermal and the non-isothermal process is investigated by DSC. The experiments are designed to induce crystallization at different temperatures and scanning rates. The crystallization process is described by the Avrami equation [28–31] as follows:

$$\ln[-\ln(1-X(t))] = \ln k + n \ln t \quad (4.2.1)$$

where $X(t)$ is the crystallization degree at time t , k the crystallization dynamical parameter and n the Avrami number that reflects the growth pattern of the crystallites. The reciprocal value of time t at $X(t) = 50\%$ is applied to express the crystallization rate, and Eq. (4.2.1) is transformed into

$$t_{1/2} = \left(\frac{\ln 2}{k}\right)^{1/n} \quad \text{or} \quad \frac{1}{t^{1/2}} = \left(\frac{k}{\ln 2}\right)^{1/n}. \quad (4.2.2)$$

4.2.2.2. Non-isothermal crystallization behavior

(1) *Non-isothermal crystallization of NPET.* The crystallization process is also described by the Avrami equation and the related time $t_{1/2}$ at 50% crystallinity degree is shown in Table 4.2.

Below MMT loads of 5% (by wt), the crystallization temperature of NPET increases with the load of MMTs. This shows an easy crystallization behavior, for example, the crystallization rate is enhanced over three times. The crystallization of NPET at isothermal crystallization condition will cause variations in the spherical crystallite morphology of PET.

(2) *Non-isothermal crystallization of NPBT.* Using the Avrami equation to calculate the non-isothermal crystallization data in DSC scanning patterns, plots of $\ln[-\ln(1-X(t))]$ vs. $\ln t$ are obtained as shown in Figure 4.15(a) and (b).

Table 4.2
Effect of clay load on crystallization for NPET under non-isothermal crystallization

Sample no.	Clay load (wt%)	T_c (°C)	$t_{1/2}$ (min)
1	0.0	174.0	1.80
2	1.5	196.0	0.72
3	2.5	197.2	0.80
4	5.0	201.0	0.60

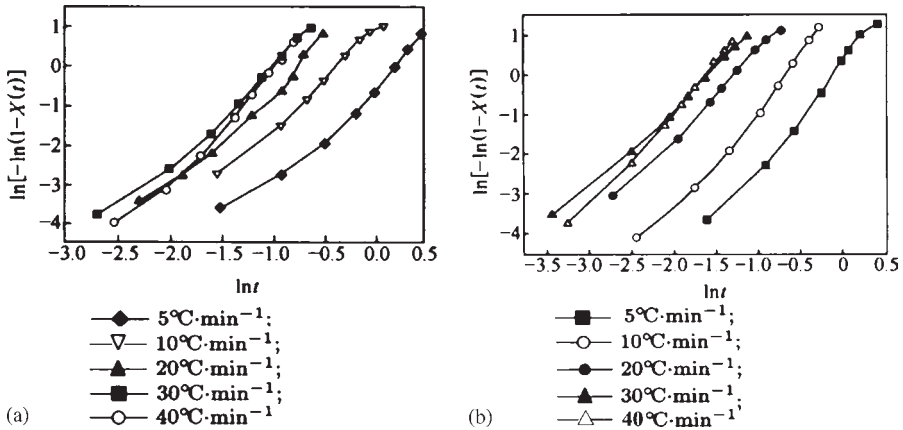


Fig. 4.15. Non-isothermal crystallization behavior for PBT (a) and NPBT (b) with a clay load of 5% (by wt) (refer Chapter 2 for preparation of PBT and NPBT).

Table 4.3

Dynamical parameters for PBT and NPBT under non-isothermal crystallization Scanning rate ($^{\circ}\text{C min}^{-1}$)

Sample		5	10	20	30	40
NPBT0	$t_{1/2}$	1.063	0.592	0.407	0.317	0.334
	N	2.24	2.38	2.34	2.36	2.69
NPBT5	$t_{1/2}$	0.832	0.478	0.262	0.191	0.187
	N	2.39	2.31	2.05	1.86	2.20

Note: NPBT0 stands for pure PBT; NPBT5 stands for PBT loaded with 5% (by wt) of clay, where clay is treated by laurylamine by using the preparation method described in Chapter 3.

Figure 4.15 shows that under non-isothermal crystallization, NPBT and PBT have slightly different crystallization processes at higher scanning rates from 20 to $40^{\circ}\text{C min}^{-1}$. For NPBT, crystallization curves from 30 to $40^{\circ}\text{C min}^{-1}$ intersect, while for PBT, curves from 20 to $40^{\circ}\text{C min}^{-1}$ intersect, both at a low scanning rate. Therefore, NPBT and PBT have similar crystallization behavior. This suggests that the clay load has a critical point.

Based on the intercept and slope from curves in Figure 4.15, the parameters k and n are calculated and listed in Table 4.3 according to Chapter 3. The plot of crystallization rate ($1/t_{1/2}$) vs. scanning rate under non-isothermal crystallization is shown in Figure 4.16.

It is seen in Figure 4.16 that the crystallization rate ($1/t_{1/2}$) for NPBT increases rapidly with the DSC scanning rate and also the slope increases with the increase in scanning rate. This observation suggests a much higher crystallization behavior of NPBT than that of PBT. The average increase in NPBT crystallization rate is about 50% higher

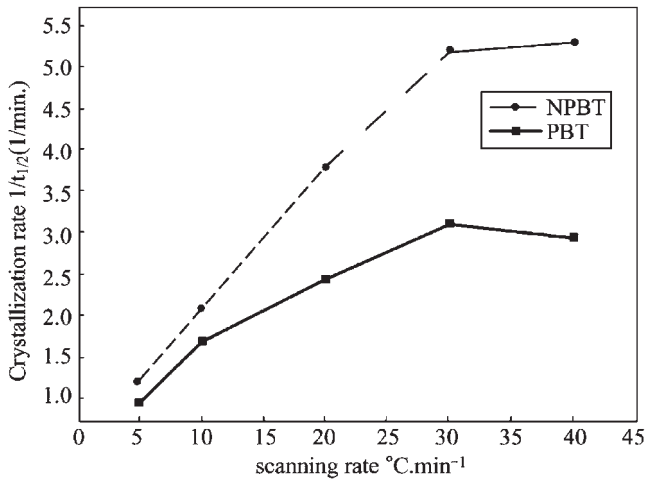


Fig. 4.16. Plot of the crystallization rate vs. scanning rate under non-isothermal crystallization for both PBT and NPBT with a clay load of 5% (by wt) (preparation conditions are similar to that in Figure 4.15).

for all non-isothermal crystallization cases, compared with PBT within 5% loading of clay. Introducing nanoparticles into the matrix to act as new nucleation centers has a direct effect on the crystallization rate. The comparison of all values of N in both PBT and NPBT listed in Table 4.3, shows that the crystallites grow in a similar manner, further implying that these nanoparticles are of similar size.

4.2.3. Phase transformation and polymorphism in crystallization

4.2.3.1. Phase transformation

In nylon6, there are two crystalline forms, α and γ . The α phase consists of fully extended planar zigzag chains, in which adjacent antiparallel chains are joined by hydrogen bonds. It is the most thermodynamically stable crystalline form obtained from the melt. The γ form is composed of pleated sheets of parallel chains joined by hydrogen bonds and is less stable than that obtained by fiber spinning at a high speed or by fast cooling from the melt.

The transition between α and γ occurs by melting and annealing the crystalline forms in a saturated-steam atmosphere without any significant loss of orientation and by applying stress at room temperature. The polymorphism transition in nylon6,6 has been widely studied [32,33]. The room-temperature triclinic structure transforms into a high-temperature pseudo-hexagonal structure at elevated temperatures. The Brill transition in WAXD shows that the two peaks at 21° and 24° merge into a single reflection peak at 21.5°. While in nylon6, the two peaks at 20.5° ((100) crystal face) and 24° ((010) + (110) crystal face), characteristic of monoclinic γ , will shift to a peak at 21.5° representative of the γ phase.

In the nanocomposites of nylon6/synthetic saponite, the used synthetic sodium saponite is endowed with a cation exchange capacity (CEC) of 71.2 mmol (100 g)⁻¹

sample. Several techniques of DSC and WAXD show the presence of polymorphism in them, which is dependent on the cooling rate from the melt and clay load. The quench of such a sample from the melt induces the formation of the γ crystal form. The high load of saponite will further induce the heterogeneous nucleation of the γ form, while inducing the α form at a low load [33].

Similarly, when layered silicates of MMT are used as the inorganic phase, the induced γ form from the exfoliated MMT layers also appears. This will be discussed later in this chapter. As for the clay, it may be prepared from natural bentonite, which is produced by Minerals Colloid BP, Southern Clay products, and Gonzales. Generally, this clay has C E C of 90 mmol (100 g)⁻¹ sample after undergoing modifications in several steps.

4.2.3.2. Polymorphism

The pure polymer of polyamide (PA)6 has many crystallization forms such as α , β and γ forms. The α form is regarded as the most stable one, while the γ form is the unstable one. The α phase consists of fully extended planar zigzag chains, in which adjacent antiparallel chains are joined by hydrogen bonds. It is thermodynamically the most stable crystalline form obtained from the melt. The α and γ forms have properties as shown in Table 4.4.

It is known that polymorphism in nylon6/clay nanocomposites is dependent on the cooling rate from the melt and clay loading. The quench from the melt induces the formation of the γ form.

4.2.3.3. Polymorphism in crystallization

In polymer-MMT nanocomposites, the introduction of exfoliated layers creates new functions but results in an unstable system. For example, in PA6–MMT nanocomposites crystallized from the melt, a γ crystal form induced from the dispersed layers appears. The same phenomenon occurs in the melting process of polymer-based nanocomposites. The unstable crystal form is believed to affect the properties of the final products, although in fact, in the PA6–MMTs, the binding force of matrix with layers of MMTs is so tight that its HDT is 100°C more than that of the pure matrix. So far, another polymer matrix whose binding force is as high as that of nylon6 has not been found (Figure 4.17).

In our investigations, we observed the existence of other polymers of polybutylene terephthalate (PBT) whose MMT nanocomposites give different patterns compared with the pure counterpart. In pure PBT polymer crystals, two types of spheres exist [34,35], one is a normal crystal, while the other is an abnormal crystal. Some condensed morphology was investigated by WAXD for both PBT and NPBT samples annealing at a temperature of 60–140°C. The WAXD patterns of these samples are shown in Figure 4.18.

Table 4.4
Comparison of crystal forms of α and γ in PA6 and PA6-clay nanocomposites

Polymorphism	Melting point (°C)	X-ray diffraction 2θ (deg)	Stability	DSC melting peak
α form	240	20,24	Good	Single
γ form	210–214	21,22	Bad	Double

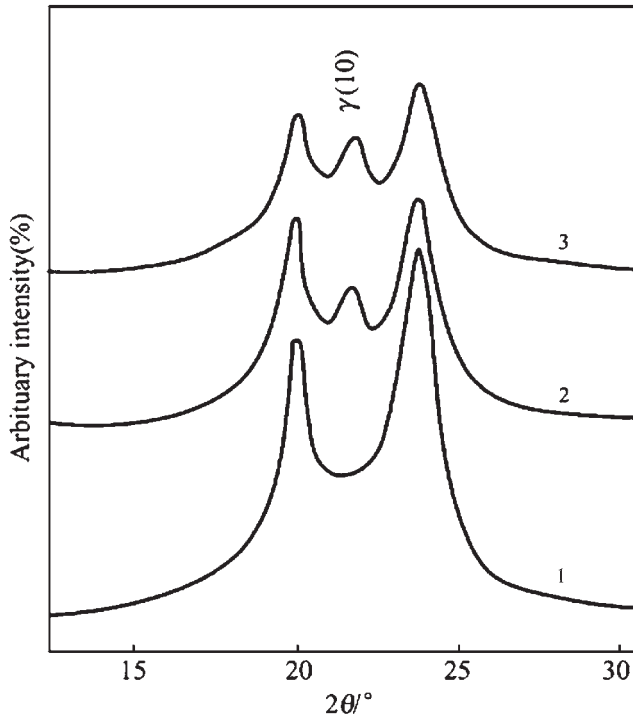


Fig. 4.17. WAXD patterns of γ polymorphism induced by MMT layers in nylon6-MMT nanocomposites: 1, PA6; 2, PA6-5% organo-clay; 3, PA6-5% organo-clay.

For samples crystallized from the glassy state, the diffraction behavior at 2θ (20° , 25°) and 2θ (25° , 35°) differ from each other. This has been observed by tracing the scanning at different temperatures. The complex morphology of PBT and NPBT leaves this problem open to further investigations. However, it has been demonstrated that the introduction of MMT layers into PBT enhances the properties of the PBT without being affected by possible unstable crystallites.

4.2.4. Crystallization degree and rate

4.2.4.1. Crystallization degree

Crystallization degree is an important parameter that describes the crystallization behavior of thermoplastic resin polymers and their nanocomposites with inorganic nanoparticles. It is expressed as $\Delta H/\Delta H_f^0$ based on DSC heating scanning, where ΔH is the heat of fusion changing as scanning rate and crystallization time and ΔH_f^0 is a heat of fusion at the equilibrium state (e.g., ΔH_f^0 is a fixed value for PBT [35]). A plot of heat of fusion vs. DSC scanning (non-isothermal crystallization) is shown in Figure 4.19.

In Figure 4.19 there is a great difference in the crystallization degree (heat of fusion) between PBT and NPBT. The ΔH for NPBT increases much more rapidly with the

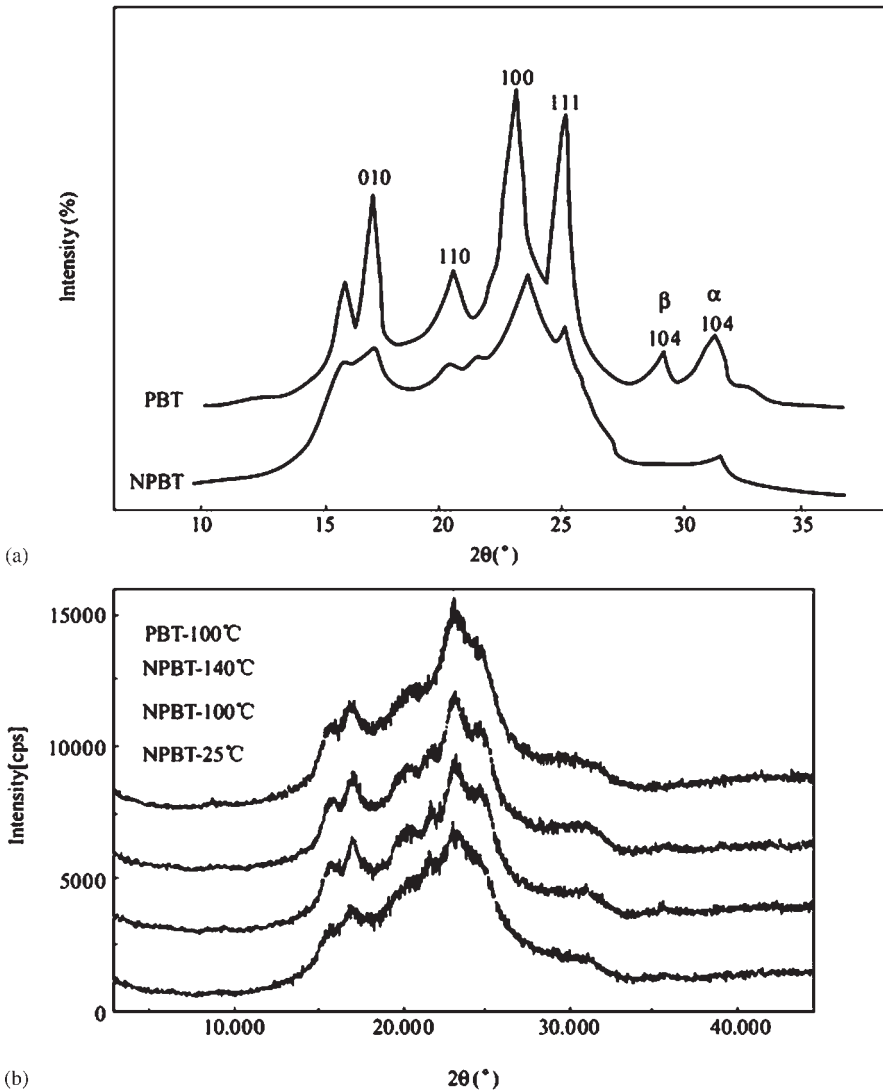


Fig. 4.18. WAXD patterns; (a) NPBT and PBT, (b) NPBT annealing at different temperature for 30 min.

scanning rate than that of PBT. The ΔH of PBT stays nearly unchanged under non-isothermal crystallization scanning, suggesting that PBT is slow to respond to the scanning rate.

4.2.4.2. Crystallization rate

The samples discussed in this section are NPET with different molecular weights and have physical and mechanical properties as shown in Table 4.5, where viscosity, molecular

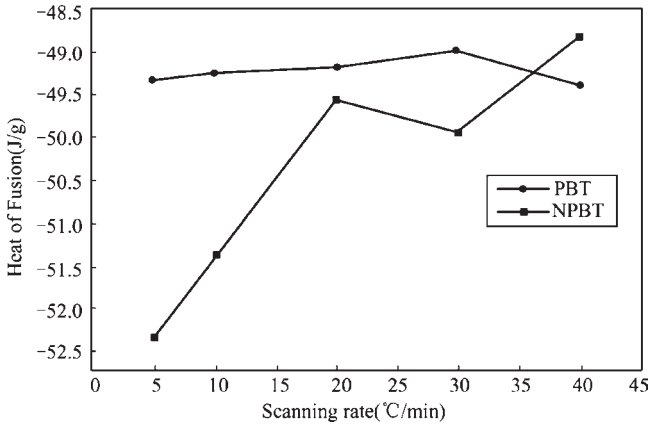


Fig. 4.19. Plot of heat of fusion (ΔH) vs. scanning rate under non-isothermal crystallization for PBT and NPBT with clay load of 5% (by wt) (its preparation is similar to that in Fig. 4.14).

Table 4.5
Molecular weight and its distribution for NPET samples

No.	MMT load (%, by wt)	M_w g/mole	M_w/M_n	η_{iv}
1	0.0	37,057	2.01	0.56
2	0.5	48,100	2.00	0.690
3	1.5	40,800	1.74	0.647
4	2.5	45,157	2.00	0.679
5	5.0	42,142	1.69	0.552

Note: η_{iv} , intrinsic viscosity.

weight and distributions of NPET samples are given. The samples are prepared according to our previously reported procedures [35,36].

The molecular weight of the polymer in the NPET is affected by introducing the MMTs, i.e., the MMTs play a role in determining the molecular weights that are obtained for the polymer. The interaction of MMT particles with the PET molecular chains will be different from that of the counterpart macroparticles acting with organic polymers [35]. The Avrami numbers for the crystallization rate calculated from isothermal crystallization are shown in Table 4.6. The crystallization dynamics parameter k is also shown. For $n > 2$, the polymer system may have secondary crystallization (primary and secondary crystallization) [36]. Table 4.6 shows the Avrami numbers of NPET samples under different isothermal crystallization temperatures [37,38].

By DSC tracing of NPET crystallized from the melt (Table 4.7), it is seen that NPET has a crystallinity rate 2–5 times higher than that of pure PET. These results show that the exfoliated MMT layers have strong interactions with PET molecular chains and act as heterogeneous nucleation sites, which accelerate the crystallization rate of PET.

Table 4.6
Effect of MMT load on its Avrami number under isothermal crystallization

T_{iso} (°C)	n_1 (0.0% (by wt) MMTs)	n_2 (1.5% (by wt) MMTs)	n_3 (5.0% (by wt) MMTs)
216	2.68	4.35	2.12
215	2.85	3.54	1.67
214	1.64	4.11	3.62
213	2.82	3.36	3.49

Note: T_{iso} , Isothermal crystallization ; $t_{1/2} = (\ln 2/k)^{1/n}$.

Table 4.7
Effect of clay load on NPET crystallization rate under isothermal crystallization

Sample no.	Clay load (wt%)	T_c -216 (°C)	T_c -215 (°C)	T_c -214 (°C)	T_c -213 (°C)
1	0.0	3.9	3.2	2.5	2.2
2	1.5	1.9	1.5	1.6	1.3
3	2.5	1.7	0.7	1.2	1.1
4	5.0	1.6	0.6	1.0	—

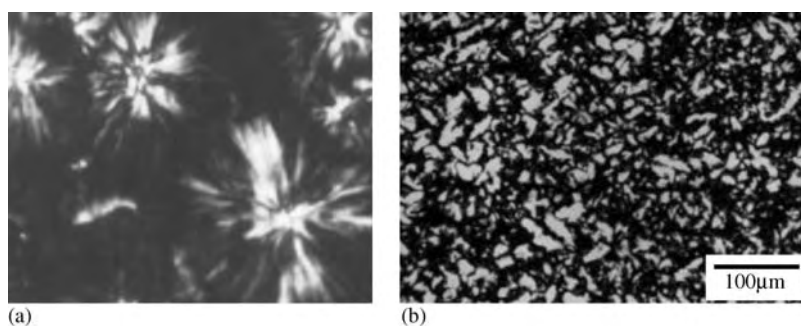


Fig. 4.20. Spheres of polypropylene (a), and polypropylene-MMT nanocomposites (b).

4.2.5. Crystallization morphology–property relationships

Nanoparticles act as nucleation sites for polymer crystallization to form crystallites. This effect is shown in Figure 4.20, where polypropylene spheres are transformed from large particles into fine particles due to the introduction of exfoliated layers. This nucleation effect has led to improved properties of polypropylene-MMT nanocomposites, as shown in Table 4.8.

4.3. Thermal properties

4.3.1. Melting behavior

The NPET and PET samples with molecular weights of 40,000 to 42,000 Da (molecular weight distribution of M_w/M_n is from 1.9 to 2.1) have been investigated. The melting

Table 4.8

Comparison of properties of polypropylene and polypropylene–MMT nanocomposites with homogeneous crystallites as in Figure 4.19.

Index	Unit	PP	PP-MMTs
Density	g cm^{-3}	0.903	0.928
Melt flow rate 230°C/2.16 N	g 10 min^{-1}	0.30	0.37
Hammer impact strength 0°C (notched)	kJ m^{-2}	2.5	9.7
Dangling impact strength 23°C (notched)	kJ m^{-2}	4.7	9.1
Tensile strength at break	N mm^{-2}	33	37
Linear expanding coefficient	K^{-1}	1.3×10^{-4}	1.7×10^{-5}
Transverse contract rate (pipe)	%	1.55	0.78
Thermal conductivity	W mK^{-1}	0.20	0.22

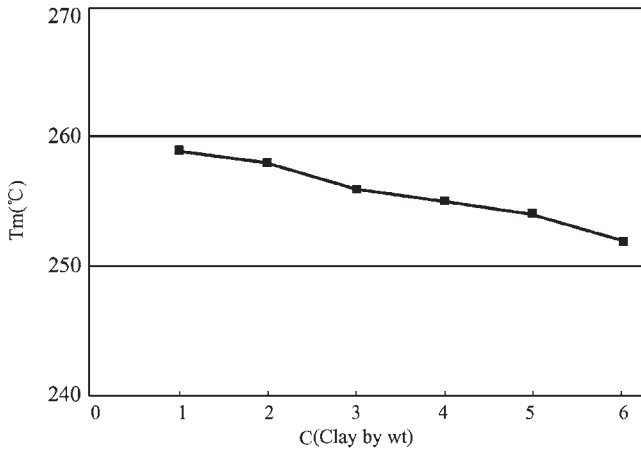


Fig. 4.21. Plot of melting point with clay concentration for nanocomposites of NPET.

points for NPET decrease with an increase in the clay load of MMTs. These trends are seen in Figure 4.21

This phenomenon is believed to result from the small-scale effect of the nanoparticles. The large specific area of the nanoparticles produces a large surface potential energy. Thus, the nanoparticles induce finer crystallized particles through nucleation, which makes the fine polymer crystallites easier to melt than the large ones. Additionally, the polymer chains are easier to polarize in NPET than in PET. Both of the above reasons explain the lower melting points in NPET than that in PET. In fact, previous investigations [39] have shown that the molecular chains near the surface of clay lamellae are harder than the other molecular chains of PET, which is evidence for polymer chain polarization. The low melting point of NPET is due to a nanoparticle effect and is beneficial for NPET processing.

4.3.2. Heat distortion temperature

HDT is either an application parameter or property index used in evaluating polymer-based nanocomposites. For example, HDT in PA6-layered silicate nanocomposite is 150°C or 100°C more than the matrix of pure PA6. The HDT of nanocomposites of PET or PBT with layered silicates of clay is 20°C–50°C more than that of the pure matrix PET or PBT. Our investigation shows that the enhancement of the HDT results from the more densely adsorbed polymer chains on the surface of the exfoliated layers.

4.3.2.1. HDT of poly(butylene terephthalate) (PBT)-based nanocomposite

The HDT of PBT's is a key technical parameter for its application to heat conditions. In the preparation of NPBT, the clay load can reach over 5% (by wt), as seen in the morphology in Figure 4.22. The addition of clay nanoparticles creates a large enhancement of HDT for PBT though some agglomerated particles are observed, and reflects a strong interaction between dispersed clay layers with the PBT matrix. The molecular chain length and their bonding reaction with PBT also have a significant effect on HDT of NPBT. The organic reagents or intercalation reagents are listed in Table 4.9. HDT of NPBT is enhanced from 30 to 50°C over PBT within 5% (by wt). It is pointed out that this increase in the level of HDT is even greater than that seen in NPET [40,41]. Thus, a new type of PBT material is produced.

The effect on HDT for three kinds of intercalation reagents, selected for treating the clay of MMTs, is shown in Table 4.9. The HDT of NPBT samples increase by 30–50°C in comparison with pure PBT. The chain length, the chain polarity of treating reagents, and the treating agents match with polymer chains, and the loading contribute to HDT of the sample. These results are different from previous reports on other polymers–clay nanocomposites [42–48] and show that the selected reagents have certain effects on the MMT layer's dispersion of clay and its interaction with PBT molecular chains.

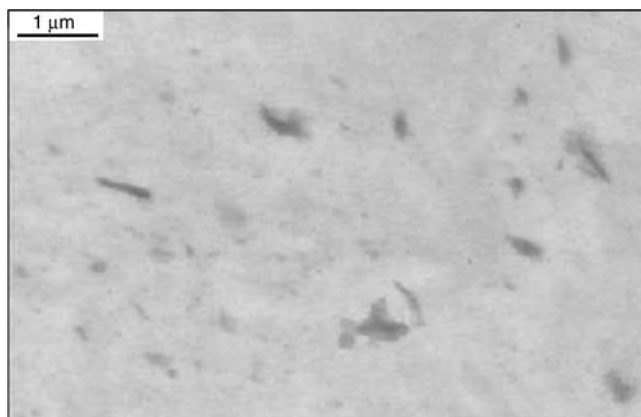


Fig. 4.22. The morphology of NPBT with high HDT of ~120°C.

Table 4.9
HDT of NPBT with different clay loads and intercalation reagents

Intercalation reagents	Clay content (% by wt)	HDT ^a (°C)
No	0.0	75
HOOC(CH ₂) ₅ NH ₂	3.0	112
HOOC(CH ₂) ₃ NH ₂	5.0	120
CH ₃ (CH ₂) ₁₁ NH ₂	3.0	116
CH ₃ (CH ₂) ₁₁ NH ₂	5.0	120
CH ₃ (CH ₂) ₁₅ NH ₂	3.0	118

^aMeasured under a load of 1.84 MPa; HDT, heat distortion temperature.

Table 4.10
Properties of HDT and films of NPET using different treating reagents

Reagents	HDT(°C)	Film transparency
EA(1%)	84	Y
EA(3%)	89	Y
EA(5%)	95	Y/N
PET	76	Y

Note: Values within parentheses are the clay loading weight; EA, Ethanolamine.

4.3.2.2. HDT of PET-based nanocomposites

The proper load of MMTs clay in NPET is 3% (by wt) based on our investigations of the thermal properties and nucleation of NPET. The overall properties of NPET are unsatisfactory if the clay load is less than 3% or more than 5% by wt. The same is true for the HDT of NPET. When an inhomogeneous distribution of the nanoparticles in the nanocomposites is detected, the effect on the HDT is observed as listed in Table 4.10. In this table, the HDT varies with the MMT load for the same reagent EA (ethanolamine). The non linear variations in HDT are due to inhomogeneous distributions of layers in the polymer melt when the load surpasses 3.0%. The proper clay load is less than 5% (by wt) for PET and other polymers such as polyamide and polypropylene.

4.3.3. Thermal degradation

Thermal gravimetric analysis (TGA) has been used to investigate the thermal degradation behavior of NPET. The overall properties of NPET and PET are enhanced when the layered silicates' load is within 10% (by wt). The thermal degradation behavior is shown in Figure 4.23.

A higher degradation temperature of NPET compared with PET is obtained. The TGA degradation temperature of NPET increases with the clay content: 410°C (0.0%

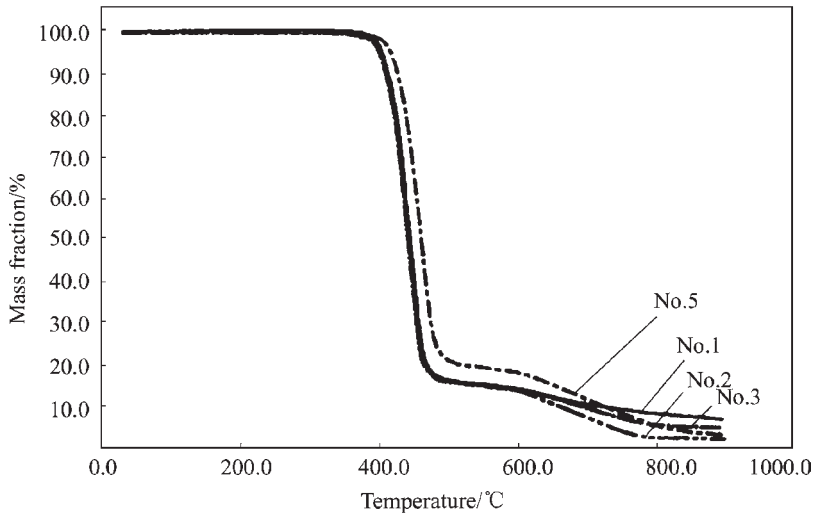


Fig. 4.23. Thermal degradation behavior of PET and NPET samples with different MMTs load (No. 1, PET; No. 2, NPET with 0.5% (by wt) clay, No. 3, NPET with 2.0% (by wt) Clay; No. 5, NPET with 5.0% (by wt) clay.

clay, by wt); 416°C (2.0% clay, by wt); 422°C (3.0%, by wt); 426°C (5.0% clay, by wt). The cross-linking of nanoparticles with the polymer PET chains causes the degradation behavior.

4.3.4. Specific heat and fireretardancy

The specific heat is defined as $C_p = [\partial H/\partial T]_p$. At constant pressure, C_p is related to the heat of fusion by

$$\Delta H = C_p \Delta T \quad (4.3.1)$$

where ΔH is the heat of fusion and ΔT the difference of temperature. According to this definition, Rupp found that nanoparticles should have materials with much higher C_p values composed of coarse crystallites (e.g., nanocrystallites of Cu with size of 8 nm have a C_p 54% higher than those of polycrystallites) [49]. The C_p values of Al_2O_3 (80 nm) and SiO_2 (20 nm) increase linearly with the annealing temperature [50]. However, when the annealing temperature is low, the increase in C_p values for these oxides is difficult to observe.

Clay of MMT is mainly composed of SiO_2 (70%) and Al_2O_3 (20%). When clay is mixed with PET by the intercalation–polymerization process, the C_p values of NPET shows a fluctuating change with clay content. In the temperature range lower than 100°C (the application temperature of NPET), the C_p value of NPET nanocomposites changes only slightly with clay content and annealing. The C_p plotted against the concentration of clay (C) is shown in Figure 4.24 for NPET.

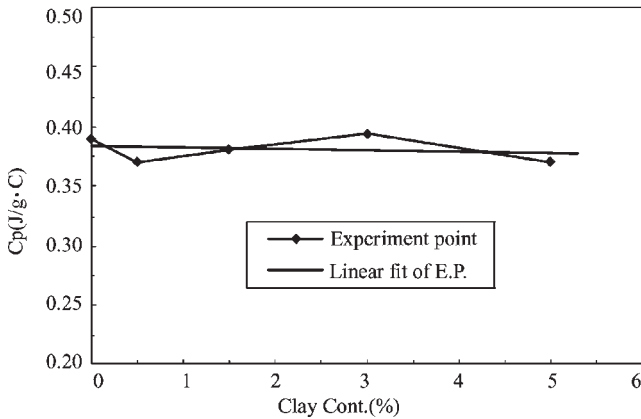


Fig. 4.24. Specific heat capacity of NPET vs. clay content.

The fluctuation of C_p for NPET is a reflection of the existence of unstable nanostructures. The presence of a fluctuation can be used as a guide to determine the quality of NPET. An NPET film should not show fluctuating behavior for C_p .

Thermal dynamics theory shows that the main parts of the contributions to C_p are vibrational entropy and configurational entropy or crystal lattice vibrations [49,50]. Based on this theory, the fluctuation of C_p in NPET nanocomposites should result from the clay lamellae interacting with polymer chains. At a low content of clay (lower than 5% MMTs (by wt)), the enthalpy of NPET changes little, and thus, the C_p value also changes slightly. The heterogeneous distribution of clay layers should contribute a great part to the fluctuation in heat capacity. TEM of NPET shows that heterogeneous distribution or agglomeration is more severe at high clay load than at a low clay load. These morphology can be observed by AFM. The fluctuation of C_p is not only seen in NPET, but in PS/clay nanocomposites [51,52] as well.

For the small amount of nanoparticles added, the nanoparticles in a PET matrix do not have an obvious heat capacity effect (experimental data errors have been excluded). The above result is not a conflict for nanocomposite properties such as fire retardancy. Nanoparticles in the polymer matrix present a barrier to oxygen diffusion, which will reduce degradation by oxygen for the PET polymer chain. Nanoparticles improve fire retardancy by preventing oxygen from penetrating into the polymer matrix.

4.3.5. Particle load–thermal property relationship

The thermal performance of nanocomposites of PBT-layered silicates of MMTs (NPBT) is listed in Table 4.11. The organo-clay of MMTs is treated by laurylamine (12-C). The thermal degradation temperature increases from 391 up to 401°C (MMT load is from 1 to 10% (by wt)), which is higher than that of 390°C for pure PBT itself. The melting point of NPBT decreases compared with that of PBT from 225 to 235°C. The degradation rate slows down when PBT is processed, due to the reduction of

Table 4.11
Thermal properties and process properties of NPBT^a

No.	MMT load (%)	HDT ^b (°C)	T_d (°C)	T_m (°C)	Inject T^c (°C)	Product surface
1	0.0	75.0	390	231	110	Bright
2	5.0	116.0	391	230	55	Bright
3	7.0	118.0	401	221	—	Bright
4	10.0	121.0	395	223	58	Little Bright

^aLayered silicate of MMTs treated by laurylamine. ^bMeasured at a load of 1.84 MPa. ^cInject T is the injection mold temperature.

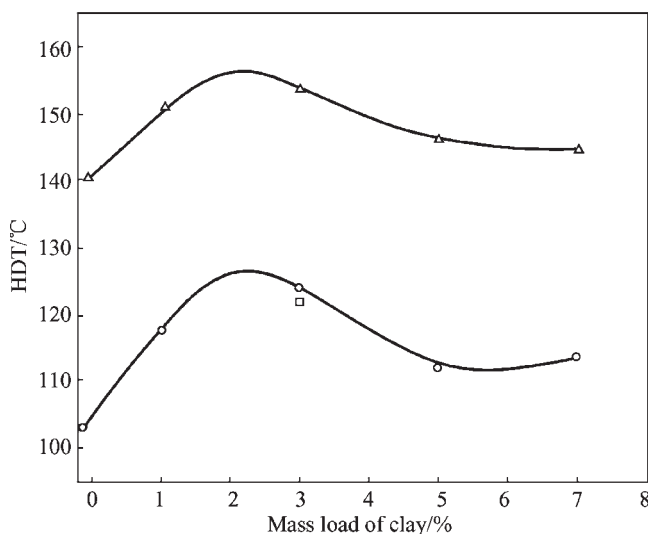


Fig. 4.25. Relationship between the HDT and the MMT load for PEO-MMT nanocomposites. Lower curve: MMTs treated by $\text{CH}_3(\text{CH}_2)_{15}\text{N}^+\text{H}_3$; upper curve: nanocomposite samples cured by tetrahydrophthalic anhydride (MeTHPA) or 4,4'-diamine diphenyl methyl (DDM).

spherulite size in PBT by the MMTs. The NPBT also has better rheological properties than PBT because of the changed surface properties in the nanocomposites.

Most properties of polymer-MMT nanocomposites increase linearly with the clay load [53–58], but there are some nanocomposites in which this does not occur. For example, in PEO-MMT nanocomposites, the HDT of the sample increases to its maximum point at 2.0% (by wt) of MMT load, but then decreases at higher load values, as shown in Figure 4.25.

Similar trends can be observed in the mechanical properties–particle load relationship.

4.4. Mechanical properties

The introduction of nanoparticles into a polymer matrix increases the mechanical properties such as tensile strength, bending modulus and related properties. The particle

distribution morphology has an effect on their final properties. When the nanocomposite samples are sheared, the exfoliated layers of MMTs in the polymer matrix take on an oriented dispersion state.

4.4.1. Tensile strength and bending modulus

The mechanical properties of NPBT, with 1.0 to 10.0% (by mass) MMTs are listed in Table 4.12. The bending modulus of NPBT (E_b) increases with an increase in the load content of MMTs, while the bending strength (σ_b) decreases slightly. The tensile strength (not shown) is enhanced two times that of PBT for a clay load of 5% (by wt).

In applications, it is important to enhance the impact strength of PET-layered silicate of MMT nanocomposites (NPET). The method of particle addition to the polymer matrix is important. A comparison of gel addition and powder addition of nanomaterials into a polymer matrix is shown in Table 4.13. The tensile strength and modulus obtained from powder addition (σ_t) are obviously better than those from gel addition.

4.4.2. Brittleness–ductility

In rigid particle reinforcing and toughening of a polymer matrix, the brittle–ductile transformation law has been established based on CaCO_3 particles [57]. These principles are

Table 4.12
Mechanical properties of NPBT with laurylamine-treated clay

LS load (%)	η (dl g ⁻¹)	Izod (J m ⁻¹)	σ_b (MPa)	E_b (MPa)
0.0	0.90	44.3	105.0	1700
1.0	0.92	45.1	110.9	2650
2.0	0.86	41.2	106.8	2900
5.0	0.87	37.4	104.0	3700
10.0	0.85	brittle	95.2	—

Note: η is the viscosity; Izod is notched izod impact strength; σ_b and E_b are bending strength and modulus.

Table 4.13
Nanocomposite properties of MMTs in situ polymerized with PET monomer

MMT load (%)	(dl g ⁻¹) η	σ_t (Mpa)	ϵ_t (%)	E_t (Mpa)	σ_b (Mpa)	E_b (Mpa)
Gel						
0.0	0.64	46.9	3.0	2510	90	2000
1.0	0.61	44.10	2.0	2920	88	2660
Powder						
0.0	0.65	61.9	7.0	2125	107.5	1700
3.0	0.67	64.1	3.0	3712	105.0	2800

Note: η is the viscosity; σ_t , ϵ_t and E_t are tensile strength, elongation at break and modulus; σ_b and E_b are bending strength and modulus, respectively.

important to understand the difference between these rigid particles and nanoparticles. There are several advantages in using the gel addition/polymerization method for NPET such as improved HDT and rheological behavior and enhancement of the crystallization rate. There are also some disadvantages such as a decrease in impact strength for MMT loads over 1% (by mass). Table 4.14 shows the nanocomposite impact properties when MMTs are loaded using the gel method.

Table 4.15 shows the properties of NPET as a function of the MMT load where each group has two samples: one is pure PET and the other is NPET. Only when the intrinsic viscosity of the NPET is above 0.60 dl g^{-1} , their impact strength is enhanced. Powder loads of 5% (by mass) will also give samples with better impact strength, which overcomes the system's sensitivity to MMT load.

4.4.3. Particle load–mechanical property relationship for PP–MMTs and PEO–MMTs

In polypropylene–MMT nanocomposites, the thermal and modulus properties are improved within 3% (by wt). The ratio of the modulus of storage energy for PP–MMT nanocomposites to PP increases as the clay load increases Figure 4.26. At a fixed temperature, the results also show that the ratio of the modulus of storage energy for PP–MMT nanocomposites to PP is not linear with clay content.

Figure 4.27 shows more aspects of the particle load–mechanical property relationship, where the modulus temperature is plotted, and the modulus is enhanced in every nanocomposite, while bending strength has a maximum.

Table 4.14
Impact strength of MMTs–PET nanocomposites using the gel loading method

No.	MMT load (%)	η (dl g ⁻¹)	Impact strength (J m ⁻¹)
1	0.0	0.60	28
2	1.5	0.65	27
3	2.5	0.68	21
4	5.0	0.56	15

Table 4.15
Comparison of MMT powder loads improving the impact strength of MMT–PET nanocomposites

No.	Load (%)	η (dl g ⁻¹)	M_n (g mol ⁻¹)	MWD	Izod Impact (J M ⁻¹)
1	0.0	0.64	4.14×10^4	2.01	30.0
2	1.0	0.61	3.97×10^4	1.90	33.0
3	0.0	0.57	3.25×10^4	1.87	20.0
4	2.0	0.55	—	—	16.0
5	0.0	0.63	4.08×10^4	2.01	28.0
6	1.5	0.61	3.91×10^4	1.74	35.0
7	0.0	0.63	4.08×10^4	2.01	28.0
8	5.0	0.59	3.5×10^4	1.70	29.0

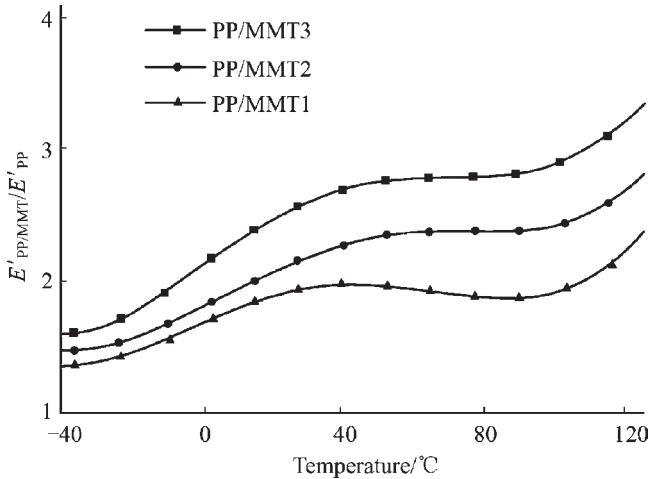


Fig. 4.26. Plot of the ratio of modulus of storage energy for PP-MMT nanocomposites to PP with temperature; PP/MMT1 is 1%, PP/MMT2 is 2%, and PP/MMT3 is 3% (by wt).

4.5. Special properties of nanocomposites

4.5.1. Assembly and self-assembly

The formation of nanostructures by assembly and self-assembly (are important topics in advanced material science) as well as techniques of preparing nanomaterials and nanocomposites. Ordered nanostructures in nanocomposites can have unique properties and these will constitute the next generation of quantum structural devices. The structures include one-dimensional (1D), two-dimensional (2D) and three-dimensional (3D) systems composed of nanoscale particles, stable molecular or atomic clusters, nanolamellae, nanotubes, nanowires, nanocables, nanosilk and nanoscale pores.

The intrinsic properties of nanoparticles are related to quantum scale and surface effects. The understanding of the physical phenomena in nanocomposite materials is still in its infancy, but progress is being made rapidly.

Investigation of nanomaterials based on their ordered arrays shows that the nanostructures can be separated into basic units (e.g., nanoparticle, nanotube and nanowire). The basic unit may possess a certain characteristic behavior that contributes to the overall properties of the nanostructure. A study of the arrangement of the basic units into nanostructures may reveal the relationship between the interdistance spacing of the units and nanostructure function. Further, the coupling effect between the units in relation to nanostructure function needs to be studied.

In industry, nanostructures or array structures can be fabricated by self-assembly, blending and doping. Included in these nanostructures are:

- emulsion systems composed of several stable surfactants (e.g., AOT and NP_x);
- porous materials (e.g., MCM-41, MCM-42 and silica carriers);

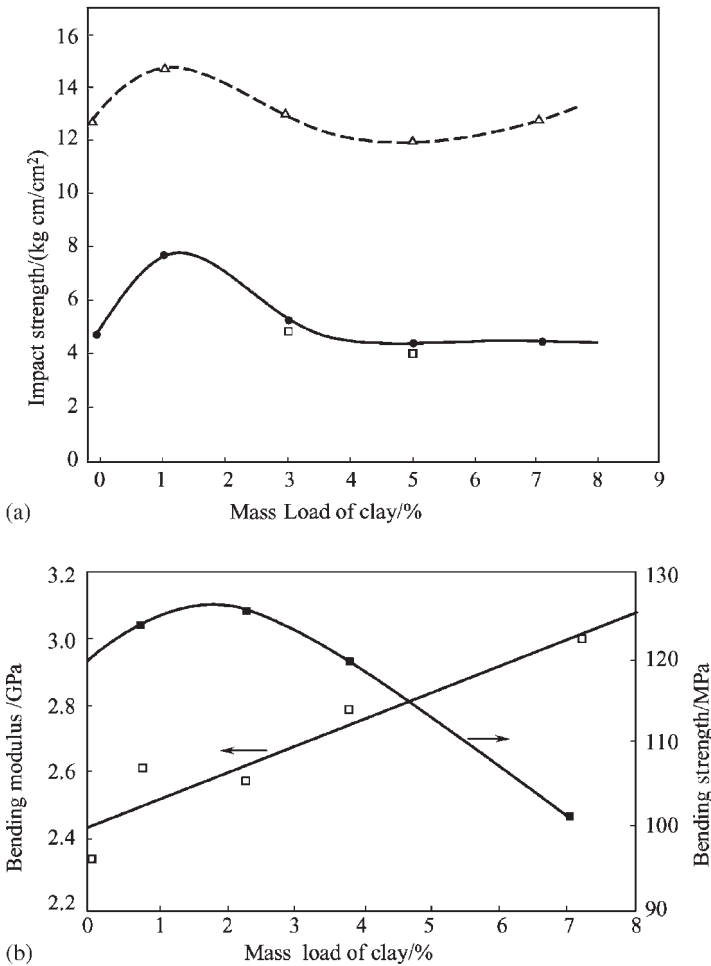


Fig. 4.27. The mechanical properties of PEO-MMT nanocomposites vs. load of MMTs. (a) Impact property vs. MMT (clay) load, where the samples containing MMTs treated with $\text{CH}_3(\text{CH}_2)_{13}\text{NH}_3^+$ are cured by either DDM (upper curve) or MeTHPA (lower curve). (b) Bending property vs. MMT (clay) load, where the samples containing MMTs treated with $\text{CH}_3(\text{CH}_2)_{17}\text{NH}_3^+$ are cured by DDM.

- film plate and template made from metals;
- polymer resin-based composite films.

Polymer–inorganic composite films are characterized by high mechanical strength, ease of processing and molding, and control of the shape of materials. At present, polymer–inorganic nanocomposites are the dominant materials for preparing practical, multifunctional and self-assembling nanomaterials with a high performance to cost ratio. This section includes the preparation of several polymer–inorganic nanocomposites with ordered arrays. We shall focus attention on the character of the array structure in these nanocomposites.

4.5.1.1. Properties of self-organized nanostructures and molecular self-organization

(1) *Colloidal crystals.* In a self-assembling nanostructure, atoms, ions and molecules assemble to form arrays and patterns by oriented non-covalent synergistic interactions (hydrogen bonds, van der Waals bonds, ionic bonds and hydrophobic bonds). The self-organization process is not a simple stacking and addition of these weak interactions, but an integrated synergistic effect. The formation of a self-assembling nanostructure has two important conditions. The first condition is the existence of a sufficient number of non-covalent bonds. The van der Waals and hydrogen bonds are weak non-covalent bonds (bond energies are 2.0934 to 4.1868 KJ / mol⁻¹); thus, a sufficient quantity of these weak bonds is needed to construct stable nanostructure systems. The second condition is that the overall process of formation of the self-organized system leads to a decrease in free energy; otherwise, the stable self-assembling system cannot form.

The creation of a molecular self-assembling system is divided into three steps:

- (1) The molecular intermediates of complicated but complete structures are constructed by ordered covalent bonds.
- (2) The molecular intermediates are transformed into large molecular aggregates by the synergistic interactions of weak intermolecular bonds.
- (3) The ordered nanostructure system is formed through a multi-repeated self-organized process, with one or several molecular aggregates acting as a structural unit. Research in self-organization synthetic methods has recently become cutting edge. For example, in the process of creating nanostructures of C₆₀Se colloidal crystals [58], C₆₀Se quantum dots of 1.5–10 nm are treated by adsorbing trialdyl phosphine chalcogenide on their surface. The crystals are then suspended in mixtures of 90% octa-alkane and 10% octa-alcohol at 80°C and ambient pressure. The pressure is then reduced to evaporate the octa-alkane, which increases the weight fraction of the nanocrystals in the mixtures and changes the solutions polarity. By this process the C₆₀Se quantum dots covered by a polar surfactant transform into a self-assembled nanostructure of planar colloids [61].

Properties of self-organized nanostructure systems are realized by adjusting their parameters with colloidal crystals. The spectra of the C₆₀Se quantum dots colloidal crystals show that light absorbing and emitting bands have a blue shift as the diameter of the quantum dot is reduced from 6.2 to 3.85 nm. If the concentration of quantum dots is increased, the interdistance between quantum dots is shortened and the enhancement of the coupling effect between crystals leads to a red shift.

(2) *Nanostructures of metal colloid by self-assembly.* Metal colloids connected with functional groups by surface treatment are capable of forming self-assembling nanostructures in organic molecular environments. Nanoparticle surfaces covered with thiol form a type of suspending solution, which can construct a dense pack of arrangements of self-organized long-range orders with a single-layer array structure on the highly oriented substrate of thermal black lead, layered MoS₂ or silica. In the suspending system, organic molecular chains connect with metal particles of Au. The physical properties of the system are controlled by the particle size of Au and the suspending concentration.

Andres et al. [59] have reported that metal particles of Au connected into a network have unusual electric current–voltage curves.

(3) *Self-organized synthesis of porous nanostructures.* The self-organization technique has been used to synthesize nanostructures of porous aragonite [60]. For example, several drops of bi-continuous microemulsions are sprayed on copper (Cu) or bronze (Cu). The substrate-containing emulsions are then submerged in a solvent of hot chloroform at 55°C or hexane at 65°C for 1–3s. Finally, the sample is withdrawn to evaporate the residual solvents in air and a white hollow mesoporous aragonite of nanostructure is obtained. The mesoporous aragonite shows an egg-like, hollow shell morphology, as observed under the microscope.

(4) *Synthesis of nanostructures by molecular self-organization.* Molecular self-organizations, which are necessary to create complex biological structures, exist in biological systems. For example, the assembly of proteins in biology is caused by molecular self-organizations. For example, acetone acid dehydrogenation enzyme coordinated compound has a diameter of about 30 nm and is composed of eight 3-polymerized units of sulfur octa-amine, 12 sulfur octa-amine dehydrogenated enzymes and 24 acetone dehydrogenated enzymes.

Molecular self-organization synthesis is summarized as:

(a) *Nanorod and nanotube.* Two units of polymer molecules result from a rigid rod block connected with a molecular soft circuit ring block, which forms a rod-like spiral wire [61]. These two units of polymer molecules can grow into long strips of aggregates by self-organization with non-covalent bond interactions. Such aggregates have lengths of about 1 μm and are several nanometers in diameter.

(b) *Multilayers of films.* By using tri-block copolymers such as polymethyl methyl acrylate-polystyrene-polytert-methyl acrylate, a supramolecular copolymer of self-organized nanostructure is prepared. Similarly, the tri-block copolymer aggregates are used as structural units, which further self-organize into nanostructures of supramolecular multilayers [62]. The aggregates are capable of self-organizing into stable nanostructures, whose aggregates are stacked, layered structure and their supramolecular films show interesting phenomena of self-generating waves transformed from red to green through control of the block segments in the main chain.

Molecular self-assembly is a new scientific field that is interdisciplinary in nature, involving physics, chemistry, biology, engineering and material science on the nanoscale. Molecular self-assembly and self-assembling nanostructures will form the basis for the next generation of nanostructure microdevices and nanomaterials.

4.5.1.2. *Synthesis of nanoparticle arrays on thick film templates*

Synthesis of nanostructures on a template provides more freedom to control its properties. A common template is a synthetic porous membrane. Compared with other preparation methods, the use of a template for assembling nanostructures has the following advantages:

- (1) The template can be used for the preparation of materials with nanostructure such as nanostructures of metals, alloys, semiconductors, conducting polymers, oxides, carbon and other materials.

- (2) The template is capable of the synthesis of nanosilk, nanotubes and their nanocomposites with high dispersions of nanoparticles.
- (3) The template can be used as an adjustor. For example, by changing the template's pore size, the diameter of the synthesized nanotubes and nanowires can be adjusted.

4.5.1.3. Template preparation and classifications

Templates of thick films are films with a high density of nanocylindrical pores. The film thickness can be several tens to hundreds of micrometers. The usual template is of two types: inorganic films with ordered pores and cavities such as membranes made from aluminum oxide, and polymer films with random pores and cavities. Other templates are porous glass plates, mesopore zeolites, proteins, MCM-41 and porous metal templates.

The preparation of a nanoarray system involves the use of thick, nanoporous films as a template. By using chemical and electrochemical methods inorganic nanotubes and nanowires can be grown inside the template. Sol-gel, chemical polymerization and chemical vapor deposition methods are also used to form inorganic and organic particles or structures inside the pores of the template. The preparation of the template is the first step in the further synthesis of nanostructural material.

(1) *Alumina template.* A sheet of alumina with high purity (99.999%) is submerged in butyl acid or sulfuric acid solution at a low temperature to corrode the positive pole and to obtain a porous template of alumina [63–65]. The pores are of hexa-angular, cylindrical shape and are vertical to the template film surface in ordered parallel arrangements. The pore size can be from 5 to 200 nm with a pore density up to 10^{11} pores cm^{-2} . The structural parameters are capable of being adjusted or varied according to type, concentration, temperature, voltage, electrolyzing time of electrolyte solution and pore-opening technique.

(2) *Polymer template.* Usually, thin films of polycarbonate (PC), polyester (PET), and polystyrene (PS) with a thickness micrometers (e.g. 6 μm) are used as templates [66]. By exposing the membrane to α particles from a radioactive source, damaged tracks are formed inside the membrane, which are then chemically etched to transform the tracks into pores. Alternatively, damaged tracks can be created by heavy ion bombardment. Cylindrical pores characterize the templates, and several pore cavities are crossed slantingly to the film surface, possibly at an angle of up to 34° relative to the surface normal of the film. The pore distribution is random and pore density is about 10^9 pores cm^{-2} .

(3) *Metal template.* The metal film is prepared by the deposition of a layer of metal on one face of the alumina template. The deposited metal film can act as a catalyst or electrode in subsequent electrodeposition.

Example 4.5.1.1. Monomers of polymethyl methyl acrylate (PMMA) are mixed with 5% (by wt) BPO drawn into the pores of an alumina template under a vacuum. The template is then heated to polymerize the monomers into PMMA cylindrical arrays under ultraviolet radiation. A metal film on the bottom of the template filled with PMMA is evaporated. This composite structure is submerged in a 10% (by wt) aqueous NaOH solution to remove the alumina template and to obtain a negative composite material of PMMA. The thin film is present on the bottom of this negative composite. The

negative-type composite is placed into the electrolyte solution, and the metal will gradually fill in the pore cavity of the negative composite by catalytic activity on the metal film or by electrodeposition with the metal film as an electrode. Finally, acetone is used to remove the PMMA. This process results in a porous metal template with the same pore size and pore arrangement as the original template. The final metal template is of low strength, which can limit its application in the catalysis of petroleum.

4.5.1.4. Template synthesis methods and their techniques

The synthesis of nanotubules or nanowires inside porous templates can be carried out by wet chemical methods. In addition, other methods including electrochemical deposition, chemical polymerization, sol-gel and chemical vapor deposition (CVD) can be used. In the case of a wet chemical method inside a template, questions such as whether the chemical precursor solution is wetting the pore walls will arise. Wettability plays an important role in allowing a reaction to take place inside the whole length of the pore. Any process that deposits material on the inside of the pore must be controlled by chemical reaction. A rapid deposition rate produces a plugging of the pore ends. Chemical reaction control can be achieved by ensuring that the mass transfer of chemicals into the pore is much faster than the chemical transformation inside the pore. The use of a low temperature can reduce the chemical reaction rate.

(1) *Electrochemical deposition.* This method has been used to assemble metal and conducting polymer fibers and tubes on the alumina and polymer templates, for example, the preparation of nanofibers (silks) and nanotube arrays from metals of Cu, Pt, Au, Ag, Ni, polypyrrole, polyaniline (PAN) and poly(trimethyl thiophene). A brief description of the preparation process is as follows: on one face of the template, a layer of metal thin film is sputtered, deposited or vaporized, and can act as the cathode in electrochemical deposition [67]. The method is also suitable for assembling conducting polymer nanowires and nanotubes. Polyaniline (PAN), polypyrrole and poly(trimethyl thiophene). By controlling the polymerization time, the nanotube wall thickness is adjusted. Polymer monomers are first polymerized in the pore wall, and form the thin wall of nanotube within a short time.

(2) *Electroless deposition.* In this method, the two important factors are sensing agent and reducing agents, with the help of which metals are assembled into template pores to prepare metal nanotubes, metal fibers and their arrays. Typical sensing agents are Sn^{2+} ions. The template is submerged into a solution of the sensing agent, and amine ($\text{H}_2\text{N}-$) on the pore wall, (carbonyl) group ($-\text{COOH}$) and hydroxyl group ($-\text{OH}$) are mixed with the sensing agent. The template with the adsorbed sensing agent is immersed in solutions containing ions of Ag^+ , and non-continuous nanoparticles of Ag cover the pore wall. Then the template is again immersed in metal electroless deposition of solution containing reducing agent. In the process, metal nanotubes are formed inside the pore. The tube wall thickness is adjusted by controlling the time of submerging [68].

(3) *Chemical polymerization.* In the chemical polymerization method [69], the monomers in the template pore cavity are polymerized into polymer tubes or wires by a chemical or electrochemical process. In this process, the template is submerged in the mixture of monomers and polymerization initiator. Then, the solutions inside the pore

of the template form an array system of polymer tube or silk by polymerization at a certain temperature and ultraviolet radiation. Generally, one face of the template is coated by metals as anode, and monomers inside the pore cavity of the template are polymerized into arrays of polymer tube or silk once the electric current is on. The formation of polymer tube or silk depends on the time, i.e., a short polymerization time produces a short nanotube. As the polymerization time increases, the thickness of the nanotube wall increases, and finally forms nanowires or nanosilk.

The electrochemical method can be used to prepare nanotubes or nanosilk arrays from conducting polymers such as poly(trimethyl thiophene), polypyrrole and polyaniline. These arrays demonstrate enhanced electrical conductivity. The finer the silk, the higher is the electrical conductivity. For example, polypyrrole nanosilk has 10 times the electrical conductivity compared with that of the bulk. The enhancement of electrical conductivity originates from regular arrangements of the polymer chain inside the nanosilk. As the diameter of the nanosilk becomes smaller, the ordered arrangements of the polymer chain have high ratio relative to the overall chains, and thus, the electrical conductivity produces more intense effects. The nanotube and nanosilk arrays in the conducting polymers are used as microelectronic devices.

Insulating plastics can be used to synthesize arrays of nanotubes or nanosilk by chemical polymerization methods. For example, an alumina template is immersed into a saturated acrylonitrile aqueous solution, to which 25 ml of 15 mmol^{-1} of $(\text{NH}_4)_2\text{S}_2\text{O}_8$ and 25 ml of 20 mmol^{-1} NaHSO_3 aqueous solution are added. The mixture is polymerized for 1–2 h at 40°C . During polymerization, N_2 gas is introduced to clean the environment and the polyacrylonitrile (PAN) is finally polymerized to produce nanotube arrays. The assembling system is heated at 750°C in air for 1 h, and then reheated in a nitrogen atmosphere for 1 h, transforming the polyacrylonitrile into a graphite nanotube array. After the alumina template is removed by solvent, the carbon nanotube is formed, and PAN tube in the nanotube will assemble. If metal of Au silk is mixed in PAN tube, the composite silks are finally obtained.

If the template is immersed into 8 ml of acrylonitrile, to which 1 mg besane nitrile is added, the acrylonitrile is polymerized into polyacrylonitrile nanosilk at 60°C in a nitrogen atmosphere. The same heating treatment method makes the nanosilk become a graphitic nanosilk array.

(4) *Chemical vapor deposition method (CVD)*. Generally, common chemical vapor deposition methods have high deposition rates, so that the pore is often plugged and prevents the vapor gas from entering the whole pore cavity. Consequently, nanosilk and nanotubes cannot be formed.

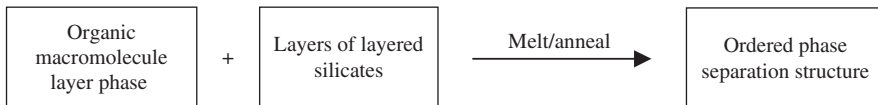
(5) *Sol-gel method*. This method is universal in several fields. Nanoparticles obtained from sol-gel synthesis are used for dipping porous Al_2O_3 template to produce inorganic arrays of nanotube and nanosilk such as nanotube arrays of TiO_2 , ZnO and WO . The alumina (Al_2O_3) template is first immersed into a sol, which allows the sol to be deposited on the wall of the template pores. By thermal treatment, nanotubes or nanosilk are formed inside the pore. Short immersion times produce nanotubes, while long merging times produce nanosilk.

The template method is a simple and a practical way of synthesizing nanostructure array systems. Furthermore, single compositions or mixtures of nanotube and nanosilk can be prepared by template methods. Suitable materials for this purpose can be metals, polymers, carbon and semiconductor or oxides. Fabrication of these nano-material arrays is not only beneficial for basic research, but have potential applications as well.

4.5.1.5. Nanocomposites and nanostructure of polymer-layered silicates and silica

(1) *Organized regular structure from melt quench.* Selection of proper organic macromolecules as matrix material is important for assembly. Recently, several examples of phase-separation structure from blending or block macromolecules have been prepared, specifically, spinodal decomposition phase patterns, which provide an extremely important matrix for forming assembling structures in polymer-inorganic nanocomposite materials. Using techniques of block copolymerization, cross-linking reaction, sulfurization and melt quench, layered phase-separation morphology in many polymers has been realized. The layered phase structure is regular and similar to the interlayer structure of MMTs.

The preparation of the regular phase structure of polymer-layered silicates is shown in the following sketch diagram, where the layer phase of the organic polymer is assembled with the layers of silicates. The mixtures then undergo a melt and step-by-step quench, and are finally annealed at a given temperature (130°C for PET-MMT nanocomposites) to form nanocomposites with an ordered pattern.



The final results from phase separation in organic macromolecules are the formation of a spherulitic phase or double continuous-phase structures, which are regularly layered phase structures on the nanoscale. For example, in PET-layered silicate nanocomposites, the ordered continuous-phase structure can be formed by a melt quench and annealing process. During annealing, the ordered layers exfoliate from layered silicates and interconnect to form a continuous structure as shown in Figure 4.28.

During phase separation and the formation of ordered structures, the loading concentration of layered silicates has a sensitive effect on the phase separation. Thus, when loading conditions (concentration and way of addition of inorganic phase, e.g., layered silicates) are determined, the design of the subsequent treatment methods will help in obtaining the formation of ordered phase separation.

Using natural MMTs with natural nanostructure to assemble with a semi-crystalline polymer with similar crystallized phase structure, a regular assembling structure has been produced. Nanocomposites are regarded as precursors of regular ordered assembling structures, and have had a significant impact on high-barrier materials, new materials of quantum dots and quantum conducting wires. The materials are also of

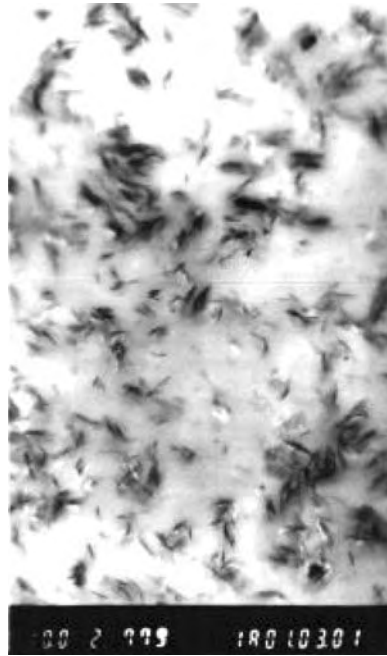


Fig. 4.28. TEM pattern of possible phase separation in PET-MMT nanocomposites (the samples are melt-quenched at first and then annealed at 130°C for 30 min).

significance in understanding natural order and controlling material structure and compositions.

(2) *Ordered structure by pillared MMTs.* MMTs pillared with silica have a stable layered structure, in which the interlayer distance is enlarged to the original basal space of pristine MMTs. This pillared structure is maintained even when it is subjected to high temperatures (500–700°C) or calcined. The preparation of MMTs with such an ordered structure is suitable for exfoliation in the melt. Using post-monomer intercalation and polymerization, the layer structure will be further exfoliated into random morphology. The pillared MMTs are regarded as precursors for the further preparation of nanocomposites with layer exfoliation dispersion morphology. Details on this technique are given in Chapter 3.

4.5.2. Optical properties

4.5.2.1. Silica colloidal crystal and its optical effects

Monodisperse colloidal silica and polystyrene spheres with diameters comparable with the wavelength of visible light can be assembled to form colloidal crystals. Studies on the optical effects of colloidal crystals have become a recent focus in the fields of optical and solid physics because of the importance of colloidal crystals in

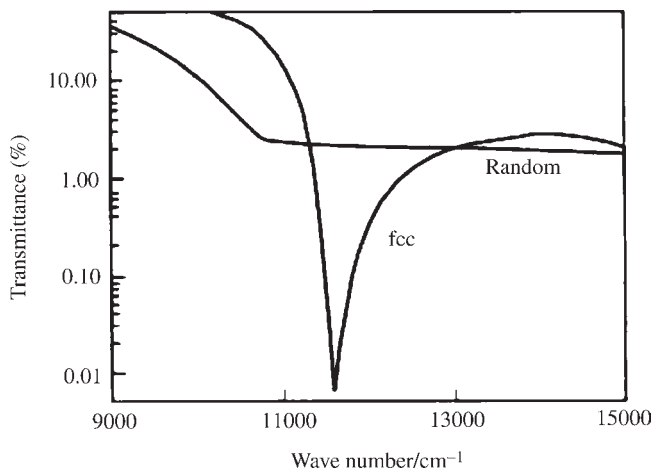


Fig. 4.29. Transmission spectra of a fcc silica colloidal crystal and a random silica suspension.

photonics and photonic crystals. This photonic crystal is a new type of material with a photonic bandgap. Structurally, it is a three-dimensional substance with periodic refractive index. The periodicity is related to the magnitude of the wavelength of light. The behavior of a photon in a photonic crystal is similar to that of an electron in an atomic crystal. We, along with our collaborators, have prepared a series of visible and near-infrared colloidal crystals made of submicron monodisperse silica spheres. The structure of silica colloidal face-centered-cubic (fcc) crystals was determined by Kossel rings analysis. The real distance between crystal planes and the positions of the high-symmetry points at the first Brillouin zone were measured. In addition, the transmission spectrum in the [111] direction, i.e., L point of the first Brillouin zone, was also measured in the visible and near-infrared regions shown in Figure 4.29. The spectrum demonstrates a sharp dip around $11,600\text{ cm}^{-1}$. This result coincides quite well with the lowest gap calculated at the L and X points for the (fcc) structure. Because of a lower SiO_2 refractive index ($n = 1.45$), the complete band gap could not be found or realized. We tried to increase the refractive index of the complex particles by coating the monodisperse silica sphere with titania (TiO_2 , $n = 2.50$). A multi-step coating procedure gives a 40 nm thick coating of titania on the silica core. Thus, the volume fraction of titania in a $\text{SiO}_2/\text{TiO}_2$ complex sphere with a diameter of 200 nm may reach 50%.

4.5.3. Liquid crystal behavior

The introduction of nanoparticles into a polymer matrix can enhance functional properties. Nanocomposite materials of polyester-MMTs and polystyrene-MMTs show liquid crystal behavior, although from several investigations, only the polystyrene-MMT nanocomposites show liquid crystalline behavior during the insitu heating process. This behavior has been discussed in Section 5.2 of Chapter 5.

4.6. Functional properties by nanoparticle assemble and doping

4.6.1. Barrier properties

The high-energy and adsorbing behavior of nanoparticles endow them with superior barrier properties to gases such as oxygen, carbon dioxide and moisture. Based on these barrier properties, the nanocomposites of polyester–MMTs, polyamide–MMTs and polyester–silica are prepared for packaging materials. The average gas permeation coefficients of the nanocomposite materials decrease to at least one-third of the coefficients of the pure polymer matrix. In PET-silica nanocomposites, some of the film materials for bottles have 5–6 times superior barrier properties to the PET itself.

To clarify the barrier mechanism, two models are suggested. According to the first model, the exfoliated layers in the nanocomposites produce an obstacle to gas transport. In the second model, known as the bulb model, the dispersed particles in the nanocomposite materials adsorb the gas passing through them to form bulbs. The details of these models are used in practical designs that are mentioned in Section 6.1 of Chapter 6.

4.6.2. Optical and reflection properties by assembly and doping

4.6.2.1. The fluorescent reinforcing effect of mesoporous solids and composites

This section, addresses several phenomena that result from the fluorescent reinforcing effects of mesoporous solids and their nanocomposites. Investigations have shown the significance of surface effects of mesoporous solids.

(1) *Assembly of nano-ZnO/mesoporous SiO₂ solids.* In an autoclave overloaded by ultra-high pressure (3–10 MPa), supercritical conditions can be created. The sol-gel process and supercritical drying techniques are used to prepare mesoporous SiO₂ solids with a porosity of 93% and pore diameters of 2–30 nm (gas gel). Aqueous ZnSO₄ solution is then drawn into the pores, to which dilute ammonia is added. A precipitate of Zn(OH)₂ is produced inside the mesoporous SiO₂. The precipitates are annealed at temperatures of 473–873 K to prepare nanocomposites of ZnO/SiO₂ with mesopore size [70]. The size of the nano-ZnO inside the mesopore can be adjusted by selecting different annealing temperatures. Measurements in the ultraviolet–visible range give a strong green light band within the visible light range; the peak position is located at about 500 nm. Compared with pure nanoparticles of ZnO black, the mesoporous solids made from aqueous ZnSO₄ solution have their light-emitting intensity enhanced 50 times (Figure 4.30).

It is interesting that the fluorescent effect of the mesoporous solid can be adjusted by controlling the concentration of the ZnSO₄ solution. The more nanoparticles inside the pore cavity, the more significant the fluorescent effect. Annealing and concentrating aqueous ZnSO₄, gives the position shift of the fluorescent band for the prepared nanocomposites. The results in Figure 4.30 show that the peak position shifts from 500 to 580 nm for samples annealing at 473 K/4 h or 473 K + 773 K/4 h. When the concentration of aqueous ZnSO₄ solution is diluted from the saturated state to 50% (by wt), the fluorescent intensity of the system is reduced from 50 times higher to 10 times higher than that of silica itself, while the peak position of the fluorescent band shifts from 500 to 480 nm.

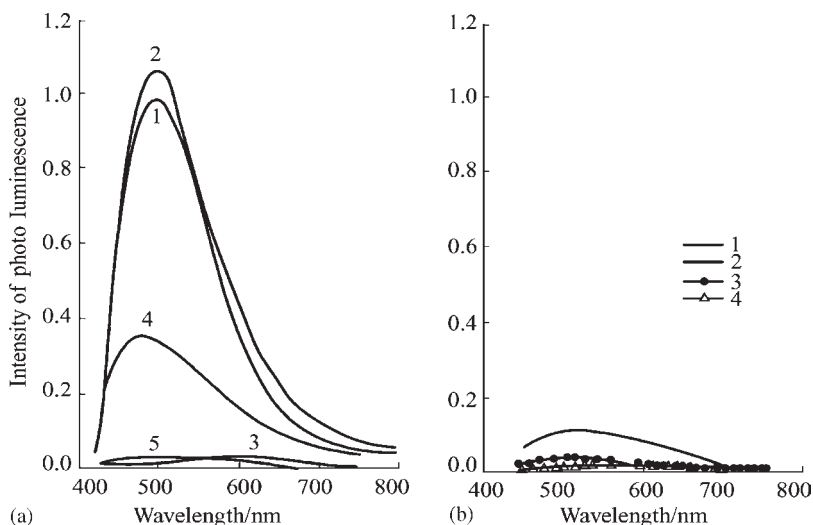


Fig. 4.30. Light-emitting spectra caused by light for samples of both mesoporous nanocomposites of ZnO/SiO₂ gas gel and nanostructure of ZnO block. (a) Mesoporous composite samples in curves 1–3 are prepared by immersing SiO₂ in aqueous ZnSO₄ solution; the mesoporous composite sample in curve 4 is made from immersing SiO₂ in aqueous ZnSO₄ solution diluted with 50% (by wt) water; the sample in curve 5 represents the corresponding pure mesoporous SiO₂ solid particle. Samples in curves 1–4 are annealed at 473 K for 4 h, 473 K for 4 h and 773 K for 4 h, 473 K for 4 h and 773 K for 4 h, and 873 K for 4 h and 573 K for 4 h, respectively. (b) Curves 1–4 represent four kinds of nanostructures from ZnO blocks annealed at 473, 573, 673 and 1423 K for 4 h.

(2) *Doping mesoporous silica.* A series of fluorescent intensity effects is found for silica matrix doped with rare earth and Al ions to form doped mesoporous SiO₂ dry gel. In the doping experiment, compounds of Ce(SO₄)₂ or Ce(NO₃)₃ and AlCl₃ are added to precursors of silica at the molar ratio of Si/Ce = 100:1 and Al/Ce = 10:1. Through hydration of these compounds and gelation, solids of Ce⁴⁺ and Ce³⁺-doped into the mesoporous silica are prepared. The fluorescent experiments show that two fluorescent bands are observed in Ce⁴⁺-doped mesoporous silica: one located at 340 nm in the ultraviolet region and the other at 650 nm in the visible region (Fig. 4.31), while in Ce⁴⁺-doped mesoporous silica solid sample (not silica dry gel), no fluorescent phenomenon is observed in the ultraviolet and visible light regions. It is seen in Figure 4.30 (curve b) that Al³⁺ doping produces a five fold increase in the fluorescent intensity. The Al³⁺-doped composites decrease in their fluorescent intensity when they are annealed at 773 K. The annealing has a trivial effect on the Ce⁴⁺/SiO₂ samples without doping (curves (c) and (e) in Figure 4.31).

The codoping of Tb³⁺ and Al³⁺ into mesoporous SiO₂ dry gel also shows intense fluorescent phenomena. An acute fluorescent peak appears in the green wave region of 546 nm (Figure 4.32).

In Figure 4.31, the intensity of the fluorescent peak can be adjusted by controlling the addition of Al³⁺. When the molar ratio of Al/Tb = 10:1, an intensified effect of green light is observed and the light intensity increases ten times (Figure 4.33).

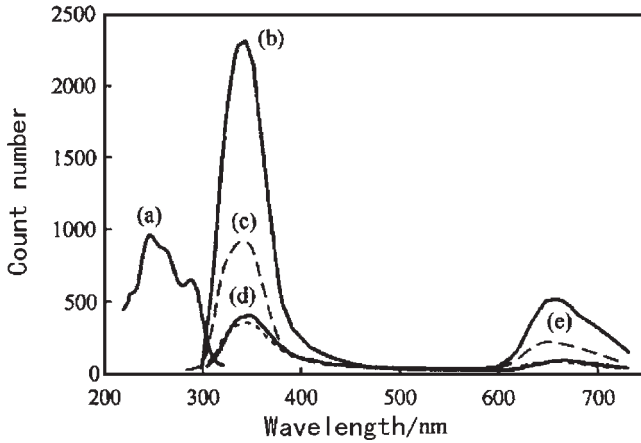


Fig. 4.31. Emission and radiation spectra of $\text{Ce}^{4+}/\text{SiO}_2$ ($E_x = 250$ nm) composites. (a) Excitation spectrum, $E_m = 345$ nm; (b) and (d) are spectra of composite samples with or without doped Al; (c) and (e) (dotted lines) correspond to emission spectra of samples annealed at 773 K for 1 h.

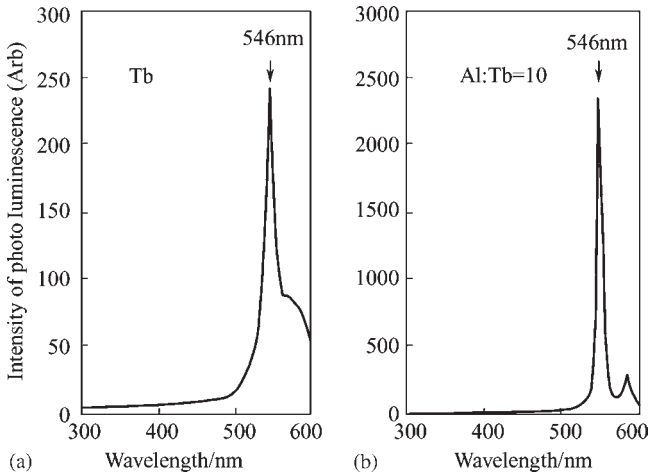


Fig. 4.32. Fluorescent spectra of Tb/SiO_2 (the back fluorescent light of SiO_2 is discounted, $E_x = 245$ nm) (a) no addition of Al and (b) molar ratio of $\text{Al}/\text{Tb} = 10$ (the fluorescent peak at 490 nm is covered by time frequency effects in the measurement, thus not shown; molar ratio of $\text{Si}/\text{Tb} = 100$ for all samples). (with the permission of Science Press of China)

The light intensity reaches a maximum value when the molar ratio is $\text{Al}/\text{Tb} = 50:1$. Some results in the literature indicate that in the Sm doping of mesoporous silica (dry gel), the maximum fluorescent intensity occurs at a molar ratio of $\text{Al}/\text{Sm} = 10:1$. However, the results of our experiment show that the intensified fluorescent peak at a molar ratio of $\text{Al}/\text{Tb} = 50:1$ is 1.5 times that at a molar ratio of $\text{Al}/\text{Tb} = 10:1$.

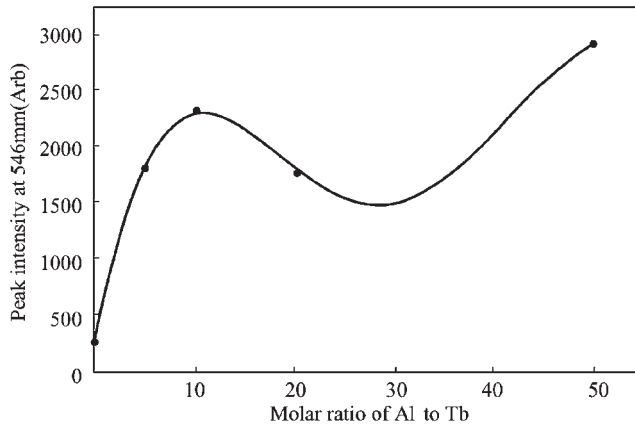


Fig. 4.33. Loading quantity of Al is related to fluorescent intensity at 546 nm of Tb/SiO₂ composites. (with the permission of Science Press of China)

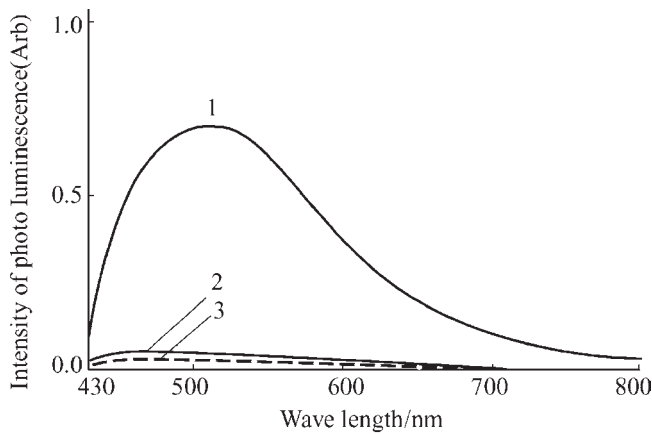


Fig. 4.34. Fluorescent spectra due to visible light of doped SiO₂ and pristine SiO₂ at several conditions: curve 1—Al³⁺-doped silica aerogel without annealing; curve 2—pure silica aerogel; curve 3—Al³⁺-doped silica dry gel annealed at 300°C for 4 h. (With the permission of Science Press of China)

The amplitude of the fluorescent intensity of doped mesoporous SiO₂ solids can be adjusted by varying the porosity. Annealing treatments modulate the fluorescent shift. The results make it possible to control the fluorescent intensity of the mesoporous solid's and fluorescent band position.

Using a sol-gel process and supercritical drying methods, Al³⁺-doped gas gel with a porosity of 93% can be prepared, in which the extremely intense fluorescent effect can be observed [71]. Furthermore, Al³⁺-doped SiO₂ aerogel can be investigated by fluorescent spectra. In Figure 4.34, the fluorescent spectra of the composites are shown, where curve 1 represents the fluorescent spectrum of SiO₂ aerogel without an annealing treatment,

curve 2 represents pristine SiO_2 aerogel Al^{3+} -doped and curve 3 is the fluorescent spectrum of silica dry gel with 50% porosity annealed at 300°C .

A broad fluorescent band from 400 to 700 nm is present for curve 1 with the peak position at 520 nm. The results show that the fluorescent intensity of Al^{3+} -doped silica aerogel is 10 times higher than that of either Al^{3+} -doped dry gel or silica aerogel without doping. The fluorescent intensity benefits from the high porosity of the aerogel.

As for Al^{3+} -doped silica samples, annealing treatment can greatly enhance the fluorescent intensity amplitude of Al^{3+} -doped SiO_2 aerogels, in which significant fluorescent behavior occurs. The broad fluorescent band is divided into two peaks when they are annealed at 773 K. Such treatments have 2–3 times the fluorescent intensity than that of untreated silica samples, 40 times the intensity of aerogel silica without doping and 32 times the intensity of Al^{3+} -doped SiO_2 dry gel, which is higher than that of porous silicon (Figure 4.35).

In curve 1, double peaks (P1, P2) of Al^{3+} -doped SiO_2 aerogel have significant red shifts of the peak position compared with the untreated samples.

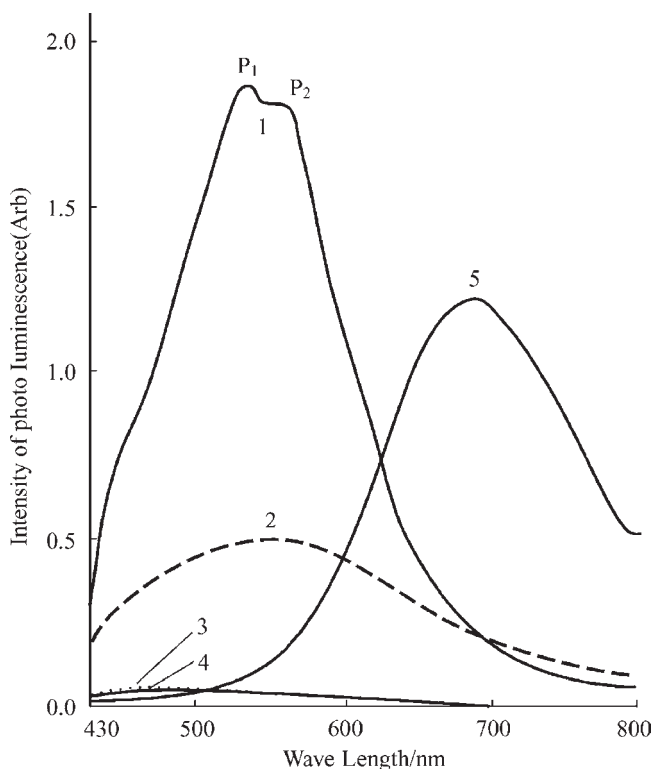


Fig. 4.35. Fluorescent spectra due to visible light: curve 1 – Al^{3+} -doped SiO_2 aerogel annealed at 500°C for 4 h; curve 2 – aluminum silicate; curve 3 – Al^{3+} -doped SiO_2 dry gel annealed at 300°C for 4 h; curve 4 – pure SiO_2 aerogel; curve 5 – porous silicon. (With the permission of Editorial office of Chinese Physics, Science Press of China)

(3) *The position modulation of the light absorption edge and band.* One of the most important characteristics of mesoporous composites is that it is possible to change the position of the light absorption edge and band by heat treatment and by control of the hetero-nanoparticle quantity in the mesopores. This character is not seen in common composites.

Nanoparticles of Cr_2O_3 are assembled in the pore cavities of porous Al_2O_3 composites, whose absorbing band position is capable of being adjusted through heat treatment. Blue or red shifts of these composites can be obtained by heat treatment or hydrogen reduction. Red shifts of the absorption band are obtained by reduction using hydrogen. The modulation of the absorption band results from the fact that the heat treatment changes the nanoparticles surface state inside the pores. The higher the temperatures, the more perfect the surface coordination of particles. This is because the condensation of oxygen, which reduces optical aberration and quantum scale effects, lead to a blue shift of the absorption band. Under a hydrogen reduction atmosphere, the particle surface is deficient of oxygen. Surface aberration increases, causing a red shift of the absorption band. The above has been extensively discussed in the literature.

A nanocomposite of Ag nanoparticles in mesoporous silica displays light absorption behavior, which is different from both the Ag nanoparticle itself and the mesoporous silica solid. This nanocomposite has some semiconductor characteristics of direct band gap, and furthermore, the position of the light absorption can be controlled through the loading quantity of Ag particles to obtain shifts from ultraviolet to red [72].

Experiments have shown that a vibration absorption peak of surface plasma at 400 nm exists for Ag nanoparticles, while such a surface coresonance absorption peak disappears when Ag nanoparticles with diameters less than 3 nm are assembled into the mesoporous silica solids. The light absorption spectra of these mesoporous composites have only left an absorption border, which corresponds to the interbands absorption of the Ag particles inside the pores. When the Ag loading reaches 5.0% (by wt), the position of the absorption band border shifts from near ultraviolet to overall visible light (Figure 4.36). As the loading weight of Ag increases, the amplitude of the red shift also becomes enhanced. The absorption border can be controlled by adjusting the loading quantity of nanoparticle (e.g., Ag) inside the pores of mesoporous composites.

Further investigation of the Ag/SiO₂ system shows that the light absorption value of mesoporous composites with different loading of Ag is related to the light wavelength, which is consistent with the light absorption equation of the direct band gap of a semiconductor,

$$\alpha\hbar\nu = A(\hbar\nu - E_g)^{1/2} \quad (6.2.1)$$

where A is the absorption value, $\hbar\nu$ is the incident light energy and A and E_g are constants. For different composite samples, the $(\alpha\hbar\nu)^2 - \hbar\nu$ plots are a series of parallel lines (Figure 4.37).

The significance of the above lies in the fact that the semi-conducting light absorption characters in nanoparticles of Ag in porous SiO₂ composites are different from those of semiconductors, the bandgap of the former can be adjusted through the quantity of nanoparticles of Ag.

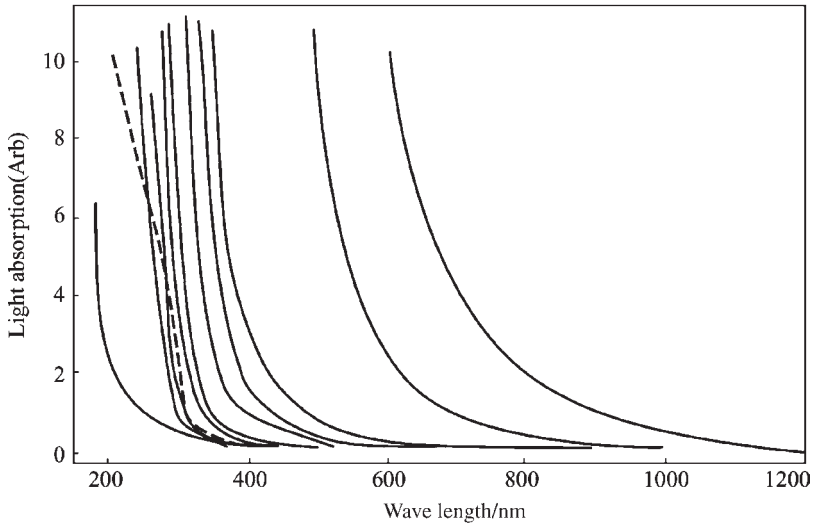


Fig. 4.36. Absorption spectra of Ag/mesoporous silica with different Ag loading when annealing at 773 K for 0.5 h. The straight line curves show the Ag loading weight fraction of 0.0, 0.25, 0.50, 0.75, 1.00, 1.23, 1.72, 2.50, 3.44, and 5.00 from left to right; The dashed line curve shows the absorption spectrum of Ag particles calculated for an Ag/SiO₂ system through effective media theory based on the media constant of the Ag interbands. (With the permission of Editorial office of Chinese Physics, Science Press of China).

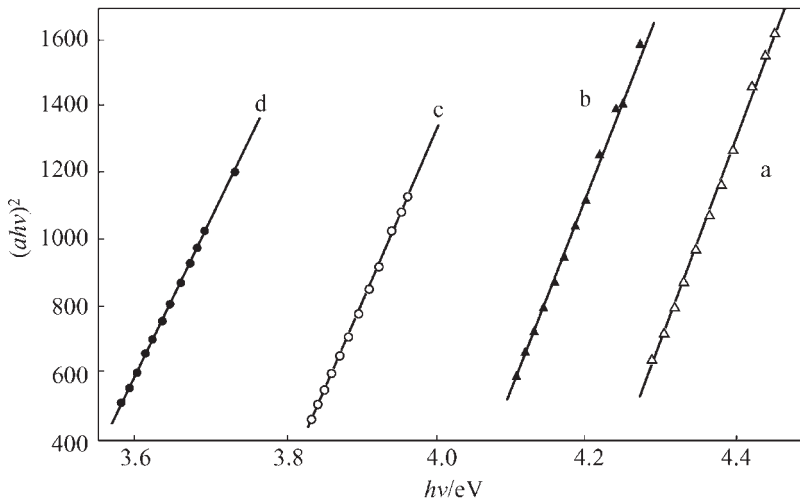


Fig. 4.37. $(\alpha\hbar\nu)^2$ vs. $\hbar\nu$ curves: Ag loading weight of a – 0.75%; b – 1.0%; c – 1.23%; d – 1.72%. (With the permission of Editorial office of Chinese Physics, Science Press of China)

(4) *Environmental sensitivity in the process of adsorption and oxidation.* The surface adsorption and oxidation in the nanoparticles inside mesoporous composites are more sensitive to the environment than other materials. At ambient conditions, oxygen in air physically adsorbs on the surfaces of Ag nanoparticles inside pores, which transforms

into a chemical adsorption to eventually produce an oxidized surface of the particles. In dry air, these composites produce only physical adsorption without oxidation. As the relative humidity increases, the oxidation process accelerates. By using differential scanning calorimetry (DSC) heating, light absorption experiments and thermodynamical analysis, the binding energy of O_2 with nanoparticles of Ag inside the silica pores, and the binding energy of Ag–O bond in the Ag_2O are obtained through a physical and chemical adsorption process of Ag nanoparticles. The experimental data on composites of nanoparticle Ag/mesoporous SiO_2 are the first to be reported till now. The significance of this work is that the oxidation on the surface of Ag particles greatly increases the width of the inner bands of the composites, and thus provides a new way to control the interband width. The blue shift of the light absorption border is related to the surface oxidation process of metal particles inside pores.

4.6.2.2. *The interface coupling effect induced by environment*

At room temperature and a relative humidity greater than 80%, some Ag_2SiO_3 forms between the particles and the pore wall, which causes the particle sample to transform from transparent to opaque. The formed interface obeys a time power function law at room temperature and high humidity. The interface starts to degrade at 573 K and completely degrades at 973 K, which makes the composite sample of Ag/silica return to its original state or transform back from opaque to transparent. Before the interface phase is completely degraded, heating this sample will not cause particles inside the pores to be coarse. If the composites are alternately exposed to air, and then heated in the temperature range from 573 to 973 K, they exhibit the same reversible optical phenomenon as above.

4.7. Rheology and dynamic behavior

The rheology and dynamic behavior of polymer–inorganic nanocomposites depend on the processing and application performance. In measuring rheological properties, the equipment used usually includes capillary meters and disc-type viscometers. The capillary types are usually INSTRON, while the disc-type is an advanced type of ARES (advanced rheometric expansion system). In capillary measurements of polyamide–MMT nanocomposites with ultra-high molecular weight polyethylene (UHMWPE), the aspect ratio of the capillary tube selected is 20:1, 40:1, 60:1 and higher. The melting temperature is 250–270°C, depending on the nanocomposite type. On the other hand, the dynamic mechanical analyzer (DMA) has been adopted to trace the dynamic behavior at different temperatures and loads. In Figure 4.38, the melt viscosities (vs. the shear rate) are compared for two samples of PA6 and the nanocomposite NPA6.

Although the melt viscosity of NPA6 is higher than that of PA6 at low shearing rates, it is lower than that of the latter at higher shearing rates (greater than 100 s^{-1}). As the shearing rate increases, the viscosity of NPA6 with 4.0% MMT load decreases rapidly. The reason for this behavior is the possible orientation of exfoliated MMT layers in the polymer melt. These oriented layers have a lubricating role for the polymer chains.

For UHMWPE–kaolinite nanocomposites (Figure 4.39), the viscosities of the nanocomposites are lower than those of pure polyethylene at high shearing rate, even when the MMT overload is as high as 15%, or 24% (by wt). At low shearing rates, there

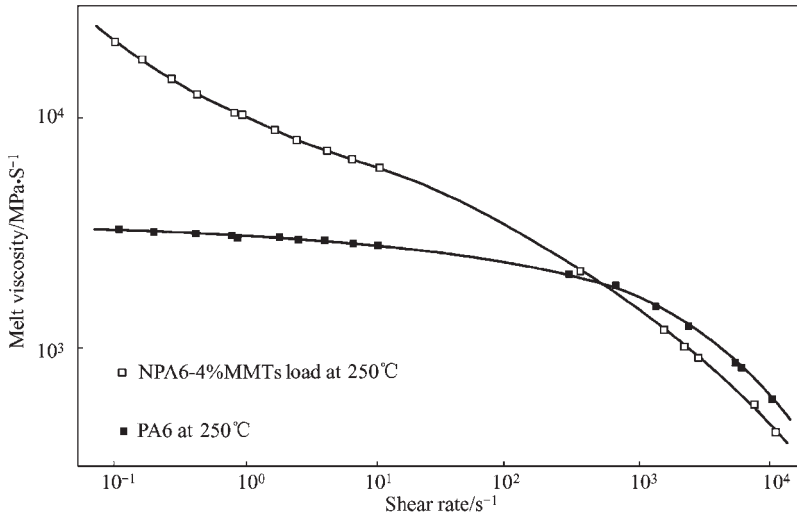


Fig. 4.38. Rheological curves of PA6 and NPA6 with a 4.0% MMT load.

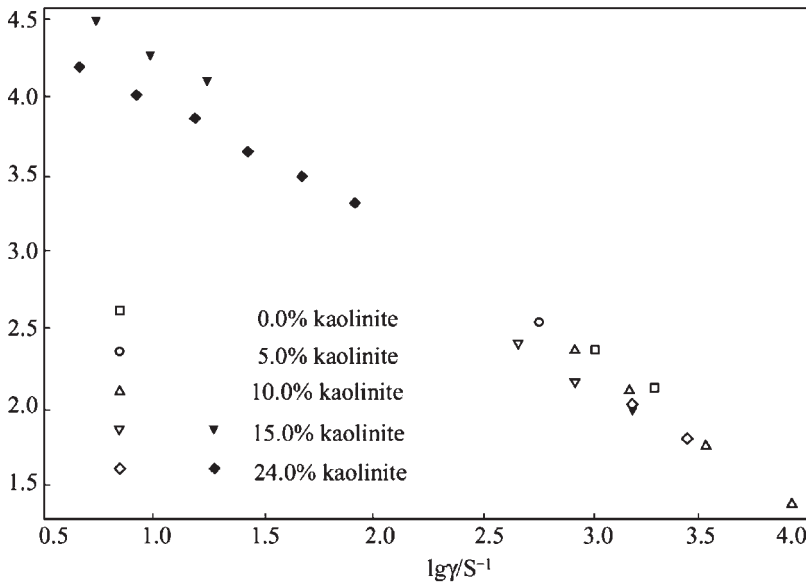


Fig. 4.39. Apparent viscosity vs. shearing viscosity for UHMPWE-kaolinite nanocomposites.

is an absence of slip phenomenon. Thus, the melt is difficult to squeeze out and there is a pressure vibration that leads to a coarse appearance of the product. It is interesting to note that the higher the load of the kaolinite, the lower the apparent viscosity of the melt in the pseudo-plastic area. The induction of kaolinite reduces the viscosity of the

high-molecular-weight polyethylene. In this way, processing problems with UHMWPE are expected to be solved.

4.8. Nucleation and order

4.8.1. Nucleation in solution, melt and annealing

The nucleation effect of polymer–inorganic nanocomposites is produced when they are dissolved in solution, and melted or annealed at different temperature, time and pressure. Research on this subject has been published elsewhere [53–55]. In this book, the nucleation behavior of nanoparticles in different dispersion morphology (exfoliated, intercalated or aggregated) in the nanocomposites of polyester–MMTs (silica), and PP–MMTs (silica) has been observed. This nucleation process and effect have been described in different sections of the book, and thus, a summary and comparison of this nucleation behavior are briefly given.

Samples of PS–MMT nanocomposites will not show liquid crystalline behavior as described in Chapter 5. However, these melt-extruded samples of PS–MMT nanocomposites do produce the liquid crystalline (LC) state from in situ heating and cooling process. When they are annealed at a temperature above 100°C, all crystalline behavior disappears.

In polyester–MMT nanocomposites, when the quenched samples are annealed at different temperatures from 130 to 200°C, ordered patterns are usually created. For example, Section 4.1.4 shows how the PBT–clay nanocomposite samples can show ordered patterns after the amorphous samples are annealed at different temperatures for different times.

In PET–MMTs, it has been observed that this nanocomposite sample shows an abnormal pattern in the diffraction position below 5° (2θ). We thought that this is either an ordered structure form produced by a new tiny crystalline transition or a new crystal form. But this phenomenon is best studied by those who are specialized in crystallization theory and practice.

Although we are aware of the significance of nucleation and order, we have to continue to find ways by which the mechanism and process are revealed. Recently, we introduced the layer-by-layer (LbL) technique [56] to treat layered clay in order to detect these new phenomena. These works may pave the way for revealing the characteristics of these effects from the nanoparticle nucleation and order.

4.8.2. Nucleation of metal oxide nanoparticles in ultrathin polymeric films

4.8.2.1. Surface modification with polymeric electrolytes: LbL films

The LbL deposition technique of building supramolecular multilayers on solid substrates by adsorbing polyelectrolytes has emerged as a simple means of producing templates of controlled thickness. The LbL technique is also a surface modification method. Decher [73,74] has established that such multilayers may be reproducibly built and that the resultant structure is mechanically and thermally stable. Such films have been utilized in the preparation of electroluminescent devices and zener diodes, and the possibility of their use in flat screen displays has also been suggested. The porous and supramolecular

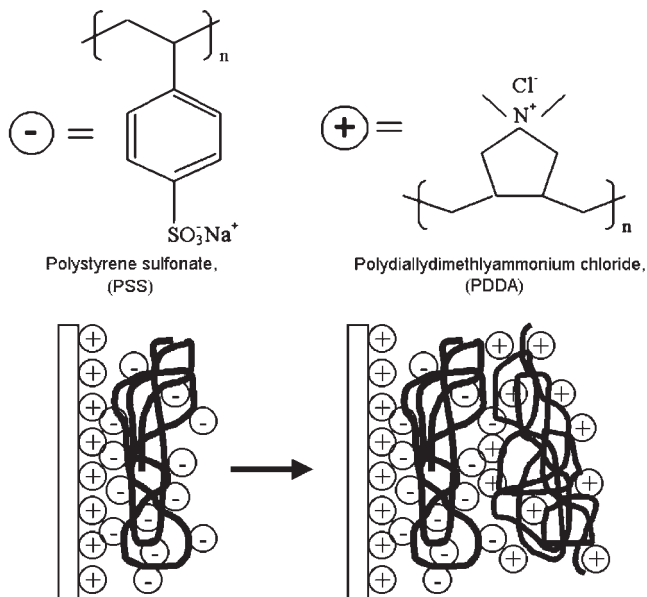


Fig. 4.40. Schematic representation of LbL deposition for a positively charged surface.

structure of these films provide opportunities for studying chemical reactions in the nanoscale regime. Figure 4.40 shows schematically an example of the LbL deposition technique for the sequential deposition of a polyanion (PSS) followed by the deposition of a polycation (PDPA) on a positively charged surface.

The procedure of LbL deposition is relatively simple. For example, poly(diallyldimethylammoniumchloride) PDPA, a polycation, and poly(styrenesulfonate) (PSS), a polyanion, can be deposited sequentially on a negatively charged surface as follows: the polyionic solutions of PDPA and PSS are prepared separately in 20 mM concentrations; the former is dissolved in deionized water, while the latter is dissolved in a 0.1 M NaOH solution, and then adjusted to a pH of 4.5 by dropwise addition of 0.1 M HCl. All concentrations are calculated based on the monomer molecular weights. Polymer films can be assembled on negatively charged substrates if one starts with PDPA. A PDPA/PSS deposition cycle is termed the deposition of one layer pair. For nanoparticle nucleation, deposition is preferably ended with the first half of a layer pair in order to terminate the film with a PDPA layer, as will be discussed later. The deposition of the LbL films can be followed by UV-visible spectroscopy as shown in Figure 4.41; the absorbance is linear with the number of layer pairs deposited. For the above conditions each layer pair is approximately 4–5 nm thick, so that a 10.5 layer pair thick nanofilm is about 50 nm in total thickness.

4.8.2.2. *In situ nucleation and growth of nanoparticles in LbL films*

Divalent and trivalent ions can bind to the negatively charged sulfonate groups in LbL polyelectrolyte nanofilms, and the adsorbed ions can be oxidized to form nanoparticles

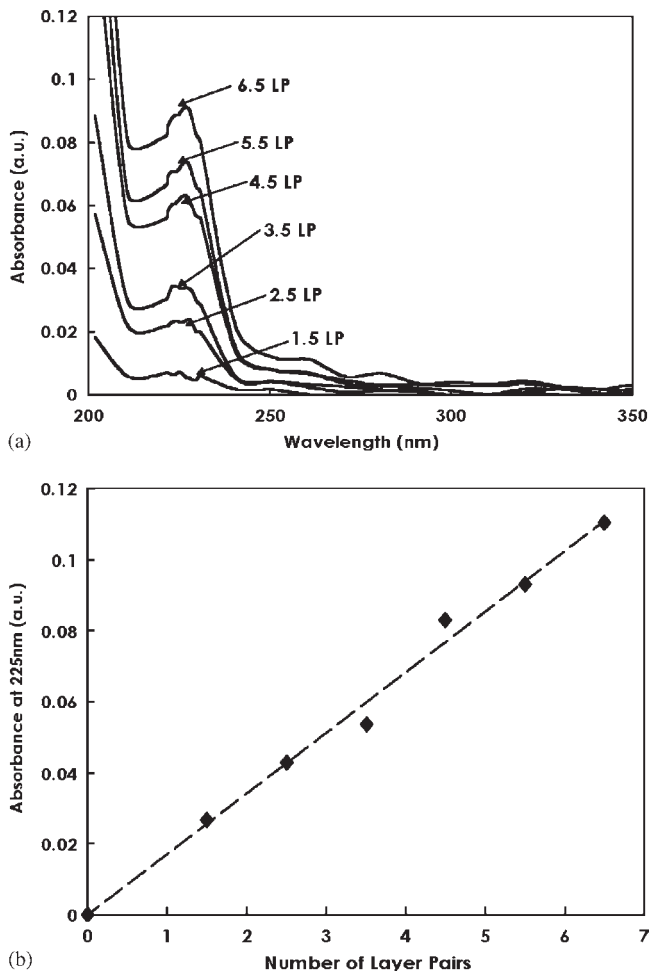


Fig. 4.41 (a) UV-visible absorption for numbers of layer pair (LP) (without absorption-oxidation cycles); (b) absorbance at 225 nm with respect to the number of layer pairs deposited.

of oxides or reduced to form nanoparticles of other compounds [75–79]. For example, nucleation of metal oxide nanoparticles within a nanofilm of polyelectrolyte occurs by cycling the polymer-coated substrates first in M^{2+} and then in NaOH or NH_4OH solution (absorption-oxidation cycles or oxidative hydrolysis cycles). The M^{2+} solution can be prepared in concentrations of 4–40 mM by dissolving an M^{2+} salt (e.g., MCl_2 or $M(NO_3)_2$) in purified water. The solutions of 0.1–1.0 M base are made using purified water. Before cycling, all solutions are vigorously sparged for 45 min with nitrogen gas to remove any dissolved oxygen in solution. In Schlenken tubes, under nitrogen gas, the polymer nanofilm on a substrate can be exposed to the M^{2+} solution for a few minutes. Typical substrates can be quartz, silicon wafers, ZnSe wafers, membranes or more

complex-shaped substrates such as catalytic particles. The substrates are rinsed with degassed and purified water to remove excess ions absorbed in the film, and then exposed to NaOH or NH_4OH solution for several minutes. Substrates are once again rinsed with degassed and purified water and dried completely before the absorption–oxidation cycle is repeated. Figure 4.42 shows that the process of oxidative nucleation and growth can be followed by UV–visible spectroscopy [75]. Figure 4.43 and the nucleation of nickel hydroxide nanoparticles with the number of oxidative hydrolysis cycles is linear. The resulting nickel hydroxide nanoparticles after x cycles are shown in Figure 4.42. Each oxidative hydrolysis cycle nucleates new nanoparticles, while nanoparticles from previous cycles grow in size.

Dante et al. [76] have demonstrated the formation of nanoparticles of akaganéite ($\beta\text{-FeOOH}$) in multilayered polymer films of PDDA and PSS produced by the LbL technique. Ferrous chloride was used as the starting metal ion solution. Uniform, needle-like nanoparticles of $\beta\text{-FeOOH}$ were obtained inside the nanofilm. Transmission electron microscopy (TEM) showed uniform needles with a diameter of 10 nm and a length of 100 nm. Deposition of the nanofilms had to be terminated with the last layer

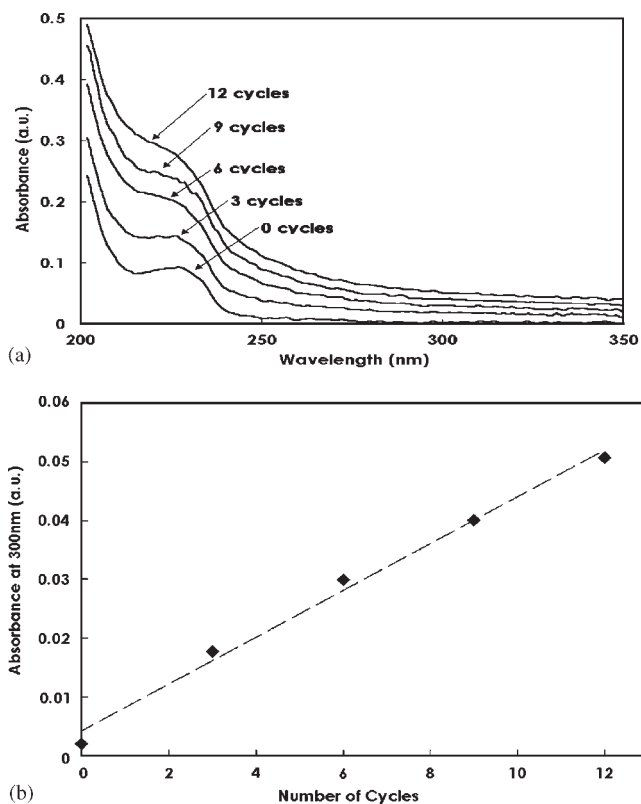


Fig. 4.42. (a) UV–visible absorption spectra for 6.5 layer pairs cycled in a 40 mM $\text{NiCl}_2 \cdot 6\text{H}_2\text{O}$ solution and in 1.0 M NaOH solution; (b) absorption at 300 nm with respect to number of oxidative cycles.

role in determining the structural and morphological characteristics of iron oxyhydroxides, although their chemical compositions are the same.

Nucleation and growth of lead sulfide (PbS) nanoparticles in a PDDA–PSS film produced by the LbL deposition technique has been studied by Dutta et al. [78]. Interest in PbS arises from the fact that it is a semiconductor having a small bandgap (0.41 eV) and large exciton diameter (18 nm) that permits size-quantization effects to be observable even for large-sized particles or crystallites. Moreover, the non-linear optical (NLO) properties of PbS nanoparticles show large differences in their optical limiting behavior below and above the absorption edge suggesting that such systems may be utilized in high-speed switching [79]. Chemical reaction within the polymer film was initiated by Dutta et al. [78] by absorbing Pb^{2+} from an aqueous solution of $\text{Pb}(\text{NO}_3)_2$ followed by exposure of the film to H_2S gas. Electron microscopic examination of the films revealed that while nanoparticles were formed in films that were subject to one or two reaction cycles, large crystallites were formed when these films were exposed to a large number ($N = 10$) of reaction cycles. In the latter case, a broad distribution of particle sizes was observed and may perhaps be attributed to a form of Ostwald ripening occurring during the process. Detailed studies show the nucleation and growth of the PbS nanoparticles into larger crystallites. UV–visible absorption studies reveal that the absorption spectral profiles of the films are dependent on the size of the PbS crystallites. The broadened absorption spectral profile observed for films subject to a large number of reaction cycles may be attributed to the superposition of the spectral profiles of the small clusters that tend to be blue-shifted due to quantum confinement effects and the large clusters that are red shifted. Crystal size can be controlled by the number of cycles. Essentially, a single cycle gives only nanoparticles, which continue to grow in size with more cycles. Instead of using a reducing reaction, it was also possible to oxidize the Pb ions to obtain PbSO_4 particles [78].

Zhang et al. [80] reported the oxidative hydrolysis of Co^{2+} ions absorbed in organized, multilayered, polymer films to form cobalt hydroxide nanocrystals. It was found in this study that using more polymer layer pairs results in more crystal growth. Hydrolysis of the Co^{2+} ions in a nitrogen-rich environment gave rise to mainly needle-like crystallites of $\alpha\text{-Co}(\text{OH})_2$ that were initially about 100 nm in length and then increased in size with the number of absorption–hydrolysis cycles. However, in an oxygen-rich microenvironment, hexagonal crystallites were found to be predominant. X-ray diffraction (SAED) and TEM studies revealed that these hexagonal crystallites were mainly those of $\beta\text{-Co}(\text{OH})_2$. Figure 4.44 shows the transition from the α to β form as observed by TEM by changing the nitrogen-rich environment to an oxygen-rich environment during the absorption–hydrolysis cycles. These studies suggest that by varying the nitrogen to oxygen ratio, the formation of $\alpha\text{-Co}(\text{OH})_2$ and $\beta\text{-Co}(\text{OH})_2$ may be controlled.

Rubner and colleagues [81,82] have further improved the method of Dante et al. [76] by using weak polyelectrolytes such as poly(acrylic acid) (PAA) instead of a strong polyelectrolyte such as PSS. The advantage of their technique is that the linear charge density can be varied with pH. Thus, it is possible to control the charge density of the adsorbing polyelectrolyte and the charge of the previously adsorbed polymer. This technique allows the control of the thickness of the nanofilm, the composition, surface properties and the level of polymer interpenetration. Rubner and colleagues synthesized LbL nanofilms

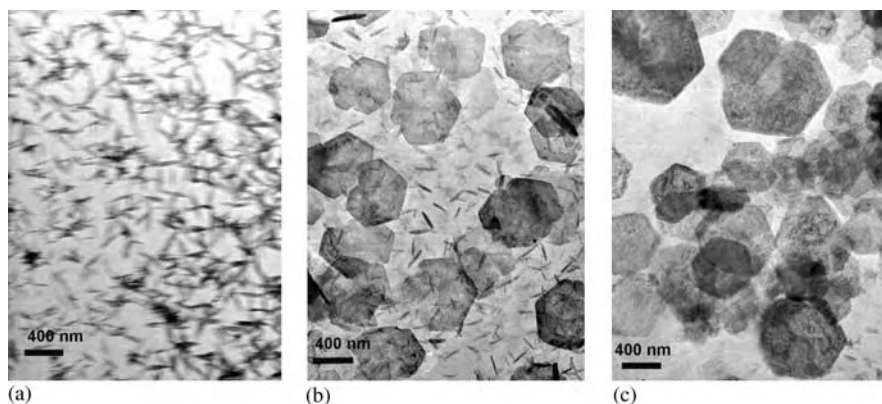


Fig. 4.44. TEM micrographs of a 3.5 layer pair of PDDA-PSS films at different stages of the absorption-hydrolysis process and different atmospheres: (a) two cycles in a nitrogen-enriched environment; (b) four cycles, where after the two cycles in (a) the atmosphere is changed from a nitrogen-rich environment to an oxygen-enriched microenvironment; and (c) eight cycles, where after the two cycles in (a) the atmosphere is changed from a nitrogen rich environment to an oxygen-enriched microenvironment. The concentrations of cobalt chloride and sodium hydroxide solutions were 4 and 10 mM, respectively. The scale bars are 400 nm.

containing silver nanoparticles and semiconductor nanoparticles. They showed that it was possible to stratify the nanofilm in layers with and without nanoparticles. Dai and Bruening [83] used post-reduction of metal ions to obtain ultrathin LbL films of catalytic metal nanoparticles with a size range of 4–30 nm. Recently, Rubner and colleagues [84] nucleated palladium nanoparticles as catalytic seeds for further growth of electroless nickel on the nanoparticle seeds. The size of the seeded nickel nanoparticles could be controlled and up to 14 nm diameter nanoparticles were obtained inside the nanofilms.

The LbL technique of depositing polyions on substrates to build nanofilms of specific thickness, composition and surface charge can be used to carry out nanoreactions inside the ultrathin films to form nanoparticle-polymer complexes. Nanofilms of nanoparticle-polymers are useful in coatings, catalysis, electrical, optical, magnetic, electrooptical and magneto-optical applications. Manipulation of film-type and reaction conditions allows for control of the nanoparticle product, distribution and size inside the ultrathin polymer matrix.

References

- [1] (a) K. Ramanan, Y. Koray, *Curr. Opin. Colloid Interface Sci.* 6 (2001) 464; (b) Y.A. Shchipunov, T.Y. Karpenko, *Langmuir* 20 (2004) 3882; (c) M.A. Osman, V. Mittal, M. Morbidelli, U.W. Suter, *Macromolecules* 36 (2003) 9851; (d) V. Bekiari, P. Lianos, U.L. Stangar, B. Orel, P. Judeinstein, *Chem. Mater.* 12 (2000) 3095; (e) A.B. Morgan, J.W. Gilman, *J. Appl. Polym. Sci.* 87 (2003) 1329.
- [2] (a) Y.C. Ke, Z.B. Yang, C.F. Zhu, *J. Appl. Polym. Sci.* 85 (2002) 2677; (b) Y.C. Ke, *Reports of PET-Inorganic Nanocomposite to CNPC*, 2004, p. 7; (c) Z.N. Qi, Y.C. Ke, Y.K. Ding, *Chin. Pat. Bull. CN 1187506 A*, 1998; (d) C.J. Yan, MS Dissertation, University of Petroleum, China, 2004, 5.
- [3] A. Monnier, F. Schuth, Q. Huo, *Science* 261 (1993) 1299.
- [4] W.P. Cai, L.D. Zhang, *Physics (Chin.)* 26 (4) (1997) 213.

- [5] Y.H. Li, C.M. Mo, L. Yao et al., *J. Phys. Condensed Matt.* 10 (7) (1998) 1655.
- [6] (a) M.D. Dvorak, B.L. Justus, D.K. Gaskill et al., *Appl. Phys. Lett.* 66 (7) (1998) 804. (b) R.S. Shiriitt, *Phys. Rev.* B35 (1987) 8113.
- [7] V. Vendange, P. Colombus, *Mater. Sci. Eng.* A168 (1993) 199.
- [8] Fudan university(Ed.), *Probability Theory*, People's education press, Beijing, 1981.
- [9] (a) P. Dong, *Acta Physico-Chimica Sinica*, 14 (2) (1998) 109; (b) R.Y. Zhao, P. Dong, W.J. Liang *Acta Physico-Chimica Sinica*, 11 (7) (1995) 612.
- [10] S.L. Chen, P. Dong, G.H. Yang et al., *Ind. Eng. Chem. Res.* 35 (1996) 4487.
- [11] Y.C. Ke, T.B. Wu, *Acta Polymerica Sinica*, 2005 (in press).
- [12] Y.C. Ke, *The meeting on the Industrialization of Polymer-Inorganic Nanocomposites*, Beijing, 2004, 4.
- [13] T.B. Wu, Y.C. Ke et al., *Assemble of monodispersed PS and silica particles and the related properties*, *Particuology*, 1 (2003) 247–252.
- [14] Y.C. Ke, *Polymer-Inorganic Nanocomposites*, Chem. Ind. Beijing, 2003.
- [15] P.M. Chaikin, T.C. Lubensky, *Principles of Condensed Matter Physics*, Cambridge University Press, Cambridge, 1995.
- [16] P.G. de Gennes, *Rev. Mod. Phys.* 64 (1992) 645.
- [17] F S. Bates, G.H. Fredrichson, *Phys. Today* 52 (1999) 33.
- [18] A.K. Khanpur, S. Foster, F.S. Bates et al., *Macromolecules* 28 (1995) 8796.
- [19] M.W. Matsen, F.S. Forster, *Macromolecules*, 29 (1996) 7641.
- [20] M.W. Matsen, F.S. Bates, *J. Chem. Phys.* 106 (1997) 2436.
- [21] Y. Mogi, M. Norman et al., *Macromolecules* 27 (1994) 6755.
- [22] T. Goldacker, V. Abetz, R. Stadler et al., *Nature*, 398 (1999) 137.
- [23] T. Goldacker, V. Abetz, *Macromolecules* 32 (1999) 5165.
- [24] E. Helfand, Z.R. Wasserman, *Macromolecules* 9 (1976) 879.
- [25] A.F.M. Barton, *CRC Handbook of Polymer-Liquid Interaction Parameters and Solubility Parameters*, CRC Press, Boston, 1990.
- [26] A.R. Vaia, D.J. Klaus, J.K. Edward, E.P. Giannelis, *Macromolecules* 28 (1995) 8080.
- [27] P.F. Green, E.J. Kramer, *J. Mater. Res.* 1 (1986) 202.
- [28] M. Avrami, *J. Chem. Phys.* 9 (1941) 177.
- [29] M.J. Avrami, *J. Chem. Phys.* 8 (1940) 212.
- [30] Y.C. Ke, C.F. Long, Z.N. Qi, *J. Appl. Polym. Sci.* 71 (1999) 1139.
- [31] Y.C. Ke, *Polym. Mater. Sci. & Eng. (Chin.)*, 20 (3) (2004) 88.
- [32] Q. Li, *Postdoctoral Reports*, Institute of Chemistry, China Academy of Sciences, 1996.
- [33] T-M Wu, C-S Liao, *Macromol. Chem. Phys.* 201 (2000) 2820.
- [34] M.G. Brereton, G.R. Dowies, R. Fakeways, *Polymer* 19 (1) (1978) 17.
- [35] (a) I.H. Hall, M.G. Pass, *Polymer* 17(1976)807. (b) Y.C. Ke, *Chin. J. Chem. Engin.* 6 (11) (2003) 701; (c) Z.N. Qi, Y.C. Ke, Y.Z. Zhou, *Chin. Pat. Appl.* 97104055.9, Vol. 4, 1997.
- [36] B. Wunderlich, *Macromolecular Physics*, Vols. 2-3, Academic Press Inc., New York, 1976, p. 35.
- [37] Y.C. Ke, C.F. Long, Z.N. Qi, *J. Appl. Polym. Sci.* 71 (1999) 1139–1146.
- [38] M. Avrami, *J. Chem. Phys.* 7 (1939) 1103.
- [39] B.Z. Jiang, *International Microsymposium on Polymer Physics*, Guilin, Vol. 12, 1997.
- [40] Y.C. Ke, *Postdoctoral Research Report*, Institute of Chemistry, CAS, 1998, p. 11.
- [41] Y.C. Ke, *Patent Office of China*, Pat. Appl. 01131141.8 (2001).
- [42] J.K. Lu, Y.C. Ke, X.S. Yi, Z.N. Qi, *J. Polym. Sci. Part B: Polym. Phys.* 39 (2001) 115.
- [43] Y.C. Ke, J.K. Lu, X.S. Yi, J. Zhao, Z.N. Qi, *J. Appl. Polym. Sci.* 18 (4) (2000) 808.
- [44] Y. Kojima, A. Okada, *J. Appl. Polym. Sci. Part B: Polym. Phys.* 32 (1994) 625.
- [45] Y. Kojima, A. Usuki, M. Kawasumi, A. Okada, Y. Fukushima, T. Kurauchi, O. Kamigato, *J. Mater. Res.* 8 (1993) 1185.
- [46] Y. Kojima, A. Usuki, *J. Polym. Sci. Part A: Polym. Chem.* 31 (1993) 1755.
- [47] A. Usuki, Kabushiki Kaisha Toyota Chuo Kenkyusho, US4889885, 1989, p. 12.
- [48] Hutton, Jr., *Monadnock Paper Mills, Inc.*, US49201714, 1990.
- [49] J. Rupp, R. Birringer, *Phys. Rev.* B36 (1987) 7888.
- [50] L.D. Zhang, Q.M. Mo, *Nanomaterial Science*, Press of Liaoning science & technology, ShenYang 1994.
- [51] Q. Li, *Postdoctoral Report*, Institute of Chemistry, CAS, 1996.

- [52] S.J. Wang, Q. Li, Z.N. Qi, F.S. Wang, *Chin. J. Polym. Sci.* 8 (1) (1996) 29.
- [53] Y.C. Ke, *China Particuology*, 1 (2003) 247.
- [54] Y.C. Ke, G.F. Yang, D.Y. Zheng, submitted to the proceedings of Inter. Conf. Mater. for Adv. tech. (ICMAT 2005), Singapore 3–8, July, 2005 (www.mrs.org.sg).
- [55] Y.C. Ke, *Chem. Eng. Oil & Gas (Chin.)* 33 (1) (2004) 50.
- [56] G.M. Chen, Z.N. Qi, *J. Mater. Res.*, 15 (2) (2000) 351–356.
- [57] G.M. Chen, Q. Li, Z. N. Qi, F. S. Wang, *Polym. Bulletin (Chin.)* 4 (1999) 1–10.
- [58] J.K. Li, Ph. D. Dissertation, Institute of Chemistry, CAS, 1997.
- [59] R.P. Andres, J.D. Bielefeld, J.I. Henderson et al., *Science* 273 (1996) 1690.
- [60] K. Walsh, S. Mann, *Nature* 377 (1995) 320.
- [61] L.H. Radzilowski, S.I. Stupp, *Macromolecules* 27 (1994) 7747.
- [62] (a) G. Li, L.B. McGown, *Science* 264(1994)249. (b) S.I. Stupp, V. LeBonheur, K. Walker et al., *Science* 276 (1997) 384.
- [63] A. Espic, V.P. Parkhutik, in: J. O. Bockris, R.E. White, B.E. Corway, (Eds.), *Modern Aspects of Electrochemistry*, Plenum Press, New York, 1989 (Chapter 6).
- [64] (a) C. A. Foss Jr., G.L. Hanyak, J.A. Stockert et al., *J. Phys. Chem.* 98 (1994) 2963; (b) C.A. Foss Jr., G.L. Hanyak, J.A. Stockert et al., *J. Phys. Chem.* 96 (1992) 7497.
- [65] H. Masuda, K. Fukuda, *Science* 268 (9) (1995) 1446.
- [66] C.J. Brumilk, V.P. Menon, C.R. Martin, *J. Mater. Res.* 9 (1994) 1174.
- [67] S.K. Chakarvarti, *J. Phys Res.* B62 (1991) 109.
- [68] R. Parthasarathy, K.L.N. Phani, C.L. Martin, *Adv. Mater* 7 (1995) 896.
- [69] G.S. Chen, L.D. Zhang, Y. Zu et al., *Appl. Phys. Lett.* 5(1999) 2455.
- [70] F. Yan, M. Bao, W. Wu et al., *Appl. Phys. Lett.* 67 (23) (1995) 3471.
- [71] Y.H. Li, C.M. Mo, L. Yao, L.D. Zhang et al., *J. Phys. Condensed Mat.* 783 (8) (1998) 4389.
- [72] R. Morino, T. Mizshina, Y. Volagawa et al., *J. Electrochem. Soc.* 137 (7) (1990) 2340.
- [73] G. Decher, in: Sauvage, J.P. (Ed.), *Comprehensive Supramolecular Chemistry*, Pergamon Press, NY, 1996.
- [74] G. Decher, *Science* 277 (1997) 1232.
- [75] A.M. Fojas, E. Murphy, P. Stroeve, *Ind. Eng. Chem. Res.* 41 (2002) 2662.
- [76] S. Dante, Z. Hou, S. Risbud, P. Stroeve, *Langmuir* 15 (1999) 2176.
- [77] A. Dutta, G. Jarero, L. Zhang, P. Stroeve, *Chem. Mater.* 12 (2000) 176.
- [78] A. Dutta; T. Ho, L. Zhang, P. Stroeve, *Chem. Mater.* 12 (2000) 1042.
- [79] V.L. Colvin, M.C. Schlamp, A.P. Alivisatos, *Nature* 370 (1994) 354.
- [80] L. Zhang, A. Dutta, G. Jarero, P. Stroeve, *Langmuir* 16 (2000) 7095.
- [81] S. Joly, R. Kane, T. Radzilowski, A. Wang, R.E. Cohen, E.L. Thomas, M.F. Rubner, *Langmuir* 16(2000) 1354.
- [82] T.C. Wang, M.F. Rubner, R.E. Cohen, *Langmuir* 18 (2002) 3370.
- [83] J. Dai, M.L. Bruening, *Nano Lett.* 2 (2002) 497–500.
- [84] T.C. Wang, M.F. Rubner, R.E. Cohen, *Chem. Mater.* 15 (2003) 299.

This page intentionally left blank

CHAPTER 5

Characterization and Techniques

OUTLINE

- Introduction 276
- 5.1. Particle characterization 276
 - 5.1.1. *Multiple morphology* 276
 - 5.1.2. *Surface morphology* 277
 - 5.1.3. *Particle measurements and statistics* 278
- 5.2. Structure and properties 278
 - 5.2.1. *Theories* 278
 - 5.2.2. *Mechanical properties* 282
 - 5.2.3. *Thermal properties* 283
 - 5.2.4. *Barrier properties* 283
 - 5.2.5. *Other properties* 284
- 5.3. Characterization techniques for structure and properties 285
 - 5.3.1. *Introduction* 285
 - 5.3.2. *X-ray* 285
 - 5.3.3. *Light scattering for particles and molecular weight* 289
 - 5.3.4. *TEM* 295
 - 5.3.5. *AFM* 296
 - 5.3.6. *Scanning Electron Microscopy* 300
 - 5.3.7. *DSC and TGA* 301
 - 5.3.8. *Computer modeling* 302
 - 5.3.9. *Coulter particle size analyzer* 306
 - 5.3.10. *Surface plasmon resonance (SPR) spectroscopy* 306
- 5.4. Multiple structures of nanocomposites 308
- 5.5. Relationship between structure and property 310
 - 5.5.1. *Introduction* 310
 - 5.5.2. *Nucleation and crystallization* 311
 - 5.5.3. *Layer nanostructure* 311
- 5.6. Nanoeffects in nanocomposites 312
 - 5.6.1. *Nanoeffects in thermal behavior* 312
 - 5.6.2. *Nanoeffects in condensed state aspects* 314
 - 5.6.3. *Nanoeffects from assembly and self-assembly* 323
- References 326

In this chapter, the relationship between structures and properties in nanocomposites, their characterization and related characterization techniques are dealt with. This chapter focuses on the nanoeffects in composites of different phases.

Introduction

Characterization of nanostructures is a crucial factor in understanding the structure of nanoparticles in nanocomposite materials. As more and more products based on nanocomposite structures make their entry into the industry, the control of product quality becomes increasingly important. Given that the nanoparticles have an infinite number of morphologies and shapes, their accurate description seems almost impossible. This situation demands that many traditional techniques be used for measuring nanostructures and their properties. Such techniques include X-ray diffraction (XRD) and scattering, light scattering for particle size, morphology and molecular weights, microscopy methods for particle dispersion and multiple structure, dynamic scanning calorimetry (DSC), temperature degradation gravimetric analysis (TGA) and related calorimetry for thermal properties of nanocomposites. When the characterization technique cannot detect the nanoscale structures, computer modeling can be used to predict possible nanostructures.

Particle morphology usually affects particle dispersion in the polymer melt and its final properties. Therefore, particle morphologies should be systematically investigated using different techniques. New phenomena and unique properties resulting from the combination of nanoparticles and polymer matrixes are referred to as nanoeffects, and will be discussed further. Although most of these nanoeffects may not have yet a perfect description, they are introduced here because of their unique position in polymer science and nanotechnology.

5.1. Particle characterization

5.1.1. Multiple morphology

Nanocomposites, generally have multiple morphology, especially nanocomposites with layered silicates. Particle morphology can be classified into roughly three groups. The first group consists of round-shaped structures (a few SEM examples will be given later in this chapter) or fiber-like particles (e.g., TEM image in Figure 5.1). The second group consists of structures of multiple-layered morphology, which are characterized by their interlayer distance (Figure 5.1). The third group is made of assembled or ordered structures. This last group can be seen in the same PET-MMT nanocomposites by TEM characterization.

In Figure 5.1(c), a few regular patterns are seen, which suggest the existence of a long-range order (bright domains) in the direction of 45° to the y -axis. These regular patterns of quenched NPBT are a mixture of PBT polymer crystallites and dispersed layers or clay crystal layers, and reflect a molecular order resulting from the adsorption of polymer chains to the surface of clay.

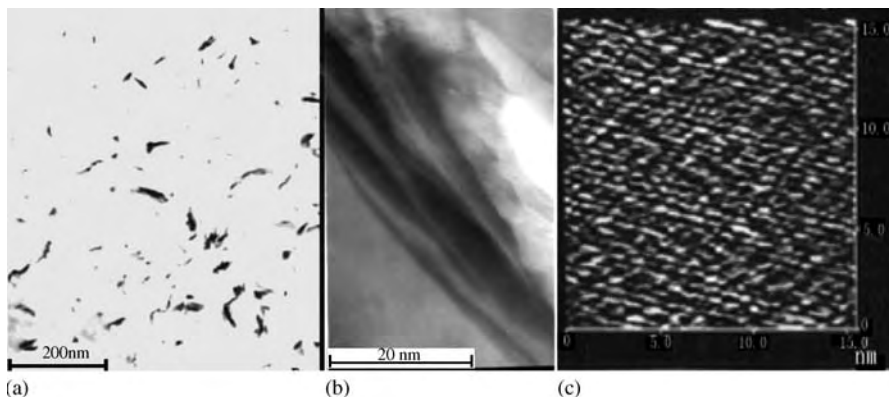


Fig. 5.1. Multiple morphology of polymer-MMT nanocomposites: (a) first morphology, particles with different morphology in PET-MMT nanocomposites; (b) second morphology, particles with layered structure in PET-MMT nanocomposites; (c) Third morphology, particle dispersion and ordered structure in PBT-MMT nanocomposites. (a) and (b) By TEM, (c) by AFM.

5.1.2. Surface morphology

Most silica is of neutral charge, but it is charged in particle form. In silica nanoparticles there are a lot of dangling bonds or unsaturated bonds, which will adsorb opposite charges in solution by Coulombic forces, and form the so-called electrical double layers. Electrical double layers have been described by the Stern model in this book. Similarly, the double electrical layers in nanoparticles of silica are also expressed by the formula [1] $\psi = \psi_0 \exp(-\kappa x)$, where ψ_0 is zeta potential, and is an important parameter in describing the interface state of a nanoparticle suspending system. Further, $1/\kappa$ is defined as the thickness of the double electric layer:

$$1/\kappa \propto Z \quad \text{or} \quad 1/\kappa \propto C^{1/2} \quad (5.1.1)$$

where Z is the atomic valence and C the concentration of the strong electric analytes. This mathematical relation shows that highly concentrated solutions of ions of high valence will have thin double electric layers. In describing the interface between nanoparticles, two new models are widely used as follows:

(1) *Model of the interface order.* In nanomaterials and nanocomposites, the atoms are in order or have an ordered structure in the interface region. In this book, various ordered structures for particles in solution under the induction of liquid crystal state, spinodal phase decomposition and particle nucleation do not possess an ordered structure at the interface. All these structures can be investigated by high-resolution transmission electron microscopy (HRTEM), and ultrafine X-ray scattering techniques.

(2) *Model of the interface.* The interface of nanomaterials or nanocomposites does not normally have a single type of arrangement, but has multiple morphologies.

For example, nanoparticles may organize into nanoparticles assemblies inside pores. In this case, the ordered interface structure can have both hydrophilic and hydrophobic properties.

5.1.3. Particle measurements and statistics

Two kinds of distribution diagrams can be plotted in particle measurements and statistics, one of which is called the particle size–volume distribution curve, and the other the particle number–volume distribution curve. In our investigations, frequency distribution of particles and the accumulation distribution of particles based on TEM morphology statistics are used. In TEM measurements, the particles with different shapes are modeled as spherical particles. For example, we take the following equation to express the size of different particles:

$$D_{\text{avg}} = \left(\sum_1^n d_i/n \right) k_i$$

where D_{avg} is the average value, n the total numbers of particles, d_i the different size parameters of the particles and k_i are the correction coefficients. When D_{avg} is obtained, it is used to plot the frequency–log particle size curve [2] and accumulation density–clay particle size curve as shown in Figure 5.2.

5.2. Structure and properties

5.2.1. Theories

Theories related to the structure and properties of nanocomposites are used to reveal new phenomena, mechanisms, processes and effects. At the present time, these basic

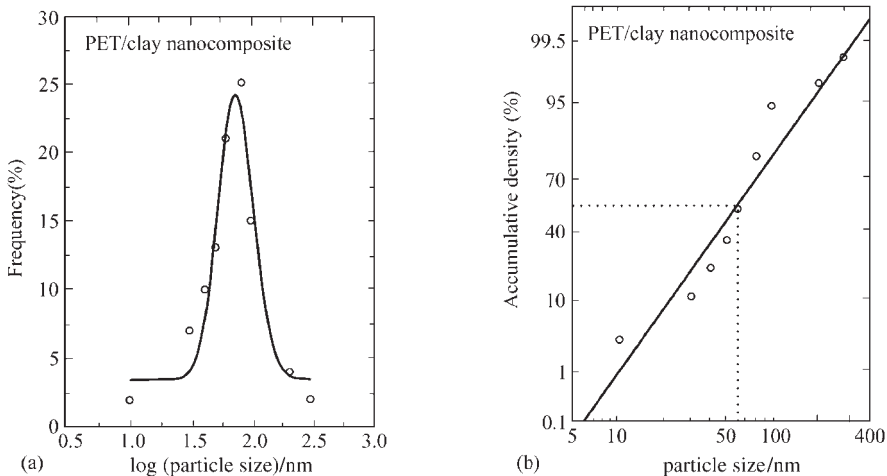


Fig. 5.2. Examples of the distribution curves of the (a) frequency and (b) accumulation distribution of particles. (With the permission of John Wiley in the article, Y.C. Ke, Z.B. Yang, C.F. Zhu, *J. Appl. Polym. Sci.*, 85 (2002) 2677–2691)

aspects related to nanoparticle science are still not systematically studied. Therefore, the existing relationships related to micrometer size particles are usually used for nanoscale characterization. For example, in many cases, the impact strength is not enhanced in nanocomposites but reduced, and this issue is still open to debate. To better understand and properly design new systems of nanocomposites with overall enhanced properties, the Halpin-Tsai [3] equations for designing composites with different shapes are introduced. This theory describes how to obtain isotropic properties from an anisotropic system. The composite module for a two-phase system is expressed here. The shape factor ζ of inorganic phase added to the polymer matrix stated in the Halpin-Tsai equation is in the form

$$P/P_m = (1 + \zeta\eta\phi)/(1 - \eta\phi) \tag{5.2.1}$$

where $\eta = (P_f/P_m - 1)/(P_f/P_m + \zeta) = (M_R - 1)/(M_R + \zeta)$, P is the modulus (property) of composites, P_f the modulus of the inorganic phase (e.g., fiber), P_m the modulus of the pure matrix, ζ the shape factor of the inorganic phase and ϕ the volume fraction of inorganic fillers. Depending on the inorganic fillers, several forms of the above equations are obtained.

For very rigid particles, $\eta = 1$,

$$P/P_m = (1 + \zeta\phi)/(1 - \phi). \tag{5.2.2}$$

As for layers of MMTs, ζ is the aspect ratio ($=L/R$), where L is a length of the layered filler, e.g., layer of MMTs and R is its radius. The plot of P/P_m vs. ϕ is shown in Figure 5.3 for a fixed ζ . As shown in the figure, when ϕ decreases, the curves move toward the direction of the arrow and finally approach a line with a slope of ϕ .

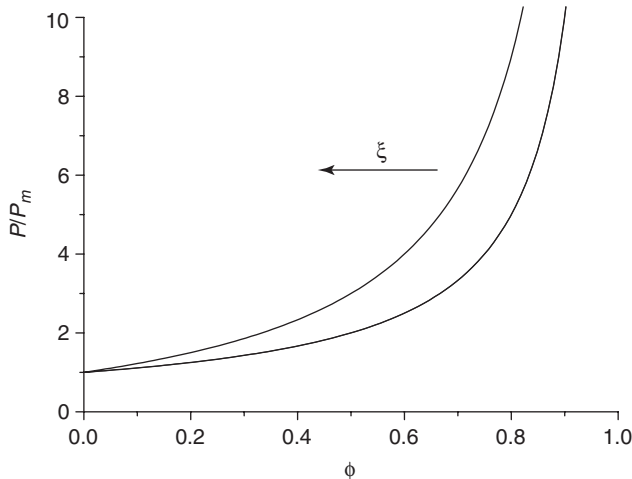


Fig. 5.3. Plot of P/P_m vs. ϕ .

For continuous fiber reinforcement, $\zeta = \infty$, and this gives the formulae.

$$P = \phi P_f + (1 - \phi)P_m \quad \text{or} \quad P/P_m = \phi(P_f/P_m - 1) + 1. \quad (5.2.3)$$

The Halpin-Tsai equation 5.2.1 is in the same form for discontinuous layers or lamellae-shaped reinforcements. According to these equations, the volume fraction (ϕ) and the filler's shape or morphology (ζ) are the key factors the modulus of composites.

5.2.1.1. The modulus

Eq. (5.2.1) can be applied to predict the modulus (property)–MMT load relationship in nearly all types of polymer–MMT nanocomposites, e.g., in polyurethane–MMT nanocomposites. The composite modulus vs. MMT load graph shown in Figure 5.4 confirms the similarity between the experimental curve and that obtained from theoretical prediction.

5.2.1.2. Heat distortion temperature

The heat distortion temperature (HDT) of composites is closely related to the modulus of composites, i.e., $\text{HDT} \propto E_c$ (composite modulus). For micrometer particles, the Halpin-Tsai equation is used to predict the modulus and HDT of the composites, especially for composites with $\phi \geq 20\%$ (by vol). For example, the HDT of PBT reinforced by very high load (60%, by wt) of glass fiber filler can surpass 300°C (test at 1.84 MPa, data and products from “Polymer Resources Inc.”), while nanocomposites cannot reach such a high HDT. However, nanocomposites can provide a new raw resin for further modification. The HDT of nanocomposites is generally different from that of blending materials reinforced by fillers. As reported for most of the polymer nanocomposites with clay, the clay load is usually rather low (e.g., less than 10%, by wt), but they significantly affect nanocomposite moduli such as the HDT.

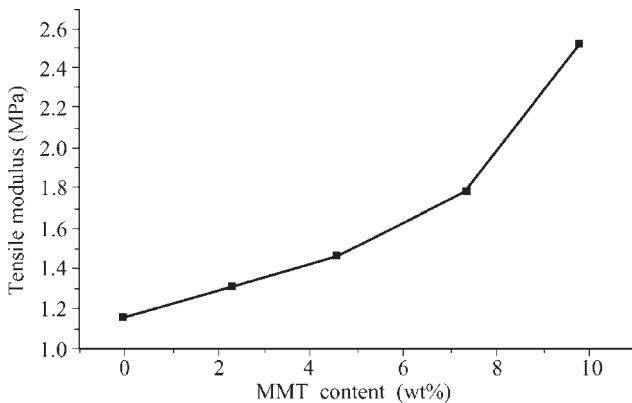


Fig. 5.4. Plot of tensile modulus vs. MMT load content.

On the other hand, for high clay loads (10% or more by wt), some of the clay without complete exfoliation will form discontinuous filler rather than nanoparticles. Therefore, the same clay will have different morphology or shapes (ζ) in the nanocomposites. This morphology will be related to the nucleation of particles, and will directly affect the molecular conformation. Additionally, there is a close relationship between the HDT properties and the polymer chain rigidity. Computer modeling results and previous literature [4] have shown that the polymer chains near the particle surface possess a higher density and/or rigidity than those far away from the surface, which results in the enhancement of HDT of PBTs [5–7]. Figures 5.5 and 5.6 show that the

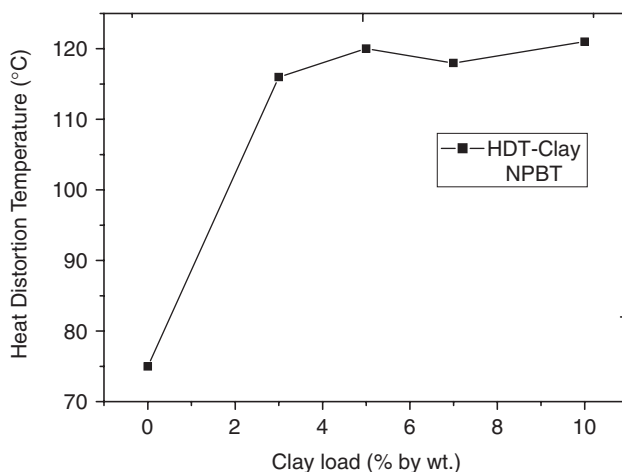


Fig. 5.5. Plot of HDT vs. clay load for PBT-MMT (clay) nanocomposites (NPBT).

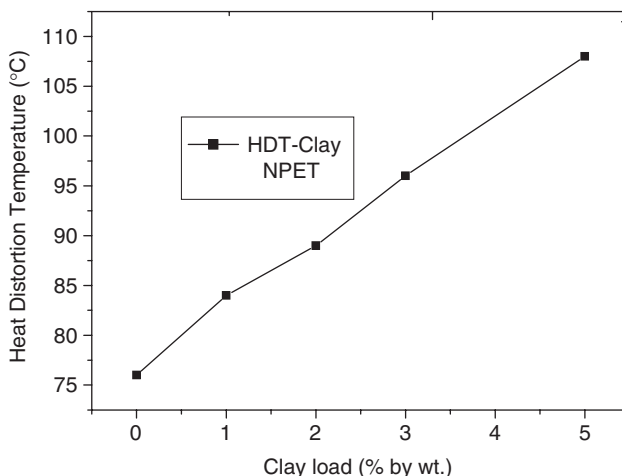


Fig. 5.6. Plot of HDT vs. clay load for PET-MMT (clay) nanocomposite (NPET).

HDT value of the nanocomposites increases as ϕ increases, which is also consistent with the prediction given by the Halpin-Tsai equation. Thus, the filler effect of clay on the HDT is significant.

5.2.2. Mechanical properties

The mechanical tests and measurements are usually related to existing standards. Although there are no such standards for nanocomposites, their mechanical properties are obtained by referring to the ones for pure polymer matrix. For example, the flexing (bending) and breaking strength measurements of a given nanocomposite are performed according to ASTM 790, while their notched izod impact strength is obtained according to ASTM D256.

Typical plots of mechanical properties vs. clay load for PET-MMT nanocomposites are shown in Figure 5.7. Bending strength decreases as the amount of MMT clay increases, while the modulus of the nanocomposites typically increases as clay load increases. Both of these trends are also seen in other types of polymer–clay nanocomposites. The mechanical behavior presented in Figure 5.7(a) is not easily explained, but is thought to result from the separation of inorganic phase from the polymer matrix due to the incompatibility at molecular level and compatibility between polymer and nanoparticles. Therefore, new theoretical approaches to nanoscale mechanisms emphasizing the interface compatibility are needed to guide the design of nanocomposites.

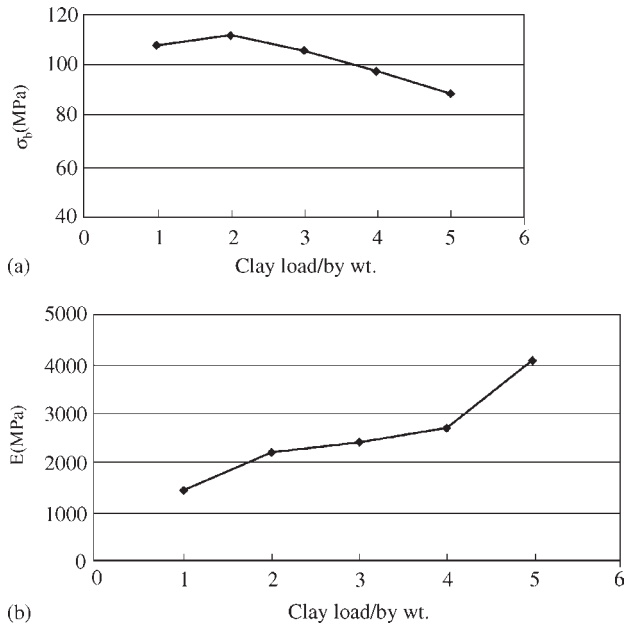


Fig. 5.7. Mechanical properties vs. concentrations of clay load of PET-clay nanocomposites: (a) bending strength (σ_b)–clay load; (b) Young's modulus (E) – clay load.

5.2.3. Thermal properties

5.2.3.1. HDT

HDT is an important parameter for evaluating nanocomposite materials subjected to mechanical force under certain temperature conditions. In order to determine the HDT, nanocomposite samples should have the standard dimensions of 120 mm × 10 mm × 12 mm size according to GB-1634-79. In practice, polydialkylsiloxane is used as the medium (referred to as ASTM D648). Data are obtained under exerted pressure. The usual pressure exerted is 1.84 MPa. The final result is the average of two samples measured at the same time.

5.2.3.2. Thermal behavior due to nanoparticles

Nanoparticles do not only exert a confinement effect on the molecular chains inside the interlayer space, but also produce a thermal shielding effect by cross-linking. The degradation temperature of NPET is usually higher than that of PET although their thermal degradation behavior is similar.

The most intense nanoeffect of polymer–clay of MMT nanocomposites is the increase in HDT (Figure 5.8). At low loads, the thermal degradation temperature increases 30°C or more than that of pure PET.

It can be seen that the high surface energy of nanoparticles causes a reduction in the melting point of NPET. The surface effect will produce smooth surfaces of the final products, and improve its process performance. Additionally, other factors such as the type of treating reagents, their chain length and polarity and the treating method, affect the increase in the HDT of the nanocomposites (Figure 5.9).

5.2.4. Barrier properties

Silica particles dispersed in the polymer matrix have barrier properties that allow them to prevent gas permeation. Lowered gas permeation will protect the materials inside the

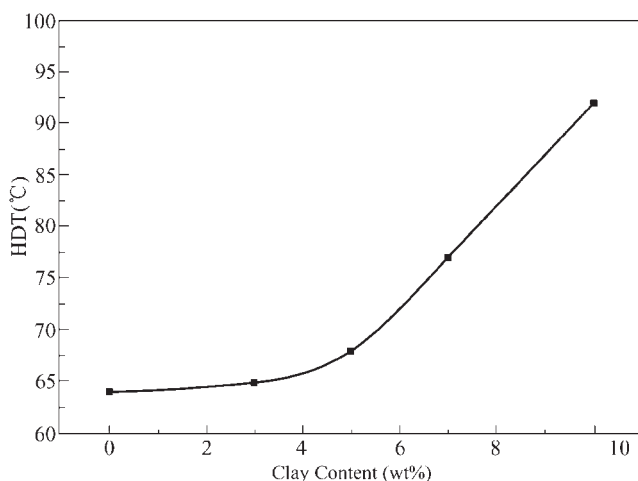


Fig. 5.8. HDT vs. the clay load for PP by melt intercalation with MMTs.

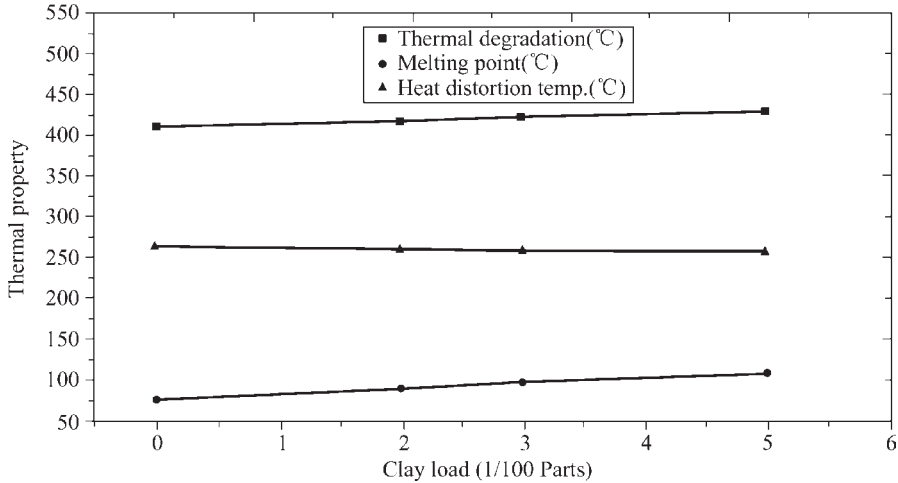


Fig. 5.9. Plot of thermal properties (T_d , T_m , HDT) vs. the clay load.

package of nanocomposites from being degraded by oxygen and other foreign gases. But silica particles are not always the best choice for effectively stopping gas permeating into materials used for packaging. Results show that a silica load of up to 5% (by wt) does not sufficiently lower the effective barrier properties to protect against oxygen gas. Recently, polyesters filled with MMTs have been shown to have better barrier properties against oxygen. Among nanocomposites PET–MMTs, PETG–MMTs and PEN–MMTs, the best results were obtained for PEN–MMTs. These nanocomposite films improved the barrier properties by reducing the oxygen permeability to one-third of its original value. Similarly, different intercalation agents affect the barrier properties. Results have shown that octa alkyl quaternary ammonia is the poorest in stopping oxygen from penetrating into composites, while diethyl oxy octa-alkyl ammonia is the best intercalant used in barrier materials. These basic resins easily become yellow because of the instability of the MMTs. In practice, MMTs are usually replaced by nanoparticles such as ZnO, TiO₂ or nanocomposite particles such as ZnO/SiO₂, SiO₂/Al₂O₃, SiO₂/Co₂O₃.

5.2.5. Other properties

Rheological properties of the polymer matrix are improved if there is complete exfoliation of the layer structures. For example, if the nanocomposites of PS–MMTs, (MMTs treated with an oligomer PS) are melt-sheared, the result is the complete exfoliation of the layer structure, as revealed by TEM. These nanocomposites usually have a viscosity at high shearing rate lower than that of the pure counterpart, which makes the surface of the final product smooth and bright (discussed in Chapters 3 and 4). Nowadays, ARES equipment (advanced rheometric expansion system) is used to measure the behavior of complex viscosity–shearing rate relationships, and can be used to measure a unique phenomenon such as thinning-by-shearing in rheological behavior of nanocomposites. For example, the rheological properties of PA6–MMT nanocomposites are better than those of PA6 itself at

high shearing rate, as measured by capillary rheometers. Rheological measurements show that nanocomposites have improved processing properties over pure polymers.

5.3. Characterization techniques for structure and properties

5.3.1. Introduction

The structure of nanocomposites comprises interfaces, crystals, polymorphism, nanostructures, multiple phases and nanoparticles and their distribution. Nanoparticle interactions with the polymer matrix, morphologies and multiple phases are the main objectives of structure investigations, and these factors are closely related to the properties of the nanocomposite. Nanoparticles are either spherical or non-spherical. The size of the spherical-like particles is given by their diameter. The size of monodisperse silica particles (SiO_2) is their diameter. The size of non-spherical particles is often expressed by a representative spherical-like particle. Such a measurement or expression method is called relative quantity of diameters [8]. For two-dimensional layered structures with spherical-like morphology, the relative quantity of diameters is not usually used. The particles are expressed by statistics of the average scale of the layer-like particles, or expressed by projection diameters using TEM techniques. Usually, the Feret and Krumbein diameter [8] is used to express particles without spherical shape. The Feret diameter refers to the separation between two parallel lines of a particle's projection. The Krumbein diameter, also called the maximum diameter in a definite direction, refers to the maximum project length of a particle in one direction. It is worth mentioning that spherical- and non-spherical-like morphologies are often relative. Depending on the technique used to characterize the particles, the same particles may have different shapes. The most obvious examples are SEM and TEM techniques. The layered silicate particles of MMTs are round spheres when observed by SEM, and the same particles are fiber-like when observed by TEM.

There are several characterization techniques to determine nanostructures and morphologies. With the rapid development of both nanotechnology and nanomaterials, the corresponding techniques for nanostructure characterization are also rapidly being upgraded. For example, dynamic laser scattering equipment can measure the average diameter and size distribution of particles sized 1–1000 nm. Automatic analysis equipment for microparticles (e.g., the Coulter Counter) can measure particles of 0.1–10 μm along with their mass distribution and average particle size or diameters. Microscopy with electroswimming devices can measure particles of 0.1–10 μm , their charge distribution and zeta potential. Companies such as Malvern and Brookhaven make nanoparticle measurement equipment. Traditional equipment such as rheometers can also be used to obtain information about nanocomposite properties. Interfacial tension equipment can be used to measure the surface tension and obtain information on the nanostructure of molecules at interfaces.

5.3.2. X-ray

5.3.2.1. Crystallite size and the Bragg equation

(1) *Crystallite size.* XRD is the usual method for measuring the structure of layered silicates. In X-ray measurements, the diffraction peak position, half-width and identification

of peaks are the main parameters used to describe materials. The X-ray data are also used to calculate other parameters such as the size of crystallites, crystallization degree, inter-layer distance, etc:

$$D = C\lambda/B \cos \theta \quad (5.3.1)$$

In the above equation, D is the size of the crystallites, λ the X-ray wavelength in XRD experiments (usually, the line of the radiation in metallic copper is used), C a constant ($C = 0.89$), 2θ the diffraction peak position, and B the widening degree of half-width of XRD curves. $B^2 = B_M^2 - B_S^2$, where B_M is a widening factor of experimental measurements in half-width of diffraction curves and B_S is a widening factor of the equipment itself ($B_S = 0.1-0.15$). In order to obtain an accurate B value, the peak position for measuring B_S values should be as close as possible to the position of B_M . When the size of the crystallites is less than 100 nm, the widening effect on the peak due to the crystallites themselves is significant. Under such circumstances, the calculated results of widening data should be carefully analyzed.

(2) *Bragg equation.* The Bragg equation is used to calculate the parameters of the crystal lattice and has the form of

$$\lambda = 2d \sin \theta \quad (5.3.2)$$

where d is the separation of unit crystal layers or planes. For layered compounds or silicates, d is the interlayer distance. The other parameters in Eq. (5.3.2) have the same definitions as in Eq. (5.3.1).

Example 5.3.2.1. Calculation of interlayer distance. A sample of layered silicate of MMT containing some water has an XRD peak at 7.5° . The MMT is further treated or intercalated with dodecyl-alkyltrimethyl chloric ammonia by a cation exchange reaction, which gives a treated MMT sample with XRD at 15° . The variation of the inter-layer distance for MMT before and after intercalant treatment is calculated as follows:

$$\begin{aligned} 2\theta = 7.5^\circ, \quad \lambda = 0.1542 \text{ nm}, \quad d_1 = \lambda/2\sin\theta = 1.18 \text{ nm} \quad (\text{Before treatment}) \\ 2\theta = 15^\circ, \quad \lambda = 0.1542 \text{ nm}, \quad d_2 = \lambda/2\sin\theta = 5.89 \text{ nm} \quad (\text{After treatment}) \end{aligned}$$

The difference of the interlayer distance before and after intercalant treatment of MMT is

$$\Delta d = d_2 - d_1 = 5.89 - 1.18 \text{ nm} = 4.71 \text{ nm}.$$

The Bragg equation based on XRD patterns is generally used to detect layer expansion of MMTs in nanocomposites. Let us consider a nanocomposite of epoxy resin with clay, as an example. The epoxy resin and 7% (by wt.) organo-clay load are mixed together at 225 and 235°C for different time intervals, and then the curing agent tetrahydro phthalic anhydride (MeTHPA) and accelerator of *N,N*-benzyl dimethyl amine (BDMA) are

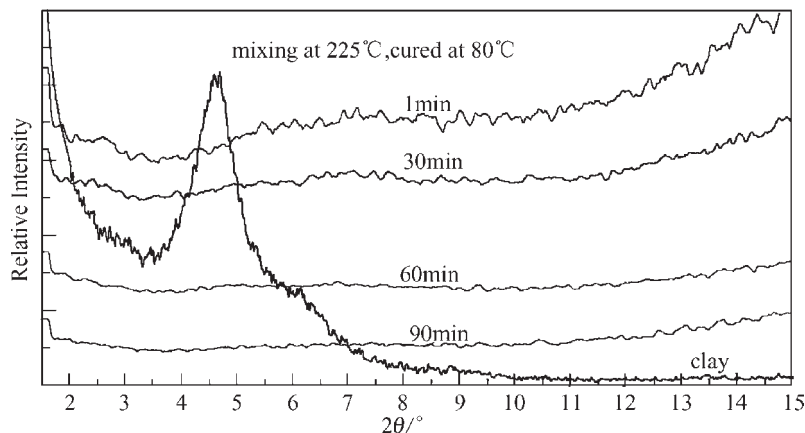


Fig. 5.10. XRD of nanocomposites of epoxy–clay (7%, by wt.) mixed at 225°C for different time intervals and cured at 80°C for 2 h.

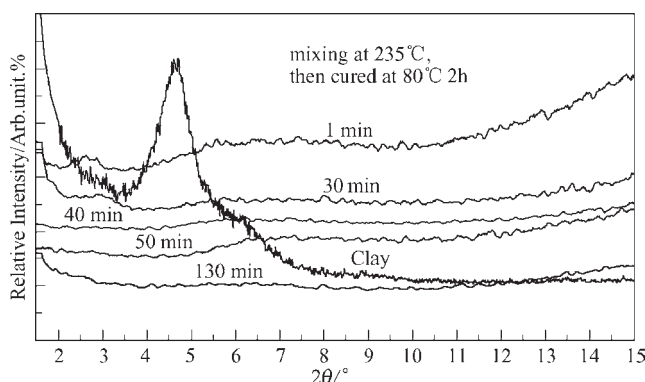


Fig. 5.11. XRD of nanocomposites of epoxy–clay (7% by wt.) mixed at 235°C for different time intervals and cured at 80°C for 2 h.

added for curing at 80°C for 2 h. The X-ray spectra for these nanocomposites are shown in Figures 5.10 and 5.11.

In this case, if the mixing time at 225°C is less than 60 min, only the intercalated composites are obtained after curing (the residual diffraction peak of d_{001} still exist), but their layers can be completely exfoliated. When the mixing time is 60 min or more, there is no residual d_{001} diffraction peak. If the mixing temperature increases to 235°C, complete exfoliation of the nanocomposite is obtained when the mixing time is shortened to 40 min. In particular, when mixing is performed at any temperature between 180 and 260°C, followed by curing at 80°C for 2 h, the critical mixing time will always be found. The clay will be completely exfoliated when mixing takes longer than the critical time; otherwise, only an intercalated mixture can be obtained. The results show that the mixing time has a critical effect on the layer exfoliation of the nanocomposites.

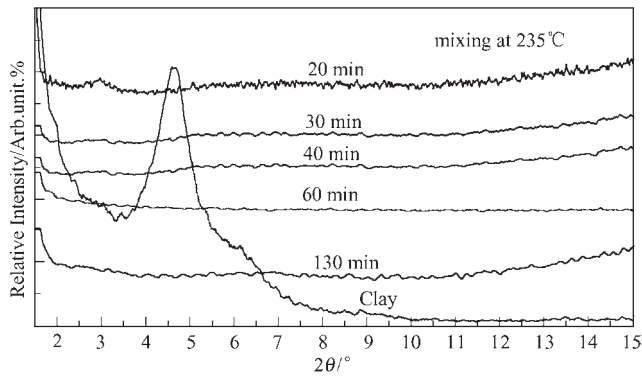


Fig. 5.12. XRD patterns of nanocomposites of epoxy–clay (7% by wt.) (sample preparation conditions: mixing at 235°C for different times, curing at 80°C for 2 h, and again post-curing at 160°C for 3 h).

At temperatures lower than 80°C, the curing process is not complete. Therefore, the post-curing process is necessary to spread and activate the curing epoxy molecules. Both the curing process and its measurements are very important for practical applications. There is the question of whether or not the epoxy molecules penetrate into the interlayer gallery of clay during the post-curing process, causing the layers to swell. To answer this question, the factor of curing time is taken into consideration. Results have shown that the critical mixing time is shortened for clay layer exfoliation during the post-curing process as shown in Figure 5.12.

Mixing conditions (e.g., mixing time and temperature) have a significant effect on organo-clay intercalation and exfoliation, which is influenced by the gelation time of the epoxy resin's at curing. In epoxy–clay systems, the transition from intercalation region behavior to exfoliation region takes place under specific mixing conditions, which are optimized by considering the three factors of mixing: temperature, time and gelation transition. In practice, to obtain complete exfoliation of PEO-based nanocomposites, the mixing temperature and time for a selected epoxy should be chosen within the “liquid–solid transition” area of the exfoliation curve from experimental data. It is worth mentioning that the mixing temperature should not be too high because the mixture becomes too viscous. On the other hand, the temperature of the mixture should not be too low and the mixing time should not be delayed too long. Generally, mixing at 200–235°C is the best condition for the nanocomposite of epoxy resin/organo-clay. The effect of an organic agent on the layer exfoliation of epoxy–clay nanocomposites will be dealt with further.

Example 5.3.2.2. Polymorphism peak induced by MMT layers. In nanocomposite samples, polymorphism peaks are often observed, [10–11] which reflect a polymorphism transition. In Figure 5.13, nylon6–MMT nanocomposites have exfoliated layers and induce a polymorphism peak at $2\theta = 21.7^\circ$, which is a λ -form crystal.

In another layered silicate–PBT nanocomposite, the X-ray patterns also show abnormal diffraction at 2θ positions larger than 30° . In “as-polymerized” samples of NPBT

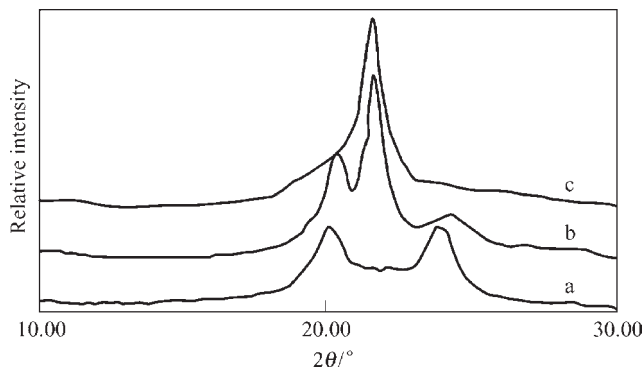


Fig. 5.13. λ -form crystals in nylon6–MMTs nanocomposite induced by MMT layers: nylon6; (b) nylon6-MMT (annealed); (c) nylon6-MMT (not annealed).

and PBT, the NPBT annealed at different temperatures for 30 min show a crystal form transition. The two peaks with their locations of $2\theta > 30^\circ$ are transitional due to the crystallization temperature and layered platelets of MMTs.

5.3.2.2. X-ray crystallization degree

XRD patterns were obtained on a Rigaku D/MAX/2400 X-ray diffractometer; the Cu $K\alpha$ radiation light is used. In this measurement, the scanning rate depends on the requirements of the data collection, usually ranging from 1° to 3° min^{-1} . In many measurements by X-ray techniques, the crystallization degree is an essential parameter to describe the crystallization behavior and state of polymer-based nanocomposites due to exfoliated layers or dispersed particles. The crystallization degree (X) equation for XRD is shown as follows:

$$X(\%) = W_a / (W_a + W_c) \times 100 \% \quad (5.3.3)$$

where W_a and W_c are weight fractions of the amorphous and crystallized parts, respectively, in the whole semi-crystallized nanocomposite [9]. So far, the two-phase model (amorphous and crystallized) is usually used to calculate and investigate the crystallization degree of samples.

5.3.3. Light scattering for particles and molecular weight

5.3.3.1. Laser scattering for particles

In many statistical methods, particle size is a key parameter. When superfine particles are measured by laser scattering, they are usually dissolved in solvents. In these media, the particle size measured is not the “true size” of the particles because the size measured by laser scattering includes both the inorganic (in the core) and the organic (in the shell) parts. The core stands for the real size of the particle, but the laser scattering method usually gives the size of both core and shell, or core–shell. This shell size cannot be accurately determined so far. In this book, the particle size is referred to as the core–shell structure. The particle size with “core” and “shell” is shown in Figure 5.14.

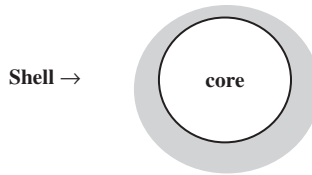


Fig. 5.14. The core-shell of superfine particles in media.

The real shape of particles in media (e.g., H_2O) takes at least three forms of core-shell structure, i.e., non-round, round and non-circular shell shapes. In measuring particle size, a dispersing agent is necessary to create a homogeneous system. The dispersing agent will prevent particles from aggregating during the measurement of the system.

5.3.3.2. Principles of light scattering and optical omitting

(1) *Principle.* In this technique, particle size (or diameter) is measured or determined by measuring the intensity of the scattering light, vibrations of particles and quantity of light, or light intensity. In modern equipment, a large area detector is used for small particles with large scattering angle and a small area detector for large particles with small scattering angle. The area of detectors is designed to be inversely proportional to the intensity of the scattering light of particles. Usually, detectors are arranged at forward angles (Malvern [12]). Once the light scattering has been measured, it is necessary to calculate the particle size distribution. This is done by mathematically fitting the data using optical scattering theories. Theories that analyze data for particulate materials are based on the Mie theory. Early laser diffraction systems with limited optical configurations could not make use of the Mie theory and used approximations or subsets of this theory such as Fraunhofer's approximation. Fraunhofer's approximation assumes that the particles are opaque discs (similar to a coin) and all light is scattered around the particle. Fraunhofer's approximation gives good results if the particle size is greater than about $50\ \mu\text{m}$. For particles smaller than about $50\ \mu\text{m}$, the Mie theory offers the best solution. In this method, the light energy is plotted against the particle size and light-scattering angle. The particles' size and distribution are determined by calculation of the scattering angle distribution, which varies as the particles size varies.

(2) *Sources and light decay.* In laser scattering equipment, the laser beam goes through a group of prisms and its light from a He-Ne laser source is enlarged into parallel light with a diameter of about 8 mm. The laser beam penetrates the particle aggregates and creates diffractions. A multi-electronic detector is placed in a post-focus plane of a Fourier transforming prism (the receiver). Inside the receiver there are six groups of prisms arranged at different focus distances. In measuring large-size particles, a long focus distance is used. The optical-electrical detector is made of 30 concentric semi-circles, which record the light passing quantity of the diffraction pattern within the focusing plane.

The latest laser scattering equipment can measure particle sizes from 0.002 to 2000 μm . Light decay is used to measure the particle size by measuring the particle groups

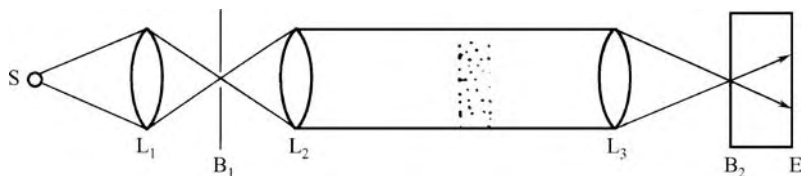


Fig. 5.15. Sketch map of optical decay road.

light scattering and the light intensity decay after it is absorbed by particles in the incident direction of light. In light decay, the optical road map is shown in Figure 5.15.

In the Figure 5.15, monochromatic light with an intensity I_0 and wavelength λ originates from light source S , becomes a strip of parallel light by a focusing prism L_1 and diaphragm B_1 and becomes quasi-straight at L_2 . The laser S is of high intensity and monochromatic. The parallel light penetrates gas or liquid solutions with dispersed particle groups, and, in turn, goes through prism L_3 and light B_2 ; finally, optical–electrical detector E receives it. The principle for the light transmitting process is described by the Lambert–Beer equation

$$\ln(I_0/I) = nKaL \text{ or } G = \lg(I_0/I) = (\lg e)nKaL \quad (5.3.4)$$

where G is the optical density or light decay, I the intensity of penetration light, I_0 the intensity of empty light, L the thickness for a light going through the sample region, n the particle number, a the area of particle facing light, K the coefficient of particle decay, which is related to the refractive relative rate m to the media and also the particle size parameter. As for particles with diameter size equal to D , and with concentration C (or overall particle weight for each unit volume),

$$G = (\lg e)3CK1/2D\rho. \quad (5.3.5)$$

For monodisperse particle groups and the measurement of their light decay G , the particle's diameters are calculated from a wavelength of λ , light decay coefficient of K and diameter of D under refractive index of m .

The advantages of light scattering and light decay are high speed, easy-to-realize optical–electrical transformation measurements and automatic analysis of data. Light scattering has wide applications in the measurement of nanoparticles.

(3) *Factors affecting final results.* There are several factors affecting the measured results.

(a) *Sampling.* The suspending solution of layered silicates of clay is sticky. This makes sampling difficult. To correct the final results, we usually mix the samples from the reaction in a bowl, sample randomly from any part of the bowl, and place the sample in the solution with matched surfactants. In the case of a dry powder sample, one uses the riffle sampler, by which the samples of large and small particles are mixed homogeneously in the sample trays. The sampling process also gives a homogeneous sample.

(b) *Media*. Selection of the proper media for wet particle measuring is often one of the key factors determining the final result data. For example, in deionized water, the zeta potential for $\gamma\text{-Al}_2\text{O}_3$ is -80 mV, while it is -20 mV in tap water. To obtain consistent results, the media used for measuring most oxide particles is deionized water.

To measure sticky systems, the solution is designed as a mixture of water and surfactant or a microemulsion of water with oxidized ethylene ether. Polyoxide ethylene such as, NP_x ($x = 4, 6, 8, \dots$) is often used.

(c) *Morphology or state*. In some cases, material in the dry state is used to measure the final distribution. However there are limitations, such as the material to be measured should not be sticky (e.g., layered silicate of clay, of montmorillonite, kaolinite, etc.). The material size to be measured should neither be too large for easy free flowing, nor too small (e.g., $< 1 \mu\text{m}$ for SiO_2 , TiO_2).

When a material is unsafe, poisonous or explosive when exposed to air, it should not be measured by the dry method. The shape or state of the measured particles can affect the final results. Most particles are all not round, and mixtures are of different sizes and shapes, such as disc-, fiber-, and sphere-like. Under such conditions, we suppose that TEM is the best method to characterize the particle structure and its dispersion because it can resolve particle morphology and give correct statistical results.

(d) *Stability*. In measuring ultrafine particles, the suspension's stability is the main condition for obtaining correct size data. To obtain stable systems, the common method is dispersing with ultrasound. The technique is successful for some particles with micrometer size and non-sticky properties, such as silica. However, it is an absolute failure for layered silicates of clay such as MMT particles, attapulgite particles, etc. An example is shown in Figure 5.16, where TiO_2 particles in deionized water are measured in the Malvern mastersizer analyzer. Different particle dispersion patterns have been seen during different measuring times.

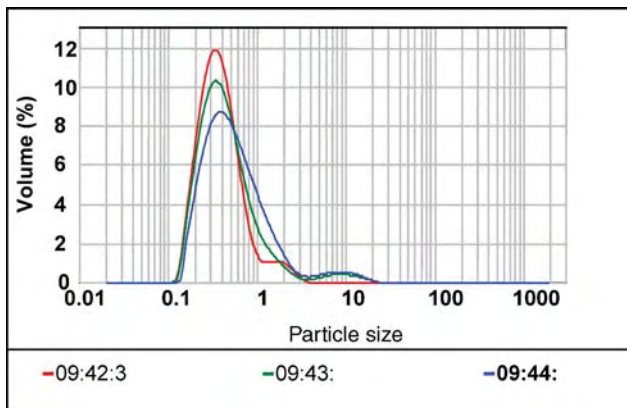


Fig. 5.16. The dispersion pattern of TiO_2 particles dispersed with ultrasound in deionized water for different time intervals as measured with the Malvern mastersizer analyzer: times are given in h:min:s. Particle size in μm . (With the permission of Malvern Co. in the specifications attached with the equipment.)

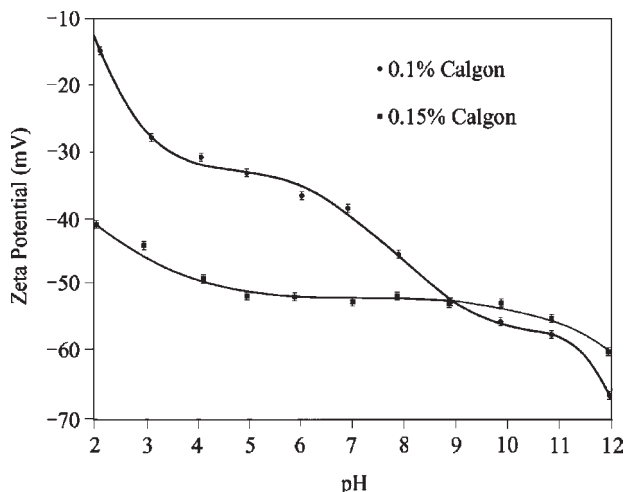


Fig. 5.17. Plot of zeta potential vs. pH for TiO_2 particles in deionized water. (With the permission of Malvern Co. in the specifications attached with the equipment.)

In order to stabilize the system to obtain consistent size data, charges such as a Lewis base, are usually added. Presently, there are additives such as Calgon, $(\text{NaPO}_3)_6$ or $\text{Na}_6(\text{PO}_3)_6$. Calgon 0.10 and 0.50% (by wt), is added to the above oxide suspension with different pH values [13]. The plot of zeta potential vs. pH is as shown in Figure 5.17. According to this plot, the results are nearly the same for 0.1 and 0.15% Calgon in the pH range 9–11, and this is the region where the TiO_2 particles should be analyzed for size data. A 0.15% (by wt) Calgon and TiO_2 particles were dispersed in a solution with a pH 11. The dispersion patterns for such a solution are shown in Figure 5.18, where the green and red curves are the same as the blue curve. Thus there is no effect of time.

5.3.3.3. Molecular weight and viscosity

For small molecules except polymers, the sample scattering intensity can be described using the Rayleigh expression established by Debye [13]:

$$\frac{KC}{R_\theta} = \frac{1}{M} + 2A_2C \quad (5.3.6)$$

where K is an optical constant, C the protein concentration, R_θ the Rayleigh ratio of the analyte intensity to the incident intensity, M the weight-average molecular weight of analyte, and A_2 is the second virial coefficient. As suggested by this equation, a plot of KC/R_θ vs. C should be linear, with an intercept equivalent to $1/M$ and a slope that is proportional to the second virial coefficient. This type of single angle molecular weight analysis is known as a Debye plot, and is shown in the Figure 5.19. The intercepts in both plots are consistent with the known molecular weight of 14.7 kDa. As seen in Figure 5.19, the second virial coefficients are strongly dependent upon the type of buffer used.

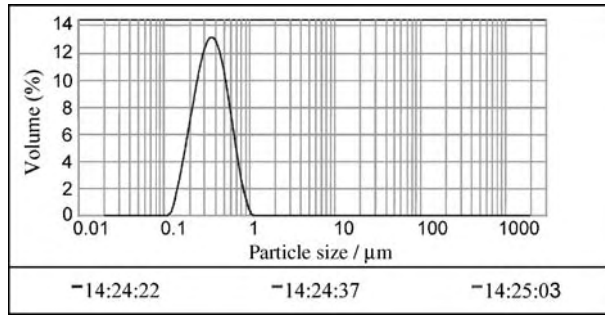


Fig. 5.18. The dispersion pattern of TiO_2 particles dispersed with ultrasound in deionized water and 0.15% Calgon for different time intervals as measured with the Malvern mastersizer analyzer. (time is given in h:min:s). (With the permission of Editorial office of China Particology, Science press of China.)

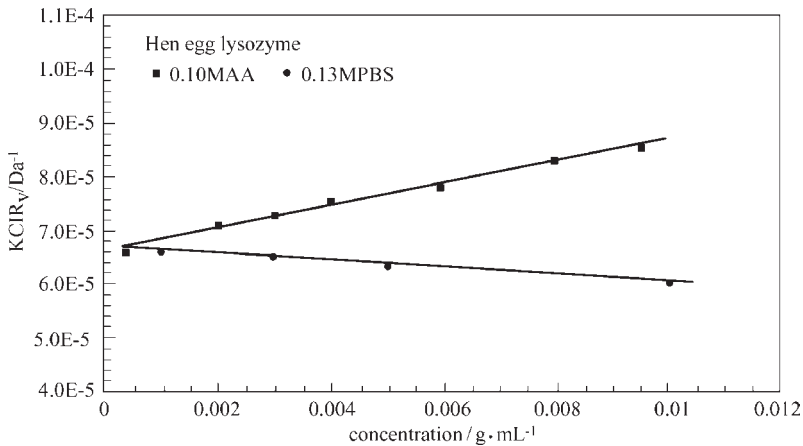


Fig. 5.19. Debye plots for lysozyme in 0.10 M acetic acid buffer and 0.13 M phosphate-buffered saline.

The greatest difficulty in measuring the molecular weight of polymer–MMT nanocomposites is that the inorganic phase in them affects the measured results. These inorganic particles cannot be filtered out because they form a homogeneous phase with the organic matrix (see the Malou experiment [14]). The molecular weight of the nanocomposite should be measured by a gel permeation chromatography (GPC) to give the molecular weight and distribution of the medium containing the inorganic phase, but is difficult to separate the inorganic phase.

For practical applications, it is better to characterize the nanocomposite by its viscosity. For example, an NPBT sample is dissolved in mixed solvents of 50/50 (w/w) of 1,1,2,2-tetrachloro ethane ($n_0^{25} = 1.5250$) and phenol, and then measured using an Ullman viscometer at a concentration of $0.1 \text{ g (100 ml)}^{-1}$ and temperature of $25 \pm 0.1^\circ\text{C}$:

$$[\eta] = \left(1 + \frac{\eta_{sp}}{0.7C}\right)^{\frac{1}{2}} - 1 \quad (5.3.7)$$

where η is the intrinsic viscosity, $\eta_{sp} = (t - t_0)/t_0$, t and t_0 are times for sample solution flow and pure solvent flow in the viscometer and C is the concentration of the solution (from 1×10^{-3} to 10×10^{-3} g ml⁻¹). The viscosity of NPBT samples of 0.0, 1.0 and 5.0% (by wt) clay is measured by this process. Their viscosity data are 0.90, 0.92 and 0.87 (dl g)⁻¹, respectively. In fact, the viscosity of both NPET and NPBT samples can be measured by this process.

5.3.4. TEM

Transmission electronic microscopy TEM uses electron penetration into particles, which will give particle's size and cubic dispersions. Analysis of the image is used to measure the particle's size or diameter. Several methods, such as crossing methods [1] and average particle size method of peak value are also used. The crossing methods require that at least 600 particles cross length are measured and their arithmetic or number average data of are then obtained. These average data on multiplying by a coefficient of 1.56 give a final average size of the particles, where 1.56 is a statistical coefficient.

In some viewpoints, to get an average result of particle size, there is a need to take at least 10,000 pictures, which is accurate for statistical calculations. In practice, this is difficult to achieve. Thus, in TEM measurement, the above coefficient method might be a suitable and empirical method for correctly estimating the final distribution of particles in different media.

In modern TEM equipment, software is attached to make statistical calculations of the particles, which is helpful for obtaining the average size and the distribution of particles. Usually, 100 particles are measured for statistical calculations [15,16].

In modern TEM equipment, the particle crystallite diameter–particle number curve is usually obtained in the final results. This curve is called the particle distribution pattern, in which the particle size corresponding to the peak of the curve is used as the mean particle size.

5.3.4.1. Preparation of samples for TEM

Several special methods for preparing samples for TEM have been reported, including the microtome method, the dyeing method, and the epoxy wrapping method. In the microtome method, a diamond knife is used, by which a thin film of thickness less than 100 nm is obtained. For PBT and NPBT samples, the samples are first embedded in epoxy. Then the microtome is used to section thin films (50–100 nm) by cutting with the microtome diamond knife. The films are moved to the copper grids of TEM. TEM observation is conducted at a voltage of 200 kV on a Hitachi S-800H. To improve the color difference of the thin film, the sample for TEM is usually dyed by vapor of solvents such as OsO₄ (highly toxic) under a protecting gas. The dyeing method is popular in preparing samples of many researches, and is quite easy to do [17]. For soft samples, toughened or easily cracked samples, an epoxy wrapping sample's method is used [18]. Obviously, the method is used when the epoxy morphology does not affect the real distribution of nanoparticles. To improve the contrast (difference), the microtomed slides are usually placed on the copper grid substrate, and then the sample is treated by carbon vapor deposition under vacuum. The sample surface covered by carbon is

beneficial for electron transmission experiments because it produces strong contrast, which helps to give an objective and complete morphology of the sample.

5.3.5. AFM

The atomic force microscopy (AFM) method is a technique that is used to investigate atoms and their interactions on an atomic level. The principle of AFM is based on the interaction force between two approaching objects. The precursor to AFM is scanning tunneling microscopy (STM) invented by IBM scientists (G. Binnig et al.) in 1986. In recent decades, the rapid development of AFM has led to a series of scanning probe microscopies such as frictional force microscopy (FFM), surface electronic potential microscopy (SEPM), electrostatic force microscopy (EFM) and electrochemical atomic force microscopy (EC-AFM) (R. Vidu et al.).

5.3.5.1. Principle

Considerable literature has described the principle of AFM. The interaction force between the probing tip and the sample's surface is related to the distance. The force–distance curve is important in AFM observation and is called the F/S curve. Figure 5.20 is a typical force–distance curve measured for a single silicon crystal surface by an Si_3N_4 probing tip.

It is seen from Figure 5.20 that, when the probing tip of the AFM approaches the sample's surface, the attracting force is first detected at point A. After the tip makes contact with the surface at point B, the repulsive force increases, and the increasing rate is related to the mechanical force characteristics of the sample's surface, the surface interacting force and the geometrical shape of the probing tips. When the probing tip is gradually withdrawn from the sample's surface starting from the repulsive force region (point C), the maximum adhesion force is observed (point D). By using AFM one can

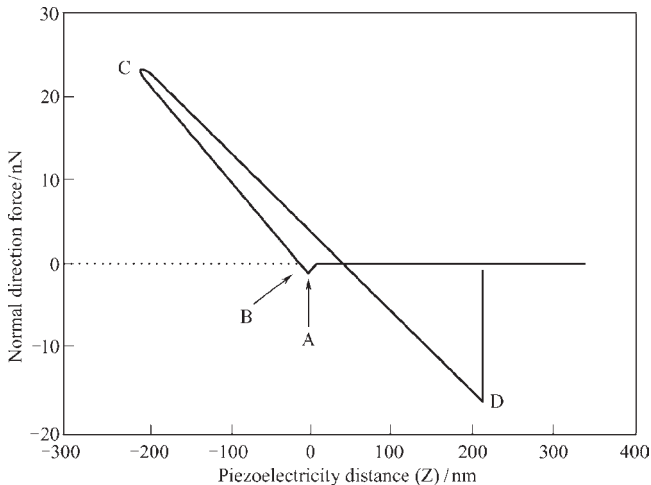


Fig. 5.20. Typical force–distance curve of a sample (single silicon crystal surface) by a Si_3N_4 tip.

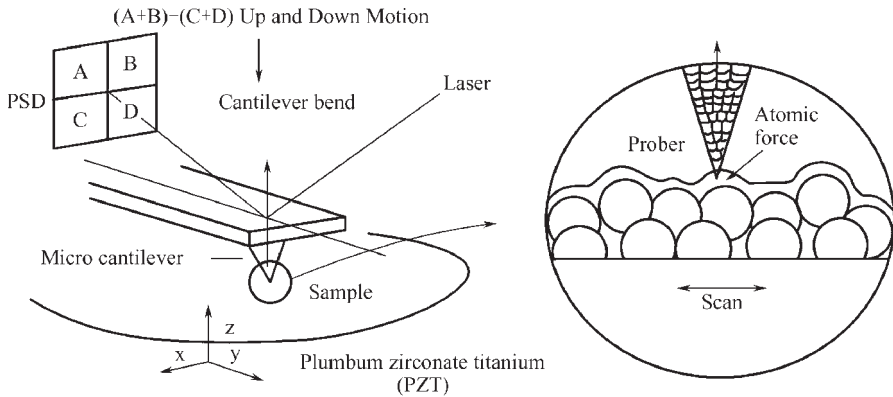


Fig. 5.21. Diagrammatic representation of the principle of atomic force microscopy.

observe either repulsive regions or attractive regions. In AFM observations, the interaction between sample and probe tip is obtained from the F/S curve.

In Figure 5.21, the sample is fixed on an opto-electric ceramic scanner. The sample can be moved with accuracy higher than 0.1 nm in the directions of x , y , and z -axis. The probe (tip) is then fixed on the end of the bending arm, which is made to approach the sample's surface as close as possible in order to detect the interaction force between the sample and the tip. In Figure 5.22, an Au film covers the back of the bending arm. Bending arm movement is detected by the position sensitive detector (PSD) by reflecting laser light on the back of the bending arm. In AFM observation, a feedback electric circuit is used to apply a fixed force between the sample and the tip (constant-force mode). By scanning in x and y directions, the morphological map of the sample surface is obtained by measuring the scanner movement in the z -direction on the bending arm.

In addition to the constant-force mode the AFM also has a constant-height mode. In the constant-height mode, the scanner is required to keep a constant height in the z direction when it scans in the x and y directions, while a measurement is made by recording the movement in the z direction. Such a mode is usually used to observe maps of atoms and molecules.

There is another approach, which is known as the tapping mode. When the tapping mode is used, the cantilever in the z direction is driven to synchro-vibration. When the scanner is in the both x and y directions, it keeps a certain amplitude or phase location difference, and produces the sample surface's morphology by recording the scanner's movement in the z direction. Depending on the amplitude, the contact between the probe and sample can be a periodical or non-periodical. Such a mode reduces the interaction between the probe and the sample, and thus it is widely applied to softer and easily deformed samples.

5.3.5.2. Application fields (examples)

(1) *Phase separation of PBT-layered silicate nanocomposites (NPBT)*. In investigating the nanostructure of NPBT, the constant-force mode has been used and the morphologies obtained from the ASFM measurements are shown in Figure 5.22.

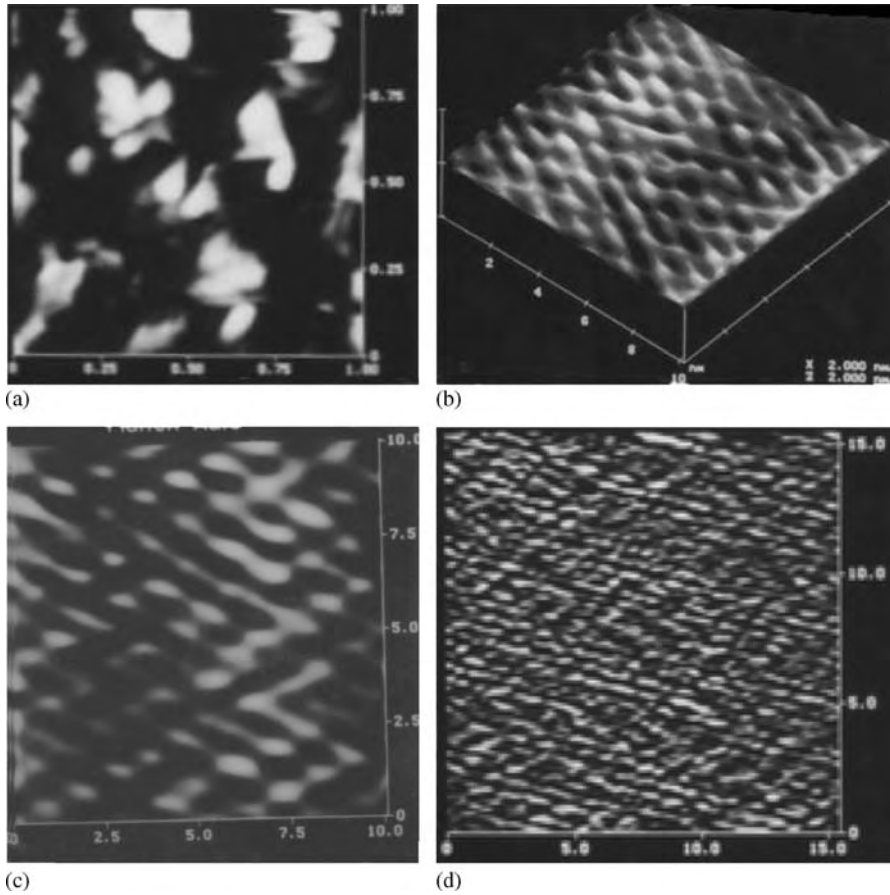


Fig. 5.22. AFM morphology of PBT-layered silicates nanocomposites: (a) phase separation on a large-scale region; (b) nanoparticle and polymer microcrystallite composite on a small-scale region; (c) phase separation on small scale (the parallel textures are polymer's crystalline chain in the direction of 45°) and (d) nanoparticles and their composites with polymer microcrystallites on a small scale.

(2) *Nucleation morphology of FeO(OH) crystals on a molecular deposited single monolayer.* By using a precursor of $\text{Fe}(\text{NO}_3)_3 \cdot 9\text{H}_2\text{O}$ to prepare nanoparticles of FeO(OH), the nucleation of FeO(OH) on a single monolayer of an acidic thiol on a gold surface can be observed. The FeO(OH) particles are grown on the thiol monolayer by adsorption of Fe^{3+} ions from an $\text{Fe}(\text{NO}_3)_3 \cdot 9\text{H}_2\text{O}$ solution in water and then the Fe^{3+} ions are oxidized with a hydroxide solution. The nucleation and growth of the FeO(OH) particles on the thiol monolayer are observed by AFM using the constant-height mode as shown in Figure 5.23.

(3) *EC-AFM.* Electrochemical AFM has recently been developed to measure electrochemical surfaces in liquid electrolyte as shown in Figure 5.24. Here, electrochemical surfaces can be investigated under different electrical potentials by AFM. The surface is the

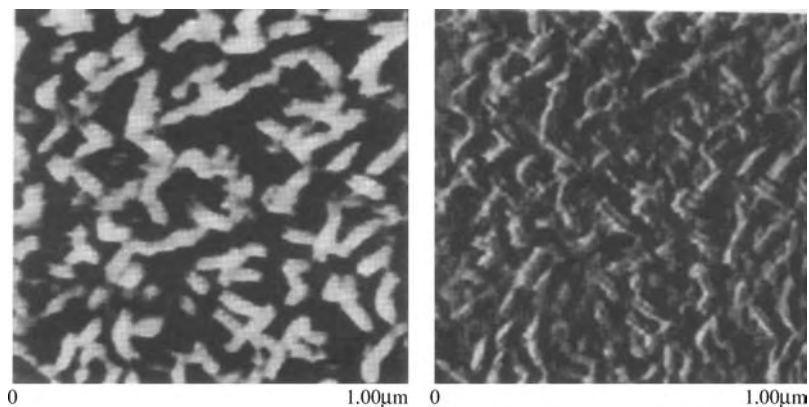


Fig. 5.23. AFM morphology of FeO(OH) crystallites on a thiol monolayer.

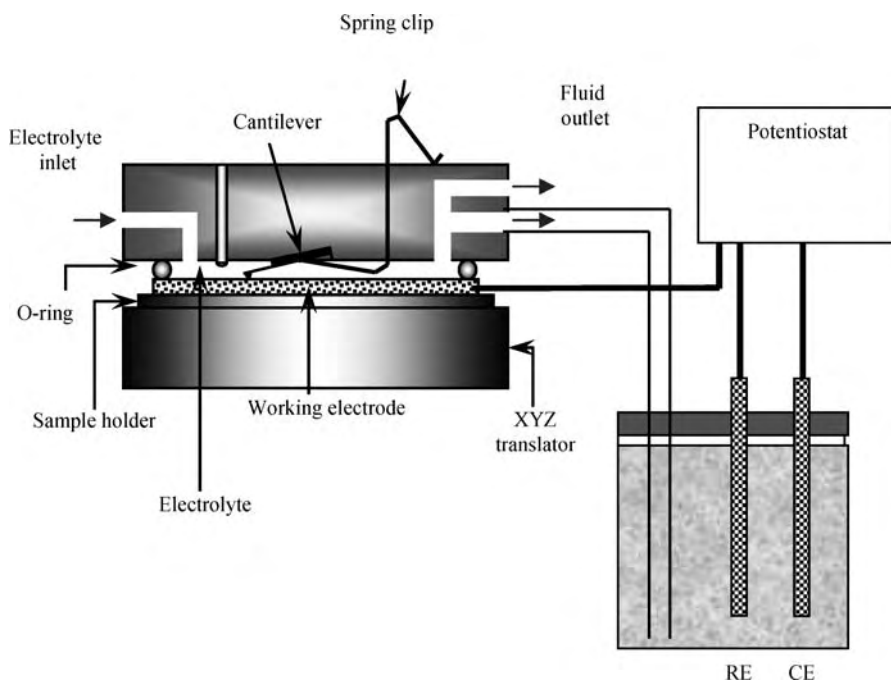


Fig. 5.24. EC-AFM mode of investigation of electroic deposition and dissolution (from R. Vidu et al.)

working electrode, and the counter electrode (CE) and the reference electrode (RE) are in electrical contact through an electrolyte salt bridge. The potential on the working electrode is set by the potentiostat and the current can be measured. The setup is attractive for studying the growth and dissolution of nanoparticles on an electroic surface

due to electrochemical reaction. By scanning in time, the dynamic growth or dissolution of nanoparticles on the electrode surface can be studied.

5.3.6. Scanning Electron Microscopy

SEM for studying the morphology of nanocomposites is quite different from TEM. In SEM, electrons are emitted in a direction parallel to the sample's surface. The method used to prepare a sample is of great importance for detecting the nanostructure with SEM. The first method is a fragile-breaking method for samples in liquid nitrogen (N_2). The sample to be investigated is frozen in liquid N_2 , where it becomes fragile and can then be broken to make a fresh surface. Afterwards, Au metal is deposited on the fresh surface to obtain a sample for SEM measurement. In the second method, a microtomed sample is obtained for SEM. Samples with thicknesses of 100–500 nm are suitable for detection with SEM. The sample is then placed on a copper grid for Au metal deposition on its surface. Finally, the particle's distribution is characterized on the surface of a selected film, whose preparation includes the selection of wrapping resins. The resins selected must not change with the morphology of the sample. Figure 5.25 shows the SEM morphology of the NPET sample. Results show the particle distribution and the particle projection as a sphere.

In modern SEM equipment, particle analysis is available. The typical measurement range for SEM is from 1 nm to 1 μm . Usually in an image, the morphology of particles is shown in a gray scale. To analyze the image the computer software performs hole-filling, noise removal and auto-cut, by which interconnected particles are cut into single ones. Through this analytical treatment, each single particle can be observed, measurements of area, circle length and shape parameter are made, and, in turn, the corresponding particle size is computed [19].

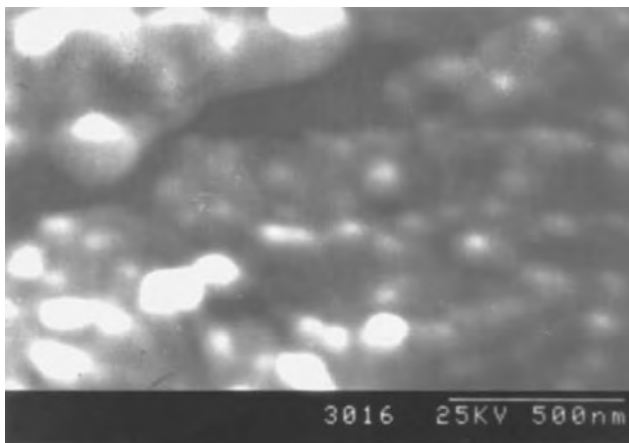


Fig. 5.25. SEM morphology of particle and particle distribution in the NPET sample with 3.0% (by wt.) clay load. Here, particles project like spheres.

5.3.7. DSC and TGA

The specifications on both DSC and TGA have been clearly described in the products made by commercial companies. The heat released from the sample detected is recorded by DSC through a comparison with the standard sample. A brief introduction to DSC working principle is shown in Figure 5.26. The sensor is a kind of μ -sensor in which the recording is a $0.02 \mu\text{W}/\text{digit}$. In TGA, the weight loss or change from the evaporation, decomposition or interaction with the atmosphere for a sample detected during the heat scanning is recorded in situ in a sensor calculated from a weight balance. For detailed specifications of TGA one may refer to the literature and products from Perkin-Elmer or Netzsch [20,21].

To obtain practical DSC patterns of nanocomposite samples, trial and error experiments are carried out in advance in order not to destroy these precious samples before they are investigated. For example, NPBT samples are set to scan from 30 to 270°C (NPBT has a melting point of 235°C) with a rate of $10^\circ\text{C min}^{-1}$ held for 2–5 min. for a complete melting. Many experiments prove that the degradation occurs during this heat scanning. The data errors are $\pm 2^\circ\text{C}$ for the melting point, and $\pm 5\text{--}10\%$ for ΔH .

As shown in Chapters 3 and 5, isothermal and non-isothermal crystallization experiments are capable of being carried out by DSC. In most of our experiments, pellet nanocomposite samples with weights from 2 to 6 mg are sampled in an aluminum crucible (or platinum crucible for polymer-silica nanocomposite samples, which protects the sample cell from being broken by silica). In cases of NPET, NPBT, NPA6, their crystallization behaviors are designed in different scanning processes. For example, in a non-isothermal crystallization experiment cycle of NPET sample, the sample is scanned from 30 to 300°C, held at 300°C for 3 min and cooled from 300 to 30°C under different rates (from 5 to $40^\circ\text{C min}^{-1}$). To protect the sample from degradation, the samples are protected by N_2 gas with a flow rate of 40 mls^{-1} . The results are

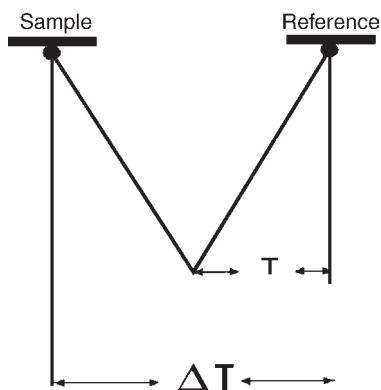


Fig. 5.26. DSC working principle in the area contacts between thermocouples and crucibles, where T is a temperature change of reference sample as furnace heating increases and ΔT is the temperature difference between measured sample and reference sample (indium, tin).

corrected using standard tin after each sample. Similarly, for this sample, TGA experiments are run from 50 to 1000°C with a scanning rate of 10°C min⁻¹ and sample weights between 8 and 12 mg.

5.3.8. Computer modeling

5.3.8.1. Calculation methods

The calculations of polymer-layered silicate nanocomposites need model parameters. Once the optimization of the initial model (by using the smallest repeat unit of a polymer chain (2 or 3 chain unit)) is established, then the calculations of the optimized model by dynamics method with ensembles of NVT (normal invariable volume and temperature), Nose (compensating the temperature variance during calculation [22]) method for controlling temperature at 298 K, the calculation steps are 1 fs, and modeling lasting for 200 ps. Similar calculations are applied to the other BHET molecules with ensembles of NVT at temperatures of 300 and 400 K, calculus step of 1 fs lasting for 80 ps.

5.3.8.2. BHET molecules

The molecular force-type parameter and atomic charges for the BHET monomers under a COMPASS force field (see Figure 5.27) can be calculated [22]. The COMPASS force field integrates the molecular force field based on the ab initio quantum calculation. The COMPASS force field has a similar form to CFF force field in its potential functions [22] (Table 5.1).

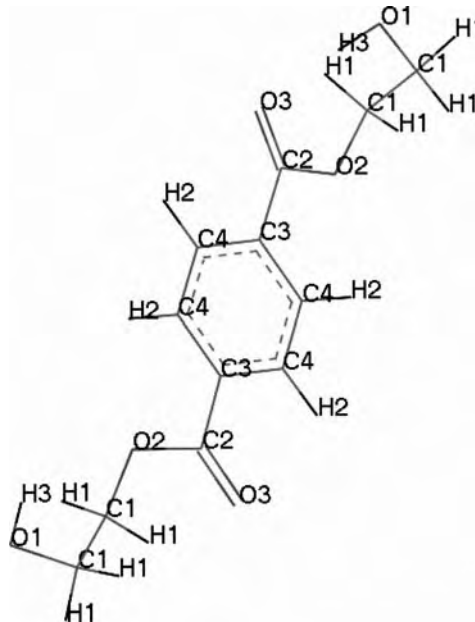


Fig. 5.27. The molecular structure of BHET monomers.

Table 5.1
Parameters and charges of BHET monomers under
calculation force

Atom type	Force field parameters	Charges
C1	C4o	0.054
C2	C3'	0.597
C3	C3a	-0.035
C4	C3a	-0.1268
O1	O2h	-0.57
O2	o2s	-0.272
O3	o1=	-0.45
H1	h1	0.053
H2	h1	0.1268
H3	h1o	0.41

Table 5.2
Calculated model parameters for hydrated MMTs

Model	No. of water molecules	Interlayer distance (nm)	Water content (gg^{-1} MMTs)
1	32	12.08	0.1
2	64	15.28	0.2

5.3.8.3. Models of the intercalation and bulk polymers

In the intercalation model, the intercalant of $\text{CH}_3\text{CH}_2\text{CH}_2\text{CH}_2\text{NH}_3^+$ is used to neutralize the negative charges inside the layers. The bulk polymer phase includes the same quantity of molecules of $\text{CH}_3\text{CH}_2\text{CH}_2\text{CH}_2\text{NH}_2$ in order to make a comparison with the material inside the layers. Three MMT models are established whose model parameters are shown in Table 5.2.

The crystal cell and coordinate parameters of MMTs are necessary for establishing the calculating model. The crystal space group of $\text{C}_{2h}^5\text{-P2/m}$ and cell parameters $a = 0.518$ nm, $b = 0.914$ nm, $c = 1.25$ nm for MMTs are adopted. In the computer calculation of the practical MMT unit cell model, the atomic charges [22b] based on the space group C2/m are used in our calculations.

Model 1 from Table 5.2 is taken to form Model 1-LAYER, i.e. Model 1 provides its interlayer as a location where the intercalant molecule intercalation occurs. Similarly, Model 2-BODY means that the intercalant molecules in the bulk polymers interact in the interlayer space of MMTs. Comparison of the results shows that the initial material inside the layer gallery in the Model 1-LAYER is the same as in Model 1-BODY. The initial Model 2-LAYER has the same material as the Model 2-BODY. In all initial models, BHET and the intercalant are introduced without any set conditions (see Tables 5.3 and 5.4).

Table 5.3
Parameters of the intercalated model

Model	Minimum repeat unit (nm)			BHET ^a in the minimum repeat unit
	A	b	d	
Model 1-LAYER	2.112	1.828	2.322	8
Model 2-LAYER	2.112	1.828	3.337	16

Note: d, interlayer distance;

^aBHET Molecular numbers in the minimum repeat unit.

Table 5.4
Parameters in the bulky calculation model

Model	Minimum repeat unit (nm)			BHET in the minimum repeat unit
	A	b	d	
Model 1-BODY	2.112	1.828	1.332	8
Model 2-BODY	2.112	1.828	2.425	16

5.3.8.4. Interaction between BHET monomers and layer surfaces

5.3.8.4.1. Formation of hydrogen bonds The OH group at the end of BHET molecules will form hydrogen bonds with oxygen on the surface of the MMTs. The comparison of Model 1-LAYER and Model 1-BODY shows that the hydrogen density is different between the two models Figure 5.28. In the BHET matrix, the end hydrogen atoms tend to be continuous. The hydrogen density changes significantly as the dynamic calculation proceeds. The hydrogen atom has a large motional freedom in the bulk. Inside the layers, the end hydrogen atoms tend to accumulate and show large density near the layer surface. As time proceeds, the density varies less. When the shape of the density curve becomes stable, it means that one (or two ends) of the BHET molecule (Figure 5.29) is (are) confined within the MMT layers, or has (have) formed a hydrogen bond. Such a density distribution of hydrogen atoms is beneficial for polymerization reactions.

5.3.8.5. Confinement of BHET molecules inside the layers

Hydrogen atoms in the bulk BHET ends and near the MMT layers are compared with their movements within 80 ps. Results show that the hydrogen atoms in the bulk BHET are mobile with large regions for movement (Figure 5.30). Hydrogen atoms near the MMT layers have confined space for movement and reduced mobility. The hydrogen mobility vertical to the layers is much lower than its mobility parallel to the layers. Under such conditions, the hydrogen atoms have jumping characteristics. At a low temperature of 300 K, the jumping movements are significant. The jumping behavior is characteristic of hydrogen bonding.

5.3.8.6. Order distribution of BHET molecules in the surface of the layers

The hydrogen bond formation of BHET with the layer surface of MMTs will not only confine the monomers, but also play a role in the polymerization process in bulk BHET.

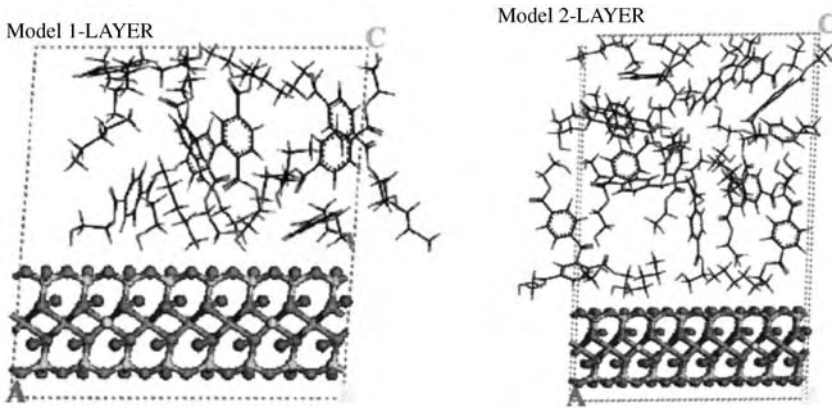


Fig. 5.28. Comparison of Model 1-LAYER and Model 2-LAYER. The upper part represents the molecular morphology of BHET, and the lower part the unit cell of MMTs.

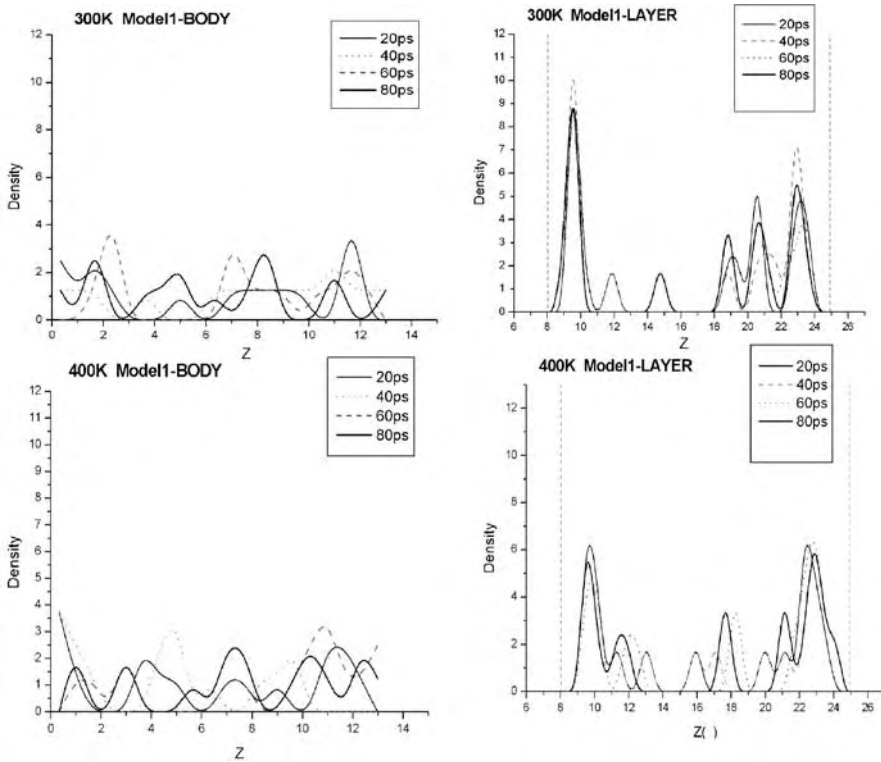


Fig. 5.29. Density comparison of hydrogen atoms in the bulk matrix and along the *c*-axis (*z*-axis shows a distance along the vertical direction to layers (or *c*-axis). The absolute is related to the mono-cell in unit of Å; vertical axis is molecular density).

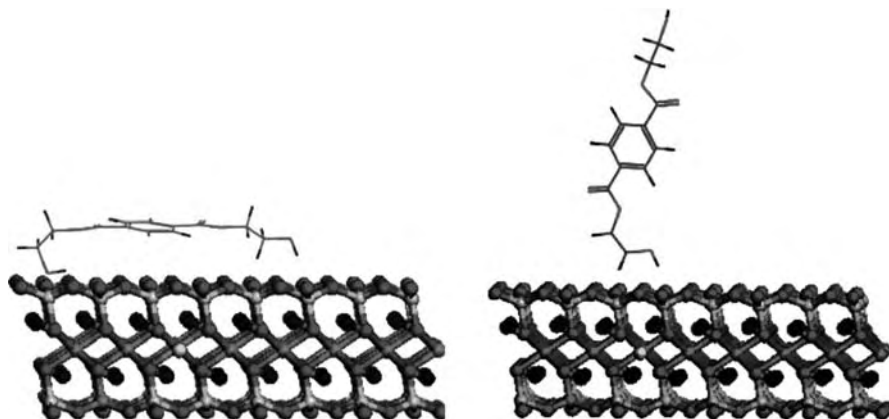


Fig. 5.30. Morphology of BHET molecules inside the MMT layers.

In Figure 5.31, the calculations of Model 2-LAYER and Model 2-BODY show that the bulk BHET has its carbon of the benzene ring in a random state along the *c*-axis. The curve distribution at 300 K is more stable than that at 400 K. While the carbon atoms of the benzene rings inside the layers show valuable density distributions, such as two narrow peaks on two sides showing hydrogen bonds between its end groups and layers (Figure 5.31), the two broader peaks in the middle are for only one end hydrogen forming a bond with the layers. Before the polycondensation reaction, the BHET molecules have random orientation. The formation of polymer chain segments is uncertain, while the BHET inside the layers form selective orientations before polycondensation. Even though the MMT load in the nanocomposites is low, the large specific surface area of the MMTs has a profound effect on the properties of the nanocomposites, such as accelerating the crystallization rate of PET and improving their mechanical properties.

5.3.9. Coulter particle size analyzer

With the Coulter particle size analyzer, or Coulter Counter, one can measure the particle size and number in a suspending solution. The measurement limitation is from 0.3 to 20 μm in size, which requires that the particle distribution be relatively narrow. In the Coulter Counter, the particle suspension in an electrolyte solution flows through a small orifice, which will cause the electrical conductivity across the orifice to vary whenever a particle passes through the orifice. The peak value of the conductivity is related to the passing particle's size. By recording the electric conductivity for many particles passing through the orifice, the particle size distribution is obtained. This method is suitable for measurement of suspended particles in water. In principle, the Coulter Counter gives the particle's volume as the raw data, from which the particle size is calculated.

5.3.10. Surface plasmon resonance (SPR) spectroscopy

SPR spectroscopy can be used to monitor deposition or growth of materials, such as nucleation and growth of nanoparticles on an interphase. SPR spectroscopy is a powerful

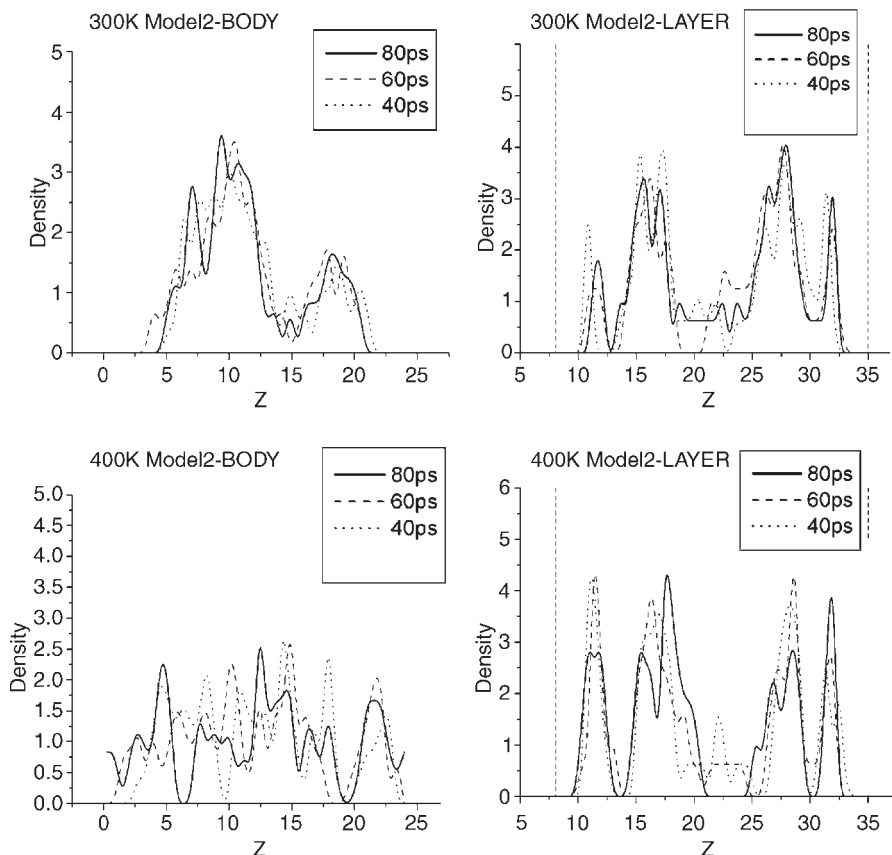


Fig. 5.31. The density distribution comparison of carbon atom number of the benzene ring in the BHET matrix and inside the layers of MMTs along the c -axis.

technique for measurements of ultrathin films in a variety of media; it results from the interplay of two interfacial phenomena. A beam of light that goes through an interface will be partially reflected and partially transmitted across the interface. In the regime of total internal reflectance, the refracted light turns into an evanescent wave with a decay length that is typically of the order of 200 nm. Oscillations in the electron cloud at a noble metal–dielectric interface (medium) are called surface plasmons. When the energy and momentum coupling conditions are satisfied, the electron cloud in the metal can be turned into a resonator driven by p-polarized light in the evanescent wave, resulting in the absorption of energy at the interface. This condition will also be manifested in the appearance of a minimum in the angular spectrum of the intensity of the reflected light. The location of this minimum, the resonance angle, is strongly influenced by changes in the dielectric properties of the medium within the decay length of the evanescent wave. The shift in resonance angle is proportional to the amount of material adsorbed at the interface, and SPR can be used to measure the formation of very thin adlayers (down to 0.1 nm)

with very fast sampling times (~ 0.1 s). The “Kretschmann” configuration is normally used to attain the energy and momentum matching conditions between the incoming light and the surface plasmons at the gold–medium interface. Monochromatic p-polarized light from a laser is used as the light source. The intensity of the reflected laser light is captured by a photodiode whose output is sent to a lock-in amplifier and then to a PC for data handling and storage. A θ – 2θ goniometer is used to perform scans of the intensity of the reflected light as a function of the incident angle. The SPR curves (reflectivity vs. internal angle) can be modeled using the characteristic formalism for homogeneous stratified dielectric media to yield the thickness of films or materials formed on the noble metal interphase. The kinetics of particulate film growth on the noble metal interphase can be followed by fixing the detector at a given angle and monitoring the reflectivity as a function of time. Typically, this angle is chosen 0.5° – 2° less than the resonance angle so that changes in reflectivity are linearly related to the shift in resonance angle or, alternatively, to the change in adsorbed layer thickness. Figure 5.32 shows the change of the reflectivity with time for the growth of a lepidocrocite nanoparticulate film on a sulfonic acid surface on gold as a function of pH.

The sulfonic acid surface on gold was created by chemisorption of a sulfonic acid thiol on the gold surface. First, ferric ions in solution were adsorbed on the sulfonic acid groups and then the ferric ions were oxidized to lepidocrocite by exposing the surface to a basic solution. Independent AFM measurements showed a film of lepidocrocite nanoparticles.

5.4. Multiple structures of nanocomposites

A polymer structure has multiple levels: the first level is for chain structure, the second is for the chain conformation and the third is for the condensed structure. When the

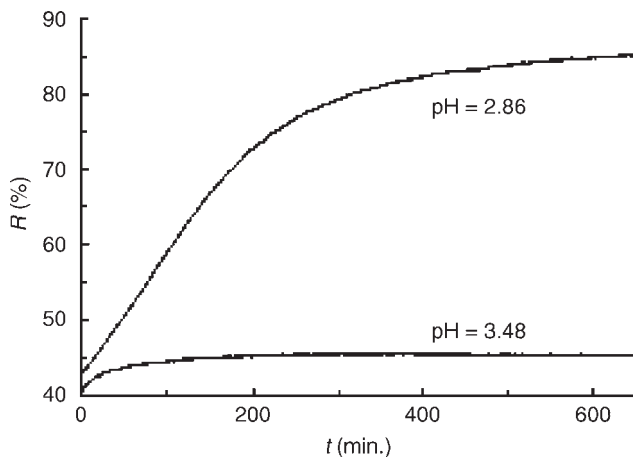


Fig. 5.32. Time and pH dependence of surface plasmon resonance reflectivity for growth of a film of lepidocrocite nanoparticles on a sulfonic acid surface on gold.

polymer polymerizes with nanoparticles, several new structure types appear which cannot be expressed by the original polymer's microstructure. The overall characterization of these structures is necessary. Thus, the multiple level structure model is used to describe the polymer–inorganic nanocomposites. The first level of structure refers to the nanoparticle dispersion (aggregation or agglomeration), which is easily identified by electronic microscopy (SEM in Figure 5.33).

The second level of structure for the polymer–inorganic nanocomposites is their inner structure, such as particle separation, the interphase between particles, and particle exfoliation of layered silicates. This structure is revealed with TEM (Figure 5.34) or AFM.

In morphological pictures obtained by TEM, dark lines represent MMT layers oriented vertical to the sample's surface (Figure 5.34). MMT layers exfoliated from NPET have strip-belt morphology with an interlayer distance of 1.4–3.7 nm, which is consistent with that calculated from X-ray diffraction. Sometimes, a fiber- or silk-like morphology around the dispersed layers is observed, closely resembling “polymer brushes”. These polymer brushes are partly inside and partly outside the layers. Similarly, in PA 6–MMT nanocomposites, the average diameter of the layers is measured as (160 ± 30) nm or (70 ± 20) nm, depending on the method of preparation. The interdistance of the layers is 35–45 or 40–60 nm, depending on the sample. In these two polyamide-based nanocomposites, 2–3 layers of particles are observed. This structure is in a secondary level of morphology whose definition is not similar to that reported [23].

The third level of structure in polymer–layered nanocomposites is the assembling structure of the interface. This structure is often related to the nanocomposites' heat distortion performance and to other properties. To reveal this third-level structure, SAXS technique is used. With SAXS, the long-range order scale of LS can be obtained from the scattering intensity (I) of experimental curves with integrated factors (q) or the

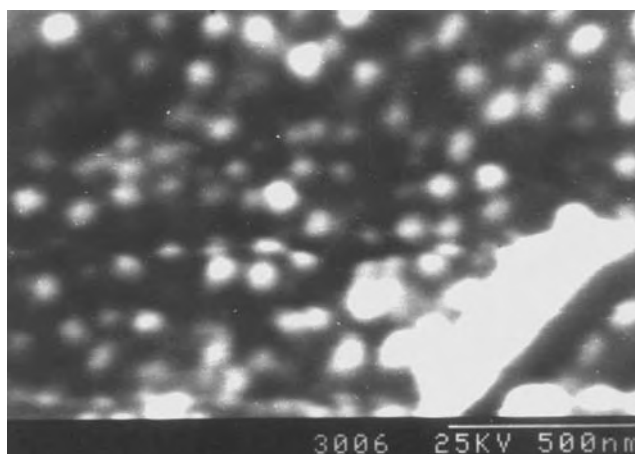


Fig. 5.33. SEM morphology of nanoparticles dispersed in a polymer matrix.

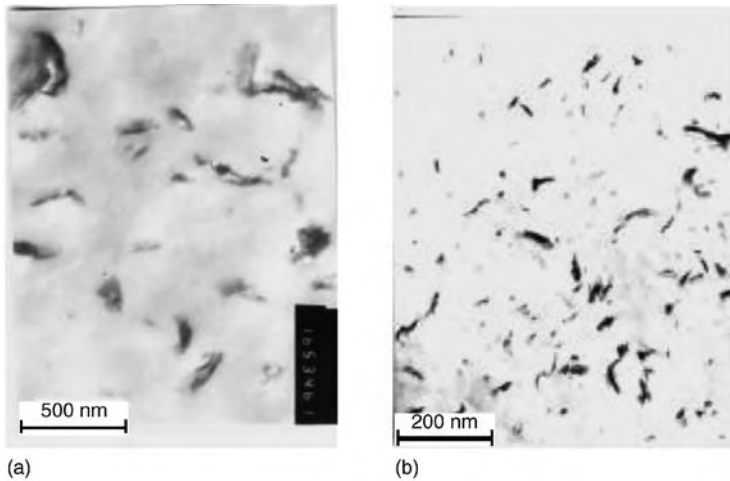


Fig. 5.34. TEM morphology of a polymerized NPET film: (a) NPET with 2.5% MMT load by ethanolamine; (b) NPET with 2.5% MMT load by laurylamine.

relationship of $\lg I$ vs. $\lg q$. In the third level of structure, the polymer's crystal form is in transition and crystal morphology or crystal induction is observed. For example, in pure PA6, the α -crystal form dominates, but in PA6-MMT nanocomposites, polymorphism of PA6 is induced by the introduction of MMT layers into the PA6 matrix. The α -phase in PA6 is thought to have a higher modulus at temperatures below T_g , but the modulus reduces more rapidly at temperatures above T_g than that of γ -phase crystallites. This shows that γ -phase crystallites of PA6 have higher HDT.

5.5. Relationship between structure and property

5.5.1. Introduction

The inter-relationships between structure and property for nanocomposites are investigated by chemical analysis and physical techniques such as AFM, STM, and TEM. Nanostructure is characterized by the morphology of nanoparticles, their arrangement order or self-assembled patterns. The difference between the nanostructure and microstructure of traditional materials is important in providing an insight into the property's effects, which is also a reference point for the further design of material patterns.

Samples for measurement may have several forms such as films, block, chips, pellets and shapes, according to the standards of GB (China) and ASTM. Sample preparation and measurement should be properly designed. For example, samples for DSC are cut into pellets or chips from the melt-extruding process. This technique needs a scanning rate of $10\text{--}20^\circ\text{C min}^{-1}$, and the measured results of the samples need to be corrected by standard materials of In and Zn.

Other samples for microscopy might be microtomed films. Similarly, samples for AFM observation might be prepared from melt pressing in a hydraulic compress or equipped with a heating device. Samples of thickness 50–100 nm can be cut with a diamond knife, for TEM and SEM. Obviously, the thin films are quite suitable for AFM investigation.

5.5.2. Nucleation and crystallization

Crystallization process originates from the nucleation of crystallites. The dynamics process has been briefly described by several investigators [23–26]. The crystallization behavior of the prepared nanocomposites is revealed or investigated in this section.

5.5.3. Layer nanostructure

In NPET, particle morphology and layer structure in intercalations, and exfoliation state are observed by TEM as shown in Figure 5.35, where (a) is pristine layer structure of MMTs, (b) is the layer structure of blending PRT resins with MMTs and (c) shows possible brushes of polymers in NPET.

Figure 5.35(b) shows that the layer textures are not parallel and exhibit an irregular dispersion state, with the interlayer distance less than 30 nm [27,28]. Some interlayer distances are only about 1.5 nm. In Figure 5.35(a) the layer textures are basically parallel, which shows the disadvantage of the simple blending of PET resins with layered

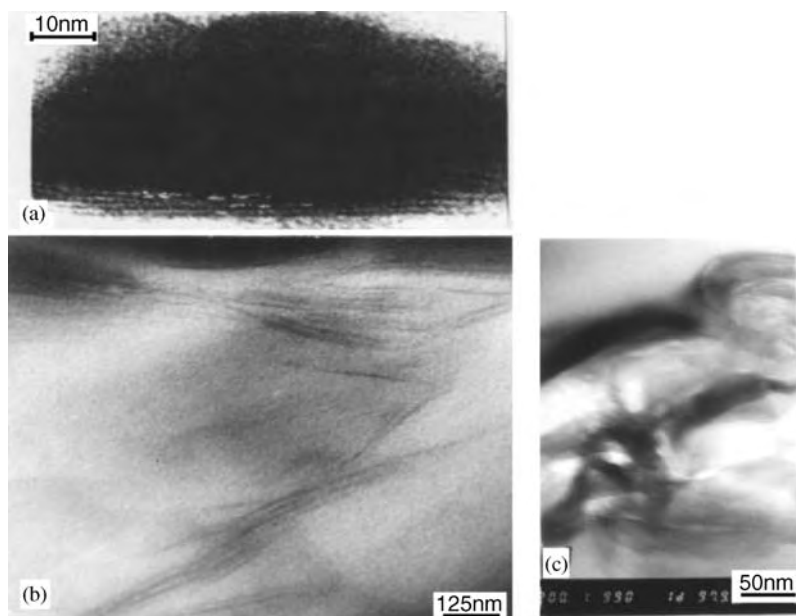


Fig. 5.35. TEM morphologies of MMT layers in PET matrix: (a) blending materials of PET-MMTs; (b) NPET samples; (c) possible polymer brush in NPET.

silicates. In Figure 5.35(c), layer-stacking morphology is observed and polymer brush-like layers are seen with a non-homogeneous interlayer distance. These layer exfoliation morphologies are also seen in epoxy-MMT nanocomposites (Chapter 3), and other kinds of polymer-layered silicate nanocomposites [28,29].

5.6. Nanoeffects in nanocomposites

5.6.1. Nanoeffects in thermal behavior

5.6.1.1. Double-melting behaviors resulting from nucleation

Double melting is a phenomenon observed in DSC patterns for polymers where two melting peaks occur, one at a high melting position (real melting point) and the other at a low melting position. Previous studies have given insights on the formation of the double-melting peak, which are summarized as follows:

- (1) The double-melting peak is a result of the melt-recrystallization process of the initial crystallization morphology due to prior crystallization history [30,31].
- (2) The double-melting peak arises from the presence of two distinct populations of crystalline lamellae [32,33].
- (3) It originates from the formation of two different morphologies of spherulitic and crystal aggregate-like structures [34].

The double-melting behavior for two different sizes of crystallites has been investigated for PET [35] and PE [36]. In these papers, the double-melting behavior of PET-clay nanocomposites has also been studied. In PET and NPET samples, DSC patterns of annealed samples are as shown in Figure 5.36.

Double-melting behavior is an important characteristic of DSC curves [37,38]. The abnormal behavior of the disappearance of the double-melting peaks suggests that the nanoparticles affect the thermal and melting behaviors of polymers. This is a result of the nucleation step during crystallization. For short times in isothermal crystallization, the small peaks at the low position of the original double-melting behavior do not appear. However, as the annealing time is prolonged, the small peak at a lower position appears, although not very clearly, which suggests an unstable behavior of the nanoparticles (Figure 5.37). The phenomenon in NPET is completely different from pure PET. The appearance of small melting peaks in DSC patterns is due to the different crystal sizes dispersed in the PET matrix.

The nucleation behavior for silica-PET nanocomposites annealed at 130°C for 45 min by DSC is shown in Chapter 3. The double-melting point peaks do not disappear, but shrink for different silica loads showing that silica-PET has relatively low crystallization rates compared to layered silica-PET; such results arise from the slightly inhomogeneous dispersion of silica.

The nucleation behavior of the cores of SiO₂ particles (in core-shell structure) shows that the percolation rate of SiO₂ in PET is very slow, while layered silica (LS) particles can rapidly form a homogeneous dispersion and an in situ exfoliation of the layers. The morphology of LS cores is not easily achieved by treating with simple surfactants, implying that bi-hexaethylene terephthalate (BHET) oligomer of PET as a treating film

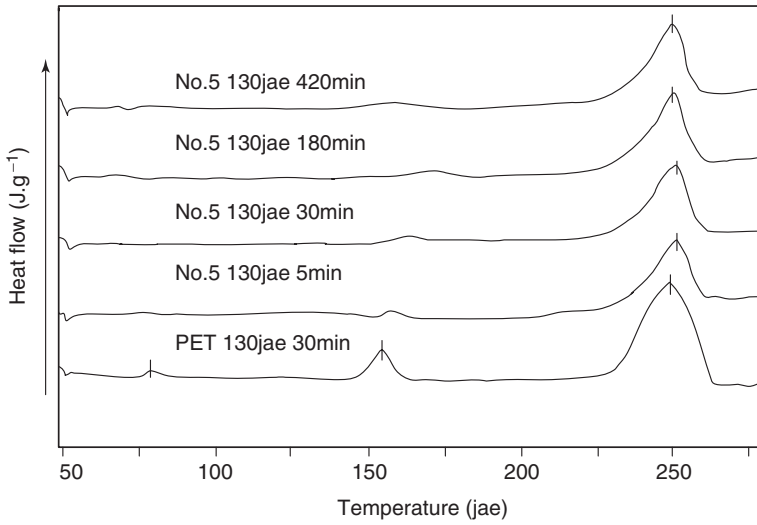


Fig. 5.36. DSC patterns for PET and NPET annealed at 130°C for different times. Sample no.5 is a NPET with 5.0% (by wt) clay.

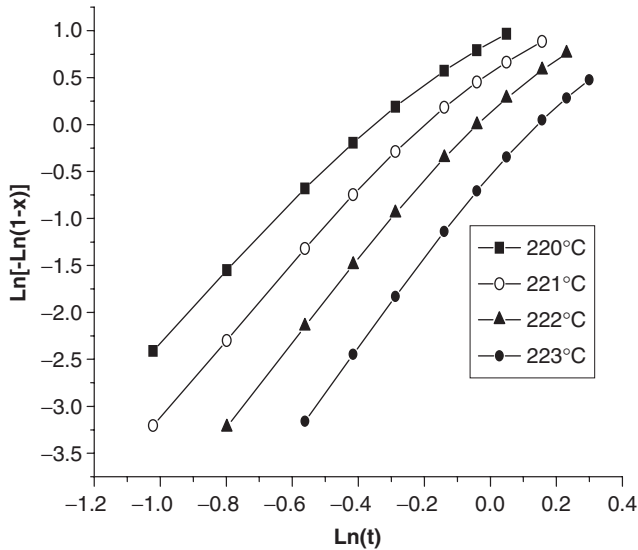


Fig. 5.37. Avrami curves for the isothermal crystallization of NPET (3.0% MMT load).

for core-shell particles is good. The nucleation morphology of SiO₂ particles is similar to that of PET, but they are not easily percolated. The LS particles can further form the exfoliated layers, as observed by AFM (not shown). When LS is mixed with PET to form LS-PET nanocomposites during this process, many nucleation centers form from

the exfoliated LS and are interconnected. This shows that exfoliated LS layers are easier to percolate than silica particles.

5.6.1.2. Effect comparison of different nanoparticles

To compare the nanoeffects from different particles, silica and layered silicate (LS)-based nanocomposites are prepared. When the LS load is from 0.5 to 1.5 wt%, and the silica load is from 0.5 to 1.5 wt%. The crystallization degree of PET-silica nanocomposites is much lower than that of PET-LS. Both of them have lower values of $t_{1/2}$ than that of PET ($t_{1/2}=1.8$ min for PET; $t_{1/2}=0.81$ min for PET-silica; $t_{1/2}=0.72$ min for PET-LS). These data indicate a rapid crystallization of PET-LS (or silica) nanocomposites. The transparency of the films is affected by the inorganic particle load so that the load is kept below 1.5 wt%. The barrier properties to oxygen can be improved 2–4 times the original PET film (for details please contact Y.C. Ke by key@cup.edu.cn).

5.6.1.3. Different crystallization behavior from nanoparticles nucleation

The Avrami equation can be used to investigate the crystallization behavior of polymer-inorganic nanocomposites. Taking NPET samples as an example, the isothermal crystallization behavior described by the Avrami equation is shown in Figures 5.37 and 5.38, where the crystallization behavior is compared for samples of PET, NPET (1.0% (by wt) of MMTs) and NPET (3.0% (by wt) of MMTs).

The plots of $\ln[-\ln(1-x(t))]$ vs. $\ln t$ are shown in Figures 5.37 and 5.38(a) and (b), which are results for isothermal crystallizations.

It can be seen from Figure 5.37 that there appear bending curves showing a transition in crystallization behavior. There are two stages of crystallization: one stage in the linear section called primary crystallization and the other in the bending section called secondary crystallization. In comparing Figure 5.38(a) with (b), it is found that only primary crystallization behavior of the linear crystallization process occurs, at the critical point for the MMT load of 3.0% for preparing nanocomposites of NPET. At this critical point, there is a nucleation effect from the heterogeneous phase. Beyond this point, the properties of PET nanocomposites decrease as the MMT load increases. The critical concentration or load of 3.0% ($c=3.8\%$, by wt) is suitable for designing other polymer-layered silicate nanocomposites, such as PA66-MMT nanocomposites, PS-MMT nanocomposites and PA6-MMT nanocomposites. However, this critical point is not a universal factor in designing other polymer-layered silicate nanocomposites, such as PBT-MMT nanocomposites and PA6-MMT nanocomposite engineering plastics.

5.6.2. Nanoeffects in condensed state aspects

5.6.2.1. Spherulitic morphology

In polymer-layered silicate nanocomposites, variety in the spherical morphology is a factor that shows how the nanoeffect affects the composite properties. Adding only a few layers of silicate (e.g., MMT, 5 wt% (by mass)) into polymer, e.g., poly(butylene terephthalate) (PBT), the nanocomposites of PBT-MMT (NPBT) show an increase in the HDT, which is caused by their layer exfoliation and their crystallization nucleation. This thermal effect resulting from the nanometer-sized layers should be

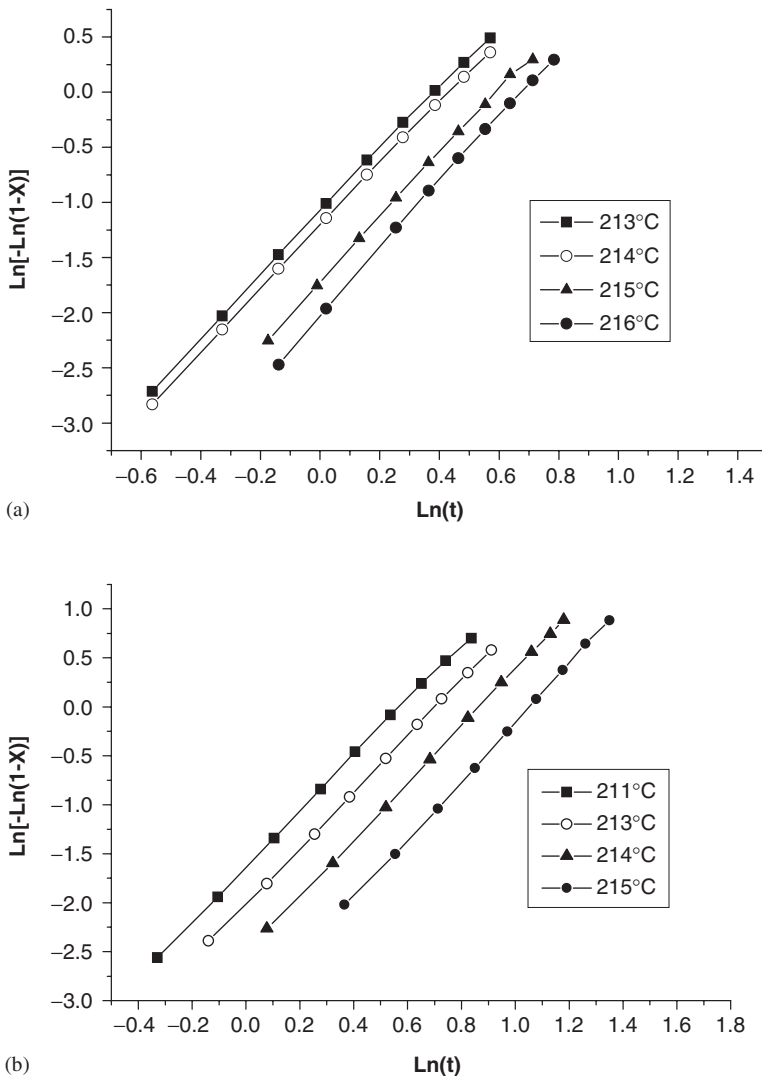


Fig. 5.38. Comparisons between NPET and PET in isothermal crystallizations by Avrami equation (a) NPET (1.0% MMT load), (b) pure PET.

thought of as nanoparticle effect or nanoeffect. As more layers exfoliate from the MMTs, more surface hydroxyl groups are exposed, and these layers interact stronger with the polymer matrix.

Figure 5.39 shows the TEM images of crystallized samples of pure PBT and NPBT. The addition of MMTs helps forming nucleation centers from the exfoliated layers and exerts a noticeable effect on the spheres' growth: the nanoparticles can either grow or stop growing (see Figure 5.39(b) and (c)).

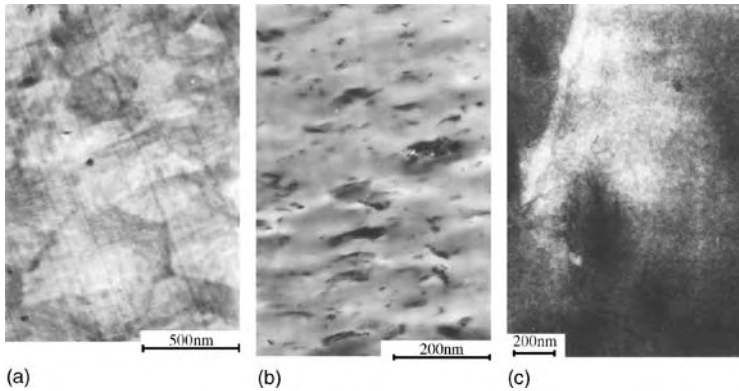


Fig. 5.39. (a) TEM of sphere morphology of PBT and (b) NPBT (2% (by wt) ethanolamine-treated LS), and (c) NPBT (2% (by wt) laurylamine-treated LS).

The morphology may change when reagents of various lengths of chain are chosen to treat MMTs. For example, when a short chain of ethanolamine is used to treat MMTs, agglomerated particles are obtained and the exfoliation effect with layered silicate is weak although it has a polarized effect on the polymer matrix. When a long chain of laurylamine is used to treat the LS, it results in a strong exfoliation effect. Therefore, the agents used for treating LS to form the layered structure should have a certain length. In this way, the nucleation center may form and stimulate the interaction with PBT molecular chains, and enhance the HDT of the nanocomposites.

5.6.2.2. The fluctuation of crystallization activation energy

In the isothermal crystallization process, as the MMT loading increases, the nucleation effect becomes more obvious. Under some load (i.e., critical point), this nucleation effect or interaction reaches the maximum level. In Figure 5.40, relative activation energy E_r ($E_r = E_a(\text{NPET})/E_a(\text{PET})$) vs. MMT loading (c) is plotted. The ratio of the absolute activation energy for PET (0% (by wt) MMTs), NO_1 -NPET (1.0% by mass of MMTs), NO_2 -NPET (1.5% by mass of MMTs), NO_3 -NPET (2.5% by mass of MMTs), NO_4 -NPET (3.0% by mass of MMTs), and NO_5 -NPET (5.0% (by wt) MMTs) over that of pure PET is plotted against the clay load. On the curve shown in Figure 5.40, there is a maximum value at 3.0% (by wt) MMT load (a critical point for MMTs load in PET). The change in trend for this curve at a MMT load of 3.0% (by wt) suggests a change in mechanism. When the MMT load is <3.0% (by wt), its crystallization dynamic is governed by spherical growth mechanism in NPET nanocomposites. At this MMT load, the calculated Avrami number is 2.85 and the interaction of layered silicate layers with polymer PET molecular chains will make it difficult for spherical crystallites to grow, i.e., E_r increases as the MMT load increases. When the MMT load is >3.0%, its crystallization dynamics is governed by a nucleation mechanism, where the nucleation of the exfoliated silicate layers occur, and then E_r decreases as the MMT load increases. Such a phenomenon has been observed in PA6-MMT nanocomposites [39].

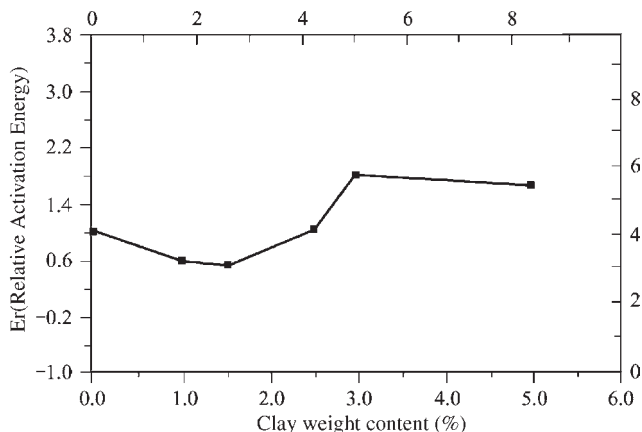


Fig. 5.40. The plot of relative active energy (E_r) vs. MMT load.

The polymer matrix and molecular chains might produce some cross-linking. In such a case, the introduction of nanoparticles into the polymer matrix will produce an intercalation interaction with layered silicates, which will lead to a polarization of the polymer chains. The polymer chains will enter into the interlayer space and cross-link the exfoliated layers. As a result of cross-linking, the HDT increases.

5.6.2.3. Acceleration effect of crystallization rate due to nucleation

(1) *DSC patterns.* The crystallization rate of nanocomposites is characterized by thermal dynamic parameters such as the glass transition temperature (T_g) and the peak temperature for a sample that is crystallized from glassy state (T_{gc}). At present, the difference between T_{mc} and T_{gc} is also accepted as a parameter in the characterization of the crystallization rate (T_{cr}):

$$T_{cr} = T_{mc} - T_{gc}$$

where T_{mc} is the crystallization rate for a sample that crystallizes from its melting state. T_{cr} is always greater than zero, and the difference is shown in the DSC patterns in Figure 5.41. The crystallization peaks of NPET samples crystallized from melt state are observed to move from a lower to a higher position as the MMT load increases.

(2) *Rescanning for crystallization rate.* To further investigate the nanocomposites' crystallization behavior, a special experiment is designed. In this experiment, the first step consists of scanning the samples from glassy state to 30°C above their melting points, waiting for 2 min and then followed by rapid cooling from that position to room temperature. Finally, a rescanning from the glassy state to a temperature that is 30°C

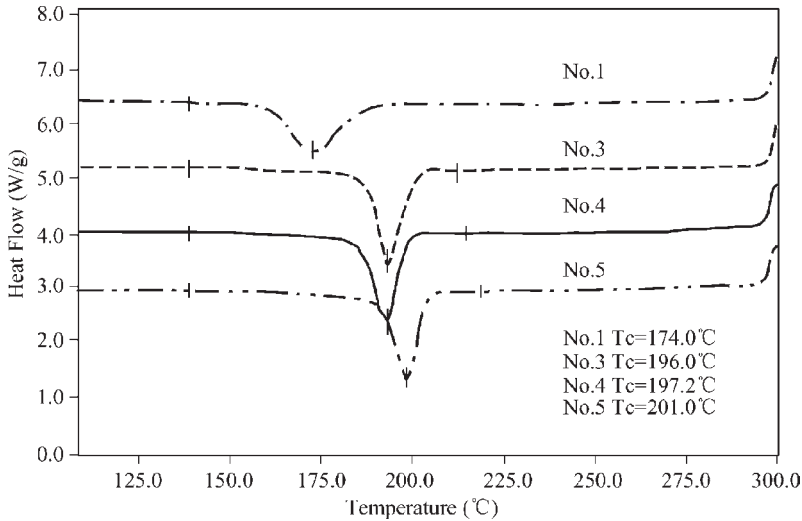


Fig. 5.41. The DSC pattern of NPET samples crystallized from the melting state. The samples have different content of clay (No.1 – pure PET, No.3 – 1.0% (by wt) clay, No.4 – 3.0% (by wt) clay, No.5 – 5.0 (by wt) clay).

above the melting point. The entire process presented above is called a “round trip”. In the second step, the round trip scanning is repeated. The round trip scanning runs using DSC have revealed that there are no cold crystallization peaks in NPET samples, while there are cold crystallization peaks in the pure PET samples.

The experiments show contrary results. The scanning curves for NPET go straight through forward melting points without any intermediate curves of cold crystallization. This process can be described in another way. After the first heat scanning and cooling, with a rescanning from room temperature to a higher temperature, the complete equilibrium state of a hybrid system will rapidly return to a new equilibrium level without an intermediate cold crystallization process for NPET. Such an intermediate stage occurs in PET crystallization. In other words, PET has a slow crystallization rate; therefore, in each thermal scanning, a real or absolute equilibrium cannot be reached quickly but could be reached in a long time.

In conclusion, nanoparticle exfoliation has significant nanoeffects on the nucleation and crystallization processes. It is assumed that the exfoliated nanoparticles are centers of nucleation and the confined molecular chains adsorbed on the interlayer space promote crystallization and accelerate the process.

(3) *Comparison of the crystallization rate.* The crystallization rates ($1/t_{1/2}$) of NPET and PET with MMTs, NPET and PET with silica, and pure PET are compared using the DSC experiments. The PET-MMT nanocomposites have a higher rate than the PET-silica nanocomposites, whose crystallization rate is higher than that of the pure PET. The plot of ($1/t_{1/2}$) vs. MMT load is shown in Figure 5.42. When the MMT load exceeds 5% (by wt), the crystallization behavior of NPET is not as obvious as shown there. The

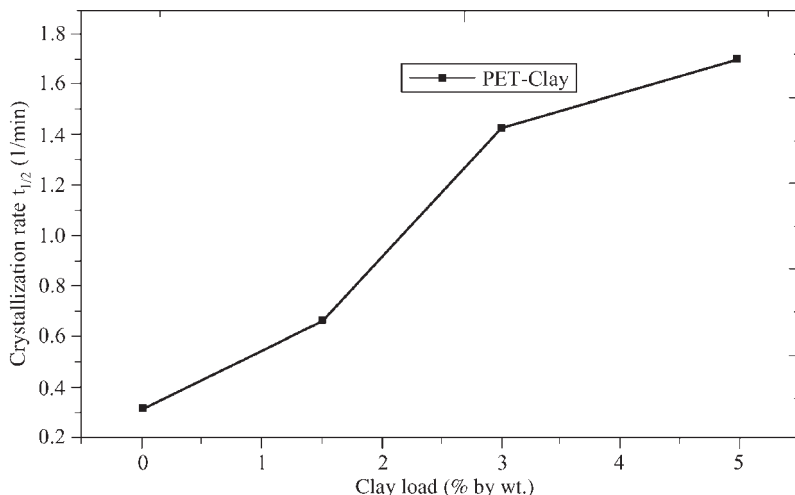


Fig. 5.42. Plot of NPET isothermal crystallization rate vs. MMT load at 214° C. A comparison of PET with NPET is shown in Figure 5.43 (a) and (b).

results in Figure 5.43 show that the NPET tends to crystallize at once while the pure PET goes through a cold crystallization process.

5.6.2.4. Nanoeffects in induced liquid crystal-like behavior

Whether the nanoparticles induce phase transformation in nanocomposites is still an open debate. Additionally, the induced liquid-like behavior in PS-MMT nanocomposites should be mentioned. Such a phenomenon is found in their extruded samples. As PS is amorphous, it is interesting to observe its melting behavior in PS-MMT nanocomposites in injected mold or extruded form (Figure 5.44).

The melting behavior is directly observed by the X-RD patterns of the PS-MMTs extruded samples. The X-RD spectrum shows a series of phase transformations in the diffraction angle below 10° (2θ) (Figure 5.45).

The polarized optical microscopy (POM) is used to trace the phase transformation process. In Figure 5.46, when an extruded PS-MMT nanocomposite sample is melted under the POM observation, phase movements or transformations are seen from (a) to (b) or (c).

Phase transformation does not result from the simple orientation of the particles by the exerted force induced by the extruder but rather from the ordered structure generated by the oriented layers dispersed in the PS matrix. There are additional examples related to the PS-MMT nanocomposites with exfoliated layers and self-assembling morphology [40,41]. The formation of ordered structure can be produced under different conditions. The formation of a complete exfoliation morphology and the assembly of particles with polymer chains require a number of conditions, such as a high molecular weight of PS, grafting of ammonia groups at the ends of the PS and the use of shearing or extruding forces. Examples of PS-MMTs with ordered structure are given below.

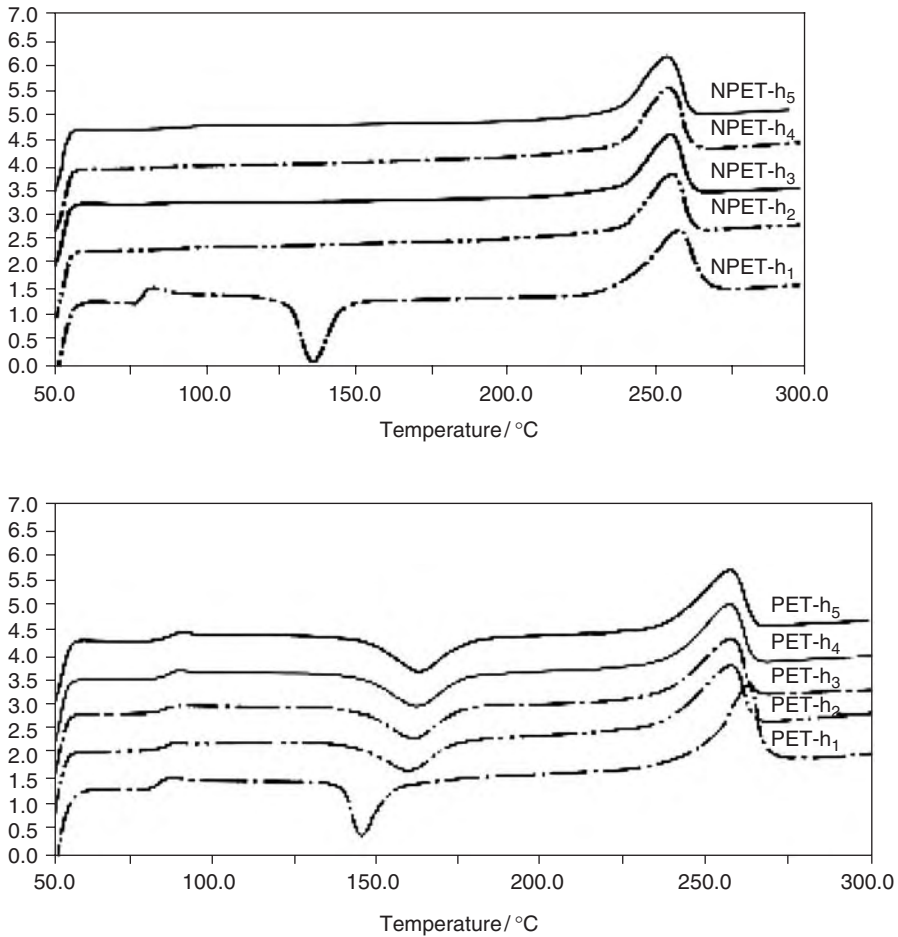


Fig. 5.43. DSC patterns of thermal and crystallization behavior of NPET-3.0% (by wt) clay (a) and pure PET (b). h_1 - h_5 stand for a scanning circle. Starting from room temperature to 300°C (h_1), then cooling to room temperature (h_2), and again scanning from room temperature to 300°C (h_3) and so on. The heating scanning rate is 10°C min⁻¹ and the cooling rate is 20°C min⁻¹.

Example 5.6.2.1. Preparation of PS-MMT nanocomposites. The MMTs are first treated with 16-alkyl trimethyl bromide ammonia. The treated MMTs are directly dispersed into PS monomers. Then, *p*-sulfide ammonia and 12-alkyl sulfide potassium are added to the system, resulting in a stable water-based emulsion. The emulsion is reacted with styrene. The polymerization reaction is at 70°C under nitrogen gas. The powder is then filled into a Brabender mixer, or a CS-183 type MMX minimax molder, to be extruded. Pellets of nanocomposites with oriented structure are obtained as observed by TEM measurements.

Example 5.6.2.2. Preparation of samples of PS-MMT nanocomposites with ordered structure. The PS-MMT nanocomposite samples with ordered structure are prepared

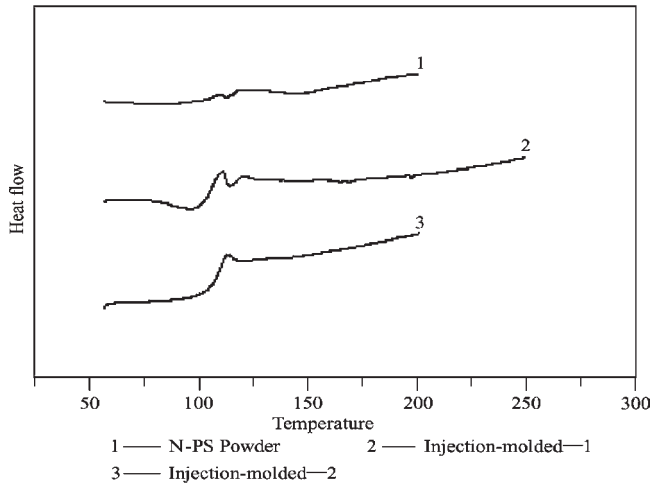


Fig. 5.44. DSC patterns of PS-MMT nanocomposite samples of different forms.

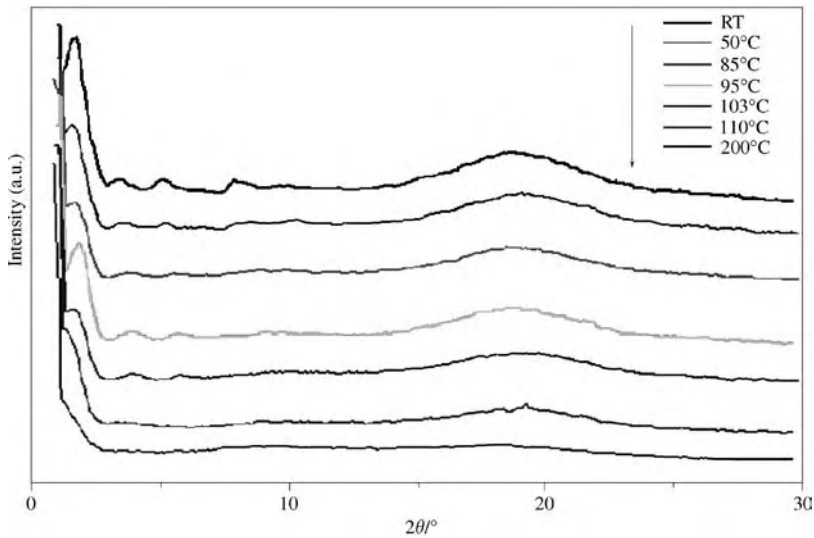


Fig. 5.45. XRD patterns of in situ heating extruded sample of PS-5.0% (by wt) MMT nanocomposite in the attached heating platform.

between two glass plates. The PS-MMT nanocomposite materials are melted at 200°C inside the two plates, and a rapid reaction occurs between the two species. In this way, sample sizes of 40 mm × 20 mm × 10 μm can be prepared. The samples are then quenched in cold water and the amorphous state is obtained. Finally, the samples are annealed under a fixed temperature to obtain samples with ordered structures.

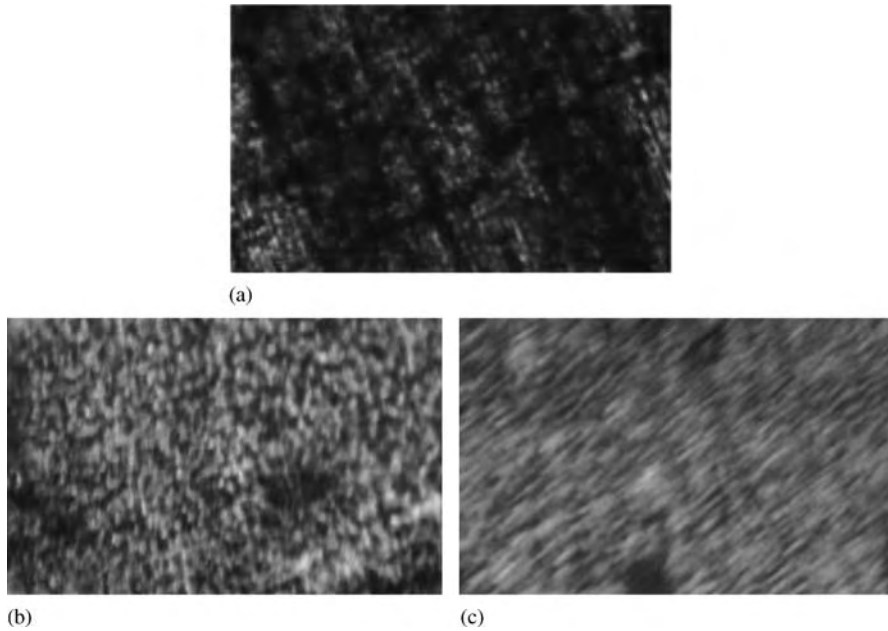


Fig. 5.46. POM observation of phase transformation of the extruded sample of PS-5.0% MMT nanocomposites made from the extruder as in Figure 5.45. (a) Room Temperature; (b) 90°C; (c) 100°C.

Example 5.6.2.3. Preparing ordered structure samples by applying hydraulic pressure. Pellet samples of PS-MMTs can be molded under hydraulic press in their melted state. Then, by an in situ process, the melted samples are cooled from their melting state to room temperature and are isothermally crystallized for 5 to 200 min. By this process, a sample with initial order structure is prepared.

5.6.2.5. Particle morphology and aggregation. As shown previously, the size of the spherulites is refined by the introduction and nucleation of nanoparticles. During this process, a part of the exfoliated particles have a tendency to aggregate again. Some aggregated particles may form irreversible coarse particles as seen in Figure 5.47.

Some dissociated SiO_2 particles that naturally exist in the layered silicate accounting for less than 0.5% (by wt.) may also disperse in the exfoliated layers by an electrostatic effect. These SiO_2 particles may have created the agglomerated particles in layered silicates. The exfoliated particles are seen in Figure 5.47(a). Some scattered particles still maintain a stacking state or are composed of 2–10 layers of layered silicates. These silk-like layers formation and their interphase indicate strong interactions between them. Unlike Figure 5.47(a), 5.47(b) shows some blocks and a few parallel structures, whose particle sizes are 1–10 μm , accounting for 3–4% (by number) of all the dispersed particles. The exfoliated and/or aggregated particles are related to the intercalant chain length. Experimental results suggest that the bonding interaction between intercalants and layered silicates is not the unique factor that affects the

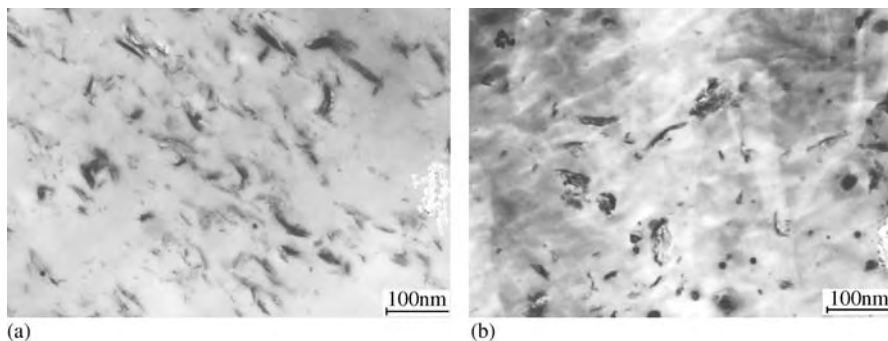


Fig. 5.47. TEM aggregated particle morphology of layered silicates in NPET. (a) exfoliated particles with a few agglomerate particles; (b) agglomerated particles.

exfoliation. For example, by using ethanolamine and laurylamine as intercalants for treating MMTs for polybutylene terephthalate (PBT) polymerization, the PBT-MMT nanocomposites have different dispersed particle morphology and corresponding properties depending on the intercalant used. The long chain of laurylamine leads to adequate exfoliation of the layered structure, but the short chain and the polar group of ethanolamine creates agglomerations of particles. A large number of exfoliated particles enhances the nanocomposites, HDT or related thermal behavior.

5.6.2.6. Assembly or self-assembly

The interphase of self-assembling structures. Nanoeffects resulting from particle exfoliation and their assembling or self-assembling behavior have been investigated. It is widely accepted that there can be self-assembled morphology in polymer-layered silicate nanocomposites. Molecules that have both hydrophilic and hydrophobic properties and ordered aggregation behavior interact with the inorganic nanoparticle interphases. The interactions at interphases can create nanoeffects, which have an impact on the optical and crystallization aspects of nanocomposites. It is now accepted that assembling or self-assembling structures are the cause of nanoeffects in quantum scale materials.

5.6.3. Nanoeffects from assembly and self-assembly

5.6.3.1. The assembly between surfactant and molecularly deposited films

Surfactant and molecular deposits have charged end groups, which cause them to be adsorbed on the nanoparticles. Depending on the amount of charge on the particle surface, these surfactant and molecular deposit films are designed so that the final nanocomposites have an assembling, organizational structure. The regular assembling patterns of these nanocomposites have special properties and functions compared to their original state. For example, films on the particles have low friction, special optical properties, special rheological properties and resistance to high temperature. The combination of layered silicates of clay with MD films is used to gain insight into the nature of life.

5.6.3.2. Self-assembly in polymer-layered silicate nanocomposites

(1) *Self-assembly characterized by X-ray patterns.* Wide-angle X-ray diffraction (WAXD) technique is chosen to investigate ordered or crystallized structure in annealed samples of NPET. X-ray patterns of annealed NPET are shown in Figure 5.48. Figure 5.48 shows the typical triclinic crystal diffraction patterns for PET together with splitting peaks. As a distinctive phenomenon in the small-angle region of the diffraction patterns, several small diffraction peaks appear. These small peaks vary with the annealing time. The peak in diffraction position at $2\theta = 5.0^\circ$ is a residue of unexfoliated layers of MMTs, while the peak in a position less than 5.0° is a possible liquid state. The appearance of peaks in the small-angle region of 2° – 3° is still under debate. The exfoliated layers will be self-organized in the polymer matrix. The self-assembly process is also observed in PS-MMT nanocomposites, where a similar possible liquid order structure is formed because pristine PS prepared by free radical initiation is not crystalline but amorphous.

(2) *The ordered or irregular structure revealed by AFM.* The basis of AFM scanning imaging has been presented in the previous sections. Taking PET as an example, its molecular chain unit is $-(OC-\phi-COOCH_2CH_2O)-$ where ϕ is the benzene ring. Figure 5.49 shows the AFM images of PET-layered silicate of clay (NPET) and pure PET structures.

The morphological variations of different NPET samples can be characterized by AFM techniques. Particle dispersion in the polymer matrix is best characterized in amorphous samples because the particles are separated from the matrix by a melt-quenching process. With this treatment, similar ordered morphology in either the entire area or in limited regions has been obtained. The ordered structures result from the assembly of crystalline microdomains of polymer matrix and the exfoliated layers, which are dispersed in polymer matrix. In practice, it is noted that the pure polymer PET has many

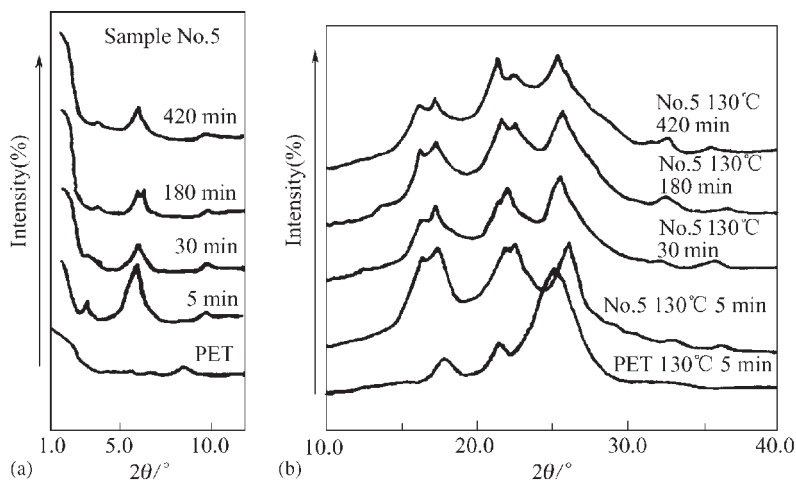


Fig. 5.48. X-ray patterns of annealed NPET: (a) diffraction patterns in small-angle region; (b) diffraction patterns in wide-or large-angle region.

random microdomains of crystallites, although the sample went through a melt-quench process (Figure 5.49(b)). The introduction of exfoliated layers into the polymer matrix has enlarged its molecular separation up to about 1.0 nm (Figure 5.49(a)). The separation of pure PET obtained from Figure 5.49(b) is only 0.4 nm. The transition from molecular interactions in PET to molecular–nanoparticle interactions demonstrates that the original interaction forces are replaced, and also that the assembly is varied.

The separation between two phenyl rings is calculated to be 0.28 ± 0.02 nm and agrees with that obtained from experimental data. A large load of MMTs (Figure 5.49(a)) will have an exfoliation efficiency lower than that of a low load because the separation between molecules due to intercalations is smaller than that observed for low loads.

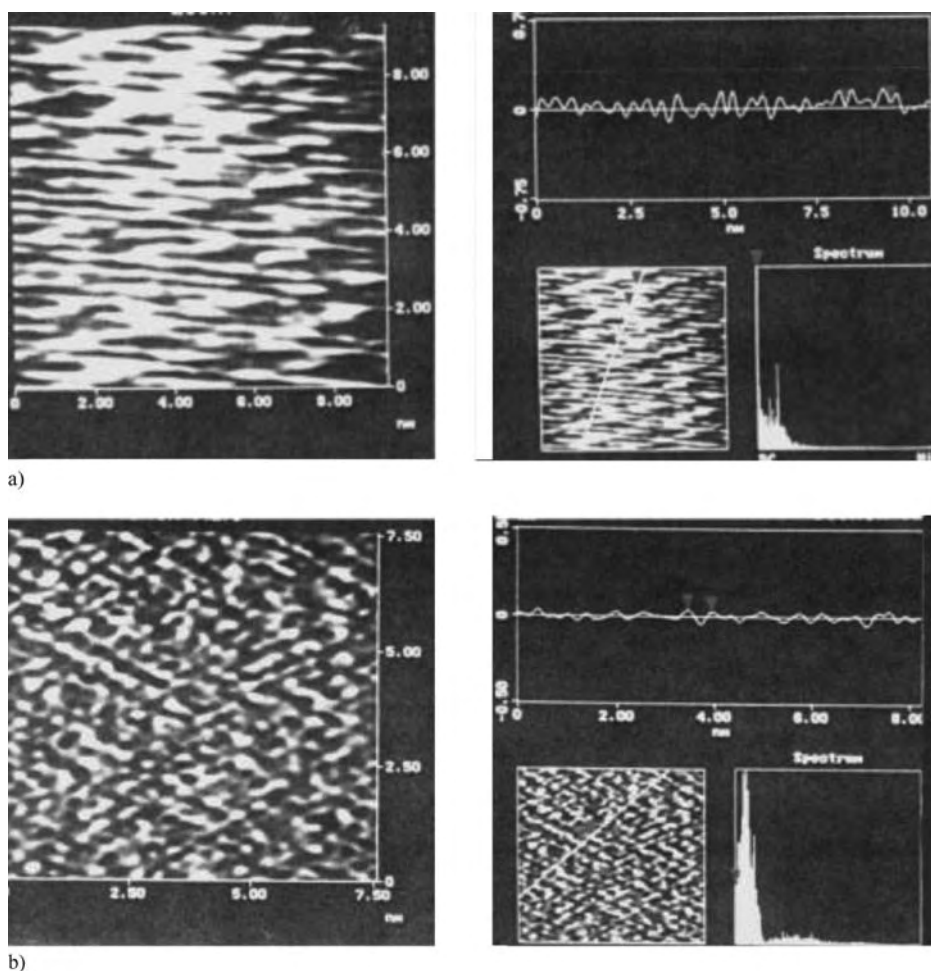


Fig. 5.49. AFM morphology of NPET and PET samples obtained using a melt-quench process: (a) NPET (1.0% MMT load); (b) pure PET.

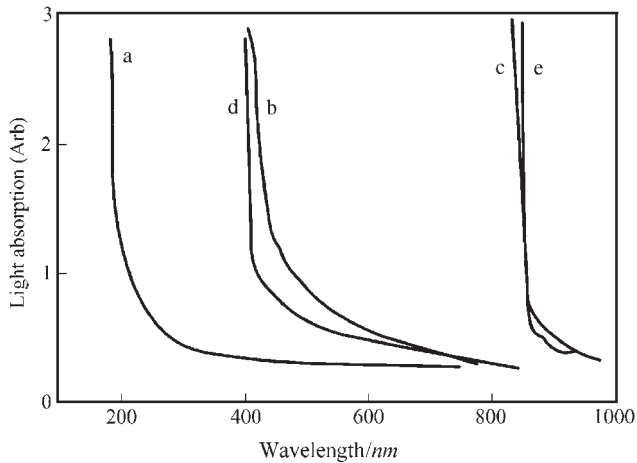


Fig. 5.50. Light absorption spectra of reference samples and composite samples: a – reference sample (mesoporous SiO_2 solid); b – composite sample annealed at 623 K for 2 h; c – sample b exposed to room temperature in air for 12 h under relative humidity of 60–65% d – sample c annealed at 580 K for 10 min; e – Ag_2O powders with diameter of 50 nm.

5.6.3.3. Sensitivity to the environment

Specially designed structures of mesoporous composites are sensitive to the environment. Composites of nanoparticles of Ag/mesoporous SiO_2 are extremely sensitive to humidity. For room temperature and low humidity (e.g., less than 30%), such composites are stable. However, when the humidity is higher than 60%, these composites become unstable and produce a series of new phenomena that are not found in either Ag or Ag/SiO_2 composites. More recently, our research team as well as other groups have found that similar nanostructures can reversibly switch between transparent and opaque properties. For example, when the nanoporous composites based on silica transform from transparent to opaque, the colors of these materials change from light yellow to black as soon as they are exposed to a humidity higher than 60%. Afterwards, these samples return to transparent light yellow from black color after annealing at a temperature higher than 500 K, and then this phenomenon can be repeated again. The phenomenon can be described using the shift of light absorption. Investigations have shown that this phenomenon is a result of the surface structure variation of Ag nanoparticles inside the pores, when the Ag surface is oxidized to Ag_2O at high relative humidity. On the other hand, Ag_2O is changed back to Ag when annealed at 500 K. Thus, the nanoscale of Ag promotes oxidation of the Ag surface and, vice versa, the nanoscale promotes degradation of these oxides at high temperatures (Figure 5.50).

References

- [1] L.D. Zhang and C.M. MO, *Nanomaterials and Nanostructure*, Science Press (China), Beijing, 2000.
- [2] Y.C. Ke, *Postdoctoral Reports*, Institute of Chemistry, China Academy of Sciences, 1998.
- [3] J.C. Halpin-Tsai and J.L. Kardos, *Polym. Eng. Sci.* 16 (5) (1976) 344.

- [4] Y.C. Ke, Z.B. Yang, and C.F. Zhu, *J. Appl. Polym. Sci.* 85 (13) (2002) 2677.
- [5] Z.N. Qi, Y.C. Ke, and Y.Z. Zhou, *Chin. Pat. Appl.* 971041964.
- [6] Y.C. Ke, and C.F. Long, *International Symposium on Polymer Physics Guilin City, China*, 25–29, p. 158. (1997).
- [7] Y.C. Ke, Z.N. Qi, and C.F. Long, *J. Appl. Polym. Sci.* 71 (1999) 1139.
- [8] S.C. Lu, *Processing Technologies of Powders*, China Light Industry Press, Beijing, 1999.
- [9] Y.C. Ke, Y.B. Zheng and Z.W. Wu, *J. Mater. Sci. (China)* 10 (2) (1996) 205.
- [10] Q. Li, *Postdoctoral Report*, Institute of Chemistry, China Academy of Sciences, 1996.
- [11] Y.C. Ke, C.F. Zhu, and Z.N. Qi, *Symposium on Polymer Science Hefei, China*, 1997, 1910.
- [12] M. Kaszuba, M. Connah & K. Mattison, *Malvern Co. Labplus international sept*, 2004 (www.malvern.co.uk)
- [13] (a) M. Connah, *An introduction to the principle of particle sizing*, Specifications for Malvern Co. (b) P. Debye, *J. Phys. Colloid Chem.* 51 (1947) 18–32.
- [14] (a) L.M. Liu, *MS Dissertation*, Institute of Chemistry China Academy of Sciences, 1998 (b) L.M. Liu, Z.N. Qi, F.S. Wang et al., *J. Appl. Polym. Sci.* 71 (1999) 1133.
- [15] M. I. Mendelson, *J. Am. Ceram. Soc.* 52 (8) (1969) 443.
- [16] Y.C. Ke, *Reports on PET- Clay Nanocomposites*, Reports to BASF, 1998.
- [17] V. Aegutz and T. Goldacker, *Macromol. Rapid Commun.* 21 (2000) 16.
- [18] Y.C. Ke, *J. Appl. Polym. Sci.* 85 (13) (2002) 2677–2691.
- [19] S.C. Lu, *Powder Processing Techniques*, China Light Industry Press, Beijing, 1999.
- [20] Y.C. Ke, *Polymer-Inorganic Nanocomposites*, Chemical Industry Press of China, Beijing, 2003.
- [21] (a) P. X. Sun, *Netzsch Specifications for DSC and TGA*, Beijing, 2003.
- [22] (a) F.-R. C. Chang, N.T. Skipper, and G. Sposito, *Langmuir*, 11 (1995), 2734; (b) N.T. Skipper, F.-R. C. Chang, and G. Sposito, *Clay and Clay Minerals*, 43 (1995) 285; N.T. Skipper, F.R.C. Chang, and G.Sposito, 43 (1995) 294; (c) F.-R.C. Chang; N.T. Skipper, and G. Sposito, 13 (1997) 2074; F.R.C. Chang, N.T. Skipper, and G. Sposito, 14 (1998) 1201; (d) Group of the Guiyang Geochemical Institute, China Academy of Sciences, *The Handbooks for Identifying the Mineral Powder Crystallites by X-ray*, Press of Science, China, 1978, p. 283; (e) C.J. Yan, *Master Degree Dissertation*, University of Petroleum, Beijing, 2004; (f) M. O'keefe, N.E. Brese, *J. Am. Chem. Soc.*, 113 (1991) 3226. (g) H. J. Sun, *Phys. Chem. B.*, 102 (1998) 7338.
- [23] D.M. Lincoln, R. A. Vaia, Z.G. Wang, B.S. Hsiao, *Polymer* 42 (2001) 1621.
- [24] Y.C. Ke, *Chin. J. Chem. Eng.* 11 (6) (2003) 701.
- [25] Y.C. Ke, T.B. Wu, C.M. Xu et al., *China Particology* 1 (6) (2003) 247.
- [26] Z.N. Qi, Y.C. Ke, Y.Z. Zhou, et al., *Chin. Pat. Appl.* 97104055.9 (1997).
- [27] Y.C. Ke, *Chem. Eng. Oil & Gas (Chin.)* 33 (1) (2004) 50.
- [28] D.B. Zax, D.K. Yang, R.A. Santos, H. Hegemann, E.P. Giannelis, and E. Manias, *J. Chem. Phys.* 112 (6) (2000) 2945.
- [29] E. Manias, H. Chen, R. Krishnamoorti, J. Genzer, E. J. Kramer, and E.P. Giannelis, *Macromolecules*, 33 (2000) 7955.
- [30] S.S. Chang, *Polym. Commun.* 29 (1987) 138.
- [31] Y. Lee and R.S. Porter, *Macromolecules*, 20 (1987) 1336.
- [32] S.Z.D. Cheng, *J. Polym. Sci. Polym. Phys. Ed.* 28 (1990) 655.
- [33] M. Yagpharov, *J. Therm. Anal.* 31 (1986) 1073.
- [34] N. Alberola, *J. Mater. Sci.* 26 (1991) 1856.
- [35] P.J. Holdsworth, A. Turner-Jones, *Polymer* 12 (1970) 195.
- [36] H. Marand and A. Prasad, *Macromolecules* 25 (1992) 1731.
- [37] S.M. Aharoni *J Appl. Polym. Sci.* 29 (1984) 853.
- [38] A. Gary and M. Gilbert, *Polymer* 17 (1976) 44.
- [39] Z. D. Zhao, *PhD Report*, Institute of Chemistry, China Academy of Sciences, 1995.
- [40] B. Hoffman, C. Dietrich, R. Thomann, and R. Friedrich, *Mulhaupt, Macromol. Rapid Commun.* 21 (2000) 57.
- [41] Y.T. Lim and O.O. Park, *Macromol. Rapid Commun.* 21 (2000) 231.

This page intentionally left blank

CHAPTER 6

Applications and Products

OUTLINE

- Introduction 330
- 6.1. Applications of nanocomposites 330
 - 6.1.1. *Barrier materials and packages* 330
 - 6.1.2. *Fire-retardant materials* 334
 - 6.1.3. *Engineering plastics* 337
 - 6.1.4. *Films and clothes* 339
 - 6.1.5. *Coatings* 341
 - 6.1.6. *Electronics* 348
 - 6.1.7. *Catalysts and carriers* 349
 - 6.1.8. *Additives* 363
- 6.2. Products of nanomaterials 368
 - 6.2.1. *Products in industry* 368
 - 6.2.2. *Product processing technology* 371
 - 6.2.3. *Product quality control* 375
 - 6.2.4. *Product markets* 377
- 6.3. Nanocomposites and traditional industries 378
 - 6.3.1. *Chemical materials and additives* 378
 - 6.3.2. *Construction materials* 380
 - 6.3.3. *Reformation of traditional industries* 380
- 6.4. Prospects 384
 - 6.4.1. *Membrane and film materials* 384
 - 6.4.2. *Applications of the monodisperse particles* 384
- References 387

In this chapter, we discuss how nanoparticles are made into a series of new products for applications in engineering materials, functional materials, coatings, etc. Some unique and potential industrial applications of nanomaterials are also introduced.

Introduction

There is an increasing need for polymer-based nanocomposite materials due to the developments in traditional industry and advanced materials. These needs pave the way for a unique and new market for improving traditional products [1–3]. At present, the diverse organic polymers with high yield find their applications in fibers, resins, rubbers and their composites including polymer–polymer and inorganic reinforcing polymer composite. Due to difficult dispersion behavior, the composites of nanoparticle filling polymer develop relatively slowly, while the polymer–inorganic nanocomposite materials by in situ polymerization technology increase rapidly. There is a great potential to modify traditional materials. So far, the in situ intercalation polymerization technique is thought to be one of the best choices for dispersing nanoparticles in the polymer melt. It may provide a very large number of new products for daily life and industrial applications.

Nanocomposites have several advantages. Loading small amounts of inorganic nanoparticles usually produces superior properties in nanocomposites. For example, in nylon6-MMT nanocomposites with a load as less as 5% (by wt), the heat distortion temperature (HDT) increases to 150°C compared to the 65°C of pure nylon6, while its density remains nearly unchanged. The barrier properties of some polymers as polyester and polypropylene can be enhanced 3–6 times over the pristine polymer resins. In our daily life, the materials or products of films or membranes, containers such as bottles, cans, boxes, etc. urgently need improved barrier performance to protect the contents inside them from being spoiled.

From a theoretical point of view, the nanoeffects from the nanoparticles in the nanocomposites provide an important window to modify traditional petrochemicals and related materials, and thus play an important role in reforming traditional industry. In other words, polymer–layered silicate and silica nanocomposite materials can be applied to those fields where pure polymer materials have been used.

6.1. Applications of nanocomposites

6.1.1. Barrier materials and packages

6.1.1.1. Introduction

Several barrier materials for packaging products exist which are made by applying either multiple layer coextrusion techniques or coating techniques. The nanocomposite materials for these packaging applications are designed to provide high barrier properties to oxygen (O₂) and carbon dioxide (CO₂) and to be recycled after applications. The modified nanocomposite materials are endowed with a long term, shelf-storage period and thus are suitable for the beer (or wine) bottle industry in keeping with shelf longevity and product freshness.

To improve the bottle's barrier properties based on organic polymers, 10–40-nm-thick layer coatings on the inner and outer wall of the polymer containers by plasma techniques are used. In addition to the multiple layered composites, the use of a homopolymer of PEN or the copolymer of PEN–PET, by a coextrusion process, is also

a choice for barrier materials. All these techniques have been seen in the products from different corporations. The Crowns Co. (Europe) creates a beer bottle using a technique of “an integration of blowing-pumping (pouring) of polyester resin.” The bottle product has achieved a high shelf-life of 6 months but is expensive. The nanoparticle coating is unstable.

The development of plastic bottles shows a great trend in the replacement of the traditional glass beer bottle, which have many disadvantages such as, being unsafe, heavy weight and being inconvenient to transport.

In 2001, the overall number of containers produced in the world for beer were 3030×10^8 , where 71% were glass bottles, and the rest were metal bottles. In China, glass bottles account for 80% of the beer containers. In 2002, the total yield of beer in China was 23.84 million tons which accounted for one-fifth of the world's beer production. Means to reduce the bottle weight for beer or liquor is becoming an important issue. A 640 ml bottle weighs up to 460–540 g or 600 g, while the same plastic bottle weighs 42–65 g, only one-tenth (1/10) of the glass one.

To improve the bottle's properties and seek an alternative solution, plastic bottles have been tried in the beer package industry. Table 6.1 gives the data from our investigations. In practical applications, 3–6 months of shelf-life for a beer package is required (Table 6.2). So far, both the multiple layer coextrusion and coating technologies are used to prepare nanocomposite materials as barrier materials (Table 6.3).

The total yield of PET for beer packages in 2004 in the leading countries of the world is 0.4 million tons, which produce 12×10^8 500 ml bottles. The shelf-life of a plastic beer bottle is 6 months. Nanocomposite materials used for bottle manufacture solve problems such as the beer colloids instability including biological and non-biological aspects, oxygen (O₂) permeation and bad taste due to light exposure.

For barrier material used in bottles, there are many choices such as polymers of PVDE, MXD₆, PET and PA. All these are suitable to improving the barrier properties to gas (O₂, and CO₂). PA6 itself has unsatisfactory barrier properties to O₂ and CO₂,

Table 6.1
The PET-based composite materials and their barrier properties to gas

No.	Company Names	Barrier resins	Processing or (°C)	Shelf life (mo)	Effect v/v
1	Honeywell	Aegis OX + nylon6	280	6 mo	Barrier O ₂ , CO ₂
2	CMB(GB)	OXBAR + PET/MXD6	280–300	24 mo	Barrier O ₂ , CO ₂
3	Leydold(GER)	PET/SiO _x coat	EB/8–90 μm	3 mo	Barrier
4	ULVAC	PET/C coat	EB/vacuum coat	6 mo	Barrier
5	Superex	PET/LCP	10–15%LCP	6 mo	Barrier, 2 times
6	Amoco/Shell	PEN, PEN/PET	Coextrude	6 mo	Barrier, 4 times
7	Eastman	PET/MMTs	In situ polymerization or Coextrude	3 mo	Barrier, 4 times

Note: nylon6, polyamide 6; MXD₆, a special kind of nylon; processing, processing temperature; Mo, month; PET, polyester; LCP, liquid crystalline polymer; mo, months; EB, electronic beam; effect v/v, the ratio of shelf life for composite bottle to pure material bottle.

Table 6.2

General data for plastic beer bottle of PET in industrialization

No.	Beer producer Industrialization	Capacity	Material for beer bottles	Shelf life
1	Anheuser Bush, US, 1998.7 try	16 oz	100% PEN	2 mo
2	Bass Breweries, UK, 1997.12	0.33 l	3-PET/EVOH	5 mo
3	Danone, France, 1998 try	0.33 l	3-PET/EVOH	5 mo
4	Carlton United Breweries Australia, 1998.12	0.5 l	PET/epoxy amine coat	100 day
5	Heineken, Netherlands, 1998.12 try	0.5 l	5-PET/nylon/adsorbent	6 mo
6	Karlsberg, Germany, 1998.11 try	0.5 l	PET/12% nylon	9 mo
7	Miller, US, 1998.11 try	16/20 oz	PET/nylon/O ₂ adsorbent	4 mo
8	Old Manor, UK, 1996 try	3 l	PET or PVDC coat	3 mo
9	Otchakovo, Russia, 1998 try	2 l	PET	28 day

Note: Oz, ounce; l, liter; PEN, a polyester of polyethylene tere-naphthylate; EVOH, an ethyl-vinyl ester copolymer resin; PVDC, polyvinyl dichloride; try, in process to be industrialized; mo, Month.

Table 6.3

The yield of beer in PET packages of the world

Beer yield (tons)	USA	Japan	Germany	Italy	France	Britain	Australia	Canada	China
In 2000	73,500	35,000	28,000	30,600	34,000	16,300	15,400	14,000	27,050
In 2004	114,000	50,000	46,000	51,000	38,000	25,700	15,400	20,800	36,000

while the PA6 (or MXD6)-layered silicate nanocomposites are very popular as a barrier layer in the multiple layer system.

6.1.1.2. The beer bottle

In different locations of the bottle, the formaldehyde content is not homogeneous. The color of the beer bottle depends on the processing technology. Several measurements are taken to solve such problems by copolymerization of monomers of *p*-terephthalate (PTA) with *m*-terephthalate (MTA) to reach a homogeneous crystallization and control the wall thickness during processing. The resin's crystallinity is a special factor to be considered. The different locations in the beer bottle from its neck to the bottom have different degrees of crystallization. To obtain a homogeneous bottle, better processing technology is needed.

Based on a series of commercial nanoscale particle precursors (NPP) invented by us, several kinds of polyester nanocomposite materials for barrier bottles are under trial applications. We are investigating their applications. Bottles made from NPET materials are shown in Figure 6.1.

A practical example of a nanocomposite material is PA6-5% (by wt). MMTs (NPA6). NPA6 has a HDT of 96–120°C (56–65°C for PA6) and an O₂ permeability coefficient of 0.65–0.67 (1.2–2.0 for PA6). The measuring conditions are: HDT at 18.5 kg cm⁻¹, O₂ permeability coefficient at 23°C, RH 60%; units are cm³ m⁻²-24 h Pa. NPA6 can serve as a barrier layer in different types of bottles such as PET-NPA6-PET and PET-PET-NPA6-PET-PET.

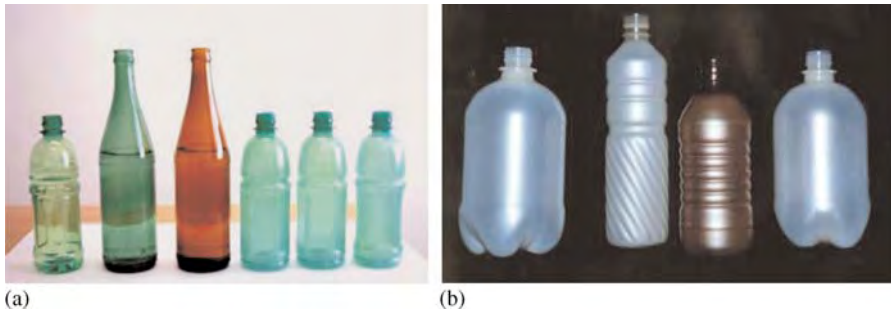


Fig. 6.1. Bottles made from NPET (PET-MMTs nanocomposites) materials: (a) left to right: the first is a PET bottle, the second and third are green and brown glass bottles, and the other three are bottles of NPET materials; (b) left to right: bottles with different shapes and colors; the first, second and fourth are NPET bottles, and the third is a PET bottle.

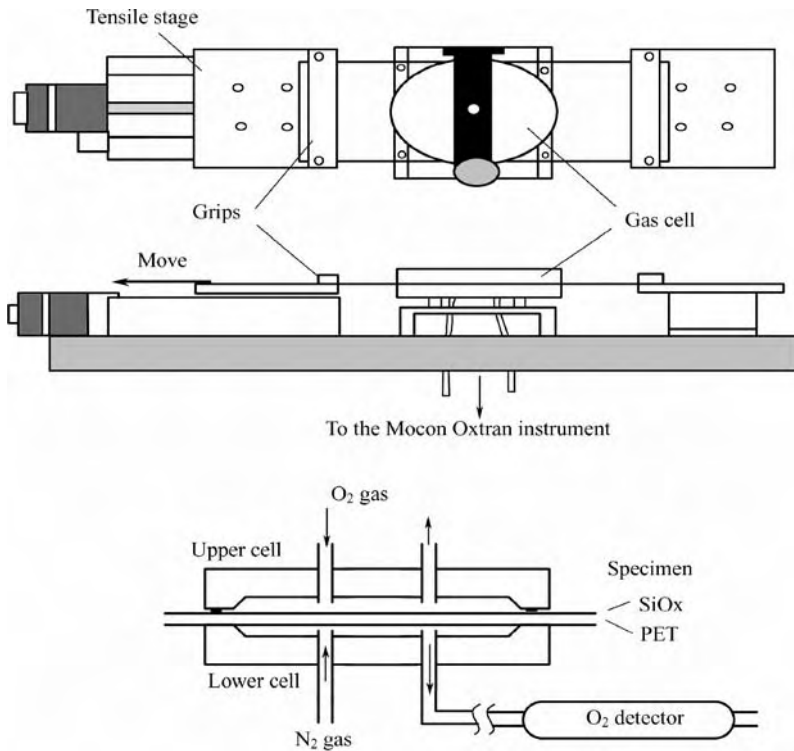


Fig. 6.2. Measurement equipment for barrier materials.

The barrier properties of these materials are measured in the equipment drawn roughly in Figure 6.2, where the round film sample with radius of 80 mm is firmly compressed in the gas cell. The cell room is then deflated and oxygen gas is permeated through the film sample. The cell has a projected picture in the lower part of Figure 6.2.

By measurements, we often get 3–6 times the barrier property for the nanocomposite films over the pure polymer resins, which is suitable for practical applications. The data are calculated from the China standard of GB/T1038-2000.

6.1.1.3. The diffusion of silica

Silica aggregates with an open (fractal) structure can percolate at lower volume fraction than non-aggregated hard spheres, which has been investigated in the literature [4]. The influence of 10-nm-diameter silica particles on oxygen diffusion and oxygen permeation in two different films is compared. When most of the dye (platinum octa-ethyl porphin) is bound to the silica surface in this composite film, the diffusion coefficients (D) decrease with an increase in silica content, but the diffusion effects are rather small; D_{O_2} ranges from 2.2×10^{-5} to $1.4 \times 10^{-5} \text{ cm}^2 \text{ s}^{-1}$ when the silica load increases to a large extent. Thus, in applications, the silica particles are mainly used as carriers that adsorb oxygen to enhance the barrier properties of the nanocomposites. When the nanocomposite films are used as sensors, the layered silicates or silica also act as carriers of luminescent dye. In this application, the layered silicates are even more effective than that of the silica. The particles in the composite effect the response of the sensor to gas in a way that is poorly understood so far.

6.1.1.4. The mechanism of nanoparticles providing barriers to gas

We use two geometrical models for explaining gas transport in barriers. These models are shown in Figure 6.3(a) and (c). In model A there are complex pores in the dispersed nanoparticles of the nanocomposites providing a long path for gas to pass through (see Figure 6.3(a)). Similarly, when gas passes through the particles in the nanocomposites, it is adsorbed by the particles forming diverse bubbles and provide a barrier to the gas (Figure 6.3(c)).

6.1.2. Fire-retardant materials

6.1.2.1. Layered silicates as retardant material

Layered silicate acting as a retardant material provides a shielding layer insulating oxygen from the polymer matrix. Layered silicates of clay such as MMTs and

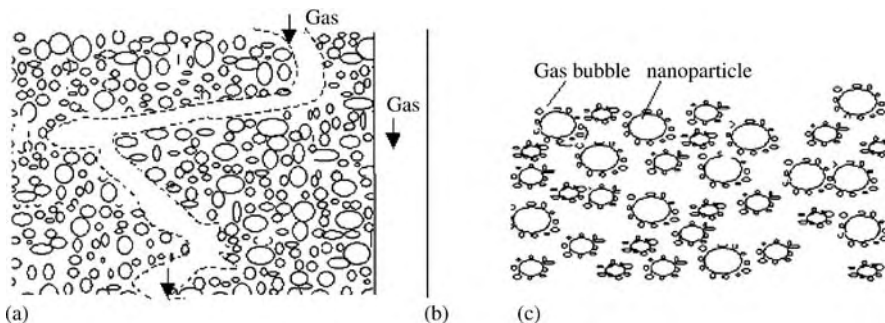


Fig. 6.3. Geometrical models of nanoparticle providing a barrier to gas in the nanocomposite: (a) Complex pore model of the space in the dispersed nanoparticles; (b) Straight pore without nanoparticles; (c) Adsorbing bubble model of nanoparticles providing a barrier to gas.

attapulgites have been treated with retardant materials in nanocomposites using a mixing technology. The retardant reagent is intercalated into the layer space, then they are blended with a polymer matrix or in situ polymerized together to obtain a new nanocomposite material. The nanocomposites are suitable for reinforcing engineering plastics with retardant function. Some of these reinforced nanocomposites of MMTs with PET polymers with glass fibers are shown in Table 6.4.

The glass fiber-reinforced engineering plastics based on nanocomposite materials of PET show a fire-retardant grade of *V-0*. When processing the reinforced composites of NPET, the quantity of retardant reagents required is lesser than that in traditional plastics. The thorough dispersion of both retardant reagents and nanoparticles has effects on the performance of the final composites. With their development and wide applications, they (including carbonate or titanium salt) can become choices in replacing phosphorous retardants.

6.1.2.2. Layered double hydroxides (LDHs) as a retardant material

The LHDs are also called hydrotalcite and have a large amount of bonding water in their interlayer space. They discharge water and carbon dioxide (CO_2) when subjected to heat to retard fire. After the release of H_2O and CO_2 , the nanostructured LDHs is transformed into porous solid base with high specific surface area, which strongly adsorbs smoke and organic acid gas during burning. LDHs itself have no toxic content and thus are safe retardant materials. A highly effective retardant LDHs is obtained by introducing free radicals trapping reagents in it. Hydrotalcite and hydrotalcite-like compounds have layered structures. The LDHs have a structure similar to hydromagnesite.

According to the calcination temperature T_c , the progress for calcinating hydrotalcite is divided into several stages. In the first stage, when T_c is lower than 200°C , the water inside the gallery is lost, but the layered structure is maintained. At the second stage, when $T_c = 250\text{--}450^\circ\text{C}$, the $-\text{OH}$ on the plate surface is degraded; the degradation of CO_3^{2-} discharges CO_2 gas. In the third stage, at temperatures from 450 to 550°C , the $-\text{OH}$ groups are completely lost according to experimental analysis and form the products of $\text{Mg}\text{--Al}\text{--O}$ mixed oxides (layered double oxide (LDO)). At this point, the hydrotalcite inorganic system has a maximum specific surface area and pore volume [5].

Table 6.4

Properties of NPET as engineering plastics reinforced by different loads of glass fibers

Properties	Standards	NPETG10	NPETG20	NPETG30
Tensile strength (MPa)	GB/T1040	90	121	140
Tensile modulus (GPa)	GB/T1040	5.5	7.2	8.1
Extension at break (%)	GB/T1040	5.6	3.0	1.7
Bending strength (MPa)	GB8341	158	180	200
Bending modulus (GPa)	GB9341	5.1	7.5	10.2
Izod impact (J m^{-1}) at 23°C	GB1843	54	69	75
HDT (at 1.82 MPa)	GB1634	190	210	218
Melting point ($^\circ\text{C}$)		250–260	250–260	250–260
Degradation temperature ($^\circ\text{C}$)		469	453	448
Fire-retardant grade UL94		V-0	V-0	V-0

Usually, when T_c is within 550°C , the mixed metal compounds retain some humidity (or water) and CO_2 (or carbonate), and thus they can restore to double-layered hydroxides, once again showing good “memory” behavior. LDO has good thermal stability in acting as a fire-retardant material.

Anions are adsorbed in layer gallery of LDHs and often react with the materials containing ions such as, CO_3^{2-} , PO_4^{4-} and I^- . The layer structure is seen in Figure 6.4.

The chemical compositions of LDH layers can be adjusted depending on the requirements. This leads to variation of ion type and quantity by recognition between the native layer and foreign material. The crystallite size of LDHs is capable of being adjusted from 20 to 60 nm, and thus LDHs can show diverse practical functions acting as barrier reagents for ultraviolet light, fire retardancy, thermal stability, catalyst carrier, environmental-friendly materials and possible shielding materials for red light.

By using hydrotalcite containing magnesium and aluminum, initial degradation temperature of LDHs is either in the lower or higher temperature range, which widens the scope of its retardant applications. LDHs have advantages of retardant such as, eliminating smoke and filling aspects by both hydroxyl aluminum and hydroxyl magnesium compositions. LDHs are regarded as new chlorite-free fire retardants with high effectiveness [6].

When LDHs are mixed with a polymer matrix, the degraded hydrotalcite containing magnesium and aluminum helps discharge the CO_2 gas and moisture, diluting the concentration of burning gas and diminishing fire. Further, MgO and Al_2O_3 from the degraded products act as layers of heat insulation. Meanwhile, absorbing heat in the degradation of LDHs reduces the temperature on the polymer surface. The wider degradation temperature of the LDHs is more close to that of the protected polymers, which shows a better retarded oxidation or fire effect [6].

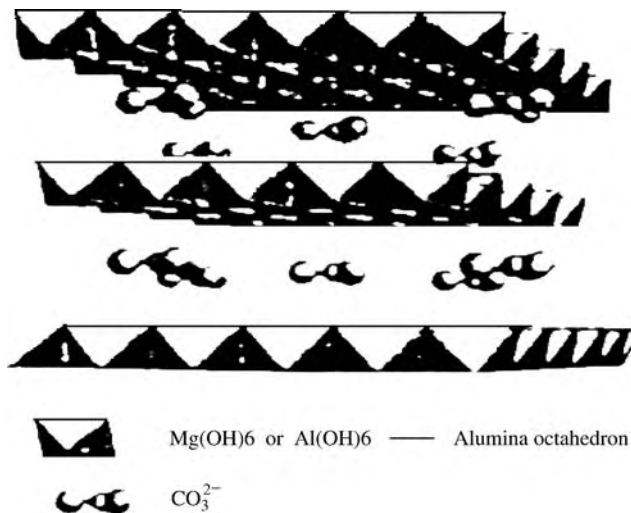


Fig. 6.4. Proposed layer structure of synthetic LDHs.

6.1.3. Engineering plastics

Most nanocomposites have applications in engineering fields, e.g. PET–MMT (silica) nanocomposites are used as engineering plastics. The applications include reinforced materials, retardant materials, functional materials in electronic industry, chemical fibers, molding parts, etc. For the case of MMTs treated with laurylamine ammonia salt, the PET–MMT nanocomposite-engineering plastics have shown good toughness features (Figure 6.5).

6.1.3.1. Polyester cloth or film

Poly(methyl methyl acrylate) (PMMA) itself is low in hardness and high in abrasive property. To further improve the polymer matrix properties, 3% (by wt) of nm-SiO₂ (nanometer-sized SiO₂) is mixed with the polymer. The PMMA–silica nanocomposite have shown good property resistance to abrasion, It has an ideal transparency compared with the PMMA matrix. The PMMA–silica nanocomposites are usually safe to contact food and therefore are used to prepare materials for cloth or films in different food packaging. In the case of silica, it is treated with coupling agents such as KH570 in hexane under its boiling temperature and used to prepare nanocomposites safely for contacting food.

The unsaturated polyester is often used to make gel film or gel cloth, which protects food. To improve functional properties such as barrier to gas, absorbing harmful light, a composite material of polyester film covering on nanoparticle SiO₂ was prepared. The data for the composite are shown in Table 6.5. The composite also has favorable properties of anti-aging from harmful light.

Nanocomposites of SiO₂ nanoparticles with unsaturated polyesters are used to cover the surfaces of materials with the aim of protecting or decorating the articles, which make them look more beautiful than before. The preparation of SiO₂ nanoparticles with unsaturated polyester is simple except for the preliminary silica treatment. The nanocomposite is obtained by first mixing the nanometer silica with monomers of the selected unsaturated polymers, and then initiating its polymerization. The raw product is prepared by washing the mixture in the solvent of an alcoholic compound. This nanocomposite can be cast, using a casting machine, to prepare the final film products.

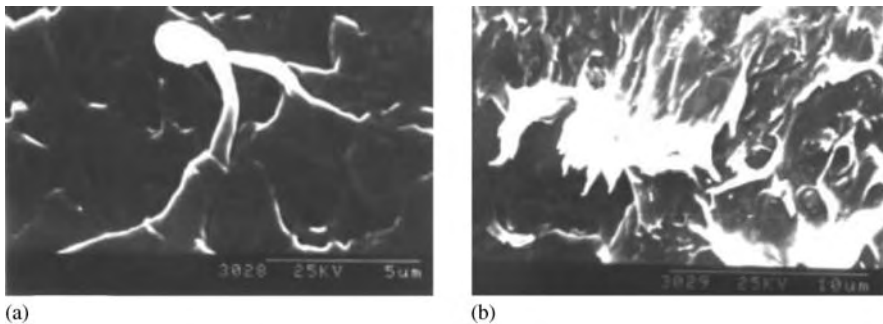


Fig. 6.5. Toughness features of PET–MMT nanocomposites (MMTs treated with laurylamine ammonia salt): (a) region; (b) surface.

Table 6.5

Physical properties of nanocomposites of SiO₂ nanometers with unsaturated polyester

Items with SiO ₂	Original gel film	The nanocomposite gel film
Abrasion loss per unit (mg cm ⁻²)	4.07	1.23
Mo's hardness	2.2 grade	2.9 grade
Tensile strength (kg cm ⁻²)	133	277
Resistance to hot water (90°C)	94 h	>720 h
Impact	Crushing (first impact)	No cracking (repeated three times)

Note: Specific surface area of silica is 640 m² g⁻¹; particle size is 10 nm.

6.1.3.2. Reinforcing plastics

Universal plastics have vast amount of yields, wide applications, and low cost. At present, the properties of polymer resins and engineering plastics cannot meet the diverse requirements of engineering materials. By addition of nanoparticles to universal plastics, it is possible to obtain the required level of engineering plastics performance. For example, nanoparticles of SiO₂ are used to modify polypropylene; the properties of these nanocomposites reach the level of nylon6, while its cost is only one-third of the latter.

Addition of nanoparticles to plastic matrixes can improve the plastic's toughness. For example, on mixing nanoparticles of SiC/Si₃N₄ mixed particles treated by C₁₀-acid with LDPE (with a particles weight of 5%), the impact strength of the nanocomposite reaches the level of 55.7 KJ m⁻², which is two times that of the pure LDPE. Such a nanocomposite material does not break on stretching to 625% of the original size. The extension value at breaking is five times that of the pure LDPE. Similarly, 25% (by wt) of nm-CaCO₃/HDPE nanocomposites has a maximum impact strength 1.7 times that of the pure HDPE, while the composite has an extension value at breaking of 660%. When the CaCO₃ load reaches 16% (by wt), all the mechanical properties of the nanocomposite are much better than that of pure HDPE.

6.1.3.3. Functionalized plastics and fibers

Functionalized nanoparticles are mixed with plastics to prepare nanocomposites with functional properties such as bacteria-killing and antielectrostatic behavior. For example, nm-ZnO carried on MMT particles acts as antielectrostatics reagents for PET, PC and saturated polyesters and other polymers such as PP. Functionalized chemicals mixed with the polymer fibers provide nanocomposites with improved performance for far-infrared-reflection, bacteria-killing and a capability of sequestering odors. For example, nm-ZnO or nm-ZnO carried on silica is added to polyester fibers used for insulation against ultraviolet light and for eliminating toxicity and odors. Further, nanocomposite fibers provide bacteria-killing properties if fabricated from Ag carried on SiO₂ or MMT particles by precursors such as TEOS, or reagent-treated particles. These composites are used as materials in home appliances. We have prepared mixed composites of nanoparticles of ZnO and SiO₂ on a polyaniline matrix to produce fibers for clothes, which show antibacterial properties and antielectrostatic shielding.

The technologies for these materials are similar, including the melt-, the reaction- and the injection-extruding techniques. All these techniques melt the nanocomposites.

Resins of unsaturated polyester and polyurethane generally form nanocomposites by post-curing techniques after thorough mixing with nanoparticles.

6.1.3.4. UHMWPE–MMT nanocomposite plastics

Ultra-high-molecular-weight polyethylene (UHMWPE) itself has good abrasive, high-impact, self-lubricating and impact absorbing energy properties. However, the extremely high viscosity makes it difficult to process UHMWPE. Nanocomposite technology provides a practical way to solve this problem by melt-mixing UHMWPE with organic clay. This technology originates from one of our inventions. UHMWPE is mixed thoroughly with the layered silicates producing exfoliated layers with lower frictional coefficient, which in turn reduces the molecular entanglement of UHMWPE. The reduced entanglement itself plays a good self-lubricating role in melt processing. In fact, the mixture of UHMWPE-organic clay can be processed by using common extrusion technology and equipment. For example, the mixture can continuously produce pipes and different forms of bulk materials with better rheological properties than that of the pristine resin. The UHMWPE–MMT nanocomposites enhance the properties of pipes made from the pure resins. The nanocomposites have better performance–cost ratio than iron pipes, aluminum, plastics or other common pipes.

6.1.4. Films and clothes

6.1.4.1. Preparation of polymer–layered silicate nanocomposite films

The production of nanocomposite films or membranes follow previous techniques:

- *In situ polymerization.* Polymer monomers are intercalated into the interlayer space of layered silicate, which further swell or exfoliate into thin layers and then scatter by post-polymerization
- *Melt exfoliation.* The precursors of treated layered silicate are melt-mixed in a double-spinning roller of an extruder machine. Under mechanical forces of a spinning roller, squeezing and high temperatures, the pieces of layered silicate are separated apart and form polymer–layered silicate nanocomposites
- *Emulsion polymerization.* Layered silicate are dispersed thoroughly in a water phase to form an emulsion system; then polymer monomers are added to the system to initiate polymerization and form polymer–layered silicate emulsions. These nanocomposites are used as precursors for preparation of membranes and films

6.1.4.2. Polypropylene–layered silicate nanocomposite films

Polypropylene resins are blown or biaxially oriented into thin films, which are used for applications in electronics, packaging and food storage. The biaxially oriented PP films (BOPP) create a series of products such as electronics films, printing films, magnetic films, decoration films, heat-sealing films, money paper films and metal electronic deposition films.

Traditional polypropylene resins themselves have disadvantages such as easy degradation, poor-melt rheological behavior, defect morphology and poorly controllable isotacticity index, which directly leads to products with fluctuating size, heterogeneous

film transparency, poor barrier to gas (such as O₂, CO₂ and H₂O) and separation of residuals or additives from the PP matrix.

6.1.4.3. PP nanocomposite films

(1) *PP-layered silicate nanocomposite films.* In the preparation of the nanocomposite film, PP oligomers are grafted with maleic acid, forming a composite precursor with treated layered silicate (e.g. MMTs). Then, this precursor is melt-mixed with PP resins in an extruder at 220–240°C. The pellets of PP-layered silicate nanocomposites become the film materials. In practice, PP-layered silicate nanocomposite films are blown into shape with a width of 1/6 m. From investigation of the PP-layered nanocomposite films, PP has become a choice for barrier materials. This can be done by mixing its resin with either the nanoparticles or other polymers with good barrier performance such as polymers PVDC, PET and PA6. PA6 is often used to melt-mix with PP or PP-based nanocomposites, where the nanoparticles could be either layered silicate or a silica precursor. Other methods to prepare nanocomposite materials and films have appeared in the literature [7–10]. We have made PA6-MMT nanocomposites into films for food packaging.

(2) *PP-silica nanoprecursor films.* Silica is often used as an antiadhesive for PP films. The silica is usually added to the PP in an indirect way, e.g. the superfine nanoparticles of SiO₂ are mixed with PP resins by using its nanoprecursor. This precursor is made from SiO₂ particles with surface treatment. In its application, it is possible for the nm-SiO₂ to react with water-soluble polyacrylamide (PAA) and mix with polyester oligomers. In this method, the silica nanoprecursor has 20% (by wt) of silica load, which can then be directly melt-blended with PP resins to make the pellet products by a double-spinning roller extruder at a temperature of 220–240°C. The pellets are then hot-blown into films with several millimeters thickness. Physical and mechanical properties of the films are shown in Table 6.6.

6.1.4.4. Fibers and clothes

The fibers made of NPET materials have higher modulus and HDT than those of PET itself. However, the dry strength is decreased. The NPET fibers are endowed with good properties in presswork or print and far-infrared reflection. NPET is also used to weave clothes with good insulating properties.

Table 6.6
Properties of films from PP-silica nanocomposites

No.	Load (by wt)	Film thickness (mm)	σ_b (MPa)	E_b (MPa)	T_h (mm °C ⁻¹)	T_l (°C)	Haze
1	1%	4	30.7	1,231	0.68	90.5	68.2
2	3%	4	29.0	1,110	0.62	87.1	87.1
3	1%	4	31.5	1,134	0.65	87.7	82.8
4	3%	4	30.1	1,134	0.82	78.7	90.1
5	0%	4	30.2	1,202	0.66	92.6	55.3

Note: T_t , transparency; σ_b , bending strength; E_b , bending modulus; T_h , film thickness in measuring its haze, T_l , light transmission percentage.

Nylon6–MMT nanocomposites (NPA6) have enhanced properties over the pristine polymer. Thus, NPA6 has higher strength, modulus, resistance to heat or higher HDT and a higher barrier to gas, while it has lower wettability adsorption properties over the PA6. The fibers are used for tire-reinforcing threads. Similarly, the fine fibers are also materials for clothes and functional covers. The NPA6 film materials have better functions such as transparency, which is thought to be from the nanoparticle effect. Products of NPA6 are shown in Figure 6.6.

6.1.5. Coatings

6.1.5.1. General description

A large number of industries have developed coating products. Modern coatings have more requirements on environmental protection. In these coatings, synthetic products account for 60% (by wt) of the whole yield in China.

At present, China has a total yield of 1.2 millions of tons of coating from 150 companies including alcoholic acid resin coating, acrylic resin coatings, building coatings, ship coatings, steel coatings, appliance coatings and dry powder coatings. On the basis of these coatings, nanoparticles have a large number of applications and provide many new functions including optical, magnetic and electrical.

Superfine coatings have been applied to airplane parts since the early 1990s. They have created new functions such as “shielding shell” for different wavelengths of light; “shielding shape” functions protect the flying object or vehicle from being discovered by detecting devices or equipment such as radar. Research on these special coatings is extensive in both university and industry. The application techniques are easier than that of dry powder such as PEEK (for military applications) [11].

Nanoparticles introduced into coatings create many positive effects in the properties and highly improve the quality. They provide new functions such as absorbing light, insulating sounds, barrier properties to gas and liquid and effective transmitting properties. Coatings containing nanoparticles are called nanocomposite coatings and include liquid-state and powder solid-state coatings. They mainly aim at solving the existing



Fig. 6.6. Products made from NPA6 materials (left to right: threads and fibers; films are shown at the back).

problems such as “color suspending,” low stability, poor thixotropic properties and low resistance to aging. The coatings containing nm-SiO₂ and nm-TiO₂, (especially, nanocomposite coatings of alcoholic acid resin–nm-SiO₂ (TiO₂) or acrylic resin–nm-SiO₂ (TiO₂)) have applications in automobiles, appliance, ships, etc.

The dry powder solid-state coating is one of the coatings introduced for nanoparticles. This coating has excellent physical and chemical aspects.

6.1.5.2. Network and nanostructure in nanocoatings

Based on our investigation of the surface of SiO₂ nanoparticles, pristine silica particle surface is usually covered by hydrogen bonds from hydroxyl groups. On its surface, unsaturated broken or dangling bonds, hydroxyl and hydrogen bonds in different bonding states exist. The bonds are interconnected and supposed to be in a tridimensional conformation (or tridimensional network, tridimensional silica structure, etc.). The structures are shown in Figure 6.7. Generally, the aggregated hydrogen bonds on its particle surface have no strong interactions between them and are easy to be separated with an external shear force. The hydrogen bonds return rapidly to their original state once the external forces are removed; this make their structure reorganize. Such an interaction acts similar to a spring.

The shear force and its weakening reaction resort rapidly to the original state depending on the interaction time and exerted force, which is called “thixotropic” or “shear thinning behavior.” The shear thinning behavior is an important factor on the coating properties of nm-SiO₂ particles and other particles. To trace the quality of these

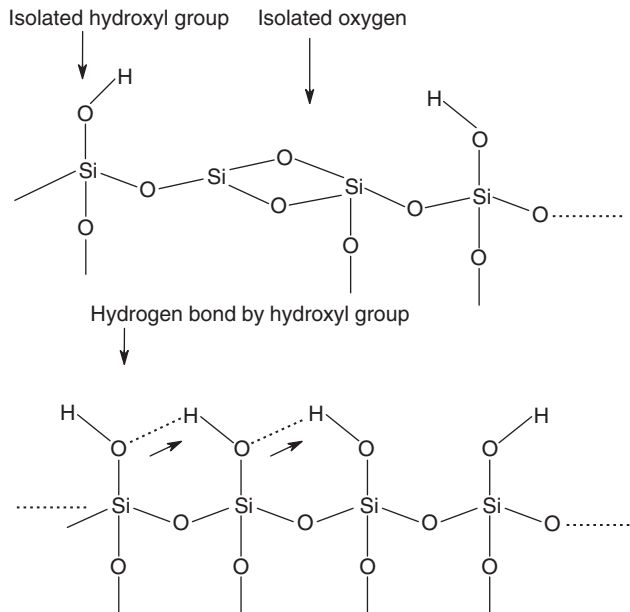


Fig. 6.7. Three-dimensional conformation chain structure in nanoparticle silica.

silica nanocomposite materials, their nanostructures are characterized by the FTIR technique. The hydrogen bonds are at regions 3,000–4,000 or 1000–2000 cm^{-1} . The commonly used nm-SiO₂ coatings are listed in Table 6.7.

FTIR along with Raman spectrum is used to characterize the physical properties of the nanoparticles, including surface hydroxyl groups, particle size and their interconnected state. The TEM technique further reveals aggregated or agglomerated state of particles in silica coating suspended system. These characterizations are important to quantify particle properties.

6.1.5.3. Some index for coatings containing nanoparticles

(1) *Ecological reasons protect coatings with magnetic behavior.* Special coatings are designed for ecological reasons to protect the environment. By adding some special nanoparticles to the coating, magnetic particles are mixed with silica in the coatings to yield functional properties from both magnetic and ecological aspects. The coatings containing these nanoparticles form either a single composition or a double composition type of coating. The single composition coating is with single material composition such as, coatings of nm-SiO₂/Fe₂O₃ with a single resin, which has the quality standards as shown in Table 6.8.

Compared to single composition coating, the double composition coating refers to two material compositions such as coating of nm-SiO₂-TiO₂/Fe₂O₃ with two

Table 6.7
General physical properties of nm-SiO₂

Commercial name	Specific surface area ($\text{m}^2 \text{g}^{-1}$)	Hydroxyl groups on surface (%)	Mean size (nm)	Ultraviolet reflection (%)
S-SiO ₂	160 ± 5	36	15	>85
P-SiO ₂	640 ± 5	48	20	>80

Note: S-SiO₂, a kind of spherical particle, P-SiO₂, a kind of porous particle suitable for surface adsorption, total impurities content ≤0.5%.

Table 6.8
Quality requirements for single composition coating

Requirements	Standards
Meet the quality requirements of the traditional coatings	GB1720-89, GB/T (1730-1734)-93
Extremely stable color	GB (6749-52)-86
Resistance to atmosphere or weather (Florida longevity under sunshine)	≥30 months
Ecological protecting behavior	Heavy metal weight ≤0.1% (by wt) organic
Resistance to wettability and heat	Organic solvent: trace
Resistance to invasion of bacteria	GB 1765-89

mixed resins. The double composition coating has the quality standards as shown in Table 6.9.

(2) *Nanopowder coatings.* Our dry powder coatings contain few or no solvents; the application method is quite different from that of the liquid coating in that they are capable of being hot-sprayed on the surface of objects and have their own standards as shown in Table 6.10.

The nanoparticles added to coating systems are usually aggregated and form pseudoagglomerated secondary particles with particle sizes of micrometers. But, aggregation behavior has no effect on their nanostructure when hot-sprayed on the surface of objects. The nanostructure is maintained in a hot-spraying method. Thus, the nanopowder coatings can be made on several types of solid surfaces such as TV screens, automobile glass and other objects.

Example 6.1.5.1. Nanopowder coatings for automobiles. Based on its special performance in optical, mechanical, electrical and catalytical aspects, the 10 nm-TiO₂ is used in coatings when it is carried on silica. In such a composition, nm-TiO₂ particles show scattering behavior at visible light, a strong shielding effect in ultraviolet light and superior transparency. This sensitive effect produces quite mysterious color and unique optical property that is very popular in automobile coatings, and has found wide applications to different cars and trucks with their special properties as shown in Table 6.11.

Table 6.9
Quality requirements for double composition coating

Requirements	Standards
Meet the traditional coatings	GB1720-89;GB/T(1730-1734)-93
Extreme stability of color	GB(6749-52)-86
Resistance to weather or atmosphere (Florida longevity under sunshine)	≥30 months
Ecological protecting behavior	Overall heavy metal weights ≤0.1% (by wt) Organic solvent: trace
Far-infrared light reflection rate	Capable of resistance to radiation light or aging
Resistance to the invasion of microbes	≥80%

Table 6.10
Quality standards for dry powder coatings

Requirements	Standards
Meet traditional coating quality requirements	GB1720-89; GB/T (1730-1734)-93
Particle maximum diameter	≤20 μm
Resistance to foggy salt	ASTM B1177
Resistance to ultraviolet light	Yes
Resistance to heat (200°C for over 1 h)	Yes
Resistance to weather (Florida longevity under sunshine)	≥50 months
Smooth and clean surface	GB 9754-85
Self-cleaning performance	Good

Table 6.11
Properties of coatings of silica – TiO₂ nanocomposites

Properties	Components	Specifications
Appearance	White powder	Depends
Organic additives	Lauryl acid/dodecyl acid	
Particle	SiO ₂ /ZrO ₂ /Al(OH) ₃ /Fe(OH) ₃	
Mean size (nm)	14/25/35/55	
pH	6–8	
Polymorphism	Rutile/acute/mixed	Depends
Moisture (%)	0.05	
Burning residual (%)	0.3	
Surface property	Hydrophilic/hydrophobic	Depends
SSA (m ² g)	50–70	
SSA before treatment (m ² g)	90	
Purity (%)	>98.5	Depends
Heavy metals (ppm)	As <0.5/Pb <0.5/Hg <0.01	

Note: SSA, specific surface area.

The TiO₂ mineral exhibits polymorphism, an acute and a rutile type of crystal form, and usually exists in a mixture form. In silica carried on the TiO₂ particle, different crystal forms and relative content can be adjusted according to practical requirement that show the different covering behavior or shielding force. The mixed coatings have wide applications in cosmetics, plastic films, lubricants, catalysts and electronics.

Example 6.1.5.2. Nanocomposite coatings with functions. In the organic–inorganic nanocomposite coatings, the organic phase is selected from di-block copolymers, triblock copolymers and quarter-block copolymers of polyesters, providing resistance to abrasion and film-forming behavior. The coating is endowed with different functions depending on the additives. For example, the additive Ag-ion nanoparticle provides bacterial-killing behavior, while the additive titania particle imparts resistance to ultraviolet and chemical erosion. These functions find applications or coatings of underwater pipes, gas pipelines and construction materials.

Prime examples of applications are those of polyester or polypropylene matrix mixing with selected TiO₂ or Ag particles followed by hot-spraying, to make coatings on TV or computer screens to prevent the emission of harmful light. The functional coatings of polyaniline based on nanocomposites will be discussed later.

6.1.5.4. Inorganic coatings and their applied standards

Besides GB standards, we may refer to the ASTM quality standards for common inorganic particle coatings containing nanoparticles. By using hot-spraying techniques, the nanopowder coatings disperse homogeneously on the surface. Nanopowder coating techniques are ecologically benign. Harmful solvents, toxic polymer resins and additives of colors and dyes are partly or completely replaced by the powder-coating technique. In designing and preparation of the nanoparticles coatings (including the control of the composition and quality), it is suggested to refer to the correspondence standards based on those shown in Table 6.12.

Table 6.12
Some indexes and their standards for nanopowder coatings

Coating properties	Observing standards
Color	ASTM-D718, D1208
Water solubility	ASTM-D2448, D422
Oil solubility	ASTM-D1483
Expansion of adsorbing water	ASTM-D 6083
Weight variation of adsorbing water	ASTM-D 471

In waterproof coatings, the water absorption rate (or percentage) is necessary for application. In practical application to waterproof materials, the inorganic coating is selected to make the water adsorption rate to be zero. The present reference standards for this is ASTM-D6083, which requires the water adsorbing rate $\leq 20\%$, and thus needs revision. As for waterproof materials for building roof materials, the ASTM-D471 standard is used to measure the water absorption rate of the coating film under different controlled conditions (Table 6.13).

The water adsorbing rate for a waterproof coating is measured and calculated using Eq. (6.1.5), where the sample size is selected as $25 \times 50 \times 2$ (mm³) and the sample thickness is designed to be less than 2 mm. By measuring the sample's weight variation, the water adsorption rate is obtained:

$$\Delta W = (W_2 - W_1)/W_1 \times 100 \quad (6.1.5)$$

where ΔW is the water adsorbing percentage of the coated sample (if the time is fixed, ΔW is a adsorbing rate); W_2 or W_1 is the weight after or before adsorbing water of the coated sample, respectively.

6.1.5.5. Surfactant and treatment agents for nanoparticle coatings

Most nanoparticles are of high specific surface area and surface free energy, but are thermally unstable in coating systems. When they mix with dye or color, some surfactants act as treatment agents to improve the compatibility with the coating by converting between hydrophilic or hydrophobic properties.

By controlling the broken or unsaturated bonds on the surface of nanoparticles, and reducing the interface defects, the coating adhesive force with organic matrix reverses its wettability. Some of these surfactants and treatment agents necessary to reach these goals are selected from Table 6.14.

6.1.5.6. Dispersion techniques and technologies of nanoparticle coatings

Our recently invented nanoparticle precursor powder (NPP) [12] has application in several coatings, some of which are used to prepare nanomaterial coatings on the outside surface of the automobiles. For example, MMT-PS [13] or MMT-PCL systems [14] are used to simply mix with additives of color or surfactants such as KH-570 to prepare homogeneous coatings.

Three traditional techniques including milling, abrasion and supersonic (ultrasound) techniques are used to disperse the nanoparticles in the coating mixture. The colloid

Table 6.13
Reference time standard for waterproof coating resistant to water according to ASTM-D 471

Temperatures of water or vapor (°C)		Time (h)
-75	85	22
-55	100	46
-40	125	70
-25	150	166
-10	175	670
0	200	1,006
23	225	2,998
50	25	4,990

Note: The data error is ± 2 .

Table 6.14
Surfactant and treatment agents for nanoparticles in coatings

Silicon compounds	Ester compounds	Polymer	Grafting agents
KH-550	Titanium acid ester	PEG	ROH
KH-560	Aluminum acid ester	PVA	RNH ₂
	C ₁₂ -C ₁₈ acid or ester	PVP	ROOR ₁
KH-570		PC	
		PS	SH group propyl acid

Note: PEG, polyethylene glycol; PVA, polyvinyl alcohol; PVP, polyvinyl pyridine; PC, polycarbonate; PS, polystyrene.

millers is suggested for preparation of nanocomposite coatings. By adopting the tri-rollers or multi-rollers of this machine and using reciprocating abrasive milling, most of the nanoparticles can be homogeneously dispersed in the coatings. The ball miller is another technique for dispersing particles into coatings, where collisions and friction between balls or between the ball and the cylinder wall may occur. The aggregated particles are broken or crushed and dispersed in situ. The abrasive machine can feed continuously, thus the nanopowder slurry in the cylinder is violently collided and sheared by sand particles. After a period of abrasive interaction between nanoparticles and sand particles, the nanoparticles change homogeneously into slurry of coatings. Supersonic vibration is also a means to disperse nanoparticles into the polymer matrix. In the method, the pH of the mixture is adjusted to match the electric charges between nanoparticles and the coating itself. The brief flowchart for such a technology of dispersing nanoparticles in different coatings is shown in Figure 6.8. The nanoparticles treated with reagents can be transformed into nanoparticle precursor (NPP), which is an intermediate and exfoliated again during its mixing with coatings. By physical and chemical processes, homogeneously dispersed morphology of nanoparticles is observed [15].

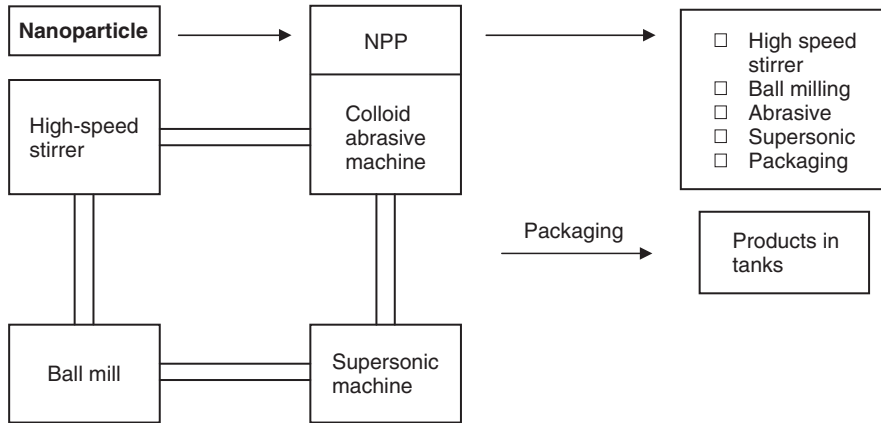


Fig. 6.8. Flow chart of nanomaterial coating preparation.

6.1.5.7. Advantages of nanomaterial coatings in applications

Simple methods of preparation, application and cost reduction are the advantages of nanocomposite coatings. These are the most important aspects that have to be recognized in practical applications. The introduction of nanoparticles into traditional coatings improve their properties in areas such as suspending, adhesive strength, functionality, resistance to aging and ecological protection. Further, the coating quality or grade is enhanced to a higher level.

The nanoparticles create functions such as shielding harmful light, far-infrared reflection (keeping warm), adsorbing ecological noise, dissipation of heat, self-cleaning and optical-magnetic properties in their applications to automobile surfaces, house walls and metal surfaces. According to our investigations, the coatings are not difficult to fabricate. However, the long time stability of the nanoparticles in the coatings, which should be an important factor for practical application, is not clearly understood. The study of designing methods and characterizing the stable coating system is an emerging field.

6.1.6. Electronics

6.1.6.1. Layered silicate as materials for conducting electricity

Natural layered silicate has regular nanostructure and interlayer space, which is used as a capacitor. For example, layered silicate of mica is used as an electronic capacitor. The ordered layer structure is a natural template or reactor for preparation of information material. For example, in Li batteries based on MMTs, Li ion carried on MMTs produces a composite cell as shown in Figure 6.9.

So far, the use of Li-MMTs as a cell material does not provide a perfect cell and probably results from its residual impurity ions such as Na^+ , Ca^{2+} and Mg^{2+} . The interactions of different compositions in this battery make the dielectric conducting behavior more complicated. The polyaniline–MMT nanocomposites are used as conducting

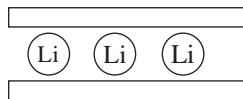


Fig. 6.9. Li ions carried on MMTs form a battery.

materials and antistatic electrical additives in polyester and polypropylene films; some products of these films will soon be seen in the market.

6.1.7. Catalysts and carriers

6.1.7.1. Preparation and application of model catalysts

For particle surfaces, especially their inner surface, the morphology is very complicated and needs investigation by common electronic probes and scanning electron microscopy at a molecular or atomic level. To improve the probing intensity, resolution and accuracy for the surface of single crystals, flat plates and films act as carriers for model catalysts.

(1) *Design of model carrier and catalysts.* The model carriers and catalysts are for characterizing and investigating the nanomaterials. While most of these structured materials are 2D, the information on their 3D structure is either difficult to detect or low to resolve. The specific surface area of the 2D materials is rather low; this limits their selectivity. It is not easy to observe the diffusion process and the mass transformation in the reactions. Designing a solid monodisperse particle system whose surface is treated by an active material is a good choice to solve the problem. In such a system, monodisperse particles are assembled into model catalysts with homogeneous pore diameter and characterized with the following:

- (a) Dispersion state of the active material on a carrier such as silica, its crystallite size and distribution.
- (b) Accurate information on the 3D nanostructure and its pore diameter distribution, and a flexible adjustment of pore size in a wide range.
- (c) High specific surface area of the model carrier, and the catalyst activity and distribution.

(2) *Preparation of model carrier.* Model catalyst carriers are prepared by assembling solid monodisperse silica spherical particles. The gap between the particles constitutes the homogeneous passageway of pores of the model carrier. The pore diameter distribution is extremely narrow. The pore size and specific surface area are a function of particle diameter. The practical pore diameter distribution ranges from 0.14 to 0.50 times the particle diameter; porosity percentage is 26–35% for a range of pore diameters. A pore size of 6–300 nm or higher can be selected. A model carrier is characterized by SEM in Figure 6.10, where 300 nm microspheres have been assembled into a model carrier.

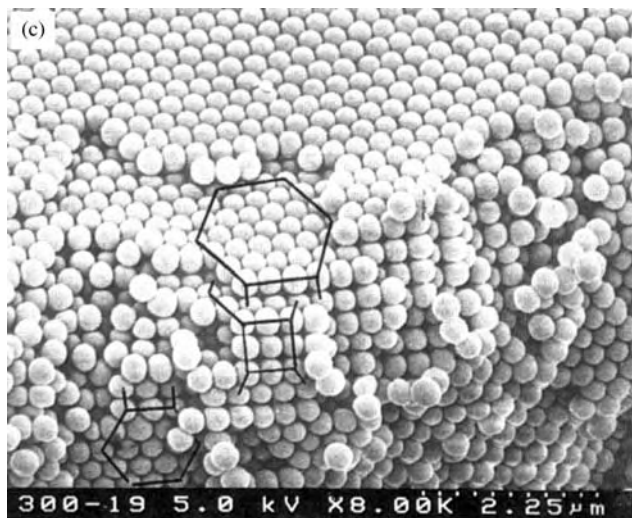


Fig. 6.10. SEM morphology of model carrier assembled by monodispersed particles.

The active component is transformed on the particle surface and the carrier after or before assembly. Several active components to modify the particles of silica include active materials such as Al_2O_3 , TiO_2 , NiO and MoO_3 . These model catalysts are tested on our continuous micro reactors to measure activity. For example, a model catalyst carrying 2.1% (by wt) of MoO_3 is used to refine directly fractioned diesel, resulting in a desulfurization rate of 95.1% and a denitrogen rate of 87.2%.

(3) Application of model catalyst.

(a) *The effect of pore structure on diffusion of reaction molecules.* The model catalysts are applied to residual grade at 110°C from Daqing by pressure reducing subtraction techniques. The residual molecule scale is calculated using the maximum probability of pore diameters from 6.6 nm to 85.8 nm according to equivalent sphere diameters of 1.79 nm by selecting a model with adsorption and diffusion behavior.

The molecular distribution of the residual is measured by dipping in pores with different sizes by gel permeation chromatography (GPC) at a catalyst/petroleum ratio of 1:2. If the carrier of small diameters produces a confining effect on the diffusion of raw materials with large size, it is reflected by the enhancement of the relative mean molecular weight (M_w) of the residual. This experimental result is shown in Figure 6.11. It is found from these curves that the residual still diffuses in the model carrier with 20 nm pore diameter consistent with the calculations of Pawar [16].

(b) *Dispersion of active component on the catalyst surface.* The monolayer quantity of NiO and MoO_3 carried on silica measured by X-ray photo electronic spectroscopy (XPS) is described. According to Kerkhof [17], when active components disperse in a monolayer distribution, the ratio of XPS peak intensity to its carrier is proportional to

the ratio of atoms in the bulk. In our prepared model product, the dispersing content of NiO is calculated to be 0.03g NiO/100 m² SiO₂ from the curve of content vs. I_s (see Figure 6.12). Similarly, MoO₃ content carried on SiO₂ surface is calculated to be 0.02 g MoO₃/100 m² SiO₂ (see Figure 6.13).

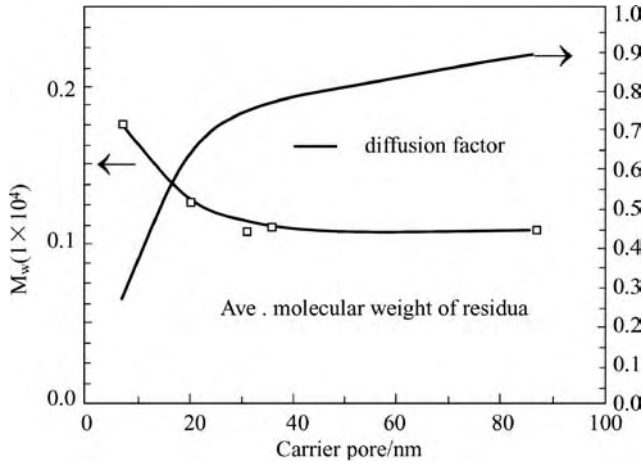


Fig. 6.11. Plot of carrier pore size vs. relative mean molecular weight (M_w) and diffusion factors in confining space for residuals.

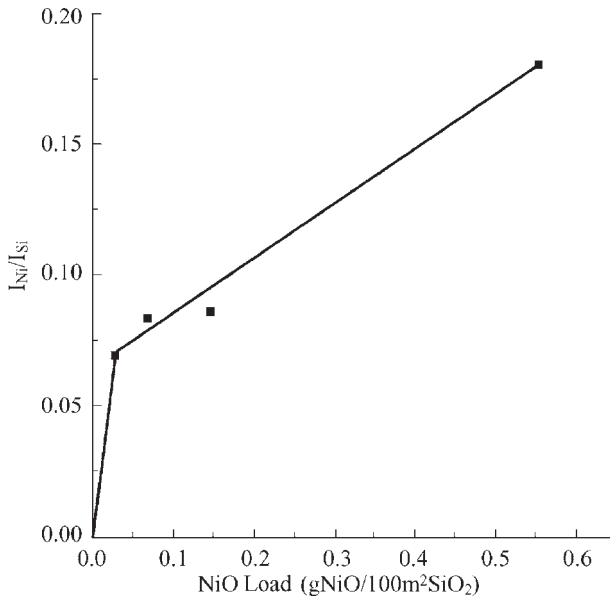


Fig. 6.12. Dispersing content of NiO.

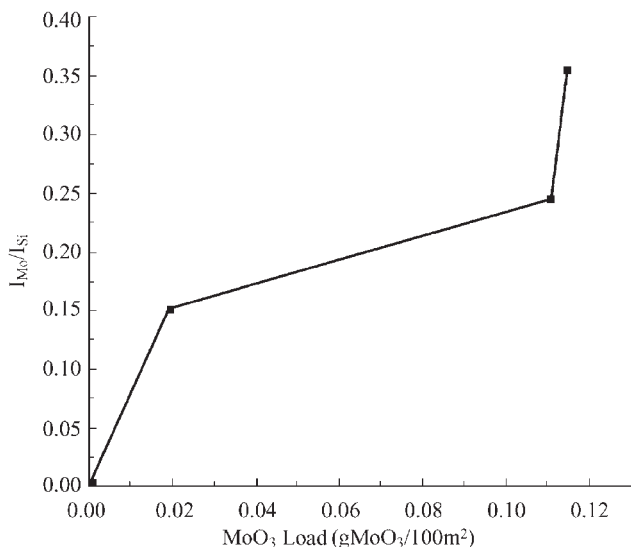


Fig. 6.13. Dispersing content of MoO₃.

(c) *Carrying the active material.* The sphere-like silica is equivalent to a microcarrier. The active crystallites on its surface are observed by TEM. The silica is capable of being observed in precession at a very high strength. The morphology of active MoO₃ on the 150 nm silica carrier is shown in Figure 6.14. Experiments show that such a model catalyst is suitable for revealing the diffusion behavior of reactive molecules (especially macromolecules) inside the pore, which provide data for designing the catalyst pore structure and the selectivity. Meanwhile, by accurately characterizing and controlling the active component dispersion, their crystallite size and relations with a designed reaction, the optimized reaction rate and selection are obtained.

6.1.7.2. Catalysts based on layered silicate carriers

Attapulgite serves as a catalyst of superstrong acids. It has the following superior characteristics:

- (1) It has a zeolite gateway inside the crystallites and has fine porous structure in its crystallite aggregates.
- (2) It has several Lewis acid and base active centers due to non-equivalent isomorph substitution between cations, less OH⁻, OH₂⁻ groups in octahedral coordination system and broken bridge bonds (e.g. -O-Si bonds).
- (3) It has strong mechanical properties and thermal stability under heat treatment. Attapulgite meets not only the requirements for micropores and surface performance in heterogeneous catalyst, but also produces synergistic effects of acid-base catalysts. Heterogeneous catalyst has direct effects on its activation energy and the reaction grade and form positive carbon ion on its transformation in reaction. Also, attapulgite has shape-selection (enantiomorphic) performance

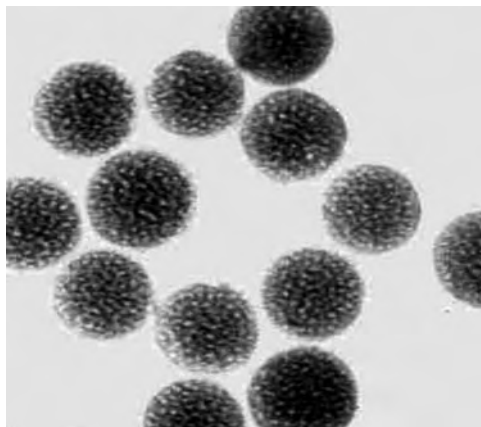


Fig. 6.14. TEM morphology of MoO_3 on the silica particle carrier.

in cracking olefins as in molecular sieves. In cracking butylene, attapulgite on post-treatment acts by depolymerizing of butylene bonds and produces isomerization effects.

Attapulgite can also carry other active metals or metal cations such as Pt, Ni and Cu, which disperse homogeneously on its surface or inside the gateway of the pores. For example, active compositions of AlCl_3 – CuCl – KCl catalysts carried on attapulgite particles are a catalyst in cracking ethylene gas. This system catalyzes the reactions of ethylene and chlorites forming 1,2-dichloric ethane with yield of 99% (by wt).

In the preparation of polyolefins using Ziegler–Natta catalysts, the traditional carrier is MgCl_2 . To prepare nanocomposites based on attapulgite, in situ polymerization is attempted. For example, the active compositions of TiCl_4 , the electronic donor and other additives are carried together on the ethanol-treated attapulgite to prepare catalysts for ethylene polymerization.

6.1.7.3. Carriers

The nanoparticle carriers here refer to carriers whose size or diameter and porosity structure are on the nanometer scale. Thus, carriers with porosity size less than 100 nm are also included in the nanoparticle carrier. Most of the traditional catalysts are nanoparticle carriers because of their pore diameter, which ranges from 1 to 50 nm. As for the polyolefin industry, it developed from the early single functional Ziegler–Natta catalysts to the one integrating the functions of polymerizing and modifying polymer properties. In Table 6.15, the diverse carriers for polyolefins are listed.

As for nm- SiO_2 as a carrier, not only its particle sizes but also the content of its surface hydroxyl group (OH) are controlled. In this way, silica particles provide the best coordination interaction with active centers or compositions on the catalyst. On the surface of SiO_2 particle, the hydroxyl group can reach 30%. A later section in the book discusses the process of carrying catalysts on the silica nanoparticles.

Table 6.15
Diverse carriers for polyolefin

Inorganic types	Organic types
MgCl ₂ , layered silicate, SiO ₂	Starch, cyclodextrins, polystyrene
MCM-41, Zeolite(VPI-5), ZSM-5	PS-diethylene phenyl copolymers
	Sulfonated diethylene phenyl copolymers

6.1.7.4. Approaches of carrying MAO on SiO₂

In the 1980s, metallocene catalysts appeared to enhance greatly the above traditional catalysis activity. The methyl aluminum oxide (MAO) acts as an additive catalyst. The preparation of the metallocene catalysts and additives on SiO₂ carrier is shown here.

(1) *The preparation of metallocene catalysts based on silica and layered silicates.*

(a) *MAO/SiO₂.* Nano-SiO₂ particles are first suspended in methyl benzene solvent, then washed and finally filtered out the treated particles, to which MAO is added. Under certain circumstances, the treated carriers are calcinated under N₂ atmosphere with temperature ranging from 200 to 500°C. This calcination temperature is a factor for the catalyst activity. A trial-and-error method is often used to optimize the best conditions and compositions of the final catalysis.

(b) *SiO₂/MAO/Cp₂ZrCl₂.* On the surface of SiO₂/MAO, the active components of Cp₂ZrCl₂ or Et(ind)ZrCl₂ (Et = ethyl bridge, ind = indene group) with indene group are carried (Figure 6.15). The compositions of the catalyst further dehydrogenates at 200–400°C with hydroxyl groups below 30% (by wt) and the catalyst in mass ratio of Al/Zr = 4,000, which is made at conditions of pressure at 0.6 MPa and a temperature of 60°C.

(c) *Reduction of MAO quantity.* The high cost of metallocene catalysts is mainly due to the consumption of large quantities of MAO. To reduce the MAO quantity, MMTs of proper moisture content are tried as a carrier for MAO. The precursor of additive catalyst of Al(RO)₃ are made from the reagent of AlR₃ (R = Et, Me, etc.) and is carried on the granulated particles of Li-MMTs by in situ formation of MAO caused by a hydration reaction of the water in the carrier.



However, water in the interlayer of Li-MMT hydrates AlR₃ into the mixtures of MAO or HMAO (MMAO). So, careful control of the AlR₃ hydration integrates the carrying process with the production of MAO, which not only reduces the intermediate process, but also the consuming quantity of MAO.

MMT particles as carriers are beneficial for forming a homogeneous distribution of polyolefin particles. The size of the shaped carrier has a linear relationship with polyolefin particle distribution. This requires control of the particle size and distribution of the catalysis.

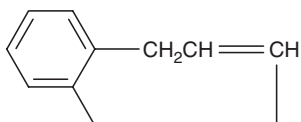


Fig. 6.15. The molecular structure of indene group.

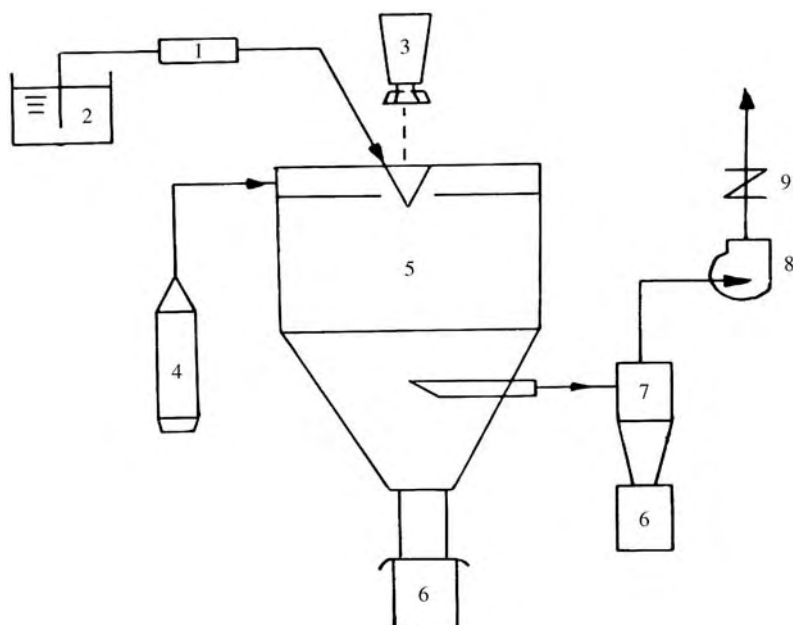


Fig. 6.16. Schematic representation of a spray dryer. 1 – pump adding raw suspending system; 2 – tank; 3 – spray head of centrifugal type; 4 – air dryer; 5 – drying room; 6 – product container; 7 – spinning separator; 8 – centrifugal air; 9 – air adjustor.

(d) *Shape up device.* The large-scale shaping up the carrier particles with nanostructure is made in a spray dryer shown in Figure 6.16. The process is as follows: the slurry of layered silicates (or silica) treated with organic compounds is pumped from tank 2 to a spray head 3 through tube 1. Due to hot air in room 4, the wet particles are dried in room 5 and the products are collected in container 6. Only a few product powders go through separator 7 and are stored in container 6. There are two types of dryers: centrifugal dryer and pressure dryer. The centrifugal dryer is suitable for the preparation of fine particles with a homogeneous distribution; however the dried particles have unsatisfactory flow property. The pressure dryer is suitable for shaping up particles with good shape and flow properties.

(2) *Propping layered silicates.* The interlayer structure of layered silicates provides a space for other organic molecules or metal oxides to penetrate into the silicates. The mixtures use propping agents (small molecules of amine or metal compounds) intercalating

into the interlayer space and an enlarged interlayer distance is usually produced. Natural or synthesized clay (e.g. bentonite, MMT, bentonite of MMT isomerization, talc and Li-MMTs) is suitable for the preparation of the propping structure. The synthesized clays of fluoro-MMTs, Li-MMTs, fluoro-mica, synthetic hydroxyl-talc, sodium-mica (NaTSM) and synthetic strip-mica are also choices as propping structures.

Propping agents usually include the organic compounds, metal oxides and their precursors. Organic compounds are mainly amines such as alkyl amine, amine with olefin chains or other groups. Metal oxides are selected from single oxide or their composites such as Al_2O_3 , SiO_2 , ZrO_2 , GaO_2 , $\text{SiO}_2\text{-Al}_2\text{O}_3$ and $\text{SiO}_2\text{-TiO}_2$. The most common oxides are ZrO_2 , Al_2O_3 , etc. Metal oxide precursors are alcoholic compounds such as TEOS and TBTT. Using the propping agent, the interlayer distance of the layered silicates reaches up to 1.5–2.5 nm.

(a) *Preparation of propping layered silicates.* The preparation of propping layered silicates is similar to the process of intercalated reaction. Propping clay for carriers is prepared by an exchange reaction between the ions in the clay's interlayer and the ions in the propping agent. The solvents are usually water, ethanol, methanol or their mixtures with designed proportions.

The selected propping agents are alcoholic compounds of metals such as aluminum, zirconium, silicon and chromium with alcoholic compounds such as $\text{M}(\text{OEt})_n$ (where $\text{M} = \text{Al, Zr, Si, Cr, Fe}$ and Ga ; $n = 4$). After they replace the exchangeable cations in the gallery of clay, the propping clay is obtained and calcinated. Finally, the propping structure of a further enlarged interlayer distance is obtained with a micropore passage of 0.6–1.4 nm.

Propping clay in dry or wet state is used to carry on active components or metals (especially precious metals) such as Pt, Pd, Mo, Cr and Mn. The compositional metals such as Pt/Pd, Ni/W, Co/Mo and Cu/Co/Mo are used for a hydrogenation catalyzing process with concentrations up to 0.1–20%.

(b) *Some index characterizing propping layered silicates.* The indexes for different catalysts are for reference. Some indexes for propping layered silicates are determined depending on their application and condition. In the hydrogenation transferring process, the indexes for the catalysts carried on the layered silicates are given as shown in Table 6.16.

(c) *Preparation of active metal catalysts on the carriers.* The dehydrogenation catalysts are also prepared by carrying the active components on the layered silicates SiO_2

Table 6.16
The physical properties of clay-based catalysts

Properties	Data
Surface area ($\text{m}^2 \text{g}^{-1}$)	100–400
Micropore volume (ml g^{-1})	0.05–1.5
Mean pore diameter (nm)	2–30
Bulk particle size (m)	2–20
Microscopy particle size (nm)	500–1000

and Al_2O_3 particles. Mixing the Al_2O_3 with SiO_2 or layered silicates increases the acidity degree of catalysts, which makes a catalyst “aluminized” or “acidity increased.”

Example 6.1.7.1. Preparation of Zr catalysts on commercial carriers. The catalysts used to crack oil wax are prepared on the usual commercial carriers of Al_2O_3 and SiO_2 with nanopores. Pd (0.5%, by wt) from its precursor PdCl_2 disperses in the mixture carrier of 70% (by wt) $\text{SiO}_2/\text{Al}_2\text{O}_3$ (12% Al_2O_3) from a sol–gel process and 30% (by wt) of Al_2O_3 as adhesive. Also, tetra-amine palladium solution is mixed with 80% (by wt) Y-zeolite and 20% (by wt) Al_2O_3 , by an initial dipping technique, and then calcinated at high temperature (<600°C) and inert gas atmosphere.

Example 6.1.7.2. Preparation of Zr-MMT catalysts. Commercial MMTs are used to prepare catalysts by mixing them with acetic zirconium and pillared layered silicate catalyst (PILC). Then 500 ml of Zr $(\text{CH}_3\text{COO})_2$ solution containing 22% ZrO_2 is diluted in 2.8 l of distilled water. To this solution, 50.0 g of bentonite is added. This suspension is stirred for 3 h at room temperature, and the filtration cake is obtained by a centrifugal machine and washed 6–8 times with 4 l of water. The solid particles are dried in the oven at 120°C for 48 h. Then, the temperature is raised to 200°C at a rate of 100°C min^{-1} and held for 2 h. Following this, the temperature is raised to 400°C at a rate of 100°C min^{-1} and held for 2 h. The Zr-MMTs or Zr-bentonite thus obtained has its characteristic indexes and results as shown in Table 6.17. For similar processes one can refer to US patent no.5248644.

(3) *Preparation of carrier for olefin polymerization.* The Ziegler–Natta catalysts are carried on layered silicates for olefin polymerization. Some indexes for their structure are shown in Table 6.18.

Table 6.17
Properties of Zr-MMT catalysts

Properties	Data
Layer interdistance (nm)	2.05 (X-ray)
Surface area ($\text{m}^2 \text{g}^{-1}$)	372 (BET)
Micropore volume (ml g^{-1})	0.138 (BET)
Elements (by wt)	Zr 19.5%, Si 19.2%, Al 7.25% Fe 1.6%, Mg 0.90%, Na 0.07%

Table 6.18
Properties of the polyolefin catalysts based on clay

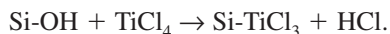
Items	Data
Surface area ($\text{m}^2 \text{g}^{-1}$)	100–800
Micropore volume (ml g^{-1})	0.03–2.5
Mean pore diameter (nm)	2–30
Bulk particle size (m)	2–20
Microscopy particle size (nm)	500–1,000
Cations residue (ppm)	<1,000

The high surface area of clay particles is beneficial for adsorbing metal elements or oxides. A Ti content of 4–15% (by wt) is required for olefin polymerization, while Ni or Pd content less than 0.5% (by wt) is needed for olefin cracking. The residual cations of Na^+ and Ca^{2+} in the clay may affect the activity of polyolefin catalysts. There is no evidence that residual cations effect the cracking reactions of $\text{C}_4\text{--C}_5$ into $\text{C}_2\text{--C}_3$ in petroleum, except for forming high residue carbons.

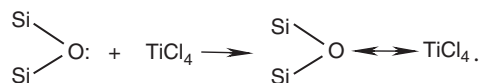
In our work, composite carriers of $\text{MgCl}_2/\text{SiO}_2$ are shaped particles, which are suitable for polyethylene polymerization (gas or slurry phase). The MMT carrier propped by MgCl_2 in ethanol, silica in water or their mixtures in ethanol solvent is one of the choices as carrier. The aggregated layers from clay are exfoliated into nanoparticles forming nanocomposites during polymerizations which are shown in Figure 6.17 for the polyethylene–MMT nanocomposites based on the above mixing carrier.

(4) *Ziegler–Natta catalyst on the silica particles.* The carrying technique for Ziegler–Natta catalyst on silica particles is either a ball milling or dipping method. A bond between the active components of catalyst and the groups on the carrier forms in a similar way to carrying TiCl_4 on silica [10]. The reactions are:

First reaction:



Second reaction:



The second reaction cannot form the active centers in the polymerization because the TiCl_4 is adsorbed. The first reaction is an effective carrying process of TiCl_4 and the hydroxyl group on silica reacts with TiCl_4 in an unequal ratio. The molecules of TiCl_4

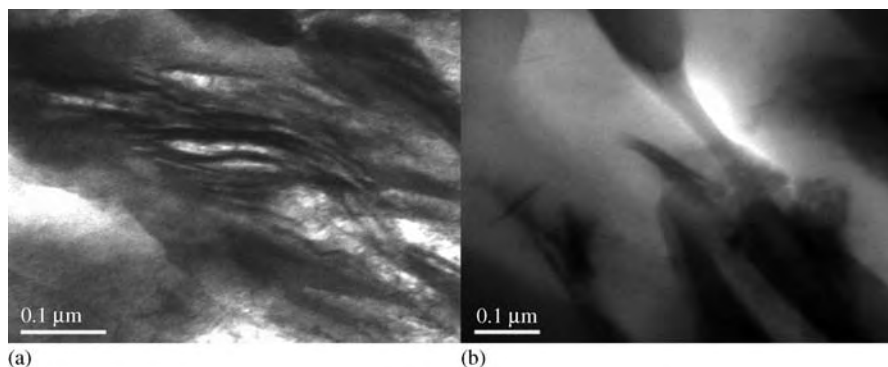
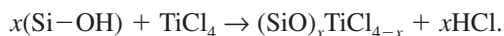


Fig. 6.17. Propping carrier exfoliated morphology in the polymerization: (a) the exfoliated and propping layer morphology; (b) the layer fiber-like dispersion morphology.

react strongly on the silica when particles of sizes 2–5 nm are used. One molecule of TiCl_4 reacts with several hydroxyl groups on silica as



In other words, the previously formed species further react with vicinity hydroxyl groups reducing the Ti load on the surface. The thermal activation temperature controls the TiCl_4 reaction process on the silica surface. When the temperature is lower (350°C), the silica surface has a higher density of hydroxyl group; TiCl_4 then has tri-replacement reaction with hydroxyl groups. When the temperature is even higher (650°C), the surface hydroxyl group density decreases and the reaction mainly is di-replacement and single replacement.

6.1.7.4. Preparation of porous heterogeneous structure by propping and templating methods

(1) *Heterogeneous structure of layered silicate.* In powder crystalline clay particles, propping layered silicates retain their original layer structure even when the metal oxide is used. The structure changes only after the metal oxide, neutral amine and quaternary salt are applied to treat the layered silicate. After calcination, the porous and the heterogeneous structure of layered silicate are created. To form a heterogeneous structure, several cations are mixed to cause an exchange reaction with the ions in the interlayer space, along with the neutral amine or neutral inorganic oxide precursor as a template. In the case where TEOS is selected as a precursor or a template, a mesostructure of SiO_2 forms in its interlayer space. By removing surfactants, a mesoporous structure with a surface area of $100\text{--}900\text{ m}^2\text{ g}^{-1}$ and a pore diameter of 1.2–4.0 nm is obtained. This structure in the heterogeneous catalyst zeolite and adsorbent is prepared in a similar process as to the above-mentioned template.

(2) *Selection of agents for heterogeneous structure.* Table 6.19 lists several reagents for selection.

The molar ratio of onium (cation amine salts)/amine/precursors is 1/5/50, or a C 1/(5–30)/(50–250). Based on this ratio of different reagents, layered silicate of MMT, talc or mica are selected as candidates for pillared layered silicate hybrid (PLSH) corresponding to lattice space of 2.5–7.5 nm. The particles have a pore diameter of 1.2–4.0 nm and a surface area of $100\text{--}900\text{ m}^2\text{ g}^{-1}$. There is also a debate on PLSH, in which the metal precursors in crystal lattice of 2:1 type mica is, in fact, cross-linked by hydrogenation. Due to this cross-linking behavior, the pillared layered silicate are called “hybrid.”

Table 6.19
Choices of amine reagents for heterogeneous inorganic structure

Types	Examples
Amine	Primary amine, secondary amine, tertiary amine, their mixtures. Amine with more than six carbons e.g., laurylamine
Quaternary amine salts	Cation amine salts, e.g., laurylamine chloric acid
Precursors for metal oxides	TEOS, TBTT, $\text{Zr}(\text{OH})_2$, $\text{Al}(\text{OH})_3$, etc.

(3) *Synthesis of crystalline intermediates of organic–inorganic layered metal oxides.* The synthesis of crystalline intermediates of organic–inorganic layered metal oxides is composed of several designed steps.

- (a) Selection of a layered silicate with 2:1 type structure. This structure produces a nanoscale pore morphology with or without ordered patterns. A 2:1 type mica crystal structure is selected.
- (b) Selection of inorganic metal oxide precursors, which include metals with valence states of 2, 3, 4, 5 or 6, or mixtures, e.g. Zr^{4+}/Al^{3+} mixtures. These metal oxides prove to be superior pillared agent. A proper composite of the metal oxides generally produces pillared layered silicate carrying active compositions.
- (c) Selection of quaternary amine salt as a template, while neutral amine as cotemplate. They have proper mixing ratio as mentioned above and are optimized depending on reaction conditions.

The mixtures produce intermediates with different morphology. By a calcination process of the intermediates, the heterogeneous structure is prepared. The other method to prepare heterogeneous structure of layered silicate is suggested to be by subtraction of intermediates in ethanol chloric acid (HCl) solvents.

Examples 6.1.7.3. Preparation of organic MMT derivatives. To a 1% (by wt) MMT suspension, 0.3 mol l^{-1} of ammonia salts ($C_{16}H_{33}N^+(CH_3)_3$, $C_{10}H_{21}N^+(CH_3)_3^-$ or $C_{12}H_{25}N^+(CH_3)_3$) is added. Then, the suspending solution is stirred at 50°C for 2 h. In this way, a cation exchange product of MMTs or CE-MMTs is prepared. Finally CE-MMTs are separated by centrifugation in ethanol several times (6–8) to remove extra cations. The collected filtrates are dispersed again in water to prepare the CE-MMTs. The obtained powders are dried under room temperature.

Example 6.1.7.4. Preparation of solvated organic MMT derivatives and its heterogeneous structure. The first step is the preparation of amine-solvated organic-MMTs, where amine with different chain lengths ($C_nH_{2n+1}NH_2$, $n = 6-18$) is added to CE-MMT solution with molar ratio of amine/CE-MMTs = 20:1 (amine/CE-MMTs = 20/1). This suspending solution is stirred at 50°C for 30 min. The obtained slurry is used for the preparation of pillared silicate hybrids. The second step is the preparation of porous heterogeneous structure of MMTs, where, the molar ratio of CE-MMTs/amine/TEOS = 1: (5–10) : (30–50). The amines used are $C_{10}H_{21}NH_2$, $C_{12}H_{25}NH_2$ and $C_{16}H_{33}NH_2$. The mixtures are sealed in a container after vigorously stirring at room temperature for 4 h. The final intercalates are dried in air at room temperature without washing with water to stimulate a further hydration of TEOS in the interlayer space. The dried products are calcinated at 650°C for 4 h to remove the template surfactants of amine giving a porous crystalline heterogeneous structure of MMTs.

These mixtures give heterogeneous structure with nanopore size of 1.5–50 nm. On comparing the interlayer distance of dried powders and calcinated samples, it is found that the mixtures have their interlayer distance decreased from ~ 2.7 to 0.3 nm. The results show that all products are intercalates of SiO_2 and carbons of calcinations.

6.1.7.5. Nanometer catalysts

Most of traditional catalysts have their active sites from several nanometers to tens of nanometers. They are naturally called nanometer catalysts. For example, $\text{Rh}_6(\text{CO})_{16}$ carried on Al_2O_3 was used to prepare $n\text{-Rh}/\text{Al}_2\text{O}_3$ catalysts, where Rh particles are 2 nm in size. These kinds of nanometer catalysts are briefly discussed below:

(1) *Nanometer active compositions carried on large particles.* The particles are talc, Al_2O_3 , SiO_2 , etc. The active compositions originate from PdCl_2 , $\text{Ni}(\text{CO})_8$ and $\text{Rh}_6(\text{CO})_{16}$, forming nanoparticles after calcinations of their precursors. The nanoparticles of Pd or PdO, Ni or NiO, and Rh or Rh_xO_y are easily detected in the catalysts.

(2) *Nanometer active compositions carried on nanometer particles.* Several nanometer particles such as nm- $\text{SiO}_2/\text{TiO}_2$ are used to prepare nanometer catalysts. For example, dispersing SiO_2 in 100 nm of boehmite gel (0.5–5%, by wt) gives a mixture for calcination, and 80% (by wt) of boehmite is transformed into a loose morphology of $\alpha\text{-Al}_2\text{O}_3$. The $\alpha\text{-Al}_2\text{O}_3$ aggregated particles are milled or crushed into superfine powders with particle size of 20–50 nm and specific surface area of at least $50\text{ m}^2\text{ g}^{-1}$ (See USP6048577, 2000, Norton company).

SiO_2 particles can be coated by nm- Al_2O_3 . The codeposition method is used to prepare the nanometer catalysts with this coating. For example, precursors of Rh ($\text{OCH}_2\text{CH}_2\text{O}$) and $\text{Si}(\text{OC}_2\text{H}_5)_4$ are mixed in water to prepare a sol. Then, the gel forms are calcinated under high temperature, to form nanocomposites of $n\text{-Ni}/\text{SiO}_2$, $n\text{-Co}/\text{SiO}_2$, $n\text{-Rh}/\text{SiO}_2$ or $n\text{-Rh}/\text{Al}_2\text{O}_3$.

(3) *Nanometer active compositions carried on particles with nanometer pore structure.* The pore size for nanoparticles ranges from <2 to >50 nm. The traditional carriers such as ZSM-4(5), SAPO, Zeolite, MCM-41(42), etc., have pore diameters of 2 nm. The pore structure is suitable for cracking oil and wax.

(a) *Cation exchange methods.* The carriers are first treated by an ion or cation exchange reaction. For example, the Zeolites (SiO_2 or silicates) first have their surface acidified or treated by chloric acid (HCl) and then the ions of H^+ , Na^+ , etc. are formed on the surface. The acidified carriers are mixed with composite cations of, e.g. $[\text{Rh}(\text{NH}_3)_5\text{Cl}]^{2+}$ in solutions to prepare $n\text{-Rh}/\text{Zeolite}$ (SiO_2 or silicates) nanometer catalysts. The noble or precious metal nanoparticles carried on the carriers are used in hydrogenation reaction, desulfurization and cracking reaction thus providing high activity and selectivity. The $\text{Rh}(\text{Pd}, \text{Pt})/\text{Al}_2\text{O}_3(\text{C}, \text{SiO}_2)$ catalysts have been used in organic synthesis, petrochemicals and environment-friendly cars.

(b) *Template synthesis.* Nanosize pores are prepared on template agents of selected surfactants. In the preparation of ordered pores, the surfactants are synthesized independently. The hydrothermal synthesis method is used to create pores. With appropriate strength the preparations provide carriers of ZSM-4(5) or SAPO with pore size of 2 nm. They in turn become a good template used in the preparation of precious metal nanometer particles; for example, 2 nm of Rh deposited in solvents gives metal particles homogeneously distributed on the carrier when immersed in the same solvents.

6.1.7.6. Photocatalysis

Photocatalyst of titania materials has a highly ordered structure of solid particle system, which is necessary for achieving a high efficiency and selectivity [18–19]. The activity of the titania component for photocatalysis depends on its particle morphology. The layered gallery of LDHs forming a complex-layered oxides [20] provides the proper morphology for photocatalysis. In other practices, several functional complex of the *trans*- ReO_2 (pyridine) $_4^+$ ions are used to intercalate into the hectorite or fluorohectorite to exhibit photocatalysis. Similarly, *trans*- ReO_2 (CN) $_4^{3-}$ intercalated into the positive layer of LDHs (Mg/Al) also shows performance of photocatalysis. ReO_2 (pyridone) $_4$ -hectorite and ReO_2 (pyridine) $_4$ -fluorohectorite complexes exhibit high light-emissive characters and are thus capable of acting as photocatalytic supports. Uranyl clay, uranyl-containing pillared clay and uranyl zeolites have been found to exhibit photo catalytic performance, and the proper control of structure parameters like pore size and surface area of supports lead to photocatalytic selectivity and activity [21]. The titania–MMT compounds are formed when the pillared MMTs are intercalated by TiO_2 particles. The TiO_2 -pillared MMTs have 0.58 eV blue shift in the adsorption and fluorescence spectra compared with pristine TiO_2 particles [22]. The growth of ZnS and CdS particles in a silica-pillared layered phosphate has been used for photocatalysis. In the preparation of CdS and CdS-ZnS mixtures in the interlayer gallery of MMTs, LDHs (Mg/Al) or saponite, the Cd^{2+} ions are intercalated into the interlayer space of MMTs by a cation exchange reaction. Then the particles obtained are treated with H_2S , which gives a nanocomposite of CdS/MMTs. The CdS particles are confined to the interlayer space of MMTs. Their non-linear optical properties as semiconductor particles doped in the layered material have potential use as photofunctional material [23]. Ultrafine Ni particles (0.5 nm) are more suitable for catalysis than larger Ni metal particles in water-photocatalyzing decomposition [24].

6.1.7.7. Thermal resistance

Attapulgit is used as heat-insulating material. Attapulgit has interconnected open pores replaced by sealed pores, which reduces thermal conducting and exchange by interflow; fiber diameters reduce thermal contacting resistance. Compared with other layered silicates of illite, MMTs, Na-bentonite, etc., attapulgit has low thermal conducting coefficients i.e., $0.06 \text{ W m}^{-1} \text{ }^\circ\text{C}^{-1}$ with a water content of 12% (by wt) and bulk density of 1.6 g cm^{-3} . The density parameter in layered silicate family is one of the main factor responsible for improving their thermal conducting coefficients at a fixed constant solid load. The smaller the density the better the thermal conducting performance of the corresponding layered silicate of the attapulgit. This is due to the different effects of density on the thermal conduction by air, radiation and convection with the increase in the density, the smaller pore diameters reduce the thermal convection by radiation, interexchange or interflow. The heat-conveying quantity by a solid phase increases with the contacting rate between solid particles.

Thus, attapulgit as a heat-insulating material is unique and it is used in engineering fields. At present, refinery plants consume as much as 15.0 millions m^3 thermal insulating materials, including attapulgit.

6.1.8. Additives

6.1.8.1. Nanoparticles used for stabilizing emulsions

When clay particles are applied to stabilize emulsions, the particle size is designed to be about 200 nm. The dispersed layers from layered silicates stabilize the interphase of the nanoparticles in solution. Hydrophobic MMTs stabilize the interphase of W/O or O/W/O emulsions, while hydrophilic MMTs stabilize the interface of O/W or W/O/W system. In addition to uses in polymerization media, these emulsions have applications in oil field drilling and separating liquids from oil in oil recovery plants. In the preparation of PS-MMT nanocomposites, MMT layers serve to stabilize the emulsions of PS monomers. The practical products of MMT-stabilizing emulsions are coatings used for electrostatic shielding, high insulation and magnetic properties. These coatings have better properties than coatings using kaolinite. Similar reports on nanoparticle stability effects are also seen [25–27]. It is found that silica particle stabilizes oil-in-water emulsions, while carbon black stabilizes water-in-oil emulsions. However, whenever appropriate quantities of silica and carbon black are mixed, the resulting mixture does not stabilize any emulsion. Similar results have been achieved by others [26].

Tsugita et al. [27] reported an oil–water emulsion using a combination of Na-MMT and polar organic compounds such as glycerol monopalmitate and ethylene glycol monostearate. The complexes formed between the particles and organic compounds surround the oil droplets, and the droplets are fixed by a network structure from the interaction of Na-MMT platelets in the aqueous phase. Several investigators had created oil–water system using clay particles. Menon et al. [28] observed that the stability of water-in-oil emulsions stabilized by clay particles depends on the formation of complex structures at the oil–water interface. Such structures effectively retain the particles at the oil–water interface. The particles tend to remain at the oil–water interface when the contact angle is 90° according to Tadros et al. [29] The fine particles (especially nanoparticles) can adsorb on the interface of an oil droplet in a continuous aqueous medium and the adsorbed particles act as a barrier protecting the oil droplets from coalescence. When particles agglomerate and submerge into one of the bulk phases, droplet coalescence occurs. Such a process requires additional energy when the particles provide a barrier to coalescence. Almost all particles have a tendency to be adsorbed at the oil–water interface since the particles transfer from a bulk phase to an interface [30]. A novel way to disperse the powder is to use supersonics (ultrasonics) to prepare stable drops. In addition to providing steric hindrance to drop–drop coalescence, the adsorption of particles at the oil–water interface also affects the rheological properties of the interfacial region [31,32]. At a sufficiently high concentration of particles, the particle-packed interface exhibits viscoelastic behavior. The viscoelastic interface affects the emulsion stability by retarding the rate of film drainage between the coalescing emulsion droplets or by increasing the energy required to displace particles from the contact region between the droplets.

Kaolinites treated with asphaltens have been used to study the particle partitioning between the phases of an oil-in-water emulsion and the oil–water interphase. The nanoparticles adsorbed at an oil–water interface are very stable. The core–shell structure is extremely strong when the interfacial film thickness is controlled.

6.1.8.2. Modifications of clay particles with asphaltens

Kaolinite particles with 200 nm are treated with asphaltene. Asphaltenes are first extracted from Alberta athabaskan bitumen by adding excess hexane to the bitumen. The volume ratio of hexane/bitumen is 4:1. The mixture of bitumen and hexane is stirred in a beaker for 30 min, and left undisturbed for 2 h. The asphaltenes precipitate and settle at the bottom of the beaker. They are then filtered and dried at room temperature for 24 h. A known amount of asphaltenes is then dissolved in mixed solvent of *n*-heptane/toluene at a volume ratio of 1:1. The kaolinite (10 g l^{-1}) is added to the mixture and stirred for 24 h. Finally, the treated clay particles are filtered and dried for 24 h at room temperature. The procedure is similar to that published by Menon and Wasan [28]. The treated clay particles are applied in mud drilling or in waterproofing.

6.1.8.3. Emulsion preparation

Reverse osmosis water is used to prepare the emulsion. A known amount of the treated clay particles (W_i) is first added to a given volume of water with a specified pH value and sheared using a homogenizer for 30 min at 3000 rpm. This initial clay concentration in water is denoted by C_t . The emulsion is prepared by adding a known volume of oil to the clay in water suspension and shearing it using the same homogenizer at a predetermined speed for 10 min. The total volume of the oil and water is 852 ml. A light mineral oil is used as the dispersed phase. It has a density of 780 kg cm^{-3} and a viscosity of 2.4 mPa s at 25°C. The oil volume fraction of the obtained emulsion is set to be 0.126. The emulsion stability is controlled by either the droplet size or their contact angle. The d_{32} (Sauter mean diameter) is used to quantify the average size of the oil droplets. The pH of the aqueous phase is adjusted by adding dilute hydrochloric acid or sodium hydroxide solutions to the emulsion. Then the contact angle of θ vs. pH is plotted.

6.1.8.4. Antibacterial nanocomposites for engineering plastics

Ag ion is an element capable of killing bacteria when carried on other nanoparticles such as SiO_2 . The nanocomposite particles are then mixed with plastics to produce advanced engineering plastics with antibacterial activity. The commercial inorganic nanocomposite, known as MF350 composed of Ag and SiO_2 is characterized with high effective, rapid and durable antibacterial behavior. MF350 has a stable and reliable effect on killing over 36 types of bacteria. The properties are listed in Table 6.20. This

Table 6.20
Antibacterial nanocomposite particles based on the Ag system^a

Physical parameters	Property index
Mean particle size (nm)	<90
Apparent density (g cm^{-3})	2.6 ± 0.3
Temperature resistance (°C)	950
SiO_2 content (%)	>90
Al_2O_3 content (%)	4.5 ± 0.5
Ag content (%)	≥ 3.0
Impurities (%)	≤ 0.03

^aCommercial name is MF350.

unique rapid-killing bacteria property makes it widely applicable in porcelain, chemical fibers, plastic products, appliance, coating and medical cosmetics.

The antibacterial nanocomposites of Ag and SiO₂ particles have been applied in making appliances. From 1999, these antibacterial particles have been used to prepare a new generation of special materials for refrigerators. The antibacterial effects are compared and listed in Table 6.21.

The nanosilica particles used for carrying the antibacterial composition are commercial products. The mixed silica particles with active compositions have good compatibility with most of the organic polymer matrixes. The polymer–silica nanocomposite products have high strength, toughness and resistance to aging compared with the pure polymer matrix when the inorganic load is controlled. Similarly, in polyethylene–5% (by wt) SiO₂ nanocomposites, the tensile strength is enhanced twice than pure PE; they have superior properties to PA6, and will probably in future replace PA6 in engineering plastics.

6.1.8.5. Adsorbing agents

The zeolite gateway inside attapulgite has a very large inner specific surface area. The single crystallites are fine rod-, needle- and fiber-like. During its dispersion, the rod-like fibers are multidimensional and of higher surface charge. The fibers deposit randomly and produce a heterogeneous distribution among the aggregates after drying. Attapulgites have a characteristic specific surface of up to 215 m² g⁻¹. The size of the zeolite gateway inside the attapulgite is homogeneous, which is beneficial for molecular sieves. Thus, chemical adsorption dominates in attapulgite.

The properties of attapulgite is to act as a filtration agent, deodorant, and bleaching agent or as a carrier. It has strong selective adsorption to cations, since the Coulomb force dominates during adsorption. The ability for attapulgite to adsorb cations depends on its electronegativity and atomic radius as shown in Table 6.22.

Table 6.21
Comparison of the antibacterial effects

Types	Samples	Killing rate (%)	Standards
Large-intestine bacillus	Refrigerator door seal	92.7, 91.6, 93.6	AATCC100-1993
Golden grape coccus		94.5, 93.8, 95.3	
Large-intestine bacillus	Inner liner, dish and handle in Refrigerator	91.3, 92.0, 92.4, 92.8	GB15981-1995
Golden grape coccus		92.7, 92.8, 94.1, 94.8	

Note: Data were measured in the Institute of Environmental Sanitation and Sanitation Engineering, Academy of China Disease Defense and Medicals. (Meilin Corporation Hefei, China)

Table 6.22
Electronegativity and radii of metal cations (in Angstroms)

Metal	Cu	Zn	Pb	Mn	Cr	Cd
Atomic radius	1.90	1.65	2.33	1.55	1.66	1.69
Ionic radius	1.35	1.35	1.80	1.40	1.40	1.55

The cation adsorbing order for ions on the attapulgite from strong to weak is



Attapulgite's adsorbing behavior agrees with theoretical predictions. A saturated adsorption value exists at which further addition of cations reaches equilibrium. Attapulgites adsorbing effect is related to several factors as size, type, polarity and hydrophilic behavior. It has high ability to adsorb small molecules such as NH_3 , pyridine and acetone. In their adsorption process, small molecules of ethanol and pyridine enter into the inner gallery replacing part of the zeolites' water and form hydrogen bonds with the residual water in the zeolite. The dielectric performance and the presence of inner gateway inside the crystallites of attapulgite make it to have wide applications. Besides hydroxyl groups, unbalanced charge and broken bonds (e.g. Si–O–Si bond) on crystal lattice defects, are all possible sites adsorbing foreign materials. The attapulgite has four kinds of possible adsorbing centers:

(1) *Isomorph substitution.* Oxygen atoms in the silica tetrahedron by isomorph substitution. These atoms provide a weak interaction with adsorbing molecules.

(2) *Hydrogen bond.* Negative water molecules (H_2O) coordinated with metal ion of Mg^{2+} on the fiber edge form a hydrogen bond with adsorbing nuclei.

(3) *Covalence bond.* The broken Si–O–Si bridges form Si–OH groups accept ions and combine with adsorbing ions to form covalent bonds.

(4) *Electroadsorbing centers at unbalanced locations.* The substitution of isomorph but non-equivalent valence for the same crystal compositions (e.g. $\text{Al}^{3+} \rightarrow \text{Mg}^{2+}$, $\text{Fe}^{3+} \rightarrow \text{Mg}^{2+}$ substitution) and the loss of coordination water (H_2O^- , OH^-) provide electroadsorbing centers of unbalance charge.

In summary, attapulgite has three kinds of adsorbing effects: cations inside the tetrahedral system, structural edge water coordinated with Mg^{2+} and Si-OH groups. Most of the adsorption occurs on the external surface of attapulgite or empty locations where crystal defects grow. The adsorption does not completely occur inside its gateway.

6.1.8.6. Rheological additives

(1) *Attapulgite.* As one of the nanoprecursors, attapulgite has its exfoliated layers parallel to the axis of the crystal fiber. Its fine crystallites of crystal structure and rod-like fibers provide a thorough exfoliation under external pressures or force (shear force). Under a low shear force, the suspended attapulgite forms a gel. As the shear force increases, the liquid suspension resorts to a viscosity as low as water. Compared to MMTs, attapulgite is more suitable for producing slurries in saturated salt solution, where its slurry swelling rate reaches $24 \text{ m}^3 \text{ t}^{-1}$; while that of fiber-like attapulgite reaches $50 \text{ m}^3 \text{ t}^{-1}$, measured at a viscosity of 15 mPa s and a shear rate of 1020 s^{-1} . The factors on its swelling behavior are given below.

(a) *Surface electronegative performance.*

(b) *The higher the surface electronic potential, the stronger the hydration capacity.*

- (c) *Surface perfectness.* Attapulgite has an imperfect surface, a lower crystallinity degree, more broken bonds and unbalanced points of charge and the stronger hydration.
- (d) *Cation-type occupying locations by octahedral.* Isomorphic substitution between cations of trivalent Al^{3+} and divalent Mg^{2+} is a beneficial for creating active locations on the crystal surfaces and enhancing the hydration capacity.
- (e) *Desegregation of its aggregates.* Electronic microscopy shows the coexistence of minerals with fiber attapulgite and crystals. In contrast, the minerals coexisting with earth-like attapulgite are not crystallites; the earth-like attapulgites have an increase slurry yield under strong shear forces.
- (f) *Length of fibers.* The length of single fibers is more suitable for net formation with large empty space.

(2) *LDHs.* Its two-dimensional layered plates have weak interactions between them and are easily exfoliated under external forces. Thus, it has superior thixotropic properties for coatings. In polymer-LDH nanocomposites, layer exfoliation provides a composite film with excellent enhanced mechanical properties and good transparency. For example, in PVC, LDHs act as a plasticizing agent and antismogging drop agent. The regular layered structure provides a mesopore structure with particle size of 10–50 nm.

(3) *Structure memory effect of LDHs.* Nanostructured LDHs has a unique “structure memory effects.” Its structure resumes the original structure after certain conditions are exerted. This characteristic is used to intercalate the necessary guests into LDHs interlayer space to assemble to a functional layer structure. Under the controllable external interaction, LDHs can completely discharge the guest materials in its interlayer space. Under the conditions of excess air and water, LDHs react with carbon dioxide (CO_2).

When LDHs act as carrier of free enzyme and related active components, an enzyme carrying catalyst is obtained. LDHs are an excellent carrier for agricultural medicines and fertilizers and can release the active components at specific time and quantity. This can be done by controlling the chemical properties of the layer-plate structure.

(4) *Layer-plate structures and their controlling properties.* LDHs is a derivative of talc minerals, and it has overcome the talc's disadvantages of high interlayer charges, and difficult exfoliation of their layers. The modified product of talc mineral is a type of hydrotalcite, which is obtained by reacting metal chloric salts with CO_2 .

In the layer-plate structure of LDHs, there are anions in the interlayer space, which react with anionic compounds by an anion exchange process. Due to the exchange reaction, the layer structure is exfoliated into random particles with sizes of several tens of nanometers. LDHs have their layer composition changed as the reaction proceeds. The layer charge on LDHs is positive; this adsorbs negative charges such as, CO_3^{2-} , SO_4^{2-} and Cl^- . This is a special characteristic.

- (a) *Adjustable layer-plate compositions.* As stated above, layer-plate compositions of LDHs can be adjusted depending on the application. By adjusting the compositional ratio of the initial raw materials, the layer-plate compositions can be varied to obtain different layer-plate chemical properties and electronic charge densities. For example, if the initial raw materials are MgO (SiO_2) or Al_2O_3 (BaO), the layer charges of LDHs are quite different.

- (b) *Adjustable ions type and quantity in the interlayer space.* By assembling the molecules by an intercalation and ion exchange in LDHs, the ion type and quantity in LDHs can be varied. This will change the properties of LDHs to a great extent.
- (c) *Adjustable crystallite size and the distribution.* By controlling synthetic conditions, the crystallite size can be adjusted accurately to 20–60 nm. The size distribution of the crystallite particles is narrow.

There are several obvious advantages of LDHs properties such as structure, size, property and applications. The layered LDHs as a nanoprecursor has a length of 20–40 nm and width of 30–60 nm. This size can be modulated within a wide range. Finally, the ease of processing nanocomposites of LDHs-PP (PE) provides an excellent material for fabricating high-performance materials with superior antiaging, mechanical, barrier, antielectrostatic and dust-proof properties.

6.2. Products of nanomaterials

The literature shows that there are more than 200 different nanoparticles or powders produced in industry. The production lines for these powders have increased rapidly in China. Superfine particles such as ZnO, ZrO₂, SiO₂, CaCO₃, and layered silicates, are available. The nanopowders are often used in products for cosmetics, optical-electric components, packaging materials, coatings, etc. Nanoparticles in these products and fields generally improve the properties of the products. Some are listed below:

- (1) Enhancing the activity of catalysts, and reducing the quantity of the active catalyst material.
- (2) Producing homogeneous dispersions and distributions of particles.
- (3) Enhancing the stability of a suspending system and improving its properties such as adjustment of the interfacial tension.
- (4) Enhancing the resistance properties to ultraviolet light or other radiation; and anti-aging and antioxygen degradation.
- (5) Enhancing the heat resistance properties.
- (6) Enhancing a film's barrier and fire-retardant properties.
- (7) Enhancing general polymer functionalities such as optical, sound, electronic and magnetic.
- (8) Enhancing application properties of polymers, such as transparency, and ease of processing.
- (9) Enhancing other properties related to field of polymers materials, batteries and energy.

6.2.1. Products in industry

6.2.1.1. MMT gel and powders for nanoparticle precursors

(1) *MMT gel for nanoprecursors.* Large-scale preparation of nanoprecursor particles based on MMTs is of significance; these are produced by several companies. Industries often use traditional equipment and techniques such as autoclaves, depositing tanks, Ramond millers, spray-drying and ball milling. The preparation technology for nanoprecursor particles is divided into several steps such as raw material preparation,

pretreatment and post-treatment. Layered silicates of clay undergo a pretreatment process. The raw minerals are crushed, washed and selected by floating separation for pretreatment reactions in intercalation and spray-drying. The equipment used is universal and only a couple of examples are given below.

Example 6.2.1.1. Preparation of MMT nanoprecursor particles. Na-MMTs (5 kg) is dispersed in 50 l autoclave for 0.5 h, keeping water temperature at 80°C. Then, 0.01 kg of NaNZy (a specially designed salt with Na⁺) is added to suspending system, diluted and deposited for 24 h to separate the upper gel from the residues at the bottom. The upper suspending systems contain 2.0 kg of solid, to which 243.1 g of caprolactum phosphorous quaternary ammonia dissolved in 1000 g of water is added. The gel is prepared by stirring this solution, which is spray-dried at 5 kg h⁻¹ in a vaporizing machine to obtain the powder.

Example 6.2.1.2. Preparation of MMT nanoprecursor particles. Na-MMTs (25 kg) is suspended and stirred in a 1,000 l autoclave for 0.5 h, with the solution maintained at a temperature of 80°C. Then 0.05 kg of NaNZy is added to the suspending solutions and deposited in a tank for 24 h, during which the separation of the upper gel and lower residues occur. The upper suspension (gel) with solid content of about 20 kg is pumped into the second 1000 l autoclave, to which 2431.1 g of caprolactum phosphorus quaternary ammonia aqueous solution dissolved in 10.0 kg of water is added. The suspension is stirred for 6–12 h and then the gel is dried at a rate of 25 kg h⁻¹ with a spray-drying machine. The properties of pristine and treated clay are listed in Table 6.23.

The spray-drying method is often employed for these powders when the powders are used in polymer-grade MMTs. MMTs go through purification steps to ensure that they meet the specifications for purity. In production, the treated MMTs are often used in flow processes. A Teflon bag is then used to prevent generation of smoggy powder and to improve recovery.

(2) *Drying polymer-grade powders.* The dissociated sand in the powder is controlled to be <0.5% (by wt) and then dried on a spray drier (Figure 6.18), which is found to be quite successful in controlling the quality of the final products. However, it is energy-consuming. When the yield capacity of powder reaches 1000 tons, the drying method may be replaced by using a Remond miller as shown in Figure 6.19.

Table 6.23
Properties of pristine MMTs and treated MMTs

Properties	Pristine MMTs	Treated MMTs
CEC (mmol (100 g) ⁻¹)	70–110	>90
Free sand content (%)	<0.1	<0.05
Whiteness (by spectrophotometer)	>70	>80
Fe ₂ O ₃ + FeO (%)	<0.5	<0.1
Solid content in gel (%)	5	5–15
Viscosity (ϕ 600)	>20	~200

Note: Hardness of water: [Ca²⁺, Mg²⁺] < 100 ppm; [Cl⁻] < 20 ppm.



Fig. 6.18. The partial device for preparing MMT powder in industry.

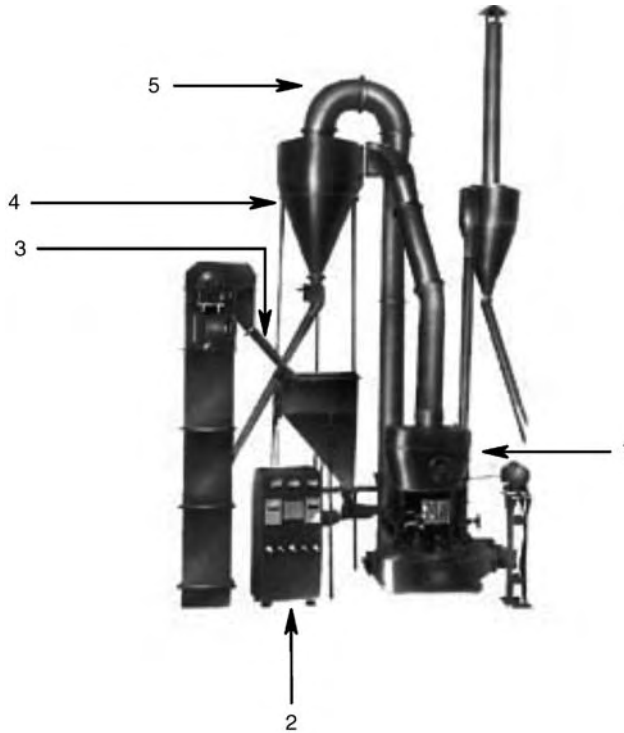


Fig. 6.19. Sketch of a Remond mill: 1 – main motor, 2 – controlling cabinet, 3 – product powder, 4 – separation area (fine powder separated from coarse one), 5 – returning area (the coarse particles returning to the main motor).

When MMT powders are prepared on a large scale, Remond millers can be used. The miller crushes the coarse particles of MMTs into fine ones. For example, the large particles of MMTs enter into the main motor 1 for milling. Then some of the fine qualified particles are separated in area 4 to become the final products while some coarse particles return to the original main motor for further milling.

6.2.2. Product processing technology

6.2.2.1. Selection of equipment

To meet industrial needs, proper selection of equipment type is a factor for designing a production line. Selection of the Remond miller type according to the yield is appropriate. Parameters of some Remond millers are listed in Table 6.24 where “*R*” is a factor for selecting a particular miller. The MMT powders from such millers have particle sizes of about 100 μm . To make them suitable for preparing polymer–inorganic nanocomposites, these coarse particles need to be further treated with ion exchange reaction.

6.2.2.2. Porous silica

Preparation of porous silica proceeds in two steps: preparing particles and calcinations in a one-pot or an autoclave. Its advantage ensures that the nanoparticle powder materials are homogeneous or dispersed homogeneously in the polymer matrix. Depending on the practical requirements, several choices are available for preparing the silica particles with round surfaces, porous structures or multi-porous structures. Some routes for large-scale preparation of nm-silica are given below.

(1) *Non-surfactant template*. This route is for preparing inorganic materials with micropores or mesopores. The tri-block copolymer of polyethylene oxide (PEO)–polypropylene oxide (PPO)–polyethylene oxide (PEO) has been used [33] as a template for synthesizing mesoporous silica materials. Based on this technology, polymer–silica nanocomposites are prepared on a large scale. The silica precursor or tetraethyl oxide silane (TEOS) is used. The TEOS reacts with bi-(triethyl methyl oxide silane) aromatic monomer or acetylene monomer, in which a network-like polymer–silica nanocomposite is obtained [34]. Results show that the silica has heterogeneous pore distribution.

(2) *Surfactant template*. In a template of cetylalkyltrimethylammonia bromide (CTABr)/sulfo compound, the sulfo compound makes a blockage inside the particle’s passageway. In a mixture of bi-(tri-ethyl oxide methyl silane) ethane (BTE)/TEOS, the CTABr serves

Table 6.24
Remond millers and their parameters

Parameter/type	3R1410	3R2115	3R2615	3R2715	4R2715	4R3016	4R3216
Feed particle size (mm)	5–8	15	20	20	15–25	15–25	25
Product size (mm)	—	—	0.125–0.044	—	—	—	—
Yield/8 h (Tons)	1–10	1–18	2–25	2–28	3–30	3–36	3–38
Axial rotate speed (rpm)	280	180	170	170	170	187	130
Miller ring ID (mm)	ϕ 405	ϕ 640	ϕ 780	ϕ 830	ϕ 830	ϕ 880	ϕ 970
Miller roller D (mm)	ϕ 140	ϕ 210	ϕ 260	ϕ 260	ϕ 270	ϕ 300	ϕ 320
Roller and ring H (mm)	100	150	150	150	150	160	160

Note: ID, inner diameter; D, diameter; H, height of both miller roller and ring.

as a template to prepare organic–silica composites (or silica treated with organic surfactant) with ordered and periodical mesoporous structure or patterns [35]. In an integrated process of particle preparation and surface treatment, the final product contains bridged ethylene groups in the silica particles. The silica in the composites has large porosity, which is advantageous for different chemical reactions, and is widely applicable in membrane separation, selective catalysts, microelectronics, oil cracking and optics.

(3) *Emulsion template.* The emulsion generally contains water and oil phase along with a surfactant stabilizing its drops, which forms a thermally stable system. Emulsion technology is popular in preparing silica nanoparticles because of its homogeneity, where the dispersing phase size is in 5–50 nm. The self-assembled nanoparticles interact with polymer (e.g. polystyrene) as a template or structural component when the polymers are hydrophobic. Both hydrophilic and hydrophobic reagents are used to reduce the polarization difference between the polymer particles and polar dispersion phase. In an oil/methyl amide emulsion template without ethanol, the superfine silica particles are prepared by a sol–gel process [25], and the silica pore size is controlled within 50 nm.

(4) *Porous silica applied to preparing functional materials.* In the application of fiber-like mesoporous silica [36,37] for the olefin carrier in a polymerization reaction, stretched chain crystals of polyethylene fibers are prepared. Similarly, using mesoporous silica as a carrier, ordered ruthenium cluster carbonyl compounds have been prepared [25]. These are used to catalyze hexane and cycle octane for polymerization in a hydrogen environment.

6.2.2.3. Silica powders and drying

Several practical methods for collecting silica powders have been developed such as use of supercritical fluids, spray-drying, cold-freezing drying, common heating drying milling methods. A good example is the preparation of NPP with core-shell structure size of 20–40 nm using silica as the core material. When it is prepared in a solvent of ethylene glycol (EG) by a sol–gel method, it is collected by a supercritical drying method as shown in Figure 6.20. The critical conditions for EG are $T_c = 372^\circ\text{C}$, $P_c = 76 \text{ atm}$, $Z_c = 0.27$ and $\rho_c = 0.334 \text{ g cm}^{-3}$. At the end of the sol–gel reaction, the product is obtained from the outlet shown in Figure 6.20. The silica has some EG chains and hydroxyl groups adsorbed on its surface and therefore can be directly applied to other polymers to prepare nanocomposites. The silica can also be melted with oligomers of polyester or polyamide to prepare NPP particle products.

The cold-freezing drying method is suitable for preparing small amounts of silica and is not suitable for large-scale preparations. The common heating drying methods are widely used but will produce some agglomerated silica particles.

6.2.2.4. Products based on nanosilica

(1) *Products of nanosilica-rubber composites.* Silica nanoparticle materials are mixed with copolymer rubber of butylenes and styrene (PBS) or polychlorinated ethylene (PCE). They can carry tan antiaging agent and colorful dyes to produce colorful waterproof paper materials. The modifications improve the properties and these are similar to or surpassing the universal products of tri-unit rubbers of EPR (ethylene copolymer with polypropylene) (Table 6.25).

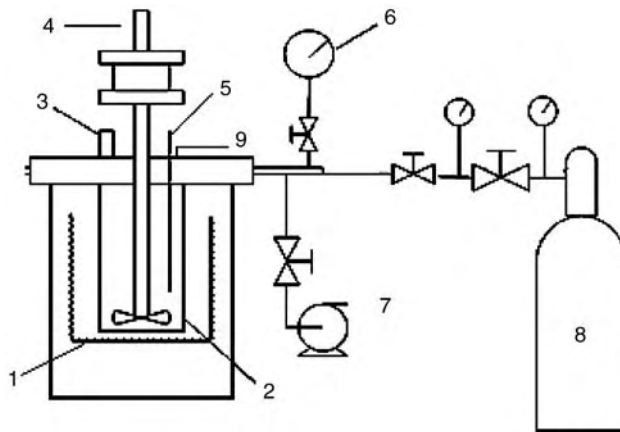


Fig. 6.20. Simple supercritical fluids for drying nanosilica particles: 1 – heating resistance; 2 – high-pressure autoclave; 3 – feed inlet; 4 – stirrer; 5 – thermocouple; 6 – pressure meter; 7 – vacuum pump; 8 – nitrogen; 9 – outlet for product.

Table 6.25

Comparison of properties between nm-SiO₂ modified waterproof paper-like material of EPR and EPR rubber matrix material of tri-units

Properties	nm-SiO ₂ modified EPR waterproof material	EPR matrix material of tri-units
Penetration of water (0.3 MPa)	No	No
Tensile strength (MPa)	≥10.1	≥7.35
Elongation at break (%)	≥661	≥450
Strength at elongation of 300% (MPa)	≥6.1	≥2.9
Tearing strength at 90°(kN m ⁻¹)	≥42.5	≥24.5

The tearing strength of modified colorful waterproof materials with 5% load (by wt) of nm-SiO₂ surpasses that of EPR rubber. Instead of micron-sized SiO₂, nm-SiO₂ mixed with EPR to produce tires for automobiles reduces inorganic content and enhances tire properties. nm-SiO₂ has indexes similar to micro-SiO₂ particles presently used in the automobile tire industry. It is expected that MMTs will replace micron-sized silica in automobile tires.

(2) *Products of polypropylene–nanosilica composites.* The products have many forms, one of which is PP–nanosilica plate materials for packaging. The processing technology of propylene–nanosilica composite raw material usually uses melt-casting technology as shown in Figure 6.21, where the silica nanoparticles carrying some additives, such as antioxygenization and nucleation, are mixed with PP resins. Then at temperatures of 180–210°C and a gap of 0.6 mm, a thick plate is cast and formed. The products have superior properties such as in higher HDT, lower shrinkage and relatively higher transparency compared to the pure PP.



Fig. 6.21. Processing line for plate materials of polypropylene-silica nanocomposites.

6.2.2.5. Preparing nanocomposite products based on different technologies

(1) *Deposition.* Active components in catalysis can be directly deposited on the chosen carriers by CVD-PVD and plasma deposition. Under inert gas atmosphere, these techniques are used to prepare nanoparticle metal powders or nanocomposite particles on the carriers. By using dielectric deposition in solution, composite metal precursors are used to prepare nanoparticles of Ni-Fe, Ni-P, and Ni-Zn. The detailed processing technologies are similar to the traditional ones, except that the carriers have both nanoparticle size and nanopores.

(2) *Nanofibers as carriers.* Nanofibers of nanocarbon black has superior activity and selectivity for the carrier or catalysts of the Ni/ γ -Al₂O₃ system. Chevron, USA, Inc. (CA, USA) has prepared a type of aluminum silicate zeolite, in which the weight ratio of m (SiO₂)/ m (Al₂O₃) is ≥ 500 with pore diameters >705 nm. The first oxides are SiO₂, GeO₂ or their mixtures; the second oxides are Al₂O₃, GaO₂, Fe₂O₃, InO₂ or their mixtures (see US patent US6103215). These catalysts are used in the transformation reaction of olefin compounds. We have used nanocarbon black as a carrier for Ni catalyst to remove sulfur in gasoline and diesel. Due to attapulgites nanofiber-like structure, it is also a useful choice. In the case of MMTs as a carrier of olefin catalyst, the activity reaches 10–100 g product g catalyst⁻¹, when the inorganic phase load is 1–10% (by wt).

(3) *Drying technology.* In emulsion of W/O with aluminum hydrous solution and organic compounds, no alcoholic salts of metals are used to reduce the cost of catalysts. Using spray-drying and calcination technology, one can prepare nanoparticles with multipores and an extremely thin covering of several nanometers. The metal solutions are Al(OH)₃, Cr(OH)₃, ZnCl₂ and ZrCl₂. The catalyst carriers are amorphous and of very large surface area and resist high temperatures. They maintain their original high surface area over a long time.

(4) *The significance of nanomaterial catalysts.* Nanomaterial catalysts are significant since they contain nanoscale in both particle and pore size and a nanostructured array that can be controlled by appropriate preparation techniques. Presently, nanomaterial

catalysts are replacing traditional precious metals. This replacement can compensate for the shortage of precious metals.

6.2.3. Product quality control

6.2.3.1. Layered silicates and their quality control

Several commonly used layered silicates are listed in the previous tables (Table 1.18, Table 2.2, Table 6.23) along with other synthesized artificial products such as V_2O_5 , magadiite and LDHs.

(1) *Quality control.* The diverse applications of layered silicates require quality control, supervision and evaluation to avoid practical problems. Some standards and related parameters have been established to characterize nanoparticle and their precursors. Due to unstable and varying compositions of layered silicates, complicated purifying processes are used. Under such conditions, the composition of nanomaterial precursors must be characterized by chemical analysis. In addition, the following properties described below are used to evaluate the layered silicates and their precursors.

(2) *Water adsorption property.* Water adsorption is a property that characterizes the interaction or intercalation behavior of MMTs with reagents. MMTs as a nanoparticle precursor expand 8–15 times their original volume when adsorbing water quantities equal to 10–20 times their own mass. The water adsorption rate (W_{ar}) is used to express water adsorption quantity of MMTs or a quantity that the unit weight of MMTs adsorb:

$$W_{ar} = W_w / W_M$$

where W_w , and W_M are the weights of water and MMTs, respectively.

(3) *Expansion property.* The expansion property is similar to that of water adsorption for MMTs. The expansion property is expressed as the expansion capacity or volume. The expanding volume (V_e) is defined as a final volume after the MMTs are dissolved in dilute hydrochloric acid:

$$V_e = V_T / W_M$$

where V_T is the total expanding volume for overall weight of layered silicates (W_M). From this, it is shown that the Na-MMTs have higher V_e than that of Ca-MMTs or acidified MMTs. Similarly, in the same type of MMTs, it is found that the higher the content of MMTs in layered silicates the higher V_e , which is an index for evaluating MMTs' quality and type.

(4) *Discoloring by adsorption.* Layered silicates can adsorb gas, liquid and organic matters. The discoloring rate or capability is used for characterizing layered silicates' adsorption behavior using the expression

$$T = T_0 \times W_2 / W$$

where T is the sample's discoloring capability, T_0 the discoloring capability of a standard sample (e.g. MMTs), W the standard sample's weight, and W_2 the sample's weight.

Generally, when layered silicates are treated or activated by acid, they gain superior capacity to discolor.

A certain amount of MMTs is used to discolor a bitumen solution in kerosene. The difference in light absorbing value before and after its discoloring will give the ratio of light absorbed, which is defined as

$$A = (E_0 - E_2)/E_0 \times 100\%$$

where A is the discoloring rate (%), E_0 the light absorbing value of standard kerosene solution and E_2 the light absorbing value after discoloring bitumen kerosene solution.

(5) *Gel valence.* Under most circumstances, layered silicates disperse into suspending gel solution, which has certain viscosity, lubrication and rheological properties. To determine the gel behavior, a dispersing agent such as MgO (magnesium oxide) is used to prepare a gel system. The gel valence (value) is used to express the dispersing property. Then the layered silicates (e.g. MMTs) are mixed with a known amount of water to which a known amount of MgO is added. Then the suspending solution is allowed to stand for 24 h to form a gel system and the final volume, called the gel valence (GV), is given by

$$GV = V_T(15)$$

where $V_T(15)$ is the total volume for 15 g of sample. GV is an index to evaluate gel behavior of layered silicates and is an integrated characterization of the sample's properties at dispersion and its expanding aspect. Previously, GV was mainly used to characterize the content of MMTs in a sample. Higher content of MMTs leads to a higher gel valence. Na-MMTs has higher GV than that of Ca-MMTs and acidified-MMTs.

(6) *Other properties essential for the quality control.* In preparing superfine particles, the slurry viscosity is used to predict the expansion behavior or the volume value of the suspending solution in which the viscosity reaches 15 mPa s for a certain sample. In the petrochemical industry, there are other properties such as free acid, activity degree, particle size, porosity, etc. that are used to characterize the particle performance as a catalyst or an additive, and to characterize the effects of water treatment and coatings. So far, these properties are mainly used for the raw materials of nanoparticles. Some of the related standards are established while many new standards need to be created for nanomaterials.

6.2.3.2. *The application approach*

The sol-gel process for the preparation of layered silicates on a large scale is combined with particle surface treatment. The treated particles are used to make products immediately after their preparation. This approach reduces costs and ensures the use of freshly prepared materials in the manufacture of specific composites. The following common approaches and processes are all suitable for the combinations in the preparation of nanoparticles with surface treatment.

(1) *Sol-gel process.* In an industrial scale using nanoparticles by a sol-gel process, the inorganic raw materials, organic compounds and additives are placed in a container or

autoclave. These are then mixed in a mixer or reactor. Finally, homogeneous suspending solution is prepared which is a sol. The sol suspension forms a gel on heating or when subjected to pressure. The gel goes directly to a spray dryer to prepare superfine powders; meanwhile, the surface is treated by the reagents needed for specific applications. In other cases, the treated or intercalated layered silicates react with monomers forming a suspending solution, which is then initiated to polymerize under similar conditions used for the bulk polymers. Different additives are used in this suspending system to obtain the nanocomposites of polymer-layered silicates. Similarly, the obtained gel particles are washed with proper solvents and dried in a spinning dryer, and are crushed by a milling machine and calcinated.

(2) *Emulsion method.* In a mixed solvent emulsion solution, the mixtures undergo nucleation of microbulbs, aggregations, agglomerations and heat treatment (or post-calcination) to prepare nanoparticles. These emulsions are media that are normally used for polymerization of bulk polymers (e.g. PS). The nanoparticles are obtained post-calcination. This does not avoid the particle's agglomerations or heterogeneous distribution of particle size.

(3) *Intercalation polymerization.* This method has already been described in detail and it is used to make nanomaterials for different applications.

6.2.4. Product markets

6.2.4.1. Layered Double Hydroxides (LDHs)

LDH particles have been used in different emulsions by the petroleum industry, which consume 10–50 ktons year⁻¹. In the coating industry, LDHs as suspending reagents are consumed at 5–50 ktons year⁻¹. In the ceramic and catalytic fields, each year several hundreds of tons of LDHs particles are used as additives and carriers. As for the engineering plastics, LDHs as fillers are used to prepare high-performance nanocomposites and consume 10–100 ktons a⁻¹. LDHs as reinforcement agents in rubber and rubber-plastic fields consume 10–100 ktons a⁻¹.

6.2.4.2. MMTs

At present, nanopowder companies in China produces 10–100 ktons of MMTs year⁻¹ and 20–80 ktons of nanoscale silica per year according to data from the Information Center of China Chemicals (data before the end of October 2000).

6.2.4.3. Kaolinite

Ultrafine powder of kaolinite is one of the earliest products used on an industrial scale. In China, this type of layered silicate is mainly used as diverse kinds of carriers in catalyzing raw petroleum, refining diesel, de-sulfurization, etc.

6.2.4.4. Silica

The industrially produced nanopowders are ZrO₂, SiC, Si₃N₄ and SnO₂/SiO₂. A yield of nm-ZnO has a production capacity over 300 tons year⁻¹. A yield of nm-CaCO₃ can reach 10 ktons.

6.2.4.5. Market predictions

At present there is a remarkable increase in the yield of nanopowder materials every year. In further, for these nanopowders, silica and layered silicates will become the products

with the largest yields and it is predicted that silica will reach several hundred tons per year and the layered silicates will reach several thousands of tons per year before 2007.

6.3. Nanocomposites and traditional industries

Nanotechnology aims at improving and replacing traditional materials. In the long term, it will bring out many new materials and devices that, in turn, will result in large-scale changes in the traditional industries. It is predicted this change will stimulate the reformation of the traditional industries. Nanotechnology is energy-saving and less energy dissipating as the traditional industries. Further, nanocomposite materials may avoid many ecological problems.

6.3.1. Chemical materials and additives

6.3.1.1. Industrial slurries of layered silicates

(1) *Layered silicate slurries and standards.* In the past, clay was largely used as common material for adsorbents, slurries and metallurgy. Modified clay is used as nanoprecursors or as inorganic phases in nanocomposites. There are relative indexes or standards based on the traditional standards (e.g., American Petroleum Index (API) standard for oil drilling slurries). Several indexes of clay are listed below for nanoprecursor of MMT particles:

- Water content $\leq 8\%$ (by wt)
- pH value = 7–10 (5% (by wt) suspending solution)
- Whiteness $\geq 80\%$
- Pb content $\leq 20 \times 10^{-6}$
- As content $\leq 2 \times 10^{-6}$

These data for MMTs deal with their slurry properties, appearance, environmental protection requirements and hygienic aspects. Traditional viscometers such as NDZ-6 and NDG-29 are used to measure the MMTs' slurry viscosity based on their $\phi 600$ values.

(2) *MMTs transformed into nanoprecursors.* Raw materials of MMTs have different compositions depending on the locations of the ores in nature. Through a floating selection and screw-mixing with sodium salt (Na_2CO_3), they transform into intermediates of high quality with stable compositions and serve as high-quality nanoprecursors for nanomaterials. The reagents selected from different quaternary ammonia for treating layered silicates depend on both the dispersion and flocculation behavior as needed for specific applications.

6.3.1.2. Additives for petroleum and petrochemical engineering

The additive raw materials in drilling and oil recovery engineering are of various types. In each of these additives, nanoparticles or nanoprecursors are added by proper mixing to form the nanocomposites used in the application.

(1) *Acid washing-off reagents.* When MMT or silica is used as an additive, it needs surface treatment by using the techniques described previously. The acids such as H_3PO_4 , H_2SO_4 and HCl are usually used as washing-off reagents for oil recovery fluids.

(2) *Cation polymers.* In preparing fluids for drilling, polymers with high molecular weight serve as covering agents and those with low molecular weight act as stabilizing reagent for MMTs or mixtures of nanoparticles of CaCO_3 /silica. The common water-soluble polymers fluids can be stabilized by nanoparticles and applied to drilling fluids or emulsions in oil recovery.

(3) *Inorganic treatment agents.* Inorganic agents, e.g. $\text{Na}_3\text{Cr}_2\text{O}_7$, act as diluting agents, while the oxides of MgO , ZnO and polymers of polyacrylic amide (PAA) and carboxylic methyl cellulose (CMC) act as flocculation reagents in petroleum working fluids. They are used with dispersion reagents such as NaOH and Na_2CO_3 .

In these working fluids and emulsions used in the petroleum industry, the above additives exert different effect on the stability and on the rheological properties by stabilizing the double electric layers of MMTs or silica layered particles.

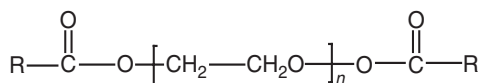
(4) *Antioxidation agents.* These additives are mainly applied to polymers or petrochemicals. They are commercial agents produced by companies. The superfine or nanoparticles act as carriers for the active antioxidation additives. Typical carriers are acidified MMTs or their mixtures with silica.

(5) *Nucleation agents.* Nucleation agents play a role in improving polymer crystallization behavior and processing properties. For example, polyester of PET is easy to degrade thermally during processing. Addition of some nucleation agents to polyester of PET remarkably improves its processing and molding behavior. Among these various traditional nucleation agents, the treated MMTs are the most effective.

6.3.1.3. Tubes and pipes based on nanocomposites

Polypropylene resin is obtained in large yield and is used as an engineering plastic, including tubes and pipes in the transportation of fluids and oils. The nanoparticle-modified polypropylene resin has improved properties such as brittleness and degradable behavior.

Example 6.3.1.1. Preparing nanoprecursors of layered silicates treated with organic molecules for PP tubes and pipes. The preparation process is divided into several steps. First, the organic treated layered silicates are prepared: 10 g of MMTs with of $95 \text{ mmol} (100 \text{ g})^{-1}$ CEC is mixed with 490 ml of water at 60°C , stirred and formed into a 2% (by wt) water slurry. Then 1 g of di (2-hydroethyl)-methyl tallow chloric ammonia reagent is added to the slurry, stirred vigorously for 1 min and the residuals are filtered. The filtrates are washed several times and dried at 60°C for 16 h under circulating gas flow, to obtain the product organo-MMTs. Second, the MMT-extending reagent mixture is prepared. The extending reagent is



where the R group is selected from epoxy (oligomers, EPON-828), PA6 or branched polyethylene (PE) and polypropylene (PP). The extending reagent and 40% (by wt) of organic MMTs are then blended together in methylene chloride (CH_2Cl_2). The extended MMTs are prepared by evaporating the solvents. Third, the extending MMTs are melt-blended with polypropylene resins to prepare pellets. This product is suitable for preparing PP-based pipes and tubes.

The processing of the PP-MMTs in an extruding machine to make pipes is slightly different from that of a PP matrix. The same is true for polyethylene. It is difficult to process UHMWPE into pipes and tubes. Addition of some treated MMTs to UHMWPE improves its flowing behavior and rheological properties. By in situ polymerization of PE with organic kaolinite, UHMWPE-based nanocomposites can be prepared, which has superior resistance to environmental temperatures, aging and degradation. The nanocomposites of MMT-UHMWPE and kaolinite-UHMWPE have been used to prepare tubes and pipes in the petroleum industry.

6.3.2. Construction materials

Construction materials have disadvantages such as releasing poisonous gases, penetration of water, poor insulation and easy degradation in the environment. Several rubber materials and their mixtures with nanoparticles have been used to make construction materials.

6.3.2.1. Nanocomposites as chemical building materials

Nanoparticles with rubber matrixes can be chosen to enhance their properties such as mechanical strength, abrasion and resistance to aging. Traditional carbon black is generally used to modify rubber in order to prepare high-performance composites. The "white carbon black" (mixed silica of nanometer and micrometer size) has become an industrial filler in preparing composites for waterproof materials, coatings and decoration paper used in construction. In these materials, nanosilica particles are designed to carry pigments or dyes providing colorful rubber products. These modifications make new rubber building materials of versatile color and appearance. The use of nano- SiO_2 as a reinforcing reagent mixed with color components provides a product with superior properties. These composites also show excellent performance in antiaging and antioxidation. Especially, the nanosilica-EPR (ethylene-propylene copolymer) composite materials have greatly improved waterproofing and antitearing properties compared with the traditional rubbers.

6.3.3. Reformation of traditional industries

6.3.3.1. Prospects

From the versatile applications of the nanocomposite materials, it is recognized that nanomaterials and nanotechnology may cause reformation of the traditional industries including the petroleum industry. Nanomaterials have influence on biomaterials, biology, medicine, information technology, ecological protection and trade affairs. The petroleum industry as a traditional industry needs urgently a reformation of new technologies. Applications of nanoparticles to lubricants, catalysts and polymer-based nanocomposite are important to develop new materials for the petroleum industry.

6.3.3.2. Energy resources

Besides liquid oil, natural gas is an important energy source. In the transformation of natural gas into liquid chemicals, several kinds of metal films such as Ni–Mo or Ni–W are used as catalysts on carriers such as ZSM5, MMTs or nanoprecursors of layered silicate with controlled porosity. These nanoparticles substitute the precious or noble metals Pd and Pt. Similarly, nanoparticles of Ni–Mo–Al, Ni–Mo–Ti, etc. have replaced the noble metals in catalyzing hydrogenation reaction, desulfurization and cracking of long-chain olefins or alkyl chains.

The energy industry has used several types of catalysts for polymer synthesis. The layered silicates of MMTs (Li-MMTs), attapulgite and kaolinite have been used as catalyst carriers. The active metals of Cr, Ti and Zr on these carriers improve the catalyst activity for polymerization.

Catalyst pairs such as MAO–Li–MMTs (metallocene catalyst), Cr–Na–MMTs (Ziegler–Natta catalyst) and Ti–kaolinite (Ziegler–Natta catalyst) are found to be practical. Recently, the Ti–attapulgite catalyst system for polyethylene polymerization was found to be quite satisfactory [38]. Our inventions of MMT–Ziegler–Natta catalysts and nm-SiO₂–MAO for metallocene catalysis have been shown to be effective catalysts [38].

Recent developments demonstrate that the “one-pot” technology can be used for preparing nanocomposites of polyolefin–inorganic nanoparticles or nanoprecursors. This discovery will cause an impact in the polyolefin industry and provide new species of modified olefin polymers.

6.3.3.3. Materials

We predict that the use of nanocomposites will cause a revolution for materials such as metals, non-metals and polymers.

(1) *Metals*. At present, nearly all metals can be crushed into superfine powders. Nanoparticles made from metal compounds of Ti, Cr, rare earth elements or layered silicates are mixed with metals of Fe to produce new series of alloys with lightweight and high strength.

Nanocomposites of metal oxide mixtures of SnO₂/SiO₂, ZnO/SiO₂, Fe/ZrO₂, etc. [39] have applications in the preparation of special alloys with high abrasion and strength but are lightweight. In some cases, the use of metal nanoparticles lowers cost. For example, Ag metal nanoparticle electronic circuits reduce the printing circuit cost to one-third of the original. The miniaturization progress in modern electronics is growing rapidly. Microcomputer storage units are being made from metal nanoparticles and show advantages in property–cost aspect. In this age of recycling, up to 40% of the metals are currently recycled. Nanoparticles can be made from recycled metals, which will provide environmental benefits.

(2) *Non-metals*. Carbon nanotubes based on nanoparticle catalyst have shown great industrial potential. They have diverse functions and high specific surface area in energy storage, e.g. the storage of hydrogen. Similarly, the preparation of tube-like clay is in progress. The layered silicate and silica have been introduced into ceramic materials with metals as additives. The brittle properties of the ceramic material are expected to be overcome. Several attempts have shown that if nanoparticles of layered silicate,

SiO_2 and ZrO_2 , are mixed with ceramics (CaO , MgO and Al_2O_3), a series of new ceramic materials are produced with enhanced ceramic toughness.

(3) *Polymers.* The layered silicate and silica have the highest potentials when applied to organic polymers to obtain improved properties. There appears a trend to synthesize layered silicate by imitating their natural compositions and structure in order to obtain a stable composition of nanoprecursors. This man-made synthesis will overcome the existing disadvantages of unstable and different compositions in the layered silicates. For example, SiO_2/NaOH , $\text{MgO}/\text{CO}_3^{2-}$ systems are synthesized into magadiite and LDHs, etc. The uniform layered silicate have profound effects on nanocomposites performance, polymer modifications and their large-scale production. Due to the large market of organic polymers, thousands of new polymer-based or modified materials can be created.

6.3.3.4. *Biology*

The bones of man have a natural nanostructure. They are inorganic–organic composites. At present, hydrocalcite nanoparticles and their nanocomposites with polymer adhesives are used to replace or repair natural bones. Hydrocalcites are quite compatible with human organs such as skin, blood and bones. These materials are being used for clinical applications. The research focuses on nanoparticles of ZrO_2 and SiO_2 to reinforce the man-made bone's strength [34]. In earlier times, we studied UHMWPE as a key material for man-made skin and junctures. At present, other polymer candidates for such applications are polylactic acid (PLA), polyglucine acid (PGA) and polyamide.

6.3.3.5. *Medicine*

Nanomaterials of silica and MMTs can serve as carriers of medicines, which will allow the active component to be transported more conveniently into the body. The so-called talent medicines covered by several layers of nanoparticles (e.g. MMTs, SiO_2) can enter the body and affect the biological activity, such as lowering the reactivity of a specific enzyme.

Purified MMT layers by themselves are made to act as a medicine for curing dysentery and filtering out bacteria. Chinese medical research has attempted to carry medicine on the nanoparticles of SiO_2 and other nanoparticles to enhance drug effectiveness. The medicine carried on nanoparticles is adsorbed gradually and directly by the skin without the need of injecting. The MMTs gradually release their active compositions, which extends the curative effect.

6.3.3.6. *Information technology*

Developing higher storage density materials in much smaller microfunctional devices has become a new goal. Nanoparticles of magnetic materials are of small size, single magnetic field structure or magnetic domain, but with high magnetic induction strength. They are used as magnetic recording media to enhance the recording density, increase the sound to noise ratio and improve the picture's quality. In Fe/Cr multiple films, a superparamagnetic effect was found for the first time in 1988. This opened the door for creating a new electronic magnet and, in addition, a new field for research and development of nanomagnetic materials. In 1994, the read-write magnetic head with magnetic resistance effects was first developed by IBM, in which the magnetic record

density was enhanced 17 times to reach 5 Gb in^{-2} (recently 11 Gb in^{-2}). This made the magnetic discs dominate over the optical disc since the 1980s.

The traditional cooling agent of fluorine chlorine olefin (Flion) has damaged the ozone layers and its low cooling effect has become a big problem. To solve this problem, a substitution of magnetic cooling materials is being considered.

According to quantum mechanics principles, electrons will penetrate through a "wall" and escape from it. This phenomenon predicts that new generation of chips, logical units, will not be connected by wires but interrelated, which needs new designs to connect single electronic devices into integrated circuits. In another aspect, the chips movement will not be controlled under such condition. Electrons will be regarded as "waves," not as "particles." However, the industrial applications of the above have a long way to go. The electrons capped in a small size or space has another contribution in making the related materials emit light. "Quantum dot-line lasers" or "grade-connecting lasers" are of extremely small size but emit a very high intensity of light. A very low electronic voltage will drive these lasers to emit a blue or green light, which is used to read or write optical disc with, enhanced storage density. If "capped" atoms are made from small particles or quantum dots, the storage degree will be enhanced hundred thousands of times and will cause a revolution in information technology.

6.3.3.7. *Ecological protection*

Semiconductor-made nanomaterials have been shaped into diverse sensors for accurate measurement of temperature, wettability and gases in the atmosphere or the environment. The sensors also find applications in automobiles. Due to cost and exchangeable features, the sensors for automobiles are made from metal oxides and active catalysts. Silica-or silicate-carried active metals of Cu, Ni and Co has been used for sensors.

6.3.3.8. *Impact and change in traditional industries*

The development of nanomaterials has a great impact on the following aspects of traditional industries:

(1) *Intellectual rights.* The present patents on traditional materials will be continuously replaced by new patents based on "nanometer" technology (e.g. existing catalyst carrier will be substituted by their counterpart nanoparticles).

(2) *Special materials.* Materials of special applications based on new nanocomposites will appear continuously (e.g., composites of PP and PE with inorganic phase).

(3) *Essential variations of energy and ecological protection.* Nanoparticles have features to "save" energy. Nanotechnology disposes off old and traditional processes for new and environmental friendly ones.

(4) *Impact on existing processing technology.* Through nanotechnology, materials are arranged at atomic and molecular levels. In the nanomaterials surface, the interdistance between two blocks of materials is close so that atoms on the surface produce chemical bonds and friction barrier forces by intermovement.

6.3.3.9. Other aspects

(1) *Military applications.* Nanoparticle powder produces great repulsion force in application to rocket solid fuels, and it can be used as a strong explosive powder. Some materials in tanks can be replaced by nanoparticle steel and aluminum materials. The tanks made of these nanomaterials have high strength but less weight (one-tenth of the original weight). Several ceramic materials for military aims can be made by nanocomposites of different nanoparticles such as ZrO_2 , MgO and SiO_2 . These can bear extreme high temperature as high as $1,000^\circ C$ without deformation.

(2) *Trade.* Nanocomposites have become significant components of materials, which will become important in trade. Naturally, the trade itself is of different applications of nanomaterials. The traditional trade of steel, raw ores of layered silicates and other minerals will be replaced by trade of different superfine powders.

6.4. Prospects

6.4.1. Membrane and film materials

Nanocomposites can be used to fabricate membranes. Organic membrane technology is used to design membranes for separating synthetic gas from natural gas. The transformation of natural gas into liquid materials requires design of inorganic membrane catalysts.

The polymer–MMT nanocomposite films have unstable colors that affect or limit their applications as films. In polymer–silica nanocomposites, the light shielding effect becomes one of its disadvantages. Silica particles have the highest shielding effect on visible light and thus their nanocomposites reduce the transparency.

6.4.2. Applications of the monodisperse particles

The monodisperse latex (e.g. polystyrene) spheres have been used as the standard particles to calibrate particle analyzers. But the latex spheres have some shortcomings such as their size and undesirable changes in organic solvents. It is difficult to calibrate the particle analyzers of sedimentation type with water because their specific gravity is close to unity. The composite nanoparticles of PS-silica will replace the sub-micron latex standard particles.

6.4.2.1. The standard particles for calibration

Using our synthesized $1\ \mu m$ and nanoscale monodisperse silica particles, a series of suspensions samples are used to model water. The known particle concentration and size are used to study the suspending solid particles to model oil reservoirs. The results provide a base for setting up the standard of water quality in water flooding for oil field recovery. In addition, the influence of silica solubility in water on the size of particles can be eliminated at extremely dilute condition of 10^{-4} wt% concentration. The number-average diameter of monodisperse silica particles obtained by a calibrated TEM is consistent with the most probable diameter measured on a Coulter counter calibrated by

polystyrene standard particles. The submicron monodisperse silica particles are used successfully as standard model dust particles to calibrate the first 0.1 μm dust particle counter made in China. The effectiveness of the particles is the same as that of the standard provided by particle measuring systems and the Duke Scientific Corp.

In these standard particles, it has to be noted that partial aggregation will cause serious error such that the particle analyzers cannot give the most probable diameter (e.g. sedimentation type particle analyzers). The 1 μm particles, e.g. S10-1, are prepared and aggregated for calibration usage. The results from TEM, the disc centrifuge particle analyzer (e.g. BI-XDC) and the dynamic laser scattering (DLS) particle analyzer (e.g. ZetaPlus) are presented in Table 6.26.

The data from different apparatuses are very similar although they work on different principles and are expressed in different ways. Recently, the S10-1 standard particles have been used for calibration of LKY-3 disc centrifuge particle analyzers for nanoparticles or submicron particles made in China. It is hoped that the monodisperse particles will be widely applied as standards.

6.4.2.2. As HPLC packing for separation of biopolymers

There are different columns for analysis, separation and preparation of usual organic compounds, especially oil cracking fractionations. Some related columns with silica are listed in Table 6.27.

Table 6.26
Diameter of S10-1 measured by different ways

Techniques	Method	Diameter (nm)
TEM	Number-average diameter	1037
	Most probable diameter	1033
	Mass median diameter	1031
Disc centrifuge	Volume-average diameter	1080
	Geometric-average diameter	1040
DLS	Effective diameter	1053

Table 6.27
Products of chromatograph columns

Columns for analysis	Size	Columns for chiral separation	Size
AT.Phenyl (Spherical silica)	S-S-M	AT. Cellulose chiral column	S-S-M
AT.CN (Spherical silica)	S-S-M	AT. Amylose Chiral column	S-S-M
AT.ROR (Spherical silica)	S-S-M	AT. Cyclodextrin Chiral column	S-S-M
AT.DiOl (Spherical silica)	S-S-M		
AT.C18 (Spherical silica)	S-S-M		
AT.C8 (Spherical silica)	S-S-M		
AT.C1 (Spherical silica)	S-S-M		
WLZ.NH2 (Spherical silica)	S-S-M		
AT.SiO2 (Spherical)	S-S-M		

Note: S-S-M: (50–150 mm) \times (2–5 mm) \times (3–7) μm .

Columns for preparing organic compounds, such as AT.C18 (spherical silica), are used for different purposes. As for the separation properties of the columns used in oil cracking fractionation, the traditional packing of high-pressure liquid chromatograph (HPLC) with internal pores has high mass transfer resistance and low column efficiency for the separation of biopolymers, e.g. proteins. Non-porous, monodisperse fine silica particles after surface modification are used as HPLC packing. The silica particles give close packing and form uniform pores among the particles in the column. The size of the pores is about 100 nm and it is a function of the particle diameter. The separation of solutes occurs on the external surfaces of the particles. This type of novel packing effectively overcomes the shortcomings of traditional packing and becomes an important material for high-speed separation of biopolymers. Several sizes of monodisperse silica particles are synthesized as listed in Table 6.27, and non-polar stationary phases bonded by C_8 and C_{18} aliphatic radicals are prepared and treated by the hydrothermal method to close the pores, which were treated with octodecyltrichlorosilicate and octyldimethylchlorosilicate, respectively [40]. The chromatograms of five varieties of proteins under gradient elution on two kinds of non-porous packing (NPS- C_{18} , NPS- C_8) and a macroporous packing (Chromagabond- C_4) are shown in Figure 6.22. The figure demonstrates that the peaks of two proteins with higher molecular weight (BSA and Ova) in the macroporous packing expand; however, the peaks in the non-porous packing are narrowed. Moreover, the column length with non-porous packing is reduced to one-third of that with macroporous packing, thus the time for analysis is shortened.

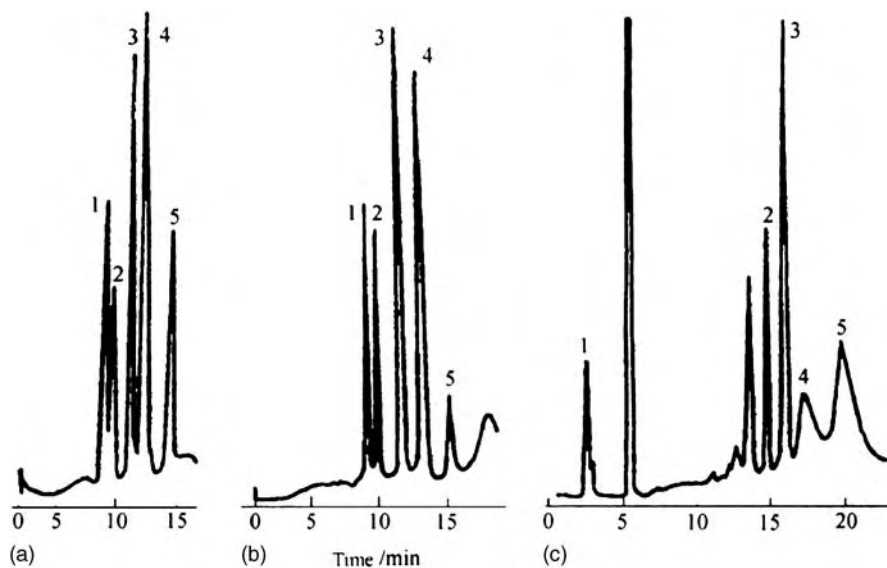


Fig. 6.22. Protein separation on non-porous packing and a macroporous packing chromatographic columns: (a) NPS- C_{18} , 2.1 μm , 50 \times 5 mm i.d.; (b) NPS- C_8 , 2.1 μm , 50 \times 5 mm i.d.; (c) Chromagabond- C_4 , 150 \times 4.6 mm i.d. Peaks: 1 – ribonuclease-A; 2- insulin; 3- lysozyme; 4- bovine serum albumin (BSA); 5-ovalbumin (ova).

Monodisperse silica with nanometer size is used to separate oil cracking and fractionation of other compounds. Their high effectiveness results either from the silica porous structure or its active surface. When the silica diameter is less than 300 nm, the monodispersity is not easy to control and a separation effect is not expected. The 100 nm monodisperse silica is used for these separations.

6.4.2.3. Model catalysts with controlled pore size for heavy oil conversion

Design and development of catalysts with suitable macropores are required for heavy oil conversion. A series of model catalysts with uniform and adjustable pore size are prepared. Their size ranges from 6 to 1000 nm. It is proposed that novel catalysts for heavy oil cracking and hydrogenation [41,42] will be developed, and their active surface can be changed depending on the requirements. Using these model catalysts, the following were achieved: (1) the mechanisms of catalytic reaction of heavy oil; (2) the effect of pore structure of the catalyst on the reactant molecular diffusion and the relationship between the pore structure and selectivity as well as the reactivity; (3) the match of the pore structure of the catalytic supporter with the stock molecule; and (4) the single catalytic behavior of the active surface without diffusion.

Aggregates of non-porous monodisperse silica particles form uniform interstitial pores [41]. Their most probable pore diameter is a function of particle diameter and the range of the pore size distribution is 0.14–0.50 times the particle diameter. The porosity range is 26–35% and roughly independent of the particle diameter. The active components can deposit on the silica surface before or after the accumulation of the particles. Al_2O_3 , TiO_2 , NiO and MoO_3 are used to modify the surfaces of monodisperse silica particles or model supports [42]. Their pore diameter ranges from 6.6 to 85.8 nm. The supports with a pore diameter of 20 nm have restrictive diffusion of the residual oil molecules, which thus need enlarging according to calculations for restrictive diffusion factor [43,44].

References

- [1] Y.C. Ke, Barrier materials for packages, The Meetings of Plastics and Its Processing, Asia and Pacific regions, Shanghai, 2003, p.11.
- [2] Y.C. Ke, Chin. Pat. Appl. 02157993.8, vol. II, 2002.
- [3] Z. Qi, Y.C. Ke, Chin. Pat. ZL97 1 04055.9.
- [4] D.M. Lincoln, R.A. Vaia, Z.-G. Wang, B.S. Hsiao, Polymer 42 (2001) 1621.
- [5] W.T. Reichle, S.Y. Kang, D.S. Everhardt, J. Catal. 101 (1986) 352.
- [6] Q.L. Ren, Q. Luo, H.C. Wu, J. Insulating Mater. 6 (2001) 22.
- [7] A. Usuki, J. Appl. Polym. Sci. 63 (1997) 173.
- [8] Y. Kurokawa, J. Mater. Sci. Lett. 151 (1996) 481.
- [9] T.J. Pinnavaia, Chem. Mater. 6 (1994) 2216.
- [10] M. Kawasumi, Macromolecules 30 (1997) 6333.
- [11] Y.C. Ke, Ph.D. Dissertation, Jilin University, China, 1996.
- [12] Y.C. Ke, J. Chin. Plast. 17 (9) (2003) 43.
- [13] Z.N. Qi, J. Shanghai Jiao Tong Univ. 32 (9) (1998) 130.
- [14] G. Jimenez, N. Cyata, J. Appl. Polym. Sci. 11 (1997) 2211.
- [15] C.M. Ke, H.Z. Wang, Paint Coat. Ind. 33 (3) (2003) 14.
- [16] Y. Pawar, Ind. Eng. Chem. Res. 32 (1993) 743.
- [17] F.P.J.M. Kerkhof, J. Phys. Chem. 83 (1979) 1612.

- [18] D. Makoto, K. Kazuyuki, *Chem. Rev.* 95 (1995) 399.
- [19] M. Gratzel, *Energy Resources through Photochemistry and Catalysis*, Academic Press, New York, 1983.
- [20] M.D. Newsham, E.P. Giannelis, T.J. Pinnavaia, K.G. Nocera, *J. Am. Chem. Soc.* 110 (1988) 3885.
- [21] S.L. Suib, J.F. Tanguay, M.L. Occelle, *J. Am. Chem. Soc.* 108 (1986) 6972.
- [22] H. Yoneyama, S. Nippa, *Chem. Lett.* 11 (1988) 1807.
- [23] T. Cassagneau, G.B. Hix, D.J. Jones, P. Maireles-Torres, M. Rhomari, J. Rozeere, *J. Mater. Chem.* 4 (1994) 189.
- [24] A. Kudo, K. Sayama, K. Asakura, K. Domen, K. Maruya, T. Onisi, *J. Catal.* 120 (1989) 337.
- [25] (a) W.Z. Zhou, J.M. Thomas, D.S. Shephard, et al., *Science* 280 (1998) 705; (b) A. Imhof, D.J. Pine, *Nature* 389 (1997) 948.
- [26] M. Van Boekel, P. Walstra, *Colloid Surf.* 3 (1981) 109.
- [27] A. Tugita, S. Takemoto, K. Mori, Y. Otami, *J. Colloid Interface Sci.* 95 (1983) 551.
- [28] V.B. Menon, D.T. Wasan, *Sep. Sci. Technol.* 23 (1988) 2131.
- [29] T.F.M. Tadros, B. Vincent, in: P. Becher (Ed.), *Encyclopedia of Emulsion Technology*, Vol. 1, Marcel Dekker, New York, 1983, p. 272.
- [30] S. Levine, E. Sanford, *Can. J. Chem. Eng.* 58 (1985) 622.
- [31] D.E. Tmabe, M.M. Sharma, *J. Colloid Interface Sci.* 157 (1993) 244.
- [32] D.E. Tambe, M.M. Sharma, *J. Colloid Interface Sci.* 162 (1994) 1.
- [33] D.Y. Zhao, J.L. Feng, Q.S. Huo, et al., *Science* 279 (1998) 548.
- [34] K.J. Shea, D.A. Loy, O. Webster, *J. Am. Chem. Soc.* 114 (1992) 6700.
- [35] T. Asefa, M.J. MacLachlan, N. Coombs, et al., *Nature* 402 (1999) 867.
- [36] C.T. Kresge, M.E. Leonowicz, W.J. Roth, et al., *Nature* 359, (1992) 710.
- [37] K. Kageyama, T. Tamazawa, J-ichi, *Science* 285 (1999) 2113.
- [38] (a) Y.C. Ke, J.R. Hu, H. Wang, *Chem. Ind. & Eng. Prog.* 22(12) (2003) 1308; (b) J.F. Rong, Ph.D. Dissertation, Institute of Petrochemical Science and Technology, Sinopec, Beijing, 1999.
- [39] M.R. Towler, I.R. Gibson, S.M. Best, *J. Mater. Sci. Lett.* 19 (2000) 1689.
- [40] P. Dong, P. Ren, *Proceedings of the 11th National Conference on Chromatography*, Dalian, 1997, pp. 55–56, (in Chinese).
- [41] P. Dong, Y. Zhu, in: S.Y. Chen, et al. (Eds.), *Collection in Technical Basis for Preparation of Catalysts*, Hangzhou University Press, Hangzhou, 1997, pp. 93–97 (in Chinese).
- [42] X.C. Guo, P. Dong, *Langmuir* 15(17) (1999) 5535.
- [43] Y. Pawar, L. Anderson, *Ind. Eng. Chem. Res.* 32 (1993) 743.
- [44] D.Z. Zhang, *Physics* 23(3) (1994) 141.

Subject Index

A

Active component dispersion, 350
Additives, 122, 363, 378
 petroleum, 378
 petrochemical engineering, 378
Adsorbing agents, 365
Adsorption behavior, 35
AFM (atomic force microscopy), 296
 application fields, 297
 principle, 296
Antibacterial nanocomposites, 364
Applied standards, 345
Application approach, 376
Assembly, 256
 mesoporous SiO₂, 256
 nano-ZnO, 256
 self-assembly, 323, 246
Attapulgite, 366
Avrami equation, 180

B

Barrier
 materials, 330
 properties, 256
Beer bottle, 332
Bending modulus, 244
BHET molecule, 302
Biology, 382
Blending
 melting, 172
 in situ polymerization, 173
 media, 173
Bragy equation, 286

C

Carriers, 353
 olefin polymerization, 357
 particles, 361
 nanometer pore structure, 361
Carrying MAO on SiO₂ approaches, 354
Catalysts, 349
Cation exchange methods, 361
Calibration standard particles, 384
Caprolactum, 121

Chemical

 building materials, 380
 materials, 378
Classification, 6
 nanocomposite, 6
 polymer-inorganic, 6
 silicate, 8
 layered silicate, 8
 polymer-inorganic nanocomposites, 51
 related compounds, 8
Clay particles, 364
 asphaltenes modifications of, 364
Clothes, 340
Coagulation, 39
Coatings, 341
Colloid stability, 39
 aggregation stability, 40, 41
 dynamic stability, 39
Composite, 6
 materials, 6
 organic-inorganic, 6
Computer modeling, 302
Condensed structure, 29
Conducting electricity, 348
Construction materials, 380
Controlled pore size, 387
 model catalysts, 387
 heavy oil conversion, 387
Controlling properties, 367
Copolymer, 223
 blending of, 224
 block, 223
 nanoparticle array, 249
 self-assembling of, 224
 tri-block, 223
Coulter particle size analyzer, 306
Crystal
 chlorite, 17
 clay minerals, 11
 kaolinite, 11
 mixed-layer minerals, 19
 montmorillonite, 13
 ollote, 16
 sepiolite, 18
 size, 285
 structure, 11

Crystallization, 228, 311, 314
 acceleration effect, 317
 comparison, 319
 degree, 289
 rate, 317, 318, 319
 activation energy, 316
 rescanning, 318
 Curing reagents, 136

D

Degree, 234, 374
 Debye-Huckel equation, 38
 Deposition, 251
 approach, 57
 chemical vapor, 252
 electrochemical, 251
 electroless, 251
 sol-gel, 252
 Discoloring by adsorption, 375
 Dispersion
 degree, 34
 techniques, 346
 phase and media, 33
 redispersion of, 79
 solvent intercalation, 105
 steric effect, 80
 surface treatment of, 77
 surfactant, 78
 DLVO theory, 43
 Doping, 256
 environmental sensitivity, 262
 interface coupling effect, 263
 mesoporous silica, 257
 position modulation, 261
 rheology, 263
 dynamic behavior, 263
 Double-melting behaviors, 312
 Drying polymer-grade powders, 369
 DSC, 301

E

Ecological protection, 383
 Electronics, 348
 Emulsion
 preparation, 364
 method, 377
 Crystal structure, 10
 layered silicates, 10
 clay minerals, 10
 Energy resources, 381
 Engineering plastics, 337
 Epoxy
 intercalation behavior, 142

monomer, 136
 nanocomposite additive, 137
 Equipment selection, 371
 Esterification
 direct, 174
 indirect, 175
 Exfoliation behavior, 145
 Expansion property, 375

F

Factors
 affecting final results, 291
 sampling, 291
 media, 292
 morphology, 292
 stability, 292
 Fibers, 340
 Films, 339
 materials, 384
 polymer-layered silicate, 339
 polymer-silica, 201
 polymorphism of, 232,233
 PP-layered silicate, 340
 PP nanocomposite films, 340
 PP-silica films, 340
 polyester, 337
 Fire-retardant materials, 334
 Flocculation, 39
 Fluorescent reinforcing effect, 256
 Functionalized, 338
 plastics, 338
 fibers, 338

G

Gel valence, 376
 General aspects for nanocomposite, 54
 dry method, 54
 evaporating method, 54
 free energy variation, 153
 sedimentation method, 54
 wet method, 54

H

Halpin-Tsai equation, 279
 Heat distortion temperature (HDT), 280, 283
 HPLC packing, 385
 Heterogeneous structure agents, 359

I

Information technology, 382
 Inorganic coatings, 345

- In situ polymerization composites, 55
- Intercalation
chemistry, 60
dynamics of, 226
melt, 100, 178
oligomer, 111, 117
polymerization, 377
polymer-MMT nanocomposites of, 61
solvent, 176
technology of, 382
isothermal, 230
emulsion, 107
granule, 71
media, 101
monomer, 106
- K**
- Kaolinite, 377
- L**
- Lambert-beer equation, 291
- Layered, 10
silicate structure, 10
alumina octahedron, 11
octahedral crystal sheet, 11
combination of, 11
crystal sheets, 11
composition, 70
dispersion behavior, 116
double hydroxides, 335
particle exfoliation, 82
plate structure, 367
precursor intermediate, 101
silica tetrahedron, 10
silica crystal sheet, 10
- LDHs, 367, 377
structure memory, 367
- Light scattering, 289
TEOS tracing hydrolysis, 24
- Light decay, 290
- M**
- Materials, 381
- Magnetic behavior, 343
- Mechanical properties, 243
- Medicine, 382
- Membrane, 384
- Metallocene catalyst preparation, 354
- Microemulsion approach, 56
- Mixing ethylate approach, 55
alcoholic sodium approach, 56
ethanol-ammonia approach, 56
- MMT, 368
gel and powders, 368
MMTs, 377
- Models
carrier preparation, 349
catalysts preparation, 349
intercalation, 303
bulk polymers, 303
- Molecular
self-organization, 248
viscosity, 293
weight, 293
- Monodisperse silica, 25, 84
dispersion behavior of, 115
electric rheological fluid, 89
microsphere selection of, 90
reselection of, 91
particle applications of, 384
- Multiple structure, 44
chain, 44
second level, 45
nanocomposites structures, 308
structure of polymers, 44
condense state, 45
- N**
- Nanocoatings, 342
- Nanocomposite applications, 330
- Nanocomposite morphology
complete exfoliation of, 171
PS-MMTs, 170
poly(ethylene terephthalate)(PET), 172
- Nanocomposite preparation methods, 52
blending methods, 52
intercalation methods, 52
filling methods, 53
nanoprecursor methods, 52
sol-gel methods, 52
- Nanocomposite properties
HDT, 179
mechanical, 179
PEO-clay, 154
physical, 179
PI-MMT hybrids, 200
polyethylene-MMT, 166
polystyrene-inorganic, 167
PS-MMTs, 169
- Nanocomposites, 253, 377
PMMA-based, 197
polyamide-silicate, 120
polyaniline-silicate, 190
polyester-silicate, 172
polyethylene oxide-MMTs, 136
polyethylene oxide-silicate, 135

polyimides-based, 198
 polymer-layered silicate, 253
 polymer-silica, 253
 polyolefin-silicate, 155
 Nanocomposites tubes, 379
 Nanoeffect, 7
 critical scale, 7
 nanocomposites, 7, 312
 assembly, 324
 self-assembly, 324
 condensed state, 315
 thermal behavior, 312
 Nanomaterial catalysts significance, 374
 Nanomaterials products, 368
 Nanometer, 3
 Nanofibers as carriers, 374
 Nanoparticle, 228
 growth of, 266
 Nanoparticle coatings technologies, 346
 Nanoparticle precursor, 135
 Nanopowder coatings, 344
 Nanoscale, 3
 nanomaterial, 3
 nanoparticle, 3
 Nanosilica products, 372
 Nanostructure, 3, 212, 253
 Unit of, 61
 assembled, 221
 composite, 215
 distribution, 215
 layer, 311
 mesoporous solid, 215
 metal colloid, 248
 phase separation, 222
 pore, 215
 self-organized, 248
 specific surface area, 216
 spinodal phase decomposition of, 221
 surface atomic numbers, 216
 synthesis of, 249
 Nanotechnology, 3
 Non-isothermal, 230
 Nucleation, 265, 311
 annealing, 265
 in-situ, 266
 LBL film, 265
 melt, 265
 metal oxide, 265
 solution, 265
 polymeric electrolytes, 265

O

Optical properties, 254
 Organo-clay, 140

P

Packages, 330
 Particle, 212
 application of, 220
 morphology, 212, 228
 order, 226
 phase separation of, 221
 size deviation of, 217, 220
 statistical distribution of, 212
 surface morphology of, 212
 Particle and porosity, 32
 Particle measurement, 278
 Particle morphology, 276
 assembled structure, 276
 ordered structure, 276
 multiple-layered, 276
 round-shaped structure, 276
 aggregation, 323
 Particle preparation, 86
 PE-inorganic nanocomposite, 162
 Phase, 33
 Phase interface, 33
 Phase transformation of, 232
 Photo catalysis, 362
 PI-MMTs
 flow chart, 198
 recipe, 198
 Plasma deposition approach, 57
 PMMA-silica nanocomposite, 197
 Polyamide, 120
 PA11, 120
 PA6, 120
 PA66, 120
 Polyaniline (PAN), 190
 Polypropylene, 155
 Polystyrene, 167
 Polyester cloth, 337
 Polymer-based nanocomposites, 50
 Polymer classification, 47
 biopolymers or biomacromolecules,
 49
 functional, 49
 universal usage of, 48
 special type of, 49
 high performance of, 49
 Polymerization
 casting nylon, 133
 ethylene, 159
 nylon, 66, 126
 PAN, 192
 polyamide, 124
 polypropylene, 158
 Polymerization intercalation, 101
 Pore structure effect, 350

Porous heterogeneous structure, 339
 preparation, 359
 Precursor, 22
 Silica, 22
 tetra ethylene oxide silicon, 23
 Preparation, 25
 MMTs/oxide composite carrier, 155
 monodisperse SiO₂, 25
 nylon66 nanocomposite, 126
 PA6-MMTs nanocomposites, 124
 Polybutyleneterephthalate-clay,
 nanocomposite, 182
 polyester-clay nanocomposite, 173
 polyethyleneterephthalate-clay, nanocomposite,
 179
 polystyrene-inorganic nanocomposite, 167
 PS-MMTs nanocomposites, 168
 silica colloid crystal, 32
 SiO₂ opals, 25
 Submicrospheres, 25
 nanocomposite products, 374
 Product markets, 377
 Product processing technology, 371
 Product quality control, 375
 Properties
 barrier properties, 283
 mechanical properties, 283
 thermal properties, 283
 Propping layered silicates, 355
 Prospects, 380, 384

Q

Quality control, 375

R

Rate, 234
 colloidal crystal, 248
 Rayleigh expression, 293
 Reinforcing plastics, 338
 Relationship of, 245

S

Schulze-Hardy principle, 43
 Sedimentation, 36
 Sedimentation equilibrium, 36
 Silica, 377
 drying of, 372
 porous, 371, 372
 powders of, 372
 Silica modification, 84, 88
 oligomer treatment of, 107
 particle grade of, 84

 self-assembly mechanism, 98
 silica diffusion, 334
 Silicates, 3, 334
 purification, 71
 dispersion, 77
 modification, 70
 epoxy nanocomposite, 140
 Sol-gel approach, 54
 Sol-gel process, 376
 Sources of light, 290
 Specific surface area, 34
 Spherulitic morphology, 315
 Stabilizing emulsion nanoparticles,
 363
 Structure, 253
 optical effects of, 254
 ordered, 253, 254
 silica colloidal crystal, 254
 silicate heterogeneous, 359
 Surface morphology, 277
 interface model of, 277
 interface order model of, 277
 Synthesis, 360
 crystalline intermediates, 360
 layered metal oxides, 360
 nanometer catalysts, 360
 organic-inorganic, 360

T

Template, 250
 alumina, 250
 emulsion, 371
 metal, 250
 non-surfactant, 371
 polymer, 250
 surfactant, 371
 synthesis methods of, 251
 Template synthesis, 361
 Tensile strength, 244
 Thermal properties, 237
 crystallization degree, 186
 fire retardancy, 241
 heat distortion temperature, 184,
 239
 non-isothermal crystallization, 185
 relationship of, 242
 specific heat, 241
 thermal, 237
 thermal degradation, 240
 thermal degradation and melting, 186
 Theories, 278
 diffusion, 36
 electromotion potential, 36

thermal dynamics, 242
Averami equation, 181, 230,
231
light scattering, 290
optical omitting, 290
Traditional industries, 377

W

Water adsorption property, 375

Z

Zeta potential, 38
Ziegler-Natta catalyst, 358